REFINEMENT OF PTR-MS METHODOLOGY AND APPLICATION TO THE MEASUREMENT OF (O)VOCS FROM CATTLE SLURRY.

EMILY HOUSE

A thesis submitted to the University of Edinburgh, College of Science and Engineering for the degree of Doctor of Philosophy.

2008

Declaration of Originality

The work in this thesis is the original work of the author throughout the text, except where otherwise acknowledged, and has not been presented previously, wholly or in part, for the award of any degree in any university.

Acknowledgements

Abstract

Oxygenated volatile organic compounds ((O)VOCs) contribute to ozone formation, affect the oxidising capacity of the troposphere and are sources of growth, and in some cases formation, of aerosols. It is therefore important to identify and quantify sources of (O)VOCs in the troposphere. In the late 1990s a unique technique for quantification of organic trace gas species, proton transfer reaction mass spectrometry (PTR-MS) was developed. PTR-MS potentially offers rapid response and high sensitivity without the need for sample pre-concentration. Concentrations can be derived from the PTR-MS either by calibration or can be calculated from measured ion count rates and kinetic considerations.

In this work, the methodology of PTR-MS application is critically assessed. The uncertainties and inaccuracies associated with each parameter employed in the calculation of concentrations are reviewed. This includes a critical appraisal of models for the calculation of the collisional rate constant currently applied in the field of PTR-MS. The use of a model to account for the effects of the electric field, available in the literature but not previously applied to the PTR-MS, is advocated. Collisional rate constants employing each of the models discussed have been calculated for the reactions of H_3O^+ with over 400 molecules for PTR-MS.

In PTR-MS it cannot be assumed that the product ion occurs only at the protonated non-dissociated mass. Few product distributions obtained from PTR-MS are cited in the literature, and even then the reaction chamber conditions (pressure, temperature and electric field strength) are not always specified. A large volume of product distributions for trace gases with H_3O^+ in select ion flow tube mass spectrometry (SIFT) exists in the literature and is reviewed. In SIFT, no electric field is applied to the reaction chamber and the extent and even nature of fragmentation can differ in PTR-MS. In addition to the application of an electric field, the energy in the reaction chamber can be increased by increasing the temperature or by variation of the reagent ion. In this work, the increase in energy *via* the three methods is approximated to enable a comparison of product distributions. The review of product distributions in PTR-MS, select ion flow drift tube mass spectrometry (SIFDT), variable temperature select ion flow tube mass spectrometry (VT-SIFT), SIFT, proton transfer reaction time of flight mass spectrometry (PTR-TOF-MS), proton transfer reaction ion trap mass spectrometry (PTR-ITMS) and electron ionisation mass spectrometry (EI-MS) is used alongside thermodynamic considerations to collate a list of potential contributors to a range of mass to charge ratios (m/z) in the PTR-MS. The need for further measurements of product distributions as a function of temperature, pressure and electric field strength for a

wider range of (O)VOCs is highlighted. This enables dissociation to be better used as a tool for compound identification rather than being considered a hindrance.

The collation of likely product distributions is applied to identify possible contributors to m/z observed during PTR-MS measurements of emission from cattle slurry. Field measurements were made during fertilisation of a grassland site south of Edinburgh in 2004 and 2005 and in laboratory-based measurements in 2006. Contextual reasoning, previous measurements and isotope ratios are used to narrow the list of possible contributors. Large concentrations of m/z cautiously identified as alcohols followed by a latter peak in carboxylic acids were observed during laboratory measurements. Increases in the corresponding m/z were also observed during the fertilisations. Other tentatively identified compounds emitted included phenol, methyl phenol, trimethylamine, and various sulphur containing compounds.

Contents

Appendices

Electronic Format

1 Introduction

(Oxygenated) volatile organic compounds (O)VOCs include pure hydrocarbons and organic compounds containing oxygen. These compounds may include other elements such as sulphur or halogens. (O)VOCs are found at trace levels (mixing ratios of parts per billion and less) in the troposphere. The troposphere is the lowest level of the atmosphere extending from Earth's surface up to an altitude of 10 to 15 km (Seinfeld and Pandis 1998).

(O)VOCs are released in to the troposphere through anthropogenic and biogenic activities. Anthropogenically produced (O)VOCs include large quantities of alkanes, alkenes and alkylbenzenes emitted as the result of their use in industry, for example as solvents, and due to the treatment, storage, distribution and combustion of fossil fuels (Freidrich and Obermeier 1999). Major biogenic (O)VOCs include methane, 2-methyl-1,3-butadiene (isoprene), monoterpenes and dimethylsulphide (Fall 1999). Guenther *et al* (1995) estimated that 2-methyl-1,3-butadiene comprises 44 % of natural global non-methane VOC flux, with monoterpenes constituting a further 11 %. Total global annual emissions of 2-methyl-1,3-butadiene were estimated by Guenther *et al* (2006) to be 600 Tg.

Oxygenated volatile organic compounds (OVOCs) are also produced as a result of tropospheric oxidation of volatile organic compounds (VOCs). For example Singh *et al* (2000) estimated that 28 Tg yr^{-1} of acetone is produced from the oxidation of propane, *iso*-butane, *iso*-pentane, *iso*-butene, *iso*-pentene monoterpenes and methylbutenol constituting ~50 % of the global source of acetone (~ 56 Tg yr^{-1}).

(O)VOCs are oxidised in the troposphere by reaction with hydroxyl radicals (*OH*), nitrate radicals (*NO₃*) and ozone (*O₃*). The chemistry of *OH* radicals in the troposphere is complex and details can be found elsewhere (e.g. Derwent 1999, Seinfeld and Pandis 1998). Briefly, *OH* radicals are mainly produced in the troposphere by photolysis of *O₃* (λ < 310 nm) followed by reaction of the resulting singlet oxygen atom with water vapour, but they are also produced by the reaction of hydroperoxy radicals (*HO₂*) with nitric oxide (*NO*), and photolysis of nitrous acid (*HONO*), methanal (*HCHO*) and higher aldehydes. *OH* radicals are interconverted with *HO₂*. *OH* radicals are removed by reaction with nitrogen dioxide (*NO₂*) to form nitric acid (*HNO₃*) (e.g. Seinfeld and Pandis 1998, Derwent 1999). The reactions of (O)VOCs with *OH* generally dominate during the day. However due to the photolytic nature of *OH* radical production the reactions of (O)VOCs with *NO₃* and to a lesser extent *O₃* become important during the night (e.g. Atkins 2000).

The reaction of VOCs with *OH* can result in O_3 formation in the troposphere. O_3 in the troposphere is a health hazard to humans and plants, and is formed by the reaction of molecular oxygen (O_2) and atomic oxygen (O) (Eq. 1.1). Atomic oxygen is formed in the troposphere by the photolysis of NO_2 also producing *NO* (Eq. 1.2). In turn, *NO* removes O_3 by reaction to form NO_2 and O_2 (Eq. 1.3).

$$O_2 + O \xrightarrow{\quad M \quad} O_3 \qquad\qquad (1.1)$$

$$NO_2 \xrightarrow{\quad h\nu \quad} NO + O \qquad\qquad (1.2)$$

$$O_3 + NO \rightarrow NO_2 + O_2 \qquad\qquad (1.3)$$
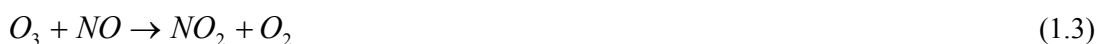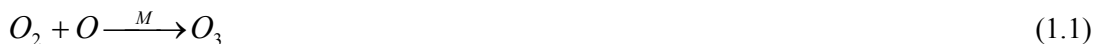
The oxidation of VOCs can provide an alternative route of *NO* reaction, thereby effectively reducing O_3 removal by reaction with *NO* (Eq. 1.3), the reaction of a VOC, *R*, with *OH* and subsequently O_2 initially produces a peroxy radical (RO_2). In the presence of *NO* the peroxy radical reacts with *NO* to form NO_2 and an alkoxy radical (*RO*). This alkoxy radical may subsequently react with O_2 forming HO_2 and an OVOC. The HO_2 may then react with *NO* to form *OH* and NO_2 and the OVOC may react with *OH* is a similar manner to the original VOC (as described above) (Derwent 1999, Seinfeld and Pandis 1998, Atkins 2000). Methane, for example, reacts with *OH* by hydrogen abstraction producing a methyl radical (CH_3) and water. The methyl radical subsequently reacts with oxygen, *via* a termolecular process, forming a methyl peroxy radical (CH_3O_2). The methyl peroxide radical can subsequently react with *NO* producing NO_2 and a methoxy radical. The methoxy radical may react with oxygen producing HO_2 and methanal. Methanal may subsequently be photolysed producing *OH* or may react with *OH*. This HO_2 can subsequently react with *NO* to form *OH* and NO_2. Thus two molecules of NO_2 are potentially produced from one molecule of methane in this process. This NO_2 can subsequently react *via* Eq. 1.2 and Eq. 1.1 to form O_3 (Derwent 1999).

In addition, the products of oxidation of some (O)VOCs have been linked to aerosol formation. Some of the oxidation products have low volatilities and condense onto existing aerosol particles partitioning between the gas and particulate phases. Anthropogenic VOCs including benzene, toluene and dimethylbenzene (xylene) have been shown to form secondary organic aerosol (e.g. Forstner *et al* 1997, Hurley *et al* 2001, Kleindienst *et al* 2004, Martín-Reviejo and Wirtz 2005). Aerosol formation from the major biogenic VOCs, 2-methyl-1,3-butadiene (isoprene) and the monoterpenes, has also been observed (e.g. Kroll *et al* 2005, Ng *et al* 2006, Lee *et al* 2006). The ability of an (O)VOC to contribute to aerosol formation in this manner depends on the concentrations present, its chemical reactivity, the vapour pressure of its products and the nature and mass of existing aerosol onto which the

products may condense (Seinfeld and Pandis 1998). Some (O)VOCs also contribute to the formation of new aerosol. For example, the oxidation of many volatile organic sulphur containing compounds (VOSCs), such as dimethylsulphide, results in the formation of sulphuric acid (H_2SO_4) which can nucleate to form H_2SO_4-H_2O particles (e.g. Charlson *et al* 1987, Seinfeld and Pandis 1998). A number of (O)VOCs are also a human health hazard, for example, benzene and several polyaromatic hydrocarbons are carcinogens (e.g. Sterner 1999).

Using proton transfer reaction mass spectrometry (PTR-MS), (O)VOCs can potentially be detected at trace (ppt, part per trillion) concentrations with fast response times and without the need for sample pre-concentration. PTR-MS is a chemical ionisation mass spectrometry technique in which H_3O^+ reagent ions are employed to ionise trace (O)VOCs under the influence of an electric field. The molecules of sampled air which do not react with H_3O^+ act as the buffer gas. Concentrations can be derived by calibrating the instrument with the relevant (O)VOC over a range of concentrations to determine a value of ion count rates per ppb of (O)VOC. However, in the case of OVOCs such as the carboxylic acids, which are observed in emissions from animal waste, the comparably low volatility and sticky nature of the species prevent the development of stable calibration standards in the ppt to ppb range. In addition, a huge number of (O)VOCs are present in the troposphere and can be detected by PTR-MS, so calibration for every species is not possible. Alternatively, concentrations can be calculated theoretically from kinetic considerations using the rate constant for the reaction of the (O)VOC with H_3O^+, the reaction time, the experimentally-derived detection efficiencies of the ions and the measured count rates of the reagent and product ions.

The main objective of this thesis is to assess and improve upon the theory and methodology of PTR-MS and to apply the technique to qualitatively assess (O)VOCs emitted from cattle slurry. Chapter 2 describes the PTR-MS, methods of operation, the associated uncertainties and inaccuracies and possible approaches for their reduction. The background to PTR-MS development (§ 2.1), the principles of operation (§ 2.2) and instrument configuration (§ 2.3) are initially outlined. A critical assessment of the parameters employed in the calculation of concentrations, the manner of their derivation, and other factors possibly affecting the calculation follows. This includes a discussion of the applicability of theories for the derivation of collisional rate constants. The possible effect of the electric field on collisional rate constants is discussed. The use of the results of trajectory calculations of collisional rate constants, parameterised for dependence on the energy of the ion in the presence of an electric field and the temperature of the neutral (Su 1994), to reduce inaccuracies in the calculation of concentrations in the PTR-MS is proposed for the first time.

In Chapter 3 the nature and extent of reactions in the PTR-MS are discussed. The existing literature documenting fragmentation in the PTR-MS is critically reviewed. Measurements of product distributions in the PTR-MS literature are scarce. Published product distributions observed from reactions with H_3O^+ in select ion flow tube mass spectrometry (SIFT) are utilised to hypothesise possible fragmentations in the PTR-MS. No electric field is applied in SIFT and the consequent reduction in energy results in reduced fragmentation. In addition to the increase in levels of fragmentation compared to those observed in SIFT, new pathways of reaction may become energetically viable in the PTR-MS. As well as application of an electric field around the reaction chamber, energy may be elevated by increases in temperature, or the use of an alternative protonating reagent ion to increase the enthalpy of reaction. A novel method is employed to estimate product distributions in the PTR-MS from those observed from reactions with H_3O^+ in variable temperature select ion flow tube mass spectrometry (VT-SIFT) and from SIFT where alternative protonating ions have been used. This approach involves the approximation of the change in energy relative to reaction with H_3O^+ at 298 K. Assumptions and limitations of this approach are discussed. The use of electron ionisation mass spectrometry (EI-MS) to assist deduction of fragmentation patterns has been suggested in some PTR-MS literature (e.g. Malekina *et al* 2007) and is discussed. Thermodynamic considerations are used to aid interpretation of existing data and to discuss the likelihood of potential reaction pathways. The enthalpies of several reactions are estimated for the first time. In the case of reactions other than non-dissociative proton transfer, thermodynamic considerations are limited in the absence of activation energies, some available activation energies are reviewed. Published product distributions measured in select ion flow drift tube mass spectrometers (SIFDT), proton transfer reaction time-of-flight mass spectrometers (PTR-TOF-MS) and proton transfer ion trap mass spectrometry (PT-ITMS) are included in the appraisal. Finally the results of the preceding discussion are collated in a mass chart summarising potential contributors to a range of mass to charge ratios (m/z) in PTR-MS.

In Chapter 4 the results of Chapter 3 are utilised to interpret measurements of (O)VOCs emitted from cattle slurry. The results of measurements made using PTR-MS during fertilisation of a grassland site south of Edinburgh in 2004 and 2005 and from laboratory based cuvette measurements in 2006 are reported. Isotope ratios, contextual reasoning and previous measurements in the literature, using alternative techniques such as GC, are employed to identify likely candidates at m/z at which elevated concentrations were observed.

References

Atkins, R (2000) Atmospheric chemistry of VOCs and NO_x, *Atmospheric Environment*, **34**: 2063-2101.

Charlson, R. J., J. E. Lovelock, M. O. Andreae, S. G. Warren (1987) Oceanic phytoplankton, atmospheric sulphur, cloud albedo and climate, *Nature*, **326**: 655 – 661.

Derwent, R. G. (1999) Chapter 7: Reactive Hydrocarbons and Photochemical Air Pollution. In: *Reactive Hydrocarbons in the Atmosphere*, edited by C. N. Hewitt, pages 267-291. Academic Press, London.

Fall, R (1999) Chapter 2: Biogenic Emissions of Volatile Organic Compounds from Higher Plants. In: *Reactive Hydrocarbons in the Atmosphere*, edited by C. N. Hewitt, pages 41-91. Academic Press, London.

Forstner, H. J. L., R. C. Flagan, J. H. Seinfeld (1997) Secondary organic aerosol from the photooxidation of aromatic hydrocarbons: Molecular composition, *Environmental Science and Technology*, **31**: 1345 – 1358.

Fredrich, R., A Obermeier (1999) Chapter 1: Anthropogenic Emissions of Volatile Organic Compounds. In: *Reactive Hydrocarbons in the Atmosphere*, edited by C. N. Hewitt, pages 1-39. Academic Press, London.

Guenther, A., C. N. Hewitt, D. Erickson, R. Fall, C. Geron, T. Graedal, P. Harley, L. Klinger, M. Lerdau, W. A. McKay, T. Pierce, B. Scholes, R. Steinbrecher, R. Tellamraju, J. Taylor, P. Zimmerman (1995) A global model of natural volatile organic emissions, *Journal of Geophysical Research*, **100**: 8873-8892.

Guenther, A., T. Karl, P. Harley, C. Wiedinmyer, P. I. Palmer, C. Geron (2006) Estimates of global terrestrial isoprene emissions using MEGAN (Model of Emissions of Gases and Aerosols from Nature), *Atmospheric Chemistry and Physics*, **6**: 3181 – 3210.

Hurley, M. D., O. Sokolov, T. J. Wallington, H. Takekawa, M. Karasawa, B. Klotz, I. Barnes, K. L. Becker (2001) Organic aerosol formation during the atmospheric degradation of toluene, *Environmental Science and Technology*, **35**: 1358 – 1366.

Kleindienst, T. E., T. S. Conver, C. D. McIver, E. O. Edney (2004) Determination of secondary organic aerosol products from the photooxidation of toluene and their implications in ambient $PM_{2.5}$, *Journal of Atmospheric Chemistry*, **47**: 79 – 100.

Kroll, J. H., N. L. Ng, S. M. Murphy, R. C. Flagan, J. H. Seinfeld (2005) Secondary organic aerosol formation from isoprene photooxidation under high-NO_X conditions, *Geophysical Research Letters,* **32**: L18808: 1 – 4.

Lee, A., A. H. Goldstein, J. H. Kroll, N. L. Ng, V. Varutbangkul, R. C. Flagan, J. H. Seinfeld (2006) Gas-phase products and secondary aerosol yields from the photooxidation of 16 different terpenes, *Journal of Geophysical Research*, **111** (D17305): 1 – 25.

Malekina, S. D., T. L. Bell, M. A. Adams (2007) PTR-MS analysis of reference and plant-emitted volatile organic compounds, *International Journal of Mass Spectrometry*, **262**: 203-210.

Martín-Reviejo, M., K. Wirtz (2005) Is benzene a precursor for secondary organic aerosol?, *Environmental Science and Technology*, **39**: 1045 – 1054.

Ng, N. L, J. H. Kroll, M. D. Keywood, R. Bahreini, V. Vautbangkul, R. C. Flagan, J. H. Seinfeld (2006) Contribution of first- versus second-generation products to secondary organic aerosols formed in the oxidation of biogenic hydrocarbons, *Environmental Science and Technology*, **40**: 2283 – 2297.

Seinfeld, J. H., S. N. Pandis (1998) *Atmospheric Chemistry and Physics From Air Pollution to Climate Change*, John Wiley & Sons, Inc., United States of America.

Singh, H., Y. Chen, A. Tabazadeh, Y. Fukui, I. Bey, R. Yantosca, D. Jacob, F. Arnold, K. Wohlform, E. Atlas, F. Flocke, D. Blake, N. Blake, B. Heikes, J. Snow, R. Talbot, G. Gregory, G. Sachse, S. Vay, Y. Kondo (2000) Distribution and fate of selected oxygenated organic species in the troposphere and lower stratosphere over the Atlantic, *Journal of Geophysical Research*, **105** (D3): 3795-3805.

Sterner, O (1999) *Chemistry, Health and Environment*, WILEY-VCH, Weinheim.

Su, T. (1994) Parameterization of kinetic energy dependences of ion-polar molecule collision rate constants by trajectory calculations, *Journal of Chemical Physics*, **100** (6): 4703.

2 Proton Transfer Reaction Mass Spectrometry (PTR-MS)

2. 1 The Background to PTR-MS Development

PTR-MS combines chemical ionisation (CI) with swarm based techniques to enable quantification of trace species with rapid response times. Chemical ionisation (CI) developed by Munson and Field (1966) produces ions for mass spectrometer analysis *via* ion-molecule reactions (IMR) in the gas phase. The advantage of CI over alternative ionisation techniques, such as electron impact or photoionisation, for application to atmospheric trace species measurement is the comparatively low degree of fragmentation (refer to Lindinger *et al* 1993). Minimising fragmentation facilitates allocation of masses and quantification of individual compounds when analysing a mixture of many compounds. Swarm based techniques and their progression have been comprehensively reviewed elsewhere (Lindinger 1986a, Graul and Squires 1988, Ferguson 1992, Bohme 2000). The following section provides only a brief overview. This does not include the advances and variability in the nature of ion source generation which was addressed in detail by Graul and Squires (1988).

Swarm techniques were developed for the study of kinetics of low energy ion-molecule reactions. Subsequent instrument developments, namely the addition of electric field (already employed for the study of ion mobilities) and/or temperature variability have enabled determination of the energy dependency of reaction rates and product distributions. These studies continue to be key to the understanding of ionospheric chemistry as reviewed by Viggiano, 2006 and Ferguson 2007 with some application in tropospheric ion-molecule chemistry (e.g. Eisele *et al* 2006) and astrophysics (e.g. Španěl *et al* 1995a).

Stationary swarm/stationary afterglow techniques are used to determine ion − molecule reaction rate constants. 'Afterglow' refers to light emission observed in these instruments which occurs as a result of recombination of excited ions and electrons resulting in emission of photons. Ions are produced by spiking of inert buffer with traces of particular gases e.g. N_2 which is introduced the microwave discharge to produce e.g. N_2^+ and N^+. Ions (A^+) are discharged in a low pressure chamber filled with inert buffer. Neutral molecules (B) are then introduced. The concentration of ions in the absence of B is dependent on diffusion alone. On addition of B the chemical reaction of A^+ with B also effects A^+ concentration. Thus the rate constant can be determined from time dependencies of $[A^+]$ with and without B in a given volume. The rate equation for such a chemical reaction, Eq. 2.1, is given by Eq. 2.2. The concentration of B, $[B]$, is maintained by flow into the chamber and $[B]>>>[A^+]$.

Integrating Eq. 2.2 between time, $t = 0$ and $t = $ t, treating $[B]$ as a constant, gives Eq. 2.3 (Lindinger, 1986a).

$$A^+ + B \xrightarrow{\quad k \quad} P \qquad (2.1)$$

$$-\frac{d[A^+]}{dt} = k[A^+][B] \qquad (2.2)$$

$$[A^+]_t = [A^+]_0 \exp(-kt[B]) \qquad (2.3)$$

where $[A^+]_0$ is the concentration of A^+ at time $t = 0$, and $[A^+]_t$ is the concentration of A^+ at $t=$t. k can therefore be determined from the decay of the ion signal with time.

It is experimentally easier to convert the time dependency of A^+ concentration into a function of spatial co-ordinate. Flow tubes were developed so volume, V, in which the reaction is occurring moves with known velocity, v, along the x axis of known length and so Eq. 2.3 becomes Eq. 2.4. There is a constant rate of ion production (unlike the stationary technique which relies on the time decay of ions) though ion density remains much less than reactant gas density ($[B]>>>[A^+]$) and $[B]$ is ~ constant.

$$[A^+]_l \approx [A^+]_0 \exp(-k(l/v)[B]) \qquad (2.4)$$

or

$$\log[A^+]_l \approx \log[A^+]_0 - k(l/v)[B] \qquad (2.5)$$

where $[A^+]_l$ denotes the ion density detected at the end of the reaction chamber after traveling length l at velocity, v and $[A^+]_0$ denotes the ion density at the point of reactant gas (B) addition (Goldan *et al* 1966, Lindinger 1986a). By varying reactant gas density a plot of $\log[A^+]_l$ versus $[B]$ can be obtained the gradient of which is $-k(l/v)$. In flow tubes v is determined by buffer gas velocity (v_b) alone ($v=v_b$). v_b can be measured (Fehsenfeld *et al* 1966) or calculated for a given buffer flow, reaction chamber dimensions and known temperature and pressure (e.g. Smith and Španěl, 2005). For a given drift tube length the reaction rate constant can therefore be obtained from $-k(l/v)$. Eq. 2.4 and 2.5 are approximations as loss of ions by diffusion to the walls are not included, these loses can be determined from the diffusion coefficient (Fehsenfeld *et al* 1966).

There are two types of flow tube depending on whether the ion source is upstream of the reaction region, flowing afterglow, FA (Fehsenfeld *et al* 1966) or a separate region in the vacuum chamber with ion pre-selection, select ion flow tube, SIFT (Adams and Smith 1976). FA spectra are often complicated by the presence of more than one reagent ion, the use of SIFT simplifies spectra interpretation and reduces uncertainty associated with measured rate constants.

To enable the range of energies over which ion-molecule reactions could be studied to be extended FA was modified by the addition of a homogenous electric field applied around the reaction region. A reaction region with such a homogenous electric field is termed a drift tube and these instruments are referred to as flow drift tubes, FDT (McFarland *et al* 1973a). The homogenous electric field results in a bulk ion velocity in the direction of the drift tube, denoted drift velocity, v_d, (§ 2.4.1.5). In this case v_d is usually much greater than v_b thus $v \approx v_d$. Loss of ions by diffusion to the walls is relatively small and is generally neglected. The validity of this neglection in the drift tube of PTR-MS has recently been critically reviewed by Keck *et al* (2007) (§ 2.7). FDT were later modified by combination with the separate ion creation chamber and ion pre-selection of SIFT producing a select ion flow drift tube, SIFDT (Smith and Adams 1979).

High temperature flowing afterglow (HTFA) and variable temperature, (VT-SIFT) and SIFDT instruments have been developed to further the investigation of the effects of increasing internal and translational energy and changes in distribution of energy on ion-molecule reaction kinetics and fragmentation for understanding of the ionosphere (Viggiano and Morris 1996, § 2.9, Chapter 3). Such applications are also of use in determining the suitability of various ions for detection of specific VOCs at elevated energies and fragment ratios with potential relevance to PTR-MS (e.g. Arnold *et al* 1998, Chapter 3).

CI and swarm drift techniques were first applied to trace gas quantification at the University of Innsbruck by Lagg *et al* (1994) using SIFDT. The need to improve sensitivity (restricted to 0.1 ppm in SIFDT), detection limits and portability lead to the development of PTR-MS (Hansel *et al* 1995, Lindinger *et al* 1997, 1998a, b). In 1998 Ionicon Analytik was formed as a spin-off company from the Institute for Ion Physics at the University of Innsbruck supplying commercial PTR-MS for use in environmental, food and medical research.

2. 2 PTR-MS and Trace Gas Density Calculations

In PTR-MS a fraction of trace gas constituents (*M*) are chemically ionised in a drift tube by proton transfer from H_3O^+ (Eq. 2.6).

$$H_3O^+ + M \rightarrow MH^+ + H_2O \tag{2.6}$$

Product ions are subsequently analysed *via* a quadrupole mass spectrometer and an electron multiplier.

Proton transfer is used, as opposed to charge transfer for example, because of the comparably low level of fragmentation. H_3O^+ is a suitable reagent ion for detection of trace gases in air since its reaction with the major components of air is not thermodynamically favourable. H_3O^+ does react with most trace (O)VOCs but does so at relatively low energies. Therefore, fragmentation is generally minimal, e.g. loss of water from protonated C_2 and C_3 alcohols (§ 3.3), compared to chemical ionisation through more energetic reactions, such as protonation with H_3^+ or charge transfer, or hard ionisation techniques such as electron ionisation mass spectrometry (EI-MS). It should be noted however that the energy available for reaction is increased by the electric field; there are few cases in which no fragmentation occurs and from which the product ion occurs at the compound mass +1 alone (Chapter 3). The soft chemical ionisation techniques do not enable molecules of the same molecular mass (isobaric) to be distinguished. If fragmentation is well characterised as a function of the reaction chamber conditions (e.g. energy available in the reaction chamber, pressure and temperature) this can potentially be used as an aid to identification of isobaric compound and fragment contributions (Chapter 3 and 4) rather than serving merely to complicate mass spectra interpretation (e.g. Wyche *et al* 2005). NH_4^+ ions can also be produced with high purity at the ion source employed in commercial PTR-MS by using NH_3 in place of H_2O. However proton transfer is less thermodynamically favourable and fewer trace species can be detected (Lindinger *et al* 1998a).

Similarly to FA, FDT, SIFT and SIFDT the total trace gas concentration, $[\sum M]$, in the drift tube is much greater than the concentration of reagent ion $[H_3O^+]$. Due to the short residency of air in the drift tube, only a small concentration of trace gas reacts. The total protonated trace gas concentration, $[\sum MH^+]$, is much less than reagent ion concentration, $[H_3O^+]$, and trace gas concentration is approximately unchanged. Combined with the short residence time of H_3O^+ ions, it can be assumed that the concentration of H_3O^+ does not change either:

$$[\sum M] \gg [H_3O^+] \gg [\sum MH^+]. \tag{2.7}$$

$$[\sum M]_0 \approx [\sum M]_t \tag{2.8}$$

$$[H_3O^+]_0 \approx [H_3O^+]_t \tag{2.9}$$

where $[\ ]_0$ denotes concentration at time zero at the drift tube entrance and $[\ ]_t$ denotes concentration at time t at drift tube exit. In these conditions a trace gas volume mixing ratio (VMR) can be calculated by reversal of the method for rate coefficient measurement described in § 2.1. A known rate constant of proton transfer and reaction time is combined with primary and product ion signals to determine trace gas density by calculation according to Eq. 2.10; derivation of this equation is given in Appendix A.

$$[M] = \frac{(MH^+)}{(H_3O^+)} \frac{T_{H_3O^+}}{T_{MH^+}} \frac{1}{kt} \frac{10^9}{N} \qquad (2.10)$$

where $[M]$ is the volume mixing ratio (VMR) of the trace gas species i.e. (O)VOC of interest in units of parts per billion (by volume), ppb. (MH^+) and (H_3O^+) are the observed ion counts of H_3O^+ and MH^+ respectively in units of counts per second (cps). N is the number density of molecules in the drift tube and under normal operating conditions is $\sim 4.58 \times 10^{16}$ particles cm^{-3}. k is the reaction rate constant for proton transfer from H_3O^+ to the trace gas of interest, Eq. 2.6, and is typically in the order of 10^{-9} cm^3 s^{-1} (§ 2.4). t is the residence time of H_3O^+ ions in the drift tube i.e. reaction time. Under normal operating conditions this is $\sim$100 μs (§ 2.5). $T_{H_3O^+}$ and T_{MH^+} are the mass dependent detection efficiencies for H_3O^+ and MH^+ respectively (§ 2.7).

Sensitivity (S, counts per second per ppb, ncps ppb^{-1}) is defined as the observed ion counts of MH^+ obtained at a VMR of 1 ppb, and normalized to H_3O^+ ion counts of 10^6 cps. Therefore

$$S = 10^{-3} \frac{T_{MH^+}}{T_{H_3O^+}} ktN \qquad (2.11)$$

the accuracy and precision of calculated concentrations and sensitivities is dependent on the inaccuracies and uncertainties associated with reaction rate constant, reaction time, and the detection efficiencies. Hansel *et al* (1995, 1999) estimate an uncertainty of 20 % in calculated rate constants, and an error of up to 10 % is estimated in the reaction time under dry conditions increasing with humidity (Keck *et al* 2007, § 2.5 and 2.6). Uncertainty in indirectly determined detection efficiencies, § 2.7, are estimated to be 20 % (Keck *et al* 2007). The sources of inaccuracies and uncertainties of these values are addressed in § 2.4, 2.5 and 2.7 respectively. Accuracy also depends on how the (O)VOC reaction with $H_3O^+.(H_2O)_n$ clusters (where applicable) is treated in the concentration calculation, this is discussed in § 2.6.

Sensitivity can be increased by maximising H_3O^+ density, reaction time (§ 2.5), and improving the ability of the quadrupole mass spectrometer and electron multiplier to collect and detect reagent and product ions (§ 2.7). Concentration detection limits are determined by sensitivity, the signal-to-noise ratio and instrument background. The signal-to-noise ratio is dependent on the dwell time (Hayward *et al* 2002). The precision and accuracy with which instrument background is quantified affects that of the concentration measurements (Steinbacher *et al* 2004a,b). Response times of the PTR-MS are determined by a number of factors including residence time of air in the drift tube, memory effects, dwell times

employed at the quadrupole, the number of masses measured and time spent switching between masses at the quadrupole.

Sensitivity and detection limits were improved relative to the SIFDT by the use of a novel hollow cathode ion source and consequent eradication of ion pre-selection (*via* a quadrupole mass filter) to produce a high density of hydroxonium ions (Lindinger *et al* 1998a). The hollow cathode differs from that used in SIFDT by the addition of a source drift region, § 2.3.1, and adjustments to the geometry of the source itself (private communication with A. Jordan, July 23 2007). In order to maintain the high density of hydroxonium ions the common components of air are used as the buffer exploiting their lack of reaction with H_3O^+. In the model of PTR-MS used here Ionicon Analytik made minor modifications to further improve sensitivity. The drift tube diameter and volume was reduced thereby decreasing residence time of air and improving response time. An additional vacuum chamber between the drift tube and quadrupole was introduced resulting in higher ion detection efficiencies (de Gouw and Warneke 2007). A H_3O^+ signal of ~ 1 x 10^7 cps is readily obtainable in this model of the PTR-MS compared with ~ 4 x 10^6 cps in the original PTR-MS. High sensitivities with low detection limits (10-100 ppt) and rapid response times (~0.2 s) important for flux measurements can now be achieved.

The accuracy of VMRs is also dependent on the extent of reaction between H_3O^+ and MH^+ and specificity of the PTR-MS. Fragmentation and clustering of MH^+ complicate mass spectra and without knowledge of product ratios under varying drift conditions or the use of complementary techniques, such as GC-MS or GC, mass spectra become hard to interpret. This can result in underestimation of trace gas mixing ratios. Issues regarding fragmentation and clustering are discussed in § 2.6, § 2.9 and Chapter 3. Clustering of H_3O^+ molecules with H_2O reduces the H_3O^+ signal. Compounds such as benzene and toluene do not react with clusters and sensitivity is consequently reduced (Warneke *et al* 2001, de Gouw and Warneke 2007). Reaction of some compounds, for example monterpenes and amines, with $H_3O^+(H_2O)_n$ clusters is thermodynamically favourable (Tani *et al* 2003 & 2004). In this case the cluster can be included in Eq 2.10 as a reagent ion, as discussed in § 2.6.

The level of fragmentation and clustering depends on energy available in the drift tube as well as the bond strengths and exoergicity of reaction. The energy of neutrals is dependent on primarily on temperature. Energy of the ions is dependent on the ratio of electric field strength, *E*, and number density of particles in the drift tube, *N*, i.e. pressure and temperature in the drift tube (§ 2.4.1.5). *E/N* is usually specified in Townsend, Td, 1 Td = 10^{-17} V cm^2. Initially PTR-MS measurements were normally performed at *E/N* of 140 Td. However,

Warneke *et al* (2001) reported increases in typical sensitivities from 10-20 cps ppbv^{-1} to 40-50 cps ppbv^{-1} by decreasing *E/N* to 120 Td and thereby increasing reaction time. The effect on cluster distribution was minimal. PTR-MS measurements are normally performed at an *E/N* of between 120 and 130 Td in this study. This region is optimal for the reduction of fragmentation and maximising the residence time whilst minimising cluster formation (§ 2.6 and 2.9). In third body reactions in which the buffer molecule is involved, variations in pressure at fixed *E/N* will effect product ion distributions. Variation of temperature at fixed *E/N* may also effect product distributions due to the consequent variation in energy of the neutral (Chapter 3). The degree of clustering of ions with H_2O is also dependent on the density of water vapour in the drift tube and thus sensitivity may depend on the humidity of sampled air (§ 2.6).

The reaction time is dependent on inverse *E/N* (§ 2.5). Therefore from Eq. 2.10 and 2.11, sensitivity is dependent on pressure squared. At fixed *E/N* (necessary to prevent varying fragmentation and clustering), thus constant reaction time, sensitivity is linearly dependent on pressure. As pressure increases the number density of particles in the drift tube and frequency of reaction is increased (de Gouw *et al* 2003a). The increase in pressure is limited by pumping speeds and the difficulty in increasing electric field strengths to maintain constant *E/N*. Also at high voltages, discharges can occur across the drift tube (de Gouw *et al* 2003a, de Gouw and Warneke 2007). The sensitivity can also potentially be increased by increasing the length of the drift tube and thereby *t*. An increased voltage is required with length to achieve the same electric field strength and length is therefore limited by the consequent voltage discharges (de Gouw *et al* 2003a, de Gouw and Warneke 2007). Length (de Gouw *et al* 1999, 2000) and pressure (Hanson *et al* 2003); modified versions of the PTR-MS have been developed.

An alternative to trace gas mixing ratio calculation by Eq. 2.10 is to calibrate the PTR-MS over a range of known concentrations at ambient humidity, or, preferably over a range of humidities. A measured sensitivity is obtained by taking the gradient of a plot of measured normalised cps against actual (e.g. gravimetrically determined) concentration. The concentration of the corresponding species in subsequent measurements of samples of unknown concentration, of the same humidity, can be calculated by division of measured normalised cps by this sensitivity (cps ppb^{-1}). In this manner linearity over a concentration range and throughout a measurement campaign can be assessed. The extent of fragmentation, under given drift tube conditions can also potentially be determined from calibration gas sampling depending on the number and nature of components.

The uncertainty of concentrations and sensitivities derived in this manner essentially depends only on the uncertainty associated with the calibration gas and the instrument background. This method is generally less erroneous than calculation of concentrations using Eq. 2.10. Hewitt *et al* (2003) estimated that use of calibration gas could reduce inaccuracy by up to 15 %. Hansel *et al* (1995, 1999) estimated that the uncertainty of a volume mixing ratio calculated *via* Eq. 2.10 is ± 30 %. Uncertainties associated with calibration standards employed are typically around ± 20 % (e.g. Sprung *et al* 2001, Warneke *et al* 2001, Ammann *et al* 2004, Sprig *et al* 2005). There are a large number of examples of calibration of PTR-MS in the literature (e.g. Hayward *et al* 2002, de Gouw *et al* 2003b, Steinbacher *et al* 2004b).

Ammann *et al* (2004) reported good agreement between calculated and gravimetrically determined calibration standard concentrations for a range of (O)VOCs with a maximum deviation of 16 %. De Gouw *et al* (2003a) compared calculated (Eq. 2.11) sensitivities with those measured using a calibration mixture for acetonitrile at *E/N* of ~ 95 – 145 Td varied by drift tube pressure variation (~1.7 to 2.6 mbar) and at a fixed *E/N* of 106 Td and increasing pressure (~1.7 to 2.6 mbar). A reasonable agreement was observed between measured and calculated values. In the former case optimal agreement was observed at an *E/N* of 120 Td, i.e. normal operating conditions, or higher, measured values were increasingly greater than calculated with decreasing *E/N*. In the later case the greatest agreement was seen at ~ 2.3 mbar, discrepancy increasing either side of this. The pressure dependence of detection efficiency was suggested as a reason for both variations. In the case of varying *E/N* some of the deviation was attributed to the decrease in ion energy. At lower ion energies, increased $H_3O^+.H_2O$ cluster formation is expected. $H_3O^+.H_2O$ ions were not included as reagent ions in the sensitivity calculation, the reagent ions were therefore underestimated in the calculation. An inclusion of clusters in the sensitivity calculation (§ 2.6) and measurement of detection efficiencies at each of the drift tube conditions would be expected to improve sensitivity. The reaction time used was calculated and a fixed value of ion mobility (§2.5) and fixed rate constant (method of derivation not specified) employed (§2.4).

Warneke *et al* (2003) compared measured and calculated sensitivities for 40 compounds in PTR-MS at *E/N* of 106 Td. Uncertainties in the calculated values were estimated at 30 % compared with 20 % uncertainty in the calibration gas produced from a diffusion system. A selection of the presented results is shown in Table 2.1.

Table 2.1: A comparison of PTR-MS sensitivities for a selection of (O)VOCs measured with calibration gas standards and calculated from Eq 2.11 (Warneke *et al* 2003).

Compound	Measured PTR-MS (ncps ppb^{-1})	PTR-MS Calculated (ncps ppb^{-1})
Propanone (Acetone)	41.5	45.0
Acetonitrile	49.5	51.3
Toluene	35.0	27.2
2-methyl-1, 3-butadiene	25.8	19.8
Ethanol	3	25.9

A reasonable agreement was observed for many compounds; however some sensitivities did not compare favourably, a few differing by more than the estimated 30 %, e.g. ethanol. This was attributed to stability in the calibration standard and overlooked fragmentation, for example fragmentation of ethanol at m/z 19. Knowledge of product distribution at given *E/N* is improving (Chapter 3) e.g. Ammann *et al* (2004) observed fragmentation of 2-methyl-1, 3-butadiene (isoprene) at m/z 41 (16%) at *E/N* $\approx$ 130 Td with resultant improvement between calculated and calibrated sensitivities.

Methods for calibration gas generation have been reviewed by Barratt (1981) and Naganowska-Nowak (2005) and are not addressed in detail here. Compounds such as benzene, toluene and 2-methyl-1, 3-butadiene which are less volatile and less polar, can be calibrated with increased ease than oxygenated compounds. Certified commercial standards of the former less reactive compounds are readily available at the ppb level. The interaction, adsorption and memory effects associated with serial dilution of such standards are relatively small. Cylinders of calibration standards of some alcohols and aldehydes are available at the ppb level though with a limited lifetime and high cost.

As commercial standards of OVOCs are less readily available, diffusion (McKelvey and Hoelscher 1957, Altshuller and Cohen 1960) or permeation systems (Scaringelli *et al* 1970) are employed. Application of diffusion and permeation systems for VOC calibration in atmospheric chemistry is widely reported (e.g. Possanzini *et al* 2000, Kommenda *et al* 2003, Tani *et al* 2003, 2007 and Washenfelder *et al* 2003, Ammann *et al* 2004). The generation of stable and low concentration of such volatile polar compounds by diffusion or permeation is restricted by interaction, adsorption and memory effects. The degree of uncertainty associated with standards also depends on the precision and reliability of the balance used to weigh standards. Long periods of stabilisation and constant temperature and pressure conditions are required for diffusion and permeation systems (Gautrois and Koppmann 1999, Washenfelder *et al* 2003). This hampers deployment at short-term measurement sites. The

humidity dependence of PTR-MS sensitivity necessitating constant or known (and varied) humidity of calibration gas, further complicates generation of standards. However if these problems can be overcome, a mixture of a large number of (O)VOCs can be obtained at comparably little expense. Ideally generated calibration gas concentrations should be verified by GC or GC-MS. Gas standards of carboxylic acids are notably difficult to generate and calculation of sensitivities or qualitative analysis is necessary (von Hartungen 2004, Spanel and Smith 1998a, 2000, 2001, Shaw *et al* 2007).

Given the difficulty in calibrating a number of (O)VOCs, the reduction of inaccuracies associated with calculation of mixing ratios (Eq 2.10) and sensitivities (Eq 2.11) remains important. The sensitivities discussed above were calculated using reaction rate constants for reactions in the absence of an electric field (§ 2.4), calculated reaction times (§ 2.5), and excluding $H_3O^+.(H_2O)_n$ clusters as reagent ions (§ 2.7). The inclusion of the effect of the electric field on rate constants and inclusion of reagent clusters in Eq 2.10 and 2.11 are discussed in § 2.4 and 2.6.

Before a more detailed discussion of the factors affecting sensitivities, and accuracy of reported concentrations outlined above, a brief overview of the instrumentation configuration is provided.

2.3 PTR-MS Instrumental Configuration

A schematic of the PTR-MS used in this study is shown in Figure 2.1. The instrument consists of 3 main components; an ion source, drift tube and ion detector, differentially pumped by three turbopumps.

2.3.1. The Ion Source and Source Drift Region.

A description of the ion source used in the PTR-MS has been given elsewhere (Hansel *et al* 1995) and details of a number of similar ion sources developed at Innsbruck University have been published (e.g. Lindinger 1973, Märk *et al* 1972, Lindinger *et al* 1979). A schematic of the PTR-MS ion source is shown in Figure 2.2.

The ion source consists of a cathode, cathode fall and negative glow region. Electrons emitted from the cathode are attracted to the negative glow which is axial to the cylindrical cathode between the two anodes and is close to anode potential. In doing so the high energy electrons undergo ionising collisions with neutrals.

Water vapour in

(A)

V_{600}

V_1
V_2

Anode

Cathode

Anode plate

Heated inlet, this restrictive capillary (0.1 mm inner diameter) results in a further pressure drop in the drift tube which is usually at ~ 2.0 mbar (depending on the pressure set at the pressure controller upstream). Flow into the drift tube is ~18 STP cm^3 min^{-1}.

Sample inlet
via a solenoid valve

V_3
Vdrift

Thermocouple

Resistors

(B)

Thermocouple

Pressure at this T-piece is maintained by the pressure controller. The pressure is set in the software and is usually ~ 600 – 700 mbar

Ballest inlet

Heated drift tube.

Pressure gauge

A water vapour flow of 0 – 20 STP cm^3 min^{-1} is possible, flow is usually between 6 and 8 STP cm^3 min^{-1}

Vacuum chamber & nose cone

Varian V70 Turbopump

Ion lenses

Pressure gauge

Varian V70 Turbopump

Mass flow controller

Pressure controller

Varian V300 Turbopump

(C) Quadrupole mass filter (QMF)

Electron multiplier

Deflection plates

Radio frequency and direct current

Exhaust – turbopump 1 evacuates the ion source removing water vapour. This exhaust air therefore has a high water vapour content

Water resevoir containing doubly distilled water for the ion source

IN   IN   OUT

Diaphragm pump

Dry air flows to the diaphragm pump

Condensation bottle

Exhaust

Figure 2.1: A schematic of the PTR-MS. The PTR-MS consists of: **(A)** a hollow cathode ion source and source drift region (§ 2.3.1), **(B)** a reaction region incorporating a temperature controlled drift tube (§ 2.3.2) and **(C)** the detection region (§ 2.3.3).

17
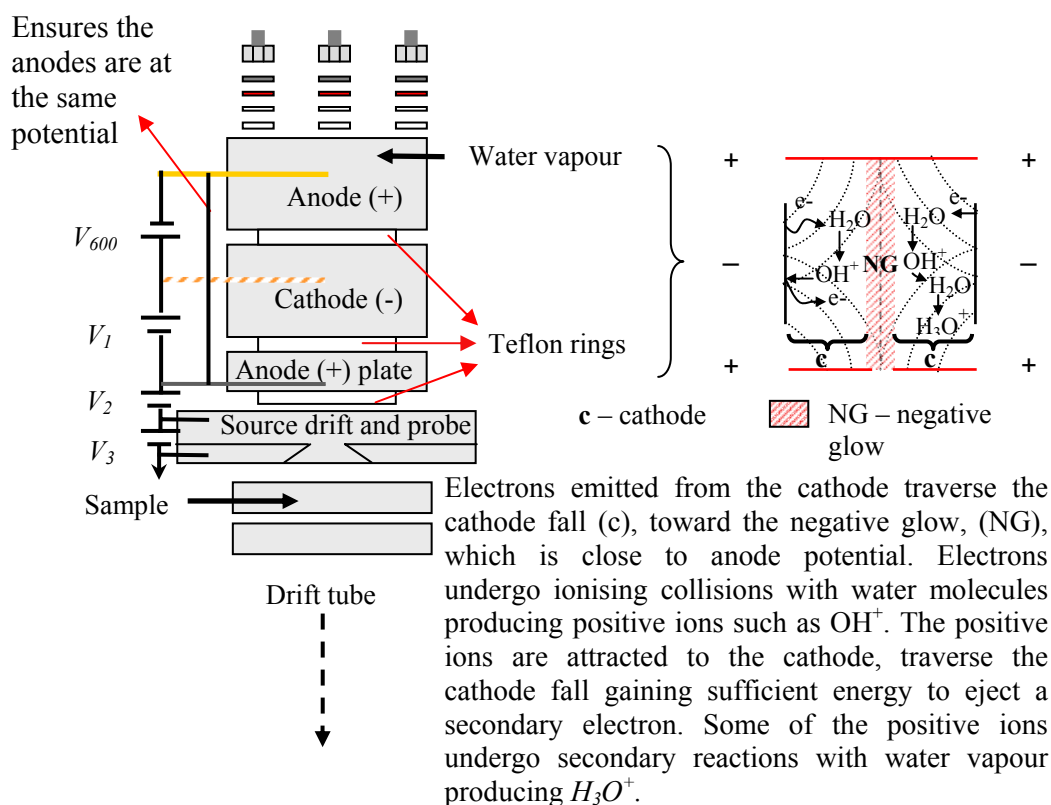
Figure 2.2: The ion source and (inset) the processes occurring within the ion source.

In this case a constant flow of water vapour flows into the ion source and the neutrals are water molecules. Water vapour flow into the ion source is controlled *via* a $0 - 20$ STP cm^3 min^{-1} (STP denotes standard temperature and pressure i.e. 273.15K and 1013.25 mbar respectively) mass flow controller. Water vapour flow is normally between $6 - 8$ STP cm^3 min^{-1}, an optimum for minimising $H_3O^+(H_2O)_n$ cluster formation (usually < 5 % depending on sample humidity and E/N, § 2.7) and maximising H_3O^+ signal. Electron impact of water molecules produces O^+, H^+, H_2^+, OH^+ and H_2O^+ ions. The positive ions are attracted to the cathode and traverse the cathode fall where sufficient energy is gained to eject a secondary electron. The secondary electron is attracted to the negative glow and traverses the cathode fall undergoing ionising collisions in the process. Hence, a plasma, a highly ionised gas in which the number of free electrons is approximately equivalent to the number of cations, of relatively high density ($10^{10} - 10^{11}$ cm^{-3}) exists (Hansel *et al* 1995).

The majority of positive ions produced by electron impact of water vapour molecules undergo further reactive collisions with H_2O neutrals producing H_3O^+ (Hansel *et al* 1995):

$$O^+ + H_2O \rightarrow H_2O^+ + O \tag{2.12}$$

$$H^+ + H_2O \rightarrow H_2O^+ + H \tag{2.13}$$

$$H_2^+ + H_2O \rightarrow H_3O^+ + H \tag{2.14}$$

$$H_2^+ + H_2O \rightarrow H_2O^+ + H_2 \tag{2.15}$$

$$OH^+ + H_2O \rightarrow H_3O^+ + O \tag{2.16}$$

$$OH^+ + H_2O \rightarrow H_2O^+ + OH \tag{2.17}$$

$$H_2O^+ + H_2O \rightarrow H_3O^+ + OH \tag{2.18}$$

The anode, cathode and anode plate voltages are determined by V_{600} and V_1 (Figure 2.1). The voltage at V_1 is fixed at ~200 V. V_{600} can be controlled *via* a potentiometer and is usually left at the maximum of 600 V. The current is controlled by a second potentiometer, the maximum current is 10 mA. In this study the ion source has been operated at 8 - 9 mA. Because the ion source is being burned continuously, a higher current may be required to maintain ignition as the ion source ages.

Ions emerge from the plasma through a small aperture (diameter 1.0 nm) in the anode plate. The ions are drawn into the source drift by its cathode potential. The source drift is a water vapour filled region where any remaining primary ions are reacted to produce H_3O^+ according to Eq. 2.12 – 2.18. The addition of the source drift therefore eliminates the need for quadrupole mass filter to pre-select ions. This region also enables the excited ions to become thermalised, it is assumed that ions enter the drift tube in ground state.

H_3O^+ is produced from the source drift with ~ 95 % purity; the impurities are NO^+ and O_2^+. O_2^+ is produced in the source drift region by charge transfer from H_2O^+ ions to O_2 diffusing from the reaction region. O_2 is less electronegative than H_2O thus it is better able to stabilize the positive charge. Further reactions with H_2O do not occur to produce H_3O^+ as in the case of O^+, H^+, H_2^+, OH^+, H_2O^+ and N_2^+ or N^+ (resulting from back flow of N_2 from the drift tube). Ions exit the source drift through a probe and enter the drift tube. The potential at the source drift and the probe where ions are selected for entrance to the drift tube is determined by voltages V_2 and V_3. V_2 and V_3 are varied to reduce O_2^+ and NO^+ and maximise H_3O^+ signals. The variability of H_3O^+, O_2^+ and NO^+ signals with V_3 at fixed V_2 is indicated in Figure 2.3. $H_3O^+.H_2O$ was monitored and showed a slight increase. Relative humidity of sampled air was monitored at the PTR-MS inlet and within standard deviation showed little variation. As seen in Figure 2.3, an increase in V_3 results in an increase in all signals but a relative increase in O_2^+ and NO^+.

V_3 is generally limited to keep O_2^+ at < 3 %, and at the time of the measurements shown in Figure 2.3, was normally operated at ~ 60 V. The trends highlighted in Figure 2.3 are in agreement with those presented by de Gouw and Warneke (2007). A similar increase in H_3O^+, O_2^+ and NO^+ signals is seen with increasing V_2 though no relative increase in impurities results. Optimal values of V_2 and V_3 vary with humidity and the cleanliness of electrodes and so the ion source is optimised on a regular basis. As the cleanliness of the ion source deteriorates it becomes difficult to achieve the necessary H_3O^+ ion counts and is therefore cleaned regularly (usually every 2 – 3 months when continually operated).
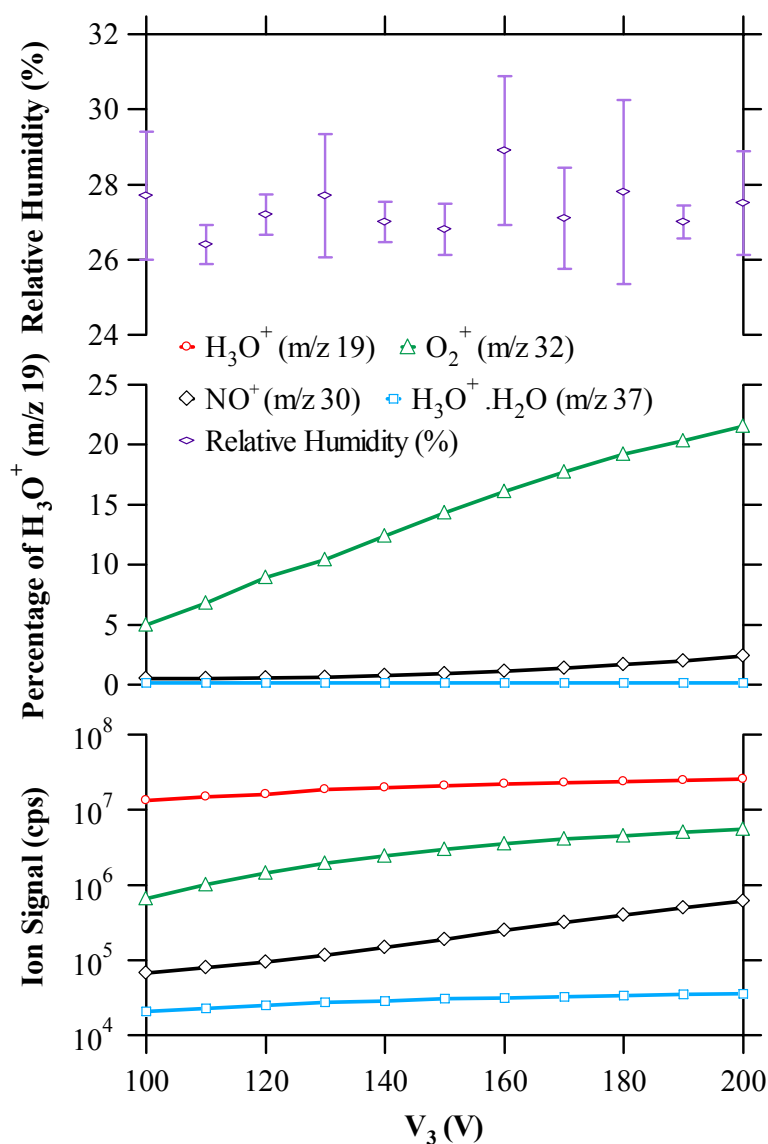
Figure 2.3: The variation of H_3O^+, O_2^+, NO^+, and $H_3O^+.H_2O$ signals with V_3 at $V_2 = 127$ V. High purity air (Sigma Aldrich BTCA 178 <100 ppb hydrocarbon) was sampled. Dew point temperature (Mitchell 3000 mirror monitor) and temperature (Type K thermocouple) of the sampled air were measured at the PTR-MS inlet enabling relative humidity to be derived.

2.3.2 Sample Air Flow and The Drift Tube

Sample air enters the PTR-MS *via* a needle valve; the maximum attainable flow is 350 STP cm^3 min^{-1}. However unless an inlet pressure higher than atmospheric pressure is employed, the needle valve of the inlet is effectively only an open/close valve. Flow into the drift tube is controlled down stream. In order to maintain a constant pressure in the drift tube, which does not vary with ambient, the pressure of the inlet is kept constant. This is achieved by T-ing the inlet line. One outlet goes to the drift tube and the other goes to an off-line pressure controller (0 – 1000 mbar), which controls the pressure at the T-junction region. By removing a varying amount of the flow at the T-junction the pressure controller achieves a constant pressure. This pressure is referred to as the bypass pressure. The bypass pressure can be set in the software and is usually between 600 and 700 mbar. A restrictive capillary takes the inlet gas to the drift tube from the T-junction. The capillary provides the further drop in pressure to 2 mbar in the drift tube. The inner diameter (0.1 mm) and length (50 cm) of the capillary controls the actual flow into the drift tube, which is ~ 18 STP cm^3 min^{-1}. Sample air enters the drift tube near the ion source exit (Figure 2.1).

The drift tube consists of 10 stainless steel rings connected to a resistor network which divides the overall drift voltage (*Vdrift*) to produce a homogenous electric field inside the drift tube. The drift tube rings are electrically isolated by Teflon rings. The drift tube length is 9.5 cm and its volume is 12.5 cm^3. The drift tube and inlet can be heated up to 353 K.

There is a second inlet, the ballast inlet. Air is drawn into the ballast inlet and sample inlet (*via* the pressure controller) by the diaphragm vacuum pump (Figure 2.1). The purpose of the ballast inlet is to supply dry air to the pump. This is necessary to prevent condensation in the pump as the water vapour from the ion source is removed to this pump (Figure 2.1).

2.3.3 The Detection Region

Ions exit the drift tube into a pre-quadrupole intermediate vacuum chamber. This chamber, not present in the original PTR-MS, enabled the sampling orifice in front of the quadrupole to be enlarged and higher detection efficiencies to be achieved (de Gouw and Warneke 2007). The majority of air is pumped away from the intermediate chamber by a turbopump. The small number of ions exiting the intermediate chamber through the enlarged orifice and nose cone are guided by ion lenses to the detection system. The detection system consist of a quadrupole mass filter (Pfeiffer Vacuum QMA 400) connected to a secondary electron multiplier (Pfeiffer Vacuum SEM-217) coupled to an ion count pre-amplifier (Pfeiffer

Vacuum CP 400). The SEM is operated in pulse counting mode. A Pfeiffer Vacuum QMH 400 is used for radio frequency and direct current generation. Mass to charge ratio (m/z) 21 ($H_3{}^{18}O^+$) and 107 (dimethylbenzene) peak resolution and position are regularly (and always following instrument transport) checked and adjusted as necessary at the QMH 400; resolution may also be adjusted in the software (Pfeiffer Vacuum Quadstar). The detection system pressure is ~ 2 x 10^{-5} mbar. This pressure is required to maximise the mean free path of ions and minimise SEM aging due to oxidation.

The quadrupole is normally operated in a multiple ion detecting (MID) mode where the quadrupole switches between a few select masses each measured at a specified dwell time. Short scan bargraph (SB) measurements, where the quadrupole sweeps over a large range of masses at a specified uniform speed per m/z, are performed intermittently to identify unexpected compounds. The time spent switching between masses is reduced in the SB mode compared to MID when working with 10 to 100 ms dwell times. This is due to differing communication times between the computer and QMS (private communication with A. Jordan 25 July 2007). The response time is dependent on the number of masses measured, the dwell on each mass and the time spent switching between masses.

Ions from the quadrupole are guided through deflection plates to the SEM where they are attracted to the large negative voltage. A Pfeiffer Vacuum HV 420 (0 – 3.5 kV) supplies a voltage of 2.4 – 3.5 kV to the SEM. The SEM consists of a series of electrodes. On impact with the first electrode ions release electrons which are accelerated to another electrode which releases another electron. Additional electrons are subsequently emitted in the same manner consequently amplifying the signal. The 90° off-axis positioning of the SEM reduces sensitivity but is necessary to prevent large numbers of photons hitting the SEM with resultant electron release and poor signal-to-noise ratio. If photons are reaching the SEM a signal (dark counts) is seen at m/z 25 where no counts would otherwise be expected. The SEM position also prevents molecules reaching the SEM and condensing or reacting thereby reducing the SEM gain (Lester 1970).

Pulses from the SEM are amplified and monitored at the CP 400. To prevent electrons resulting from any remaining photons being counted, there is a threshold of peak intensity below which electron pulses are not counted at the CP 400. A standard plot of H_3O^+ ion counts versus SEM voltage is shown in Figure 2.4. The appropriate voltage is that at the start of the plateau, where the change in counts between the chosen and subsequent voltage is between 15 and 20 % (private communication with A. Jordan, September 21 2004), as

indicated. At this point a large percentage of all pulses produced by ion collision are above the threshold and are detected, below this point not every ion produced pulse is detected.

Count rates of greater than $\sim 3 \times 10^6$ pulse frequency are too great for pulses from individual ions to be distinguished. Since typical $H_3{}^{16}O^+$ signal counts are $\sim 1 \times 10^7$ cps, the hydroxonium ion signal is measured at the ^{18}O isotope ($H_3{}^{18}O^+$; m/z 21) to prevent this SEM saturation. The $^{18}O/^{16}O$ isotope ratio is $\sim 0.20\%$ (Manura and Manura 1996) and the $H_3{}^{18}O^+$ signal has to be multiplied by 500 to obtain the $H_3{}^{16}O^+$ signal. Reducing the count rates also reduces aging of the SEM, to this end the $H_3O^+(H_2O)$ signal can be measured at the $H_3{}^{18}O^+(H_2{}^{16}O)$ isotope (m/z 39). The $^{18}O/^{16}O$ ratio is $\sim 0.40\%$ (Manura and Manura 1996) and the $H_3{}^{18}O^+(H_2{}^{16}O)$ signal has to be multiplied by 250 to get the $H_3{}^{16}O^+(H_2{}^{16}O)$ cps. Ammann *et al* (2004) compared m/z 19 cps measured directly with 500 x m/z 21 cps over a range of m/z 19 count rates (varied by V3 adjustment) with two SEM. At count rates less than 1×10^6 cps, a 1:1 relationship was observed, but deviation was $> 20\%$ at 3×10^6 cps demonstrating the aforementioned SEM saturation.
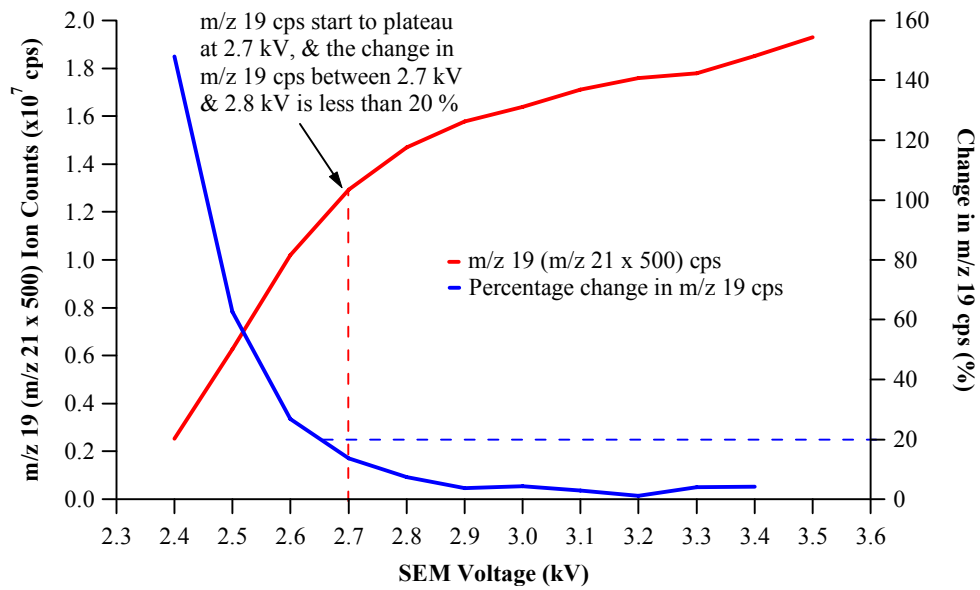
Figure 2.4: An example of the dependence of m/z 19 (m/z 21 ($H_3{}^{18}O^+$) x 500) count rates on SEM voltage. The voltage at the start of the plateau (2.7 kV in this case), where the change in count rate is less than 20 %, is the optimum SEM voltage. At lower voltages many electron pulses resulting from $H_3{}^{18}O^+$ fall below the CP400 threshold and are not counted. At higher voltages signal-to-noise is reduced and the SEM ages rapidly.

As the SEM ages, the plateau shifts to higher voltages and signal versus voltage plots (Figure 2.4) must be performed regularly to determine the optimum voltage. Although applying unnecessarily high voltage ages the SEM, during intensive measurement campaigns,

it has been necessary to optimise the SEM voltage in this manner on at least a weekly basis. Intensities of count rates decrease faster at larger masses hence unless the SEM voltage is optimised at low and high masses, the detection efficiencies (Eq 2.10) must be measured at each SEM voltage (Sugiura 1962, Ammann *et al* 2004). Given the frequency of SEM voltage changes during periods of continuous measurement, the time required for detection efficiency measurement and the consequential increase in instrument background it is favourable to optimise the SEM at a higher mass. Therefore a tedlar bag of human breath is periodically connected to the inlet to supply a continuous concentration of 2-methyl-1,3-butadiene (isoprene) (m/z 69) and the count rates at m/z 69 with increasing SEM voltage are measured (alongside H_3O^+ cps) to identify the optimum SEM voltage (Figure 2.5).
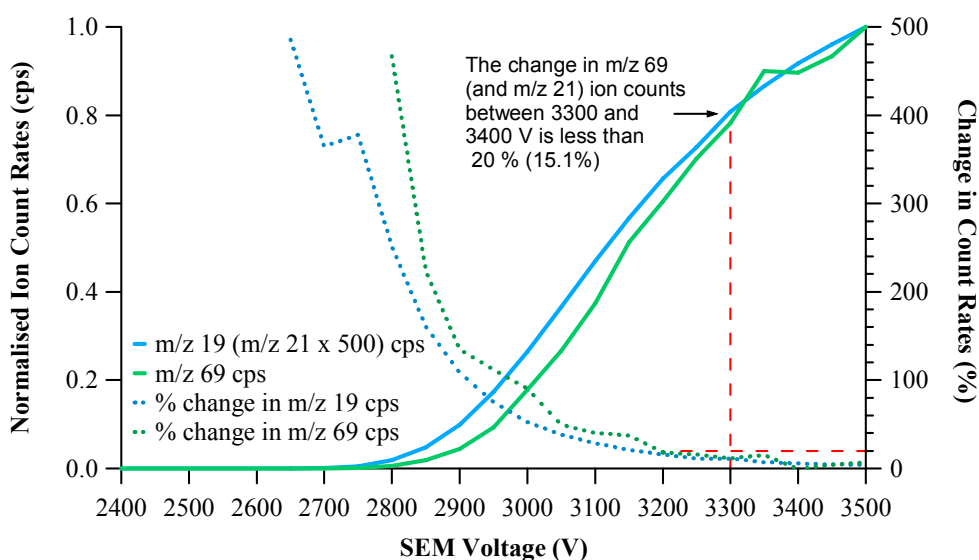
Figure 2.5 An example of SEM optimisation at m/z 19 (m/z 21 x 500) and m/z 69.

2.4 Reaction Rate Constants

The rest of this chapter provides a discussion of the factors affecting sensitivity, and the accuracy of calculated concentrations and sensitivities. The greatest source of uncertainty and inaccuracy associated with calculated concentrations and sensitivities arises from the rate constants. Calculated collisional rate constants or experimentally determined rate constants may be utilised in Eq. 2.10. However there are two issues affecting the suitability of calculated collisional rate constants:

a) The efficiency of reaction; the application of a calculated collisional reaction rate constant assumes that the reaction is efficient and proceeds at collisional rate, i.e. that every collision (as defined below) results in a reaction.

b) The accuracy of the model of calculation of the collisional rate constant and the associated uncertainties.

In the first case it has been experimentally and theoretically demonstrated that non-dissociative proton transfer reactions, such as Eq. 2.6, proceed efficiently when the Gibbs free energy of reaction is less than ~ -0.21 to -0.43 eV (Bohme *et al* 1980, Bouchoux *et al* 1996) under thermal conditions. This is discussed further in § 2.9 and Chapter 3. The effect of the occurrence of reactions other than non-dissociative proton transfer and possible effects of the elevated energies resulting from an electric field on reaction efficiency are discussed.

2.4.1 Calculation of Reaction Rate Constants

2.4.1.1 Collisional Rate Constants

The rate of reaction depends on the number of reactive collisions occurring in a unit time. The criterion for a collision is briefly outlined below. Consider a neutral approaching an ion at a fixed position. The mass of the neutral can be regarded as the reduced mass, μ. The separation distance is denoted r and the relative velocity, v. The perpendicular distance between the neutral and ion at infinite separation, is the impact parameter, b (Figure 2.6).
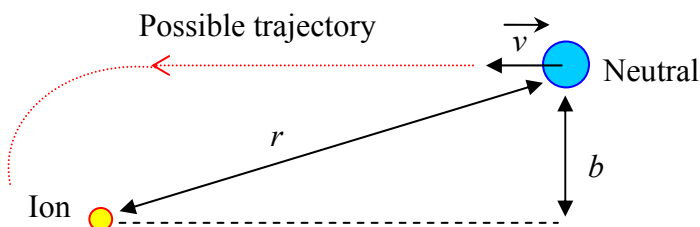
Figure 2.6: An ion molecule collision and the associated parameters.

The relative energy, E_r, of the particles is given by:

$$E_r = E_{trans} + U_{eff} \tag{2.19}$$

where E_{trans} is the translational kinetic energy and U_{eff} the effective potential energy defined by:

$$U_{eff} = U(r) + \frac{L^2}{2\mu r^2} \tag{2.20}$$

$U(r)$ is the potential energy. The second term is the centrifugal or rotational energy, the energy required to enforce conservation of angular momentum. L is the angular momentum,

$$L^2 = \mu^2 v^2 b^2 \tag{2.21}$$

At infinite separation the relative energy of the system exits solely as translational kinetic energy, $\frac{1}{2}\mu v^2$. The distribution of this energy between translational, centrifugal and potential energy changes as the neutral approaches the ion. Centrifugal energy decreases as r decreases. The various methods of determining the collisional rate constant vary in their characterization of the potential energy and thereby U_{eff}, Eq. 2.20.

Langevin theory (Langevin 1905, Gioumousis and Stevenson 1957) assumes there is no permanent dipole and interaction is through an induced dipole. Average Dipole Orientation (ADO) theory (Su and Bowers 1973b and c), and parameterized trajectory calculations (Su and Chesnavich 1982) account for a permanent dipole with varying degrees of rigour. The Langevin and Average Dipole Orientation (ADO) theory have been extensively reviewed (Bowers and Su 1975, Su and Bowers 1979, Shirts 1986, McDaniell *et al* 1970). Zhao and Zhang (2004) published ADO values for proton transfer at 298 K from H_3O^+ to (O)VOCs using quantum chemical calculations of dipole moments and polarizabilities for use in the PTR-MS. An interactive COLRATE program (Lim 1994) has been published for calculation of ion-molecule rate constants from Langevin theory, ADO and Su and Chesnavich theory in the absence of an electric field (given known dipole polarizability and moment of inertia). All three theories are applied by PTR-MS users (Lindinger *et al* 1986a, Hansel *et al* 1995, Steinbacher 2004a, de Gouw and Warneke 2007). The following section is a brief overview of these theories and a discussion of their application in a drift tube under a homogenous electric field. A fourth theory developed by Su (1994) in response to increasing application of drift tube instrumentation and interest in effects of independent variation of internal and translational energy is discussed. No examples of its previous application in the field of PTR-MS could be found in the literature. The suitability of all four theories for PTR-MS measurements (where calibrations are not available) is discussed.

2.4.1.2 Langevin Theory.

Langevin theory (Langevin 1905, Gioumousis and Stevenson 1957) defines the potential energy, $U(r)$, as the potential energy between an ion and neutral with an induced dipole as:

$$U(r) = -\frac{\alpha Q^2}{2(4\pi\varepsilon_0)^2 r^4} \tag{2.22}$$

where α is the polarizability of the neutral, Q the charge of the ion and ε_0 is the vacuum permittivity. The relative energy of the system is described by:

$$E_r = E_{trans} + \frac{\mu v^2 b^2}{2r^2} - \frac{\alpha Q^2}{2(4\pi\varepsilon_0)^2 r^4}$$ (2.23)

A neutral approaching at a large b has a large centrifugal energy (Eq. 2.20 and 2.21). As $U(r)$ decreases as r^{-4} while the centrifugal potential energy increases as r^{-2}, the centrifugal energy increases more rapidly than the attractive potential energy. The translational energy is converted to centrifugal energy and the effective potential equals the initial kinetic energy ($E_r = \frac{1}{2} \mu v^2$) at large r before the attractive potential energy is much greater than zero. In this case the rate of change in effective potential energy with r at the point when it equals $\frac{1}{2} \mu v^2$, is negative, there is a positive force acting on the neutral and it is deflected (Figure 2.7).
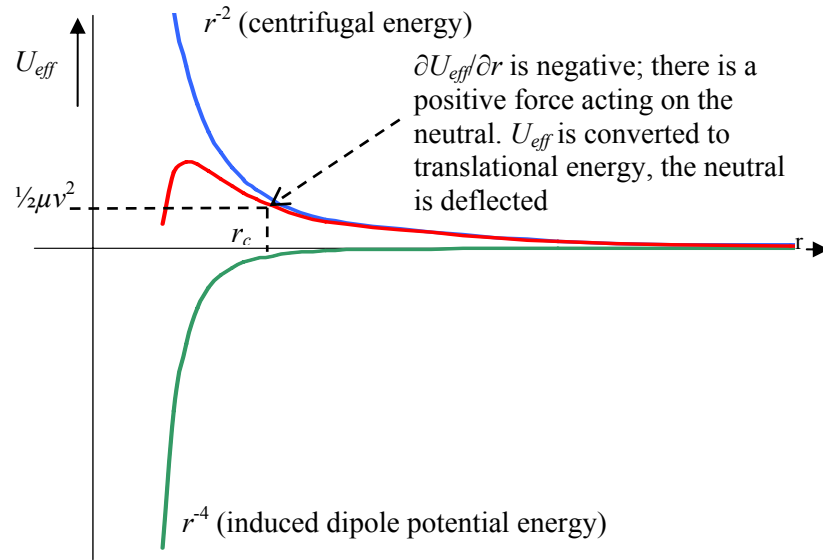
Figure 2.7: Schematic of the terms contributing to U_{eff} (red line) at a large impact parameter. The system's energy is converted to effective potential energy at large r where there is an outward force on the neutral. The effective potential energy is converted to translational energy as the particle is deflected. r_c denotes the distance of closest approach.

At a point where effective potential energy equals E_r but the derivative of U_{eff} does not equal zero, the neutral and ion are at there closest distance of approach, r_c. This is denoted a turning point, and the subsequent change in direction is defined by the deflection angle, θ_d (Figure 2.8).
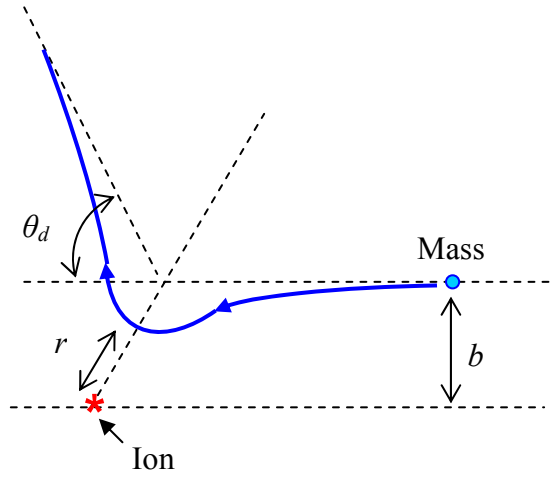
Figure 2.8: Approaching particles reaching a turning point. Adapted from Shirts (1986) and Hirschfelder *et al* (1954).

At small *b*, the centrifugal energy is small. The attractive potential is sufficient to prevent the effective potential energy reaching $\frac{1}{2}\mu v^2$ up until electron-electron, nucleus-nucleus repulsion (neglected in Eq. 2.22) is felt at small *r* (Figure 2.9).

At a critical impact parameter, *b**, the effective potential energy equals E_r at the maximum in the effective potential profile of the trajectory (Figure 2.10). The instantaneous rate of change of effective potential with *r* is zero at this point, i.e. net force is zero. The attractive potential acting on the neutral as a result of the ion equals the centrifugal force repelling it and the neutral orbits the ion at this distance, *r**.

A schematic of trajectories at varying impact parameters is shown in Figure 2.11; note that the initial relative velocity is constant. The initial energy and angular momentum, therefore centrifugal energy, increase with increasing relative velocity. The value of *b** decreases as relative velocity increases.
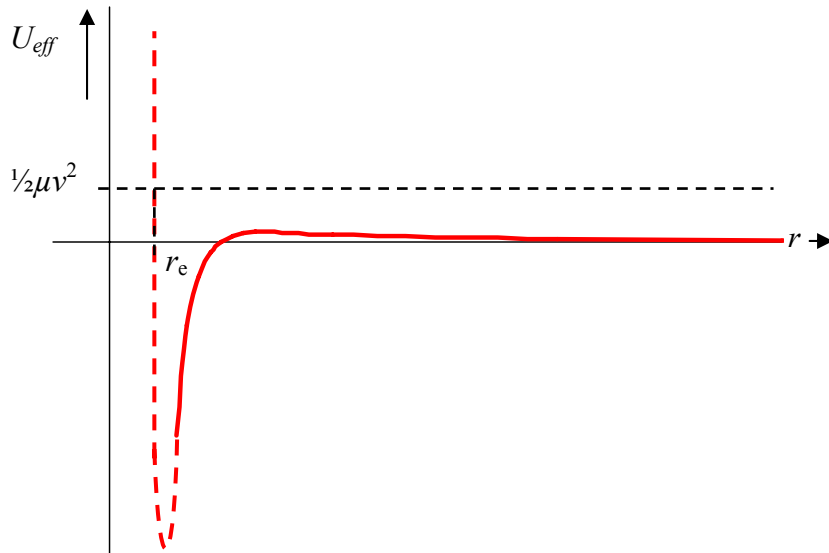
Figure 2.9: The effective potential energy at small impact parameters. No turning point occurs until the exponential electron-electron and nucleus-nucleus repulsion is experienced. This distance of closest approach for such impact parameters is denoted r_e.

r^{-2} (centrifugal energy)

$\partial U_{eff}/\partial r = 0$; there is no net force, the centrifugal force equals the attractive force. All the systems energy is in use in U_{eff} and the neutral orbits the ion at r^*

r^{-4} (induced dipole potential energy)
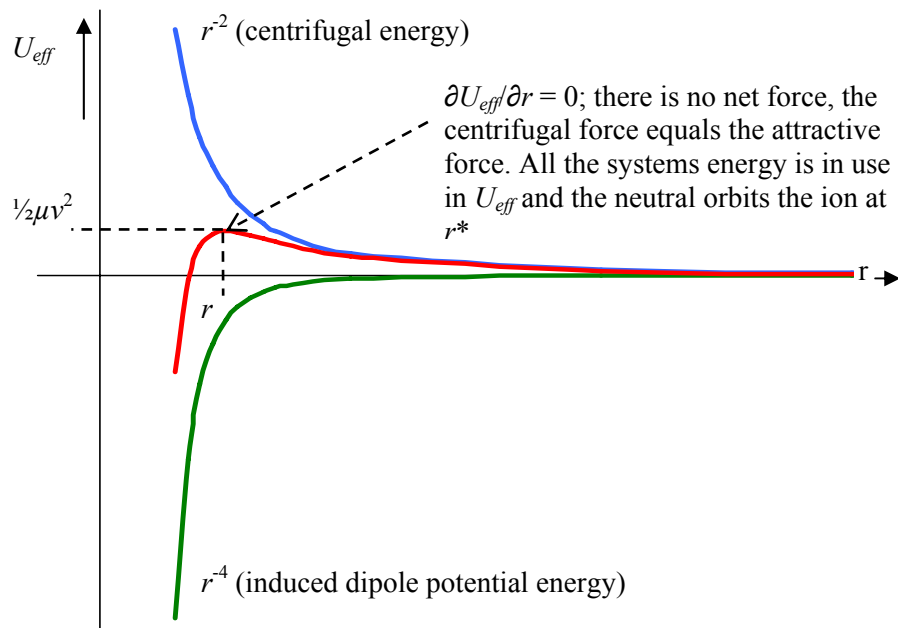
Figure 2.10: The effective potential energy profile at $b = b^*$
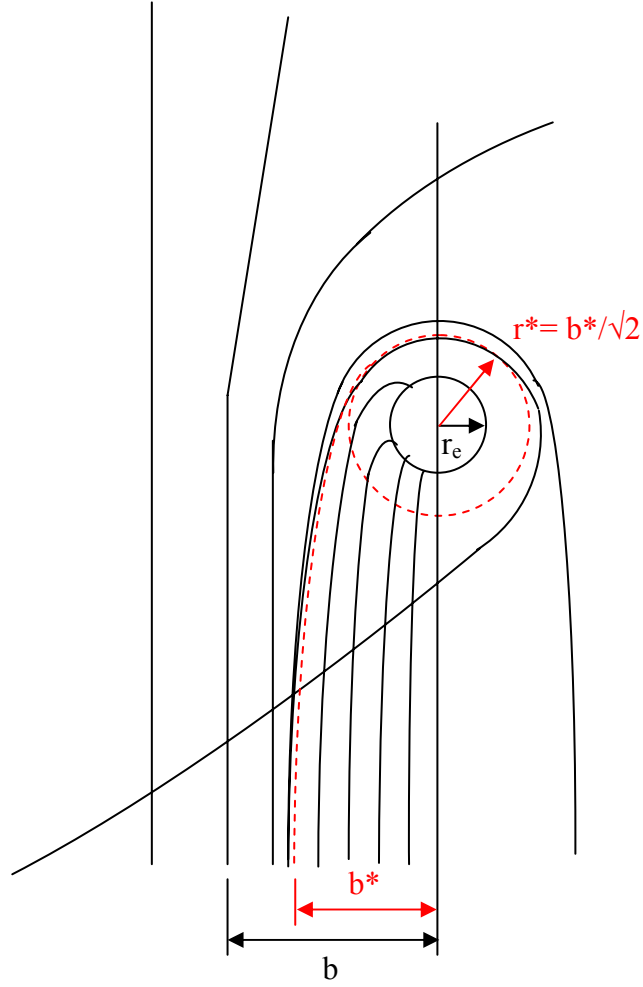
Figure 2.11: Trajectories of neutrals approaching an ion at constant initial relative velocity. Those ions with an impact parameter less than b^* have a small enough angular momentum, thus centrifugal potential energy, that the attractive potential of ion-induced dipole interaction results in an effective potential energy less than the initial kinetic energy of the system up until the repulsive wall of the potential energy occurs. r_e indicates the distance at which the repulsive potential (due to electron-electron repulsion) dominates, i.e. r_c for neutrals with b less than b^*. It is assumed that all collisions where b is less than b^* will be reactive collisions. At b^* the effective potential equals the energy of the system at the peak in the potential energy profile. The centrifugal force is equal to the attractive force of the ion-induced dipole interaction and the neutral orbits the ion at distance $r^*=b^*/\sqrt{2}$ (Eq 2.30). At impact parameters greater than b^*, the centrifugal energy is equal to the initial kinetic energy at large r before any attractive potential energy becomes important. Adapted from Gioumousis and Stevenson (1957) and Lindinger (1986b).

Collisions with an impact parameter lower than b^* can be assumed to be reactive and are referred to as capture collisions. Thus at infinite separation, all neutrals approaching the ion within a circle of radius b^* perpendicular to the line of collision will collide reactively. The cross-section of this circle is termed the capture collision cross-section, σ:

$$\sigma = \pi b^{*2} \tag{2.24}$$

To obtain an expression for $b*$ an expression for $r*$ is first derived. Recall that at $b*$, the systems energy is all effective potential energy, Eq. 2.20, and the net force on the neutral is zero i.e. $\partial U_{eff}/\partial r$ is zero (Figure 2.10).

$$E_r = \frac{1}{2}\mu v^2 = U_{eff} = -\frac{\alpha Q^2}{2(4\pi\varepsilon_0)^2 r*^4} + \frac{\mu v^2 b*^2}{2r*^2} \tag{2.25}$$

$$\frac{\partial U_{eff}}{\partial r} = \frac{2\alpha Q^2}{(4\pi\varepsilon_0)^2 r*^5} - \frac{\mu v^2 b*^2}{r*^3} = 0 \tag{2.26}$$

Multiplying Eq. 2.25 by $2r^{-1}$ gives an expression in the form of Eq. 2.26 and the equations can be solved simultaneously to give:

$$\frac{2E_r}{r*} = \frac{\alpha Q^2}{(4\pi\varepsilon_0)^2 r*^5} \tag{2.27}$$

Multiplying by $r*$ and making $r*$ the subject gives:

$$r*^4 = \frac{\alpha Q^2}{(4\pi\varepsilon_0)^2 2E_r} \tag{2.28}$$

An expression for $b*$ can be obtained by rearrangement of Eq. 2.26, substituting $\frac{1}{2}\mu v^2$ with E_r this gives:

$$b*^2 = \frac{2\alpha Q^2}{(4\pi\varepsilon_0)^2 r*^2 2E_r} \tag{2.29}$$

To enable substitution of the expression for $r*^4$, Eq. 2.29 is squared before substitution of Eq. 2.28 to give:

$$b*^4 = \frac{2\alpha Q^2}{(4\pi\varepsilon_0)^2 E_r} \tag{2.30}$$

Note, given Eqs. 2.28 and 2.30, $r*$ can be defined in terms of $b*$ as,

$$r* = b*/\sqrt{2} \tag{2.31}$$

Taking the square root of Eq. 2.30 and substituting E_r for $\frac{1}{2}\mu v^2$ gives an expression of $b*^2$ which can be used in the expression for capture cross-section, Eq. 2.24.

$$\sigma = \frac{2\pi Q}{(4\pi\varepsilon_0)v}\left(\frac{\alpha}{\mu}\right)^{\frac{1}{2}} \tag{2.32}$$

Since $b*$ is dependent on the relative velocity, the cross-section is a function of relative velocity. The collisional rate constant, k, is the number of collisions (where $b < b*$) per unit time and can be defined as (Su and Bowers 1979):

$$k = v\sigma \tag{2.33}$$

Substituting in Eq. 2.32 gives the Langevin rate constant:

$$k_L = \sigma v = \frac{2\pi Q}{(4\pi\varepsilon_0)}\left(\frac{\alpha}{\mu}\right)^{\frac{1}{2}} \tag{2.34}$$

where k_L is the Langevin or non-polar rate constant. The Langevin rate constant has units of cm^3 s^{-1} as in the literature, and the following units are therefore employed in Eq. 2.34. Charge, Q, Coulombs (C), polarizability, α, in g^{-1} s^4 A^2, reduced mass, μ, in g, and $4\pi\varepsilon_0$ is 1.113 x 10^{-19} cm^{-3} g^{-1} s^4 A^2. The Langevin rate constant is independent of the average relative velocity and thus temperature.

2.4.1.3 Locked Dipole and Average Dipole Orientation (ADO) Theory

In the Langevin theory the potential energy contains an ion-induced dipole term only and it is not applicable to neutrals with a permanent dipole. The potential energy for a dipole-ion interaction is given by:

$$U_D = \frac{\mu_D Q}{4\pi\varepsilon_0 r^2}\cos\theta \tag{2.35}$$

where μ_D is the dipole moment, θ is the angle of orientation between the charge and the centre of the dipole. A derivation of this equation is given in Appendix B. When the ion and molecule with the permanent dipole are at infinite separation, the molecule rotates freely. As the ion approaches, its inhomogeneous electric field exerts a force on the neutral, attracting the opposite charge of the dipole and repelling the like-charge, thereby restricting rotation, Figure 2.12.

Repulsive force F $^-$ is less than the attractive force F$^+$, there is a resultant attractive force toward the ion and higher field density
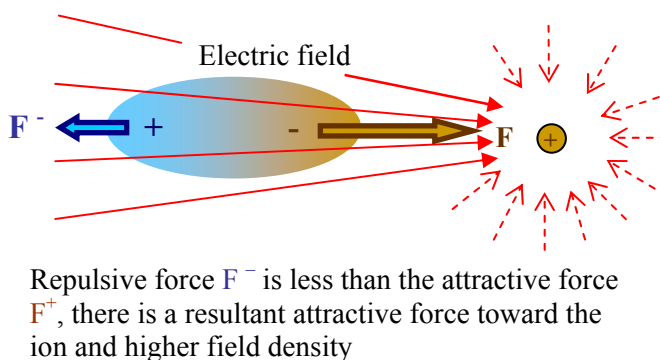
Figure 2.12: The effect of the electric field of an ion on the orientation of a molecule with a dipole. Adapted from Lindinger (1986b)

The extent to which alignment occurs depends on the rotational energy of the polar molecule relative to the attractive potential energy from the ion. The force between the ion and dipole is an average over the possible dipole orientations. If $\theta = 0$ (Eq. 2.34), the opposite charge of the dipole is aligned with the ion (Figure 2.13b) with a resultant attractive contribution to the

potential ($\cos \theta = +1$). If $\theta = 180^{\circ}$ the like charge of the dipole is aligned with the ion making a repulsive contribution to the potential energy ($\cos \theta = -1$) as shown in Figure 2.13c.

Theard and Hamill (1961) and Moran and Hamill (1963) made the simplifying assumption that the dipole either remains freely rotating, in which case only the induced-dipole contributes to potential energy, or the dipole locks on to the ion at zero degrees. Therefore, the expression for effective potential energy and its differential with respect to r at $b*$ (analogous to Eq. 2.25 and 2.26 respectively in the Langevin theory) are given by:

$$E_r = \frac{1}{2}\mu v^2 = U_{eff} = \frac{\mu v^2 b *^2}{2r *^2} - \frac{\alpha Q^2}{2(4\pi\varepsilon_0)^2 r *^4} - \frac{\mu_D Q}{4\pi\varepsilon_0 r *^2} \qquad (2.36)$$

$$\frac{\partial U_{eff}}{\partial r} = -\frac{\mu v^2 b *^2}{r *^3} + \frac{2\alpha Q^2}{(4\pi\varepsilon_0)^2 r *^5} + \frac{2\mu_D Q}{(4\pi\varepsilon_0) r *^3} = 0 \qquad (2.37)$$

Solving Eq. 2.36 and 2.37 simultaneously for $r*$ and substituting into Eq. 2.37 before rearranging results in the following expression for $b*^2$

$$b *^2 = \frac{2Q}{(4\pi\varepsilon_0) v}\left(\frac{\alpha}{\mu}\right)^{\frac{1}{2}} + \frac{2\mu_D Q}{(4\pi\varepsilon_0)\mu v^2} \qquad (2.38)$$

The locked-dipole rate constant, k_{LD}, is therefore

$$k_{LD} = v\sigma = \pi b *^2 = \frac{2\pi Q}{(4\pi\varepsilon_0)}\left(\frac{\alpha}{\mu}\right)^{\frac{1}{2}} + \frac{2\pi Q\mu_D}{(4\pi\varepsilon_0)\mu v} \qquad (2.39)$$

Noticeably, in contrast with the Langevin theory, the ion dipole contribution is dependent on the relative velocity. The experimental (ensemble) rate constant is an average over all possible relative velocities. Assuming there is a Boltzmann distribution in the drift tube (§ 2.4.1.7) a Maxwell - Boltzmann distribution of velocities (Atkins 1999, Hill 1962) can be used to obtain a mean relative velocity along the axis of approach, giving (Gupta *et al* 1967)

$$k_{LD} = \frac{2\pi Q}{(4\pi\varepsilon_0)}\left(\frac{\alpha}{\mu}\right)^{\frac{1}{2}} + \frac{2\pi Q\mu_D}{(4\pi\varepsilon_0)\mu}\left(\frac{2\mu}{\pi k_B T}\right)^{\frac{1}{2}} \qquad (2.40)$$

where k_{LD}, as is in the literature, has units of cm^3 s^{-1}. The units are charge, Q, in Coulombs (C), polarizability, α, in g^{-1} s^4 A^2, reduced mass, μ, in g, $4\pi\varepsilon_0$ is 1.113 x 10^{-19} cm^{-3} g^{-1} s^4 and the dipole moment, μ_D, in C cm. k_B *is* the Boltzmann constant (1.38066 x 10^{-16} g cm^2 s^{-2} K^{-1}) and T is temperature (K).

Comparisons with experimental data show that the locked-dipole rate constants overestimate the rate constant due to the overestimation of the dipole effect (Gupta *et al*. 1967, Bowers and Laudenslager 1972, Su and Bowers 1973a – c, 1974). Bowers and Laudenslager (1972)

included a parameter, C, the dipole locking constant, to account for the degree of dipole locking in the rate equation, C is $\sim \cos\theta$. C has values from zero to one. A value of zero indicates the dipole continues to freely rotate in the presence of the ion, i.e. there is no ion-dipole potential energy contribution. A value of one indicates locking of the dipole at zero degrees i.e. $\theta = 0$ as in the locked-dipole theory.

$$k_{ADO} = \frac{2\pi Q}{(4\pi\varepsilon_0)}\left(\frac{\alpha}{\mu}\right)^{\frac{1}{2}} + \frac{2\pi QC\mu_D}{(4\pi\varepsilon_0)\mu}\left(\frac{2\mu}{\pi k_B T}\right)^{\frac{1}{2}}$$ (2.41)

where k_{ADO} is the average dipole orientation rate constant (cm^3 s^{-1}) and units are as for the locked-dipole rate constant, Eq. 2.40 (C is unitless). Initial values of the dipole-locking constant were obtained by comparison of experimental rate constants for charge transfer to isomers with the same polarizability but varying dipole moments (Bowers and Laudenslager 1972, Su and Bowers 1973a). The ratio of rate constants for reaction of a molecule with a dipole to that without a dipole is equivalent to the ratio of the Langevian rate constant (induced dipole, Eq 2.34) with the ADO rate constant (Eq. 2.41). The effectiveness of charge dipole locking and contribution of the dipole potential term can be determined from Eq. 2.34 and 2.41:

$$\frac{k_{polar}}{k_{nonpolar}} \approx \frac{k_{ADO}}{k_L} = 1 + C\left[\frac{2^{1/2}\mu_D}{(k_B T\alpha\pi)^{1/2}}\right]$$ (2.42)

$$C = \frac{(k_B T\pi\alpha)^{1/2}}{\mu_D 2^{1/2}}\left(\frac{k_{polar}}{k_{non-polar}} - 1\right)$$ (2.43)

where k_{polar} and $k_{non-polar}$ are experimental values for the ion-molecule system studied.

Dipole locking is dependent on the strength of the dipole and is molecule specific thus these experimentally determined values of C are of limited value. A theoretical model was subsequently developed by Su and Bowers (1973a and b) to enable C to be obtained for any ion-dipole interaction. This was done by evaluating the rate constant *via* the capture-cross section and the velocity calculated from $b*$ similarly to the Langevin and locked-dipole rate constant derivation. The rate constants derived from this theoretical model were calculated for a range of dipoles and polarizabilities and input into Eq. 2.41 to obtain C. At a given temperature, C was observed to be a factor of $\alpha^{1/2}\mu_D$ only (Su and Bowers 1973c). Values of C as a function of $\alpha^{1/2}\mu_D$ at temperatures of 150 K to 500 K have been published (Su and Bowers 1973c, 1975). Average dipole orientation rate constants can therefore be calculated simply from Eq. 2.41, using these tables.

(a) +Q

Schematic of the geometry of a dipole and its alignment with an ion

r

θ

d_1 d_2

$- q$ $+ q$

(b) +Q

θ r

$- q$

$+ q$

The negative charge of the permanent dipole, -q, is close to alignment with the positive charge of the ion, +Q and θ is close to zero. There is an attractive potential energy.

(c) +Q

r

$+ q$

θ

$- q$

The positive charge of the permanent dipole, +q, is close to alignment with the positive charge of the ion, +Q and θ is close to 180°. There is a repulsive potential energy contribution.

Figure 2.13: Schematics illustrating the effect of a change in dipole locking angle, θ, as a polar molecule rotates with respect to an ion.

The principles of the theoretical model used by Su and Bowers (1973a and b) to determine the theoretical rate constants are outlined in the following section: $b*$ and relative velocities for the theoretical ADO rate constants were calculated from expressions for the effective potential energy at $b*$ and its derivative with respect to $r*$. In this case the full ion dipole potential energy term is included (Su and Bowers 1973a - c, Su and Bowers 1979):

$$E_r = \frac{1}{2}\mu v^2 = U_{eff} = \frac{\mu v^2 b*^2}{2r*^2} - \frac{\alpha Q^2}{2(4\pi\varepsilon_0)^2 r*^4} - \frac{\mu_D Q}{4\pi\varepsilon_0 r*^2}\cos\overline{\theta}(r) \qquad (2.44)$$

The complication in the calculation is introduced in the need to assess the average dipole orientation, $\overline{\theta}(r)$. Note that an average orientation determined as a function of r is employed; the average orientation at $r*$ is critical to the rate constant calculation. The probability of a given orientation at a distance r is dependent on the number of ways of arranging the dipole to give that orientation and the total energy of the rotating system, E_{rot}, in the plane of collision. E_{rot} is dependent on the rotational kinetic energy, KE_{rot}, in the plane of collision and the ion-dipole interaction energy, U_D, as defined in Eq. 2.35.

$$E_{rot} = KE_{rot} + U_D \qquad (2.45)$$

Two cases are identified by Su and Bowers, one where the rotational energy is less than the dipole interaction potential and the other where rotational energy is greater than dipole interaction. In the first case the dipole rotation is restricted and motion is oscillatory, in the second the dipole can freely rotate in a full circle (non oscillatory motion). The average energy of molecules with rotational energy less than the dipole interaction is denoted E_1 and average energy of molecules with rotational energy greater than the dipole interaction E_2. The average orientation as a function of r is then given by

$$\overline{\theta}(r) = \overline{\theta}_1(r)F_1 + \overline{\theta}_2(r)F_2 \qquad (2.46)$$

where F_1 and F_2 are the fraction of molecules with energy less than and greater than U_D respectively. $\overline{\theta}_1(r)$ and $\overline{\theta}_2(r)$ are determined from E_1 and E_2 respectively. E_1, E_2, F_1 and F_2 are evaluated by application of the Boltzmann distribution using:

$$P(e_r)de_r = (1/kT)e^{-e_r k_B T}de_r \qquad (2.47)$$

where e_r is the rotational energy of the neutral given by (Su and Bowers 1973b, Banwell and McCash 1994, Richards and Scott 1994)

$$e_r = E_J = J(J+1)h^2/8\pi^2 I \qquad (2.48)$$

where J is the quantum number, h is Planck's constant and I is the moment of inertia. Substituting $\overline{\theta}(r = r*)$ and $\partial\overline{\theta}/\partial r$ into equations for the capture-cross section and relative velocity gives the theoretical rate constant. As established in the locked-dipole case, the rate

constant is dependent on velocity and Maxwell-Boltzmann mean thermal velocity distribution is invoked. An additional temperature dependence is introduced in C indicating the decrease in dipole locking with increased temperature (Su and Bowers 1979).

2.4.1.4 Su and Chesnavich Trajectory Calculations

Chesnavich *et al* (1980) and Su and Chesnavich (1982) calculated a thermal ion-dipole capture rate constant, k_{SC}, using variational transition theory and classical trajectory analysis. The resulting capture rate constant was shown to be related to the Langevin rate constant by two reduced parameters, T_R and I^*:

$$\frac{k_{SC}}{k_L} = K_{cap}(T_R, I^*) \tag{2.49}$$

$$T_R = \frac{2\alpha k_B T}{\mu_D^2} \tag{2.50}$$

$$I^* = \frac{\mu_D I (4\pi\varepsilon_0)}{\alpha Q \mu} \tag{2.51}$$

3000 trajectories for each combination of T_R and I^* showed that at low values of I^*, K_{cap} is dependent only on T_R. The region in which this is true is defined by:

$$I^* < \frac{0.7 + x^2}{2 + 0.6x} \tag{2.52}$$

where $\quad x = \frac{1}{\sqrt{T_R}} = \frac{\mu_D}{(2\alpha k_B T)^{\frac{1}{2}}} \tag{2.53}$

If Eq 2.52 is satisfied, K_{cap} can be determined from the following empirical fit of the trajectory curve.

$$K_{cap} = \begin{cases} 0.4767x + 0.6200; x \geq 2 \\ \dfrac{(x + 0.5090)^2}{10.526} + 0.9754; x \leq 2 \end{cases} \tag{2.54}$$

The Su and Chesnavich rate constant, $k_{SC,}$ is in units of cm^3 s^{-1}, the other units are as for the locked dipole rate constant in Eq. 2.40 and moments of inertia, I, are g cm^2. Although the derivation of the trajectory calculation was for linear molecules it can be used for non-linear molecules, with more than one moment of inertia, by using a mean moment of inertia to calculate I^* (private communication with T. Su, June 14, 2007). If Eq. 2.52 is not satisfied the parameterisation does not apply and a rate constant cannot be calculated by this method.

2.4.1.5 The Effect of the Electric Field on Collisional Rate Constants

The theories discussed so far do not consider the effect of a homogenous electric field, as in the drift tube of PTR-MS, on rate of reaction.

The translational energy of ions is increased by the electric field as the ion is attracted to the opposite charge and repelled by the like-charge of the field. Since the electric field is homogenous, the forces on the positive charge of a dipole or induced dipole are equal to the forces on the negative charge and there is no change in the translational energy of the dipole (when at infinite separation from the ion) (Figure 2.14).
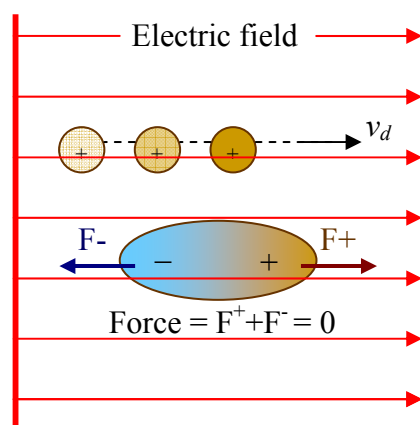
Figure 2.14: The effect of a homogeneous electric field on an ion and polar molecule (adapted from Lindinger 1986b). The velocity of the ion is increased in the direction of the field. There is no net force on the polar molecule and its translational energy is unchanged.

The ion motion in the direction of the field is superimposed on fast random motion and anisotropic diffusion. Random motion is contributed to by thermal energy and the conversion of ion energy provided by the field to random energy in ion-neutral collisions. The average velocity of the ions perpendicular to the field is close to zero (§ 2.4.1.7 and 2.7). The average velocity in the direction of the electric field is the drift velocity, v_d. (McDaniel *et al* 1970 Meisels 1974, Mason and McDaniel 1988)

The Langevin rate constant is independent of velocity (Eq 2.34). To derive the ion-dipole collsional rate constant knowledge of the **average relative** velocity is required. The average dipole orientation and trajectory rate constants for ion-polar reactions decreases as relative velocities increase with increasing temperature. The distribution of velocities is assumed to be unchanged by the electric field and is taken to be a Maxwell-Boltzmann distribution (§ 2.4.1.7). The effect of the electric field on the collisional rate constant may be viewed as akin to a selective increase in temperature (of the ion and only affecting the translational energy

directly). In this case, an effective internal ion temperature can be calculated and used in place of the reaction chamber temperature in Eq. 2.41 and 2.53.

To derive an effective temperature to determine mean relative velocities in the drift tube, the mean centre-of-mass kinetic energy of the ion-neutral, $KE_{c.m.}^{r}$, must be known. To determine $KE_{c.m.}^{r}$ knowledge of the kinetic energy of the ion is required. Wannier (1953) derived an expression for the mean ion kinetic energy in a drift tube:

$$KE_{ion} = \frac{1}{2}M_i v_d^{\ 2} + \frac{1}{2}M_b v_d^{\ 2} + \frac{3}{2}k_B T \tag{2.55}$$

M_i is the ion mass, M_b is the buffer mass, in the case of PTR-MS the buffer is air and the average molecular weight of air of 28.9 g mol^{-1} is employed as an approximation of M_b. The units of KE_{ion} are kg m^2 s^{-2} (kg m^2 s^{-2} = 1 J) and the following units are employed: M_i and M_b in kg particle[-1], drift velocity, v_d in m s^{-1}, temperature, T, in K and the k_B, the Boltzmann constant is 1.38066 x 10^{-23} kg m^{-2} s^{-2} K^{-1}. KE_{ion} is given in eV here (§ 3), where 1 eV is an energy and is 1.6022 x 10^{-19} kg m^2 s^{-2} (McGlashan 1971). The first term in Eq. 2.55 is the energy due to velocity in the field direction, the second term is energy due to ion neutral collisions in the field and the third term is thermal energy. This equation is a reasonable approximation at low and high field strengths (McFarland 1973b)

The drift velocity, v_d, is preferably an experimental value but can be calculated to a first approximation from:

$$v_d = K \times E \tag{2.56}$$

where E is the electric field strength, normally between ~ 5800 and 6300 V m^{-1} here, and K is the ion mobility (m^2 V^{-1} s^{-1}). The electric field strength is obtained from the ratio of the voltage at the drift tube, V_{drift}, (usually 550 – 600 V) and the length of the drift tube, l_d, (0.095 m in this case). K is usually given as a reduced mobility, K_0 (m^2 V^{-1} s^{-1});

$$K_0 = \frac{P_{dt}}{P_0}\frac{T_0}{T_{dt}}K = K\frac{N}{N_0} \tag{2.57}$$

where P_{dt} is the drift tube pressure, P_0 is the standard pressure (101325 Pa), T_{dt} is the drift tube temperature (K), T_0 is the standard temperature (273.16 K), N_0 is the number density of particles at standard temperature and pressure (2.687 x 10^{23} particles m^{-3}) and N is the number density of particles at experimental temperature and pressure (particle m^{-3}). Mobility is itself dependent on E/N, experimental values at the appropriated E/N are used. Substituting Eq. 2.57 into Eq. 2.56 gives:

$$v_d = K_0 N_0 \left(\frac{E}{N} \right)$$ (2.58)

Thus, increasing the electric field strength or decreasing the pressure or temperature of the drift tube increases the drift velocity and subsequently the kinetic energy of the ions (Eq. 2.55). It follows from the E/N dependence of KE_{ion} that varying levels of fragmentation and clustering are observed at different E/N (§ 2.6, 2.9 and Chapter 3). Therefore, E/N must be specified with PTR-MS results and PTR-MS measurements performed at significantly different E/N are not comparable (§ 2.6, 2.9 and Chapter 3).

The centre-of-mass kinetic energy for an ion neutral pair is given by (McFarland, 1973b):

$$KE_{c.m.}^r = \frac{M_r}{M_r + M_i} \left(KE_{ion} - \frac{3}{2} k_B T \right) + \frac{3}{2} k_B T$$ (2.59)

where M_r is the molecular mass of the reactant molecule. The units of $KE_{c.m.}^r$ are kg m^2 s^{-2} (1 kg m^2 s^{-2} = 1 J) and the following units are employed: KE_{ion} in kg m^2 s^{-2}, M_i and M_r in kg particle^{-1}, T, in units of K and k_B, the Boltzmann constant is 1.38066 x 10^{-23} kg m^{-2} s^{-2} K^{-1}. $KE_{c.m.}^r$ is given in eV here (§ 3), where 1 eV is an energy and is 1.6022 x 10^{-19} kg m^2 s^{-2} (McGlashan 1971). The effective temperature is defined as (McFarland 1973b)

$$T_{eff} = \frac{2 KE_{c.m.}^r}{3 k_B}$$ (2.60)

Note that this temperature only relates to the increase in translational energy of the ion in the field. This T_{eff} does not consider the impact on the internal energy of the ion due to field induced ion-buffer collisions (§ 2.9). The reduction due to energy loss in inelastic collisions (§ 2.9) is neglected. Anisotropic diffusion terms are neglected in this derivation of T_{eff} (as are they in Eq. 2.10 as discussed in § 2.7). Viehland *et al* (1981) have derived more thorough treatments of T_{eff} in the case of polyatomic ions in monatomic and diatomic buffers. The use of these more comprehensive T_{eff} expressions in ion-polar collisonal rate constant theories discussed still provides only a first approximation. Although expressions for T_{eff} purposefully do not assume a Maxwell-Boltzmann distribution of ion velocities, use in the rate equations as discussed, does assume a Maxwell-Boltzmann ion velocity distribution which is not necessarily the case (§ 2.4.1.7). Eq. 2.60 has been widely employed by PTR-MS users (Steinbacher 2004a,b, de Gouw and Warneke 2007) and is employed for comparison of rate constants here.

Unlike an increase in temperature, the electric field does not affect the energy of the neutral. The translational energy of the neutral reactant is unaffected by the field and therefore

collisions with the buffer and thus the internal energy is also approximately unchanged. Since the rotational energy of the polar neutral is not affected by the electric field, the temperature of the dipole locking constant in the ADO theory (§ 2.4.1.3) remains the drift tube temperature. T_{eff} is only used to calculate mean velocity in Eq. 2.41. In the more developed Su and Chesnavich trajectory calculation (§ 2.4.1.4), it is not possible to select a separate rotational temperature to the ion temperature. The use of T_{eff} results in an overestimation of the rotational energy and therefore underestimation of dipole-locking and the corresponding rate constant.

Su (1994) published a method to calculate collisional rate constants based on trajectory calculated results relating the Langevin rate constant to the capture rate constant by a factor, K_c, parameterised by $KE_{c.m.}^r$ and rotational temperature (T_{rot}):

$$\frac{k_{KE_{c.m.}^r}^{T_{rot}}(T)}{k_L} = K_c(\tau, \varepsilon) \tag{2.61}$$

$$\tau = \frac{\mu_D}{\sqrt{\alpha T_{rot}}} \tag{2.62}$$

$$\varepsilon = \frac{\mu_D}{\sqrt{\alpha KE_{c.m.}^r}} \tag{2.63}$$

$k_{KE_{c.m.}^r}^{T_{rot}}$ is the collisional rate constant calculated *via* this method (cm^3 s^{-1}) when units are, polarizability, α, in Å^3, dipole moment, μ_D, in Debye (D), rotational temperature, T_{rot}, in K and $KE_{c.m.}^r$, in electronvolts (eV). The rotational temperature is taken as the drift tube temperature. The empirical fit of 6000 trajectories showed:

$$K_c(\tau, \varepsilon) = 1 + c_1 \tau^{0.4} \varepsilon^2 S + c_2(1 - S) \times \sin[c_3\{c_4 + \ln(\tau)\}] \tau^{0.6} (\varepsilon - 0.5)^{\frac{1}{2}} \tag{2.64}$$

where c_1=0.727143, c_2=3.71823, c_3=0.586920, c_4=4.97894 and

$$S = \begin{cases} \exp[-2(\varepsilon - 1.5)]; \varepsilon > 1.5 \\ 1; \varepsilon < 1.5 \end{cases} \tag{2.65}$$

As discussed above, the use of drift tube temperature as rotational temperature assumes no effect of the electric field on the rotational energy of the dipole. There will be little effect *via* collisions (as there is with the ion) however, in the same way that the ion affects rotational energy of the polar neutral, the direct effect of the electric field will restrict rotation. This may be considered to enhance alignment with the ion since there may be less neutral molecules with sufficient energy to overcome the ion-dipole interaction. The effect may be more complex since particular rotations may be favoured over others in the field. However a

comparison of the relative field strengths of the ion (considered as a point charge here) at distances in the order of r^* (§ 2.4.1.2) (Table 2.2), with the electric field strength of $\sim 50 - 60$ V cm^{-1} in the drift tube show that the exclusion of these effects is likely to be a limited source of error. Statistical thermodynamic considerations also indicate that alignment of the dipole with the field is very slight when field strengths of the magnitude used in the PTR-MS and thermal temperatures are applied (Hill 1962).

Table 2.2: Ion field strength at various distances, r, calculated from Coulomb's law treating H_3O^+ as a point charge (1.60×10^{-19} C).

r (Å)	Ion Field Strength (10^7 V cm^{-1})
2	35.99
4	9.00
6	4.00
8	2.25
10	1.44
12	1.00
14	0.73
16	0.56
18	0.44
20	0.36

Steinbacher (2004a) reports consistently better agreement between calculated and calibrated concentrations with the PTR-MS when no effective temperature was used in rate constant calculation (refer also to Steinbacher *et al* 2004b). Rate constants were calculated *via* the ADO theory (§ 2.4.1.3) and Su and Chesnavich trajectory theory (§ 2.4.1.4). The underestimation of rate constants with T_{eff} may be in part due to an overestimation of rotational temperature with the Su and Chesnavich calculation. Another more general reason for an underestimation of collisional rate constant in drift tubes has been previously noted: Lindinger *et al* (1975a) reported experimental rate constants for four fast exothermic proton transfer reactions to polar molecules which occur at collisonal rate at thermal temperatures (§ 2.9) measured using a flowing afterglow drift tube over a range of E/N. The experimental rate constants showed an increase with $KE_{c.m.}^r$ contrary to the decrease predicted by e.g. ADO theory (with effective temperature). Bei *et al* (1989) suggested that at the high translational energies or (effective) temperatures in the drift tube, the r^* (§ 2.4.1.2) distance as defined by Langevin theory may become less than the hard sphere diameter, d_{HS}, (r^* decreases as relative velocities and centrifugal energy increase § 2.4.1.2). In this case a collision will occur at d_{HS} where $b > b^*$ and use of b^* as defined by Langevin theory alone will result in an underestimation of the collisional cross section and therefore the collisonal rate constant. Also at these smaller separations, the assumption that d_1 and d_2 (Figure 2.13 a)

are equal as used in the derivation of the ion-dipole potential (Eq. 2.35, Appendix B) is no longer valid.

Bei *et al* (1989) derived theoretical rate constants from a new ion-polar interaction potential including a dependence on dipole dimensions and taking in to account collisions at the hard sphere radius as reactive for the exothermic reaction of H_3^+ with NH_3. These theoretical rate constants varied with $KE_{c.m.}^r$ in a comparable way to the experimental data of Lindinger *et al* (1975a).

None of the ion-polar collisional rate constant theories discussed include hard sphere radius and dipole dimensions in the potential energy of interaction (private communication with T. Su, June 27 2007). There does not appear to be a generally applicable theory for ion-polar rate constant calculation which does so. Calculated ion-polar rate constants may therefore underestimate the collisional rate as $KE_{c.m.}^r$ (and therefore *E/N*) increases.

Glosik *et al* (1993) defined a parameter, β, for the variation of collisional rate constants with $KE_{c.m.}^r$. β was obtained from the ratio of measured thermal rate constants to rate constants measured at elevated $KE_{c.m.}^r$ for a number of reactions which are fast and efficient at thermal temperatures where an increase in rate (i.e. collisonal rate) is observed with $KE_{c.m.}^r$. β increased from 1.0 at $KE_{c.m.}^r$ of 0 eV to ~0.1 eV up to ~2.0 at $KE_{c.m.}^r$ of 1.1 to 1.2 eV. At the values of $KE_{c.m.}^r$ normally applied in the PTR-MS (0.2 to 0.3 eV) this is a relatively small factor, though converse to the decrease expected in $k_{KE_{c.m.}^r}^{T_{rot}}$. The obtained $\beta(KE_{c.m.}^r)$ values have been applied to a number of inefficient reactions to determine the true energy dependence of reaction efficiency (distinct from collisional rate dependence) in SIFDT measurements (Glosik *et al* 1993, 1995). Multiplication of thermal collisional rate constants (where β=1), i.e. k_{SC} at 298 K or rate constants measured using SIFT at 298 K, for H_3O^+, reaction with polar molecules by β at the appropriate $KE_{c.m.}^r$ should therefore provide reasonable approximations of the rate constant at elevated energies if the hard sphere diameter is the dominating factor in rate constant determination. β variation with $KE_{c.m.}^r$ incorporates translational energy dependence of the reaction rate constants, the hard sphere radius inclusion and changes in possible assumptions about dipole dimensions. Since $\beta(KE_{c.m.}^r)$ values are dependent on hard sphere radius, polarizability and the dipole moment, and given that the values obtained by Glosik *et al* (1993) were measured in SIFDT in a

helium buffer rather than PTR-MS, values obtained in this manner are subject to some uncertainty. However the deviation of β for the individual reactions of varying hard sphere diameter and polarizability was small. The reactions used to derive the average $\beta(KE_{c.m.}^r)$ included $Kr^+ + CS_2$, CS_2 has a polarizability similar to many of the (O)VOCs (8.74 Å^3) and the hard sphere diameter is comparable to that of a number of (O)VOC + H_3O^+ systems.

The decrease in $r*$ at elevated energies and consequent need to consider d_{HS} also applies to ion-non-polar collision (§ 2.4.2). Exclusion of hard sphere collisions may lead to underestimation of the rate constant at high translational energies ($/T_{eff.}$). Smith *et al* (1990) derived an integral for calculation of rate constants including both Langevin and hard sphere collision parameters. In the case that $r*$ is greater than d_{HS}, this integral reduces to the Langevin collisional rate constant (Eq 2.34). At higher effective temperatures, where $r*$ is smaller than d_{HS}, it reduces to the hard sphere collisional rate coefficient.

There do not appear to be any investigations into the $KE_{c.m.}^r$ dependence of rate constants for reaction of H_3O^+ with non-polar (O)VOCs in a drift tube (§ 2.9). Midley *et al* (2002) investigated the variation of rate constants of H_3O^+ reaction with toluene, ethylbenzene and *n*-propylbenzene with temperatures from 500 – 1000 K using HTFA and VT-SIFT. Measured values where within experimental error of those calculated using Su and Chesnavich theory (§ 2.4.1.4). No increase in rate constant was observed suggesting that at these energies, hard sphere diameter, ion charge and VOC polarizability, the hard sphere diameter is not less than $r*$ as defined by Langevin theory. Given that the hard sphere radius of other VOCs of interest with relatively small dipole moments and similar polarizabilities, e.g. 2-methyl-1,3-butadiene (isoprene), and H_3O^+ is similar to that of toluene and H_3O^+, it is assumed that the hard sphere radius is less than $r*$ in the PTR-MS under normal operating conditions and the collisional rate constant can be best approximated by excluding the hard sphere collision diameter. It is notable that T_{eff} is generally greater than 1000 K under normal operating conditions in the PTR-MS and in the absence of investigation of rate constant variation in a drift tube at varying *E/N*, the point at which the hard sphere diameter dominates the collisional rate constant cannot be defined.

There are limited investigations of the variation of rate constants with $KE_{c.m.}^r$ or temperature for reactions of H_3O^+ with non-polar molecules quantifiable with PTR-MS (§ 2.9, Chapter 3) (Warneke *et al* 1996, Lagg *et al* 1994). The rate constants of those reactions studied showed a decrease with increasing $KE_{c.m.}^r$ as expected given the elevated translational energy. If it is assumed that the decrease is entirely due to the increase in translational energy and that the

measured reaction rate constant is the collisional rate constant at all energies (§ 2.4.1.7), it appears the hard sphere diameter is not important at these energies, polarizabilities and dipole moments. The collisional rate constant is therefore better approximated by $k_{KE^r_{c.m.}}^{T_{rot}}$ than by multiplication of thermal rate constants by β at the corresponding $KE^r_{c.m.}$.

2.4.1.6 A Comparison of Calculated Rate Constants

Collisional rate constants were calculated with each of the discussed methods for a range of VOCs observed using the parameters displayed in Table 2.3. The moments of inertia used to derive the mean moments of inertia (Table 2.3) for the Su and Chesnavich trajectory calculation are shown in Table 2.4. The calculated rate constants are collated in Table 2.5.

As expected the rate constants of non-polar molecules, e.g. benzene, are the same with each method (note the $KE^r_{c.m.}$, T_{rot} parameterised rate constant cannot be calculated for molecules without a dipole moment). Rate constants of polar molecules calculated *via* Langevin theory are less than k_{ADO} and k_{SC} since the ion-dipole interaction is not accounted for. Values of k_{ADO} and k_{SC} calculated at effective ion temperatures are less than those at drift tube temperatures. As expected the $KE^r_{c.m.}$, T_{rot} parameterised rate constant is greater than k_{SC} calculated at an effective temperature.

It is proposed that, where m/z can be unambiguously identified, k_L values for non-polar molecules and $k_{KE^r_{c.m.}}^{T_{rot}}$ for polar molecules are used in the calculation (Eq. 2.10) of concentrations in the PTR-MS.

Table 2.3: Polarizabilities, α, and dipole moments, μ_D, used to calculate collisional rate constants as presented in Table 2.5.

Compound	α (Å^3)	μ_D (D)	I_m (10^{-40} g cm^2)	T_{eff} (K)	$KE^r_{c.m.}$ (eV)
Benzene	10.78[a]	0[a]	196.7[c]	1731	0.22
Toluene	11.80[b]	0.375[b]	322.2[c]	1775	0.23
1, 2 – DMB	14.90[b]	0.64[b]	-	1808	0.23
1, 4 – DMB	15.08[a]	0.081[a]	485.7[d]	1808	0.23
1, 3 – DMB	15.03[a]	0.271[a]	592.0[d]	1808	0.23
1, 3, 5 – TMB	17.16[a]	0.047[a]	628.7[d]	1835	0.24
1, 2, 3 – TMB	17.09[a]	0.66[a]	-	1835	0.20
1, 2, 4 – TMB	17.17[a]	0.291[a]	-	1835	0.20
Methanol	3.32[b]	1.7[b]	25.3[e]	1421	0.18

Table 2.3 is continued on the following page.

Compound	α (Å^3)	μ_D (D)	I_m (10^{-40} g cm^2)	T_{eff} (K)	$KE^r_{c.m.}$ (eV)
Ethanol	5.11[b]	1.69[b]	72.4[e]	1562	0.20
Propanone (acetone)	6.39[b]	2.88[b]	117.4[f]	1642	0.21
Ethanal (acetaldehyde)	4.59[b]	2.75[b]	63.3[f]	1545	0.20
2-methyl-1,3-butadiene (isoprene)	10.22[a]	0.25[a]	200.1[g]	1692	0.22
3-Buten-2-one (MVK)	8.18[a]	3.11[a]	191.7[h]	1700	0.22
2-Methyl-2-propenal (MACR)	8.3[b]	2.68[b]	196.3[i]*	1700	0.22
Methanoic acid	3.4[b]	1.425[b]	54.1[j]*	1562	0.20
Ethanoic acid	5.1[b]	1.7[b]	106.9[j]	1653	0.21
Propanoic acid	6.9[b]	1.75[b]	197.9[j]	1716	0.22
Butanoic acid	8.58[b]	1.65[b]	-	1763	0.23
Pentanoic acid	10.41[b#]	1.61[b]	-	1799	0.23
2-methylphenol	13.84[b]	1.045[a]	-	1812	0.23
3-methylphenol	13.83[b]	1.033[a]	-	1812	0.23
4-methylphenol	13.89[b]	1.301[a]	-	1812	0.23
Phenol	9.94[b]	1.224[b]	-	1780	0.23
Trimethylamine	7.78[b]	0.612[b]	120.3[k]	1647	0.21
Acetonitrile	4.48[b]	3.92519[b]	-	1519	0.20

Note: I_m are average moments of inertia (Table 2.4), used to determine whether Su and Chesnavich parameterised trajectory could be applied. $KE^r_{c.m.}$ (Eq. 2.59) and T_{eff} (Eq. 2.60) refer to the centre of mass kinetic energy and effective temperature of ions in a drift tube at 2.0 mbar, 318.15 K and a V_{drift} of 550 V ($E = 57.89$ V cm^{-1}). The majority of measurements in this study were performed under these operating conditions. The values of T_{eff} shown were used for the calculation of $k^{T_{eff}}_{ADO}$ and $k^{T_{eff}}_{SC}$ values presented in Table 2.5. The values of $KE^r_{c.m.}$ were used for calculation of $k^{T_{rot}}_{KE^r_{c.m.}}$ values shown in Table 2.5. Polarizability and dipole values were taken from [a] Zhao and Zhang (2004) and [b]CRC Handbook of Chemistry and Physics, (2002 – 2003). [b#]A polarizability value of pentanoic acid could not be found and the value of the two other $C_5H_{10}O_2$ compounds listed in [b] were used. Moments of inertia were derived from [c]Ronne *et al* (2000), [d]by calculation using bond lengths and angles given in Kovacs (2000), [e]Allinger *et al* (2003), [f]Langley *et al* (2003), [g]Chhiba and Vergoten (1994), [h]Foster *et al* (1965), [i]Durier (1999), [j]Lii (2002), [k]Chen *et al* (2007), * indicates that a mean of isomeric values was used. TMB refers to trimethylbenzene, DMB refers to dimethylbenzene (xylene), MVK denotes methylvinylketone, MACR refers to methacrolein.

Table 2.4: Moments of inertia, I_a, I_b, I_c and mean moment of inertia, I_m, (10^{-40} g cm^2).

Compound	I_a	I_b	I_c	I_m	Reference
Benzene	147.1	147.1	294.3	196.2	Tokmakov and Lin, 2002[a]
	147.5	147.5	295.0	196.7	Ronne *et al*, 2000[a]
	147.2	*147.2*	*293.6*	*196.0*	*Ellis et al, 1999*
Toluene	151.6	334.4	480.7	322.2	Ronne *et al*, 2000[a]
	151.4	*330.0*	*480.8*	*320.7*	*Pang et al,1980*

Table 2.4 is continued on the following page

Compound	I_a	I_b	I_c	I_m	Reference
1, 4 – DMB	*157.0*	*570.4*	*729.8*	*485.7*	*Kovacs et al, 2000*
1, 3 – DMB	*315.7*	*539.9*	*920.3*	*592.0*	*Kovacs et al, 2000*
1, 3, 5 – TMB	*478.1*	*469.0*	*939.0*	*628.7*	*Kovacs et al, 2000*
Methanol	6.6	34.0	35.2	25.3	Allinger et al, 2003[b]
Ethanol	24.1	89.7	103.4	72.4	Allinger et al, 2003[b]
Propanone	82.9	98.2	170.8	117.4	Langley et al, 2003[b]
Ethanal	14.8	82.7	92.3	63.3	Langley et al, 2003[b]
2-methyl-1,3-butadiene (Z)	99.0	203.9	297.5	200.1	Chhiba &Vergoten,1994[c]
	98.4	201.1	294.4	198.0	Chhiba &Vergoten,1994[d]
MVK	93.9	196.3	284.9	191.1	Foster et al, 1965[e]
MACR (Z)	96.6	197.2	288.4	194.7	Durier et al, 1999[c]
MACR (E)	86.6	213.0	294.1	197.9	Durier et al, 1999[c]
Methanoic acid (Z)	11.0	69.8	80.7	53.8	Lii, 2002[b]
Methanoic acid (E)	9.7	71.9	81.6	54.4	Lii, 2002[b]
Ethanoic acid	74.1	88.8	157.9	106.9	Lii, 2002[b]
Propanoic acid	82.3	219.2	292.1	197.9	Lii, 2002[b]
Trimethylamine	96.2	96.2	168.5	120.3	Chen et al, 2007[b]

Note: Values in italics were calculated from first principles, bond angles and lengths were obtained from the corresponding reference, moments of inertia were otherwise obtained from the specified reference. [a] Values were obtained from Gaussian molecular mechanics programmes (B3LYP/6-311++(d,p) and B3LYP/6-31G*), [b] molecular mechanics MM4 calculated values, [c] values calculated with SPASIBA molecular mechanics programme, [d] experimental values [e] values derived from microwave spectra. Structural data was not available for the higher carboxylic acids and moments of inertia are unknown. TMB refers to trimethylbenzene, DMB refers to dimethylbenzene (xylene), MVK denotes methylvinylketone, MACR refers to methacrolein.

2.4.1.7 Ion Speed Distributions in the Drift Tube

All of the collisional rate constant theories assume a Maxwell-Boltzmann distribution of ion / molecule velocities in the drift tube. Inherent in these theories are the assumption that the mean free path of an ion is sufficiently small in the drift tube for steady state to be achieved (in each direction), i.e. that the concept of a distribution is valid and for a Maxwell-Boltzmann distribution that the velocity is asimtopic. The ion velocity parallel to the field is primarily determined by the electric field whereas perpendicular to the field it is a function of diffusion and random thermal motion only (both relatively minor parallel to the field) therefore the asimtopic nature of velocity and therefore Maxwell-Boltzmann speed distribution is questionable. Experimental measurement of ion distributions is difficult (Albritton et al 1977) and no experimental studies of H_3O^+ ion velocity or speed distributions in drift tubes could be found. Theory (Lin and Bardsley 1977) and experimental (Albritton et al 1977, Dressler et al, 1987, 1988) evidence indicate that velocity distributions of ions in a helium buffer are close to a Maxwell distribution. There appear to be no experimental data investigating ion velocity distributions in air, nitrogen or oxygen. Monte

Table 2.5: Collisional rate constants (10^{-9} cm^3 s^{-1}), calculated for normal operating drift tube conditions of P_{dt} 2.0 mbar, T_{dt} 318.15 K, V_{drift} 550 V, E 57.89 V cm^{-1}, and therefore E/N 127 Td.

Molecule	k_L (10^{-9} cm^3 s^{-1})	θ (°)	$k_{ADO}^{T_{dt}}$ (10^{-9} cm^3 s^{-1})	$k_{ADO}^{T_{eff}}$ (10^{-9} cm^3 s^{-1})	$I*$	$I*_{UL}^{T_{dt}}$	$k_{SC}^{T_{dt}}$ (10^{-9} cm^3 s^{-1})	$I*_{UL}^{T_{eff}}$	$k_{SC}^{T_{eff}}$ (10^{-9} cm^3 s^{-1})	$k_{KE_{c.m.}^r}^{T_{rot}}$ (10^{-9} cm^3 s^{-1})
Benzene	1.97	90.00	1.97	1.97	0.00	0.35	1.97	0.35	1.97	-
Toluene	2.03	88.94	2.04	2.03	0.08	0.38	2.13	0.35	2.06	2.04
1, 2 – DMB	2.25	87.31	2.32	2.28	-	0.43	2.44	0.35	2.31	2.28
1, 4 – DMB	2.27	90.00	2.27	2.27	0.02	0.35	2.28	0.35	2.27	2.27
1, 3 – DMB	2.26	90.00	2.26	2.26	0.04	0.34	2.29	0.35	2.27	2.27
1, 3, 5 – TMB	2.40	90.00	2.40	2.40	0.01	0.35	2.40	0.35	2.40	2.40
1, 2, 3 – TMB	2.39	87.48	2.45	2.42	-	0.43	2.58	0.35	2.45	2.42
1, 2, 4 – TMB	2.40	90.00	2.40	2.40	-	0.35	2.46	0.34	2.42	2.40
Methanol	1.24	77.49	2.19	1.69	0.14	2.73	2.62	1.01	1.67	2.27
Ethanol	1.44	78.52	2.26	1.81	0.22	2.01	2.63	0.74	1.78	2.24
Propanone	1.56	76.71	3.12	2.25	0.46	3.59	3.84	1.18	2.25	3.19
Ethanal	1.38	76.28	2.97	2.10	0.36	4.23	3.70	1.43	2.14	3.06
2-methyl-1,3-butadiene	1.94	89.92	1.94	1.94	0.04	0.36	2.00	0.34	1.97	1.95
MVK	1.73	76.88	3.36	2.44	0.61	3.37	4.10	1.09	2.41	3.41
MACR	1.75	77.50	3.08	2.32	0.53	2.72	3.69	0.90	2.28	3.10
Methanoic acid	1.18	78.35	1.88	1.49	0.21	2.10	2.19	0.77	1.47	1.87
Ethanoic acid	1.39	78.48	2.19	1.74	0.31	2.03	2.55	0.73	1.71	2.14
Propanoic acid	1.58	79.14	2.34	1.91	0.42	1.72	2.68	0.63	1.87	2.20
Butanoic acid	1.74	80.14	2.37	2.01	-	1.37	2.65	0.54	1.98	2.18
Pentanoic acid	1.89	80.90	2.46	2.13	-	1.17	2.70	0.50	2.11	2.24

Table 2.5 is continued on the following page.

Molecule	k_L (10^{-9} cm^3 s^{-1})	θ (°)	$k_{ADO}^{T_{dt}}$ (10^{-9} cm^3 s^{-1})	$k_{ADO}^{T_{eff}}$ (10^{-9} cm^3 s^{-1})	I^*	$I^*{}_{UL}^{T_{dt}}$	$k_{SC}^{T_{dt}}$ (10^{-9} cm^3 s^{-1})	$I^*{}_{UL}^{T_{eff}}$	$k_{SC}^{T_{eff}}$ (10^{-9} cm^3 s^{-1})	$k_{KE^r_{c.m.}}^{T_{rot}}$ (10^{-9} cm^3 s^{-1})
2-methylphenol	2.17	84.54	2.39	2.26	-	0.62	2.55	0.38	2.28	2.27
3-methylphenol	2.17	84.61	2.38	2.26	-	0.62	2.54	0.38	2.28	2.26
4-methylphenol	2.17	83.20	2.51	2.31	-	0.77	2.70	0.41	2.32	2.34
Phenol	1.86	82.52	2.21	2.01	-	0.87	2.39	0.43	2.01	2.05
Trimethylamine	1.72	85.94	1.82	1.77	0.08	0.51	1.94	0.37	1.79	1.77
Acetonitrile	1.38	74.95	3.90	2.53	-	6.92	4.95	2.39	2.73	3.92

Note: A superscript 'T_{dt}' indicates the drift tube temperature was used to calculate the rate constant. A subscript 'T_{eff}' indicates the rate constant was calculated at the ion effective temperature (Eq. 2.60) corresponding values of effective temperature are shown in Table 2.3. k_L are rate constants calculated from Langevin – Gioumousis – Stevenson theory, Eq 2.34, (Gioumousis and Stevenson, 1957) § 2.4.1.2. k_{ADO} are rate constants derived from average dipole orientation theory, Eq. 2.41, (Su and Bowers 1973b and c) §2.4.1.3. The dipole locking constants and thereby dipole locking angles, θ (°) were derived from tables of $\alpha\mu_D^{1/2}$ versus dipole locking constant at 300 K published in Su and Bowers (1975). k_{SC} are rate constants calculated using the results of Chesnavich *et al* (1980) and Su and Chesnavich (1982) parameterized trajectory calculations, Eq. 2.49 – 2.54, §2.4.1.4. I^* values and the upper limit of I^*, $I^*{}_{UL}^{T_{efft}}$, where the parameterisation is applicable are shown. All rate constants where moments of inertia were derived are within the limits of the parameterisation. I^* values were calculated from moments of inertia shown in Table 2.4. $k_{KE^r_{c.m.}}^{T_{rot}}$ are rate constants calculated from trajectories parameterised by rotational temperature, T_{rot}, and centre-of-mass kinetic energy between the ion and reactant VOC, $KE^r_{c.m.}$, Eq. 2.61 – 2.65, (Su, 1994) §2.4.1.5. T_{rot} is taken as the drift tube temperature (318.15 K). The corresponding values of $KE^r_{c.m.}$ dipole moments and polarizabilities used are given in Table 2.3. TMB is trimethylbenzene, DMB is dimethylbenzene, MVK is methylvinylketone, MACR is methacrolein.

Carlo based methods have been used to determine theoretical ion speed distributions as a function of *E/N* for certain ion-buffer combinations (Lin and Bardsley 1977). Theoretical studies relating rate constants measured in drift tubes, where non-Maxwellian distributions exist, to rate constants at thermal temperatures for monatomic and polyatomic systems have been published (e.g. Viehland *et al* 1981). This is an extensive area of research in itself and its application to the PTR-MS is beyond the scope of this study.

However, some indication of the speed distribution can be inferred by comparison with helium where a Maxwell distribution is assumed. Ion speed distributions are determined in part by the mass of the buffer relative to the mass of the ion and scattering potentials (Albritton *et al* 1977, McDaniel and Mason 1973). The mass of air is greater than H_3O^+ while helium is less. A comparison of scattering potentials is derived by comparison of mobility, *K*, dependence on *E/N* in the two buffers. H_3O^+ mobilities in nitrogen are used. H_3O^+ mobilities in nitrogen and helium were taken from Dotan *et al* (1976, 1977) and are normalised by the reduced Langevin mobility. Langevin mobility is the theoretical mobility at zero field and 298.15 K, based on an ion-induced dipole potential between the buffer and ion. Figure 2.15 shows the calculated reduced ion mobility normalised by Langrvin mobility.

Figure 2.15: H_3O^+ reduced ion mobility, $K_0 = (P \times 273.15/T \times 101325)K$ normalised by Langevin mobility, $K_L = 13.876/(\alpha\mu)^{1/2}$ as a function of *E/N* in helium, nitrogen and argon buffer. Mobility, *K*, data taken from Dotan *et al* 1976, 1977 and Böhringer *et al* 1983.

The variation in *E/N* dependencies in helium and nitrogen may be indicative of deviation of ion speed distributions from Maxwellian in nitrogen. However, some dampening of the increase in mobility with *E/N* is due to a variation in the extent of conversion of translational energy to internal energy in inelastic collisions. Investigations of monatomic O^+ reactions in

helium and argon (Albritton *et al* 1977) indicate that speed distributions in argon are not Maxwellian. Argon has a similar mass and polarizability to nitrogen and the differences in *E/N* dependencies of normalised reduced mobilities in argon and helium (Albritton *et al* 1977) are comparable to those shown in Figure 2.5.

Studies into the H_3O^+ speed distribution in air within the PTR-MS seem worthy of future attention. However, any deviation from Maxwell-Boltzmann distribution will increase with *E/N* and it is assumed that at the relatively low *E/N* employed in the PTR-MS, the distribution is close to Maxwellian.

2.4.2 Experimental Reaction Rate Constants

A vast number of rate constants for reaction of (O)VOCs with H_3O^+ have been experimentally determined using SIFT (§ 2.1) (for example Španěl and Smith 1995a,b, 1997 1998b, Michel *et al* 2005). The accuracy of the experimentally derived rate constants is ~ 20 % (Michel *et al* 2005). Table 2.6 shows some experimental values, compared with theoretical rate constants calculated at 298.15 K using the dipole moments and polarizailities listed in Table 2.3. All the theoretical rate constants compare reasonably with experimental values for molecules with little or no dipole moment. Langevin rate constants (Gioumousis and Stevenson 1957) are markedly lower than experimental (and other theoretical) values for molecules with a large dipole moments (e.g. methanol, propanone, ethanal), this is expected given that no ion-dipole potential is accounted for in the Langevin theory. The locked-dipole reaction rate constants for ion dipole reactions (Theard and Hamill 1961, Moran and Hamill, 1963) are greater than other theoretical values and measured values indicating the overestimation of the extent of dipole locking. Reaction rate constants obtained from average dipole orientation theory (Su and Bower 1973b and c) and Su and Chesnavich parameterized trajectories (Chesnavich *et al* 1980, Su and Chesnavich 1982) compare well with experimental values, though Su and Chesnavich values show a slightly improved comparison (e.g. methanol, ethanol, propanone).

The uncertainties of theoretical rate constants will increase as uncertainty in the dipole moments and polarizabilities increase. Indeed dipole moments of some molecules such as higher amines are not available and must be estimated from other values. The sticky nature of compounds such as carboxylic acids and the difficulty in obtaining low concentration samples mean that experimental rate constants are not available, and no comparison can be made with theoretical values. It is noted that while the accuracy of the model to determine *k*

is improved by utilising $k_{KE_{c.m.}^{r}}^{T_{rot}}$ the uncertainty is increased compared to simpler models due to dependence on a larger number of factors, e.g $KE_{c.m.}^{r}$, with their associated uncertainties.

Table 2.6. Rate constants at 298.15 K.

Compound	k_L (10^{-9} cm^3 s^{-1})	k_{LD} (10^{-9} cm^3 s^{-1})	k_{ADO} (10^{-9} cm^3 s^{-1})	k_{SC} (10^{-9} cm^3 s^{-1})	k_{exp} (10^{-9} cm^3 s^{-1})
Benzene	1.97	1.97	1.97	1.97	1.90[a]
Toluene	2.03	2.90	2.04	2.13	2.20[a]
1, 2 – DMB	2.25	3.72	2.32	2.45	2.40[a]
1, 4 – DMB	2.27	2.45	2.27	2.28	2.20[a]
1, 3 – DMB	2.26	2.56	2.26	2.29	2.30[a]
1, 3, 5 – TMB	2.40	2.50	2.40	2.40	2.30[a]
1, 2, 3 – TMB	2.39	3.89	2.46	2.59	2.50[a]
1, 2, 4 – TMB	2.40	3.06	2.40	2.47	2.40[a]
Methanol	1.24	5.77	2.22	2.68	2.70[b]
Ethanol	1.44	5.69	2.29	2.69	2.70[b]
Propanone	1.56	8.57	3.18	3.93	4.10[c]
Ethanal	1.38	8.33	3.03	3.79	3.50[c]
2-methyl-1,3-butadiene	1.94	2.54	1.94	2.01	2.00[a]
MVK	1.73	9.14	3.41	4.20	3.50[d]
MACR	1.75	8.13	3.13	3.78	3.50[d]
Phenol	1.86	4.69	2.23	2.42	2.70[b]

Note: k_{exp} are rate constants derived experimentally from SIFT measurements reported in, [a] Španěl and Smith 1998b, [b] Španěl and Smith 1997, [c]Španěl and Smith 1995b, [d]Michel *et al*, 2005. k_L are rate constants calculated from Langevin – Gioumousis – Stevenson theory (Gioumousis and Stevenson, 1957). k_{LD} are calculated using locked dipole theory (Theard and Hamill 1961, Moran and Hamill, 1963). k_{ADO} are rate constants derived from average dipole orientation theory (Su and Bowers 1973b,c). The dipole locking constants were derived from tables of $\alpha\mu_D^{1/2}$ versus dipole locking constant at 300 K published in Su and Bowers (1975). k_{SC} are rate constants calculated using the results of Chesnavich *et al* (1980) and Su and Chesnavich (1982) parameterized trajectory calculations. Dipole moments and polarizability used to calculate the rate constants are given in Table 2.3. TMB refers to trimethylbenzene, DMB refers to dimethylbenzene (xylene), MVK refers to methylvinylketone, MACR refers to methacrolein.

The ion-polar reaction rate constants measured in SIFT at 298 K are likely to be an overestimation of rate constants in PTR-MS due to the elevated energy of the ion in the presence of the electric field (§ 2.4.1.5). There is no comparable inventory of reaction rate constants in the PTR-MS or SIFDT, only a small number of measurements exist (Lag *et al* 1994, Warneke *et al* 1996, Tani *et al* 2003). Assuming that the distribution of energy is not important for proton transfer reactions, rate constants obtained at a comparable average total energy by temperature elevation in VT-SIFT rather than by electric field application may provide an approximation.

Values of measured rate constants for the reaction of H_3O^+ with a variety of compounds are collated in Chapter 3. A Microsoft® EXCEL file for the calculation of k_L, k_{LD}, $k_{ADO}^{T_{dt}}$, $k_{ADO}^{T_{eff}}$, $k_{SC}^{T_{dt}}$, $k_{SC}^{T_{eff}}$ and $k_{KE_{c.m.}^r}^{T_{rot}}$ is attached in an electronic form. This includes values of these rate constants and dipole and polarizabilities for over 400 molecules.

2.5 Reaction time.

Reaction time can be calculated from:

$$t_d = l_d / v_d \tag{2.66}$$

where t_d is the residence time of H_3O^+ ions in the drift tube in units of s, the drift tube length, l_d, is in units of cm. The drift velocity (§ 2.4.1.5) is calculated from ion mobilities at the appropriate E/N according to Eq 2.56 – 2.58 and is in units of cm s^{-1}. Since the residence time of the reagent ions is much shorter than the residence time of the reactant (O)VOCs (§ 2.2) it is assumed that:

$$t = t_d \tag{2.67}$$

where t is the reaction time. Reaction times employed in this study are calculated values. Measured reaction times can be obtained using Eq. 2.10. Reaction times derived in this manner are subject to the inaccuracies and uncertainties associated with the reaction rate constant and measured detection efficiencies (§ 2.7). Tani *et al* (2003) derived an experimental reaction time by sampling a known volume mixing ratio of toluene and using Eq. 2.10 with a rate constant of 2.2 x 10^{-9} cm^3 s^{-1} as measured by Španěl and Smith (1998b). This assumes that the rate constant is unchanged at elevated ion energies and that fragmentation does not occur. The dipole of toluene is small and variation in rate constant is expected to be minimal (§ 2.4). Midey *et al* (2002) measured rate constants and branching fractions for reaction of H_3O^+ and toluene at 298 – 500 K using VT-SIFT (§ 2.1) and 900 K – 1200 K using HTFA (§ 2.1). Measured rate constants were approximately constant and equal to the collisonal rate constant at all temperatures. No fragmentation was observed at 298 – 500 K and limited fragmentation was observed at 900 – 1100 K (98 % of the product was on m/z 93 at 900 K and 81 % at 1100 K). Toluene fragmentation has not been observed in the PTR-MS under standard conditions (de Gouw and Warneke 2007). Further discussion of the dissociation of the alkylbenzenes is given in § D.2.

Alternatively reaction time can be measured by applying short (~10μs) voltage pulses at the entrance and exit to the drift tube and monitoring time of arrival at the detector (Lindinger *et al* 1998a, Warneke *et al* 2001). Warneke *et al* (2001) have shown that in practice in humid

air an individual H_3O^+ ion undergoes several clustering and subsequent dissociation reactions with H_2O so that part of the time traversing the drift tube is spent as H_3O^+ and part as $H_3O^+.H_2O$. Thus the measured reaction time and associated mobility (Eq 2.58) is a weighted average, where weights relate to number density of H_3O^+ and $H_3O^+.(H_2O)_n$ $(n=1-5)$. Warneke et al (2001) showed that at high E/N (140 Td relative humidity 39 %) the mobility derived from measured residence time is close to literature values of H_3O^+ mobility derived in dry nitrogen, at low E/N (~70 Td at relative humidity of 39 %) it is close to that of $H_3O^+.H_2O$.

2.6 The Effects of the Presence of Water in the Drift Tube

In the presence of water in the drift tube association reactions occur between H_3O^+ reagent ions and water (Eq. 2.68) (e.g. Bohme et al 1979, Lau et al 1982, Španěl and Smith 1995c, Španěl and Smith 2000, Midey et al 2000, Midey et al 2002, Warneke et al 2001, de Gouw and Warneke 2007).

$$H_3O^+(H_2O)_n + H_2O \xrightarrow{\ B\ } H_3O^+(H_2O)_{n+1} \qquad (2.68)$$
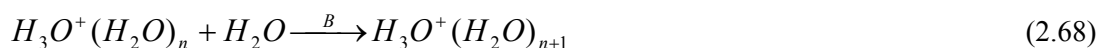
where B denotes a third-body, namely a buffer molecule such as nitrogen. The degree of formation of the $H_3O^+(H_2O)_n$ $n{\geq}1$ clusters is dependent upon the relative humidity of the air sampled, the ion-molecule centre-of-mass kinetic energy and the pressure in the drift tube. If dry air is sampled $H_3O^+(H_2O)_n$ $n{\geq}1$ are still observed as a result of water from the ion source reaching the drift tube. Warneke et al (2001) estimate that ~ 5% of the water flow in the ion source reaches the drift tube. As the E/N and the ion-molecule centre-of-mass kinetic energy is reduced the rate of association increases and the association complexes are increasingly stable (e.g. Warneke et al 2001, de Gouw and Warneke 2007). Conversely at low pressures if the pressure is reduced (at constant E/N) stabilizing collisions with the third-body (B) are reduced and the rate of cluster formation decreases (e.g. Lau et al 1982, private communication with A. Viggiano 14 March 2008 and C. Warneke 13 March 2008). Ion source parameters will also affect cluster formation (§ 2.3.1). In example Steinbacher et al (2004b) measured $H_3O^+(H_2O)/H_3O^+$ ratios of 1 to 15 % between dry air and 100 % humidity at E/N of 132.3 Td, T_{dt} 323 K, P_{dt} 2.08 mbar, E ~61.6 V cm^{-1}. Models for the calculation of $H_3O^+(H_2O)_n$ (n = 1 to 5) have been developed but cannot yet accurately describe distributions (Warneke et al 2001, Steinbacher et al 2004b, private communication with C. Warneke 13 March 2008)

Analogous association reactions are observed between some protonated species resulting from the reaction of (O)VOCs and water (Eq. 2.69) (e.g. Španěl and Smith 1995c, Španěl and Smith 2000, de Gouw and Warneke 2007).

$$MH^+ + H_2O \xrightarrow{\quad B \quad} MH^+(H_2O) \tag{2.69}$$

Two possible reactions may occur between the $H_3O^+(H_2O)_n$ $n\geq1$ clusters and (O)VOCs; proton transfer (Eq. 2.70) and/or ligand switching (Eq. 2.71) (e.g. Bohme *et al* 1979, Španěl and Smith 1995c, Španěl and Smith 2000, Midey *et al* 2000, Midey *et al* 2002, Warneke *et al* 2001, de Gouw and Warneke 2007).
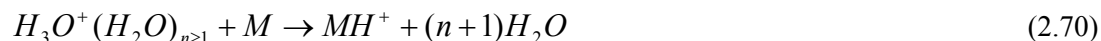
$$H_3O^+(H_2O)_{n\geq1} + M \rightarrow MH^+ + (n+1)H_2O \tag{2.70}$$

$$H_3O^+(H_2O) + M \rightarrow (M)H_3O^+ + H_2O \tag{2.71}$$

The product of ligand switching (Eq. 2.71) may subsequently dissociate possibly to MH^+ and H_2O between the reaction chamber and the detection chamber. The products of reaction Eq. 2.69 and Eq. 2.71 are indistinguishable.

The exothermicity of the proton transfer reaction (Eq. 2.70) from $H_3O^+(H_2O)_n$ to a given trace species increases as n increases thus some (O)VOCs that do undergo proton transfer with H_3O^+ do not do so with $H_3O^+(H_2O)_n$ $n\geq1$. Experimental measurements indicate that the occurrence of the ligand switching reaction (Eq. 2.71) is linked with the polarity of the (O)VOC, a larger dipole favouring reaction (Španěl and Smith 1995c).

Non-polar molecules with proton affinities less than those of $H_3O^+(H_2O)_n$ $n\geq1$ and which are non-polar, e.g. benzene, do not therefore react with the $H_3O^+(H_2O)_{n\geq1}$ clusters and Eq 2.10 and Eq. 2.11 are applicable (if the true count rates of H_3O^+ in the drift tube are known). In this case the sensitivity of the PTR-MS with respect to the (O)VOC is decreased as the concentration of H_3O^+ molecules is effectively reduced with formation of $H_3O^+(H_2O)_n$ $n\geq1$ clusters (Steinbacher *et al* 2004b, Warneke *et al* 2001). In addition sensitivities calculated *via* Eq. 2.11 may be inaccurately greater than sensitivities measured using a calibration standard and concentrations calculated from Eq. 2.10 lower than the true concentration. This is due to the dissociation of $H_3O^+(H_2O)_n$ $n\geq1$ clusters to H_3O^+ and H_2O in the region between the drift tube and detection chamber (Warneke *et al* 2001, Tani *et al* 2003).

In the case of molecules which do undergo reactions with the $H_3O^+(H_2O)_n$ $n\geq1$ clusters the sensitivity is unaffected by the formation of $H_3O^+(H_2O)_n$ $n\geq1$ clusters. If MH^+ ions are produced by proton transfer reactions with $H_3O^+(H_2O)_n$ $n\geq1$ clusters (Eq. 2.70) as well as H_3O^+ the concentration calculated from Eq. 2.10 will be an inaccurate overestimate. The

sensitivity calculated from Eq. 2.11 would be inaccurate and less than the measured sensitivity.

A possible method of including $H_3O^+(H_2O)$ ions as reagent ions has been suggested by Tani *et al* (2003) (for quantification of monoterpenes), whereby concentrations are approximated from Eq. 2.72.

$$[M] \approx \frac{(MH^+)}{\{(H_3O^+)+(H_3O^+.H_2O)\}} \frac{1}{k_{average}t_{average}} \frac{10^9}{N} \tag{2.72}$$

where ( ) denotes detection efficiency corrected ion count rates, [ ] denotes VMR in units of ppb, N is the number density of molecules in units of particles cm^{-3}. $k_{average}$, in units of cm^3 s^{-1}, and $t_{average}$, in units of s, are the average reaction rate constant and average reaction time weighted for H_3O^+ and H_3O^+ (H_2O).

As discussed above the true values of H_3O^+ and H_3O^+ (H_2O) in the drift tube are difficult to determine due to dissociation of H_3O^+ (H_2O) between the drift tube and detection chamber. Further the measured $H_3O^+(H_2O)$ count rates do not normally exceed 5 % of the sum H_3O^+ and $H_3O^+(H_2O)$ count rates. Consequently Tani *et al* (2003) suggest that Eq. 2.72 is simplified by the assumption that $k_{average}$ does not differ significantly from the rate constant for reaction with H_3O^+ alone and that the $t_{average}$ is reasonably approximated by the reaction time of H_3O^+ (Eq. 2.73).

$$[M] \approx \frac{(MH^+)}{\{(H_3O^+)+(H_3O^+.H_2O)\}} \frac{1}{kt} \frac{10^9}{N} \tag{2.73}$$

where k is the rate constant for the reaction of H_3O^+ with the trace species and t the reaction time derived from the H_3O^+ mobility (§2.5, Eq. 2.66 and 2.67). Consider the validity of these assumptions assuming that $H_3O^+(H_2O)$ forms 5 % of the total cps from H_3O^+ and $H_3O^+(H_2O)$. The variation in t arises from the variation in the mobilities of H_3O^+ and $H_3O^+(H_2O)$ (§ 2.5). Taking the mobilities of H_3O^+ and $H_3O^+(H_2O)$ in nitrogen from Dotan *et al* (1976) there is a difference of < 1% between the average mobility (assuming 5 % $H_3O^+(H_2O)$) and the mobility of H_3O^+ at normal operating E/N of ~ 120 to 130 Td. In the case of the rate consider the example of trimethylamine at 127 Td (P_{dt} 2.00 mbar, T_{dt} 318 K, E 57.9 V cm^{-1}): $k_{KE_{c.m.}^r}^{T_{rot}}$ (Su 1994, § 2.4.1.5, Eq 2.61 to 2.65) for reaction with H_3O^+ is 1.81 x 10^{-9} cm^3 s^{-1} that with $H_3O^+(H_2O)$ is 1.44 x 10^{-9} cm^3 s^{-1} resulting in a difference of 1.10 % between $k_{average}$ (assuming 5 % $H_3O^+(H_2O)$) and the rate constant for reaction with H_3O^+ alone.

This method does not take into account proton transfer reactions with higher hydrates, ligand switching (Eq 2.71) or association reactions (Eq. 2.69). The ligand switching and association reactions do not necessarily proceed at collisional rate (as non-dissociative proton transfer reactions do, Bouchoux 1996, § 2.9).

The use of an experimentally determined humidity dependent compound specific correction factor, X_R, to correct for the variation in sensitivity with humidity has been demonstrated in the literature (e.g de Gouw *et al* 2003b, de Gouw and Warneke 2007). In this case a sample of the (O)VOC of interest at varying relative humidities is passed into the PTR-MS and count rates of MH^+ derived as a function of relative humidity. X_R is the factor required for normalised ion counts to become independent of humidity and reflects the difference in rate coefficients and detection efficiencies of H_3O^+ and $H_3O^+(H_2O)$. A detailed description of this method is given elsewhere (de Gouw *et al* 2003b, de Gouw and Warneke 2007).

There have been a limited number of studies of the reactions of $H_3O^+(H_2O)_n$ $n{\geq}1$ clusters with (O)VOCs, particularly in the case of ligand switching reactions (Eq. 2.71). Likewise the reactions of H_2O with protonated (O)VOCs and their fragments (Eq. 2.69) in the PTR-MS have received little attention. The potential reactions of a number of species in the presence of water are discussed utilizing existing data from SIFT, VT-SIFT and PTR-MS in Chapter 3. It should be noted that the lower energies in SIFT result in greater production of $H_3O^+(H_2O)_n$ $n{\geq}1$ (Eq 2.68) and $MH^+(H_2O)$ (Eq 2.69) association complexes and that the presence of water vapour has a greater impact on SIFT measurements. Analysis procedures to account for the presence of water vapour in SIFT have been developed and it is estimated that the associated error has consequently been decreased from 15 % to 2 % (Španěl and Smith 2000, Michel *et al* 2005).

2.7 Detection Efficiencies, Losses due to Diffusion and Variabilities in Momentum Flux in the Direction of the Electric Field.

The efficiency with which ions are detected depends on the ability of ions to traverse the drift tube, losses occurring between the drift tube and quadrupole, factors associated with the quadrupole operation (transmission) and efficacy of deflection to the SEM (Steinbacher *et al* 2004a,b).

The detection efficiencies in Eq. 2.10 are effectively constants of proportionality relating the detected ion currents to the actual ion densities at the exit of the drift tube. These terms do not consider the variation in the ability of ions to traverse the drift tube.

The efficiency with which ions are detected following exit from the drift tube is assumed to be mass dependent. Losses due to diffusion are likely in the chamber between the drift tube and quadrupole. Diffusion is greatest for smaller ions and higher masses may therefore be expected to travel between the drift tube exit and quadrupole with increased efficiency, in a similar manner to the diffusion observed in SIFT-MS reaction chambers and to a lesser extent in the drift tube (Španěl and Smith 2001, Keck *et al* 2007). Conversely discrimination against heavier ions is often observed in quadrupole filters. This is due to the longer periods heavier ions spend in the fringing fields and is largely dependent on resolution and ion velocity (Dawson 1986). The efficiency with which ions are deflected towards the SEM is not well characterised. It is not possible to quantify each of these effects individually therefore detection efficiencies (Eq. 2.10) are obtained to correct for the combination of mass discriminatory effects.

Values of detection efficiencies are obtained by introducing a sample of a stable concentration of a single trace gas component, *M*, giving an MH^+ VMR which is sufficient to result in a significant decrease in H_3O^+ (m/z 19 or m/z 21) count rates. In this case rate equations for Eq. 2.6 were originally (given the logic of Appendix A) assumed to be:

$$\frac{d[MH^+]}{dt} = k[M][H_3O^+]$$
(2.74)

$$\frac{d[H_3O^+]}{dt} = -k[M][H_3O^+]$$
(2.75)

Therefore:

$$\frac{d[MH^+]}{dt} = -\frac{d[H_3O^+]}{dt}$$
(2.76)

$$\frac{d[MH^+]/dt}{-d[H_3O^+]/dt} = 1$$
(2.77)

Thus the ratio of change in observed MH^+ ion counts to change in observed H_3O^+ ion counts gives an indication of detection efficiency according to:

$$T_{MH^+}^{RAW} = \frac{d(MH^+)}{-d(H_3O^+)}$$
(2.78)

where $T_{MH^+}^{RAW}$ is the raw detection coefficient of MH^+, $d(H_3O^+)$ is the (negative) change in detected H_3O^+ count rates and $d(MH^+)$ is the change in detected MH^+ count rates including the isotope contribution calculated from isotope proportions available in the literature (e.g. Manura and Manura 1996). The reasoning being that if detection efficiencies of H_3O^+ and MH^+ between the drift tube exit and CP were equal, the ratio of measured change in MH^+ to

the positive change in H_3O^+ would be 1 and by definition the raw detection efficiency is 1 at m/z 21 ($H_3^{18}O^+$) (or m/z 19 if $H_3^{16}O^+$ is measured directly). Inherent in this rationalisation is the assumption that ions traverse the drift tube with equal efficiency. The measurement is repeated with non-fragmenting trace gas compounds over a range of masses. The range of raw detection efficiencies are subsequently normalised to the highest measured raw detection efficiency and a curve fitted from which detection efficiencies for all masses are obtained.

The count rates at m/z 19 or m/z 21 ($H_3^{18}O^+$) x 500 are reduced to ~ 5 x 10^5 cps before the measurement to prevent SEM saturation (§ 2.3.3) or excessive trace gas VMR. The trace gas VMR must be sufficient to produce an MH^+ VMR in excess of H_3O^+ but not greater than the VMR of the buffer (the unreactive components of air) which would result in a change in ion mobility and pressure in the drift tube thus yielding transmission values not applicable to normal operating conditions. The H_3O^+ ion counts must remain greater than zero when the trace gas sample is added i.e. all of the trace gas must be protonated so that the level of VOC in the drift tube is known and not excessively high. (private communication with M. Possell, 01 and 02 November 2004) The appropriate VOC concentration is achieved by trial and error this is a time consuming process.

The trace gas sample must be high purity, because impurities reacting with H_3O^+ would result in an underestimation of the detection coefficient. O_2^+ and NO^+ must be minimised, as in normal operation or else their reaction with the trace gas would result in an overestimation of the transmission coefficient.

Transmission measurements were performed in this study each time the instrument was moved and where possible when the SEM was changed (transmission measurements were not performed mid-campaign due to the large periods of time required for transmission, the associated elevated and changing instrument background and consequent time not measuring). Due to the difficulty in obtaining measurements where no fragmentation or impurities and low O_2^+ and NO^+ at low H_3O^+ ion counts occurred full transmission curves could not be obtained from each measurement set. The transmission curve used here (Figure 2.16) was obtained from measurements made in the period from November 2004 to May 2006. 29 measurements (out of 85 attempted measurements) were used to obtain the curve. The SEM was changed five times during this period. The manufacturer supplied transmission data with the instrument, this is also shown in Figure 2.16.
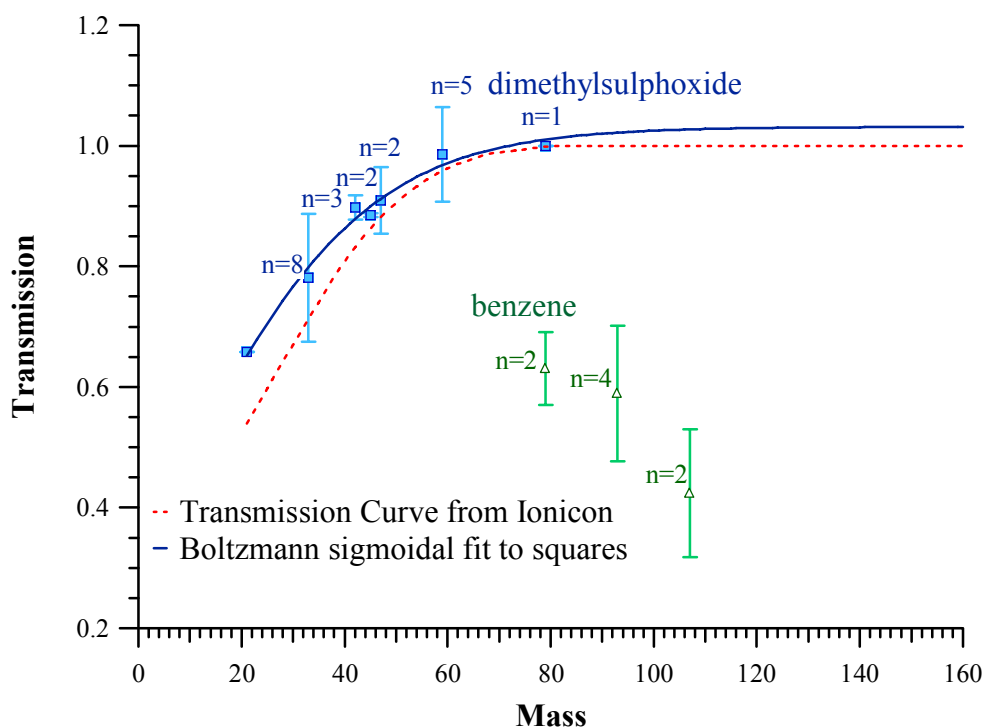
Figure 2.16: Normalised detection efficiencies. The markers are experimental values and error bars are the relative error. The number *n* specifies the number of measurements averaged. A Boltzmann sigmoidal curve was fitted to the experimental values. Values at m/z 79 were obtained using dimethylsulphoxide (■) and benzene (Δ) as indicated. The values of benzene (m/z 79), toluene (m/z 93) and dimethylbenzene (m/z 107) - symbol Δ were not used in the curve fit (see in text). The dashed line shows the detection efficiencies originally supplied by the manufacturer.

The compounds used to obtain detection efficiencies used for the fit were: methanol (m/z 33), acetonitrile (m/z 42), ethanal (m/z 45), methanoic acid (m/z 47), propanone (m/z 59) and dimethylsulphoxide (m/z 79). It is likely that the reason for the outlying values (diamonds) in Figure 2.16 is the lack of reaction of the corresponding molecules with $H_3O^+(H_2O)$: Methanol, acetonitrile, ethanal and propanone have been shown to react with $H_3O^+(H_2O)$ (Warneke *et al* 2001, Midey *et al* 2000 and 2002, de Gouw and Warneke 2007, refer to § 2.6 and Chapter 3). The proton transfer reaction from $H_3O^+(H_2O)$ to dimethylsulphoxide is exothermic (§ 3.4.2). Benzene and toluene do not react with $H_3O^+(H_2O)$ in PTR-MS (Warneke *et al* 2001). The proton transfer reactions from $H_3O^+(H_2O)$ to benzene and toluene are endothermic (§ D.2.2) and the ligand switching reaction (Eq. 2.71) does not occur (e.g. Španěl and Smith 1995c). The proton transfer reaction from $H_3O^+(H_2O)$ to the dimethylbenzenes are also endothermic (§ D.2.2) and the isomers are relatively non-polar therefore reaction with $H_3O^+(H_2O)$ is unlikely (§ 2.6). If the measured change in MH^+ count rates is due to the reaction of *M* with $H_3O^+(H_2O)$ as well as H_3O^+ Eq. 2.76 and Eq. 2.77 no longer hold and if applied result in an artificially high detection efficiency. Hayward (2003)

also observed an outlying value of detection efficiency for benzene in similar measurements, though toluene and dimethylbenzene lay on the fitted curve. In the absence of sufficient values for compounds which do not react with $H_3O^+(H_2O)$ the fitted curve shown in Figure 2.16 was utilised, this method has been employed elsewhere (e.g. Steinbacher *et al* 2004a,b, Ammann *et al* 2004).

The scatter in the values may arise from the methodology of determination or actual variation in the detection efficiency of the PTR-MS. Similarly the variation between the curve determined here and that supplied by the manufacturer may result from inaccuracy of experimental detection efficiencies, variation in the instrument's detection characteristics or differences in the PTR-MS settings during measurement.

In actuality, as recently pointed out by Keck *et al* (2007), ions do not traverse the drift tube with the same efficiency. Eqs 2.74 and 2.75 neglect momentum flux of ions in the direction of the electric field and more accurate expressions are:

$$\frac{d[MH^+]}{dt} = -\frac{\partial(v^{MH^+}[MH^+])}{\partial x} + k[M][H_3O^+] \tag{2.79}$$

$$\frac{d[H_3O^+]}{dt} = -\frac{\partial(v^{H_3O^+}[H_3O^+])}{\partial x} - k[M][H_3O^+] \tag{2.80}$$

where $x=0$ at the ion source exit and $x=l_d$ at the reaction chamber exit (the drift tube exit in the case of PTR-MS). v^{MH^+} is the velocity of the MH^+ ion and $v^{H_3O^+}$ is the velocity of H_3O^+ ions. More generally when in normal measurement mode with i trace gas species (rather than that for detection efficiency measurement) rate equations for Eq. 2.6 are:

$$\frac{d[MH^+]}{dt} = -\frac{\partial(v^{MH^+}[MH^+])}{\partial x} + k[M][H_3O^+] \tag{2.81}$$

$$\frac{d[H_3O^+]}{dt} = -\frac{\partial(v^{H_3O^+}[H_3O^+])}{\partial x} - \sum_i k_i[M_i][H_3O^+] \tag{2.82}$$

where M denotes a single trace gas species (one of i trace gas species). If the velocities of MH^+ and H_3O^+ ions are equal, as in SIFT-MS where velocities are governed by the fast flow of the buffer, Eq. 2.74 and 2.75 hold. In the PTR-MS $v^{H_3O^+}$ and v^{MH^+} are the drift velocities of the corresponding ions, calculated in the usual manner from the ion mobility at the appropriate E/N (§ 2.4.1.5, Eq 2.56). Since ion mobilities vary with e.g. ion-buffer reduced mass and polarizability (§ 2.4.1.7) drift velocities vary with ion type and Eqs. 2.79 and 2.80 cannot be reduced to Eq. 2.74 and 2.75 in the PTR-MS. Keck *et al* (2007) have shown that the solution of Eq. 2.81 and 2.82 leads to modification of the equations for the calculation of

M_iH^+ volume mixing ratio and sensitivity (Eq. 2.10 and 2.11) to give Eq. 2.83 and 2.84. Variations between ion counts at the drift tube exit and detected ion counts (i.e. detection efficiencies) are initially neglected.

$$[M_i] = \frac{[M_iH^+]_{l_d}}{k_i t [H_3O^+]_{l_d}} \frac{K_{M_iH^+}}{K_{H_3O^+}} \tag{2.83}$$

$$S = 10^{-3} ktN \frac{K_{H_3O^+}}{K_{MH^+}} \tag{2.84}$$

where $[]_{l_d}$ denotes concentration at the drift tube exit, $K_{M_IH^+}$ and $K_{H_3O^+}$ denote ion mobilities of M_iH^+ and H_3O^+ at the appropriate E/N. Similar principles result in a revised definition of the ratio of detection efficiencies as defined in the introduction to this section and derived in the manner described (Eq. 2.85)

$$\frac{T_{H_3O^+}}{T_{M_KH}} = -\frac{K_{H_3O^+}}{K_{M_KH^+}} \frac{\partial(H_3O^+)}{\partial(M_KH^+)} \tag{2.85}$$

where M_k is a trace gas species used in the measurement of the detection efficiency. Including this ratio of detection efficiencies in the revised equation for concentration calculation (Eq. 2.83) to account for the differences in ion counts at the drift tube exit and at detection gives Eq. 2.86.

$$[M_i] = \frac{1}{k_i t} \frac{(M_iH^+)}{(H_3O^+)} \frac{K_{M_iH^+}}{K_{M_KH^+}} \left(-\frac{\partial(H_3O^+)}{\partial(M_KH^+)} \right) \tag{2.86}$$

This is the same as Eq. 2.10 modified by a correction factor equalling the ratio of mobility of the protonated molecule of interest, M_iH^+, to the mobility of the trace gas species used to derive the detection efficiency in the manner described above, M_kH^+. If the trace gas species of interest, M_i, is used to derive the detection efficiency so that $M_i = M_k$, Eq. 2.10 applies (Keck *et al* 2007). If $M_i \neq M_k$, Keck *et al* (2007) demonstrate that the deviation of the mobility ratio from unity and therefore uncertainty in VMR derived by applying Eq. 2.10 may be more than 20 % even where M_i and M_k vary by only a few m/z. This error will increase as the difference in M_i and M_k increases due to the ~ inverse mass dependence of mobilities (as described by the Langevin mobility at low field strengths, § 2.4.1.7).

As highlighted by Keck *et al* (2007) the effects of transverse diffusion in the drift tube are not taken account of in the equations for calculation of concentrations to date (Eq. 2.10 and 2.86). This effect is converse to that resulting from difference in ion mobilities since diffusion is greatest for smaller masses.

A detailed derivation of Eq. 2.83 to 2.86 can be found in Keck *et al* (2007). Further discussions of treatments of differences in the ability of ions to traverse the drift and from the drift tube to detection in the absence (SIFT) and presence of an electric field (PTR-MS) can be found in Španěl and Smith (2001), Španěl *et al* (2006) and Keck *et al* (2007).

2.8 Some Concurrent and Subsequent Developments in Chemical Ionisation Mass Spectrometry Instrumentation

Development of select ion flow tube mass spectrometry (SIFT) instrumentation for (O)VOC trace gas analysis has occurred alongside the development of PTR-MS (e.g. Španěl and Smith 1996 Smith and Španěl 2005). In SIFT O_2^+, NO^+ or H_3O^+ reagent ions are generated by microwave or radiofrequency discharge in air. A quadrupole mass filter between the ion source and reaction chamber is used to pre-select the reagent ion before entrance to the flow tube *via* a venturi orifice. The reaction chamber is operated at 298 K and ~0.7 mbar. There is no electric field around the reaction chamber and the velocity of ions is dependent on the fast flowing separate buffer (usually helium or a helium argon mixture) in which Maxwell-Boltzmann distribution of ion speed is assured. The fast flow requires a large pump and combined with the additional buffer reduces portability of the instrument. Transport properties/detection efficiencies of ions in the flow tube and between the flow tube exit and detection are well characterized compared to PTR-MS (Keck *et al* 2007, § 2.7). Methods to account for the resultant varying efficiency with which ions traverse the drift tube and are detected have been developed (Španěl and Smith 2001, Španěl *et al* 2006).

In the absence of an electric field the reduced energy results in decreased fragmentation (Chapter 3). An extensive library of product distributions from the reactions of O_2^+, NO^+ and H_3O^+ with various trace gas species in SIFT exits and is available in the literature (Chapter 3). Conversely the level of association and therefore the presence of $H_3O^+(H_2O)$ in clusters (if H_3O^+ is employed) is increased relative to PTR-MS (§ 2.6). Corrections to account for the effects of humidity have been developed (e.g. Španěl and Smith 2000, Smith *et al* 2001, § 2.6). At the thermal energies in SIFT the Su and Chesnavich (1982) collisional rate constant (§ 2.4.1.4) can be applied to the proton transfer reactions. In addition numerous measurements of reaction rate constants for the reactions of O_2^+, NO^+ (which are not always efficient) and in some cases of H_3O^+ have been made (e.g. Španěl and Smith 1995a,b, Španěl and Smith 1997, Španěl and Smith 1998a, Španěl and Smith 1998b, Michel *et al* 2005, Smith and Španěl 2005 and references therein, refer to Chapter 3).

The time response of the SIFT is similar to the PTR-MS (Španěl and Smith 1996). In the most recent commercially available version of SIFT (2007), 1 ms dwell times are achievable (private communication with B. Prince 20 July 2007). Sensitivity, though improved, is lower than the PTR-MS at 1-10 cps ppb^{-1}. A relatively low detection limit of 190 ppt of phosphine in a 10 s measurement has recently been reported (Milligan *et al* 2007). However, particularly given that this will be increased at the lower measurement times required for virtual disjunct eddy covariance flux measurement, this is not yet sufficient for atmospheric flux measurements (e.g. Karl *et al* 2002, Sprig *et al* 2005, Ammann *et al* 2006).

The PTR-MS technique has also evolved over the last decade: Blake *et al* (2004) demonstrated measurements of VOCs using a proton-transfer reaction time-of-flight mass spectrometer (PTR-TOF-MS). This instrument differs from the PTR-MS not only by the use of a time of flight mass spectrometer but also a radioactive ion source. The drift tube of the PTR-TOF-MS is 10 cm long and is generally operated at 6 to 7 mbar (Blake *et al* 2004, refer to Chapter 3). The drift tube is generally operated at slightly higher *E/N* (~ 147 to 190 Td) than in normally operated PTR-MS (~120 to 140 Td) in order to minimize $H_3O^+(H_2O)$ formation and aid identification of isobaric molecules (e.g. Wyche *et al* 2005). The use of a TOF-MS enables a large number of mass channels to be monitored simultaneously. In addition the mass resolution of PTR-TOF-MS is increased (*m/Δm)*, where *m* is the full width at half-maximum of a peak, is 1200 – 1500) compared to PTR-MS employing QMS (*m/Δm* is ~100) (Blake *et al* 2004). The PTR-TOF-MS is limited by the duty cycle; the length of duty cycle is determined by the length of time required for ions to traverse the flight tube during which time no further ions can be injected into the flight tube (Blake *et al* 2004, Inomata *et al* 2006). Blake *et al* (2004) estimated a 3 % duty cycle for a 0-100 Da scan resulting in 97 % of ions being rejected. The highest H_3O^+ count rates that could be achieved by Blake *et al* (2004) without detector saturation was ~1 x 10^4 s^{-1}. The resulting sensitivity in the PTR-TOF-MS was ~ two orders of magnitude lower than similar PTR-MS instruments at ~1 count min^{-1} ppb^{-1}. Linearity of response was demonstrated in the 5 – 53 ppm range on a one minute time scale. It is noted that this sensitivity was derived from calibrations with hydrogen sulphide which may have resulted in some underestimation (refer to § 3.4).

The use of the radioactive ion source (of the PTR-TOF-MS described above) to produce clean NO^+, O_2^+ and NH_4^+ in addition to H_3O^+ without the need for pre-selection of ions (as is required in SIFT) has subsequently been demonstrated (Wyche *et al* 2005, Blake *et al* 2006). This technique is therefore more aptly named chemical ionization reaction time-of-flight mass spectrometry (CIR-TOF-MS). The use of the additional reagent ions (as in SIFT) as a tool for the identification of contributions of isobaric molecules to mass spectra has been

demonstrated (Wyche *et al* 2005, Blake *et al* 2006). Product distributions from the reaction of these ions with a number of (O)VOCs at specified drift tube conditions have been reported in the literature (e.g. Wyche *et al* 2005, Blake *et al* 2006, refer to Chapter 3). Blake *et al* (2006) derived calibrated sensitivities of CIR-TOF-MS for 1-butene of $6.3_7 \pm 0.0_3$ ncps ppb^{-1} with H_3O^+, $5.9_3 \pm 0.0_2$ ncps ppb^{-1} with NO^+ and 7.8 ± 0.1 ncps ppb^{-1} with O_2^+. The lower sensitivity compared to PTR-MS was attributed to a reduction in the H_3O^+ count rates achieved from the radioactive ion source compared to those from the hollow cathode source in the PTR-MS (§ 2.3.1) . The CIR-TOF-MS has recently been deployed for measurements of 14 (O)VOCs at VMR of ~ 0.6 – 10.0 ppb in environment chamber measurements (Wyche *et al* 2007). Measured sensitivities in the range of 6.6 to 57.4 ncps ppb^{-1} were demonstrated with precisions of 5 – 30 % at VMR of 5 – 80 ppb on the one minute time scale. The ability of CIR-TOF-MS to measure chemical weapons simulants and agents (sulphur mustard and sarin) has recently been established (Cordell *et al* 2007). In these measurements an increased electric field was applied at the final two electrodes of the drift tube to reduce association reactions. Sensitivities were obtained as a function of the two *E/N* values and as a function of humidity. Increased humidity was shown to cause a modest decrease in sensitivity. Sensitivities decreased with increasing *E/N* (due to decreased selectivity); optimum sensitivities of ~ 40 ncps ppb^{-1} for sulphur mustard and 50 – 90 ncps ppb^{-1} for sarin were achieved.

Variations of the PTR-TOF-MS have been developed elsewhere: Ennis *et al* (2005) developed a PTR-TOF-MS using a hollow cathode ion source. Limits of detection were 10 ppb for integration times of 10 to 60 s with a sensitivity of 3.7 ncps ppb^{-1} for toluene and 28 ncps ppb^{-1} for propanone. This PTR-TOF-MS did not include a venturi inlet and H_3O^+ and thus sensitivity was reduced as a consequence. Inomata *et al* (2006) developed PTR-TOF-MS with a hollow cathode ion source with orifice plate similar to that in commercial PTR-MS (QMS). Increased H_3O^+ ion count rates were consequently achieved (~5 – 7 x 10^5 counts at 1 minute integration time duty cycle 1 %, or ~ 1.7 x 10^6 cps) and sensitivities were comparable with those observed in the PTR-MS and detection limits at the sub-ppb level for 1 minute integration. Linearity of response has been demonstrated at VMR of 0-100 ppb (Tanimoto *et al* 2007). The instrument was also operated with a commercially available radioactive ion source but with reduced sensitivity. The hollow cathode PTR-TOF-MS has subsequently been deployed for the measurement of alkyl nitrates and their product distributions with count rates of 4 x 10^6 cps H_3O^+ (*E/N* 147 Td) being achieved (Aoki *et al* 2007).
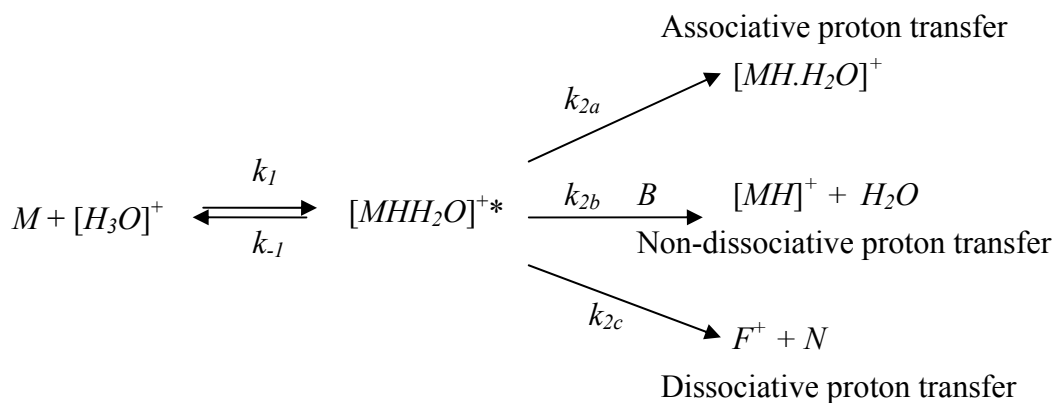
Proton transfer reaction ion trap mass spectrometers (PTR-ITMS) in which the QMS is replaced with an ion trap mass spectrometer and the reaction chamber is either a drift tube or flow tube have been developed, deployed and intercompared with PTR-IT-MS (e.g. Prazeller *et al* 2003, Warneke *et al* 2004, Warneke *et al* 2005a, Warneke *et al* 2005b, Karl *et al* 2005). The duty cycle of these instruments is improved (95 % at accumulation times of 200 ms and scan times of 10 ms) compared to conventional PTR-MS and depends upon time for accumulation of ions and scan time. The PTR-ITMS can effectively acquire a full mass scan (typically m/z 30 to 150) in the time required to scan one mass in conventional PTR-MS. This potentially enables modified eddy covariance flux measurements of a large number of species. In addition, use of IT-MS facilitates identification of isobaric molecules by use of collision induced dissociation and ion-molecule reactions in the IT (Warneke *et al* 2005a, Prazeller *et al* 2003). The sensitivity of PTR-ITMS is a factor of five lower than conventional PTR-MS. Above the limits of detection of PTR-ITMS an intercomparison with conventional PTR-MS showed agreement within less than 25 % (Warneke *et al* 2005a).

2.9 Reaction Efficiency and the Nature and Extent of Reaction Between H_3O^+ Ions and (O)VOCs in the Drift Tube.

The following section outlines factors affecting reaction efficiencies and product distributions in the PTR-MS, these principles are drawn on in Chapter 3.

Reaction efficiency is defined as the ratio of measured or true reaction rate constant to the collisional rate constant. Employing collisional rate constants as calculated above, assumes all collisions are successful and reaction efficiency is one (§ 2.4). Product distribution refers to the ratio of product ions resulting from a reaction, in this case of H_3O^+ with a trace species of interest.

The efficiency of a reaction and the product distributions from it may depend on reaction exoergicity, energy available for reaction, distribution of energy (between vibrational, rotational and translational), the nature of the buffer and pressure in the reaction chamber (e.g. Bohme 1975). Some potential reaction pathways of proton transfer are shown in Figure 2.17. If the reverse reaction occurs, efficiency will be reduced, as k_{-1} increases the forward reaction rate constant will be reduced and the rate constant for removal of H_3O^+ and R less than the theoretical collisional rate constant; the efficiency will decrease.

$$M + [H_3O]^+ \underset{k_{-1}}{\overset{k_1}{\rightleftharpoons}} [MHH_2O]^{+*}$$

Associative proton transfer

k_{2a} → $[MH.H_2O]^+$

k_{2b} B → $[MH]^+ + H_2O$

Non-dissociative proton transfer

k_{2c} → $F^+ + N$

Dissociative proton transfer

Figure 2.17: Proton transfer reaction pathways, M is the (O)VOC reactant neutral, B is a stabilizing buffer molecule, F^+ is a fragment ion and N a neutral fragment.

Efficiency of non-dissociative proton transfer reactions at thermal temperatures has been widely reported (Bohme *et al* 1980, Lindinger 1986b, Bouchoux *et al* 1996). There is little information regarding the efficiency of non-dissociative reactions or alternate reaction pathways such as hydride transfer (Jobson *et al* 2005). Product distributions from H_3O^+ reactions under thermal conditions have been extensively researched (see Chapter 3). The effect of increased translation and internal energies *via* temperature increase or electric field application on proton transfer reaction efficiencies and product distributions are less well researched. There have been a number of VT-SIFT and SIFDT studies looking at ion-molecule reaction rate constant variation with increasing energy (temperature, $KE^r_{c.m.}$ and internal energy) as reviewed by Viggiano and Morris (1996). However, the focus has been on small systems (e.g. Lindinger *et al* 1975a and b, Durup-Ferguson *et al* 1983, Viggiano *et al* 1990, Glosik *et al* 1993) and reactions such as charge transfer and hydride transfer. The variation of charge transfer reactions at increased energies in larger systems have recently received some attention (e.g. Williams *et al* 2000). Over the last decade there have been a small number of studies of elevated energy impacts on proton transfer efficiency (and product distribution) between polyatomic ions and molecules as in the PTR-MS (Lagg *et al* 1994, Warneke *et al* 1996, Hansel *et al* 1997, Arnold *et al* 1998, Midey *et al* 2000, 2002, 2003 and Milligan *et al* 2002, Chapter 3).

For the proceeding discussion it is important to distinguish possible reasons for a decrease in observed reaction rate with increased energy. As discussed in § 2.4, the collisional rate of a reaction with a polar molecule proceeding with 100 % efficiency is expected to decrease with increasing temperature or $KE^r_{c.m.}$ to some extent due to the inverse dependence on ion velocity (and in the case of temperature, reduced dipole-locking). These reactions can still be

quantified by PTR-MS assuming that the calculated rate constant factors in this energy dependence appropriately. However, if the reaction efficiency decreases with increased energy available for reaction, it will not be possible, at present, to quantify the compound with the PTR-MS since k in Eq. 2.10 cannot be theoretically derived (without employing complex transition state theory based calculations) and the backward reaction is occurring so the concentration will be an underestimation. This inefficiency would be seen as a decrease in experimental rate constant greater than the decrease predicted using for example rotational temperature and ion reactant centre of mass kinetic energy parameterised trajectories, (Su 1994), Eq 2.61 – 2.65.

Two major determinants of reaction efficiency and product distributions are discussed in the following sections; exoergicity of proton transfer reactions (§ 2.91) and the energy available for reaction in the reaction chamber (§ 2.92)

2.9.1 Exoergicity of Proton Transfer Reactions

The impact of exoergicity on reaction efficiency results in the division of non-dissociative proton transfer reactions into three groups: (a) Those which are endoergic and do not occur at thermal temperatures. It is the endoergic nature of the reaction of the major components of air such as nitrogen and oxygen with H_3O^+ which enable PTR-MS to be operated without an additional buffer gas. (b) Reactions with exoergicity greater than ~ - 0.21 eV (- 20 kJ mol^1) to - 0.43 eV (- 42 kJ mol^{-1}) at 298 K proceed with efficiency of less than one. (c) Reactions with overall change in Gibbs free energy of less than ~ - 0.21 eV to - 0.43 eV which proceed with a reaction efficiency of one under thermal conditions, (Bohme *et al* 1980, Bouchoux *et al* 1996).

The nature of the efficiency dependence on exoergicity has been attributed to the differing potential energy profiles. Those reactions with exoergicity less than - 0.43 eV are perceived to proceed with no or little activation energy barrier (Figure 2.18). A small free energy barrier is hypothesised for those reactions with overall change in free energy of greater than – 0.43 eV (Figure 2.19) (e.g. Bohme *et al* 1980).
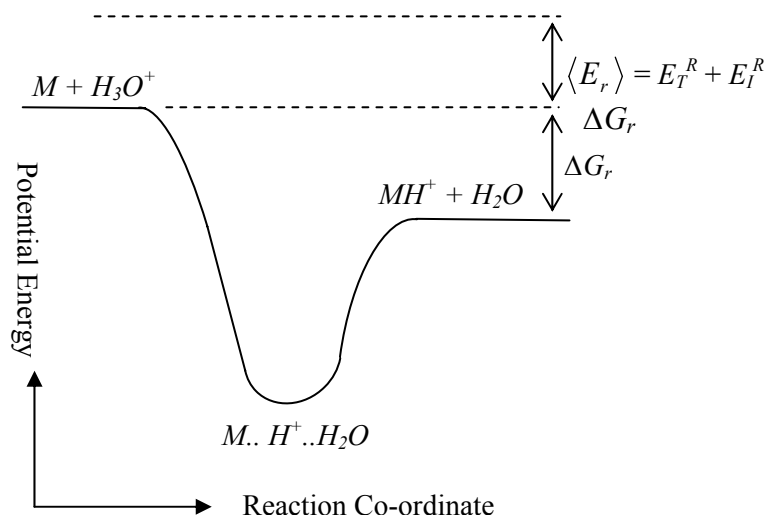
Figure 2.18: The potential energy diagram of a non-dissociative proton transfer reaction with overall change in Gibbs energy of less than $\sim - 0.43$ eV. $\langle E_r \rangle$ is the energy available for reaction, E_T^R and E_I^R are the translational and internal energy of reactants respectively (§ 2.92). ΔG_r is the Gibbs free energy of reaction. M is a trace species. Adapted from Bohme (1975).
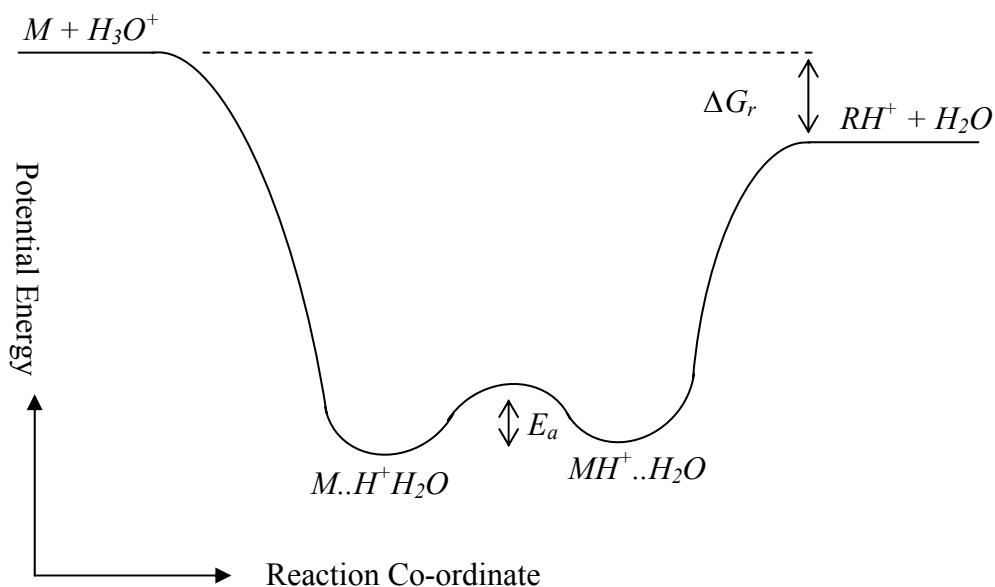
Figure 2.19: The potential energy diagram of a gas phase non-dissociative proton transfer with a change in Gibbs free energy of less than $\sim - 0.43$ eV. E_a denotes activation energy. Adapted from Uggerud (1992).

The change in Gibbs free energy of a non-dissociative proton transfer reaction is derived from gas basicities. The gas basicity (*GB*) of a species *M* is the change in standard Gibbs free energy of following hypothetical reaction:

$$MH^+ \rightarrow M + H^+ \tag{2.87}$$

The change in standard enthalpy of this reaction is termed the proton affinity (PA). The change in standard Gibbs free energy for a proton transfer reaction, such as Eq 2.6 is thus given by the difference in gas basicities of the reactant and product ions (Eq 2.88), and the change in enthalpy by the difference in proton affinities (Eq 2.89)

$$\Delta G_r^{\Phi} = GB(H_2O) - GB(M) \tag{2.88}$$

$$\Delta H_r^{\Phi} = PA(H_2O) - PA(M) \tag{2.89}$$

The standard entropy change in proton transfer reaction is generally positive and very small and is therefore often neglected, a comparison of proton affinities often providing a good approximation of the exoergicity of reaction. Gas basicities, proton affinities and Gibbs free energy of potential (non-dissociative) proton transfer reactions of H_3O^+ with the atmospherically important (O)VOCs (including some of those observed from animal waste – refer to Chapter 4), the major components of air and other potentially important VOCs are tabulated in Table 2.7. Values correspond to 298 K. Reactions are divided into the three categories discussed above. PA, GB, enthalpies and Gibbs free energies are given in eV here where eV is a molar energy equal to 96.487 J mol^{-1}.

Table 2.7: A compilation of proton affinities (PA), gas basicities (GB), potential standard enthalpy and Gibbs free energy of proton transfer from H_3O^+ for a range of compounds.

Compound (M)	PA (eV)	GB (eV)	$\Delta H^{\Phi}_{M+H_3O^+ \rightarrow MH^+ + H_2O}$ (eV)	$\Delta G^{\Phi}_{M+H_3O^+ \rightarrow MH^+ + H_2O}$ (eV)
Water	7.16	6.84		
Endoergic reactions				
Nitrogen	5.12	4.81	2.04	2.03
Oxygen	4.36	4.11	2.79	2.73
Argon	3.83	3.59	3.32	3.25
Carbon Dioxide	5.60	5.35	1.55	1.49
Neon	2.06	1.81	5.08	5.03
Helium	1.84	1.54	5.30	5.30
Methane	5.63	5.40	1.52	1.44
Exoergic reactions where $\Delta G^{\Phi}_{M+H_3O^+ \rightarrow MH^+ + H_2O}$ is $> \sim$ - 0.43 e V				
Hexane	7.02^a	-	0.14	-
Methanal	7.39	7.08	-0.23	-0.24
Hydrogen sulphide	7.31	6.98	-0.14	-0.14
Exoergic and efficient reactions, $\Delta G^{\Phi}_{M+H_3O^+ \rightarrow MH^+ + H_2O}$ is $\leq \sim$ - 0.43 Ev				
Benzene	7.78	7.52	-0.61	-0.68
Toluene	8.13	7.84	-0.96	-1.00
1, 2 dimethylbenzene	8.25	7.96	-1.08	-1.12
1, 4 dimethylbenzene	8.23	7.95	-1.07	-1.11
1, 3 dimethylbenzene	8.42	8.15	-1.25	-1.31
1,3,5 trimethylbenzene	8.67	8.38	-1.50	-1.54
Methanol	7.82	7.51	-0.65	-0.67

Table 2.7 is continued on the following page.

Compound (M)	PA (eV)	GB (eV)	$\Delta H^{\Phi}_{M+H_3O^+ \rightarrow MH^+ + H_2O}$ (eV)	$\Delta G^{\Phi}_{M+H_3O^+ \rightarrow MH^+ + H_2O}$ (eV)
Ethanol	8.05	7.73	-0.88	-0.89
Propanone	8.42	8.11	-1.25	-1.27
Ethanal	7.96	7.63	-0.80	-0.79
2-methyl-1,3-butadiene	8.56	8.27	-1.40	-1.43
Methylvinylketone	8.65	8.32	-1.48	-1.48
Methacrolein	8.38	8.05	-1.22	-1.21
Nitric acid	7.79	7.58	-0.62	-0.74
Methanoic acid	7.69	7.36	-0.53	-0.52
Ethanoic acid	8.12	7.80	-0.96	-0.96
2-methylphenol	8.62[b]	8.29[b]	-1.46	-1.45
3-methylphenol	8.72[b]	8.38[b]	-1.55	-1.54
Phenol	8.47	8.15	-1.30	-1.31
Trimethylamine	9.83	9.52	-2.66	-2.67
Acetonitrile	8.08	7.75	-0.91	-0.91

Note: Values are taken from Hunter and Lias (1998) unless otherwise specified: [a]proton affinity is from Wróblewski *et al* (2006), [b]values are from Van Beelen (2004).

The comparison of gas basicities or proton affinities assesses the exoergicity or enthalpy change for a proton transfer at 298 K. In the drift tube the ions are effectively increased in temperature. The distribution of this energy varies from that resulting from increased temperature and the neutrals are at the drift tube temperature. It is therefore difficult to determine a temperature corrected free Gibbs energy of reaction.

Midey *et al* (2002) have calculated temperature corrected enthalpies of reaction of proton transfer from H_3O^+ to benzene, ethylbenzene and propylbenzene for temperatures of 400 – 1000 K and report values within or close to maximum errors associated with the enthalpy at 298 K (±0.15 eV). The use of standard enthalpies and Gibbs energies (given that entropy is generally small thus the increase in $T\Delta S$ is small) at 298 K are therefore expected to be a good estimate of exoergicity and exothermicity of proton transfer reactions in the PTR-MS.

Bohme *et al* (1980) found that for endoergic reactions ($\Delta G_r^{\Phi} >\sim 0.07$ eV), Eq. 2.90 is applicable:

$$k_m = k_c \exp[-\Delta G_r^{\Phi} / RT] \tag{2.90}$$

where k_m is the measured rate constant and k_c is the collisional rate constant.

The input of energy in the form of temperature to the endoergic reactions results in increased rate of reaction. Increases in energy in the form of an electric field have been observed to result in an increase in rate of endothermic reactions (e.g. Hansel *et al* 1997). A decrease in rate of exoergic reactions may be expected due to the energy input under elevated

temperatures and in the presence of an electric field. The successful application of PTR-MS (though with considerable uncertainties) indicates qualitatively that the majority of reactions remain efficient at least at the *E/N* normally employed in the drift tube. Presumably in the case of most non-dissociative proton transfer reactions between H_3O^+ and trace species with $\Delta G_r^{\Phi} < \sim -0.43$ eV the rate constant for the reverse reaction (k_{-1} in Figure 2.17) is so negligible compared to that of the forward reaction (k_1 in Figure 2.17) that this reaction does not become important at energies in PTR-MS. This is not the case for those reactions with exoergic reactions with $\Delta G_r^{\Phi} > \sim -0.43$ eV (§ 3.4 and 3.6).

2.9.2. Energy Available for Reaction in the Drift Tube.

In addition to the Gibbs free energy of reaction, the average energy available for reaction contributes to the energy available for dissociation for example and is a determinant of product distributions. The degree of energy available may also affect reaction efficiencies. (e.g. Milligan *et al* 2002, Midey *et al* 2002, 2003). Average total energy available for reaction ($\langle E_r \rangle$) is given by Eq. 2.91

$$\langle E_r \rangle = \langle KE \rangle + \langle E_{rot}^{(O)VOC} \rangle + \langle E_{vib}^{(O)VOC} \rangle + \langle E_{rot}^{ion} \rangle + \langle E_{vib}^{ion} \rangle \tag{2.91}$$

where $\langle \ \rangle$ denote that values are an average over the population. $\langle E_{rot}^{(O)VOC} \rangle$ is the rotational energy of the (O)VOC neutral, $\langle E_{vib}^{(O)VOC} \rangle$ is the vibrational energy of the neutral (O)VOC. *KE* is the ion-molecule kinetic energy under the thermal conditions of SIFT this is $\frac{3}{2}(k_B T)$. $\langle E_{rot}^{ion} \rangle$ is the rotational energy of the ion, in this case H_3O^+ and under thermal condition of SIFT is also $\frac{3}{2}(k_B T)$, $\langle E_{vib}^{ion} \rangle$ is the vibrational energy of the ion. The vibrational energy of the ion and (O)VOC can be calculated from the Boltzmann distribution over 3*N*-6 modes (where *N* is the number of atoms in the molecule or ion) and the assumption that the species is an anharmonic oscillator (e.g. Maczek 1998, Midey *et al* 2003). The temperature of the flow tube is used to calculate these energies.

In the drift tube the kinetic energy, *KE*, is $KE_{c.m.}^r$ (§ 2.4.1.5, Eq. 2.59). Molecular ions in the drift tube may be rotationally and vibrationally excited by inelastic collisions with the buffer resulting in conversion of translational energy into internal energy. The level of excitation depends on the nature of the buffer and the magnitude of *E/N*. The internal energy of the ion also depends on the temperature of the drift tube. The internal energy of ions in the drift tube can therefore be approximated from the centre-of-mass kinetic energy between the ions and

buffer gas (the frequency of collisions with buffer molecules being much greater than those with neutral reactants), $KE_{c.m.}^{b}$ (e.g. Glosik *et al* 1993).

$$KE_{c.m.}^{b} = \frac{M_b}{M_i + M_b}\left(KE_{ion} - \frac{3}{2}k_BT\right) + \frac{3}{2}k_BT \tag{2.92}$$

Recall that KE_{ion} is dependent on drift velocity (Eq 2.55) and therefore E/N (Eq 2.58).

In the case of PTR-MS, the buffer is the components of air which do not react with H_3O^+ and the average molecular weight of air of 28.9 g is used alongside H_3O^+ mobility in nitrogen. The diverse nature of non-reactant molecules in air mean that $KE_{c.m.}^{b}$ is only an approximate value in the case of PTR-MS. $KE_{c.m.}^{b}$ values over a range of E/N at 318.15 K in various buffers are shown in Figure 2.20. $KE_{c.m.}^{b}$ at a given E/N is greater in the helium buffer compared with argon; this results from the higher mobility of ions in argon due to the increased reduced mass and increased polarizability of argon (§ 2.4.1.7). The higher mobility results in increased drift velocity, higher KE_{ion} and thus $KE_{c.m.}^{b}$ in argon. The $KE_{c.m.}^{b}$, thus internal energy and therefore energy available for reaction at a given E/N ,is less in a nitrogen or air buffer than a helium or argon buffer. The decreased $KE_{c.m.}^{b}$ in nitrogen, despite its lower mass (and comparable polarizability) compared with argon, is due to its diatomic nature. Some of the ion translational energy is not only converted to internal energy of the ion in ion-nitrogen collisions but also into internal energy of the nitrogen molecule. Quantitatively this results in reduced ion mobility in nitrogen (§ 2.4.1.7) and therefore reduced drift velocity, KE_{ion} and $KE_{c.m.}^{b}$.

At 127 Td and 318.15 K, $KE_{c.m.}^{b}$ is 0.18 eV, compared with k_BT of 0.027 eV at this temperature and illustrates internal excitation of the reactant ions. It is noteworthy that comparison of $KE_{c.m.}^{b}$ to k_bT enables an effective internal temperature to be calculated in a similar way to the effective translational temperature calculated in Eq. 2.58 (e.g. Viehland *et al* 1981, Durup-Ferguson *et al* 1983).

$$T_{eff}^{int\,ernal} = \frac{2KE_{c.m}^{b}}{3k_B} \tag{2.93}$$

At 127 Td and 318.15 K, $T_{eff}^{int\,ernal}$ is 1378 K. Eq. 2.93 is a first approximation (e.g. Glosik *et al* 1994) and does not apply to polyatomic ions in polyatomic buffer, a more thorough treatment in this case has been given by Viehland *et al* (1981). Alike the effective

translational ion temperature (Eq 2.60) $T_{eff}^{internal}$ values calculated *via* Eq 2.93 assumes steady state conditions exist in the drift tube (§ 2.8). If insufficient collisions occur for steady state conditions to be achieved, the ion internal temperature is likely to be closer to the drift tube temperature.
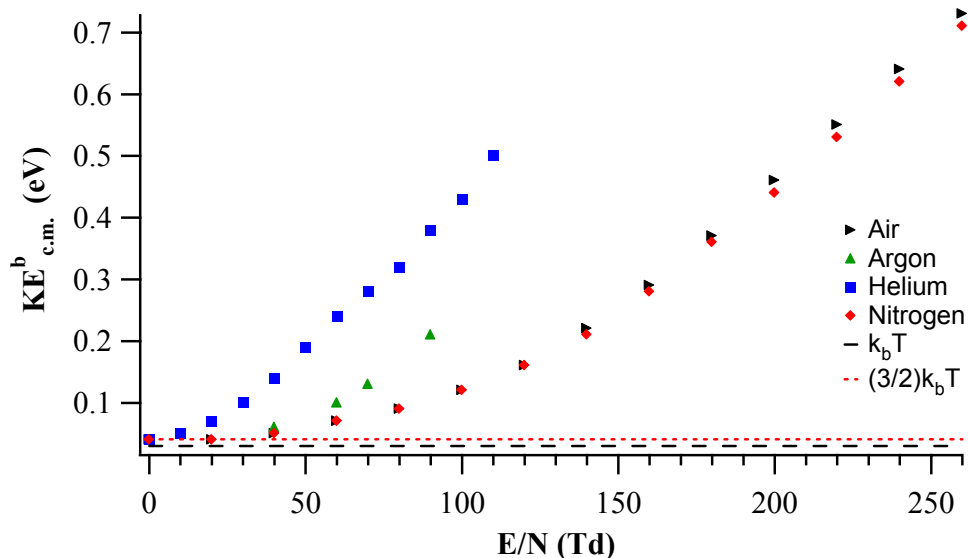
Figure 2.20: Centre of mass kinetic energy between H_3O^+ ions and buffer gas molecules, $KE_{c.m.}^b$, over a range of *E/N* in various buffers at 318.15 K. Note that $KE_{c.m.}^b$ in air was calculated using H_3O^+ mobility in nitrogen since mobility in air is unknown. H_3O^+ mobilties in helium, argon and nitrogen were taken from Dotan *et al* (1977), Böhringer *et al* (1983) and Dotan *et al* (1976) respectively.

Distinguishing vibrational and rotational energy effects in systems where the ion, reactant and buffer are polyatomic is not possible (Viggiano and Morris 1996). However the average total energy rather than the distribution of energy is generally of importance for reaction efficiency of exothermic proton transfer reactions between large molecules (private communication with A. Viggiano, June 28 2007, Viggiano and Morris 1996). Energy distributions may become important when considering product distributions.

A more in-depth discussion of the effects of increased energy on ion-molecule reaction efficiencies can be found elsewhere, e.g., Porter 1975, Chupka 1975, Bohme 1975, Lindinger *et al* 1975a,b, Meot-Ner 1979, Durup-Ferguson *et al* 1983, Viggiano *et al* 1990, Glosik *et al* 1993 and Viggiano and Morris 1996. Further experimental investigations of the effect of the electric field on reaction efficiencies is required, particularly where fragmentation and potentially alternative reaction pathways (e.g. hydride transfer) are observed.

In Chapter 3 an approximate method for estimation of the difference in $\langle E_r \rangle$ between VT-SIFT and PTR-MS is proposed. This is utilised to hypothesis product distributions and reaction efficiencies which may be observed in the PTR-MS from those measured in VT-SIFT. Limitations of this method are discussed.

References

Adams, N. G., D. Smith (1976) The selected ion flow tube (SIFT); a technique for studying ion-neutral reactions, *International Journal of Mass Spectrometry and Ion Physics*, **21**: 349-359.

Albritton, D. L., I. Dotan, W. Lindinger, M. McFarland, J. Tellinghuisen, F. C. Fehsenfeld (1977) Effects of ion speed distributions in flow-drift tube studies of ion-neutral reactions, *The Journal of Chemical Physics*, **66** (2): 410-421.

Allinger, N. L., K. Chen, J. Lii, K.A. Durkin (2003) Alcohols, ethers, carbohydrates, and related compounds. I. The MM4 force field for simple compounds, *Journal of Computational Chemistry*, **24** (12): 1447-1472.

Altshuller, A. P., Cohen, I. R. (1960) Application of diffusion cells to the production of known concentrations of gaseous hydrocarbons, *Analytical Chemistry*, **32** (7): 802-810.

Ammann, C., C. Sprig, A. Neftel, M. Steinbacher, M. Komenda, A. Schaub (2004) Application of PTR-MS for measurements of biogenic VOC in a deciduous forest, *International Journal of Mass Spectrometry*, **239**: 87-101.

Ammann, C., A. Brunner, C. Sprig, A. Neftel (2006) Technical note: Water vapour concentration and flux measurements with PTR-MS, *Atmospheric and Chemical Physics*, **6**: 4643 – 4651.

Aoki, N., S. Inomata, H. Tanimoto (2007) Detection of C_1-C_5 alkyl nitrates by proton transfer reaction time-of-flight mass spectrometry, *International Journal of Mass Spectrometry*, **263**: 12-21.

Arnold, S. T., A. A. Viggiano, R. A. Morris (1998) Rate constants and product branching fractions for the reactions of H_3O^+ and NO^+ with C_2-C_{12} alkanes, *Journal of Physical Chemistry A*, **102**: 8881-8887.

Atkins, P. W. (1999) *Physical Chemistry*. Oxford University Press, Oxford.

Banwell, C. N., E. M. McCash (1994) *Fundamentals of Molecular Spectroscopy*. McGraw-Hill, London.

Barratt, R. S. (1981) The preparation of standard gas mixtures. A Review. *The Analyst*, **106** (1265): 817-849.

Bei, H. C., P. K. Bhowmik, T. Su (1989) Trajectory calculations of high temperature and kinetic energy dependent ion-polar molecule collision rate constants, *The Journal of Chemical Physics*, **90** (12): 7046-7049.

Blake, R. S., C. Whyte, C. O. Hughes, A. M. Ellis, P. S. Monks (2004) Demonstration of proton-transfer reaction time-of-flight mass spectrometry for real-time analysis of trace volatile organic compounds, *Analytical Chemistry*, **76**: 3841 – 3845.

Blake, R. S., K. P. Wyche, A. M. Ellis, P. S. Monks (2006) Chemical ionization reaction time-of-flight mass spectrometry: Multi-reagent analysis for determination of trace gas composition, *International Journal of Mass Spectrometry*, **254**: 85-93.

Bohme, D. K. (1975) The kinetics and energetics of proton transfer. In: *Interactions Between Ions and Molecules, A NATO Advanced Study Institute*, edited by P. Ausloos, pages 489-504. Plenum Press, New York.

Bohme, D. K., G. I. Mackay, S. D. Tanner (1979) An experimental study of the gas-phase kinetic of reactions with hydrated H_3O^+ ions (*n*=1-3) at 298 K, *Journal of the American Chemical Society*, **101** (14): 3724 – 3730.

Bohme, D. K., G. I. Mackay, H. I. Schiff (1980) Determination of proton affinities from the kinetics of proton transfer reactions. VII. The proton affinities of O_2, H_2, Kr, O, N_2, Xe, CO_2, CH_4, N_2O, and CO, *Journal of Chemical Physics*, **73** (10): 4976-4986.

Bohme, D. K. (2000) Experimental studies of positive ion chemistry with flow-tube mass spectrometry: birth, evolution and achievements in the 20th century, *International Journal of Mass Spectrometry*, **200**: 97-136.

Böhringer, H., M. Durup-Ferguson, D. W. Fahey. (1983) Mobilities of various mass-identified positive ions in helium, neon, and argon, *Journal of Chemical Physics*, **79** (4): 1974-1976.

Bouchoux, G., J. Y. Salpin, D. Leblane (1996) A relationship between the kinetics and thermochemistry of proton transfer reactions in the gas phase, *International Journal of Mass Spectrometry and Ion Processes*. **153**: 37-48.

Bowers, M. T., J. B. Laudenslager (1972) Mechanism of charge transfer reactions: reactions of rare gas ions with the trans-, cis-, and 1,1-difluoroethylene geometric isomers, *The Journal of Chemical Physics*, **56** (9) 4711-4712.

Bowers, M. T., T. Su (1975) Theory of ion polar molecule collisions. In: *Interactions Between Ions and Molecules, A NATO Advanced Study Institute*, edited by P. Ausloos, pages 163-183. Plenum Press, New York.

Chen, K., J. Lii, N. L. Allinger (2007) Molecular mechanics (MM4) study of amines, *Journal of Computational Chemistry*, **00** (00) 1-22.

Chesnavich, W. J., T. Su, M. T. Bowers (1980) Collisions in a noncentral field: A variational and trajectory investigation of ion-dipole capture, *The Journal of Chemical Physics*. **72** (4): 2641-2655.

Chhiba, M., G. Vergoten (1994) The structures and vibrational frequencies of a series of linear alkanes obtained using the spectroscopic potential SPASBIA, *Journal of Molecular Structure*. **326**: 35-58.

Chukpa, W. A. (1975) Effects of Internal Energy on Ion-Molecule Reactions. In: *Interactions Between Ions and Molecules, A NATO Advanced Study Institute*, edited by P. Ausloos, pages 489-504. Plenum Press, New York.

Cordell, R. L., K. A. Willis, K. P. Wyche, R. S. Blake, A. M. Ellis, P. S. Monks (2007) Detection of chemical weapon agents and simulants using chemical ionization reaction time-of-flight mass spectrometry, *Analytical Chemistry*, **79**: 8359 – 8366.

Dawson, P. H. (1986) Quadrupole mass analyzers: Performance, design and some recent applications. *Mass Spectrometry Reviews*, **5**: 1-37.

De Gouw, J., C. J. Howard, T. G. Custer, R. Fall (1999) Emissions of volatile organic compounds from cut grass and clover are enhanced during the drying process, *Geophysical Research Letters*, **26** (7): 811-814.

De Gouw, J., C. J. Howard, T. G. Custer, B. M. Baker, R. Fall (2000) Proton-transfer chemical-ionisation mass spectrometry allows real-time analysis of volatile organic compounds released from cutting and drying of crops, *Environmental Science and Technology*, **34**: 2640-2648.

De Gouw, J., C. Warneke, T. Karl, G. Eerdekens, C. van der Veen, R. Fall (2003a) Sensitivity and Specificity of atmospheric trace gas detection by proton-transfer-reaction mass spectrometry. *International Journal of Mass Spectrometry*, **223-224**: 365-382.

De Gouw, J., P. D. Goldan, C. Warneke, W. C. Kuster, J. M. Roberts, M. Marchewka, S. B. Bertman, A. A. P. Pszenny, W. C. Keene (2003b) Validation of proton transfer reaction-mass spectrometry (PTR-MS) measurements of gas-phase organic compounds in the atmosphere during the New England Air Quality Study (NEAQS) in 2002, *Journal of Geophysical Research*, **108** (D21): 4682, art.-nr.: 10.1029/2003JD003863.

De Gouw, J., C. Warneke (2007) Measurements of volatile organic compounds in the earth's atmosphere using proton-transfer-reaction mass spectrometry, *Mass Spectrometry Reviews*, **26**: 223-257.

Dotan, I., D. L. Albritton, W. Lindinger, M. Pahl (1976) Mobilities of CO_2^+, N_2H^+, H_3O^+, $H_3O^+.H_2O$, and $H_3O^+.(H_2O)_2$ ions in N_2, *The Journal of Chemical Physics*, **65** (11): 5028-5030.

Dotan, I., W. Lindinger, D. L. Albritton (1977) Mobilities of H_2O^+ and $H_3O^+.nH_2O$ (n = 0, 1, 2) ions in He, *Journal of Chemical Physics*, **67** (12): 5968-5969.

Dressler, R. A., H. Meyer, A. O. Langford, V. M. Bierbaum, S. R. Leone (1987) Direct observation of Ba^+ velocity distributions in a drift tube using single-frequency laser-induced fluorescence, *Journal of Chemical Physics*, **67** (9): 5578-5579.

Dressler, R. A., J. P. M. Beijers, H. Meyer, S. M. Penn, V. M. Bierbaum, S. R. Leone (1988) Laser probing of ion velocity distributions in drift fields: Parallel and perpendicular temperatures and mobility for Ba^+ in He, *Journal of Chemical Physics*, **89** (8) 4707-4715.

Durier, V., A. Zanoun, A. Belaidi, G. Vergoten (1999) The *SPASIBA* force field of aldehydes. Part II: structure and vibrational wavenumbers of ethandial, propenal and 2-methylpropenal, *Journal of Molecular Structure*, **476**: 271-281.

Durup-Ferguson, M., H. Böhringer, D. W. Fahey, E. E. Ferguson (1983) Enhancement of charge-transfer reaction rate constants by vibrational excitation at kinetic energies below 1 eV, *Journal of Chemical Physics*, **79** (1): 265-271.

Eisele, F. L., E. R. Lovejoy, E. Kosciuch, K. F. Moore, R. L. Mauldin III, J. N. Smith, P. H. McMurry, K. Iida (2006) Negative atmospheric ions and their potential role in ion-induced nucleation, *Journal of Geophysical Research*, **111** (D04305): art.-nr.: 10.1029/2005JD006568.

Ellis, H., R. D. Harrison, H. D. B. Jenkins (1999) *Nuffield Advanced Science Revised Book of Data*. Longman, Singapore.

Ennis, C. J., J. C. Reynolds, B. J. Keely, L. J. Carpenter (2005) A hollow cathode proton transfer reaction time of flight mass spectrometer, *International Journal of Mass Spectrometry*, **247**: 72- 80.

Fehsenfeld, F. C., A. L. Schmeltekopf, P. D. Goldan, H. I. Schiff, E. E. Ferguson (1966) Thermal energy ion-neutral reaction rates. I. Some reactions of helium ions, *The Journal of Chemical Physics*, **44** (11): 4087-4094.

Ferguson, E. E. (1992) A personal history of the early development of the flowing afterglow technique for ion-molecule reaction studies, *Journal of the American Society for Mass Spectrometry*, **3**: 479-486.

Ferguson, E. E. (2007) Mass spectrometry in ionospheric research, *Mass Spectrometry Reviews*, **26**: 142-149.

Foster, P. D., V. M. Rao, R. F. Curl Jr, (1965) Microwave spectrum of methyl vinyl ketone. *The Journal of Chemical Physics*. **43** (3): 1064-1066.

Gautrois, M., R. Koppmann (1999) Diffusion technique for the production of gas standards for atmospheric measurements, *Journal of Chromatography A*, **848**: 239-249.

Gioumousis, G., D. P. Stevenson (1957) Reaction of gaseous molecule ions with gaseous molecules. V. Theory, *The Journal of Chemical Physics*, **29**: 294-299.

Glosik, J., D. Smith, P. Španěl, W. Freysinger, W. Lindinger (1993) SIFDT studies of the reactions of C^+, CH^+ and CH_2^+ with HCl and CO_2, and CH_3^+ with HCl, *International Journal of Mass Spectrometry and Ion Processes*, **129**: 131-143.

Glosik, J., V. Skalský, C. Praxmarer, D. Smith, W. Freysinger, W. Lindinger (1994) Dissociation of Kr_2^+, N_2Ar^+, $(CO)_2^+$, CH_5^+, and $C_2H_5^+$ ions drifting in He, *Journal of Chemical Physics*, **101** (5): 3792-3801.

Glosik, J., P. Zakouřil, V. Skalský, W. Lindinger (1995) Selected ion flow drift tube studies of the kinetics of the reactions of $Si^+(^2P)$ with C_2H_2 and C_6H_6, *International Journal of Mass Spectrometry and Ion Processes*, **149/150**: 499-512.

Goldan, P. D., A. R. Schmeltekopf, F. C. Fehsenfeld, H. I. Schiff, E. E. Ferguson (1966) Thermal energy ion-neutral reaction rates. II. Some reactions of ionospheric interest, *The Journal of Chemical Physics*, **44** (11): 4095-4103.

Graul, S. T., R. R. Squires (1988) Advances in flow reactor techniques for the study of gas-phase ion chemistry. *Mass Spectrometry Reviews*, **7**: 263-358.

Gupta, S. K., E. G. Jones, A. G. Harrison, J. J. Myher (1967) Reactions of thermal energy ions. VI. Hydrogen-transfer ion-molecule reactions involving polar molecules, *Canadian Journal of Chemistry*, **45**: 3107-3117.

Hansel, A., A. Jordan, R. Holzinger, P. Prazeller, W. Vogel, W. Lindinger (1995) Proton transfer reaction mass spectrometry: on-line trace gas analysis at the ppb level, *International Journal of Mass Spectrometry and Ion Processes*, **149/150**: 609-619.

Hansel, A., W. Singer, A. Wisthaler, M. Schwarzmann, W. Lindinger (1997) Energy Dependencies of the proton transfer reactions $H_3O^+ + CH_2O \Leftrightarrow CH_2OH^+ + H_2O$, *International Journal of Mass Spectrometry and Ion Processes*:**167/168**: 697-703.

Hansel A., A. Jordan, C. Warneke, R. Holzinger, A. Wisthaler, W. Lindinger (1999) Proton-transfer-reaction mass spectrometry (PTR-MS): on-line monitoring of volatile organic compounds at volume mixing ratios of a few pptv, *Plasma Sources Science and Technology*, **8**: 332-336.

Hanson, D. R., J. Greenberg, B. E. Henry, E. Kosciuch (2003) Proton transfer reaction mass spectrometry at high drift tube pressure, *International Journal of Mass Spectrometry*, **223-224**: 507-518.

Hayward, S., C. N. Hewitt, J. H. Sartin, S. M. Owen (2002) Performance characteristics and applications of proton transfer reaction-mass spectrometer for measuring volatile organic compounds in ambient air, *Environmental Science and Technology*, **36**: 1554-1560.

Hewitt, C. N., S. Hayward, A. Tani (2003) The application of proton transfer reaction-mass spectrometry (PTR-MS) to the monitoring and analysis of volatile organic compounds in the atmosphere, *Journal of Environmental Monitoring*, **5**: 1-7.

Hill, T. L (1962) *An Introduction to Statistical Thermodynamics*. Addison-Wesley Publishing Company, Massachusetts.

Hirschfelder, J. O., C. F. Curtiss, R. B. Bird (1954) *Molecular theory of gases and liquids*. New York: John Wiley and Sons.

Hunter, E. P. L., S. G. Lias (1998) Evaluated gas phase bascities and proton affinities of molecules: An update, *Journal of Physical Chemical Reference Data*, **27** (3): 413-656.

Inomata, S., H. Tanimoto, N. Aoki, J. Hirokawa, Y. Sadanaga (2006) A novel discharge source of hydronium ions for proton transfer reaction ionization: design, characterisation, and performance, *Rapid Communications in Mass Spectrometry*, **20**: 1025 – 1029.

Jobson, B. T., M. L. Alexander, G. D. Maupin, G. G. Muntean (2005) On-line analysis of organic compounds in diesel exhaust using a proton transfer reaction mass spectrometer (PTR-MS), *International Journal of Mass Spectrometry*, **245**: 78 - 89.

Karl, T. G., C. Sprig, J. Rinne, C. Stroud, P. Prevost, J. Greenberg, R. Fall, A. Guenther (2002) Virtual disjunct eddy covariance measurements of organic compound fluxes from a subalpine forest using proton transfer reaction mass spectrometry, *Atmospheric Chemistry and Physics*, **2**: 279 – 291.

Karl, T., F. Harren, C. Warneke, J. de Gouw, C. Grayless, R. Fall (2005) Senescing grass crops as regional sources of reactive volatile organic compounds, *Journal of Geophysical Research*, **110**: 1-11.

Keck, L., U. Oeh, C. Hoeschen (2007) Corrected equation for the concentrations in the drift tube of a proton transfer reaction-mass spectrometer (PTR-MS), *International Journal of Mass Spectrometry*, **264**: 92-95.

Kommenda, M., A. Schaub, R. Koppmann (2003) Description and characterization of an on-line system for long-term measurements of isoprene, methyl vinyl ketone, and methacrolein in ambient air, *Journal of Chromatography A*, **995**: 185-201.

Kovács, A., I. Hargittai (2000) Theoretical investigation of the additivity of structural substituent effects in benzene derivatives, *Structural Chemistry*, **11** (2/3): 193-201.

Lagg, A., A. Taucher, A. Hansel, W. Lindinger (1994) Applications of proton transfer reactions to gas analysis, *International Journal of Mass Spectrometry and Ion Processes*, **134**: 55-56.

Langevin, M. P. (1905) Une formule fondementale de theorie cinetique, *Annales des Chimie et des Physique*. **5**: 245.

Langley, C. H., J. Lii, N. Allinger (2003) Molecular mechanics (MM4) calculations on carbonyl compounds. I-IV, *Journal of Computational Chemistry*. **24** (10): 1283-1286.

Lau, Y. K., S. Ikuta, P. Kebarle (1982) Thermodynamics and kinteics of the gas-phase reactions: $H_3O^+(H_2O)_{n-1} + H_2O = H_3O^+(H_2O)_n$., *Journal of the American Chemical Society*, **104**: 1462 – 1469.

Lester, J. E. (1970) Off-axis channeltron multiplier for quadrupole mass spectrometers, *Review of Scientific Instruments*, **41**: 1513.

Lii, J. (2002) Molecular mechanics (MM4) studies of carboxylic acids, esters and lactones, *Journal of Physical Chemistry*, **106**: 8667-8679.

Lim, K. F. (1994) Programme COLRATE. QCPE 643: Calculation of gas-kinetic collision rate coefficients, *Quantum Chemistry Program Exchange*, **14** (1): 3.

Lin, S. L., J. N. Bardsley (1977) Monte Carlo simulation of ion motion in drift tubes, *The Journal of Chemical Physics*, **66** (2): 435-445.

Lindinger, W. (1973) Reaction rate constants in steady-state hollow cathode discharges: Ar + H_2O reactions, *Physical Review A*, **7** (1): 328-333.

Lindinger, W., D. L. Albritton, F. C. Fehsenfeld, A. L. Schmeltekopf, E. E. Ferguson (1975a) Flow-drift tube measurements of kinetic energy dependences of some exothermic proton transfer rate coefficients, *The Journal of Chemical Physics*, **62** (9) 3549-3553.

Lindinger, W., M. McFarland, F. C. Fehsenfelder, D. L. Albritton, A. L. Schmeltekopf, E. E. Ferguson (1975b) Translational and internal energy dependences of some ion-neutral reactions, *The Journal of Chemical Physics*. **63** (5): 2175-2181.

Lindinger, W., E. Alge, H. Störi, R. N. Varney, H. Helm, P. Holzmann, M. Pahl (1979) Investigation of ion-molecule reactions using a drift tube with separated ion source, *International Journal of Mass Spectrometry and Ion Physics*, **30**: 251-261.

Lindinger, W. (1986a) Chapter 7: Swarm methods, In: *Gaseous Ion Chemistry and Mass Spectrometry*, edited by J. H. Futrell, pages 141-151. John Wiley and Sons, New York.

Lindinger, W. (1986b) Chapter 11: Ion-Molecule Reaction Kinetics in Plasma: Rate Coefficients and Internal-Energy and Translational-Energy Effects. In: *Gaseous Ion Chemistry and Mass Spectrometry*, edited by J. H. Futrell, pages 237-257. John Wiley and Sons, New York.

Lindinger, W., J. Hirber, H. Paretzke (1993) An ion/molecule-reaction mass spectrometer used for on-line trace gas analysis, *International Journal of Mass Spectrometry and Ion Processes*, **129**: 79-88.

Lindinger, W., A. Hansel (1997) Analysis of trace gases at ppb levels by proton transfer reaction mass spectrometry (PTR-MS), *Plasma Sources Science and Technology*, **6**: 111-117.

Lindinger, W., A. Hansel, A. Jordan (1998a) On-line monitoring of volatile organic compounds at pptv levels by means of proton-transfer-reaction mass spectrometry (PTR-MS) medical applications, food control and environmental research, *International Journal of Mass Spectrometry and Ion Processes*, **173**: 191-241.

Lindinger, W., A. Hansel, A. Jordan (1998b) Proton-transfer-reaction mass spectrometry (PTR-MS): on-line monitoring of volatile organic compounds at pptv levels, *Chemical Society Reviews*, **27**: 347-353.

Maczek, A (1998) *Statistical Thermodynamics*. Oxford University Press, Oxford.

Manura J. J., D. J. Manura (1996) *Isotope distribution calculator and mass spec plotter* [online]. Ringoes. Scientific Instrument Services. Available from: http://www2.sisweb.com/mstools/isotope.htm

Märk, T., W. Lindinger, F. Howorka, F. Egger, R. N. Varney, M. Pahl (1972) A simple bakeable hollow cathode device for the direct study of plasma constituents, *The Review of Scientific Instruments*, **43** (12): 1852-1853.

Mason, E. A., E. W. McDaniel (1988) *Transport Properties of Ions in Gases*. John Wiley and Sons, New York.

McDaniel, E. W., V. Čermăk, A. Dalgarno, E. E. Ferguson, L. Friedman (1970) *Ion-Molecule Reactions*. John Wiley and Sons, New York.

McDaniel, E. W., E. A. Mason (1973) *The Mobility and Diffusion of Ions in Gases*. John Wiley and Sons, New York.

McFarland, M., D. L. Albritton, F. C. Fehsenfeld, E. E. Ferguson, A. L. Schmeltekopf (1973a) Flow-drift technique for ion mobility and ion-molecule reaction rate constant measurements. I. Apparatus and mobility measurements, *The Journal of Chemical Physics*, **59** (12): 6610-6619.

McFarland, M., D. L . Albritton, F. C. Fehsenfeld, E. E. Ferguson, A. L. Schmeltekopf. (1973b) Flow-drift technique for ion mobility and ion-molecule reaction rate constant measurements. II. Positive ion reactions of N^+, O^+, N_2^+ with O_2 and O^+ with N_2 from thermal to ~ 2 eV, *The Journal of Chemical Physics*, **59** (12): 6620-6628.

McGlashan, M. L (1971) *Physiochemical Quantities and Units*, The Royal Institute of Chemistry, Herts.

McKelvey, J. M., H. E. Hoelscher (1957) Apparatus for Preparation of Very Dilute Gas Mixtures, *Analytical Chemistry*, **29**: 123.

Meisels G. G. (1975) The determination of rate constants of ion-molecule reactions. Summary of the panel discussion led by G. G. Miesles. In: *Interactions Between Ions and Molecules, A NATO Advanced Study Institute*, edited by P. Ausloos, pages 595-618. Plenum Press, New York.

Meot-Ner M. (1979) Chapter 6: Temperature and pressure effects in the kinetics of ion-molecule reactions. In: *Gas Phase Ion Chemistry Volume 1*, edited by M. T. Bowers, pages 197-271. Academic Press, London.

Michel, E., N. Schoon, C. Amelynck, C. Guimbaud, V. Catoire, E. Arjis (2005) A selected ion flow tube study of H_3O^+, NO^+ and O_2^+ with methyl vinyl ketone and some atmospherically important aldehydes, *International Journal of Mass Spectrometry*, **244**: 50-59.

Midey, A. J., S. T. Arnold, A. A. Viggiano (2000) Reactions of $H_3O^+(H_2O)_n$ with Formaldehyde and Acetaldehyde, *Journal of Physical Chemistry. A*, **104**: 2706-2709.

Midey, A. J., S. Williams, S. T. Arnold, A. A. Viggiano (2002) Reactions of $H_3O^+(H_2O)_{0,1}$ with alkylbenzenes from 298 K to 1200 K, *Journal of Physical Chemistry A*, **106**: 11726-11738.

Midey, A. J., S. Williams, T. M. Miller, A. A. Viggiano (2003) Reactions of O_2^+, NO^+ and H_3O^+ with methylcyclohexane (C_7H_{14}) and cyclooctane (C_8H_{16}) from 298 K to 700 K, *International Journal of Mass Spectrometry*, **222**: 413-430.

Milligan, D. B., P. F. Wilson, C. G. Freeman, M. Meot-Ner (Mautner), M. J. McEwan (2002) Dissociative proton transfer reactions of H_3^+, N_2H^+, and H_3O^+ with acyclic, cyclic and aromatic hydrocarbons and nitrogen compounds, and astrochemical implications, *Journal of Physical Chemistry*, **106**: 9745-9755.

Milligan, D. B., G. J. Francis, B. J. Prince, M. J. McEwan (2007) Demonstration of selected ion flow tube MS Detection in the parts per tillion range, *Analytical Chemistry*, **79**: 2537 – 2540.

Moran, T. F., W. H. Hamill, (1963) Cross sections of ion-permanent-dipole reactions by mass spectrometry, *The Journal of Chemical Physics*, **39** (6): 1413-1422.

Munson, M. S. B., F. H. Field (1966) Chemical ionisation mass spectrometry. I. General introduction, *Journal of the American Chemical Society*, **88** (12): 2621 – 2630.

Naganowska-Nowak, A., P. Konieczka, A. Przyjazny, J. Namieśnik (2005) Development of Techniques of Generation of Gaseous Standard Mixtures, *Critical Reviews in Analytical Chemistry*, **35** (1): 31-55.

Pang, F., J. E. Boggs, P. Pulay, G. Fogarasi (1980), The molecular structure of toluene, *Journal of Molecular Structure*, **66**: 281-287.

Porter, R. F. (1975) Temperature Effects in Ion-Molecule Reactions. In: *Interactions Between Ions and Molecules, A NATO Advanced Study Institute*, edited by P. Ausloos, pages 489-504. Plenum Press, New York.

Possanzini, M., V. Di Palo, E. Brancaleoni, M. Frattoni, P. Ciccioli (2000) Dynamic system for the calibration of semi-volatile carbonyl compounds in air, *Journal of Chromatography A*, **883**: 171-183.

Prazeller, P., P. T. Palmer, E. Bocaini, T. Jobson, M. Alexander (2003) Proton transfer reaction ion trap mass spectrometer, *Rapid Communications in Mass Spectrometry*, **17**: 1593-1599.

Richards, W. G., P. R. Scott (1994) *Energy Levels in Atoms and Molecules (Oxford Chemistry Primer Series)*. Oxford: Oxford University Press.

Rønne, C., K. Jensby, B. J. Loughnane, J. Fourkas, O. F. Nielson (2000) Temperature dependence of the dielectric function of $C_6H_6(l)$ and $C_6H_5CH_3(l)$ measured with THz spectroscopy, *Journal of Chemical Physics*, **113** (9): 3749-3756.

Scaringelli, F. P., A. E. O'Keeffe, E. Rosenberg, J. P. Bell (1970) Preparation of known concentrations of gases and vapours with permeation devices calibrated gravimetrically, *Analytical Chemistry*, **42** (8): 871-876

Shaw, S., F. M. Mitloehner, W. Jackson, E. J. Depeters, J. G. Fadel, P. H. Robinson, R. Holzinger, A. H. Goldstein (2007) Volatile organic compound emissions from dairy cows and their waste as measured by proton-transfer-reaction mass spectrometry, *Environmental Science and Technology*, **41**: 1310-1316

Shirts, R. B., (1986) Chapter 2: Collision Theory and Reaction Dynamics. In: *Gaseous Ion Chemistry and Mass Spectrometry*, edited by J. H. Futrell, pages 25-57. John Wiley and Sons, New York.

Smith, D., N. G. Adams (1979) Chapter 1: Recent advances in flow tubes: Measurement of ion-molecule rate coefficients and product distributions. In: *Gas Phase Ion Chemistry Volume 1*, edited by M. T. Bowers, pages 1-44. Academic Press, London.

Smith S. C., M. J. McEwan, K. Giles, D. Smith, N. G. Adams (1990) Unimolecular decomposition of a polyatomic ion in a variable-temperature selected-ion-flow-drift tube: Experiment and theoretical interpretation, *International Journal of Mass Spectrometry and Ion Processes*, **96**: 77-96.

Smith, D., A. M. Diskin, Y. Ji, P. Španěl (2001) Concurrent use of H_3O^+, NO^+, O_2^+ precursor ions for the detection and quantification of diverse trace gases in the presence of air and breath by selected ion-flow tube mass spectrometry, *International Journal of Mass Spectrometry*, **209**: 81-97.

Smith, D., P. Španěl (2005) Selected ion flow tube mass spectrometry (SIFT-MS) for on-line trace gas analysis, *Mass Spectrometry Reviews*, **24**: 661-700.

Španěl, P., D. Smith, M. Henchman (1995a) The reactions of some interstellar ions with benzene, cyclopropane and cyclohexane, *International Journal of Mass Spectrometry and Ion Processes*, 141: 117-126.

Španěl, P., D. Smith (1995b) Reactions of H_3O^+ and OH^- ions with some organic molecules; applications to trace gas analysis in air, *International Journal of Mass Spectrometry and Ion Processes*, **145**: 177-186.

Španěl, P., D. Smith (1995c) Reactions of hydrated hydronium ions and hydrated hydroxide ions with some hydrocarbons and oxygen-bearing organic molecules, *Journal of Physical Chemistry*, **99**: 15551 – 15556.

Španěl, P., D. Smith (1996) Selected ion flow tube: a technique for quantitative trace gas analysis of air and breath, *Medical & Biological Engineering & Computing*, 34: 409 - 419.

Španěl, P., D. Smith (1997) SIFT studies of the reactions of H_3O^+, NO^+ and O_2^+ with a series of alcohols, *International Journal of Mass Spectrometry and Ion Processes*, **167/168**: 375-388.

Španěl, P., D. Smith (1998a) SIFT studies of the reactions of H_3O^+, NO^+ and O_2^+ with a series of volatile carboxylic acids and esters, *International Journal of Mass Spectrometry and Ion Processes*, **172**: 137-147.

Španěl, P., D. Smith (1998b) Selected ion flow tube studies of the reactions of H_3O^+, NO^+ and O_2^+ with several aromatic and aliphatic hydrocarbons, *International Journal of Mass Spectrometry*, **181**: 1-10.

Španěl, P., D. Smith (2000) Influence of water vapour on selected ion flow tube mass spectrometric analyses of trace gases in humid air and breath, *Rapid Communications in Mass Spectrometry*, **14**: 1898-1906.

Španěl, P., D. Smith (2001) Quantitative selected ion flow tube mass spectrometry: The influence of ionic diffusion and mass discrimination, *Journal of the American Society for Mass Spectrometry*, **12**: 863-872.

Španěl, P., K. Dryahina, D. Smith (2006) A general method for the calculation of absolute trace gas concentrations in air and breathe from selected ion flow tube mass spectrometry data, *International Journal of Mass Spectrometry*, **249-250**: 230-239.

Sprig, C., A. Neftel, C. Ammann, J. Dommen, W. Grabmer, A. Thielmann, A. Schaub, J. Beauchamp, A. Wisthaler, A. Hansel (2005) Eddy Covariance flux measurements of biogenic VOCs during ECHO 2003 using proton transfer reaction mass spectrometry, *Atmospheric Chemistry and Physics*, **5**: 465-481.

Sprung, D., C. Joost, T. Reiner, A. Hansel, A. Wisthaler (2001) Acetone and acetonitrile in the tropical Indian ocean boundary layer and free troposphere: aircraft-based intercomparison of AP-CIMS and PTR-MS measurements, *Journal of Geophysical Research*, **106** (D22): 28511-28527.

Steinbacher, M. (2004a) *Volatile Organic Compounds and Their Oxidation Products in the Atmospheric Boundary Layer: Laboratory and Field Experiments*. Thesis (PhD). Swiss Federal Institute of Technology Zurich.

Steinbacher, M., J. Dommen, C. Ammann, C. Sprig, A. Neftel, A. S. H. Prevot (2004b) Performance characteristics of a proton-transfer-reaction mass spectrometer (PTR-MS) derived from the laboratory and field measurements, *International Journal of Mass Spectrometry*, **239**: 117-128.

Su, T., M. T. Bowers (1973a) Ion-polar molecule collisions. Proton transfer reactions of H_3^+ and CH_5^+ to the geometric isomers of difluoroethylene, dichloroethylene, and difluorobenzene, *Journal of the American Chemical Society*, **95** (5) 1370-1373.

Su, T., M. T. Bowers (1973b) Theory of ion-polar molecule collisions. Comparison with experimental charge transfer reactions of rare gas ions to geometric isomers of difluorobenzene and dichloroethylene, *The Journal of Chemical Physics*, **58** (7): 3027-3037.

Su, T., M. T. Bowers (1973c) Ion-polar molecule collisions: The effect of ion size on ion-polar molecule rate constants; the parameterisation of the average-dipole-orientation theory, *International Journal of Mass Spectrometry and Ion Physics*, **12**: 347-356.

Su, T., M. T. Bowers (1974) Ion-polar molecule collisions: Nonreactive collisions of Cl $^-$ with dichloroethylene and difluorobenzene, *The Journal of Chemical Physics*, **60** (12): 4897-4899.

Su, T., M. T. Bowers (1975) Parameterisation of the average dipole orientation theory: Temperature dependence, *International Journal of Mass Spectrometry and Ion Physics*, **17**: 211-212.

Su, T., M. T. Bowers (1979) Chapter 3: Classical ion-molecule collision theory. In: *Gas Phase Ion Chemistry Volume 1*, edited by M. T. Bowers, pages 83-117. Academic Press, London.

Su, T., W. J. Chesnavich (1982) Parameterisation of the ion-polar molecule collision rate constant by trajectory calculations, *Journal of Chemical Physics*, **76** (10): 5183-5185.

Su, T. (1994) Parameterisation of kinetic energy dependences of ion-polar molecule collision rate constants by trajectory calculations, *Journal of Chemical Physics*, **100** (6): 4703.

Sugiura, T. (1962) The secondary-emission electron multiplier tube used on a mass spectrometer and its amplification of ion currents, *Bulletin of the Chemical Society of Japan*, **35** (8): 1257-1262,

Tani, A., S. Hayward, C. N. Hewitt (2003) Measurement of monoterpenes and related compounds by proton transfer reaction-mass spectrometry (PTR-MS), *International Journal of Mass Spectrometry*, **223-224**: 561-578.

Tani, A., S. Hayward, A. Hansel, C. N. Hewitt (2004) Effect of water vapour on monoterpene measurements using proton transfer reaction-mass spectrometry (PTR-MS), *International Journal of Mass Spectrometry*, **239**: 161-169.

Tani, A., S. Kato, Y. Kajii, M. Wilkinson, S. Owen, N. Hewitt (2007) A proton transfer reaction mass spectrometry based system for determining plant uptake of volatile organic compounds, *Atmospheric Environment*, **41**: 1736-1746.

Tanimoto, H., N. Aoki, S. Inomata, J. Hirokawa, Y. Sadanaga (2007) Development of a PTR-TOFMS instrument for real-time measurements of volatile organic compounds in air, *International Journal of Mass Spectrometry*, **263**: 1-11.

Theard, L. P., W. H. Hamill (1961) The energy dependence of cross sections of some ion-molecule reactions, *Journal of the American Chemical Society*, **84**, 1134-1139.

Tokmakov, I. V., M. C. Lin (2002) Kinetics and mechanism of the OH + C_6H_6 Reaction: A Detailed Analysis with First-Principles Calculations, *Journal of Physical Chemistry*, *A*, **106**: 11309-11326.

Uggerud, E. (1992) Properties and reactions of protonated molecules in the gas phase. Experiment and theory, *Mass Spectrometry Reviews*, **11**: 389-430.

Van Beelen E. S. E., T. A. Koblenz, S. Ingemann S. Hammerum (2004) Experimental and Theoretical Evaluation of Proton Affinities of Furan, the Methylphenols, and the Related Anisoles, *Journal of Physical Chemistry A*, **108**: 2787-2793.

Viehland, L. A., S. L. Lin, E. A. Mason (1981) Kinetic theory of drift-tube experiments with polyatomic species, *Chemical Physics*, **54**: 341-364.

Viggiano, A. A., R. A. Morris, F. Dale, J. F. Paulson, K. Giles, D. Smith, T. Su (1990) Kinetic energy, temperature, and derived rotational temperature dependences for the reactions of $Kr^+(^2P_{3/2})$ and Ar^+ with HCl, *Journal of Chemical Physics*, **93** (2), 1149-1157.

Viggiano, A. A., R. A. Morris (1996) Rotational and vibrational energy effects on ion-molecule reactivity as studied by the VT-SIFDT technique, *Journal of Physical Chemistry*, **100**: 19227-19240.

Viggiano, A. A. (2006) Reexamination of ionospheric chemistry: high temperature kinetics, internal energy dependences, unusual isomers, and corrections, *Physical Chemistry Chemical Physics*, **8**: 2557-2571.

Von Hartungen, E., A. Wisthaler, T. Mikoviny, D. Jaksch, E. Boscaini, P. J. Dunphy, T. D. Märk (2004), Proton-transfer-reaction mass spectrometry (PTR-MS) of carboxylic acids Determination of Henry's law constants and axillary odour investigations, *International Journal of Mass Spectrometry*, **239**: 243-248.

Wannier, G. H. (1953) Motion of gaseous ions in strong electric fields, *Bell System Technical Journal*, **32**: 170-254.

Warneke, C., J. Kuczynski, A. Hansel, A. Jordan, W. Vogel, W. Lindinger (1996) Proton transfer reaction mass spectrometry (PTR-MS): propanol in human breath, *International Journal of Mass Spectrometry and Ion Processes*, **154**: 61-70.

Warneke, C., C. van der Veen, S. Luxembourg, J. A. de Gouw, A. Kok (2001) Measurements of benzene and toluene in ambient air using proton-transfer-reaction mass spectrometry: calibration, humidity dependence, and field intercomparison, *International Journal of Mass Spectrometry*, **207**: 167-182.

Warneke, C., J. A. de Gouw, W. C. Custer, P. D. Goldan, R. Fall (2003) Validation of atmospheric VOC measurements by proton-transfer-reaction mass spectrometry using a gas chromatographic preparation method, *Environmental Science and Technology*, **37**: 2494-2501.

Warneke, C., S. Rosén, E. R. Lovejoy, J. A. de Gouw, R. Fall (2004) Two additional advantages of proton transfer ion trap mass spectrometry, *Rapid Communications in Mass Spectrometry,* **18**: 133-134.

Warneke, C., J. A. de Gouw, E. R. Lovejoy, P. C. Murphy, W. C. Kuster (2005a) Development of proton-transfer ion trap-mass spectrometry: On-line detection and identification of volatile organic compounds in air, *Journal of the American Society for Mass Spectrometry*, **16**: 1316-1324

Warneke, C., S. Kato, J. A. de Gouw, P. D. Goldan, W. C. Kuster, M. Shao, E. R. Lovejoy, R. Fall, F. C. Fehsenfeld (2005b) Online volatile organic compound measurements using a newly developed proton-transfer ion-trap mass spectrometry instrument during New England air quality study – intercontinental transport and chemical transformation 2004: Performance, intercompraison, and compound identification, *Environmental Science and Technology*, **39**: 5390 – 5397.

Washenfelder, R.A., C. M. Roehl, K. A. McKinney, R. R. Julian, P. O. Wennberg (2003) A compact, lightweight gas standards generator for permeation tubes, *Review of Scientific Instruments*, **74** (6): 3151-3154.

Williams, S., A. J. Midey, S. T. Arnold, R. A. Morris, A. A. Viggiano, Y. Chiu, D. J. Levandier, R. A. Dressler, M. R. Berman (2000) Electronic, Rovibrational and Translational Energy Effects in Ion-Alkylbenzene Charge-Transfer Reactions, *Journal of Physical Chemistry*, **104**: 10336-10346.

Wróblewski, T., L. Ziemczonek, K. Szerement, G. P. Karwasz (2006) Proton affinities of simple organic compounds, *Czechoslovak Journal of Physics*, **56** (Suppl. B): B1110- B1115.

Wyche, K. P., R. S. Blake, K. A. Willis, P. S. Monks, A. M. Ellis (2005) Differentiation of isobaric compounds using chemical ionization mass spectrometry, *Rapid Communications in Mass Spectrometry*, **19**: 3356 – 3362.

Wyche, K. P., R. S. Blake, A. M. Ellis, P. S. Monks, T. Brauers, R. Koppmann, A. C. Apel (2007) Technical note: performance of chemical ioniazation reaction time-of-flight mass spectrometry (CIR-TOF-MS) for the measurement of atmospherically significant oxygenated volatile organic compounds, *Atmospheric Chemistry and Physics*, **7**: 609-620.

Zhao, J., R. Zhang (2004) Proton transfer reaction rate constants between hydronium ion (H_3O^+) and volatile organic compounds, *Atmospheric Environment*, **38**: 2177-2185.

3 Specification of Proton Transfer Based Chemical Ionisation Mass Spectrometry.

This chapter expands the discussion of the nature and extent of H_3O^+ reaction with trace gas species begun in § 2.9. Literature values of product distributions and reaction efficiencies observed using chemical ionisation swarm based techniques including SIFT, VT-SIFT, SIFDT, PTR-MS, PT-CIMS, PTR-TOF, PT-ITMS (§ 2.1, 2.8) are reviewed for each group of trace organic compounds. The results are collated in a mass chart to indicate the level of isobaric compounds and fragments at each mass and resulting level of specificity in the PTR-MS. This mass chart has been used to identify possible contributors to important masses observed during ambient measurements alongside contextual reasoning and is referred to in chapter 4. The mass chart and compounds not utilised in chapter 4 but analysed as part of the research i.e. alkanes, alkenes, dienes, diyenes and aromatics, are included in digital format.

There are few papers specifically dedicated to the investigation of the reaction products and extent of dissociation occurring in the PTR-MS (e.g. Buhr *et al* 2002, Warneke *et al* 2003). Some fragmentation patterns have been incorporated in the discussion of ambient measurements in the wider PTR-MS literature. This chapter discusses the readily available reported product distributions; it is not a comprehensive review of the fragmentation patterns reported in PTR-MS due to the dispersed nature of the reported fragmentation patterns. Recent studies employing PTR-TOF-MS/CIR-TOF-MS (e.g. Wyche *et al* 2005, Blake *et al* 2006, Aoki *et al* 2007) and PT-ITMS (e.g. Prazeller *et al* 2003, Warneke *et al* 2005a, Karl *et al* 2005) have contributed significantly to the understanding of the nature of H_3O^+ reactions with various (O)VOC under the elevated energy conditions of the drift tube and are included here. A small number of SIFDT investigations of H_3O^+ reactions with (O)VOCs have been performed (Lagg *et al* 1994, Warneke *et al* 1996, Hansel *et al* 1997). These studies provide information about variation of both product distributions and reaction kinetics over a range of $KE_{c.m.}^r$ (Eq. 2.59). The use of a helium buffer compared with air in PTR-MS and the generally lower drift tube pressure should be considered when applying the measured product distributions to PTR-MS at similar $KE_{c.m.}^r$, particularly in the case of reactions where collisional stabilisation or activation is important.

In order to hypothesise the potential dissociation reactions in the PTR-MS where experimental data is not readily available, the thermodynamics of various non-dissociative and dissociative reactions are considered. The thermodynamics of some reactions for which

experimental data exists are used to discuss possible variations with varying drift tube conditions and $KE_{c.m.}^{r}$ (Eq. 2.59).

The Gibbs free energy released from non-dissociative proton transfer reactions, (ΔG_{r}^{Φ}) (§ 2.9.1), combined with the total energy available for reaction, $\langle E_{r} \rangle$ (§ 2.9.2) is an approximation of the energy available for dissociation (§ 2.9). Consider the reaction of propene with H_3O^+; an enthalpy profile considering the non-dissociative and one of the potential dissociation pathways is shown in Figure 3.1.
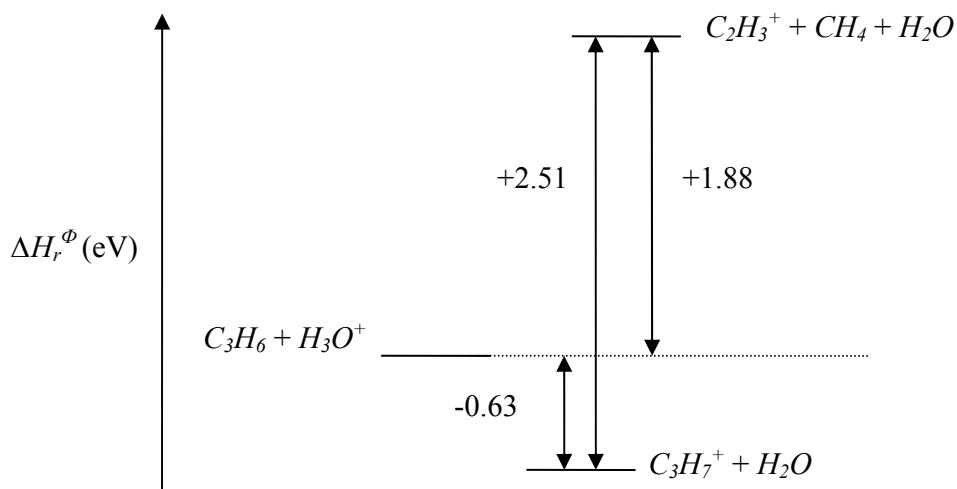
Figure 3.1: The enthalpy profile for the non-dissociative reaction of H_3O^+ with propene and the dissociative reaction to form $C_2H_3^+$.

In the H_3O^+ reaction with propene, 0.63 eV is available from the non-dissociative proton transfer, 2.51 eV is required for dissociation of $C_3H_7^+$ to $C_2H_3^+$ (assuming an in-direct mechanism), i.e. a further 1.88 eV over the enthalpy of non-dissociative reaction. Therefore if $\langle E_{r} \rangle$ is greater than 1.88 eV the reaction may proceed to $C_2H_3^+$. Note that if $\langle E_{r} \rangle$ is exactly 1.88 eV for dissociation to occur the products would be internally cold. This approach assumes that all of $\langle E_{r} \rangle$ and the energy of non-dissociative reaction is available for dissociation. That is, the distribution of $\langle E_{r} \rangle$ in reactants is not important and all forms of energy (rotational, vibrational, translation) affect reactivity equally and no energy is lost in inactive modes such as translation of transient intermediates or radiation.

Consideration of $\langle E_r \rangle$ and exoergicity alone neglects the effects of pressure and buffer which may be important, for example in reactions where collisions with buffer molecules remove energy and prevent dissociation. Whether collisional activation or stabilisation is important will depend on the mechanism of reaction and the lifetime of transient species, e.g. $(MHH_2O)^+*$, compared to collision times in the reaction chamber. In some cases experimental evidence such as the presence or lack of a dependence of product distributions on pressures (at constant reaction energies) is available to indicate the importance of collisional stabilisation or activation and is also discussed.

The thermodynamic discussion of exoergicity and $\langle E_r \rangle$ also ignores any activation energy barrier to dissociation. In some cases literature estimates of activation energies are discussed. Thermodynamic discussions of exoergicity and $\langle E_r \rangle$ generally (with the exception of reactions where collisional activation is involved) provide a lower limit for dissociation below which dissociation can not occur but above which dissociation is not certain.

Since the entropies of dissociation and non-dissociation reactions are largely unknown the standard enthalpies of reaction are generally considered in place of Gibbs free energies; this inherently assumes that entropy is negligible. In cases such as the cyclic alkanes (§ D.1.4) this may not be a valid assumption and entropy considerations are important in the dissociation reactions, where possible potential entropy considerations are discussed.

Standard enthalpies of non-dissociation reaction are calculated from the proton affinities of water and the neutral reactant as discussed in § 2.9.1. Standard enthalpies of reaction, ΔH_r^Φ, of dissociation reactions have been calculated from the relevant standard enthalpies of formation, ΔH_f^Φ, or where available from the literature as referenced. Standard enthalpies of formation of neutrals are taken from Mallard and Linstrom (2005), CRC Handbook of Chemistry and Physics (1986-1987) and Ellis *et al* (1999) as specified. The standard enthalpies of formation of ions are calculated from proton affinities and standard enthalpies of formation where possible, otherwise appearance energies and enthalpies of formation are employed. Proton affinities are taken from Hunter and Lias (1998) unless otherwise specified and appearance energies from Mallard and Linstrom (2005). The appearance energy, *AP*, is the minimum energy required to form a particular fragment ion from a precursor molecule. The calculation of standard enthalpies of a potential dissociation reactions of ethylbenzene are demonstrated below; literature values exist for this compound and are compared. A potential dissociation reaction of ethylbenzene is given in Eq. 3.1, all the reactions and

thermodynamics discussed here refer to the gas phase and (g) subscripts are omitted from equations:

$$C_8H_{10} + H_3O^+ \rightarrow C_7H_7^+ + CH_4 + H_2O \tag{3.1}$$

The standard enthalpy of reaction Eq. 3.1 is given by Eq. 3.2 – 3.3.

$$\Delta H_r^\Phi = \Delta H_f^\Phi(C_7H_7^+) + \Delta H_f^\Phi(CH_4) + \Delta H_f^\Phi(H_2O) - \Delta H_f^\Phi(H_3O^+) - \Delta H_f^\Phi(C_8H_{10}) \tag{3.2}$$

$$\Delta H_r^\Phi = \Delta H_f^\Phi(C_7H_7^+) + -74.85 + -241.8 - \Delta H_f^\Phi(H_3O^+) - 29.8 \tag{3.3}$$

Units of enthalpy values in Eq. 3.3 are kJ mol^{-1}. $\Delta H_f^\Phi(CH_4)$ and $\Delta H_f^\Phi(C_8H_{10})$ are taken from Mallard and Linstrom (2005). $\Delta H_f^\Phi(H_2O)$ is taken from Mallard and Linstrom (2005) and CRC Handbook of Chemistry and Physics (1986-1987).

$\Delta H_f^\Phi(H_3O^+)$ is derived from the proton affinity of H$_2$O, *PA(H$_2$O)*, Eq. 3.4 – 3.7:

$$H_3O^+ \rightarrow H_2O + H^+ \tag{3.4}$$

$$\Delta H_r^\Phi = PA(H_2O) = \Delta H_f^\Phi(H_2O) + \Delta H_f^\Phi(H^+) - \Delta H_f^\Phi(H_3O^+) \tag{3.5}$$

$$\Delta H_f^\Phi(H_3O^+) = \Delta H_f^\Phi(H_2O) + \Delta H_f^\Phi(H^+) - PA(H_2O) \tag{3.6}$$

$$\Delta H_f^\Phi(H_3O^+) = -241.8 + 1536.2 - 691.0 = 603.4 \tag{3.7}$$

Units of enthalpy values in Eq. 3.7 are kJ mol^{-1}. *PA(H$_2$O)* is taken from Hunter and Lias (1998). $\Delta H_f^\Phi(H^+)$ is taken from CRC Handbook of Chemistry and Physics (1986-1987) and compares with values of 1528 kJ mol^{-1} and 1530 kJ mol^{-1} in Mallard and Linstrom (2005), *PA(H$_2$O)* is taken from Hunter and Lias (1998). Hunter and Lias (1998) estimate a $\Delta H_f^\Phi(H_3O^+)$ of 592.6 ± 5 kJ mol^{-1} from the appearance energy of *(H$_2$O)$_2$* but the thermal correction of *NH$_3$* was used as an approximation and there is a large uncertainty in *(H$_2$O)$_2$* binding energies employed. The value was not used by Hunter and Lias (1998) to determine the absolute proton affinity of water due to the uncertainty and the value of 691 (±3) kJ mol^{-1} was instead derived from theoretical calculations and a proton transfer equilibrium measurement.

$\Delta H_f^\Phi(C_7H_7^+)$ is calculated from the appearance energy for formation of $C_7H_7^+$ from ethylbenzene, C_8H_{10}, Eq. 3.8 – 3.11. Accurate values of $\Delta H_f^\Phi(C_7H_7^+)$ require derivation using enthalpies of formation at 0 K alongside *AE* to give a value of the enthalpy of formation of C$_7$H$_7^+$ at 0 K with subsequent correction to 298 K. Here standard enthalpies of

formation (at 298 K) are employed alongside *AE* as an approximation. These values may differ by 12 -18 kJ mol⁻¹ from values calculated using a thorough treatment of temperature dependence (Mallard and Linstrom 2005, Lias *et al* 1988). In many cases this is a relatively small source of error compared to the range of the appearance energies.

$$C_8H_{10} \rightarrow C_7H_7^+ + CH_3 + e^-$$ (3.8)

$$\Delta H_r^\Phi \approx AE \approx \Delta H_f^\Phi(C_7H_7^+) + \Delta H_f^\Phi(CH_3) - \Delta H_f^\Phi(C_8H_{10})$$ (3.9)

$$\Delta H_f^\Phi(C_7H_7^+) \approx AE - H_f^\Phi(CH_3) + \Delta H_f^\Phi(C_8H_{10})$$ (3.10)

$$\Delta H_f^\Phi(C_7H_7^+) \approx AE - 147 + 29.8$$ (3.11)

Units of enthalpy in Eq. 3.11 are kJ mol⁻¹. $\Delta H_f^\Phi(CH_3)$ is taken from Mallard and Linstrom (2005). Note that the ion convention is employed by Mallard and Linstrom (2005) and CRC Handbook of Chemistry and Physics (1986-1987) and the enthalpy of formation of the electron are neglected. A range of *AE* values often exist for a given reaction, a review of the suitability of available *AE* values is beyond the scope of this study, instead the maximum and minimum *AE* values are used to derive the range of ΔH_f^Φ of the ion and consequently ΔH_r^Φ. It is noted that there is sometimes more than one value for the enthalpy of formation of the neutral but the range is generally small compared to that of *AE*. The minimum *AE* of Eq. 3.11 is 9.8 eV which is 945.6 kJ mol⁻¹ and gives a $\Delta H_f^\Phi(C_7H_7^+)$ of 828.4 kJ mol⁻¹, the maximum *AE* value is 11.0 eV which is 1061.4 kJ mol⁻¹ giving a $\Delta H_f^\Phi(C_7H_7^+)$ of 944.2 kJ mol⁻¹. Substituting these values and the $\Delta H_f^\Phi(H_3O^+)$ into Eq. 3.3 gives ΔH_r^Φ = -121.5 to -5.65 kJ mol⁻¹ (-1.26 to – 0.06 eV) the mean of these values is - 63.5 kJ mol⁻¹ (-0.66 eV). Midey *et al* (2002) derived a ΔH_r^Φ value of – 88 kJ mol⁻¹ (-0.91 eV); this is within the range calculated here.

Consider another dissociative reaction of H_3O^+ with ethylbenzene, Eq. 3.12. In this case the ion heats of formation can be derived from proton affinities Eq. 3.12 – 3.17

$$C_8H_{10} + H_3O^+ \rightarrow C_6H_7^+ + C_2H_4 + H_2O$$ (3.12)

$$\Delta H_r^\Phi = \Delta H_f^\Phi(C_6H_7^+) + \Delta H_f^\Phi(C_2H_4) + \Delta H_f^\Phi(H_2O) - \Delta H_f^\Phi(H_3O^+) - \Delta H_f^\Phi(C_8H_{10})$$ (3.13)

$$\Delta H_r^\Phi = \Delta H_f^\Phi(C_6H_7^+) + 52.47 + -241.8 - 603.4 - 29.8$$ (3.14)

Units of values in Eq. 3.14 are kJ mol^{-1}. $\Delta H_f^{\Phi}(C_2H_4)$ is taken from Mallard and Linstrom (2005). $\Delta H_f^{\Phi}(C_6H_7^+)$ is calculated from the proton affinity of benzene, Eq. 3.15 – 3.17

$$C_6H_7^+ \rightarrow C_6H_6 + H^+ \tag{3.15}$$

$$\Delta H_f^{\Phi}(C_6H_7^+) = \Delta H_f^{\Phi}(C_6H_6) + \Delta H_f^{\Phi}(H^+) - PA(C_6H_6) \tag{3.16}$$

$$\Delta H_f^{\Phi}(C_6H_7^+) = 82.93 + 1536.2 - 750.40 = 868.7 \tag{3.17}$$

Units of enthalpies in Eq. 3.17 are kJ mol^{-1}. *PA(C$_6$H$_6$)* is taken from Hunter and Lias (1998). $\Delta H_f^{\Phi}(C_6H_6)$ is taken from Mallard and Linstrom (2005). Substituting the value for $\Delta H_f^{\Phi}(C_6H_7^+)$ into Eq. 3.14 gives $\Delta H_r^{\Phi} = 46.2$ kJ mol^{-1} (0.48 eV). Midey *et al* (2002) derive a value of $\Delta H_r^{\Phi} = 51$ (±~15) kJ mol^{-1} (0.53 eV) in a similar manner.

There is often more than one possible structure for the ion and/or neutral resulting from dissociation. The calculated enthalpy of dissociation reactions is dependent on which structure of the product ion and/or neutral the enthalpies of formation employed correspond to. Where appearance energies for formation of the ion from the reactant neutral (O)VOC under consideration are employed to determine the enthalpy of formation of the ion it is assumed the enthalpy of formation inherently corresponds to the appropriate structure of the product ion. Little consideration has been given to the most stable structures in the proton affinity method used here and values represent first approximations; some discussion of possible ion structures are given later. Values of enthalpies of formation of various cations are also available in Lias *et al* (1984), the majority of these values were calculated from enthalpies of formation of neutrals and proton affinities also given. Enthalpies of formation for a number of cations and neutral molecules from various sources can also be found in Lias *et al* (1988). The values which would be required here from Lias *et al* (1988) were obtained mainly from various appearance energies and proton affinities from Lias *et al* (1984). Proton affinities have been re-evaluated since 1984 by Hunter and Lias (1998); thus these values have been used to calculate enthalpies of formation of cations utilised here alongside appropriate appearance energies from Mallard and Linstrom (2005) where possible. It is notable that for example absolute values of the proton affinities of propene and ethene given by Hunter and Lias (1998) were determined from the mean of experimentally derived enthalpies of formation of $C_3H_7^+$ and $C_2H_5^+$ of 798.86 kJ mol^{-1} (8.28 eV) and 901.8 kJ mol^{-1} (9.35 eV) respectively. The values of enthalpies of formation of $C_3H_7^+$ and $C_2H_5^+$ derived here from the proton affinities of propene and ethene from Hunter and Lias (1998) should therefore be 8.28 eV and 9.35 eV respectively. The values employed here were 8.34 eV and

9.41 eV the difference of ~ 0.06 eV arises from the difference in the enthalpy of formation of H^+ used here and that employed by Hunter and Lias (1998).

It is necessary to comment on the choice of units here and in the preceding chapter, values of $KE^r_{c.m.}$, $KE^b_{c.m.}$, internal energies of neutrals and ions, *PA, GB*, enthalpies, Gibbs free energies, are given in units of electron volts, eV. These units have been chosen for the purposes of ease of comparison of values of $KE^r_{c.m.}$, $KE^b_{c.m.}$ and internal energies of ions and neutrals with enthalpies and Gibbs free energies of reactions when considering dissociation possibilities. It is however important to recognize that the eV for the former $KE^r_{c.m.}$, $KE^b_{c.m.}$ and internal energies of ions and neutrals is an energy, the product of the charge of a proton, *e*, and the unit V, in SI units 1 eV $\sim$ 1.6022 x 10^{-19} J (McGlashan, 1971). For enthalpies of formation, Gibbs free energies, and associated *PA* and *GB* the 'eV' refers to a molar energy equal to $N_A e\ V$ where N_A is the Avogadro constant, under this definition, in SI units 1 eV $\sim$ 96.487 kJ mol^{-1} (McGlashan, 1971). *AE* are given in units of eV in Mallard and Linstrom (2005) where 1 eV $\sim$ 96.487 kJ mol^{-1}. 'eV' units are the frequently used to express both thermodynamic properties such as proton affinities and centre-of-mass kinetic energy values in the SIFDT and PTR-MS literature (e.g. Glosik *et al* 1993, Lagg *et al*, 1994, Hansel *et al* 1999). It is important to be aware of the changing definition of the units when using this literature i.e. whether an energy or molar energy is being considered. ΔH^{Φ}_f values in Mallard and Linstrom (2005) are given in kJ mol^{-1} and proton affinities in Hunter and Lias (1998) are given in kJ mol^{-1} and standard enthalpies of reaction are calculated in kJ mol^{-1} then converted to eV and given to 2 decimal places as in the above example calculation.

$\langle E_r \rangle$ (§ 2.9.2, Eq. 2.91) in the PTR-MS is approximately the sum of the ion neutral reactant centre-of-mass kinetic energy, $KE^r_{c.m.}$ (Eq. 2.59), the ion-buffer centre-of-mass kinetic energy $KE^b_{c.m.}$ (Eq. 2.92) and the internal energy of the neutral reactant (O)VOC (§ 2.9.2). Calculation of the rovibrational energies of the neutral (O)VOC at the temperature of the drift tube is beyond the scope of this study. $KE^r_{c.m.}$ and $KE^b_{c.m.}$ are discussed as an approximation of the ion energy available in the drift tube. The variation of $KE^r_{c.m.}$ with neutral molar mass at *E/N* of 20 to 200 Td and T_{dt} 298 K in air is shown in Figure 3.2. The variation of $KE^b_{c.m.}$ with *E/N* at T_{dt} of 298 K in air is shown in Figure 3.3. Reduced mobilities of H_3O^+ in nitrogen taken from Dotan *et al* (1976) have been employed for calculation of all KE_{ion} (Eq. 2.55 – 2.58) and thereby $KE^b_{c.m.}$ (Eq. 2.92) and $KE^r_{c.m.}$ (Eq. 2.59)

where air (conventional in PTR-MS) or nitrogen buffer has been employed. The average molecular weight of air of 28.9 g mol^{-1} was applied for calculation of KE_{ion} and $KE_{c.m.}^{b}$.
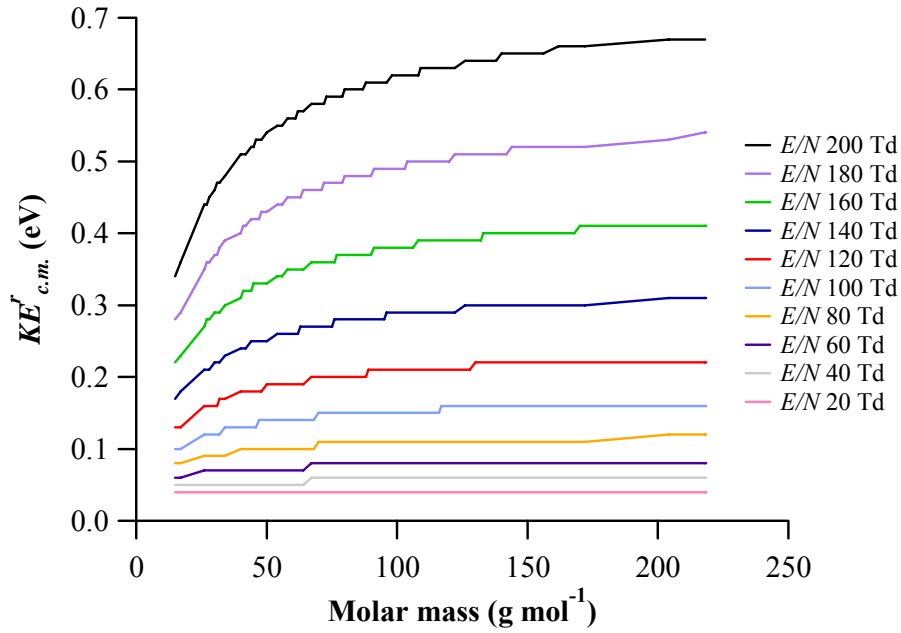
Figure 3.2: The variation of ion neutral reactant centre-of-mass kinetic energy, $KE_{c.m.}^{r}$ (Eq. 2.59) as a function of molar mass of the neutral reactant (O)VOC at various E/N at a T_{dt} of 298 K in air. Reduced mobilities of H_3O^+ in nitrogen used in the calculation of $KE_{c.m.}^{r}$ were taken from Dotan *et al* (1976).
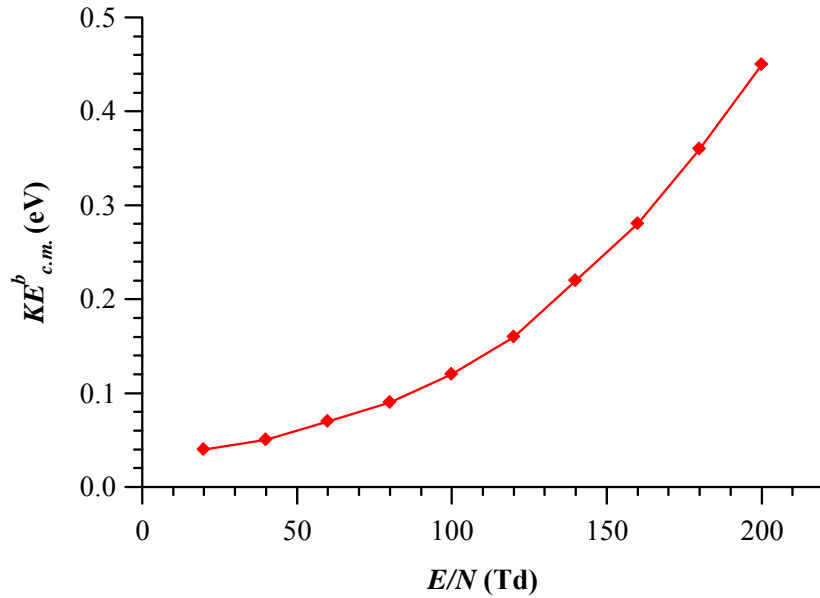
Figure 3.3: The variation of ion-buffer centre-of-mass kinetic energy $KE_{c.m.}^{b}$ (Eq.2.92) as a function of E/N at a T_{dt} of 298 K in air.

Where values of KE_{ion} (Eq. 2.55 – 2.58), $KE_{c.m.}^b$ (Eq. 2.92) or $KE_{c.m.}^r$ (Eq. 2.59) in a helium buffer have been calculated, e.g. for the discussion of SIFDT data, reduced mobilities of H_3O^+ in helium were taken from Dotan *et al* (1977).

Over the last two decades a large number of studies have been dedicated to the investigation of the kinetics and product distributions resulting from the reaction of H_3O^+ (as well as O_2^+ and NO^+) with a large number of trace gas species under the thermal conditions of SIFT at 298 K (e.g. Smith and Španěl 2005 and references within). The change in energy available for reaction, $\Delta\langle E_r \rangle$ in the PTR-MS compared to SIFT can be derived without knowledge of the rovibrational energy of the neutral assuming the drift tube is operated at ~298 K as in SIFT. Recall that in the SIFT $\langle E_r \rangle$, (§ 2.9.2), is given by Eq. 3.18 and in the PTR-MS by Eq. 3.19 (§ 2.9.2), the increase in $\langle E_r \rangle$ is derived by subtracting Eq. 3.18 from Eq. 3.19 giving Eq. 3.20

$$\langle E_r^{SIFT} \rangle = \langle KE \rangle + \langle E_{rot}^{ion-SIFT} \rangle + \langle E_{vib}^{ion-SIFT} \rangle + \langle E_{rot}^{(O)VOC} \rangle + \langle E_{vib}^{(O)VOC} \rangle \tag{3.18}$$

$$\langle E_r^{PTR-MS} \rangle \approx \langle KE_{c.m.}^r \rangle + \langle KE_{c.m.}^b \rangle + \langle E_{rot}^{(O)VOC} \rangle + \langle E_{vib}^{(O)VOC} \rangle \tag{3.19}$$

$$\Delta\langle E_r \rangle = \langle E_r^{PTR-MS} \rangle - \langle E_r^{SIFT} \rangle \approx \left[\langle KE_{c.m.}^r \rangle + \langle KE_{c.m.}^b \rangle \right] - \left[\langle KE \rangle + E_{rot}^{ion\_SIFT} + E_{vib}^{ion\_SIFT} \right] \tag{3.20}$$

where $\langle\ \rangle$ denote that values are an average over the population. $\langle E_{rot}^{(O)VOC} \rangle$ is the rotational energy of the (O)VOC neutral, $\langle E_{vib}^{(O)VOC} \rangle$ is the vibrational energy of the neutral (O)VOC both of which are approximately unchanged in the drift tube assuming the drift tube is at the same temperature as the flow tube of SIFT. *KE* is the ion-molecule kinetic energy in SIFT which is $\frac{3}{2}(k_B T)$, $\langle E_{rot}^{ion-SIFT} \rangle$ is the rotational energy of the ion in SIFT, in this case H_3O^+ and also $\frac{3}{2}(k_B T)$, $\langle E_{vib}^{ion-SIFT} \rangle$ is the vibrational energy of the ion. The $\langle E_{vib}^{ion-SIFT} \rangle$ of H_3O^+ was calculated by rearranging Eq. 3.18 and substituting the appropriate values for toluene-H_3O^+ reaction in the SIFT for which the values have been calculated elsewhere: Midey *et al* (2002) derived a value of $\langle E_r^{SIFT} \rangle$ of 0.21 eV at 298 K where the (O)VOC is toluene and the ion H_3O^+. The rovibrational energy of toluene at 300 K is 0.12 eV (Williams *et al*, 2000), the rotational energy of H_3O^+ is $\frac{3}{2}(k_B T)$ and *KE* is $\frac{3}{2}(k_B T)$, $\frac{3}{2}(k_B T)$ at 298 K is ~0.039 eV. The resultant vibrational energy of H_3O^+ at ~298 K is 0.010 eV (rovibrational energy ~0.049 eV). Substituting these values into Eq. 3.20 gives Eq. 3.21 for the change in energy in the PTR-MS at ~298 K compared to SIFT at ~298 K:

$$\Delta\langle E_r \rangle \approx \left[\langle KE_{c.m.}^r \rangle + \langle KE_{c.m.}^b \rangle \right] - 0.087 \qquad (3.21)$$

Units of all parameters in Eq. 3.21 are eV. $\Delta\langle E_r \rangle$ is displayed in Figure 3.4 as a function of the molar mass of the neutral reactant (O)VOC in the PTR-MS at 298 K with an air buffer across a range of E/N and therefore $KE_{c.m.}^r$ and $KE_{c.m.}^b$.
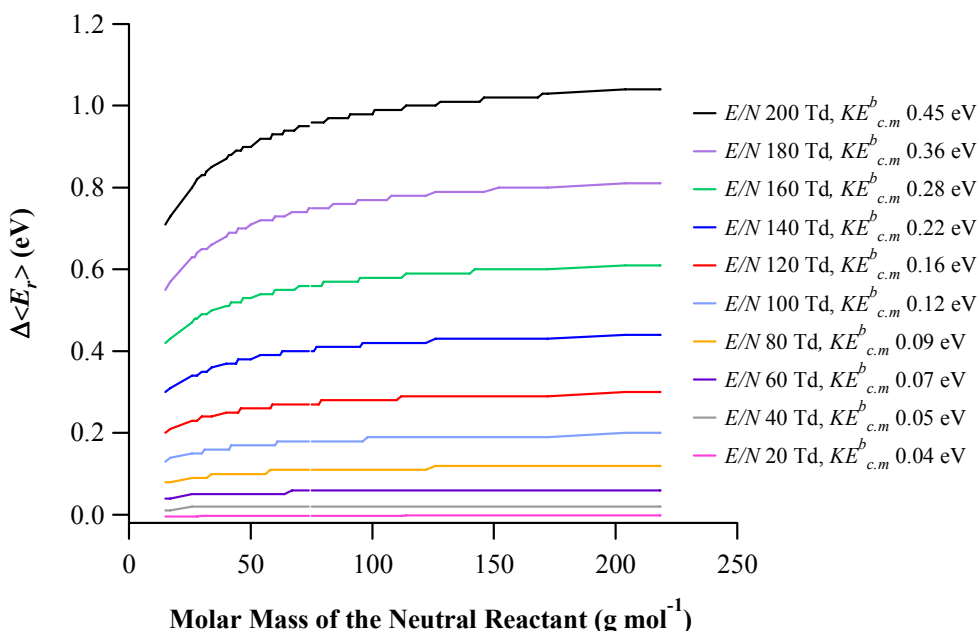
Figure 3.4: $\Delta\langle E_r \rangle$ in the PTR-MS at 298 K in air as a function on molar mass of the neutral reactant over a range of $KE_{c.m.}^r$ and $KE_{c.m.}^b$ corresponding to a range of E/N relative to the thermal conditions of SIFT at 298 K.

The temperature of the drift tube is normally operated at greater than 298 K to minimize instrument background, reduce (O)VOC losses to surfaces and sometimes to prevent water condensation. The true $\Delta\langle E_r \rangle$ is then greater than that calculated from Eq. 3.21 since the ion-molecule kinetic energy, the rovibrational energy of the ion and in this case the rovibrational energy of neutral are increased. In the model of PTR-MS used here, the maximum temperature the drift tube can be operated at is 353 K and $\Delta\langle E_r \rangle$ calculated from Eq. 3.21 is discussed as a best approximation.

The reaction of H_3O^+ with a number of trace organics has been studied at elevated temperatures in VT-SIFT (Midey *et al* 2002, 2003, Arnold *et al* 1998). Product distributions and kinetic data in the VT-SIFT are generally given as a function of $\langle E_r \rangle$ (Eq. 3.91, § 2.9.2) (Midey *et al* 2002, 2003). Results from VT-SIFT where the increase in $\langle E_r \rangle$ due to

increasing temperature is comparable to $\Delta\langle E_r\rangle$ in the PTR-MS at various E/N are used to approximate product distributions and reaction efficiencies in the PTR-MS at these E/N. The inherent assumption of this approach is that the distribution of energy ($\Delta\langle E_r\rangle$) is not important.

Another method of increasing the energy available for proton transfer is to employ a reagent ion of lower proton affinity (Milligan *et al* 2002, Španěl *et al* 1995a). In this case the energy comes from the increased exoergicity of the non-dissociative and dissociative reactions.

In this study product distributions from proton transfer reactions of a given neutral (O)VOC with H_3O^+ at increased temperatures and from reactions of that given neutral with other reagent ions are presented as a function of change in energy relative to reaction with H_3O^+ at 298 K. The product distributions of reaction with H_3O^+ at 298 K thus correspond to zero change in energy of reaction. Product distributions in the PTR-MS under varying drift tube conditions can then be approximated by comparison with distributions at similar change in energies of reaction relative to reaction with H_3O^+ at 298 K. The change in energy of reaction in PTR-MS is approximated by $\Delta\langle E_r\rangle$ derived from Eq. 3.21. In the case of H_3O^+ reactions at increasing temperature in VT-SIFT, the change in energy of reaction corresponds to $\langle E_r^{SIFT}\rangle$ at the elevated temperature minus $\langle E_r^{SIFT}\rangle$ (Eq. 3.18) at 298 K. It is assumed that any change in exoergicity resulting from the increased temperature is small and is neglected. Where energy has been increased by differing reagent ion at 298 K, the change in energy of reaction relative to reaction with H_3O^+ at 298 K corresponds to the difference in exoergicity of the reaction compared with H_3O^+ reaction ($GB(H_2O) - GB$(reagent ion)). The implicit assumption is that the change in $\langle E_r\rangle$ resulting from the change in reagent ion is small, i.e. that the internal rovibrational energy of the ion is not significantly different to that of H_3O^+. Unlike product distributions, the variation of efficiencies with the increase in exoergicity due to change in reagent ion are not compared with increases in energy due to temperature or application of the electric field. Thermodynamics, thermokinetic trends and where available VT-SIFT data are used to discuss potential variation of reaction efficiency with increased energy in the drift tube.

Dissociations discussed to this point have referred to indirect dissociation reactions proceeding through the non-dissociative product, MH^+, (e.g. Figure 3.1) as observed in many proton transfer reactions (Milligan *et al*, 2002). Some reactions such as hydrogen loss from MH^+ may actually occur directly e.g. by hydride transfer from the neutral, M (Milligan

et al, 2002, Midey *et al* 2002, Španěl *et al* 1995a). In the case of H_3O^+ reactions the neutral products resulting from the direct hydride transfer or indirect loss of hydrogen are unchanged and the reactions are thermodynamically equivalent (in the absence of energy/entropy barriers). However, consider for example the reaction of $C_2H_3^+$ with cyclopropane, $c\text{-}C_3H_6$, Španěl *et al* 1995a), indirect dissociation by loss of hydrogen from the non-dissociated product produces $C_3H_5^+$, H_2 and C_2H_2, analogous to the production of $C_3H_5^+$, H_2 and H_2O in the reaction of H_3O^+, but a direct hydride transfer reaction can occur producing $C_3H_5^+$ and C_2H_4. In this case, the indirect reaction is endothermic while the direct hydride transfer reaction is exothermic and 1.18 eV more thermodynamically favourable (neglecting entropy) than dissociative proton transfer. Thus the percentage production of $C_3H_5^+$ observed from reaction of $C_2H_2^+$ with $c\text{-}C_3H_6$ cannot be expected from H_3O^+ reaction with $c\text{-}C_3H_6$ by increasing the energy (by increasing temperature or application of an electric field) by an amount equivalent to $GB(H_3O^+)\text{-}GB(C_2H_3^+)$. Inference of product distributions in the PTR-MS by comparison with distributions resulting from similar increases in energy due to variation of reagent ion assumes that the product ions are produced *via* an analogous reaction to that of H_3O^+ with the equivalent neutral products. Where collisional stabilization or activation is involved, the product distributions may also differ from those inferred from SIFT (by variation of reagent ion) and VT-SIFT product distributions since the discussions of thermodynamic and reaction energies do not always consider changes in buffer and pressure in the reaction chamber.

Electron ionisation mass spectrometry (EI-MS) offers some insight into dissociation of positive ions of (O)VOCs and potential fragments in the PTR-MS. Some EI-MS dissociation patterns are discussed; however, the energies involved in EI-MS are much greater than those in PTR-MS. On impact with a neutral, the high energy electron beam (~70 eV) employed in EI-MS transfers ~ 20 eV, ionisation by loss of an electron requires ~ 15 eV and leaves ~5 eV for fragmentation (Harwood and Claridge 1997). This is a relatively large amount of energy compared with that available from $\langle E_r \rangle$ under normal operating conditions of the PTR-MS (e.g. ~ 0.49 eV for toluene with H_3O^+ at E/N 120 Td, P_{dt} 2.0 mbar, T_{dt} 298 K from Eq. 3.19 and roviibrational energy of toluene from Williams *et al* 2000) and the exoergicity of the non-dissociative reaction (e.g. -0.96 eV for the reaction of toluene with H_3O^+). As discussed in § 2.1, the 'soft' ionisation of chemical ionisation mass spectrometry, even in the drift tube, compared to EI is the factor which sets this technique apart from EI-MS for quantification of trace gas species (as opposed to molecular structure determination) (Munson and Field 1966). EI-MS percentage product distributions discussed here are calculated from peak tables given in JCAMP-DX EI-MS in Mallard and Linstrom (2005) and given to one decimal place.

Results of comparisons of measured *versus* calculated (Eq. 2. 11) sensitivities (§ 2.2) can provide information about fragmentation and efficiency of reaction. Comparisons must consider experimental uncertainties resulting from uncertainty in calibration and uncertainties in calculated sensitivity (§ 2.2) resulting from uncertainties in k (e.g. uncertainties in polarizability and dipole, § 2.4), t (e.g. uncertainties in drift tube length or K_0, § 2.5) and detection efficiencies (standard deviation in measured values § 2.7) and differences greater than the uncertainties are generally discussed. If the efficiency of a reaction is less than one, the measured sensitivity will be less than the sensitivity calculated using the collisional rate constant (Eq. 2.11). Likewise if fragmentation is occurring to some m/z not included with the count rates used to derive the measured sensitivity, the measured sensitivity will be less than the calculated sensitivity. Conversely if the extent of fragmentation is overestimated in the measured sensitivity, the measured sensitivity will exceed the calculated sensitivity. However, as discussed in § 2.2, a number of other factors may result in differences in the measured and calculated sensitivities: The calculated sensitivities of (O)VOCs which do not react with $H_3O^+(H_2O)_n$ clusters may be larger than the measured sensitivity due to overestimation of the H_3O^+ count rates in the calculated sensitivity as a result of $H_3O^+(H_2O)_n$ dissociation between the drift tube and detection. The calculated sensitivities of (O)VOCs which do react with $H_3O^+(H_2O)_n$ will be less than the measured sensitivity unless $H_3O^+(H_2O)_n$ are included as reagent ions or a humidity correction applied. The accuracy of the model of calculation of k, t, and detection efficiencies used to calculate sensitivities may affect agreement between calculated and measured sensitivities. For example inaccuracies in calculated sensitivities may result from the use of thermal collisional rate constant (§ 2.4.1.5), use of K_0 measured in nitrogen rather than air to derive v_d and t (§ 2.5) and/or application of detection efficiencies derived assuming ions traverse the drift tube with the same efficiency (§ 2.7).

Comparisons of ambient measurements using GC, GC-MS or alternative methods of (O)VOC measurement with PTR-MS provide insight as to whether dissociation to m/z other than those used for concentration determination may be occurring and are discussed where available in the literature. Volume mixing ratios (VMRs) derived from PTR-MS are usually compared with those from an alternative technique using a scatter plot, where the VMR of the alternative technique are plotted on the abscissa. Three important parameters are derived from linear fits of the data; the correlation coefficient, intercept and gradient (e.g. de Gouw and Warneke 2007). The intercept at the ordinate may give some indication of the accuracy of the PTR-MS background measurement. A negative intercept could be due to overestimation of the instrument background. Overestimation of the background would

result from the presence of species at the m/z of interest in the 'zero' air sampled during background measurement. The variability of instrument background and frequency of measurement may also be important. A positive intercept may indicate an underestimation of the instrument background or, more likely, contributions to the m/z of interest from other compounds. The gradient is most useful for the purposes of fragmentation discussions. A gradient of one would indicate the VMRs of the two techniques are in agreement. A gradient of less than one indicates that the PTR-MS mixing ratios are generally less than those derived from the alternative technique. Possible explanations for a gradient of less than one include the uncertainty in the PTR-MS sensitivity i.e. either uncertainty associated with calibration (§ 2.2) or uncertainty in the calculated values due to uncertainties in (§ 2.4.1), t (§ 2.5) or detection efficiencies (§ 2.7). If PTR-MS VMRs are derived by calculation, inaccuracies of the model of derivation of k_c (§ 2.4.1), t (§ 2.5) or detection efficiencies (§ 2.7) may also result in a gradient of <1. Otherwise a gradient of less than one may be indicative of fragmentation of the compound of interest to some m/z not included the calculation of VMRs of that compound. A gradient of greater than one indicates VMRs determined by the alternative technique are generally less than VMRs derived by PTR-MS. The uncertainties and inaccuracies may also contribute to a gradient greater than one, losses in the alternative technique, e.g. to canister walls in off-line GC sampling, by reaction with ozone during pre-concentration for GC measurement, or may suggest interference from another compound at the m/z used to derive concentrations of the compound of interest in PTR-MS. Uncertainties in the alternative technique may also contribute to a gradient other than one.

A brief discussion of the possibility of product ion hydrate formation (§ 2.6) and $H_3O^+(H_2O)_n$ reactions (§ 2.6) with the (O)VOCs is given for each group of compounds. The possibility of proton transfer from $H_3O^+(H_2O)_n$ is evaluated by comparison of proton affinities of the (O)VOCs with those of the $H_3O^+(H_2O)_n$ clusters. The proton affinities of $H_3O^+(H_2O)_n$ clusters have been determined in the following manner, considering the $n=1$ cluster: The proton affinity of $H_3O^+(H_2O)$ is the standard enthalpy of reaction Eq. 3.22 which is given by Eq. 3.23:

$$H_3O^+(H_2O) \rightarrow H^+ + 2H_2O \tag{3.22}$$

$$\Delta H_r^{\Phi} = \Delta H_f^{\Phi}(H^+) + 2\Delta H_f^{\Phi}(H_2O) - \Delta H_f^{\Phi}(H_3O^+(H_2O)) \tag{3.23}$$

The standard enthalpy of formation of $H_3O^+(H_2O)$ is calculated from the standard enthalpy of reaction Eq. 3.24 *via* Eq. 3.25 - 3.26

$$H_3O^+ + H_2O \rightarrow H_3O^+(H_2O) \tag{3.24}$$

$$H_f^{\Phi}(H_3O^+(H_2O)) = \Delta H_r^{\Phi} + \Delta H_f^{\Phi}(H_2O) + \Delta H_f^{\Phi}(H_3O^+) \tag{3.25}$$
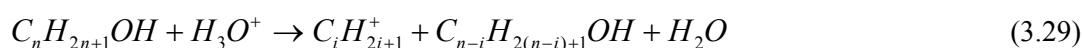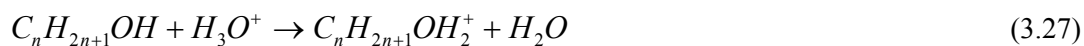
$$H_f^{\Phi}(H_3O^+(H_2O)) = -136 + +603.4 + -241.8 = 225.6 \tag{3.26}$$

The values in Eq. 3.26 have units kJ mol^{-1}. The ΔH_r^{Φ} of reaction Eq. 3.24 (-136 ± 9 kJ mol^{-1}) is taken from Mallard and Linstrom (2005) and is the average of a number of values in the literature. Substituting this value of $H_f^{\Phi}(H_3O^+(H_2O))$ and the values of $\Delta H_f^{\Phi}(H_2O)$ of -241.8 kJ mol^{-1} (Mallard and Linstrom 2005) and $\Delta H_f^{\Phi}(H^+)$ of 1536.2 kJ mol^{-1} (CRC Handbook of Chemistry and Physics 1986-1987) into Eq. 3.23 gives a ΔH_r^{Φ}, i.e. proton affinity, of 827.0 kJ mol^{-1} (8.57 eV). Applying the same method to the n=2 and n=3 clusters, taking the enthalpies of reaction of $H_3O^+(H_2O)_n$ (n= 1 and 2 respectively) with H_2O to form $H_3O^+(H_2O)_{n+1}$ (equivalent to ΔH_r^{Φ} of Eq. 3.24) from Mallard and Linstrom 2005, and using calculated $H_3O^+(H_2O)_n$ enthalpy of formation gives proton affinities of 911.0 kJ mol^{-1} (9.44 eV) and 984.0 kJ mol^{-1} (10.20 eV) respectively.

3.1 Alcohols and Diols

3.1.1 Saturated Alcohols

The available proton affinities, gas basicities and resultant standard reaction enthalpy, entropy and Gibbs free energies for the non-dissociative proton transfer reaction of H_3O^+ with various alcohols are reviewed in Table 3.1. The reaction efficiencies and product distributions of saturated alcohols in SIFT are collated in Table 3.2. The non-dissociative reactions of the alcohols with H_3O^+ are exothermic by greater than 0.43 eV (Table 3.1) and the reactions are efficient at 298 K under the thermal conditions of SIFT (Table 3.2). The proton affinity and gas basicity of the alcohols increases with increasing number of carbons and the reaction with H_3O^+ is increasingly exothermic and exoergic.

Three reactions are observed in SIFT at 298 K; non-dissociative (Eq. 3.27), dissociative elimination of H_2O (Eq. 3.28) and dissociation to a carbocation and a smaller alcohol (Eq. 3.29)

$$C_nH_{2n+1}OH + H_3O^+ \rightarrow C_nH_{2n+1}OH_2^+ + H_2O \tag{3.27}$$

$$C_nH_{2n+1}OH + H_3O^+ \rightarrow C_nH_{2n+1}^+ + 2H_2O \tag{3.28}$$

$$C_nH_{2n+1}OH + H_3O^+ \rightarrow C_iH_{2i+1}^+ + C_{n-i}H_{2(n-i)+1}OH + H_2O \tag{3.29}$$

The enthalpies of some potential dissociative reactions of alcohols with H_3O^+ are given in Table 3.3

Table 3.1: A compilation of proton affinities (*PA*), gas basicities (*GB*), potential standard enthalpy (ΔH_r^Φ), potential standard entropy (ΔS_r^Φ) and Gibbs free energies (ΔG_r^Φ) of the non-dissociative H_3O^+ reaction with saturated alcohols.

Compound	*PA* (eV)	*GB* (eV)	ΔH_r^Φ (eV)	ΔS_r^Φ (x10^{-4}eV K^{-1})	ΔG_r^Φ (eV)
Methanol	7.82	7.51	-0.66	0.42	-0.67
Ethanol	8.05	7.73	-0.89	0.21	-0.89
1-Propanol (*n*-propanol)	8.15	7.84	-0.99	0.21	-1.00
2-Propanol (*iso*-propanol)	8.22	7.90	-1.06	0.21	-1.06
1-Butanol (*n*-butanol)	8.18	7.87	-1.02	0.24	-1.03
2 -Butanol (*iso*-butanol)	8.45	8.13	-1.29	0.21	-1.29
2-Methyl-1-propanol	8.23	7.90	-1.06	-0.17	-1.06
2-Methyl-2-propanol	8.32	8.00	-1.16	0.21	-1.16
1-Pentanol	8.18[a]		-1.02		
1-Hexanol	8.29[a]		-1.13		

Note: Proton affinities and gas basicities are taken from Hunter and Lias, (1998) unless otherwise specified; [a]proton affinities from Wróblewski *et al* (2006) derived from *ab initio* calculations assuming protonation at the oxygen. ΔG_r^Φ and ΔH_r^Φ are calculated from Eq. 2.88 and 2.89, ΔS_r^Φ are calculated from $\Delta S_r^\Phi = \left[\Delta H_r^\Phi - \Delta G_r^\Phi\right]/T$.

Table 3.2: Product distributions and reaction efficiencies of H_3O^+ with various saturated alcohols in SIFT at ~298 K.

Saturated Alcohol ($C_nH_{2n+1}OH$)	P_{FT} (mbar)	T_{FT} (K)	k_m (x 10^{-9} m^3 s^1)	k_m/k_c	Observed Product Distribution : Product Ion (m/z): Percentage of Product Total, $C_nH_{2n+1}OH + H_3O^+ \rightarrow$				Reference
					$C_nH_{2n+1}OH_2^+ + H_2O$	$C_nH_{2n+1}^+ + 2H_2O$	$C_iH_{2i+1}^+ + H_2O + C_{n-i}H_{2(n-i)+1}OH$	Other	
Methanol (CH_3OH)	[a]0.67 [b]0.67 [c]0.27 [d]NS	[a]N/O [b]300 [c]NS [d]NS	[b]2.1 [c]~2.5 [d]2.2	[b]0.78 [c]0.96 [d]0.81	$CH_3OH_2^+$ (33): [a,b,c]**100**				[a]Španěl and Smith (1997) [b]Španěl *et al* (1995b) [c]Lagg *et al* (1994) [d]Lindinger *et al* (1998)
Ethanol (C_2H_5OH)	[a]0.67 [b]0.67 [c]0.27 [d]NS	[a]N/O [b]300 [c]NS [d]NS	[b]2.7 [c]~2.5 [d]2.8	[b]1.0 [c]0.96 [d]1.0	$C_2H_5OH_2^+$ (47): [a,b,c]**100**				[a]Španěl and Smith (1997) [b]Španěl *et al* (1995b) [c]Lagg *et al* (1994) [d]Lindinger *et al* (1998)
1-Propanol (n-C_3H_7OH)	[a]0.67 [b]NS [c]0.93 [d]NS	[a]N/O [b]NS [c]RT: 296 – 300 [d]NS	[b]~2.1 [d]2.3	[b]0.81 [d]0.85	$C_3H_7OH_2^+$ (61): [a]**10**, [b]**8** [c*]**20**	$C_3H_7^+$ (43): [a]**90**, [b]**92**, [c*]**75**, [c**]**45**		$C_3H_7OH.H_3O^+$ (79): [c*]**5**, [c**]**5** - also $C_3H_7OH_2^+$. H_2O $C_3H_7OH_2^+$ $(H_2O)_2$ (97): [c**]**50**	[a]Španěl and Smith (1997) [b]Warneke *et al* (1996) [c]Wang *et al* (2006) [d]Lindinger *et al* (1998)

Table 3.2 is continued on the following page.

Saturated Alcohol $C_nH_{2n+1}OH$)	P_{FT} (mbar)	T_{FT} (K)	k_m (x 10^{-9} m^3 s^{-1})	k_m/k_c	Observed Product Distribution : Product Ion (m/z): Percentage of Product Total, $C_nH_{2n+1}OH + H_3O^+ \rightarrow$				Reference
					$C_nH_{2n+1}OH_2^+$ $+ H_2O$	$C_nH_{2n+1}^+ +$ $2H_2O$	$C_iH_{2i+1}^+ + H_2O$ $+ C_{n-i}H_{2(n-i)+1}OH$	Other	
2-Propanol (i-C$_3$H$_7$OH)	[a]0.67 [b]NS [c]0.93 [d]NS	[a]N/O [b]NS [c]RT: 296 – 300 [d]NS	[b]~2.0 [d]2.8	[b]0.77 [d]1.0	C$_3$H$_7$OH$_2^+$ (61):[a]**20**, [b]**22** [c]***35,**	C$_3$H$_7^+$ (43): [a]**80**, [b]**78** , [c]***60,** [c]****45**		C$_3$H$_7$OH.H$_3$O$^+$ (79):[c]***5, [c]****15 -** also C$_3$H$_7$OH$_2^+$. H$_2$O C$_3$H$_7$OH$_2^+$ (H$_2$O)$_2$ (97):[c]****40**	[a]Španěl and Smith (1997) [b]Warneke *et al* (1996) [c]Wang *et al* (2006) [d]Lindinger *et al* (1998)
1-Butanol (n-C$_4$H$_9$OH)	0.67	N/O			C$_4$H$_9$OH$_2^+$ (75):**5**	C$_4$H$_9^+$ (57): **95**			Španěl and Smith (1997)
2-Methyl-1-propanol (C$_4$H$_9$OH)	0.67	N/O				C$_4$H$_9^+$ (57): **100**			Španěl and Smith (1997)
2-Butanol (C$_4$H$_9$OH)	0.67	N/O			C$_4$H$_9$OH$_2^+$ (75):**5**	C$_4$H$_9^+$ (57): **95**			Španěl and Smith (1997)
2-Methyl-2-propanol (t-C$_4$H$_9$OH)	0.67	N/O				C$_4$H$_9^+$ (57): **100**			Španěl and Smith (1997)
1-Pentanol (C$_5$H$_{11}$OH)	0.67	N/O				C$_5$H$_{11}^+$ (71): **100**			Španěl and Smith (1997)
3-Methyl-1-butanol (C$_5$H$_{11}$OH)	[a]0.67 [b]0.9	[a]N/O [b]296-300				C$_5$H$_{11}^+$ (71): [a]**100** [b]***100**			[a]Španěl and Smith (1997) [b]Wang *et al* (2004)
3-Pentanol (C$_5$H$_{11}$OH)	0.67	N/O				C$_5$H$_{11}^+$ (71): **100**			Španěl and Smith (1997)

Table 3.2 is continued on the following page.

Saturated Alcohol ($C_nH_{2n+1}OH$)	P_{FT} (mbar)	T_{FT} (K)	k_m (x 10^{-9}m^3 s^{-1})	k_m/k_c	Observed Product Distribution : Product Ion (m/z): Percentage of Product Total, $C_nH_{2n+1}OH + H_3O^+ \rightarrow$				Reference
					$C_nH_{2n+1}OH_2^+$ $+H_2O$	$C_nH_{2n+1}^+ +$ $2H_2O$	$C_iH_{2i+1}^+ + H_2O$ $+ C_{n-i}H_{2(n-i)+1}OH$	Other	
2-Methyl-2-butanol ($C_5H_{11}OH$)	0.67	N/O					$C_5H_{11}^+$ (71): **100**		Španěl and Smith (1997)
1-Hexanol ($C_6H_{13}OH$)	[a]0.67 [b]0.67	[a]N/O [b]~300	[b]2.6	[b]0.90			$C_6H_{13}^+$ (85): [a]**100** [b]+ ^{13}C + ^{18}O isotope:**100**		[a]Španěl and Smith (1997) [b]Custer et al (2003)
2-Heptanol ($C_7H_{15}OH$)	0.9	296-300					$C_7H_{15}^+$ (99): *****90**	$C_4H_9^+$ (57): **10**	Wang et al (2004)
2-Heptanol ($C_7H_{15}OH$)	0.9	296-300					$C_7H_{15}^+$ (99): *****90**	$C_4H_9^+$ (57): **10**	Wang et al (2004)
1-Octanol ($C_8H_{17}OH$)	0.67	N/O					$C_8H_{17}^+$ (113): **40**	$C_4H_9^+$ (57): **25** $C_5H_{11}^+$ (71): **35**	Španěl and Smith (1997)
2-Octanol ($C_8H_{17}OH$)	0.67	N/O					$C_8H_{17}^+$ (113): **75**	$C_4H_9^+$ (57): **10** $C_5H_{11}^+$ (71): **15**	Španěl and Smith (1997)

Note: Values from Lagg et al (1994) and Warneke et al (1996) were obtained in SIFDT as a function of $KE_{c.m.}^r$, however the values specified here correspond to approximately thermal conditions ($KE_{c.m.}^r \sim 3/2k_BT$) as in SIFT. P_{FT} denotes pressure in the flow tube, T_{FT} denotes temperature in the flow tube, N/O denotes normal operating conditions, in the case of T_{FT} this is ~298 – 300 K, NS indicates that a value is not specified in the cited reference. A helium carrier gas was used in all cases. Unless specified humidity is unknown: * product distributions were derived using a dry air/alcohol mixture in helium carrier gas, **values were obtained using a moist air (water vapour content ~6 %) /alcohol mixture in helium carrier gas. Wang et al (2004) obtained values in dry air as indicated but also in air at relative humidity of ~ 1.5 % and 6 %, in these cases (2-methyl-1-butanol and 2-heptanol) product distributions were unaffected by humidity since the carbocations produced do not associate with water (§ 3.1.3 and 3.3.2). k_m denotes the rate constant measured for the reaction of H_3O^+ with the saturated alcohol, k_c refers to the collisional rate constant (§ 2.4.1), k_m/k_c is the reaction efficiency. The collisional rate constant was derived using the results of Su and Chesnavich trajectory calculations (§ 2.4.1.4, Eq. 2.49 – 2.54) in the cited references, values were not given in Warneke et al (1996) and Lagg et al (1994) and were calculated here from Su and Chesnavich theory at 298 K. The rate constants were not measured by Španěl and Smith (1997) in many of the references cited here as experimental determination of rate constants is hampered by the inability to obtain known stable concentrations in the relevant range due to adsorption of the OVOCs (Španěl and Smith, 1997). The reactions are sufficiently exothermic (§ 2.9) to assume

efficient proton transfer and comparison with NO^+ and O_2^+ reaction kinetics corroborate the validity of this assumption (Španěl and Smith 1997). Lindinger *et al* (1998) specify measured thermal rate constants, no measurement conditions are specified. Uncertainty of the measured rate constants in Custer *et al* (2003) is ~ 19%, uncertainty of measured rate constants in Španěl *et al* (1995b), Lagg *et al* (1994) or Warneke *et al* (1996) were not specified but are usually ~ 15 -20 % in SIFT. Uncertainty of calculated collisional rate constants are not given but are usually ~ 20 – 25 %

Table 3.3: The standard (298 K) enthalpies of reaction of potential dissociative proton transfer reactions of various saturated alcohols with H_3O^+.

| Alcohol ($C_nH_{2n+1}OH$) $\sum KE_{c.m}^r + KE_{c.m}^b$ *	Product ion (m/z, *percentage product abundance from EI-MS*) ΔH_r^Φ (eV) $C_nH_{2n+1}OH + H_3O^+ \rightarrow$					
	$C_nH_{2n+1}^+ + 2H_2O$	$C_nH_{2n+1}O^+ + H_2 + H_2O$	$C_iH_{2i+1}^+ + H_2O + C_{n-i}H_{2(n-i)+1}OH$	$C_iH_{2i-1}O^+ + H_2O + H_2 + C_{n-i}H_{2(n-i)+2}$	$C_iH_{2i+1}O^+ + H_2O + C_{n-i}H_{2(n-i)+2}$	$C_iH_{2i+1}^+ + 2H_2O + C_{n-i}H_{2(n-i)}$
Methanol (CH₃OH) 0.33 to 0.44	CH_3^+ (15, *5*) +1.83 to +2.19[a]	CH_3O^+ (31, *40.5*) -0.62 to +0.91[a]				
Ethanol (C₂H₅OH) 0.34 to 0.47	$C_2H_5^+$ (29, *10.6*) +0.59[b]	$C_2H_5O^+$ (45, *8.2*) -0.42 to -0.15[a] -0.13[b]		COH^+ (29) +1.46 to +2.88[c] +1.52 to +3.26[b]	CH_3O^+ (31, *35.4*) +0.09 to +0.40[a]	
1-Propanol (C₃H₇OH) 0.35 to 0.48	$C_3H_7^+$ (43, *1.9*) -0.27[b] -0.34 to +0.67[c]	$C_3H_7O^+$ (59, *5.1*) -0.82 to -0.21[a] -0.29[b]	$C_2H_5^+$ (29, *8.3*) +1.22[b]	$C_2H_3O^+$ (43) -0.21 to +1.83[c] COH^+ (29) +1.64 to +3.38[b] +1.58 to +3.00[c]	CH_3O^+ (31, *46.9*) +0.25 to +2.34[a]	
1-Butanol (C₄H₉OH) 0.36 to 0.49	$C_4H_9^+$ (57, *1.2*) -0.33[b] -1.21 to +0.40[c]	$C_4H_9O^+$ (73, *0.2*) -0.38[b]	$C_3H_7^+$ (43, *10.6*) +0.37[b] +0.31 to +1.31[c]	$C_3H_5O^+$ (57) -0.54 to -0.11[c] $C_2H_3O^+$ (43) +0.01 to +1.96[c]	CH_3O^+ (31, *15.3*) +0.43 to +0.55[a]	
1-Pentanol (C₅H₁₁OH) 0.36 to 0.50	$C_5H_{11}^+$ (71, *0.8*) -1.35 to +0.21[c]	$C_5H_{11}O^+$ (87, *0.1*) -1.27 to +0.03[c]	$C_3H_7^+$ (43, *4.4*) +0.21[b] +0.14 to +1.15[c] $C_4H_9^+$ (57, *4.5*) +0.29[b] -0.59 to +1.02[c]	$C_4H_7O^+$ (71) -0.73 to +0.10[c] $C_3H_5O^+$ (57) -0.44 to +0.09[c] $C_2H_3O^+$ (43) ~0 to +1.94[c]		$C_3H_7^+$ (43) +0.71[b]
1-Hexanol (C₆H₁₃OH) 0.37 to 0.51	$C_6H_{13}^+$ (85, *0.1*) -0.85[b]	$C_6H_{13}O^+$ (101) -1.40 to +1.50[c]	$C_3H_7^+$ (43, *12.5*) +0.21[b] +0.15 to +1.15[c] $C_4H_9^+$ (57, *1.4*) +0.14[b] -0.73 to +0.88[c] $C_5H_{11}^+$ (71, *0.4*) -0.72 to +0.85[c]	$C_4H_7O^+$ (71) -0.61 to +0.22[c] $C_3H_5O^+$ (57) -0.44 to +0.09[c] $C_2H_3O^+$ (43) -0.02 to +1.93[c]		$C_3H_7^+$ (43) +0.62[b] $C_4H_9^+$ (57) +0.56[b]

Note: The m/z and percentage product distribution of the m/z in EI-MS of the alcohol are given in brackets. EI-MS percentage product distributions are in italics and were calculated from relative abundancies in Mallard and Linstrom (2005). Standard enthalpies of reaction are derived from [a]standard enthalpies of formation and appearance energies, [b]proton affinities and standard enthalpies of formation, [c]standard enthalpies of formation, ion enthalpies of formation taken from Lias *et al* 1988. [b]The enthalpies of formation of $C_2H_5^+$, $C_3H_7^+$ and $C_4H_9^+$ were calculated using the proton affinities (Hunter and Lias 1998) and standard enthalpies of formation (Mallard and Linstrom 2005) of ethene, propene and 2-butene (*PA* of 1-butene is unknown) and are 9.41 eV, 8.34 eV and 8.07 eV respectively. The enthalpies of formation of $C_2H_5O^+$, $C_3H_7O^+$ and $C_4H_9O^+$ were calculated using the proton affinities (Hunter and Lias 1998) and standard enthalpies of formation (Mallard and Linstrom 2005) of ethanal, propanal and butanal and are 6.19 eV, 5.82 eV and 5.51 eV respectively. [c]The range of values results from the range of the enthalpies of formation of the ion in Lias *et al* 1988 depending on the structure of the ion. Neutral $C_{n-i}H_{2(n-i)}OH$ molecules were taken to be linear alcohols with the *OH* attached to carbon one. $C_{n-i}H_{2(n-i)+2}$ neutrals were taken to linear *n*-isomer alkanes and $C_{n-i}H_{2(n-i)}$ to be linear alkenes with the double bond between carbons one and two. A standard enthalpy of formation of H^+ of 15.92 eV from CRC Handbook of Chemistry And Physics (1986-1987), a standard enthalpy of formation of H_3O^+ of 6.25 eV calculated as described in § 3 and by convention a standard enthalpy of formation of hydrogen of 0 were employed. All other standard enthalpies of formation were taken from Mallard and Linstrom (2005) and proton affinities were taken from Hunter and Lias (1998), appearance energies were taken from Mallard and Linstrom (2005).* $\sum KE_{c.m}^r + KE_{c.m}^b$ corresponds to *E/N* of 120 Td to 140 Td in air at T_{dt} of 298 K ($KE_{c.m}^b$ = 0.16 to 0.22 eV, Figure 3.3).

The dissociative reactions eliminating H_2O (Eq. 3.28) from methanol and ethanol are endothermic. In the SIFT at 298 K methanol and ethanol react *via* the non-dissociative pathway only (Eq. 3.27). The reactions of the C_3 and C_4 alcohols proceed predominantly by the exothermic (Table 3.3) elimination of H_2O (Eq. 3.49) to produce $C_3H_7^+$ and $C_4H_9^+$ respectively (Table 3.2). The non-dissociative product forms $10 - 20$ % of the products from C_3 alcohols and $0 - 5$ % from C_4 alcohols (Table 3.2). The elimination of H_2O is increasingly exothermic as the size of alcohol increases (Table 3.3) and the products of dissociative H_2O elimination are the only products observed in the reaction of C_5 and C_6 alcohols. Both dissociative pathways are observed for the C_7 and C_8 alcohols though the more exothermic H_2O elimination is dominant.

In EI-MS $C_nH_{2n+1}O^+$ products are observed from C_1 to C_5 alcohols with decreasing abundance as the alcohol size increases. The reactions of the alcohols with H_3O^+ to form $C_nH_{2n+1}O^+$ ions are exothermic (Table 3.3); however the lack of product ions at the corresponding m/z in SIFT at 298 K indicate an energy and/or entropy barrier to the reaction. It is possible that the product ions at for example m/z 57 and 71, correspond to $C_iH_{2i-1}O^+$ ions rather than or as well as $C_iH_{2i+1}^+$ ions. The reactions of alcohols with H_3O^+ producing $C_iH_{2i-1}O^+$ ions by elimination of hydrogen and an alkane (Eq. 3.30) are more exothermic (Table 3.3) than those producing $C_iH_{2i+1}^+$ ions (Eq. 3.29) and the lone pair of electronegative oxygen may stabilise the positive charge. However given the apparent energy/entropy barrier to elimination of hydrogen from the protonated alcohol a contribution from $C_iH_{2i-1}O^+$ ions to for example m/z 57 and 71 at 298 K, seems unlikely. It is noteworthy that the $^{13}C/^{12}C$ isotope ratios of for example m/z 57:58 signals, will vary depending if the ion was $C_iH_{2i-1}O^+$; or $C_iH_{2i+1}^+$. The correlation with the ^{18}O signal could also be used in identification. In the case of propanol, Warneke *et al* (1996) confirmed that the product at m/z 43 contains three carbons ($C_3H_7^+$) by comparing the measured m/z 43 : m/z 44 ratio with the calculated isotopic ratio $^{13}C^{12}C_2H_7^+ : {}^{13}C_3H_7^+$.

$$C_nH_{2n+1}OH + H_3O^+ \rightarrow C_iH_{2i-1}O^+ + C_{n-i}H_{2(n-i)+2} + H_2 + H_2O \qquad (3.30)$$
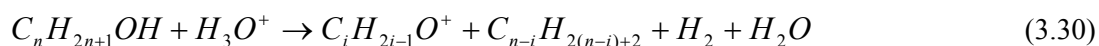
It is noteworthy that some of the $C_iH_{2i+1}^+$ product ions may be produced by dissociation of the $C_nH_{2n+1}^+$ ions by elimination of H_2O in reaction Eq. 3.28 *via* reaction Eq. 3.31 rather than directly by Eq. 3.29. However the indirect reaction (Eq. 3.31) is more endothermic and unlikely at the energies in SIFT or normally operated PTR-MS.

$$C_nH_{2n+1}OH + H_3O^+ \rightarrow C_iH_{2i+1}^+ + C_{n-i}H_{2(n-i)} + 2H_2O \qquad (3.31)$$
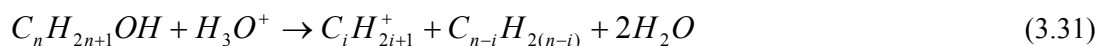
The product distributions observed from H_3O^+ reaction with various alcohols in PTR-MS, PT-CIMS, CIR-TOF and SIFDT are reviewed in Table 3.4. Under the elevated energy conditions of the PTR-MS based techniques, increased fragmentation is observed.

The non-dissociative product, $CH_3OH_2^+$ (m/z 33), was the only product observed from methanol reaction in the PTR-MS studies collated in Table 3.4. Inomata *et al* (2008) observed fragmentation to m/z 31 (CH_2OH^+) from methanol and ethanol at an *E/N* of 108 Td and T_{dt} 378 K (P_{dt} 2.1 mbar, V_{drift} 400 V, l_{dt} 9.2 cm, *E* ~43.5 V cm^{-1}), the ratio of m/z 31 to the protonated alcohol (m/z 33 and 47 respectively) was 0.0073 and 0.045 respectively (the presence or lack of other fragments was not specified). The lack of products at m/z 31 from methanol and ethanol in the PTR-MS studies collated in Table 3.4 despite the similar P_{dt} and similar or greater *E/N* may be explained by the comparably high drift tube temperature employed by Inomata *et al* (2008) and consequent increase in the energy of the neutral alcohol. Lagg *et al* (1994) studied the product distributions from the reaction of methanol with H_3O^+ in helium, P_{FT} ~0.3 mbar, as a function of energy ($KE_{c.m.}^r$) in SIFDT (Table 3.2, Table 3.4). Lagg *et al* (1994) observed only the non-dissociative product up to $KE_{c.m.}^r$ of 1 eV ($KE_{c.m.}^b$ ~0.3 eV) this is much greater than $KE_{c.m.}^r$ (and the sum of $KE_{c.m.}^r$ and $KE_{c.m.}^b$) in normally operated PTR-MS and would require an *E/N* greater than 200 Td in air (T_{dt} 298 K) (Figure 3.2). At $KE_{c.m.}^r$ greater than 1 eV a small degree of fragmentation to m/z 15 and m/z 31 was observed, m/z 15 dominating. The increase in pressure in the PTR-MS and consequent increase in destabilizing collisions relative to SIFDT may contribute to the dissociation to m/z 31 as well as the increased temperature employed by Inomata *et al* (2008). The m/z 31 (CH_2OH^+) ion is the major product from EI-MS of methanol, ethanol, 1-propanol and is the major fragment ion from 1-butanol (Table 3.3, Mallard and Linstrom 2005). The formation of CH_2OH^+ from reaction of the alcohols with H_3O^+ becomes increasingly endothermic as alkane size increases (Table 3.3) and Inomata *et al* (2008) did not observe any fragmentation to m/z 31 from propanol or butanol.

There is some evidence that there is sufficient energy for $C_2H_5^+$ (m/z 29) formation from reactions of ethanol with H_3O^+ in the PTR-MS (Table 3.4) though the degree of fragmentation is uncertain. Lagg *et al* (1994) studied the product distributions from the reaction of ethanol with H_3O^+ in helium, P_{FT} ~0.3 mbar, as a function of energy ($KE_{c.m.}^r$) in SIFDT (Tables 3.2 and 3.4).

Table 3.4: The product distributions resulting from the reaction of alcohols with H_3O^+ in the PTR-MS, PT-CIMS, PTR-TOF and SIFDT.

Saturated Alcohol	P_{dt} (mbar)	T_{dt} (K)	V_{drift} (V)	E (V cm^{-1})	E/N (Td)	Observed Product Distribution : Product Ion (m/z): Percentage of Product Total, $C_nH_{2n+1}OH + H_3O^+ \rightarrow$				Reference
						$C_nH_{2n+1}OH_2^+$ $+ H_2O$	$C_nH_{2n+1}^+ +$ $2H_2O$	$C_iH_{2i+1}^+ + H_2O$ $+ C_{n-i}H_{2(n-i)+1}OH$	Other	
Methanol	[a]NS [b]1.8 – 2.1** [c]2.4 [d]7.95* [e]1.3- 2.7** [f]0.27 [g]NS	[a]NS [b]333 [c]NS [d]313 [e]NS [f]NS [g]NS	[a]600 [b]580, [c]NS [d]2700 [e]2450 - 4900 [f]NS [g]NS	[a]NS [b]NS [c]NS [d]270 [e]35-70 [f]NS [g]NS	[a]NS [b]134 - 156 [c]106 [d]147 [e]NS [f]NS[#] [g]NS	$CH_3OH_2^+$ (33): [a]**100** [b]**~33.3**, [c]**100**, [d]**100**, [e]**100**, [f]**100**, [g]**100**			$(CH_3OH)_2H^+$ (65): [b]**14.3** $CH_3OH.CH_3^+$ (47): [b]**47.6** $(CH_3OH)_3H^+$ (97): [b]**~0.1** $(CH_3OH)_2CH_3^+$ (79): [b]**~0.1**	[a]Buhr et al (2002) [b]Malekina et al (2007) [c]Warneke et al (2003) [d]Wyche et al (2007) [e]De Gouw et al (2000) [f]Lagg et al (1994) [g]Lindinger et al (1998)
Ethanol	[a]NS [b]1.8 – 2.1** [c]2.4 [d]7.09* [e]0.27 [f]NS	[a]NS [b]313 [c]NS [d]313 [e]NS [f]NS	[a]600, [b]580, [c]NS [d]2700 [e]NS [f]NS	[a]NS [b]NS [c]NS [d]270 [e]NS [f]NS	[a]NS [b]126- 147 [c]106 [d]165 [e]NS[#] [f]NS	$C_2H_5OH_2^+$ (47): [a]**69.9**, [b]**~28.0**, [c]**50**, [d]**93**, [e]**100**, [f]**100**	$C_2H_5^+$ (29): [b]**~0.9**, [c]**50**, [d]**7**		$C_2H_5OH_2^+.H_2O$? (65): [a]**4.2** $C_2H_5O^+$? (45): [a]**25.9** $(C_2H_5OH)_2H^+$ (93): [b]**46.7** $C_2H_5OH.C_2H_5^+$ (75): [b]**21.0** $(C_2H_5OH)_3H^+$ (139): [b]**1.4** $(C_2H_5OH)_2C_2H_5^+$: (121): [b]**1.9** H_3O^+ ? (19): ?	[a]Buhr et al (2002) [b]Malekina et al (2007) [c]Warneke et al (2003) [d]Blake et al (2006) [e]Lagg et al (1994) [f]Lindinger et al (1998)

Table 3.4 is continued on the following page.

Saturated Alcohol	P_{dt} (mbar)	T_{dt} (K)	V_{drift} (V)	E (V cm^{-1})	E/N (Td)	Observed Product Distribution : Product Ion (m/z): Percentage of Product Total, $C_nH_{2n+1}OH + H_3O^+ \rightarrow$				Reference
						$C_nH_{2n+1}OH_2^+ + H_2O$	$C_nH_{2n+1}^+ + 2H_2O$	$C_iH_{2i+1}^+ + H_2O + C_{n-i}H_{2(n-i)+1}OH$	Other	
1-Propanol	[a]NS [b]7.95* [c]NS [d]NS	[a]NS [b]313 [c]NS [d]NS	[a]600 [b]2700 [c]NS [d]NS	[a]NS [b]270 [c]NS [d]NS	[a]NS [b]147 [c]NS[#] [d]NS	$C_3H_7OH_2^+$ (61): [c]**5** [d]**20**	[a]$C_3H_7^+$ (43): [a]**73.0** [c]**95** [d]**80**		[a]$C_3H_5^+$? (41): [a]**27,** [b]**51**	[a]Buhr *et al* (2002) [b]Wyche *et al* (2007) [c]Warneke *et al* (1996) [d]Lindinger *et al* (1998)
2-Propanol	[a]NS [b]2.4 [c]NS [d]NS	[a]NS [b]NS [c]NS [d]NS	[a]600 [b]NS [c]NS [d]NS	[a]NS [b]NS [c]NS [d]NS	[a]NS [b]106 [c]NS[#] [d]NS	$C_3H_7OH_2^+$ (61): [c]**13** [d]**10**	$C_3H_7^+$ (43): [a]**73,** [b]**100,** [c]**87,** [d]**90**		$C_3H_5^+$? (41): [a]**27**	[a]Buhr *et al* (2002) [b]Warneke *et al* (2003) [c]Warneke *et al* (1996) [d]Lindinger *et al* (1998)
1-Butanol	[a]NS [b]7.95*	[a]NS [b]313	[a]600 [b]2700	[a]NS [b]270	[a]NS [b]147		$C_4H_9^+$ (57): [a]**90.1 + 4.5** at the ^{13}C isotope, [b]**79**		$C_3H_5^+$? (41): [a]**5.4**	[a]Buhr *et al* (2002) [b]Wyche *et al* (2007)

Table 3.4 is continued on the following page.

Saturated Alcohol	P_{dt} (mbar)	T_{dt} (K)	V_{drift} (V)	E (V cm^{-1})	E/N (Td)	Observed Product Distribution : Product Ion (m/z): Percentage of Product Total, $C_nH_{2n+1}OH + H_3O^+ \rightarrow$				Reference
						$C_nH_{2n+1}OH_2^+$ $+ H_2O$	$C_nH_{2n+1}^+ +$ $2H_2O$	$C_iH_{2i+1}^+ + H_2O$ $+ C_{n-i}H_{2(n-i)+1}OH$	Other	
2 -Butanol	NS	NS	600	NS	NS		C$_4$H$_9^+$ (57): **89.3 + 4.5** at the ^{13}C isotope		C$_3$H$_5^+$? (41): **6.3**	Buhr *et al* (2002)
2-methyl-2-propanol	NS	NS	600	NS	NS		C$_4$H$_9^+$ (57): **90.1 + 4.5** at the ^{13}C isotope		C$_3$H$_5^+$? (41): **5.4**	Buhr *et al* (2002)
1-Pentanol	NS	NS	600	NS	NS			C$_4$H$_9^+$ (57): **89.3 + 4.5** at the ^{13}C isotope	C$_3$H$_5^+$? (41): **6.3**	Buhr *et al* (2002)
2-Pentanol /1-Methyl-1-Butanol	NS	NS	600	NS	NS		C$_5$H$_{11}^+$ (71): **39.3 + 2.3** at the ^{13}C isotope	C$_3$H$_7^+$ (43): **46.7**	C$_3$H$_5^+$? (41): **11.7**	Buhr *et al* (2002)
3-Methyl-1-butanol	NS	NS	600	NS	NS		C$_5$H$_{11}^+$ (71): **37.1 + 2.3** at the ^{13}C isotope	C$_3$H$_7^+$ (43): **45.2**	C$_3$H$_5^+$? (41): **12.2** ? (70): **3.2**	Buhr *et al* (2002)
Hexanol (isomer not specified)	1.3	NS	NS	NS	NS		C$_6$H$_{13}^+$ (85): **29**	C$_4$H$_9^+$ (57): **17** C$_3$H$_7^+$ (43): **40**	C$_3$H$_5^+$? (41): **14**	Fall *et al* (1999)

Table 3.4 is continued on the following page.

Saturated Alcohol	P_{dt} (mbar)	T_{dt} (K)	V_{drift} (V)	E (V cm^{-1})	E/N (Td)	Observed Product Distribution : Product Ion (m/z): Percentage of Product Total, $C_nH_{2n+1}OH + H_3O^+ \rightarrow$				Reference
						$C_nH_{2n+1}OH_2^+ + H_2O$	$C_nH_{2n+1}^+ + 2H_2O$	$C_iH_{2i+1}^+ + H_2O + C_{n-i}H_{2(n-i)+1}OH$	Other	
1-Hexanol	[a]NS [b]1.3 – 2.7**	[a]NS [b]NS	[a]600 [b]2450 - 4900	[a]NS [b]35-70	[a]NS [b]NS		$C_6H_{13}^+$ (85): [a]**23.7,** [b]**25**	$C_4H_9^+$ (57): [a]**16.1,** [b]**4** $C_3H_7^+$ (43): [a]**44.6,** [b]**70**	$C_3H_5^+$? (41): [a]**15.6**	[a]Buhr et al (2002) [b]de Gouw et al (2000)
2-Hexanol	NS	NS	600	NS	NS		$C_6H_{13}^+$ (85): **24.9**	$C_4H_9^+$ (57): **15.5** $C_3H_7^+$ (43): **42.9**	$C_3H_5^+$? (41): **14.2** ? (45): **2.6**	Buhr et al (2002)
1-Octanol	NS	NS	600	NS	NS			$C_5H_{11}^+$ (71): **21.2** $C_4H_9^+$ (57): **44.2** $C_3H_7^+$ (43): **25.7**	$C_3H_5^+$? (41): **8.8**	Buhr et al (2002)
2-Octanol	NS	NS	600	NS	NS			$C_5H_{11}^+$ (71): **17.9** $C_4H_9^+$ (57): **38.0** $C_3H_7^+$ (43): **22.1**	$C_3H_5^+$? (41): **8.0** ? (129): **12.2** $(C_4H_8)_2H^+$? (113): **1.9**	Buhr et al (2002)
3-Octanol	NS	NS	600	NS	NS			$C_5H_{11}^+$ (71): **19.1** $C_4H_9^+$ (57): **38.9** $C_3H_7^+$ (43): **22.6**	$C_3H_5^+$? (41): **7.4** ? (129): **10.1** $(C_4H_8)_2H^+$? (113): **1.9**	Buhr et al (2002)
2-Nonanol	NS	NS	600	NS	NS			$C_6H_{13}^+$ (85): **5.1** $C_5H_{11}^+$ (71): **13.7** $C_4H_9^+$ (57): **25.3** $C_3H_7^+$ (43): **36.1**	$C_3H_5^+$? (41): **18.1** ? (127): **1.8**	Buhr et al (2002)

Note: P_{dt} denotes drift tube pressure, T_{dt} denotes drift tube temperature, V_{drift} denotes voltage applied to the drift tube and E the electric field strength. Distributions from Buhr et al (2002) and Malekina et al (2007) are given as relative abundancies with the most abundant m/z normalised to 100 in reference and have been converted to percentage distributions here and are specified to one decimal place. Relative abundancies from Malekina et al (2007) were taken from spectra presented therein, ^{13}C and ^{18}O isotopes and unidentified m/z were not included in calculation of product abundancies. NS denotes not specified in reference. Values from Buhr et al (2002), Malekina et al (2007), Warneke et al (2003), Fall et al (1999) were derived using conventional PTR-MS. Distributions from de Gouw et al (2000) were derived using a

PT-CIMS. Values from Blake *et al* (2006) and Wyche *et al* (2007) were derived using CIR-TOF-MS. Distributions from Warneke *et al* (1996) and Lagg *et al* (1994) were derived in SIFDT (§ 2.1), a helium carrier gas was used in the drift tube. [#]Distributions are given across a range of $KE^r_{c.m.}$ in the cited reference, values corresponding to $KE^r_{c.m.}$ of 0.2 eV are tabulated here. A $KE^r_{c.m.}$ of e.g. H_3O^+-methanol of 0.14 and 0.26 eV in helium at 298 K corresponds to *E/N* of ~ 20 - 30 Td where $KE^b_{c.m.}$ is 0.07 eV - 0.10 eV and thus the sum of $KE^r_{c.m.}$ and $KE^b_{c.m.}$ is 0.21 - 0.36 eV, in the PTR-MS in air at 298 K this is comparable to the ion-molecule energy at *E/N* of ~ 100 - 120 Td where $KE^r_{c.m.}$ is 0.12 to 0.17 eV and $KE^b_{c.m.}$ is 0.12 to 0.16 eV and thus the sum of $KE^r_{c.m.}$ and $KE^b_{c.m.}$ is 0.24 and 0.33 eV .* A pressure range of 7-8 mbar is given in reference this pressure is derived from the specified *E/N, E,* and T_{dt}. **A specific value of instrumental parameter (e.g. P_{dt}) is not specified but the range of the parameter during measurements in reference is as specified. Wyche *et al* (2007) specify the percentage abundance of the ion employed for quantification of the compound in the smog chamber experiments within the reference, the remainder of the total ion signal is unspecified. Product distributions in Warneke *et al* (2003) were measured in synthetic air (humidity not specified), in Malekina *et al* (2007), Fall *et al* (1999) and Buhr *et al* (2002) product distributions were measured in ambient air (humidity not specified) and in Blake *et al* (2006) product distributions were measured in dry nitrogen (thereby reducing O_2^+). Measurements by Lindinger *et al* (1998) are assumed to be made in PTR-MS measurement conditions are not specified.

No fragmentation was observed up to $KE_{c.m.}^r$ of 0.2 eV, at $KE_{c.m.}^r$ 0.3 eV ($KE_{c.m.}^b \sim 0.1$ eV) m/z 29 ($C_2H_5^+$) formed ~ 1 % of products. In the PTR-MS (T_{dt} 298 K) in air the sum of $KE_{c.m.}^r$ and $KE_{c.m.}^b$ is ~0.4 eV at E/N of 130 Td (T_{dt} 298 K) (Figure 3.2 and 3.3). At $KE_{c.m.}^r$ of 0.45 eV and $KE_{c.m.}^b$ ~0.14 eV m/z 29 formed close to 5 % of the total product ions, the sum of $KE_{c.m.}^r$ and $KE_{c.m.}^b$ in PTR-MS in air is ~0.6 eV at E/N of 160 Td (T_{dt} 298 K). At the maximum $KE_{c.m.}^r$ of ~0.83 eV ($KE_{c.m.}^b$ ~0.23 eV) m/z 29 formed ~ 25 % of the products, in the PTR-MS (T_{dt} 298 K) in air the sum of $KE_{c.m.}^r$ and $KE_{c.m.}^b$ is ~0.98 eV at E/N of 200 Td (T_{dt} 298 K) (Figure 3.2 and 3.3). Thus the extent of fragmentation to m/z 29 in the PTR-MS (Table 3.4) generally appears to be greater than in SIFDT at a given energy ($KE_{c.m.}^r +$ $KE_{c.m.}^b$); this may be due to the increased pressure in the PTR-MS, the polyatomic nature of the buffer may also affect destabilizing collisions.

Warneke *et al* (2003) observed a difference in the calculated and measured sensitivity of PTR-MS for ethanol greater than the associated uncertainties. The measured sensitivity was derived from counts per second at m/z 47 assuming 50 % dissociation to m/z 29, as determined in laboratory experiments (Table 3.4). The difference in calculated and measured sensitivity was attributed to additional fragmentation of ethanol to m/z 19. Wyche *et al* (2007) could only observe a signal from ethanol at E/N of less than 120 Td in the PTR-MS and suggested the lack of a signal at higher E/N (and pressure) may be due to fragmentation to m/z 19. The m/z 19 ion forms 1.0 % of the total product from EI-MS of ethanol (Mallard and Linstrom 2005).

The C_3 and C_4 alcohols dissociate *via* elimination of water to $C_3H_7^+$ (m/z 43) and $C_4H_9^+$ (m/z 57) respectively. The non-dissociative reaction product seen in SIFT has not been observed in the majority of PTR-MS studies (Table 3.4). Lindinger *et al* (1998) observed minor products of non-dissociation from 1- and 2-propanol however reaction chamber conditions were not specified. Warneke *et al* (1996) studied the product distributions from the reaction of 1- and 2-propanol with H_3O^+ in helium, as a function of energy ($KE_{c.m.}^r$) in SIFDT (Table 3.2, Table 3.4). P_{FT} was not stated but it is assumed the SIFDT was normally operated and P_{FT} was in the region of 0.3 mbar. Under thermal conditions ($KE_{c.m.}^r$ ~3/2$k_B T$) m/z 61 ($C_3H_7OH_2^+$) formed ~ 8 % and ~ 22 % of product ions and m/z 43 ($C_3H_7^+$) ~ 92 % and 78 % from 1- and 2-propanol respectively; this is in good agreement with SIFT (T_{FT} 298 K) results (Table 3.2). At $KE_{c.m.}^r$ of ~0.30 eV ($KE_{c.m.}^b$ ~0.10 eV) m/z 43 formed ~ 4 % and 6 % of

product ions from 1- and 2-propanol respectively, the sum of $KE_{c.m.}^r$ and $KE_{c.m.}^b$ in PTR-MS in air is ~0.4 eV at E/N of 130 Td (T_{dt} 298 K). m/z 41 formed 100 % of products at $KE_{c.m.}^r$ ~0.8 eV and 0.4 eV from 1- and 2-propanol respectively. Hansel et al (1995) also studied the fragmentation of propanol as a function of $KE_{c.m.}^r$ and observed ~65 % fragmentation to m/z 43 at approximately thermal energies increasing to 100 % at $KE_{c.m.}^r$ ~1.5 eV.

The C_5 and C_6 alcohols dissociate by elimination of water, as in the SIFT, but the dissociation to a carbocation and smaller alcohol also becomes accessible in the PTR-MS. Dissociation to the carbocation is equal or greater than dissociation by H_2O elimination. The C_8 and C_9 alcohols react only by dissociation to carbocations and smaller alcohols, unlike in SIFT the products of dissociation by elimination of water are not observed.

An additional fragment at m/z 41 has been observed from the reaction of the $C_3 - C_9$ alcohols with H_3O^+ (Table 3.4). It is possible that this is $C_3H_5^+$ and results from further dissociation of the $C_nH_{2n}^+$ ions produced from the dissociative reactions to release hydrogen in the case of $C_3H_7^+$ and methane in the case of $C_4H_9^+$. The m/z 41 ion forms 4.0 %, 13.6 %, 10.7 %, 8.8 %, 9.3 % and 9.7 % of product from EI-MS 1-propanol, 1-butanol, 1-pentanol, 1-hexanol, 1-heptanol and 1-octanol respectively (Mallard and Linstrom 2005).

The $C_nH_{2n+1}O^+$ where n is greater than one have not been observed and it appears there is insufficient energy in normally operated PTR-MS to overcome the energy and/or entropy barrier associated with hydrogen elimination.

The reaction of alcohols with H_3O^+ are thought to proceed via formation of a nascent association complex ion $(H_3O^+.C_nH_{2n+1}OH)*$ in similar manner to longer chain alkanes (§ D.1.1). The $(H_3O^+.C_nH_{2n+1}OH)*$ association complex ion may stabilize to $H_3O^+.C_nH_{2n+1}OH$ or lose one water molecule to form the non-dissociative product (Eq. 3.6) or dissociate to the dissociative products (Wang et al 2004, 2006). Wang et al (2006) measured product distributions as a function of flow tube pressure in the SIFT. They found that at increased pressures, association relative product abundance was unchanged while the non-dissociative product decreased and the dissociative product formed by elimination of water increased. The results indicate collisions of helium carrier gas destabilize $H_3O^+.C_nH_{2n+1}OH$ resulting in increased dissociation. The increased pressure in

the PTR-MS drift tube relative to SIFT may contribute to increased fragmentation in addition to the increased energy available for reaction, though the change in buffer may also have an effect on stabilization.

Malekina *et al* (2007) observed formation of protonated alcohol dimers and trimers and fragment ions attributed to the loss of water from the proton bound alcohol dimers and trimers at high alcohol concentrations (Table 3.4). Protonated dimers, trimers and the fragments resulting from elimination of water from them constituted ~62 % of the products from the reaction of methanol with H_3O^+ and ~71 % from the reaction of ethanol (*E/N* was somewhere between 134 - 156 Td and 126 – 147 Td respectively, Table 3.4). The protonated trimer and the product of its dissociation by elimination of water were minor products in the reaction of both alcohols. Only the protonated alcohol dimer and the product of its dissociation by H_2O elimination were observed from butanol. Buhr *et al* (2002) observed a minor product ion at m/z 113 from 2- and 3-octanol; this may correspond to the protonated dimer. The formation of the dimer and trimer from ethanol and protonated ethanol are exoergic with Gibbs free energies of -1.0 eV and -0.55 eV (Feng and Lifshitz, 1995). Malekina *et al* (2007) point to the study of ethanol dimers and trimers in SIFT by Feng *et al* (1995), in this case the reaction kinetics of protonated ethanol clusters with various neutral molecules was under investigation, the dimer was produced at the ion source and the trimer was formed from the dimer by introducing ethanol into the flow tube at a flow rate of 1.5 cm^3 s^{-1} i.e. the VMR of ethanol was relatively high. Formation of protonated alcohol dimers have not been noted in the SIFT investigations of product distributions resulting from H_3O^+ reaction with alcohols referenced in Table 3.2 (concentrations not specified). The rate constant for the cluster formation is likely to show a negative temperature dependence (Meot-Ner, 1976) and can be expected to decrease with the increased energy in the drift tube. Indeed Inomata *et al* (2008) observed such a negative energy dependence for formation of the protonated ethanal dimer from ethanal reaction with H_3O^+ in the PTR-MS (§ 3.2.3).

Given the large percentage contribution of the protonated alcohol clusters and associated fragment observed from the reaction of H_3O^+ with methanol and ethanol by Malekina *et al* (2007), concentrations and sensitivities derived from m/z 33 for methanol and m/z 47 and m/z 29 for ethanol would be a significant underestimation. Warneke *et al* (2003) derived a calculated sensitivity of 25.4 for methanol and measured a sensitivity, using m/z 33 at *E/N* of 106 Td, of 15.9; this is within the uncertainties of these values. De Gouw *et al* (2003) report a good comparison between GC-MS and PTR-MS measurements of methanol at m/z 33 with a gradient of 1.028 (correlation coefficient of 0.97, intercept -110 ppb) during measurements

aboard a research ship during the New England Air Quality Study (NEAQS). The E/N used by de Gouw *et al* (2003) was not specified but V_{drift} was 710 V and P_{dt} 2.4 mbar. Warneke *et al* (2005b) compared measurements of methanol at m/z 33 aboard a research ship during the New England Air Quality Study – Intercontinental Transport and Chemical Transformation study from PIT-MS (E/N ~108 Td, V_{drift} 600 V, P_{dt} 2.4 mbar) and methanol VMRs derived with GC-MS. A gradient of 0.77 ± 0.11 (correlation coefficient of 0.96, -44 ± 21 ppt) was obtained from an orthogonal distance regression of the data. The gradient of less than one may be indicative of fragmentation or clustering of methanol to m/z other than m/z 33. However, the negative intercept indicates an overestimation of the instrument background which may contribute to the gradient of less than one. Christian *et al* (2004) observed excellent agreement between concentrations derived from an open-path Fourier transform infrared spectrometer and PTR-MS (E/N 130 Td, V_{drift} 600 V, P_{dt} 2 mbar) measurements at m/z 33 in simulated fires. The integrated methanol excess mixing ratio integrated over the fire divided by the mixing ratio from OP-FTIR was 1.04 ± 0.118; 38 fires were used in the calculation. Karl *et al* (2007) determined an average ratio of 1.1 ± 0.2 between VMR derived from m/z 33 in PTR-MS (E/N ~120 Td, P_{dt} 2.0 mbar, T_{dt} 313 K, V_{drift} ~555 V E~55.5 V cm^{-1}) and FTIR derived VMRs. As discussed above the difference between the measured and calculated sensitivity for ethanol, derived by Warneke *et al* (2003), was greater than the uncertainties. Protonated alcohol cluster formation may have contributed to this difference in addition to fragmentation to m/z 19.

The reason for the discrepancy between the results of Malekina *et al* (2007) and the good comparisons observed between PTR-MS and GC-MS and OP-FTIR measurements of methanol lies in the concentrations of methanol involved. The dependence of relative product distributions of protonated ethanol dimers and their fragments on ethanol concentration has been demonstrated in the analysis of wine headspace (Spitaler *et al* 2007, Boscaini *et al* 2004, Aprea *et al* 2007a). The alcohol dimers formed at the high concentrations in wine headspace react with (O)VOCs with proton affinities less than themselves further complicating mass spectra. The reaction of esters with the protonated ethanol clusters in addition to H_3O^+, has been investigated by Aprea *et al* (2007a). Boscaini *et al* (2004) diluted wine headspace with ethanol saturated nitrogen to generate a constantly high level of ethanol removing variability in mass spectra resulting from variable protonated cluster formation due to changing ethanol concentration but in doing so replacing H_3O^+ by the protonated ethanol dimer as the primary reagent and complicating mass spectra. Spitaler *et al* (2007) diluted wine headspace with nitrogen, reducing the ethanol concentration and thereby formation of protonated ethanol dimers. The concentrations of alcohols used by

Malekina *et al* (2007) are unknown; however it is concluded that high concentrations of VOCs could promote cluster formation. The good correlation between methanol concentrations, measured using PTR-MS and GC-MS and OP-FTIR in tropospheric air samples, indicate that at these concentrations (~0.5 to 10 ppb in the NEAQS measurements) protonated methanol clusters are a minor product of proton transfer reactions.

In summary, quantification of the higher alcohols is complicated by the isobaric nature of the product ions at m/z 43, 57, 71 and 85 all of which are also fragments and/or protonated non-dissociative products of the reaction of for example alkanes, cycloalkanes, alkenes, unsaturated aldehydes, carboxylic acids and esters (§3.5). Methanol undergoes predominantly non-dissociative proton transfer and there are few other contributors to m/z 33 thus methanol can be reasonably quantified in the absence of dimer formation. In addition to dimer formation at high concentrations and associated products, ethanol quantification is complicated by the presence of a number of isobaric compounds at the non-dissociative product m/z, e.g. methanoic acid (§ 3.5), and possibly fragmentation to m/z 19 which is masked by H_3O^+. Fragmentation of methanol and ethanol to m/z 31 requires further investigation. The formation of protonated alcohol dimers and the products of elimination of water from them as a function of alcohol VMRs (within the limit $[H_3O^+] >> [\sum RH^+]$) over varying drift tube conditions is required. This is necessary to quantify the alcohols but also to characterise interference at the m/z corresponding to the dimers, e.g., the elimination of water from the protonated methanol dimer produces *(CH₃OH)CH₃⁺* at m/z 47 which may interfere with ethanol quantification. Many of the clusters and the products of elimination of water from them contribute to the same m/z as the protonated alkylbenzenes (§ D.2.1), for example the elimination of water from the protonated methanol trimer at m/z 79, the protonated ethanol dimer at m/z 93 and the protonated propanol dimer at m/z 121.

3.1.2 The Reaction of Saturated Alcohols in the Presence of Water

Under the thermal conditions of SIFT at 298 K association products, $C_nH_{2n+1}OH.H_3O^+$, have been observed as a minor product of reaction of H_3O^+ with some alcohols in dry air samples (Table 3.2). A reduction in formation of the association products is anticipated in the PTR-MS due to the negative energy dependence of the rates of such reactions and the elevated energy levels in PTR-MS. In humid samples, protonated alcohols have also been observed to form mono- and dihydrates, $C_nH_{2n+1}OH_2^+.(H_2O)_{1,2}$ in SIFT (Wang *et al* 2004, Wang *et al* 2006, Smith *et al* 2001, Španěl and Smith 2000b), trihydrates are not formed (Španěl and Smith 2000b). Hydration of the product ions is only a consideration for the C_1-

C_3 alcohols in PTR-MS since the non-dissociative reaction is only observed from these alcohols. As discussed in § D.1.3, hydrate formation with the carbocations produced from the dissociation reactions of higher alcohols is minor and not observed in SIFT (e.g. Wang *et al* 2004, Smith *et al* 2001). Warneke *et al* (1996) report the three-body association of $C_3H_7^+$ from propanol reaction with H_3O^+ with H_2O in SIFDT. Alcohols have relatively large dipoles, and methanol and ethanol ligand switching reactions with $H_3O^+(H_2O)_n$ n=1 and 2 have been observed to proceed efficiently in SIFT at ~298 K (Smith and Španěl, 2005). Španěl and Smith (2000b) found that ligand switching was a minor route of production of MHH_2O^+ compared to association of the protonated alcohol with water for both methanol and ethanol in SIFT at ~300 K and ~0.9 mbar. Buhr *et al* (2002) observed a 4.5 % contribution at m/z 65 from the reaction of ethanol with H_3O^+ in PTR-MS which corresponds to the monohydrate and/or ligand switching product. Warneke *et al* (1996) describe the formation of a product ion at m/z 79 from the reaction of propanol under humid conditions in the PTR-MS and attribute this to $C_3H_7OH.H_3O^+$ formed *via* a switching reaction with $H_3O^+.H_2O$. Formation of the protonated alcohol hydrates and/or association products have not been noted in any of the other studies included in Table 3.3. Some dissociation of the products of ligand switching to form the protonated alcohol and water may occur at the elevated energies in the PTR-MS. The direct proton transfer will not occur efficiently. Jobson *et al* (2005) observed approximately unchanging measured sensitivity (at MH^+) with increasing humidity and an increasing measured to calculated sensitivity ratio indicative of ligand switching followed by collision induced dissociation.

3.1.3 Unsaturated Alcohols

The reaction efficiencies and product distributions resulting from the reactions of C_5, C_6 and C_8 unsaturated alcohols with H_3O^+ measured in the SIFT at 298 K are reviewed in Table 3.5. The proton affinities of the unsaturated alcohols are not known. The reactions of all the unsaturated alcohols studied are efficient indicating proton affinities are greater than that of water. Unsaturated alcohols react in a similar manner to saturated alcohols and three reaction pathways dominate; non-dissociative (Eq. 3.32 dissociation by elimination of H_2O (Eq. 3.33) and dissociation to an unsaturated carbocation and a smaller saturated alcohol (Eq. 3.34)

$$C_nH_{2n-1}OH + H_3O^+ \rightarrow C_nH_{2n-1}OH_2^+ + H_2O \tag{3.32}$$

$$C_nH_{2n-1}OH + H_3O^+ \rightarrow C_nH_{2n-1}^+ + 2H_2O \tag{3.33}$$

$$C_nH_{2n-1}OH + H_3O^+ \rightarrow C_iH_{2i-1}^+ + C_{n-i}H_{2(n-i)+1}OH + H_2O \tag{3.34}$$
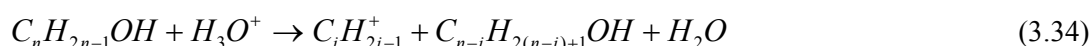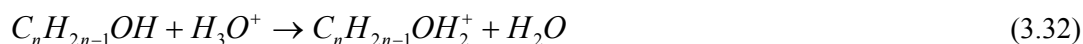
Dissociation by elimination of water (Eq. 3.33) is the dominant reaction pathway for the C_5, C_6 and C_8 alcohols in SIFT. The dissociation to an unsaturated carbocation and small saturated alcohol is only observed in the C_8 unsaturated alcohols and is < 20%. Custer *et al* (2003) observed a minor fragment from *E*-3-hexen-1-ol which may correspond to $C_5H_9^+$ formed by dissociative elimination of methanol. The non-dissociative pathway is ≤ 18 % in all of the reactions studied. The non-dissociative pathway is not observed from alcohols where the double bond is in the second position (Schoon *et al*, 2007). The increasing level of dissociation with increasing number of carbons is indicative of increasing proton affinity as in the case of the saturated alcohols. The degree of dissociation is less than that from the corresponding saturated alcohols as a result of the stabilisation of the charge by the double bond.

The product distributions from H_3O^+ reaction with C_5, C_6 and C_8 unsaturated alcohols in PTR-MS, PT-CIMS and CIR-TOF-MS are reviewed in Table 3.6. Products formed from elimination of H_2O (Eq. 3.33) remain the dominant products in PTR-MS based techniques. The products observed from H_3O^+ reaction with 1-penten-3-ol, *Z*-2-penten-1-ol and *E*-2-penten-1-ol are similar to those observed in SIFT. Fall *et al* (2001) used GC-PTR-MS to identify 1-penten-3-ol and 2-penten-3-ol (and 3-methylbutanal) at m/z 69 in air from freeze thaw treated leafs, the ^{13}C ratio of m/z 69 to 70 was 5.4 % confirming that the fragment is a C_5 compound ($C_5H_9^+$). In contrast to SIFT, dissociation to unsaturated carbocation and a saturated alcohol (Eq. 3.34) is observed from the branched C_5 alcohols (3-methyl-2-buten-1-ol, 3-methyl-3-buten-1-ol, 2-methyl-3-buten-2-ol) in the PTR-MS based instruments. However the unsaturated carbocation is a minor fragment (8-10 %) and the contributions of products from the non-dissociative and H_2O elimination reaction are similar to those in SIFT. The additional energy in the PTR-MS based techniques also enables the dissociation to an unsaturated carbocation and saturated alcohol to occur with the C_6 unsaturated alcohols. In this case the unsaturated carbocations form a greater percentage of the products (17.8 – 35.5 %) and there is a reduction in the percentage contribution of the products resulting from elimination of H_2O (Eq. 3.33). An additional fragment ion is observed from the C_6 unsaturated alcohol reactions at m/z 59. The unsaturated carbocations contribution from 1-octen-3-ol is increased by ~ 40% in the PTR-MS and an additional product ion is observed at m/z 57.

Unlike in the SIFT measurements, there is no clear difference in product distributions corresponding to position of the double bond. A greater degree of non-dissociative reaction product was observed from the branched 2-methyl-3-buten-1-ol than the other C_5 unsaturated alcohols. There is little or no difference in product distributions from different isomers of a

given unsaturated alcohol and it is not possible to distinguish isomers from PTR-MS spectra alone.

At the higher energies of EI-MS differing fragmentation patterns are observed. For example, m/z 57 is the dominant (48.7 %) product ion from 1-penten-3-ol and m/z 41 (19.8 %) and m/z 67 (11.8 %) are the dominant ions from 3-hexen-1-ol (Mallard and Linstrom 2005).

Table 3.5: Product distributions and reaction efficiencies of H_3O^+ with various unsaturated alcohols in SIFT-MS at ~298 K.

Unsaturated alcohol ($C_nH_{2n-1}OH$)	P_{FT} (mbar)	T_{FT} (K)	k_m (x 10^{-9} m^3 s^{-1})	k_m/k_c	Observed Product Distribution : Product Ion (m/z): Percentage of Product Total, $C_nH_{2n-1}OH + H_3O^+ \rightarrow$				Reference
					$C_nH_{2n-1}OH_2^+ + H_2O$	$C_nH_{2n-1}^+ + 2H_2O$	$C_iH_{2i-1}^+ + H_2O + C_{n-i}H_{2(n-i)+1}OH$	Other	
1-Penten-3-ol (C_5H_9OH)	1.50	295	2.6	0.96	$C_5H_9OH_2^+$ (87): **11**	$C_5H_9^+$ (69): **85**		$C_2H_5OH^+$ (45): **4**	Schoon *et al* (2007)
Z-2-Penten-1-ol (C_5H_9OH)	1.50	295	3	0.94		$C_5H_9^+$ (69): **99**			Schoon *et al* (2007)
E-2-Penten-1-ol (C_5H_9OH)	1.50	295	3	1.1		$C_5H_9^+$ (69): **99**			Schoon *et al* (2007)
3-Methyl-2-buten-1-ol (C_5H_9OH)	[a]1.50 [b]~0.7	[a]295 [b]RT ~300	[a]3.4 [b]2.7±0.5	[a]1.0 [b]0.87		$C_5H_9^+$ (69): [a]**98** [b]major		[b](81): major [b](85): minor	[a]Schoon *et al* (2007) [b]Custer *et al* (2003)
3-Methyl-3-buten-1-ol (C_5H_9OH)	1.50	295	3.2	1.2	$C_5H_9OH_2^+$ (87): **9**	$C_5H_9^+$ (69): **89**			Schoon *et al* (2007)
2-Methyl-3-buten-2-ol (C_5H_9OH)	[a]1.50 [b]1.50 [c]~0.7	[a]295, [b]297 [c]RT ~300	[a]2.6 [b]2.6 [c]2.2±0.4	[a]0.96 [b]0.96 [c]0.71	$C_5H_9OH_2^+$ (87): [a]**18** [b]**17 + 1** at ^{13}C isotope [c]minor	$C_5H_9^+$ (69): [a]**80**, [b]**76 + 4** at ^{13}C isotope [c]major		[c](81): major	[a]Schoon *et al* (2007) [b]Amelynck *et al* (2005) [c]Custer *et al* (2003)
Z-2-Hexen-1-ol ($C_6H_{11}OH$)	1.50	295	2.8	0.88	$C_6H_{11}OH_2^+$ (101): **3**	$C_6H_{11}^+$ (83): **96**			Schoon *et al* (2007)
E-2-Hexen-1-ol ($C_6H_{11}OH$)	[a]1.50 [b]~0.7	[a]295 [b]RT ~300	[a]3.3 [b]~3*	[a]1.2 [b]1	$C_6H_{11}OH_2^+$ (101): [b]minor	$C_6H_{11}^+$ (83): [a]**99** [b]major		[b](81) major [b](99) minor [b](95) minor	[a]Schoon *et al* (2007) [b]Custer *et al* (2003)

Table 3.5 is continued on the following page.

Unsaturated alcohol ($C_nH_{2n-1}OH$)	P_{FT} (mbar)	T_{FT} (K)	k_m (x 10^{-9} m³ s¹)	k_m/k_c	Observed Product Distribution : Product Ion (m/z): Percentage of Product Total, $C_nH_{2n-1}OH + H_3O^+ \rightarrow$				Reference
					$C_nH_{2n-1}OH_2^+ + H_2O$	$C_nH_{2n-1}^+ + 2H_2O$	$C_iH_{2i-1}^+ + H_2O + C_{n-i}H_{2(n-i)+1}OH$	Other	
Z-3-Hexen-1-ol ($C_6H_{11}OH$)	[a]1.50 [b]1.50 [c]~0.7	[a]295, [b]297 [c]RT ~300	[a]3.2 [b]3.2 [c]2.8 ±0.5	[a]1.1 [b]1.1 [c]0.97	$C_6H_{11}OH_2^+$ (101): [a]6, [b]6, [c]minor	$C_6H_{11}^+$ (83): [a]94, [b]88 + 6 at ^{13}C isotope, [c]major		[c](99) minor [c](67) minor	[a]Schoon et al (2007) [b]Amelynck et al (2005) [c]Custer et al (2003)
E-3-Hexen-1-ol ($C_6H_{11}OH$)	[a]1.50 [b]~0.7	[a]295 [b]RT ~300	[a]3.2 [b]2.5±0.4	[a]1.1 [b]0.86	$C_6H_{11}OH_2^+$ (101): [a]6, [b]minor	$C_6H_{11}^+$ (83): [a]93 [b]major	$C_5H_9^+$ (69): [b]minor	[b](99) minor	[a]Schoon et al (2007) [b]Custer et al (2003)
1-Octen-3-ol ($C_8H_{15}OH$)	1.50	295	2.5	0.86	$C_8H_{15}OH_2^+$ (129): 9	$C_6H_{11}^+$ (83): 82	$C_5H_9^+$ (69): 8		Schoon et al (2007)
6-Methyl-5-hepten-2-ol /2-Methyl-2-hepten-6-ol ($C_8H_{15}OH$)	1.50	295	2.9	0.94	$C_8H_{15}OH_2^+$ (129): 14	$C_6H_{11}^+$ (83): 68	$C_5H_9^+$ (69): 16		

Note: P_{FT} denotes pressure in the flow tube, T_{FT} denotes temperature in the flow tube. A helium buffer was used in all cases. k_m denotes the rate constant measured for the reaction of H_3O^+ with the unsaturated alcohol, k_c refers to the collisional rate constant (§ 2.4.1), k_m/k_c is the reaction efficiency. The collisional rate constant was derived using the results of Su and Chesnavich trajectory calculations (§ 2.4.1.4, Eq. 2.49 – 2.54) in the cited references. The accuracy of the rate constants measured by Amelynck et al (2005) and Schoon et al (2007) was estimated to be 25 % with precision better than 5 %. Uncertainty of calculated collisional rate constants were not given in the cited references but are usually 15 to 30 %. Product distributions are not specified by Custer et al (2003), observed product ions are classified as major and minor where minor products are less than half the intensity of major products. *uncertainty was omitted, changes in VOC flow rates caused a systematic variation in the rate coefficient measurement.

Table 3.6: Product distributions and reaction efficiencies of H_3O^+ with various unsaturated alcohols in PTR-MS, PT-CIMS and CIR-TOF-MS.

Unsaturated alcohol ($C_nH_{2n-1}OH$)	P_{dt} (mbar)	T_{dt} (K)	V_{drift} (V)	E (V cm⁻¹)	E/N (Td)	Observed Product Distribution : Product Ion (m/z): **Percentage of Product Total,** $C_nH_{2n-1}OH + H_3O^+ \rightarrow$				Reference
						$C_nH_{2n-1}OH_2^+ + H_2O$	$C_nH_{2n-1}^+ + 2H_2O$	$C_iH_{2i-1}^+ + H_2O + C_{n-i}H_{2(n-i)+1}OH$	Other	
1-Penten-3-ol (C_5H_9OH)	NS	NS	NS	NS	NS	$C_5H_9OH_2^+$ (87): **<5**	$C_5H_9^+$ (69): **95**			Fall *et al* (2001)
Z-2-Penten-1-ol (C_5H_9OH)	NS	NS	NS	NS	NS	$C_5H_9OH_2^+$ (87): **<5**	$C_5H_9^+$ (69): **95**			Fall *et al* (2001)
E-2-Penten-1-ol (C_5H_9OH)	NS	NS	NS	NS	NS	$C_5H_9OH_2^+$ (87): **<5**	$C_5H_9^+$ (69): **95**			Fall *et al* (2001)
3-Methyl-2-buten-1-ol (C_5H_9OH)	NS	NS	NS	NS	NS	$C_5H_9OH_2^+$ (87): **3**	$C_5H_9^+$ (69): **87**	$C_3H_5^+$ (41): **10**		Fall *et al* (2001)
3-Methyl-3-buten-1-ol (C_5H_9OH)	NS	NS	NS	NS	NS	$C_5H_9OH_2^+$ (87): **1**	$C_5H_9^+$ (69): **91**	$C_3H_5^+$ (41): **8**		
2-Methyl-3-buten-2-ol (C_5H_9OH)	[a]NS, [b]1.3 - 2.7* [c]2.4 [d]7.95	[a]NS [b]NS [c]NS [d]313	[a]NS, [b]2450 - 4900, [c]NS [d]2700	[a]NS [b]35-70 [c]NS [d]270	[a]NS [b]NS [c]106 [d]147	$C_5H_9OH_2^+$ (87): [a]**13,** [b]**19,** [c]**19,** [d]**16**	$C_5H_9^+$ (69): [a]**77,** [b]**81,** [c]**71**	$C_3H_5^+$ (41): [a]**10**		[a]Fall *et al* (2001) [b]de Gouw *et al* (2000) [c]Warneke *et al* (2003) [d]Wyche *et al* (2007)

Table 3.6 is continued on the following page.

128

Unsaturated alcohol ($C_nH_{2n-1}OH$)	P_{dt} (mbar)	T_{dt} (K)	V_{drift} (V)	E (V cm^{-1})	E/N (Td)	Observed Product Distribution : Product Ion (m/z): Percentage of Product Total, $C_nH_{2n-1}OH + H_3O^+ \rightarrow$				Reference
						$C_nH_{2n-1}OH_2^+ + H_2O$	$C_nH_{2n-1}^+ + 2H_2O$	$C_iH_{2i-1}^+ + H_2O + C_{n-i}H_{2(n-i)+1}OH$	Other	
E-2-Hexen-1-ol (C$_6$H$_{11}$OH)	[a]1.3 [b]1.3 - 2.7	[a]NS [b]NS	[a] NS, [b]2450 - 4900	[a]NS [b]35-70	[a]NS [b]NS	C$_6$H$_{11}$OH$_2^+$ (101): [a]0.2	C$_6$H$_{11}^+$ (83): [a]76, [b]83	C$_4$H$_7^+$ (55): [a]23, [b]17 C$_5$H$_9^+$ (69): [a]0.8		[a]Fall et al (1999) [b]de Gouw et al (2000)
Z-3-Hexen-1-ol (C$_6$H$_{11}$OH)	[a]1.3 [b]1.3 - 2.7* [c]2.5 [d]NS	[a]NS [b]NS [c]NS [d]NS	[a] NS, [b]2450 - 4900 [c]NS [d]600	[a]NS [b]35-70, [c]NS [d]NS	[a]NS, [b]NS [c]NS, [d]NS	C$_6$H$_{11}$OH$_2^+$ (101): [a]1, [b]4, [c]22	C$_6$H$_{11}^+$ (83): [a]74, [b]80, [c]78, [d] 60.2 + 4.2 at ^{13}C isotope.	C$_4$H$_7^+$ (55): [a]22, [b]9, [d]35.5	? (59): [a]5, [b]7	[a]Fall et al (1999) [b]de Gouw et al (2000) [c]Warneke et al (2002) [d]Buhr et al (2002)
E-3-Hexen-1-ol (C$_6$H$_{11}$OH)	1.3	NS	NS	NS	NS	C$_6$H$_{11}$OH$_2^+$ (101): 2	C$_6$H$_{11}^+$ (83): 70	C$_4$H$_7^+$ (55): 8	? (59): 20	Fall et al (1999)
1-Octen-3-ol (C$_8$H$_{15}$OH)	NS	NS	600	NS	NS	C$_8$H$_{15}$OH$_2^+$ (129): 5.9	C$_8$H$_{15}^+$ (111): 39.0 + 3.8 at ^{13}C isotope	C$_3$H$_5^+$ (41): 3.8 C$_5$H$_9^+$ (69): 42.4+ 2.5 at ^{13}C isotope	? (57): 2.5	Buhr et al (2002)

Note: P_{dt} denotes drift tube pressure, T_{dt} denotes drift tube temperature, V_{drift} denotes voltage applied to the drift tube and E the resultant electric field strength. A buffer of air was used except in the case of de Gouw et al (2000) where helium and air was employed. NS denotes values not specified in reference. Distributions from Buhr et al (2002) were given as relative abundances with the most abundant m/z normalised to 100, values have been converted to percentage distributions and are given to one decimal place. Values from Fall et al (1999, 2001), Warneke et al (2002, 2003) and Buhr et al (2002) were derived using conventional PTR-MS, distributions from de Gouw et al (2000) were obtained from PT-CIMS with an electron impact He/ H$_2$O ion source with a 70 cm drift tube and those from Wyche et al (2007) were measured using CIR-TOF-MS with a radioactive ion source as well as the time-of-flight detection system. Wyche et al (2007) specify the percentage abundance of the ion employed for quantification of the compound in the smog chamber experiments within the reference, the remainder of the total ion signal is unspecified. *A specific value of instrumental parameters (e.g. P_{dt}) is not specified but the range of the parameters during measurements within the reference are specified.

3.1.4 The Reaction of Unsaturated Alcohols in the Presence of Water

Amelynck *et al* (2005) and Schoon *et al* (2007) derived rate constants for the reaction of $H_3O^+(H_2O)$ with 1-penten-3-ol, *Z*-2-penten-1-ol, *E*-2-penten-1-ol, 3-methyl-2-buten-1-ol, 3-methyl-3-buten-1-ol, 2-methyl-3-buten-2-ol, *Z*-2-hexen-1-ol, *E*-2-hexen-1-ol, *Z*-3-hexen-1-ol, *E*-3-hexen-1-ol, 1-octen-3-ol, DL-6-methyl-5-hepten-2-ol in SIFT at ~298 K; in all cases the reaction rates were ~2 – 3 x 10^{-9} cm^3 molecule^{-1} s^{-1} and within uncertainties, efficient. The rate is derived from H_3O^+ and $H_3O^+H_2O$ signals at several small concentrations of unsaturated alcohol and theoretically corresponds to the rate of ligand switching and direct proton transfer. The contribution of each is unknown (Michel *et al* 2005). The MHH_2O^+ ions have been observed from the unsaturated alcohols (Schoon *et al* 2007, Amelynck *et al* 2005). Ligand switching is likely given the relatively large dipoles of unsaturated alcohols, dissociation of the resulting MHH_2O^+ to the protonated alcohol and water may occur at the elevated energies in PTR-MS. Observed MHH_2O^+ may also be formed by association of protonated alcohols from reaction Eq. 3.32 with H_2O . Association of the carbocations ions produced from the dominating dissociation reactions of the alcohols with H_3O^+ ions (Eq. 3.33 and 3.34) is minor (Schoon *et al* 2007, § D.1.3).

3.1.5 Diols

The available proton affinities, gas basicities and resultant standard reaction enthalpy, entropy and Gibbs free energies for the non-dissociative proton transfer reaction of H_3O^+ with a series of acyclic diols are given in Table 3.7 together with the product distributions from the reaction of H_3O^+ with various acyclic diols measured by Španěl *et al* (2002b) in SIFT (~300 K). The energetics of observed dissociative reactions and structures of resultant ions determined by Bouchoux *et al* (1997) are also displayed in Table 3.7

Table 3.7: The product distributions from the reaction of H_3O^+ with a series of acyclic diols measured in SIFT by Španěl *et al* (2002b)

Diol	Observed Product Distribution : Product Ion (m/z): **Percentage of Product Total,** $C_nH_{2n}(OH)_2 + H_3O^+ \rightarrow$ $C_nH_{2n}(OH)_2$ $H^+ + H_2O$	$C_nH_{2n}OH^+$ $+ 2H_2O$	PA (eV)	GB (eV)	ΔH_r^Φ (eV)	ΔS_r^Φ (x 10^{-4} eV K^{-1}) $C_nH_{2n}(OH)_2 + H_3O^+ \rightarrow$ $C_nH_{2n}(OH)_2H^+ + H_2O$	ΔG_r^Φ (eV)	ΔH_r^Φ $M + H_3O^+$ $\rightarrow 2H_2O +$ $(M-OH)^+$ (eV)	ΔH_r^Φ $MH^+ \rightarrow$ $(M-OH)^+$ $+ H_2O$ (eV)	E_c $MH^+ \rightarrow$ $(M-OH)^+$ $+ H_2O$ (eV)
1,2 ethanediol $C_2H_4(OH)_2$	$C_2H_4(OH)_2H^+$ (63): **35**	$C_2H_4OH^+$ protonated ethanal (45): **65**	8.46	8.02	-1.29	-3.93	-1.18	-1.10	+0.19	+1.03
1,2 propanediol $C_3H_6(OH)_2$	$C_3H_6(OH)_2H^+$ (77): **5**	$C_3H_6OH^+$ (59): **95**								
1,3 propanediol $C_3H_6(OH)_2$	$C_3H_6(OH)_2H^+$ (77): **30**	$C_3H_6OH^+$ protonated propanal and protonated oxetane (59): **70**	9.08	8.56	-1.92	-6.71	-1.72	-1.18 (protonated propanal) -0.43 (protonated oxetane)	+0.74 (protonated propanal) +1.49 (protonated oxetane)	+1.69 (protonated propanal) +1.49 (protonated oxetane)
1,2 butanediol $C_4H_8(OH)_2$	$C_4H_8(OH)_2H^+$ (91): **5**	$C_4H_8OH^+$ (73): **95**								
1,3 butanediol $C_4H_8(OH)_2$	$C_4H_8(OH)_2H^+$ (91): **10**	$C_4H_8OH^+$ (73): **90**								
1,4 butanediol $C_4H_8(OH)_2$	$C_4H_8(OH)_2H^+$ (91): **10**	$C_4H_8OH^+$ protonated tetrahydro-furan (73): **90**	9.49	8.86	-2.33	-10.3	-2.02	-1.53	+0.80	+1.14
1,5 pentanediol $C_5H_{10}(OH)_2$	$C_5H_{10}(OH)_2H^+$ (105): **10**	$C_5H_{10}OH^+$ (87): protonated tetrahydro-pyran **90**	9.64[a]	-	-2.48	-	-	-1.95	+0.53	+1.11

Note: The SIFT was normally operated therefore it is assumed pressure in the flow tube was ~0.6 – 1.5 mbar and the flow tube temperature was ~298/300 K. A helium carrier gas was employed and diol vapours were diluted in dry air. Rate coefficients were not measured due to the inability to determine absolute flow rates of diol vapours due to their sticky nature and lack of data on their vapour phase physical properties (Španěl *et al*, 2002b). Proton affinities (*PA*) and gas basicities, (*GB*) are taken from Hunter and Lias (1998) except [a]from Bouchoux *et al* (1997). The standard enthalpies (ΔH_r^{Φ}) and Gibbs free energies (ΔG_r^{Φ}) of the non-dissociative reactions with H_3O^+ are calculated from Eq. 2.88 and 2.89, standard entropies (ΔS_r^{Φ}) are calculated from $\Delta S_r^{\Phi} = \left[\Delta H_r^{\Phi} - \Delta G_r^{\Phi}\right]/T$. The standard enthalpies and critical energies (E_c) of the reactions; $MH^+ \rightarrow (M-OH)^+ + H_2O$ were taken from Bouchoux *et al* (1997). The standard enthalpy of the $M + H_3O^+ \rightarrow 2H_2O + (M-OH)^+$ reactions were calculated from the standard enthalpies of the non-dissociative reactions and $MH^+ \rightarrow (M-OH)^+ + H_2O$ reactions (note that in this case *M* denotes a diol). The specified structures of the *(M-OH)*$^+$ ions were determined by Bouchoux *et al* (1997).

The proton affinities and gas basicities of the acyclic diols are greater than water. Their reaction with H_3O^+ is exoergic by greater than 0.43 eV and reactions are presumed to be efficient (Table 3.7, Hunter and Lias 1998). The non-dissociative reaction (Eq. 3.35) is a minor reaction path for diols and dissociation by elimination of water from the protonated diol (Eq. 3.3) dominates in SIFT (Table 3.7).

$$C_nH_{2n}(OH)_2 + H_3O^+ \rightarrow C_nH_{2n}(OH)_2H^+ + H_2O \qquad (3.35)$$

$$C_nH_{2n}(OH)_2 + H_3O^+ \rightarrow C_nH_{2n}OH^+ + 2H_2O \qquad (3.36)$$
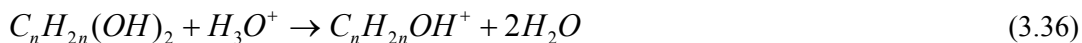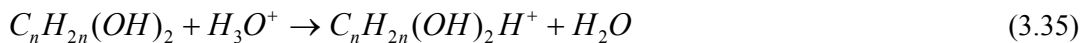
Reaction 3.36 may produce a protonated carbonyl compound or a protonated cyclic ether. Bouchoux *et al* (1997) have found that dissociation of protonated 1, 2-ethanediol produces protonated ethanal, 1, 3-propanediol produces protonated propanal and the cyclic protonated oxetane, 1, 4-butanediol and 1, 5-pentanediol produce the protonated cyclic ethers; tetrahydrofuran and tetrahydropyran. The enthalpies of the overall dissociative reactions (Eq. 3.36) are exothermic. The exothermicity of non-dissociative proton transfer is sufficient to overcome the critical energy required for dissociation of $C_nH_{2n}(OH)_2H^+$ to

$C_nH_{2n}OH^+ + H_2O$.

No measurements of product distributions from the reaction of diols with H_3O^+ in the PTR-MS could be found. At the elevated energies in the PTR-MS, the non-dissociative product may be further reduced or absent. Other dissociation pathways, for example the loss of a second water molecule from $(M-OH)^+$, may become accessible. The enthalpies of reaction for the formation of three water molecules from protonated 1, 2-ethandiol, 1, 3-propanediol, 1, 4-butanediol and 1,5-pentanediol to form $C_2H_3^+$ (m/z 27), $C_3H_5^+$ (m/z 41), $C_4H_7^+$ (m/z 55), $C_5H_9^+$ (m/z 69) respectively are ~ +1.94 eV, + 0.55 eV, +0.03 eV and -0.03 eV (where the enthalpy of formation of the ions were calculated from the proton affinities and enthalpies of formation of ethyne, propyne, 2-butyne and 2-pentyne). The lack of these product ions from the higher diols, where the reaction is approximately thermoneutral or exothermic at room temperature, indicates an energy barrier to the loss of two water molecules from the protonated alcohol greater than the exothermicity of the non-dissociative reaction. In EI-MS, CH_3O^+ (m/z 31) is a major product ion from the diols, for example m/z 31 forms 48.6 %, 16.0 %, 18.6 %, 14.0 % from 1, 2-ethanediol, 1,3-propanediol, 1,4-butanediol and 1, 5-pentanediol. CH_3O^+ may be formed in the PTR-MS by loss of alkanes from the protonated diol.

Španěl *et al* (2002b) also determined product distributions from the reaction of H_3O^+ with 1, 2-cyclopentanediol. The proton affinity of 1, 2-cyclopentanediol is 9.18 eV, the gas basicity is 8.84 eV, the standard enthalpy of the non-dissociative reaction is -2.02 eV, the standard entropy is -0.52 x 10^{-4} eV K^{-1} and the Gibbs free energy is -2.00 eV, the reaction is assumed to be efficient. The non-dissociative product formed 2 % of the product ions, the product of dissociation by elimination of water from the protonated diol formed 94 %. An additional product ion, $C_5H_7^+$, formed by loss of two water molecules from the protonated diol forms 4 % of the product ions. Španěl *et al* (2002b) suggest the ring structure is retained in all the reactions and the $C_5H_7^+$ ion is protonated cyclopentadiene and its stability is derived from its aromatic nature.

3.1.6 The Reaction of Diols in the Presence of Water.

The proton affinities of 1,3-propanediol, 1,4-butanediol and 1, 5-pentanediol are greater than that of $H_3O^+(H_2O)$ suggesting proton transfer to the diols will occur efficiently. The proton affinities of 1, 4-butanediol and 1, 5-pentanediol are also greater than that of $H_3O^+(H_2O)_2$ and proton transfer is likely to occur.

Španěl *et al* (2002b) found that the contribution of ligand switching reactions between diols and $H_3O^+(H_2O)$ to the formation of $(MHH_2O)^+$ hydrates is small compared to the contribution of association of H_2O with protonated diols under SIFT conditions. Both protonated diols and the products of dissociative elimination of H_2O were observed to associate with H_2O. The products of H_2O association with the dissociative product contributes to the m/z at which protonated ion occurs. Three-body rate coefficients for the association of water with the products of H_2O elimination from protonated diols; 1,2 ethanediol, 1,2 propanediol, 1,3 propanediol, 1,2 butanediol, 1,3 butanediol, 1,4 butanediol and 1,5 pentanediol were determined to be 2.2 x 10^{-27} cm^6 s^{-1}, 4.4 x 10^{-27} cm^6 s^{-1}, 1.8 x 10^{-27} cm^6 s^{-1}, 3.6 x 10^{-27} cm^6 s^{-1}, 2 x 10^{-27} cm^6 s^{-1}, 4.4 x 10^{-27} cm^6 s^{-1} and 5.2 x 10^{-27} cm^6 s^{-1} under SIFT conditions (in helium, P_{FT}. ~0.6 – 1.5 mbar and at a flow tube temperature ~298/300 K) This is large compared to the corresponding rate coefficient for association of H_2O with H_3O^+ of ~5.8 x 10^{-28} cm^6 s^{-1} (Španěl *et al* 2002b). Investigation of these reactions under various PTR-MS conditions as a function of humidity is required.

3.2 Aldehydes

3.2.1 The Reaction of Saturated Aldehydes with H_3O^+.

The available proton affinities, gas basicities and resultant standard reaction enthalpy, entropy and Gibbs free energies for the non-dissociative proton transfer reaction of H_3O^+ with various saturated aldehydes are reviewed in Table 3.8 The reaction efficiencies and product distributions of saturated aldehydes in SIFT are collated in Table 3.9.

Table 3.8: A compilation of proton affinities (*PA*), gas basicities (*GB*), potential standard enthalpy (ΔH_r^{Φ}), potential standard entropy (ΔS_r^{Φ}) and Gibbs free energies (ΔG_r^{Φ}) of the non-dissociative H_3O^+ reaction with saturated aldehydes.

Compound	*PA* (eV)	*GB* (eV)	ΔH_r^{Φ} (eV)	ΔS_r^{Φ} (x 10^{-4} eV K^{-1})	ΔG_r^{Φ} (eV)
Methanal (formaldehyde)	7.39	7.08	-0.23	0.49	-0.24
Ethanal (acetaldehyde)	7.96	7.63	-0.80	-0.35	-0.79
1-Propanal (propionaldehyde)	8.15	7.81	-0.98	-0.35	-0.97
1-Butanal (butyraldehyde)	8.22	7.89	-1.05	-0.31	-1.04
2-methylpropanal (*iso*-butyraldehyde)	8.26	7.93	-1.10	-0.28	-1.09
1-Pentanal	8.26	7.93	-1.09	-0.28	-1.09

Note: Proton affinities and gas basicities are taken from Hunter and Lias, (1998) ΔG_r^{Φ} and ΔH_r^{Φ} are calculated from Eq. 2.88 and 2.89, ΔS_r^{Φ} are calculated from $\Delta S_r^{\Phi} = \left[\Delta H_r^{\Phi} - \Delta G_r^{\Phi}\right]/T$.

Table 3.9: Product distributions and reaction efficiencies of H_3O^+ with various saturated aldehydes in SIFT-MS and VT-SIFT.

Saturated Aldehyde ($C_nH_{2n}O$)	P_{FT} (mbar)	T_{FT} (K)	k_m (x 10^{-9} m^3 s^1)	k_m/k_c	Observed Product Distribution : Product Ion (m/z): Percentage of Product Total, $C_nH_{2n}O + H_3O^+ \rightarrow$			Reference
					$C_nH_{2n}OH^+ + H_2O$	$C_nH_{2n-1}^+ + 2H_2O$	Other	
Methanal (formaldehyde CH_2O)	[a]0.67 [b]NS [c]NS	[a]300 [bi]150 [bii]200 [biii]294 [c]NS	[bi]4.4 [bii]3.8 [biii]3.3 [c]3.0	[bi]0.90 [bii]0.88 [biii]0.92 [c]0.91	CH_2OH^+ (31): [a,bi-iii]**100**			[a]Španěl et al (1997) [b]Midey et al (2000) [c]Lindinger et al (1998)
Ethanal (acetaldehyde C_2H_4O)	[a]0.67 [b]NS [c]NS [d]0.67	[a]300 [bi]200 [bii]294 [c]NS [d]300	[a]3.5 [bi]4.7 [bii]3.7 [c]3.6	[a]1.0 [bi]1.0 [bii]0.95 [c]0.97	$C_2H_4OH^+$ (45): [a, bi-ii,d]**100**			[a]Španěl et al (1995b) [b]Midey et al (2000) [c]Lindinger et al (1998) [d]Španěl et al (1997)
1-Propanal (propionaldehyde C_3H_6O)	0.67	300			$C_3H_6OH^+$ (59): **100**			Španěl et al (1997)
1-Butanal (butyraldehyde C_4H_8O)	[a]0.67 [b]0.93	[a]300, [b]RT			$C_4H_8OH^+$ (73): [a]**95,** [b]**95**	$C_4H_7^+$ (55): [a]**5,** [b]**5**		[a]Španěl et al (1997) [b]Španěl et al (2002a)
2-methylpropanal (*iso*-butyraldehyde C_4H_8O)	0.93	RT			$C_4H_8OH^+$ (73): **100**			Španěl et al (2002a)
1-Pentanal ($C_5H_{10}O$)	0.67	300			$C_5H_{10}OH^+$ (87): **75**	$C_5H_9^+$ (69): **25**		Španěl et al (1997)
3-Methyl-butanal (*iso*-valeraldehyde $C_5H_{10}O$)	0.93	RT			$C_5H_{10}OH^+$ (87): **70**	$C_5H_9^+$ (69): **30**		Španěl et al (2002a)
2-Methyl-butanal ($C_5H_{10}O$)	1.5	297	3.7	1.0	$C_5H_{10}OH^+$ (87): **93**	$C_5H_9^+$ (69): **4**	$C_2H_5O^+$ (45): **2** Unspecified: **1**	Michel et al (2005)

Table 3.9 is continued on the following page.

Saturated Aldehyde $(C_nH_{2n}O)$	P_{FT} (mbar)	T_{FT} (K)	k_m (x 10^{-9} m^3 s^{-1})	k_m/k_c	Observed Product Distribution : Product Ion (m/z): Percentage of Product Total, $C_nH_{2n}O + H_3O^+ \rightarrow$			Reference
					$C_nH_{2n}OH^+ + H_2O$	$C_nH_{2n-1}^+ + 2H_2O$	Other	
Pivaldehyde ($C_5H_{10}O$)	1.5	297	3.5	0.88	$C_5H_{10}OH^+$ (87): **99**		Unspecified: **1**	Michel *et al* (2005)
1-Hexanal ($C_6H_{12}O$)	0.67	300			$C_6H_{12}OH^+$ (101): **50**	$C_6H_{11}^+$ (83): **50**		Španěl *et al* (1997)
1-Heptanal ($C_7H_{14}O$)	0.93	RT			$C_7H_{14}OH^+$ (115): **80**	$C_7H_{13}^+$ (97): **20**		Španěl *et al* (2002a)
1-Octanal ($C_8H_{16}O$)	0.93	RT			$C_8H_{16}OH^+$ (129): **85**	$C_8H_{15}^+$ (111): **15**		Španěl *et al* (2002a)
1-Decanal ($C_{10}H_{20}O$)	0.93	RT			$C_{10}H_{20}OH^+$ (157): **97**	$C_{10}H_{19}^+$ (139): **3**		Španěl *et al* (2002a)

Note: Values from Midey *et al* (2000) were measured in VT-SIFT all other values were derived in SIFT at ~298 K. P_{FT} denotes pressure in the flow tube, T_{FT} denotes temperature in the flow tube. A helium buffer was used in all cases. Španěl *et al* (1997) employed air to dilute aldehyde vapours. k_m denotes the rate constant measured for the reaction of H_3O^+ with the saturated aldehyde, k_c refers to the collisional rate constant (§ 2.4.1), k_m/k_c is the reaction efficiency. The collisional rate constant was derived using the results of Su and Chesnavich trajectory calculations (§ 2.4.1.4, Eq. 2.49 – 2.54) in the cited references. The accuracy of the measured overall rate constants in Midey *et al* (2000) were estimated to be ± 25 % and the relative accuracy was estimated to be ± 10 %. The accuracy of the measured rate constants in Michel *et al* (2005) was estimated to be 20 % with a precision better than 5 %. The uncertainty associated with the collisional rate constants were not specified by Midey *et al* (2000) or Michel *et al* (2005). Lindinger *et al* (1998) specify measured thermal rate constants, but conditions were not specified.

The proton affinities and gas basicities of the $C_2 - C_5$ aldehydes are greater than that of water and the standard Gibbs free energies of reactions with H_3O^+ are less than -0.43 eV (Table 3.8). The reaction efficiencies are therefore assumed to be one (§ 2.9) and where values have been measured, they are within experimental uncertainty of one (Table 3.9). The proton affinities and gas basicities increase with increasing number of carbons for the $C_1 - C_5$ aldehydes and it is assumed that reaction of H_3O^+ with the higher aldehydes ($>C_5$) is exoergic and efficient.

In a similar manner to saturated alcohols, unsaturated alcohols and diols the protonated aldehyde (Eq. 3.37) and the product of dissociation by elimination of water (Eq. 3.38) are observed from aldehyde reaction with H_3O^+ (Table 3.9).

$$C_nH_{2n}O + H_3O^+ \rightarrow C_nH_{2n}OH^+ + H_2O \qquad (3.37)$$

$$C_nH_{2n}O + H_3O^+ \rightarrow C_nH_{2n-1}^+ + 2H_2O \qquad (3.38)$$

The extent of dissociation is reduced compared to the alcohols and diols. The extent of dissociation increases with increasing size of the aldehyde from C_1 to C_5 aldehydes.

The non-dissociative product is the only product observed from reaction of H_3O^+ with the $C_1 - C_3$ aldehydes in SIFT. The non-linear C_4 aldehyde, 2-methylpropanal, also reacts by non-dissociation alone (Eq. 3.37), however, a small level of dissociation (5%) by elimination of H_2O (Eq. 3.38) is observed from 1-butanal (Table 3.9). The dissociative product is observed from reaction of all the studied C_5 saturated aldehydes at $4 - 30$ % except pivaldehyde from which the non-dissociative product formed 99 % of the products and 1% was unassigned. Michel *et al* (2005) observed an additional minor dissociation by loss of C_3H_6 from protonated 2-methylbutanal to form $C_2H_5O^+$ at m/z 45. This may have resulted from dissociation to $C_3H_9^+$. However Michel *et al* (2005) observed hydration of the product ion at m/z 45 and therefore ruled out the aliphatic hydrocarbon ion as hydrate formation is not observed from such ions (§ D.1.3). The reaction of 1-hexanal with H_3O^+ produces the dissociative and non-dissociative product in equal quantities (Table 3.9). A decreasing amount of dissociation by elimination of water occurs with increasing aldehydes size from the C_6 to C_{10} aldehydes. The C_7, C_8 and C_{10} aldehydes react predominantly by non-dissociative reaction (Eq. 3.37), the dissociative product forming 20 % to 3 % of the total products.

Španěl *et al* (2002a) suggest by analogy with EI-MS that H_2O elimination may involve formation of a six-membered cyclic intermediate containing at least four carbons. Where a six membered ring is not possible, H_2O elimination is not observed. This may explain, for

example, the lack of dissociation from the reaction of 2-methylpropanal compared to that observed from n-butanal and the lack of dissociation from pivaldehyde compared to the other saturated C_5 aldehydes (Španěl *et al* 2002a, Michel *et al* 2005).

Product distributions from the reaction of some saturated aldehydes with H_3O^+ in the PTR-MS and CIR-TOF-MS under various drift tube conditions are reviewed in Table 3.10. Under the elevated energy conditions of PTR-MS based techniques a greater degree of dissociation is observed for the $C_2 - C_9$ saturated aldehydes.

At *E/N* of 106 Td and P_{dt} of 2.4 mbar ethanal reacts with H_3O^+ *via* the non-dissociative pathway alone (Table 3.10) as in SIFT (Table 3.9). However, at higher *E/N* of 147 and 165 Td and increased P_{dt} of ~7 - 8 mbar fragmentation occurs. The major fragments are at m/z 43 attributed to $C_2H_3O^+$ and m/z 61 attributed to its hydrated cluster, $C_2H_3O^+.H_2O$. The enthalpy for formation of $C_2H_3O^+$ from ethanal and H_3O^+ according to Eq. 3.39, is -0.72 eV to 0.081 eV, where the range arises from the variation in *AE* used to calculated the enthalpy of formation of $C_2H_3O^+$.

$$C_nH_{2n}O + H_3O^+ \rightarrow C_nH_{2n-1}O^+ + H_2 + H_2O \qquad (3.39)$$
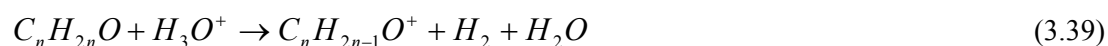
The lack of $C_2H_3O^+$ under the thermal conditions of SIFT at ~ 298 K and at lower *E/N* in the PTR-MS suggests an energy and/or entropy barrier exists. $C_2H_3O^+$ is a major product of EI-MS of ethanal forming 14.5 % of the total product ions (Mallard and Linstrom 2005) and from chemical ionisation of ethanal with O_2^+ in SIFT (45 % of product ions)(e.g. Španěl *et al* 1997). $C_2H_3O^+$ (+*HNO*) is the only product of ethanal reaction with NO^+ in SIFT (Španěl *et al* 1997). The m/z 41 ion forms a minor product from ethanal at higher *E/N* in the PTR-MS; this may arise from the loss of two hydrogen molecules from protonated ethanal to form C_2HO^+. m/z 41 is a minor product of EI-MS of ethanal forming 1.5 % of products.

Propanal similarly forms only the non-dissociative product, $C_3H_6OH^+$ (m/z 59), at *E/N* of 106 Td (Table 3.10) as in SIFT (Table 3.9). At higher *E/N,* dissociation by elimination of water (Eq. 3.38) to $C_3H_5^+$ (m/z 41) occurs. At *E/N* of 148 Td minor fragments were also observed at m/z 31 and m/z 20. Fragmentation of protonated propanal to m/z 31 and m/z 41 has also been observed in PTR-ITMS, fragment abundancies increasing by approximately similar amounts with increased FNF voltage (Prazeller *et al* 2003, Warneke *et al* 2005a). The m/z 31 ion is attributed to CH_3O^+ formed by the loss of C_2H_4 from protonated propanal (Prazeller *et al* 2003). Loss of an alkene from protonated 2-methylbutanal has been observed in SIFT (Michel *et al* 2005).

Table 3.10: The ion product distributions as percentage of the total ion signal resulting from the reaction of a series of saturated aldehydes with H_3O^+ in PTR-MS and CIR-TOF-MS.

Saturated Aldehyde ($C_nH_{2n}O$)	P_{dt} (mbar)	T_{dt} (K)	V_{drift} (V)	E (V cm^1)	E/N (Td)	Observed Product Distribution : Product Ion (m/z): **Percentage of Product Total, $C_nH_{2n}O + H_3O^+ \rightarrow$**				Reference
						$C_nH_{2n}OH^+ + H_2O$	$C_nH_{2n-1}^+ + 2H_2O$	$C_iH_{2i-1}^+$ or $C_iH_{2i-3}O^+$	Other	
Methanal (CH_2O)	[ai]2.1 [aii]2.1	[ai]378 [aii]378	[ai]400 [aii]600	[ai]43.5 [aii]65.2	[ai]108 [aii]162	CH_2OH^+ (31): [ai]**~90 +~5** at isotope [aii]**100**			$(CH_2O)_2H^+$ (61):[ai] **~5**	[a]Inomata et al (2008) [b]Lindinger et al (1998)
	[b]NS	[b]NS	[b]NS	[b]NS	[b]NS	[b]**100**				
Ethanal (C_2H_4O)	[a]2.4 [b]7.09* [c]7.95* [d]NS	[a]NS [b]313 [c]313 [d]NS	[a]NS [b]2700 [c]2700 [d]NS	[a]NS [b]270 [c]270 [d]NS	[a]106 [b]165 [c]147 [d]NS	$C_2H_4OH^+$ (45): [a]**100,** [b]**47,** [c]**47** [d]**100**			$C_2H_3O^+$ (43): [b]**20** $C_2H_3O^+.H_2O?$ (61): [b]**26** C_2HO^+ ?(41) : [b]**6** ? (39): [b]**1**	[a]Warneke et al (2003) [b]Blake et al (2006) [c]Wyche et al (2007) [d]Lindinger et al (1998)
Propanal (C_3H_6O)	[a]2.4 [b]NS [c]NS [d]NS	[a]NS [b]NS [c]NS [d]NS	[a]NS [b]600 [c]NS [d]NS	[a]NS [b]NS [c]NS [d]NS	[a]106, [b]NS [c]148 [d]NS	$C_3H_6OH^+$ (59): [a]**100,** [b]**95.2,** [c]**~80.0** [d]**100**	$C_3H_5^+$ (41): [b]**4.8,** [c]**~4.0**		CH_3O^+ ? (31):[c]**12.0** ? (20)**: [c]**4.0**	[a]Warneke et al (2003) [b]Buhr et al (2002) [c]Wyche et al (2005) [d]Lindinger et al (1998)

Table 3.10 is continued on the following page.

Saturated Aldehyde ($C_nH_{2n}O$)	P_{dt} (mbar)	T_{dt} (K)	V_{drift} (V)	E (V cm^{-1})	E/N (Td)	Observed Product Distribution : Product Ion (m/z): Percentage of Product Total, $C_nH_{2n}O + H_3O^+ \rightarrow$				Reference
						$C_nH_{2n}OH^+ + H_2O$	$C_nH_{2n-1}^+ + 2H_2O$	$C_iH_{2i-1}^+$ or $C_iH_{2i-3}O^+$	Other	
1-Butanal (C_4H_8O)	[a]2.4 [b]NS [c]NS [d]NS	[a]NS [b]NS [c]NS [d]NS	[a]NS [b]600 [c]NS [d]NS	[a]NS [b]NS [c]NS	[a]106, [b]NS [c]148 [d]NS	$C_4H_8OH^+$ (73): [a]**43,** [b]**6.3,** [d]**65**	$C_4H_7^+$ (55): [a]**57,** [b]**89.3 +**[13]**C:4.5** [c]**95.2,** [d]**35**		? (88)**: [c]**4.4**	[a]Warneke et al (2003) [b]Buhr et al (2002) [c]Wyche et al (2005) [d]Lindinger et al (1998)
1-Pentanal ($C_5H_{10}O$)	[a]2.4 [b]NS	[a]NS [b]NS	[a]NS [b]600	[a]NS [b]NS	[a]106, [b]NS	$C_5H_{10}OH^+$ (87): [a]**22,** [b]**5.0**	$C_5H_9^+$ (69): [a]**78,** [b]**71.4 +** [13]**C:5.0**	(41): [b]**15**	$C_3H_5O^+$? (57): [b]**3.6**	[a]Warneke et al (2003) [b]Buhr et al (2002)
1-Hexanal ($C_6H_{12}O$)	[a]2.4 [b]NS [c]1.3 [d]7.09* [e]7.95* [f]NS	[a]NS [b]NS [c]NS [d]313 [e]313 [f]NS	[a]NS [b]600 [c]NS [d]2700 [e]2700 [f]NS	[a]NS [b]NS [c]NS [d]270 [e]270 [f]NS	[a]106, [b]NS [c]NS [d]165 [e]147 [f]148	$C_6H_{12}OH^+$ (101): [a]**43,** [b]**3.8,** [c]**5**	$C_6H_{11}^+$ (83): [a]**57,** [b]**62.5+** [13]**C:4.4,** [c]**73,** [d]**57,** [e]**52,** [f]**~57.1**	(55): [b]**29.4,** [c]**22,** [d]**43,** [f]**~42.9**		[a]Warneke et al (2003) [b]Buhr et al (2002) [c]Fall et al (1999) [d]Blake et al (2006) [e]Wyche et al (2007) [f]Wyche et al (2005)
1-Heptanal ($C_7H_{14}O$)	[a]2.4 [b]NS	[a]NS [b]NS	[a]NS [b]600	[a]NS [b]NS	[a]106, [b]NS	$C_7H_{14}OH^+$ (115): [a]**48,** [b]**4.9**	$C_7H_{13}^+$ (97): [a]**48,** [b]**61.3 +**[13]**C:5.5**	(55): [b]**24.5** (69): [b]**3.7**		[a]Warneke et al (2003) [b]Buhr et al (2002)
1-Octanal ($C_8H_{16}O$)	[a]2.4 [b]NS	[a]NS [b]NS	[a]NS [b]600	[a]NS [b]NS	[a]106, [b]NS	$C_8H_{16}OH^+$ (129): [a]**68,** [b]**10.8**	$C_8H_{15}^+$ (111): [a]**32,** [b]**37.8 +** [13]**C:3.6**	(41): [b]**3.2** (55): [b]**2.4** (69): [b]**39.8 +** [13]**C:2.4**		[a]Warneke et al (2003) [b]Buhr et al (2002)
Nonanal ($C_9H_{18}O$)	NS	NS	600	NS	NS	$C_9H_{18}OH^+$ (143): **18.6 +** [13]**C:2.2**	$C_9H_{17}^+$ (125): **10.8**	(41): **3.2** (55): **3.6** (69): **35.8 +** [13]**C:2.2** (83): **15.1**	$C_3H_5O^+$? (57): **8.6**	Buhr et al (2002)

Note: P_{dt} denotes drift tube pressure, T_{dt} denotes drift tube temperature, V_{drift} denotes voltage applied to the drift tube and E the resultant electric field strength. Distributions in Buhr *et al* (2002) and Wyche *et al* (2005) are given as relative abundancies in reference where the most abundant m/z is normalised to 100, these values are converted to percentage distributions here and given to one decimal place. Raw count rates at each product ion m/z are displayed in Inomata *et al* (2007) and have been used to calculate approximate percentage product distributions here. Distributions in Wyche *et al* (2005, 2007) and Blake *et al* (2006) were measured in CIR-TOF (in this case with H_3O^+ ion) other values were measured in conventional PTR-MS. Wyche *et al* (2007) give only the abundance of the m/z employed in the measurements performed within the reference, usually the most abundant m/z, these values are included here for comparison. Values from Inomata *et al* (2008) were obtained using an undiluted standard (1.02 ppm) and were performed under dry conditions, i.e. only water from the ion source was present in the drift tube). Measurements by Lindinger *et al* (1998) are assumed to be made in PTR-MS but measurement conditions are not specified.

The product of hydrogen elimination *via* Eq. 3.39 is not observed from propanal at the *E/N* employed by the PTR-MS/PTR-TOF-MS studies reviewed in Table 3.8. $C_3H_5O^+$ (m/z 57) is a minor product (1.8 %) of EI-MS of propanal and a major product (50 %) of chemical ionisation of propanal with O_2^+ in SIFT and the sole product ion from reaction with NO^+ in SIFT (Španěl *et al* 1997). The formation of $C_3H_5O^+$ from propanal and H_3O^+ (Eq. 3.39) is exothermic by 0.84 eV (enthalpy of formation of the ion calculated from *AE*), the absence of the product indicates an energy and/or entropy barrier exists.

The products of *H* loss from the parent ion in EI-MS of >C_3 aldehydes are minor. Likewise the products of *H* loss from the parent ion produced from O_2^+ reaction of the saturated aldehydes are not observed from the higher saturated aldehydes in SIFT (Španěl *et al* 1997, Španěl *et al* 2002a). The product ion from reaction Eq. 3.39 are not observed from the higher aldehydes in the PTR-MS based techniques at the drift tube conditions employed by the studies collated in Table 3.9.

Formation of RCO^+ ions from carbonyl containing compounds in EI-MS is well established, the stability of such ions arises from the sharing of the positive charge between the carbon and oxygen (Duckett and Gilbert 2000). Thus HCO^+ is the predominant ion from EI-MS of ethanal (30.7 %) and propanal (24.4 %) and a major ion from the higher aldehydes (Mallard and Linstrom 2005). Formation of this ion is not observed from charge transfer reactions with O_2^+ or NO^+ in SIFT (Španěl *et al* 1997, Španěl *et al* 2002a) or from NO^+ in the drift tube of CIR-TOF-MS (Wyche *et al* 2005). HCO^+ formation by loss of an alkane from the protonated aldehydes is endothermic. The enthalpy of the reaction for ethanal is ~0.70 to 0.76 eV and for propanal is 0.93 eV, where the enthalpy of formation of HCO^+ is calculated from appearance energies. If the enthalpy of formation of HCO^+ is calculated from the proton affinity and enthalpy of formation of *CO,* assuming protonation occurs at carbon, the enthalpies of the reactions are 0.85 eV and 0.95 eV respectively. The sum of $KE_{c.m}^b$ (0.12 eV to 0.22 eV) and $KE_{c.m}^r$ for ethanal-H_3O^+ in air at *E/N* of 100 to 140 Td is 0.25 eV to 0.47 eV for propanal-H_3O^+ 0.26 eV to 0.48 eV. Thus there is insufficient energy for the reaction. In EI-MS of $C_4 - C_7$ aldehydes where γ hydrogens are present $[H_2C=CHOH]^+$ at m/z 44 formed by McLafferty rearrangement of the parent ion is the dominant ion (Harwood and Claridge 1997, Duckett and Gilbert 2000, Mallard and Linstrom 2005). The m/z 44 ion forms 17. 8 %, 27.1 %, 17.4 % and 12.4 % of the total product from EI-MS of 1-butanal, 1-pentanal, 1-hexanal and 1-heptanal respectively; but is not observed in PTR-MS.

At E/N of 106 Td the products of non-dissociative (Eq. 3.37) and dissociative elimination of water (Eq. 3.38) are formed in similar amounts from H_3O^+ reaction with 1-butanal (Table 3.9) compared to a 95% dominance of the non-dissociative product in SIFT (Table 3.8). At higher E/N the non-dissociative product dominates, constituting 95 % of the products at E/N of 148 Td and an additional minor fragment at m/z 88 is formed (Table 3.9).

In the PTR-MS based techniques, the non-dissociative product is reduced and the product of dissociation by elimination of H_2O increased for the C_5 to C_9 saturated aldehydes compared to in thermal SIFT. The additional energy in the drift tube enables a third dissociation pathway (Eq. 3.40) for the C_5 to C_9 saturated aldehydes, product ions at m/z 41, 55, 69 and 83 are produced. These ions may be $C_iH_{2i-1}^+$ and/or $C_iH_{2i-3}O^+$ potentially formed by reaction Eq. 3.40 and 3.41:

$$C_nH_{2n}O + H_3O^+ \rightarrow C_iH_{2i-3}O^+ + C_{n-i}H_{2(n-i)+2} + H_2 + H_2O \tag{3.40}$$

$$C_nH_{2n}O + H_3O^+ \rightarrow C_iH_{2i-1}^+ + C_{n-i}H_{2(n-i)+1}OH + H_2O \tag{3.41}$$
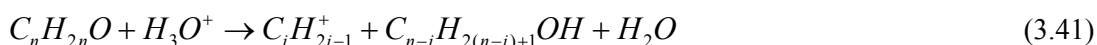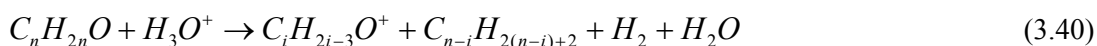
The standard enthalpies of reaction Eq. 3.40 and 3.41 for 1-pentanal, 1-heptanal and 1-octanal are given in Table 3.11. Dissociation to these m/z increases with increasing size of aldehydes.

Table 3.11 The standard enthalpies of some potential dissociation reactions of the higher saturated aldehydes with H_3O^+.

Saturated Aldehyde ($C_nH_{2n}O$)	Product ion (m/z) ΔH_r^Φ (eV) $C_nH_{2n}O + H_3O^+ \rightarrow$	
	$C_iH_{2i-3}O^+ + C_{n-i}H_{2(n-i)+2} + H_2 + H_2O$	$C_iH_{2i-1}^+ + C_{n-i}H_{2(n-i)+1}OH + H_2O$
1-Pentanal ($C_5H_{10}O$)	C_2HO^+ (41) +3.91[a]	$C_3H_5^+$ (41) +1.28[b]
1-Heptanal ($C_7H_{14}O$)	$C_3H_3O^+$ (55) +0.46[a]	$C_4H_7^+$ (55) +0.71[b]
	$C_4H_5O^+$ (69) +0.14[a]	$C_5H_9^+$ (69) +0.40[b]
1-Octanal ($C_8H_{16}O$)	$C_3H_3O^+$ (55) +0.52[a]	$C_4H_7^+$ (55) +0.78[b]
	$C_4H_5O^+$ (69) +0.20[a]	$C_5H_9^+$ (69) +0.48[b]

Note: Values are derived using enthalpies of formation of ions from [a]Lias *et al* 1988 in which the standard enthalpy of formation of C_2HO^+ and $CH_2=CHCO^+$ were derived from appearance energies, [b]proton affinities and enthalpies of formation. The enthalpy of formation of $C_3H_5^+$, $C_4H_7^+$, $C_5H_9^+$, and $C_4H_5O^+$ were derived from proton affinities and enthalpies of formation of propyne, 2-butyne, 2-pentyne and furan. $C_{n-i}H_{2(n-i)+1}OH$ molecules were taken to be straight chain alcohols with the OH attached to carbon one and $C_{n-i}H_{2(n-i)+2}$ to be straight chain alkene with double bond between carbons one and two. Enthalpies of formation were taken from Mallard and Linstrom (2005) except that of 1-pentenal which was taken from Ellis *et al* (1999). Proton affinities were taken from Hunter and Lias (1998).

Buhr *et al* (2002) also observed product ions at m/z 57 from the reaction of H_3O^+ with 1-pentanal and 1-nonanal. This may correspond to $C_3H_5O^+$ and/or $C_4H_9^+$.

3.2.2 The Reaction of $>C_2$ Saturated Aldehydes in the Presence of Water.

The proton affinities of the $C_2 - C_5$ aldehydes listed in Table 3.8 are less than those of the $H_3O^+(H_2O)_n$ $n=1 - 3$ and direct proton transfer does not occur. The rates of reaction of various aldehydes with $H_3O^+(H_2O)$ are given in Table 3.12. In SIFT ligand switching reactions between aldehydes and $H_3O^+(H_2O)$ occur rapidly and are efficient (Table 3.12, Hansel *et al* 1997). Acetaldehyde has been observed to undergo efficient ligand switching reactions with both $H_3O^+(H_2O)_2$ and $H_3O^+(H_2O)_3$ in SIFT at ~298 K forming $MH^+(H_2O)$ and $MH^+(H_2O)_2$ (Midey *et al* 2000, Španěl and Smith 1995c). MHH_2O^+ ions are also formed by three body association of H_2O with the protonated aldehydes (produced from reaction of the aldehydes with H_3O^+). The rates of these association reactions under SIFT conditions are reviewed in Table 3.12. Association of the protonated aldehydes to form the dehydrate, $MH^+(H_2O)_2$, also occurs but is much slower (Španěl *et al* 2002a).

The predominant fragment ions from H_3O^+ reaction with the aldehydes produced by loss of H_2O from the protonated aldehydes do not appear to associate with H_2O in SIFT (Španěl *et al* 2002a, § D.1.3) .

Table 3.12: Measured rate constants for the reaction of various aldehydes with $H_3O^+(H_2O)$ denoted $k_m[M + H_3O^+(H_2O)]$. The efficiency of these reactions (k_m/k_c) have been calculated from collisional rate constants cited in the specified references.

Compound	P_{FT} (mbar)	T_{FT} (K)	$k_m[M + H_3O^+(H_2O)]$ (x 10^{-9} cm^{-3} s^{-1})	k_m/k_c	$k_m[MH^+ + H_2O]$ (x 10^{-27} cm^{-6} s^{-1})
Ethanal	[a,b]NS	[a]300	[a]3.2	[a]1.07	
		[b]294	[b]3.5	[b]1.09	
1-Butanal	0.93	RT			[c]10
2-methylpropanal	0.93	RT			[c]10
3-Methyl-butanal	0.93	RT			[c]12
2-Methyl-butanal	1.5	297	[d]3.9	[d]1.18	[d]19
Pivaldehyde	1.5	297	[d]3.8	[d]1.23	[d]7.5
1-Hexanal	0.67	300			
1-Heptanal	0.93	RT			[c]10
1-Octanal	0.93	RT			[c]8
1-Decanal	0.93	RT			[c]11

Note: $k_m[MH^+ + H_2O]$ denotes the three-body rate constant for association of the protonated aldehyde with H_2O under the specified SIFT conditions. Values are taken from [a]Španěl and Smith (1995c), [b]Midey *et al* (2000), [c]Španěl *et al* (2002a) and [d]Michel *et al*

(2005). Španěl and Smith (1995c), Midey *et al* (2000) and Michel *et al* (2005) derived collisional rate constants using the results of Su and Chesnavich trajectory calculations (§ 2.4.1.4, Eq. 2.49 – 2.54). The accuracy of rate constants measured in Midey *et al* (2000) is ± 25 %, relative accuracy ± 10 %, rate constants given by Španěl and Smith (1995c), Španěl *et al* (2002a) and Michel *et al* (2005) are estimated to be accurate to ± 20 %. A helium buffer was used in all measurements.

3.2.3 The Reaction of Methanal with H_3O^+.

The reactions of methanal with H_3O^+ and $H_3O^+(H_2O)_n$ ions have been studied extensively over a range of reaction conditions by Hansel *et al* (1997), Midey *et al* (2000), Inomata *et al* (2008). The measurement of methanal in the PTR-MS is also well characterised (Steinbacher *et al* 2004, Inomata *et al* 2008) and the following section serves as a brief overview only.

The proton affinity and gas basicity of methanal are marginally greater than those of H_2O (Table 3.8). The Gibbs free energy for the reaction of methanal with H_3O^+ is -0.23 eV, this is close to the threshold of -0.21 eV (Bouchoux *et al* 1996) to -0.43 eV (Bohme *et al* 1980) above which proton transfer reactions appear to be inefficient (§ 2.6). The measured thermal rate constant is less than the calculated collisional rate constant but within the uncertainties of these values the reaction is efficient (Table 3.9). However, since the VMR of water in the PTR-MS is often much greater than that of methanal, the overall rate of the only slightly endothermic reverse reaction, Eq. 3.42, is significant.

$$CH_3O^+ + H_2O \rightarrow CH_2O + H_3O^+ \qquad (3.42)$$

In the PTR-MS additional energy is put into this endothermic reaction and the rate for the reaction therefore increases as a function of $KE_{c.m}^r$ (thus *E/N)* so that loss of protonated methanal by reaction with H_2O (Eq. 3.42) is increasingly significant. The rate constant of the forward reaction decreases as a function of $KE_{c.m}^r$ (Hansel *et al* 1997). Since some decrease in the collisional rate constant is expected as *E/N* is increased (§ 2.4.1.5), it is not clear whether a decrease in efficiency also occurs. Where non-dissociative reactions alone are considered, theoretical thermokinetic relationships suggest a positive temperature dependence of efficiency (Bouchoux *et al* 1996) though temperature dependencies of Gibbs energies should be considered. Given the input of energy into an exothermic reaction, the decrease in rate is unsurprising. Thus quantification of methanal *via* Eq. 2.10 results in an underestimation of VMRs (Hansel *et al* 1997, Steinbacher *et al* 2004, Inomata *et al* 2008).

At lower energies a three-body association reaction of protonated methanal with H_2O (Eq. 3.43) competes with the two body reverse reaction (Eq. 3.42)

$$CH_3O^+ + H_2O \rightarrow CH_3O^+(H_2O) \qquad (3.43)$$

Thus initially due to the negative energy dependence of such association reactions the overall rate of removal of CH_3O^+ decreases with increasing $KE_{c.m}^r$ (Hansel *et al* 1997).

Hansel *et al* (1997) investigated the rates of removal of CH_3O^+ and the forward non-dissociative reaction in SIFDT with a helium buffer at a pressure of ~0.3 mbar. They found that the overall rate constant for removal of CH_3O^+ decreased as $KE_{c.m}^r$ increased from 0.05 eV to 0.06 eV then increased as $KE_{c.m}^r$ was further increased. The increase in rate constant for CH_3O^+ removal with $KE_{c.m}^r$ indicating the dominance of the binary reverse reaction, Eq. 3.42. They also observed rapid ligand switching between $CH_3O^{+}(H_2O)$, produced *via* Eq.3.43, and H_2O (Eq. 3.44) at H_2O flow rates of greater than 4 standard cm^3 min^{-1}. A rate constant of 3.5 x 10^{-10} cm^{-3} s^{-1} was obtained at $KE_{c.m}^r$ of 0.05 eV corresponding to an endothermicity of ~0.06 eV. The reverse of the reaction was studied by Midey *et al* (2000) and observed to proceed with a rate of 2.3 x 10^{-9} cm^3 s^{-1} at 294 K (efficiency 0.77).

$$CH_3O^+(H_2O) + H_2O \rightarrow H_3O^+(H_2O) + CH_2O \tag{3.44}$$

Inomata *et al* (2008) derived humidity dependent sensitivities by fitting of m/z 31 (H_3CO^+) normalised count rates over a range of water vapour concentrations at a fixed known VMR of H_2CO. The reader is referred to the reference for further details and kinetic basis of the equation of the fit. This was repeated at three drift tube conditions by variation of V_{drift} (P_{dt} and T_{dt} fixed) to obtain humidity dependent sensitivities over the range of corresponding $KE_{c.m}^r$. The ratio of forward and reverse rate constants multiplied by the VMR of H_2CO was obtained from one of the fitting parameters and compared with an empirical value determined using the rate constants derived by Hansel *et al* (1997). Allowing for differences attributed to losses of C_2HO from the calibration system, the values were in approximate agreement.

Inomata *et al* (2008) observed a small degree of protonated methanal dimer formation at an *E/N* of 108 Td alongside the non-dissociative protonated methanal. The dimer was not observed at the higher *E/N* of 162 Td as expected given the negative energy dependence of association reactions. These product distributions were measured using a methanal standard with a mixing ratio of 1.02 ppm; however the dimer was also observed in a diluted sample of the standard with mixing ratio of 23.3 ppb. Further investigation of the formation of the dimer as a function of the methanal mixing ratio as well as *E/N* is required. In comparison to

the extent of dimer formation measured in the reactions of methanol and ethanol by Malekina *et al* (2007), the methanal dimer constitutes a small proportion of the products. Neglect of the methanal dimer will have a comparatively small effect on resulting mixing ratios and sensitivities. Indeed, Inomata *et al* (2008) obtained methanal VMRs using count rates at m/z 31 and the humidity dependent sensitivity derived from fitting of calibration data at *E/N* 108 Td in ambient measurement and after correction for other contributors to m/z 31 (§ 3.1.1 and 3.7) observed a good correlation between the PTR-MS derived concentrations and those measured by Multi-Axis Differential Absorption Spectroscopy (MAX-DOAS); $[HCHO]_{MAX-DOAS}=(0.99\pm0.16)[HCHO]_{PTR-MS}+(0.02\pm0.38)$ where [ ] denotes VMR.

3.3 Carboxylic Acids.

3.3.1 The Reaction of Carboxylic Acids with H_3O^+.

The available proton affinities, gas basicities and resultant standard reaction enthalpy, entropy and Gibbs free energies for the non-dissociative proton transfer reaction of H_3O^+ with various carboxylic acids are collated in Table 3.13 Measurements of product distributions and rates of reaction of H_3O^+ with a range of carboxylic acids in SIFT are also given in Table 3.13.

The proton affinities and gas basicities of methanoic acid, ethanoic acid and propanoic acid are greater than that of water. The Gibbs free energies of the non-dissociative reactions of the C_1-C_3 carboxylic acids are less than -0.43 eV and measurements indicate the reactions of H_3O^+ with methanoic and ethanoic acid are efficient. The proton affinity and gas basicities increase with increasing carboxylic acid size and it is assumed that the gas basicities of the $>C_3$ carboxylic acids are greater than that of water and reaction with H_3O^+ is efficient.

The carboxylic acids react with H_3O^+ *via* one or more of two pathways in SIFT; non-dissociation (Eq. 3.45) and dissociative elimination of H_2O (Eq. 3.46).

$$RCO_2H + H_3O^+ \rightarrow RCO_2H_2^+ + H_2O \qquad (3.45)$$

$$RCO_2H + H_3O^+ \rightarrow RCO^+ + 2H_2O \qquad (3.46)$$

The enthalpies of the dissociative reaction (Eq. 3.46) are given in Table 3.13. The thermodynamically favoured site of protonation of the carboxylic acids is the carbonyl carbon (Mackay *et al* 1978, Harrison 1992). Elimination of H_2O therefore requires a 1,3-hydrogen shift and thus involves an energy barrier governing the energy required for reaction (Harrison 1992).

Methanoic acid reacts *via* non-dissociation alone. Španěl and Smith (1998a) observed only the non-dissociative product from ethanoic acid reaction with H_3O^+. Mackay *et al* (1978) and Warneke *et al* (1996) observed a small degree of dissociative elimination of H_2O from protonated ethanoic acid. Measurements of Warneke *et al* (1996) were using SIFDT and product distributions in Table 3.13 correspond to the lowest $KE_{c.m}^r$ used; ~0.06 – 0.07 eV, this is slightly greater than KE ($3/2\,k_BT$) under thermal conditions of SIFT at ~300 K. Measurements by Mackay *et al* (1978) were using FA and SIFT and in hydrogen carrier gas rather than helium employed by Španěl and Smith (1998a).

The $>C_2$ carboxylic acids in Table 3.13 all react with H_3O^+ predominantly by dissociation and a small (10 %) degree of dissociation by elimination of H_2O in SIFT. No variation in the extent of dissociation was observed with increasing carboxylic acid size or between isomers in SIFT (Table 3.12). Dissociation is less than that observed from alcohols (§ 3.1) and higher aldehydes (§ 3.2). Španěl and Smith (1998a) observed 5 % less dissociation of the unsaturated 2-propenoic acid compared to the saturated propanoic acid.

The additional OH of lactic acid results in different fragmentation; $C_2H_5O^+$ (m/z 45) is the dominant product ion from reaction of lactic acid with H_3O^+ in SIFT. Berruyer-Penaud *et al* (2004) have shown that $C_2H_5O^+$ (m/z 45) is formed from protonated lactic acid by loss of CO followed by loss of H_2O. At higher energies loss of H_2O from protonated lactic acid was observed.

The product distributions observed from the reaction of various carboxylic acids with H_3O^+ in the PTR-MS are reviewed in Table 3.14. As in SIFT at thermal energies Lindinger *et al* (1998) observed only the non-dissociative product from methanoic acid (Table 3.14). The dissociation of all $>C_2$ protonated carboxylic acids except 2-methyl-propanoic acid is increased at the elevated energies in the PTR-MS. The dissociative product ion forms ~ 20 – 40 % of product ions from the $C_2 – C_6$ *n*-carboxylic acids at ~ E/N of ~ 120 – 145 Td (P_{dt} ~2 mbar, T_{dt} 313 – 333 K), there is no clear trend in extent of dissociation with size of carboxylic acid. Unlike SIFT, differences were observed in the extent of dissociation from different isomers in the PTR-MS. Von Hartungen *et al* (2004) observed 19 % less dissociation from the reaction of 2-methyl-propanoic acid compared to the *n*-butanoic acid isomer and 2.7 % less dissociation from 3-methyl-butanoic acid compared to pentanoic acid. Under the measurement conditions employed by those studies collated in Table 3.13 no additional dissociation pathways were observed.

Table 3.13: The reaction rates, efficiencies and product distributions from the reaction of H_3O^+ with a series of carboxylic acids measured in SIFT.

Carboxylic Acid (*ROOH*)	PA (eV)	GB (eV)	ΔH_r^{Φ} (eV)	ΔS_r^{Φ} (x 10^{-4} eV K^{-1})	ΔG_r^{Φ} (eV)	k_m (x 10^{-9} m^3 s^1)	k_m/k_c	Observed Product Distribution : Product Ion (m/z): **Percentage of Product Total,** ΔH_r^{Φ} (eV), $ROOH + H_3O^+ \rightarrow$		
								$ROOHH^+ + H_2O$	$RO^+ + 2H_2O$	Other
Methanoic acid (Formic acid)	7.69	7.36	-0.53	-0.24	-0.52	[b]2.7 [c]2.7±0.8	[b]1.0 [c]1.5	$CH_3O_2^+$ (47): [a]**100**, [c]**100**	$+1.0$ to $+1.43^e$ 1.35^f	
Ethanoic acid (Acetic acid)	8.12	7.80	-0.96	-0.03	-0.96	[b]3.0 [c]3.0±0.9 [d]0.6	[b]1.1 [c]1.4 [d]0.2	$C_2H_5O_2^+$ (61): [a]**100**, [c]**95**, [d]**95**,	$C_2H_3O^+$ (43): [c]**5**, [d]**5**, -0.42 to -0.12^e, $+0.13^a$, $+0.28^c$	
Propanoic acid (Propionic acid)	8.26	7.94	-1.10	0.00	-1.10			$C_3H_7O_2^+$ (75): [a]**90**	$C_3H_5O^+$ (57) [a]**10,** -0.63 to $+0.53^e$, -0.39^a	
n-Butanoic acid (*n*-Butyric acid)								$C_4H_9O_2^+$ (89): [a]**90**	$C_4H_7O^+$ (71): [a]**10,** $+0.03$ to $+0.23^e$	
2-Methyl-propanoic acid (*iso*-Butyric acid)								$C_4H_9O_2^+$ (89): [a]**90**	$C_4H_7O^+$ (71): [a]**10**	
Pentanoic acid (Valeric acid)								$C_5H_{11}O_2^+$ (103): [a]**90**	$C_5H_9O^+$ (85): [a]**10**	
2,2 dimethylpropanoic acid (Trimethylacetic acid, pivalic acid)								$C_5H_{11}O_2^+$ (103): [a]**90**	$C_5H_9O^+$ (85): [a]**10**	
2-Propenoic acid (Acrylic acid)								$C_3H_5O_2^+$ (73): [a]**95**	$C_3H_3O^+$ (55): [a]**5**	
2-hydroxy-propanoic acid (Lactic acid)	[gi]8.47 [gii]8.41	[gi]8.13 [gii]8.06	[gi]-1.31 [gii]-1.25	[gi]-0.66 [gii]-1.18	[gi]-1.29 [gii]-1.22			$C_3H_7O_3^+$ (91): [a]**25**		$C_2H_5O^+$ (45): [a]**75**

Note: Values from [a]Španěl and Smith (1998a) using a flow tube pressure of ~0.7 mbar (0.5 Torr) and the flow tube temperature of 300 K. A helium carrier gas was used, carboxylic vapours were diluted in dry cylinder air. Rate coefficients were not measured by Španěl and Smith (1998a) due to the inability to determine absolute flow rates of carboxylic acid vapours due to their sticky nature. Measured thermal rate constants were given by [b]Lindinger *et al* (1998) measurement conditions and uncertainties were not specified, ADO rate constants (§ 2.4.1.3, Eq. 2.41) were used to determine efficiencies in reference. [c]Values taken from Mackay *et al* (1978) were measured in FA/SIFT in a carrier gas of very dry grade hydrogen at a flow tube pressure of 0.35 to 0.61 mbar and temperature of 298 ± 2 K, acid vapours were diluted in helium, ADO rate constants (§ 2.4.1.3, Eq. 2.41) were used to determine efficiencies in reference. [d]Values taken from Warneke *et al* (1996) were measured using SIFDT in helium buffer and correspond to close to thermal conditions ($KE_{c.m.}^{r}$ ~0.06 – 0.07 eV), normal operating conditions of flow tube temperature of ~300 K and P_{FT} ~0.6 to 1.5 mbar are assumed. Efficiency was not given by Warneke *et al* (1996) and was calculated here using a collisional rate constant of 2.60×10^{-9} cm^{-3} s^{-1} derived from the results of Su and Chesnavich trajectory calculations (§ 2.4.1.4, Eq. 2.49 – 2.54). The enthalpy of the dissociative reactions are shown in italics values and were derived from specified references and [e]enthalpies of formation of neutrals from Mallard and Linstrom (2005), enthalpies of formation of RO^{+} ions derived from appearance energies in Mallard and Linstrom (2005) and a standard enthalpy of formation of H_3O^{+} of 6.25 eV calculated. [f]Value was derived from the enthalpy of dissociation of $ROOHH^{+}$ specified by Sekiguchi *et al* (2004) and the enthalpy of the non-dissociative reaction. Proton affinities (*PA*) and gas basicities, (*GB*) are taken from Hunter and Lias (1998) except [gi]experimental values from Berruyer-Penaud *et al* (2004) and [gii] computed G2(MP2) values from Berruyer-Penaud *et al* (2004). The standard enthalpies (ΔH_{r}^{Φ}) and Gibbs free energies (ΔG_{r}^{Φ}) of the non-dissociative reactions with H_3O^{+} are calculated from Eq. 2.88 and 2.89, standard entropies (ΔS_{r}^{Φ}) are calculated from

$$\Delta S_{r}^{\Phi} = \left[\Delta H_{r}^{\Phi} - \Delta G_{r}^{\Phi} \right] / T .$$

Table 3.14: The product distributions resulting from the reaction of carboxylic acids with H_3O^+ in the PTR-MS and SIFDT.

Carboxylic Acid ($ROOH$)	P_{dt} (mbar)	T_{dt} (K)	V_{drift} (V)	E (V cm^{-1})	E/N (Td)	Observed Product Distribution : Product Ion (m/z): Percentage of Product Total, $RCOOH + H_3O^+ \rightarrow$			Reference
						$RCOOHH^+ + H_2O$	$RCO^+ + 2H_2O$	$RCOOHH^+.H_2O$	
Methanoic acid (Formic acid, HCOOH)	NS	NS	NS	NS	NS	$CH_3O_2^+$ (47): **100**			Lindinger *et al* (1998)
Ethanoic acid (Acetic acid, CH$_3$COOH)	[a]2.0 [b]2.0 [c]1.3 - 2.7 [d]NS [e]1.8 – 2.1 [f]NS [g]NS	[a]313 [b]NS [c]NS [d]NS [e]303 - 333 [f]NS [g]NS	[a]555* [b]600 [c]NS [d]NS [e]580 [f]NS [g]NS	[a]55.5* [b]NS [c]NS [d]NS [e]61.1 [f]NS [g]NS	[a]120 [b]130 [c]130 [d]NS [e]122 - 156 [f]NS [g]NS	$C_2H_5O_2^+$ (61): [a]**75** [b]**70** [c]**80** [d]**100** [e]**3.8** [fi]**88,** [fii]**84** [gi]**80,** [gii]**90**	$C_2H_3O^+$ (43): [a]**25** [b]**30** [c]**20** [e]**96.2** [fi]**12** [fii]**16** [gi]**20,** [gii]**10**		[a]Karl *et al* (2007)* [b]Christian *et al* (2004) [c]Williams *et al* (2001) [d]Lindinger *et al* (1998) [e]Malekina *et al* (2007)** [f]Warneke *et al* (1996)*** [g]Vlasenok *et al* (2008)****
Propanoic acid (Propionic acid, C$_2$H$_5$COOH)	2.0	333	600	63.2	145	$C_3H_7O_2^+$ (75): **67.4**	$C_3H_5O^+$ (57) **31.7**	$C_3H_7O_2^+$.H$_2$O (93) **0.9**	von Hartungen *et al* (2004)
n-Butanoic acid (n-Butyric acid, C$_3$H$_7$COOH)	2.0	333	600	63.2	145	$C_4H_9O_2^+$ (89): **74.9**	$C_4H_7O^+$ (71): **23.7**	$C_4H_9O_2^+$.H$_2$O (107): **1.3**	von Hartungen *et al* (2004)

Table 3.14 is continued on the following page.

Carboxylic Acid ($ROOH$)	P_{dt} (mbar)	T_{dt} (K)	V_{drift} (V)	E (V cm^{-1})	E/N (Td)	Observed Product Distribution : Product Ion (m/z): Percentage of Product Total, $RCOOH + H_3O^+ \rightarrow$			Reference
						$RCOOHH^+ + H_2O$	$RCO^+ + 2H_2O$	$RCOOHH^+.H_2O$	
2-Methyl-propanoic acid (*iso*-butyric acid, $(CH_3)_2CHCOOH$)	2.0	333	600	63.2	145	$C_4H_9O_2^+$ (89): **94.4**	$C_4H_7O^+$ (71): **4.7**	$C_4H_9O_2^+.H_2O$ (107): **0.8**	von Hartungen *et al* (2004)
Pentanoic acid (Valeric acid, C_4H_9COOH)	2.0	333	600	63.2	145	$C_5H_{11}O_2^+$ (103): **74.1**	$C_5H_9O^+$ (85): **25.0**	$C_5H_{11}O_2^+.H_2O$ (121): **0.9**	von Hartungen *et al* (2004)
3-Methyl-Butanoic acid (*iso*-Valeric acid, $(CH_3)_2CHCH_2COOH$)	2.0	333	600	63.2	145	$C_5H_{11}O_2^+$ (103): **76.6**	$C_5H_9O^+$ (85): **22.3**	$C_5H_{11}O_2^+.H_2O$ (121): **1.1**	von Hartungen *et al* (2004)
n-Hexanoic acid (caproic acid $C_5H_{11}COOH$)	2.0	333	600	63.2	145	$C_6H_{13}O_2^+$ (117): **61.8**	$C_6H_{11}O^+$ (99): **37**	$C_6H_{13}O_2^+.H_2O$ (135): **1.2**	von Hartungen *et al* (2004)

Note: P_{dt} denotes drift tube pressure, T_{dt} denotes drift tube temperature, V_{drift} denotes voltage applied to the drift tube and E the electric field strength. NS denotes not specified in reference. Distributions from Malekina *et al* (2007) and von Hartungen *et al* (2004) are given as relative abundances with the most abundant m/z normalised to 100 in reference and have been converted to percentage distributions here and are specified to one decimal place. Values from Karl *et al* (2007), Malekina *et al* (2007), von Hartungen *et al* (2004), Christian *et al* (2004) and Williams *et al* (2001) were derived using conventional PTR-MS. Distributions from Warneke *et al* (1996) were derived in SIFDT (§ 2.1, 2.8), a helium carrier gas was used in the drift tube. *E was not specified in reference but to give the stated E/N of ~120 Td at the given P_{dt} of 2.00 mbar and T_{dt} of 313 K E must be approximately 55.5 V cm^{-1}. l_{dt} of ~ 10 cm was derived from the given t of 110 μs and E/N of 120 Td giving V_{drift} ~ 555 V. **A specific value of instrumental parameter was not specified but P_{dt} of 1.8 - 2.1 mbar and a temperature of 303 – 333 K was specified for measurements within the reference. The length of the drift tube was not specified, but a high sensitivity Ionicon Analytik PTR-MS was employed so a drift tube length of 9.5 cm is assumed, V_{drift} was specified. Given this temperature and pressure range and l_{dt} at a V_{drift} of 580 V E/N would have been somewhere between ~122 and 156 Td. The percentage abundancies of m/z 43 and 61 from Malekina *et al* 2007 were calculated from a specified relative abundance of 4.0 at m/z 61 assuming m/z 43 and m/z 61 were the only observed product ions. ***Distributions are given across a range of $KE_{c.m.}^r$ in Warneke *et al* (1996), values corresponding to $KE_{c.m.}^r$ [i]of 0.2 eV and [ii]0.3 eV are tabulated here. A $KE_{c.m.}^r$ of for example H_3O^+-ethanoic acid of 0.2 and 0.3 eV in helium at 298 K corresponds to E/N of ~ 20 - 30 Td where $KE_{c.m.}^b$ is 0.07 eV - 0.10 eV and the sum of $KE_{c.m.}^r$ and $KE_{c.m.}^b$ is ~0.24 - 0.41 eV, in the PTR-MS in air at 298 K this is comparable to the ion-molecule energy at E/N of ~ 100 - 140 Td where $KE_{c.m.}^r$ is 0.14 to 0.26 eV and $KE_{c.m.}^b$ is 0.12 to 0.22 eV and thus the sum of $KE_{c.m.}^r$ and $KE_{c.m.}^b$ is 0.26 and 0.48 eV. ****Vlasenko *et al* (2008) employed [gi]a helium buffer and [gii]an oxygen buffer. Product distributions in von Hatungen *et al* (2004) were obtained at 313 K. H_2O saturation and the $H_3O^+(H_2O)/H_3O^+$ was ≤ 0.25. Product distributions in Malekina *et al* (2007) were measured in ambient air (humidity not specified).

As discussed in § 3.2 in EI-MS carbonyl containing compounds, *RC(=O)M*, especially those in which no γ hydrogen exists and McLafferty re-arrangement does not occur, fragment predominantly to $[RC=O]^+$ and $[O=CM]^+$ (Duckett and Gilbert 2000). In the case of carboxylic acids *M* is *OH* and $[O=CM]^+$ is $[O=COH]^+$ at m/z 45. The C_1-C_3 carboxylic acids have no γ and $[O=CM]^+$ and $[O=COH]^+$ are the dominant fragments of the EI-MS spectra: $[O=COH]^+$ at m/z 45 forms 17.7 %, 26.9 % and 13.2 % of the total product ions in EI-MS of methanoic, ethanoic and propanoic acid respectively (Mallard and Linstrom 2005). The $[RC=O]^+$ product ions from methanoic acid, ethanoic acid and propanoic acid are CHO^+ (m/z 29), CH_3CO^+ (m/z 43) and $C_2H_5CO^+$ (m/z 57) respectively and form 37.2 %, 29.8 % and 6.8 % respectively of the product ions in EI-MS (Mallard and Linstrom 2005). The $C_2H_5CO^+$ ion from propanoic acid further dissociates to $C_2H_5^+$ (m/z 29) by elimination of *CO*, m/z 29 which forms 12.2 % of the total product ions from EI-MS of propanoic acid (Duckett and Gilbert 2000, Mallard and Linstrom 2005).

Only the $[RC=O]^+$ ions formed by the elimination of H_2O are observed from reaction of the carboxylic acids with H_3O^+ ions in SIFT and PTR-MS; no $[O=COH]^+$ ions have been observed. The enthalpy of formation of COO_2H^+ from the reaction of H_3O^+ with methanoic acid by elimination of hydrogen from the protonated ion is 1.24 eV to 1.48 eV where the enthalpy of formation of the ion is derived from *AE*. The enthalpy of formation of COO_2H^+ from the reaction of H_3O^+ with ethanoic acid by elimination of methane from the protonated ion is 1.16 eV to 1.94 eV where the enthalpy of formation of the ion is derived from *AE*. The enthalpy of formation of COO_2H^+ from the reaction of H_3O^+ with propanoic acid by elimination of ethane from the protonated ion is 1.98 eV where the enthalpy of formation of the ion is derived from *AE*. This is greater than the energy available in the drift tube (Figure 3.2 to 3.4). The formation of $[RC=O]^+$ and lack of $[O=COH]^+$ from the protonated acids is also explained by the favourability of hydrogen shift to an electronegative oxygen with a lone pair compared to hydrogen shift to an electron donating alkyl group.

Mackay *et al* (1978) investigated the product distributions from reactions of methanoic acid with HCO^+, CH_5^+ and H_3^+ as well as H_3O^+. These reagent ions result in an increase in exothermicity of 1.01 eV, 1.44 eV and 2.75 eV respectively compared to reaction with H_3O^+. The non-dissociative product ion ($HCOOHH^+$) was the only product ion observed from reactions with HCO^+ and CH_5^+. Only the reaction with H_3^+ produced the dissociative product ions (HCO^+ and H_3O^+) and in this case the non-dissociative product was not observed corresponding to an increase in energy of 2.75 eV. Even at *E/N* of 200 Td (T_{dt} 298 K in air) the $\Delta\langle E_r \rangle$ of methanoic acid is only ~ 0.89 eV, thus dissociation of methanoic acid

within the PTR-MS is unlikely. Mackay *et al* (1978) also investigated the product distributions from reactions of ethanoic acid with HCO^+ and H_3^+ in addition to H_3O^+. The results are shown in Figure 3.5
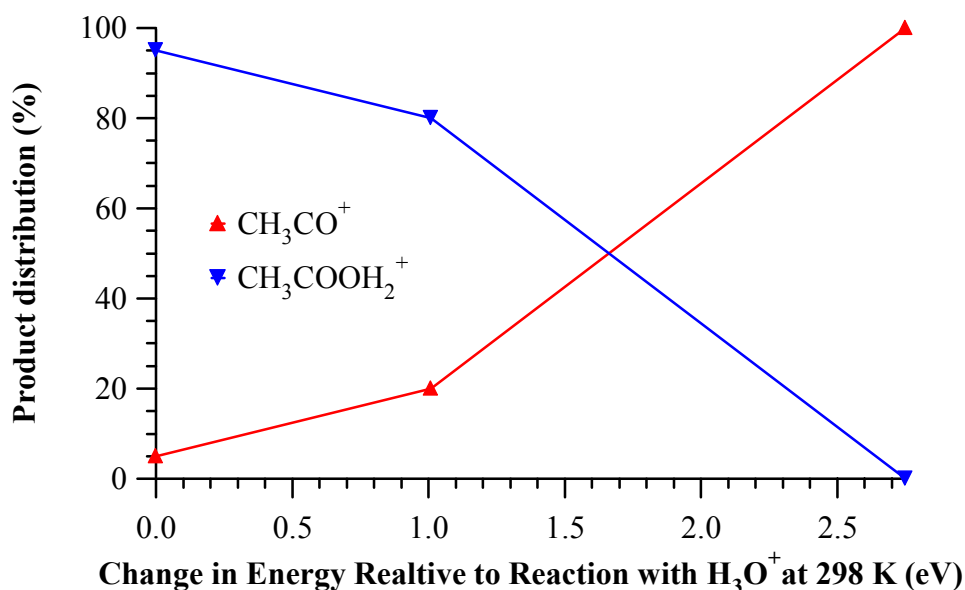
Figure 3.5: Product distributions from reactions of HCO^+, H_3^+ and H_3O^+ with ethanoic acid (~298 K in hydrogen). Change in energy relative to reaction at 298 K is *GB(H₂O) – GB (reagent ion neutral)*. Values are taken from Mackay *et al* (1978). Lines are to guide the eye only.

The $\Delta\langle E_r\rangle$ of ethanoic acid with PTR-MS in air at *E/N* of 140 Td is 0.39 ev. This suggests a dissociation of ~10 % but dissociation may not increase in a linear manner as indicated. Results compiled in Table 3.14 suggest a greater degree of dissociation although the difference in buffer and pressure may also affect the product distribution.

Mackay *et al* (1978) observed three-body association reactions resulting in the formation of protonated dimers of methanoic and ethanoic acid in reactions with H_3O^+ in hydrogen buffer in FA/SIFT. Variation in dimer formation as a function of acid VMR, *E/N* , pressure and buffer composition is unknown.

The fragmentation of protonated unsaturated $C_4H_6O_2$ carboxylic acids has been studied in high and low energy collisional experiments by Schröder *et al* (2003). In low energy collision-induced dissociation experiments at a collisional energy of 5 eV (much greater than the energy available in PTR-MS), H_2O elimination was observed from protonated 2-butenoic acid, 3-butenoic acid and methacrylic acid. The product of H_2O elimination was the

dominant product from protonated 2-butenoic acid. Loss of C_3H_6 and CO_2 were also observed from the protonated acids and the most abundant ions from protonated 3-butenoic acid. CO elimination dominated the spectra of protonated methacrylic acid and this product was minor from protonated 2- and 3-butenoic acid.

CH_4 chemical ionisation studies indicate the presence of a second interaction carbonyl group results in increased elimination of H_2O from the protonated carboxylic acid. The second carbonyl facilitates the 1, 3 hydrogen shift of the protonating hydrogen. Similarly H_2O elimination from benzoic acids with *ortho* substituents with lone pairs capable of accepting a proton and catalysing the hydrogen shift is increased (Harrison 1992).

3.3.2 The Reaction of Carboxylic Acids in the Presence of Water

The proton affinities of methanoic acid, ethanoic acid and propanoic acid (Table 3.13) are less than that of the $H_3O^+(H_2O)_n$ $n \geq 1$, thus direct proton transfer is not anticipated. Mackay *et al* (1978) observed an ion corresponding to $HCOOHHH_2O^+$ from methanoic acid and H_3O^+ in the presence of H_2O in FA (P_{FT} 0.55 mbar, T_{FT} 298 K), this was attributed mainly to the switching reaction of $H_3O^+(H_2O)$ with methanoic acid. Von Hartungen *et al* (2004) observed ions corresponding to $RCOOHHH_2O^+$ from C_2-C_6 carboxylic acids in the PTR-MS (E/N 145 Td, P_{dt} 2.0 mbar T_{dt} 333 K) at a $H_3O^+(H_2O)/H_3O^+ \leq 0.25$ at 40°C H_2O saturation, forming 0.9 % to 3.7 % of the total product ions (Table 3.14). These ions may originate from association of protonated carboxylic acids with H_2O or ligand switching reactions with $H_3O^+(H_2O)$.

3.4 Sulphur Containing Volatile Organic Compounds.

3.4.1 The Reaction of Sulphur Containing Volatile Organics with Compounds H_3O^+.

The available proton affinities, gas basicities and resultant standard reaction enthalpy, entropy and Gibbs free energies for the non-dissociative proton transfer reaction of H_3O^+ with various sulphur containing compounds are reviewed in Table 3.15. Rates of reaction, reaction efficiencies and product distributions from the reaction of H_3O^+ with various sulphur containing volatile organic compounds in SIFT are shown in Table 3.16. The product distributions observed from the reaction of H_3O^+ with various volatile organic sulphur containing compounds in PTR-MS are reviewed in Table 3.17.

Table 3.15: A compilation of proton affinities (*PA*), gas basicities (*GB*), potential standard enthalpy (ΔH_r^Φ), potential standard entropy (ΔS_r^Φ) and Gibbs free energies (ΔG_r^Φ) of the non-dissociative H_3O^+ reaction with various sulphur containing compounds. Proton affinities and gas basicities are taken from Hunter and Lias, (1998) ΔG_r^Φ and ΔH_r^Φ are calculated from Eq. 2.88 and 2.89, ΔS_r^Φ are calculated from $\Delta S_r^\Phi = \left[\Delta H_r^\Phi - \Delta G_r^\Phi\right]/T$.

Compound	*PA* (eV)	*GB* (eV)	ΔH_r^Φ (eV)	ΔS_r^Φ (x 10^{-4} eV K^1)	ΔG_r^Φ (eV)
Sulphides (*RSR*)					
Carbonyl sulphide	6.51	6.25	0.65	1.77	0.59
Carbon disulphide	7.07	6.82	0.09	2.36	0.02
Hydrogen sulphide	7.31	6.98	-0.15	-0.07	-0.14
Dimethylsulphide	8.61	8.30	-1.45	0.45	-1.46
Methylethylsulphide	8.77	8.45	-1.61	-0.07	-1.61
Diethylsulphide	8.88	8.57	-1.72	0.45	-1.73
Divenylene sulphide /Thiophene	8.45	8.13	-1.29	0.10	-1.29
Dimethyldisulphide	8.45	8.11	-1.29	-0.52	-1.27
Thiirane	8.37	8.06	-1.21	-0.42	-1.22
Thiols (*RSH*)					
Methanethiol	8.02	7.69	-0.85	-0.14	-0.85
Ethanethiol	8.18	7.86	-1.02	-0.07	-1.02
1-Propanethiol	8.24	7.91	-1.08	-0.10	-1.07
n-Propanthiol	8.33	8.00	-1.17	-0.10	-1.16
1-Butanethiol	8.31	7.99	-1.15	-0.07	-1.15
Sulphur containing oxygenates					
Methyl thiolacetate	8.59	8.27	-1.43	0.00	-1.43
Dimethylsulphoxide	9.17	8.85	-2.00	0.10	-2.01
Methane sulfonic acid	7.89	7.55	-0.73	-0.49	-0.71

The proton affinities of carbonyl sulphide and carbon disulphide are less than that of water and reactions are expected to be inefficient (Table 3.15, Bohme *et al* 1980, Bouchoux *et al* 1996, § 2.9). Španěl and Smith (1998c) measured a relatively small rate constant for the reaction of H_3O^+ with carbon disulphide of 0.25 x 10^{-9} cm^{-3} s^{-1} indicating an efficiency of 0.14. The rate of these endothermic reactions may be increased by the input of energy resulting from the drift tube in the PTR-MS, no measurements could be found.

The situation for hydrogen sulphide is similar to that of methanal (§ 3.2.3): The proton affinity and gas basicity of hydrogen sulphide are greater than those of water. However the Gibbs free energy of the non-dissociative reaction is greater than -0.43 eV to -0.21 eV and thermokinetic trends suggest a reaction efficiency of less than one (Bohme *et al* 1980, Bouchoux *et al* 1996, § 2.6). The thermal rate constants for the reaction of H_3O^+ with hydrogen sulphide derived by Williams *et al* (1998) and Lindinger *et al* (1998) are 26 % less than the collisional rate constant and that derived by Španěl and Smith (2000a) is 15 % less.

However the latter is well within the uncertainties of the measured and collisional rate constant and the former is only 1 % greater than the uncertainty in the measured rate constant. In an analogous manner to methanal (§ 3.2.3, Hansel *et al* 1997) the rate of this forward reaction is likely to decrease in the PTR-MS and more so as E/N increases due to the energy input into an exothermic reaction and the effects of the electric field on the collisional rate constant.

Although the reaction of H_2S with H_3O^+ is relatively rapid at thermal energies, the quantification of hydrogen sulphide is complicated by the significant reverse reaction (Eq. 3.47) in the presence of water VMR often in excess of hydrogen sulphide VMRs. As in the case of methanal, the rate constant of this endothermic reverse reaction is likely to increase in the PTR-MS as a function of E/N.

$$H_3S^+ + H_2O \rightarrow H_2S + H_3O^+ \tag{3.47}$$

Furthermore the switching reaction of $H_3S^+(H_2O)$ clusters, formed predominantly by three-body association of H_2O with protonated hydrogen sulphide (Eq. 3.48), with H_2O to produce $H_3O^+(H_2O)$ (Eq. 3.49) is exothermic.

$$H_3S^+ + H_2O \xrightarrow{B} H_2S(H_3O^+) \tag{3.48}$$

$$H_2S(H_3O^+) + H_2O \rightarrow H_2S + H_2O(H_3O^+) \qquad \Delta H_r^\Phi = \text{-0.53 eV} \tag{3.49}$$
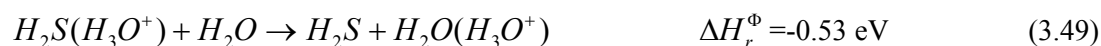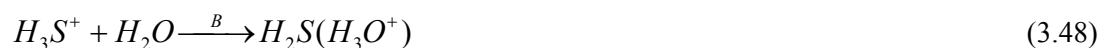
B denotes a buffer molecule. The standard enthalpy for reaction Eq. 3.49 has been derived using an enthalpy of formation of $H_3O^+(H_2O)$ of 225.6 kJ mol^{-1} (2.34 eV, § 3) and an enthalpy of formation of $H_3S^+(H_2O)$ derived from the binding energy of $H_3S^+(H_2O)$ of -71 kJ mol^{-1} (0.74 eV, Španěl and Smith 2000a), the enthalpy of formation of H_2O (Mallard and Linstrom 2005) and the enthalpy of formation of protonated hydrogen sulphide calculated from the proton affinity of hydrogen sulphide (Hunter and Lias 1998) and enthalpies of formation from Mallard and Linstrom (2005). In this respect hydrogen sulphide differs from methanal for which the analogous switching reaction is endothermic. Some dissociation of $H_3S^+.H_2O$ to H_2S and H_3O^+ may also occur; this is effectively the reverse reaction Eq. 3.47 (Španěl and Smith 2000a). Španěl and Smith (2000a) derived a termolecular rate coefficient of $2 \pm 0.8 \times 10^{-28}$ cm^6 s^{-1} in helium at number density of 2.5×10^{-16} cm^3 s^{-1} at 300 K for reaction Eq. 3.48. Despite this rate constant being only a factor of three less than that of the analogous formation of $H_3O^+(H_2O)$ from H_3O^+ and H_2O and the loss of $H_3O^+(H_2O)$ to form higher hydrates, a minor signal of $H_2S(H_3O^+)$ was observed only at large H_2O VMR indicating the loss of $H_2S(H_3O^+)$ *via* the rapid switching reaction Eq. 3.49.

Table 3.16: Product distributions and reaction efficiencies of H_3O^+ with various (oxygenated) volatile organic sulphur compounds ((O)VOSCs) in SIFT-MS.

(O)VOSC	P_{FT} (mbar)	T_{FT} (K)	k_m (x 10^{-9} m^3 s^{-1})	k_m/k_c	Observed Product Distribution : Product Ion (m/z): Percentage of Product Total, $M + H_3O^+ \rightarrow$			Reference
					$MH^+ + H_2O$	$(MH-H_2S)^+ + H_2S + H_2O$	$(MH-H_2O)^+ + 2H_2O$	
Sulphides (*RSR*)								
Carbon disulphide (CS$_2$)	0.67	300	0.25	0.14	CS$_2$H$^+$ (77) **100**			Španěl and Smith (1998c)
Hydrogen sulphide (H$_2$SH)	[a]0.67 or 1.2 [b]NS [c]0.93	[a]300 [b]NS [c]300	[a]1.4 [b]1.4 [c]1.6	0.74 [b]0.74 [c]0.84				[a]Williams *et al* (1998) [b]Lindinger *et al* (1998) [c] Španěl and Smith (2000a)
Dimethylsulphide (CH$_3$SCH$_3$)	[a]0.67 [b]0.67 or 1.2 [c]NS	[a]300 [b]300 [c]NS	[b]1.7 [c]2.1	0.62 [c]0.81	C$_2$H$_6$SH$^+$ (63) [a,b]**100**			[a]Španěl and Smith (1998c) [b] Williams *et al* (1998) [c]Lindinger *et al* (1998)
Methylethylsulphide (CH$_3$SC$_2$H$_5$)	0.67 or 1.2	300	2.4	0.89	C$_3$H$_8$ SH$^+$ (77) **100**			Williams *et al* (1998)
Divenylene sulphide (Thiophene, C$_4$H$_4$S)	0.67 or 1.2	300	1.8	0.89	C$_4$H$_4$SH$^+$ (85) **100**			Williams *et al* (1998)
Dimethyldisulphide (CH$_3$SSCH$_3$)	[a]0.67 [b]0.9	[a]300 [b]296 - 300			C$_2$H$_6$S$_2$H$^+$ (95) [a]**100** [b]**100**			[a]Španěl and Smith (1998c) [b]Wang *et al* (2004)
Dimethyltrisulphide (CH$_3$SSSCH$_3$)	0.9	296 - 300			C$_2$H$_6$S$_3$H$^+$ (127) **100**			Wang *et al* (2004)

Table 3.16 is continued on the following page.

(O)VOSC	P_{FT} (mbar)	T_{FT} (K)	k_m (x 10^{-9} m^3 s^{-1})	k_m/k_c	Observed Product Distribution : Product Ion (m/z): Percentage of Product Total, $M + H_3O^+ \rightarrow$			Reference
					$MH^+ + H_2O$	$(MH - H_2S)^+$ $+ H_2S + H_2O$	$(MH - H_2O)^+ +$ $2H_2O$	
1-3 Dithiane (SCH$_2$SCH$_2$CH$_2$CH$_2$)	0.67	300			C$_4$H$_8$S$_2$H$^+$ (121) **100**			Španěl and Smith (1998c)
Diallyl sulphide (CH$_2$CHCH$_2$SCH$_2$CHCH$_2$)	0.67	300			C$_6$H$_{10}$SH$^+$ (115) **100**			Španěl and Smith (1998c)
Diallyl disulphide (CH$_2$CHCH$_2$SSCH$_2$CHCH$_2$)	0.67	300			C$_6$H$_{10}$S$_2$H$^+$ (147) **100**			Španěl and Smith (1998c)
Thiols (*RSH*)								
Methanethiol (CH$_3$SH)	0.67 & 1.2	300	1.8	0.72	CH$_4$SH$^+$ (49) **100**			Williams *et al* (1998)
Ethanethiol (CH$_3$CH$_2$SH)	[a]0.67 [b]0.67 or 1.2	[a]300 [b]300	[b]2	0.75	C$_2$H$_6$SH$^+$ (63) [a]**100** [b]**100**			[a]Španěl and Smith (1998c) [b]Williams *et al* (1998)
1-Propanethiol (CH$_3$CH$_2$CH$_2$SH)	0.67 or 1.2	300	2.3	0.83	C$_3$H$_8$SH$^+$ (77) **100**			Williams *et al* (1998)
2-propanethiol (*n*-Propanthiol, CH$_3$CH(CH$_3$)SH)	0.67 or 1.2	300	2.3	0.86	C$_3$H$_8$SH$^+$ (77) **100**			Williams *et al* (1998)
Sulphur containing oxygenates								
Ethanethioic acid (Thiolacetic acid, CH$_3$COSH)	0.67	300			C$_2$H$_4$OSH$^+$ (77) **80**	C$_2$H$_3$O$^+$ (43) **20**		Španěl and Smith (1998c)
2-Thioethanol (SHCH$_2$CH$_2$OH)	N/O	N/O			SC$_2$H$_6$OH$^+$ (79) **5**		SC$_2$H$_5^+$ (61) **95**	Španěl *et al* (2002b)

Note: P_{FT} denotes pressure in the flow tube, T_{FT} denotes temperature in the flow tube, N/O denotes normally operated and corresponds to P_{FT} ~0.6 – 1.5 mbar, T_{FT} ~300 K. A helium buffer was used in all cases. (O)VOSC vapours were diluted with dry cylinder air by Španěl and Smith (1998c), Španěl *et al* (2002b) and Wang *et al* (2004) and with helium by Williams *et al* (1998). Wang *et al* (2004) repeated experiments adding laboratory air (RH 1.5%) and humid air (RH 6%) to the carrier gas. The reaction efficiency was not specified by Williams *et al* (1998) and was calculated here from collisional rate constants derived using the results of Su and Chesnavich trajectory

calculations (§ 2.4.1.4, Eq. 2.49 – 2.54). The rate constants measured by Williams *et al* (1998) are considered to be accurate to within ± 25 %. Lindinger *et al* (1998) specify measured thermal rate constants measurement conditions and uncertainties are not specified, efficiencies were calculated from collisional rate constants calculated from ADO theory (§ 2.4.1.3, Eq. 2.41). Španěl and Smith (1998c) derived the efficiency of the reaction of carbon disulphide with H_3O^+ from a collisional rate constant with uncertainty ± 25 % calculated using the results of Su and Chesnavich trajectory calculations, uncertainty in the measured rate constant is not specified.

Table 3.17: The product distributions resulting from the reaction of various (O)VOSCs with H_3O^+ in the PTR-MS.

(O)VOSC	P_{dt} (mbar)	T_{dt} (K)	V_{drift} (V)	E (V cm^{-1})	E/N (Td)	Observed Product Distribution : Product Ion (m/z): Percentage of Product Total, $M + H_3O^+ \rightarrow$			Reference
						$MH^+ + H_2O$	$(MH-CH_4)^+$ $+ H_2O + CH_4$	$(MH-CH_3SH)^+$ $+ H_2O + CH_3SH$	
Hydrogen sulphide (H$_2$S)	NS	NS	NS	NS	NS	H$_2$SH$^+$(35) **100**			Lindinger *et al* (1998)
Dimethylsulphide (CH$_3$SCH$_3$)	[a]2.05 [b]2.4 [c]NS	[a]323 [b]NS [c]NS	[a]520 [b]NS [c]NS	~55* [b]NS [c]NS	[a]120, [b]106 [c]NS	C$_2$H$_6$SH$^+$ (63) **[a]100, [b]100, [c]100**			[a]Aprea *et al* (2007b) [b]Warneke *et al* (2003) [c]Lindinger *et al* (1998)
Dimethyldisulphide (CH$_3$SSCH$_3$)	2.05	323	520	~55*	120	C$_2$H$_6$S$_2$H$^+$ (95) **87.7**	CH$_3$S$_2^+$ (79) **12.3**		Aprea *et al* (2007b)
Bis(methylthio)methane (CH$_3$SCH$_2$SCH$_3$)	2.05	323	520	~55*	120			C$_2$H$_5$S$^+$ (61) **100**	Aprea *et al* (2007b)
Tris(methylthio)methane (CH$_3$SCH(SCH$_3$) SCH$_3$)	2.05	323	520	~55*	120			C$_3$H$_7$S$_2^+$ (107) **100**	Aprea *et al* (2007b)
Allyl methyl sulphide	~0.1	NS	NS	NS	120 - 140	C$_4$H$_8$SH$^+$ (89): **100**			Taucher *et al* (1996)
Dimethylsulphoxide ((CH$_3$)$_2$SO)	2.05	323	520	~55*	120	C$_2$H$_6$SOH$^+$ (79) **100**			Aprea *et al* (2007b)
Benzothiazole (C$_6$H$_4$(NCHS))	2.05	323	520	~55*	120	C$_7$H$_5$NSH$^+$ (136) **100**			Aprea *et al* (2007b)

Note: P_{dt} denotes drift tube pressure, T_{dt} denotes drift tube temperature, V_{drift} denotes voltage applied to the drift tube and E the electric field strength. NS denotes not specified in reference. *l_{dt} and E are not specified; E is calculated from the specified E/N, P_{dt} and T_{dt} and corresponds to l_{dt} of ~9.5 cm. Distributions from Aprea *et al* (2007b) are given as relative abundancies with the most abundant m/z normalised to 100 and have been converted to percentage distributions here. Product distributions in Warneke *et al* (2003) were measured in synthetic air (humidity not specified), product distributions from Aprea *et al* (2007b) were measured in pure nitrogen (humidity not specified) and Taucher *et al* (1996) employed a buffer of laboratory air. Measurements by Lindinger *et al* (1998) are assumed to be made in PTR-MS but measurement conditions are not specified.

Španěl and Smith (2000a) observed an artificially high number density of H_2S under high humidities when calculating the number density from the count rates of H_2S, H_3O^+ and k and t. This was attributed to the relatively large decrease in H_3O^+ by association with H_2O compared to the decrease in H_2S due to association (Eq. 3.48). Improved quantification was achieved by consideration of the association reactions.

In the PTR-MS, the formation of $H_2S(H_3O^+)$ association complexes is likely to be reduced at a given humidity because of the negative energy dependence of the rate of association as observed in the case of $CH_2OH^+(H_2O)$ and other association reactions such as $H_3O^+(H_2O)$ formation. The elevated pressure in the drift tube results in an increase of stabilizing collisions with buffer, the change in the nature of the buffer may have an effect. The rate constant for the exothermic ligand switching reaction Eq. 3.49 may decrease at the elevated energies in the PTR-MS.

Blake *et al* (2004) calibrated a PTR-TOF-MS for hydrogen sulphide diluted in nitrogen and zero air at a VMR of 5.35 ppm to 53.47 ppm, although these are relatively large VMRs compared to atmospheric VMRs, linearity was demonstrated. A sensitivity of 0.017 counts s^{-1} ppb^{-1} was achieved at a relatively low H_3O^+ count rate of 1×10^3 counts s^{-1}. VMR ratios were calculated from the count rates of H_2S and H_3O^+ an estimated reaction time and the thermal rate constant measured by Williams *et al* (1998) (Table 3.16). At the actual VMR of 5.35 ppm the calculated concentration was 3.0 ppm, which is an underestimation of 2.35 ppm. This underestimation is greater than the 25 % uncertainty associated with the thermal rate constant and may have resulted from occurrence of the reverse reaction of protonated hydrogen sulphide with H_2O (Eq. 3.47). However other factors, such as the uncertainty in t and in the 'actual' calibration gas VMR, may have contributed to the difference. The rate constant of the forward reaction in the drift tube may also be less than the thermal rate (§ 2.4.1.5) is its use would then result in underestimation of the VMR. It is noteworthy that an E/N of 190 Td (P_{dt} 6 mbar) was employed by Blake *et al* (2004) and only minor formation of $H_3O^+(H_2O)$ was observed and was relatively insensitive to humidity. It is probable that association reactions of hydrogen sulphide were also minor at this E/N. At lower E/N and higher humidity these reactions may become important in addition to the reverse reaction (Eq. 3.47).

Although the products of hydrogen sulphide reaction with H_3O, (mainly H_3S^+) will contribute to PTR-MS, spectra quantification is not possible as yet. The measurement of rate constants for the forward reaction of H_2S with H_3O^+ and for reactions Eq. 3.47 to 3.49 as a

function of *E/N*, ideally at a range of pressures (fixed temperature) and temperature (fixed pressure) in air, is of interest. Humidity dependent calibrations at various *E/N* and development of a method for quantification of hydrogen sulphide as a function of humidity under various drift tube conditions in PTR-MS in a similar manner to that applied to methanal (§ 3.2) is required.

The proton affinities and gas basicities of the $>C_2$ sulphides, thiols and sulphur containing oxygenates in (Table 3.15) are greater than that of water. The Gibbs free energies of the non-dissociative reactions of H_3O^+ with the $>C_2$ sulphides, thiols and sulphur containing oxygenates are less than -0.43 eV and thermokinetic trends suggest efficient reactions. The measured rate constants for the reactions of H_3O^+ with the C_1-C_3 thiols, dimethylsulphide, methylethylsulphide and divenylene sulphide are approximately equal to the corresponding collisional rate constants within uncertainties (Table 3.16).

The non-dissociative product is the only product from dimethylsulphide in the PTR-MS at *E/N* of 106 Td (P_{dt} 2.4 mbar, Warneke *et al* 2003) and *E/N* of 120 Td (P_{dt} 2.05 mbar, T_{dt} 323 K, Aprea *et al* 2007b). The m/z 47 ion (CH_3S^+) is the predominant (23.5 %) fragment ion in EI-MS of dimethylsulphide (Mallard and Linstrom 2005). The enthalpy for the reaction of H_3O^+ with dimethylsulphide to form CH_3S^+ $(+CH_4+H_2O)$ is -0.36 eV to +0.14 eV the range of values corresponding to the range in *AE* employed to derive the enthalpy of formation of CH_3S^+. The lack of formation under the thermal conditions of SIFT (300K) and at the higher energies of PTR-MS at *E/N* of 106 to 120 Td (Table 3.16 and 3.17) suggest an energy barrier to this dissociation.

A small degree of dissociation of dimethyldisulphide to m/z 79 is observed in the PTR-MS at *E/N* of 120 Td (P_{dt} 2.05 mbar, T_{dt} 323 K, Table 3.17). This may be attributed to $CH_3S_2^+$ formed by elimination of methane from protonated dimethyldisulphide. The m/z 79 ion is the dominant fragment in EI-MS of dimethyldisulphide forming 17.4 % of the total product ions (Mallard and Linstrom 2005). The only products from the reaction of H_3O^+ with bis(methylthio)methane and tris(methylthio)methane in the PTR-MS *E/N* of 120 Td (P_{dt} 2.05 mbar, T_{dt} 323 K) are fragments at m/z 61 and m/z 107 respectively (Aprea *et al* 2007b, Table 3.17). These ions are possibly formed by the elimination of CH_3SH from the protonated molecules. Though the extent of fragmentation is reduced, these dissociative reactions of the protonated sulphides in the PTR-MS are akin to the dissociation of analogous ethers (*ROR*) in SIFT (e.g. Španěl and Smith 1998b) and PTR-MS (e.g. Warneke *et al* 2003).

Taucher *et al* (1996) observed no dissociation of protonated allyl methyl sulphide in the PTR-MS. They determined the rate constant for the reaction of allyl methyl sulphide with H_3O^+ to be 2.7 x 10^{-9} cm^3 s^{-1} using SIFDT with a helium carrier gas, $KE^r_{c.m.}$ not specified.

No measurements of product distributions from the reaction of H_3O^+ with thiols in the PTR-MS could be found. Analogy with alcohols suggests elimination of H_2S from the protonated thiols. The m/z 29 ($C_2H_5^+$) and m/z 43 ($C_3H_7^+$) ions are the dominant fragments from EI-MS of ethanethiol and propanethiol forming 19 % and 14.1 % of the total products respectively (Mallard and Linstrom 2005). The enthalpies of the dissociation of the protonated thiols by loss of H_2S are less favourable than those for the loss of H_2O from the analogous protonated alcohols (Table 3.3). The enthalpy for the reaction of H_3O^+ with ethanethiol to produce $C_2H_5^+$ is endothermic by 0.84 eV. The sum of ethanethiol-H_3O^+ $KE^r_{c.m.}$ (0.19 to 0.26 eV, Figure 3.2) and $KE^b_{c.m.}$ (0.16 to 0.22 eV, Figure 3.3) is 0.35 eV to 0.48 eV at *E/N* of 120 – 140 Td in air at 298 K, and on this basis elimination of hyrdrogen sulphide under these conditions is unlikely.

The enthalpy for the reaction of H_3O^+ with propanethiol to produce $C_2H_5^+$ ($+H_2S+H_2O$) is + 0.081 eV where the enthalpy of formation of $C_3H_7^+$ is calculated from the proton affinity (Hunter and Lias 1998) and enthalpy of formation (Mallard and Linstrom 2005) of propene. The sum of propanethiol-H_3O^+ $KE^r_{c.m.}$ (0.20 to 0.28 eV, Figure 3.2) and $KE^b_{c.m.}$ (0.16 to 0.22 eV, Figure 3.3) is 0.36 eV to 0.50 eV at *E/N* of 120 – 140 Td in air at 298 K. Thus provided no significant entropy or activation energy barrier exists, dissociative elimination of H_2S from protonated propanethiol is probable in normally operating PTR-MS.

In EI-MS of methanethiol CH_3^+ (m/z 15) is a minor product forming 3.3 % of the total product ions. The reaction of H_3O^+ with methanethiol to produce CH_5^+ ($+H_2S+H_2O$) is +2.88 to +2.89 eV. The range in the enthalpy arises from the range in *AE* values (Mallard and Linstrom 2005) used to determine the enthalpy of formation of CH_3^+. This reaction is therefore unlikely to occur at the energies in the PTR-MS. The pre-dominant product ion (34 %) in EI-MS of methanethiol is m/z 47 corresponding to CH_3S^+. The enthalpy for reaction of methanethiol with H_3O^+ to produce CH_3S^+ ($+H_2+H_2O$) is +0.16 eV to +0.60 eV, where the range arises from the range in *AE* values (Mallard and Linstrom 2005) used to determine the enthalpy of formation of CH_3S^+. Lindinger *et al* (2005) note that methanethiol can potentially be measured using PTR-MS and using PTR-MS coupled with GC/MS showed that the relative contribution of methanethiol to m/z 49 from coffee headspace was 100 %. No contribution to other m/z was discussed.

The non-dissociative product was the only product ion observed from the reaction of H_3O^+ with dimethylsulphoxide and benzathiazole in the PTR-MS at E/N of 120 Td (P_{dt} 2.05 mbar, T_{dt} 323 K, Aprea $et\ al$ 2007b, Table 3.17).

3.4.2 The Reaction of Sulphur Containing Volatile Organic Compounds in the Presence of Water

The proton affinity of hydrogen sulphide (Table 3.15) is much less than that of $H_3O^+(H_2O)$ (8.57 eV) and direct proton transfer is slow. Williams $et\ al$ (1998) derived a rate constant of 1.3×10^{-12} cm^3 s^{-1} for the reaction of $H_3O^+(H_2O)$ with hydrogen sulphide in SIFT (P_{FT} 0.67 or 1.2 mbar, T_{FT} 300 K), $H_2SHH_2O^+$ was the sole product ion. Ligand switching reactions between hydrogen sulphide and $H_3O^+(H_2O)$ are the reverse reaction of Eq. 3.49 and are endothermic.

Williams $et\ al$ (1998) also determined rate constants and product distributions from the reactions of $H_3O^+(H_2O)$ with methanethiol, ethanethiol, 1-propanethiol, 2-propanethiol, dimethylsulphide, methylethylsulphide and thiophene in SIFT (P_{FT} 0.67 or 1.2 mbar, T_{FT} 300 K). The reactions were rapid with rate constants in the region of 2×10^{-9} cm^3 s^{-1}.

The proton affinity of dimethylsulphide is marginally greater than that of $H_3O^+(H_2O)$. Protonated dimethylsulphide was the only product ion from reaction with $H_3O^+(H_2O)$ in SIFT, the rate constant for the reaction was 1.7×10^{-9} cm^3 s^{-1} (Williams $et\ al$ 1998). Warneke $et\ al$ (2001) determined sensitivities for dimethyl sulphide in the PTR-MS as a function of relative humidity and observed no humidity dependence. This indicates that dimethyl sulphide reacts rapidly with $H_3O^+(H_2O)_n$ n=1-3 clusters in the PTR-MS to form protonated dimethyl sulphide either via direct protonation or ligand switching followed by dissociation.

The proton affinity of methylethylsulphide is greater than that of $H_3O^+(H_2O)$. Williams $et\ al$ (1998) measured a rate constant of 2.2×10^{-9} cm^3 s^{-1} for the reaction of $H_3O^+(H_2O)$ and methylethylsulphide in SIFT (P_{FT} 0.67 or 1.2 mbar, T_{FT} 300 K); the product of non-dissociative proton transfer was the only product ion. The proton affinities of diethylsulphide, methyl thiolacetate and dimethylsulphoxide are also greater than that of $H_3O^+(H_2O)$ and rapid direct proton transfer is probable. The proton affinity of methanethiol is less than that of $H_3O^+(H_2O)$. No direct proton transfer was observed by Williams $et\ al$ (1998) only ligand switching occurred to produce $CH_3SH_2^+(H_2O)$ in SIFT (P_{FT} 0.67 or 1.2 mbar, T_{FT} 300 K). The proton affinities of the ethanethiol, 1- and 2-propanethiol are also less than $H_3O^+(H_2O)$,

however Williams *et al* (1998) observed formation of both the associative product of ligand switching and the protonated thiol in SIFT (P_{FT} 0.67 or 1.2 mbar, T_{FT} 300 K). For ethanethiol the protonated thiol formed $\leq$ 5 % of products, from 1-propanethiol 43 % and from 2-propanethiol 80 %. Several factors were suggested by the authors for the occurrence of the protonated thiol despite the endothermicity of direct proton transfer: dissociation of the $MH^+(H_2O)$ product of ligand switching, proton transfer reactions with $H_3O^+(H_2O)$ are entropy driven, a H_2O dimer is formed from proton transfer rather than two H_2O molecules and there is isomerisation the ionic products of reaction.

3.5 Amines.

3.5.1 The Reaction of Amines with H_3O^+.

The available proton affinities, gas basicities and resultant standard reaction enthalpy, entropy and Gibbs free energies for the non-dissociative proton transfer reaction of H_3O^+ with various amines are shown in Table 3.18. The proton affinities and gas basicities are greater than that of water. The Gibbs free energies of the reactions of the amines with H_3O^+ are much less than -0.43 eV and on the basis of thermokinetic trends (§ 2.9) it is assumed the reactions proceed efficiently.

Measured product distributions from the reaction of H_3O^+ with a series of primary amines in SIFT are reviewed in Table 3.19. The non-dissociative reaction (Eq. 3.50) producing the protonated amine is observed from all of the primary amines.

Table 3.18: A compilation of proton affinities (*PA*), gas basicities (*GB*), potential standard enthalpy (ΔH_r^{Φ}), potential standard entropy (ΔS_r^{Φ}) and Gibbs free energies (ΔG_r^{Φ}) of the non-dissociative H_3O^+ reaction with various amines.

Compound	*PA* (eV)	*GB* (eV)	ΔH_r^{Φ} (eV)	ΔS_r^{Φ} (x 10^{-4} eV K^{-1})	ΔG_r^{Φ} (eV)
Ammonia	8.85	8.49	-1.69	-1.25	-1.65
Primary amines:					
Methylamine	9.32	8.96	-2.16	-1.22	-2.12
Ethylamine	9.45	9.10	-2.29	-1.04	-2.26
1-propylamine	9.51	9.16	-2.35	-1.01	-2.32
2-propylamine	9.57	9.21	-2.41	-1.32	-2.37
1-butylamine	9.55	9.19	-2.39	-1.36	-2.35
1-pentylamine	9.57	9.22	-2.41	-1.04	-2.38
Benzylamine (Aniline)	9.15	8.82	-1.98	-0.31	-1.98
2-methyl-2-butylamine	9.72	9.36	-2.56	-1.11	-2.52

Table 3.18 is continued on the following page.

Compound	PA (eV)	GB (eV)	ΔH_r^{Φ} (eV)	ΔS_r^{Φ} (x 10^{-4} eV K^{-1})	ΔG_r^{Φ} (eV)
Secondary amines:					
Dimethylamine	9.63	9.29	-2.47	-0.70	-2.45
Methylethylamine	9.77	9.42	-2.60	-0.70	-2.58
Diethylamine	9.87	9.53	-2.71	-0.70	-2.69
N-ethyl-2-propylamine	9.95	9.60	-2.79	-0.80	-2.76
Tertiary amines:					
Trimethylamine	9.83	9.52	-2.67	0.07	-2.67
Triethylamine	10.18	9.86	-3.01	0.07	-3.02
N,N-diethylmethylamine	10.06	9.74	-2.90	0.00	-2.90
N,N-dimethyl-2-propylamine	10.06	9.74	-2.90	0.00	-2.90

Note: Proton affinities and gas basicities are taken from Hunter and Lias, (1998). ΔG_r^{Φ} and ΔH_r^{Φ} are calculated from Eq. 2.88 and 2.89, ΔS_r^{Φ} are calculated from $\Delta S_r^{\Phi} = \left[\Delta H_r^{\Phi} - \Delta G_r^{\Phi}\right]/T$.

Fragmentation to NH_4^+ (Eq. 3.51) is observed from all of the acyclic primary amines except 1-pentylamine. As discussed by Španěl and Smith (1999), the percentage of NH_4^+ production is correlated to the proximity of NH_2 to a CH_3 group and the number of CH_3 groups. Španěl and Smith (1999) suggest that such reactions may proceed *via* formation of the non-dissociative RNH_3 product followed by rearrangement to a carbonium ion/ammonia complex $R^+...NH_3$ when energetically accessible with further rearrangement to $(R\text{-}H)...NH_4^+$ which dissociates to the alkene and NH_4^+.

$$RNH_2 + H_3O^+ \rightarrow RNH_3^+ + H_2O \tag{3.50}$$

$$RNH_2 + H_3O^+ \rightarrow NH_4^+ + (RNH_3 - NH_4) + H_2O \tag{3.51}$$
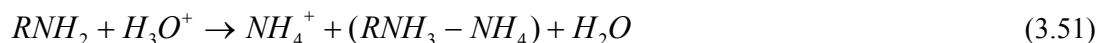
The product distributions observed from the reaction of secondary and tertiary amines in SIFT are reviewed in Tables 3.20 and 3.21 respectively. The non-dissociative product is the only product from the reaction of H_3O^+ with dimethylamine and the predominant product of H_3O^+ reaction with the other secondary and tertiary amines. Fragmentation by elimination of hydrogen is observed from secondary (Eq. 3.52) and tertiary (Eq. 3.53) amines. No production of NH_4^+ is observed from H_3O^+ reaction with secondary or tertiary amines (Španěl and Smith 1999).

$$R_2NH + H_3O^+ \rightarrow (R_2NH_2 - H_2)^+ + H_2 + H_2O \tag{3.52}$$

$$R_3N + H_3O^+ \rightarrow (R_3NH - H_2)^+ + H_2 + H_2O \tag{3.53}$$
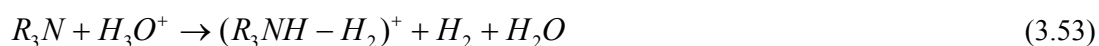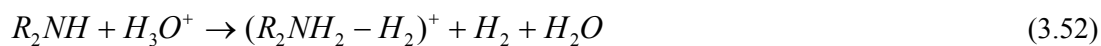
Table 3.19: Product distributions and reaction efficiencies of H_3O^+ with primary amines in SIFT-MS.

Primary Amine (RNH_2)	P_{FT} (mbar)	T_{FT} (K)	$RNH_3^+ + H_2O$	$NH_4^+ + (RNH_3 - NH_4)$ $+ H_2O$	$(RNH_3 - NH_3)^+$ $+ NH_3 + H_2O$	Reference
			Percentage of Product Total, $RNH_2 + H_3O^+ \rightarrow$			
1-propylamine ($CH_3CH_2CH_2NH_2$)	0.67	300	$C_3H_9NH^+$ (60): **90**	NH_4^+ (18): **10**		Španěl and Smith (1998d)
2-propylamine ($(CH_3)_2CHNH_2$)	0.67	300	$C_3H_9NH^+$ (60): **65**	NH_4^+ (18): **35**		Španěl and Smith (1998d)
1-butylamine ($CH_3CH_2CH_2CH_2NH_2$)	0.67	300	$C_4H_{11}NH^+$ (74): **>98**	NH_4^+ (18): **<2**		Španěl and Smith (1998d)
1-pentylamine ($CH_3CH_2CH_2CH_2CH_2NH_2$)	[a]0.67 [b]0.67	[a]300 [b]RT	$C_5H_{13}NH^+$ (88): **[a]100, [b]100**			[a]Španěl and Smith (1998d) [b]Španěl and Smith (1999)
3-methylbutylamine ($(CH_3)_2CHCH_2CH_2NH_2$)	0.67	RT	$C_5H_{13}NH^+$ (88): **>95**	NH_4^+ (18): **<5**		Španěl and Smith (1998d)
2-methylbutylamine ($CH_3CH_2CH(CH_3)CH_2NH_2$)	0.67	RT	$C_5H_{13}NH^+$ (88): **50**	NH_4^+ (18): **50**		Španěl and Smith (1999)
2-pentylamine ($CH_3CH_2CH_2CH(NH_2)CH_3$)	0.67	RT	$C_5H_{13}NH^+$ (88): **40**	NH_4^+ (18): **60**		Španěl and Smith (1999)
3-methyl-2-butylamine ($(CH_3)_2CHCH(NH_2)CH_3$)	0.67	RT	$C_5H_{13}NH^+$ (88): **30**	NH_4^+ (18): **65**	$C_5H_{11}^+$ (71): **5**	Španěl and Smith (1999)
3-pentylamine ($CH_3CH_2CH(NH_2)CH_2CH_3$)	0.67	RT	$C_5H_{13}NH^+$ (88): **30**	NH_4^+ (18): **70**		Španěl and Smith (1999)
2-methyl-2-butylamine ($CH_3CH_2C(CH_3)(NH_2)CH_3$)	0.67	RT	$C_5H_{13}NH^+$ (88): **<5**	NH_4^+ (18): > **90**	$C_5H_{11}^+$ (71): **5**	Španěl and Smith (1999)
Benzylamine (Aniline) ($C_6H_5(NH_2)$)	0.67	300	$C_6H_7NH^+$ (94): **100**			Španěl and Smith (1998d)

Note: P_{FT} denotes pressure in the flow tube, T_{FT} denotes temperature in the flow tube, RT denotes room temperature. A helium carrier gas was used in both cases. Španěl and Smith (1998d) diluted amine vapours in air, Španěl and Smith (1999) diluted amine vapours in dry cylinder air.

Table 3.20 Product distributions and reaction efficiencies of H_3O^+ with secondary amines in SIFT-MS.

Secondary Amine (R_2NH)	P_{FT} (mbar)	T_{FT} (K)	Observed Product Distribution : Product Ion (m/z): **Percentage of Product Total,** $R_2NH + H_3O^+ \rightarrow$		Reference
			$R_2NH_2^+ + H_2O$	$(R_2NH_2 - H_2)^+ + H_2 + H_2O$	
Dimethylamine (($CH_3)_2NH$)	0.67	300	$C_2H_7NH^+$ (46): **100**		Španěl and Smith (1998d)
Methylethylamine ($CH_3CH_2NHCH_3$)	0.67	300	$C_3H_9NH^+$ (60): **95**	$C_3H_8N^+$ (58): **5**	Španěl and Smith (1998d)
Diethylamine ($CH_3CH_2NHCH_2CH_3$)	0.67	300	$C_4H_{11}NH^+$ (74): **95**	$C_4H_{10}N^+$ (72): **5**	Španěl and Smith (1998d)
N-methylbutylamine ($CH_3CH_2CH_2CH_2NHCH_3$)	0.67	RT	$C_5H_{13}NH^+$ (88): **90**	$C_5H_{12}N^+$ (86): **10**	Španěl and Smith (1999)
N-ethyl-2-propylamine (($CH_3)_2CHNHCH_2CH_3$)	0.67	RT	$C_5H_{13}NH^+$ (88): **90**	$C_5H_{12}N^+$ (86): **10**	Španěl and Smith (1999)

Note: P_{FT} denotes pressure in the flow tube, T_{FT} denotes temperature in the flow tube, RT denotes room temperature. A helium carrier gas was used in both cases. Španěl and Smith (1998d) diluted amine vapours in air, Španěl and Smith (1999) diluted amine vapours in dry cylinder air.

Table 3.21: Product distributions and reaction efficiencies of H_3O^+ with tertiary amines in SIFT-MS.

Tertiary Amine (R_3N)	P_{FT} (mbar)	T_{FT} (K)	Observed Product Distribution : Product Ion (m/z):		Reference
			Percentage of Product Total, $R_2NH + H_3O^+ \rightarrow$		
			$R_2NH_2^+ + H_2O$	$(R_2NH_2 - H_2)^+ + H_2 + H_2O$	
Trimethylamine ((CH_3)$_3$N)	0.67	300	$C_3H_9NH^+$ (60): **90**	$C_3H_8N^+$ (58): **10**	Španěl and Smith (1998d)
N,N-diethylmethylamine ((CH_3CH_2)$_2$NCH$_3$)	0.67	RT	$C_5H_{13}NH^+$ (88): **70**	$C_5H_{12}N^+$ (86): **30**	Španěl and Smith (1999)
N,N-dimethyl-2-propylamine ((CH_3)$_2$NCH(CH$_3$)$_2$)	0.67	RT	$C_5H_{13}NH^+$ (88): **80**	$C_5H_{12}N^+$ (86): **20**	Španěl and Smith (1999)
Triethylamine (N(CH$_2$CH$_3$)$_3$)	0.67	300	$C_6H_{15}NH^+$ (102): **80**	$C_6H_{14}N^+$ (100): **20**	Španěl and Smith (1998d)

Note: P_{FT} denotes pressure in the flow tube, T_{FT} denotes temperature in the flow tube, RT denotes room temperature. A helium carrier gas was used in both cases. Španěl and Smith (1998d) diluted amine vapours in air, Španěl and Smith (1999) diluted amine vapours in dry cylinder air.

Table 3.22: The standard enthalpies of various dissociative reactions of C_2 to C_4 amines with H_3O^+.

Amine (M)	Parent ion: MH^+ in CI-MS M^+ in EI-MS	Product ion (m/z), ΔH_r^{Φ} (eV) $M + H_3O^+ \rightarrow$ **Percentage abundance of product ion in EI-MS,** *Percentage abundance of product ion in COH$^+$ CI-MS*, *Percentage abundance of product ion in CH$_5$$^+$ CI-MS*			
		$(MH - H_2)^+$ $+ H_2O + H_2$	$(MH - NH_3)^+$ $+ H_2O + NH_3$	$(MH - NH_4)$ $+ H_2O + NH_4^+$	$(MH - C_nH_{2n+2})^+ +$ $C_nH_{2n+2} + H_2O$
Ethylamine (primary)	**7.6**	$C_2H_6N^+$ (44): -1.49 to +1.08[b] **8.1**	$C_2H_5^+$ (29): +0.77[a] **0.5**	NH_4^+ (18): -1.02[a] **0.0**	CH_4N^+ (30): -1.37 to -0.76[b] **40.1**
Dimethylamine (secondary)	**28.3**	$C_2H_6N^+$ (44): -0.82 to -1.67[b] **44.4**	$C_2H_5^+$ (29): +0.37[a] **3.0**	NH_4^+ (18): -1.42[a] **1.4**	CH_4N^+ (30): **1.1**
1-propylmine (primary)	**6.4,** *3.8*	$C_3H_8N^+$ (58): **1.5,** *11.1*	$C_3H_7^+$ (43): -0.17[a] **1.2,** *31.6*	NH_4^+ (18): -1.23[a] **0.0,** *25.0*	CH_4N^+ (30): -1.32 to -1.30[b], **70.0,** *3.8* $C_2H_6N^+$ (44): -1.16 to 0.56[b], **0.8,** *11.7*
2-propylamine (primary)	**1.8,** *0.7*	$C_3H_8N^+$ (58): -1.82[b] **5.2,** *7.0*	$C_3H_7^+$ (43): -0.03[a] **3.3,** *25.7*	NH_4^+ (18): -1.08[a] **0.1,** *33.3*	CH_4N^+ (30): **1.0,** *28.3* $C_2H_6N^+$ (44): -2.25 to -1.94[b], **60.2,** *0.3*
N-methyl-ethylamine (secondary)	**16.9**	$C_3H_8N^+$ (58): **10.6**	$C_3H_7^+$ (43): **3.1**	NH_4^+ (18): **0.0**	CH_4N^+ (30): **9.0** $C_2H_6N^+$ (44): **40.1**
Trimethylamine (tertiary)	**23.5,** *45.3*	$C_3H_8N^+$ (58): -1.64 to -1.12[b] **34.4,** *32.4*	$C_3H_7^+$ (43): -0.65[a] **3.1,** *0.0*	NH_4^+ (18): -1.70[a] **0.0,** *0.0*	CH_4N^+ (30): -0.47 to +1.14[b], **11.1,** *0.4* $C_2H_6N^+$ (44): **1.8,** *0.0*
1-butylamine (primary)	**5.3** *3.8*	$C_4H_{10}N^+$ (72): **0.6,** *6.9*	$C_4H_9^+$ (57): -0.18[a] **0.3,** *24.2*	NH_4^+ (18): -1.18[a] **0.4,** *15.3*	CH_4N^+ (30): -1.25[b], **73.0,** *2.8* $C_2H_6N^+$ (44): -1.46 to -1.28[b], **1.3,** *1.3* $C_3H_8N^+$ (58): **0.0,** *25.4*

Table 3.22 is continued on the following page.

Amine (*M*)	Product ion (m/z), ΔH_r^Φ (eV) $M + H_3O^+ \rightarrow$				
	Percentage abundance of product ion in EI-MS, *Percentage abundance of product ion in COH⁺ CI-MS*, *Percentage abundance of product ion in CH₅⁺ CI-MS*				
	Parent ion: MH^+ in CI-MS M^+ in EI-MS	$(MH - H_2)^+$ $+ H_2O + H_2$	$(MH - NH_3)^+$ $+ H_2O + NH_3$	$(MH - NH_4)$ $+ H_2O + NH_4^+$	$(MH - C_nH_{2n+2})^+ +$ $C_nH_{2n+2} + H_2O$
2-methylpropylamine (*iso*-butylamine) (primary)	**4.4** *3.0*	$C_4H_{10}N^+$ (72): **0.6**, *9.5*	$C_4H_9^+$ (57): -0.15[a] **0.8**, *33.8*	NH_4^+ (18): -1.15[a] **0.2**, *6.8*	CH_4N^+ (30): -1.25[b], **69.7**, *5.9* $C_2H_6N^+$ (44): -1.83[b], **0.2**, *0.0* $C_3H_8N^+$ (58): **1.3**, *17.6*
2-butylamine (*sec*-butylamine) (primary)	**0.4** *0.9*	$C_4H_{10}N^+$ (72): **1.0**, *5.5*	$C_4H_9^+$ (57): +0.07[a] **0.8**, *19.0*	NH_4^+ (18): -1.07[a] **5.5**, *21.3*	CH_4N^+ (30): **2.9**, *6.6* $C_2H_6N^+$ (44): -1.76[b], **54.7**, *29.2* $C_3H_8N^+$ (58): -1.94[b], **6.3**, *0.6*
2-methyl-2-propylamine (*tert*-butylamine) (primary)	**0.0** *0.5*	$C_4H_{10}N^+$ (72): **0.0**, *1.8*	$C_4H_9^+$ (57): +0.08[a] **2.5**, *45.5*	NH_4^+ (18): -0.92[a] **0.0**, *7.3*	CH_4N^+ (30): **5.1**, *34.1* $C_2H_6N^+$ (44): **0.2**, *0.0* $C_3H_8N^+$ (58): **44.7**, *0.0*
Diethylamine (*N*-ethyl-ethylamine) (secondary)	**6.8** *23.0*	$C_4H_{10}N^+$ (72): **4.0**, *18.2*	$C_4H_9^+$ (57): -0.13[a] **0.4**, *0.9*	NH_4^+ (18): -1.13[a] **0.0**, *1.4*	CH_4N^+ (30): -2.44 to -1.71[b], **26.7**, *22.8* $C_2H_6N^+$ (44): +0.51 to +0.61[b], **8.4**, *5.1* $C_3H_8N^+$ (58): -2.14 to -1.41[b], **31.1**, *3.2*
N,N-dimethyl-ethylamine (tertiary)	**9.4** *16.6*	$C_4H_{10}N^+$ (72): **7.7**, *25.1*	$C_4H_9^+$ (57): **1.8**, *0.8*	NH_4^+ (18): **0.1**, *0.8*	CH_4N^+ (30): **4.9**, *18.8* $C_2H_6N^+$ (44): **9.0**, *3.0* $C_3H_8N^+$ (58): **37.6**, *0.5*

Note: Values were derived from enthalpies of formation of product ions derived from; [a] proton affinities and standard enthalpies of formation , [b]appearance energies and standard enthalpies of formation. A standard enthalpy of formation of H^+ of 15.92 eV from CRC Handbook of Chemistry And Physics (1986-1987) and a standard enthalpy of formation of H_3O^+ of 6.25 eV calculated as described in § 3 were employed. All other standard enthalpies of formation were taken from Mallard and Linstrom (2005) and proton affinities were taken from Hunter and Lias (1998), appearance energies were taken from Mallard and Linstrom (2005). The enthalpies of formation of $C_2H_5^+$, $C_3H_7^+$ and $C_4H_9^+$ were calculated using the proton affinities and standard enthalpies of formation of ethene, propene and 2-butene (*PA* of 1-butene is unknown) and are 9.41 eV, 8.34 eV and 8.07 eV respectively. The enthalpy of formation of NH_4^+ was calculated from the proton affinity and standard enthalpy of formation of

ammonia and is 6.60 eV. The percentage abundance of product ions in EI-MS (bold type) were calculated from relative abundancies from Mallard and Linstrom (2005); note other product ions were also observed. The percentage abundance of product ions from HCO^+ chemical ionisation mass spectra (CI-MS, bold italic) were calculated from relative abundancies given by Reiner *et al* (1986), see also Harrison (1992). Reiner *et al* (1986) derived product abundancies using either a single focussing magnetic deflection mass spectrometer or a double focussing mass spectrometer both equipped with a chemical ionisation source. The HCO^+ ions were produced from electron ionisation (70 eV) of 10%CO / 90% H_2 at 423 K and 0.4 mbar. Other minor (<10 %) product ions were observed from HCO^+ CI-MS of the amines and M^+ product ions was a major product from the reaction of *N*-ethyl-ethylamine and *N,N*-dimethyl-ethylamine, forming 16.4 % and 27.2 % of total product ions respectively. The percentage abundance of product ions from CH_5^+ CI-MS (italic) are from Whitney *et al* (1971). Measurements were made in a mass spectrometer with an ion source temperature of 423 K with methane and nitrogen pressure of ~1.33 mbar.

The reaction of ammonia with H_3O^+ has also been studied in SIFT (T_{FT} 300 K). The reaction is efficient with measured rate constant of ~2.2 x 10^{-9} cm^{-3} s^{-1} (± 20 %) and produces the non-dissociative product NH_4^+ only (Španěl and Smith 1998d, Smith *et al* 1980 and references therein). A flow tube pressure of ~0.7 mbar was employed by Španěl and Smith (1998d). Lindinger *et al* (1998) also report a thermal rate constant of 2.2 x 10^{-9} cm^{-3} s^{-1} and the non-dissociative product only but the method of measurement is not specified. In the PTR-MS large amounts of NH_4^+ are produced by the hollow cathode ion source resulting in a high background at m/z 18 and a poor detection limit (Norman *et al* 2007).

No measurements of product distributions from the reaction of H_3O^+ with primary, secondary or tertiary amines in PTR-MS based techniques, SIFDT or VT-SIFT could be found. Some of the major products from EI-MS and CI-MS employing HCO^+ and CH_5^+ protonating ions are displayed in Table 3.22. The enthalpies for the formation of these products from reaction of the corresponding amine with H_3O^+ are also given in Table 3.22. Reiner *et al* (1986) also investigated product distributions from C_5 primary, secondary and tertiary acyclic amines and similar trends to those from C_3 and C_4 amines were observed. In addition they derived product distributions from H_3^+ CI-MS of the amines. The increase in energy (Gibbs free energy) by changing the reagent ion from H_3O^+ to H_3^+ is 2.75 eV, to HCO^+ is 1.01 eV and to CH_5^+ is 1.44 eV. The increases in energy by employing HCO^+ and CH_5^+ reagent ions are closest to the increase in energy in the PTR-MS compared to SIFT; e.g. $\Delta\langle E_r \rangle$ is 0.27 to 0.40 eV in the PTR-MS at *E/N* of 120 to 140 Td (T_{dt} 298 K in air) for the C_4 acyclic amines. At the higher energies of EI-MS and HCO^+ and CH_5^+ CI-MS a greater degree of fragmentation is observed than from reaction with H_3O^+ in SIFT (Tables 3.19 - 22). As in the reaction of amines with H_3O^+ in SIFT (Tables 3.19 - 21), the extent of fragmentation of primary amines is greater than that of secondary and tertiary in EI-MS and HCO^+ CIMS (Table 3.22).

The product of elimination of H_2 from the protonated amine is a major one from HCO^+ CI-MS of secondary and tertiary amines and a minor product from primary amines as in H_3O^+ reactions in SIFT. The (*MH*- H_2)$^+$ product ion is the dominant fragment from CH_5^+ CI-MS of trimethylamine. In EI-MS these ions, produced by *H* elimination from the parent ion, are also greater from secondary and tertiary amines than primary (Table 3.20 and 3.22). (*MH*-H_2)$^+$ product ions have also been observed from CH_5^+ CI-MS of secondary and tertiary amines containing C_{14} to C_{18} n-alkyl groups, and polytertiary amines (Whitney *et al* 1971, Harrison 1992 and references therein). The increase in energy resulting from the change in reagent ion from H_3O^+ to HCO^+ results in a greater extent of fragmentation by elimination of

hydrogen from protonated diethylamine. $(MH\text{-}H_2)^+$ forms 32.4 % of the total product ions from CH_5^+ CI-MS of trimethylamine (Table 3.22) compared to only 10 % of product ions from reaction with H_3O^+ in SIFT (Table 3.19). This suggests a greater degree of dissociation by elimination of hydrogen may be observed from secondary and tertiary amines at the higher energies of PTR-MS compared to SIFT. The reactions of amines with H_3O^+ to form $(MH-H_2)^+$ are all exothermic (Table 3.22). The absence of the product ions from primary amines in SIFT (~298 K, Table 3.19) and limited production at higher energies may be due to an energy/entropy barrier to formation or competition from more thermodynamically favourable reactions.

As for the reaction of amines with H_3O^+ in SIFT, NH_4^+ is a major product ion from HCO^+ CI-MS of primary amines and minor from secondary and tertiary amines (Table 3.22). The reactions of amines with H_3O^+ to form NH_4^+ are all exothermic, however a degree of re-arrangement is required in all reactions and energy/entropy barriers are likely. Reiner *et al* (1986) calculated the potential energy diagram for dissociation of protonated 2-propylamine. The resultant values and the enthalpies of the non-dissociative and various dissociative reactions calculated here (Table 3.22) are displayed in Figure 3.6. There is an energy barrier of 1.89 eV to dissociation of protonated 2-propylamine to form NH_4^+. The energy released from the non-dissociative reaction to form the protonated amine is sufficient to overcome the barrier to dissociation to NH_4^+ and hence the observation of NH_4^+ from reaction with H_3O^+ in SIFT. Unlike in SIFT H_3O^+ reactions, the extent of dissociation to NH_4^+ in HCO^+ CI-MS of primary amines does not correlate with the number of CH_3 groups in the amine or the proximity of NH_2 to CH_3 groups; for example NH_4^+ forms 15.3 % of products from HCO^+ CI-MS of 1-butylamine and only 7.3 % from 2-methyl-2-propylamine. This may be caused by differences in the extent of competition from other dissociation channels which are accessible in reactions with these lower proton affinity ions but not in reactions with H_3O^+.

The lack of NH_4^+ from secondary and tertiary amines may result from an energy barrier to dissociation of the protonated amine requiring a greater amount of energy than that released from the non-dissociative reaction. The degree of re-arrangement (and *C-N* bond breakage) required to form NH_4^+ in the case of the secondary and tertiary amines, may result in larger critical energies and the reduced formation of NH_4^+.

Fragmentation by loss of NH_3 from the protonated amine is a major product of HCO^+ CI-MS of primary amines and a minor product from secondary and tertiary amines. Reiner *et al* (1986) found no energy barrier to NH_3 formation from the protonated primary amine 2-propylamine (Figure 3.6). Experimental investigation of the unimolecular dissociation of

metastable protonated amine ions suggest that the critical energy for dissociation to NH_3 is lower for primary amines (Reiner *et al* 1986). This is unsurprising given the rearrangement necessary for NH_3 elimination from the protonated secondary and tertiary amines. Minor abundancies of $C_5H_{11}{}^+$ were observed from the reaction of H_3O^+ with primary amines; 3-methyl-2-butylamine and 2-methyl-2-butylamine in SIFT (Španěl and Smith 1999, Table 3.19). The formation of $C_nH_{2n+1}{}^+$ ions from the reaction of H_3O^+ with amines by elimination of NH_3 is endothermic for the C_2 amines and exothermic for the majority of the higher amines. $(MH\text{-}NH_3)^+$ ions were not observed from H_3O^+ reaction with for example 2-propylamine in SIFT (Table 3.19) despite the exothermicity of the reaction and apparent lack of energy barrier. The formation of $(MH\text{-}NH_3)^+$ from the protonated primary amines are largely endothermic and would require all or nearly all of the energy released from the non-dissociative reaction (Figure 3.6). The absence of the $(MH\text{-}NH_3)^+$ from H_3O^+ reactions with the primary amines may be caused by the loss of energy released from the non-dissociative reaction into inactive modes such as radiation or in collisions with buffer molecules. The prevelance of more thermodynamically favourable frgamnetation to $NH_4{}^+$ may also contribute. A greater degree of NH_3 elimination may be expected at the higher energies of normally operated PTR-MS compared to SIFT, at least from the primary amines.

Immonium ions ($C_nH_{2n+2}N^+$) are observed from HCO^+ CI-MS of primary, secondary and tertiary amines. The immonium ions may be formed by elimination of an alkane from the protonated amines (in addition to those formed by hydrogen elimination). The immonium ions are also significant in EI-MS of the amines (Table 3.22). The reaction of H_3O^+ with the amines to form an alkane and immonium ion are all strongly exothermic (Table 3.22). The absence of immonium ions from H_3O^+ reaction with amines in SIFT indicates the enthalpy of reaction is not the critical energy. Experimental investigation of the unimolecular dissociation of metastable protonated amine ions by Reiner *et al* (1986) also suggested a significant energy barrier to alkane elimination from protonated amines. A barrier of 4.08 eV to elimination of CH_4 from protonated 2-propylamine was derived from *ab initio* calculations. To overcome such an energy barrier, 1.62 eV above the energy released from non-dissociative proton transfer from H_3O^+ to propylamine would be required (Figure 3.6). The sum of propylamine-H_3O^+ $KE_{c.m.}^r$ (0.19 eV – 0.26 eV) and $KE_{c.m.}^b$ (0.16 eV – 0.22 eV) in PTR-MS at E/N 120 – 140 Td in air at T_{dt} 298 K is 0.27 to 0.39 eV much less than the 1.62 eV required which suggests the immonium ion will not be formed in the PTR-MS. However, the exothermicity of the non-dissociative reaction of 2-propylamine with HCO^+ is
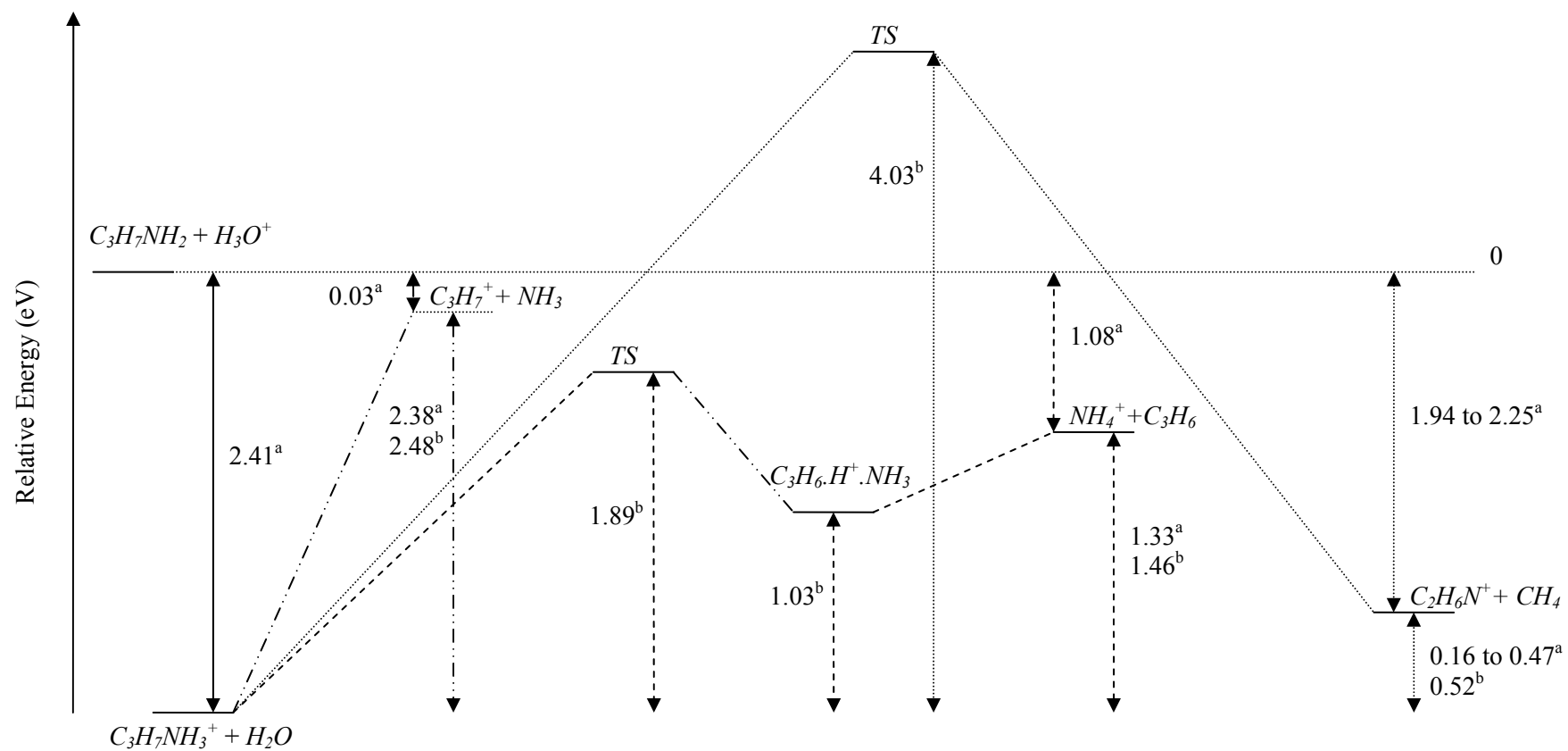
Figure 3.6: The potential energy profile for the reaction of H_3O^+ with 2-propylamine, [a]values calculated here refer to Table 3.22, [b]values taken from Reiner *et al* (1986).

3.41 eV, 0.62 eV less than the energy required for loss of alkane from the protonated amine yet the corresponding immonium ion was observed in HCO^+ CI-MS (Table 3.22). Reiner *et al* (1986) suggest that the immonium ions may be formed by direct alkide ion abstraction from the amine rather than by formation of the protonated amine followed by loss of an alkane.

In summary the reaction of primary amines with H_3O^+ produces the non-dissociative protonated amine (MH^+) and NH_4^+. The extent of dissociation to NH_4^+ is likely to be increased in the PTR-MS compared to SIFT. NH_4^+ is also the product of H_3O^+ reaction with ammonia and is produced in the ion source. Further dissociation by elimination of NH_3 from the protonated primary amine may occur at the elevated energies of PTR-MS. Secondary and tertiary amines react with H_3O^+ to produce the non-dissociative protonated amines (MH^+) and $(MH-H_2)^+$, dissociation by elimination of hydrogen is likely to increase in the PTR-MS compared to SIFT. The possibility of immonium ion formation, by alkide abstraction, from the reaction of H_3O^+ with primary, secondary and tertiary amines at the elevated energies of PTR-MS is also possible.

3.5.2 The Reaction of Amines in the Presence of Water

The proton affinity of ammonia is greater than that of $H_3O^+(H_2O)$ and Smith *et al* (1980) cite a Gibbs free energy for direct proton transfer of -0.17 eV. The proton affinity of ammonia is less than that of $H_3O^+(H_2O)_2$ and $H_3O^+(H_2O)_3$. They also give a Gibbs free energy for direct proton transfer from $H_3O^+(H_2O)_2$ to ammonia of +0.69 eV, and the reaction does not occur. Ammonia has a relatively large dipole and ligand switching reactions with $H_3O^+(H_2O)_n$ $n=1$ and 2 are exoergic. Smith *et al* (1980) cite a Gibbs free energy for ligand switching from $H_3O^+(H_2O)$ of - 0.91 eV. The Gibbs free energies for ligand switching of ammonia with $H_3O^+(H_2O)_2$ to form $NH_4^+(H_2O)$ and $NH_4^+(H_2O)_2$ are -0.04 eV and - 0.69 eV respectively. They found that the less exoergic of the possible (exoergic) channels were followed exclusively. The reaction with $H_3O^+(H_2O)$ proceeded at collisional rate (k_m = 2.2 x 10^{-9} cm^3 s^{-1}) and the sole product was that of proton transfer (NH_4^+). The reaction with $H_3O^+(H_2O)_2$ proceeded at collisional rate (k_m = 2.3 x 10^{-9} cm^3 s^{-1}) and the only product was $NH_4^+(H_2O)$. Three-body association of NH_4^+ and H_2O is possible but proceeds slowly with a measured rate constant of <0.1 x 10^{-27} cm^6 s^{-1} in SIFT at P_{FT} ~0.9 mbar T_{FT} 300 K. Thus ligand switching reactions with $H_3O^+(H_2O)$ are the main source of NH_4^+ hydrates in SIFT (Smith *et al* 1980, Španěl and Smith 2000b).

The proton affinities of the amines (Table 3.18) are greater than that of $H_3O^+(H_2O)$ (8.57 eV) and efficient proton transfer is probable. Excluding methylamine and aniline, the proton affinities of the amines are also equal to or greater than that of $H_3O^+(H_2O)_2$ (9.44 eV) indicating rapid proton transfer is likely. The proton affinities of the higher tertiary amines such as triethylamine are also greater than that of $H_3O^+(H_2O)_3$ and rapid proton transfer is expected. The polar nature of the amines suggests ligand switching reactions with $H_3O^+(H_2O)_n$ n=1 - 3 may be feasible.

3.6 Phosphines

The available proton affinities, gas basicities and resultant standard reaction enthalpy, entropy and Gibbs free energies for the non-dissociative proton transfer reaction of H_3O^+ with phosphine and methylphosphine are shown in Table 3.43. The proton affinities and gas basicities of phosphine and methyl phosphine are greater than those of water (Table 3.23). The Gibbs free energies of the reactions of phosphine and methylphosphine with H_3O^+ are less than – 0.43 eV and are expected to be efficient.

Table 3.23: The proton affinities (*PA*), gas basicities (*GB*), potential standard enthalpy (ΔH_r^{Φ}), potential standard entropy (ΔS_r^{Φ}) and Gibbs free energies (ΔG_r^{Φ}) of the non-dissociative H_3O^+ reaction with phosphines.

Compound	PA (eV)	GB (eV)	ΔH_r^{Φ} (eV)	ΔS_r^{Φ} (x 10^{-4} eV K^{-1})	ΔG_r^{Φ} (eV)
Phosphine (PH_3)	8.14	7.78	-0.97	-1.08	-0.94
Methyl phosphine (CH_3PH_2)	8.83	8.47	-1.66	-1.01	-1.63

Note: Proton affinities and gas basicities are taken from Hunter and Lias, (1998) ΔG_r^{Φ} and ΔH_r^{Φ} are calculated from Eq. 2.67 and 2.68, ΔS_r^{Φ} are calculated from $\Delta S_r^{\Phi} = \left[\Delta H_r^{\Phi} - \Delta G_r^{\Phi}\right]/T$.

Milligan *et al* (2007) studied the reaction of H_3O^+ with phosphine and demonstrated its quantification at the ppt to ppm range. A calibration standard of phosphine in nitrogen was used to derive a rate constant for the reaction of H_3O^+ with phosphine of 1.7 x 10^{-9} (±20 %) cm^{-3} s^{-1}. A helium carrier gas and P_{FT} of ~0.7 mbar was employed but the temperature was not specified although the instrument was normally operated at ~300 K. The collisional rate constant for the reaction of phosphine with H_3O^+ at 298 K derived using the results of Su and Chesnavich trajectory calculations (§ 2.4.1.4, Eq. 2.49 – 2.54), a phosphine polarizability of 4.84 Å^3 (CRC Handbook of Chemistry and Physics 2002 – 2003) and a phosphine dipole of 0.574 D (CRC Handbook of Chemistry and Physics 2002 – 2003) is
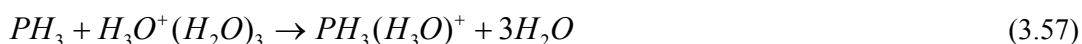
1.72×10^{-9} cm^{-3} s^{-1}. Thus the reaction is rapid and efficient and no dissociation was observed in SIFT.

Measurements of phosphines in PTR-MS based techniques could not be found. In EI-MS of phosphine, the parent ion forms 55.9 % of the total product and the most abundant fragments are observed at m/z 33 (PH_2^+) and m/z 31 (P^+) which form 18.6 % and 18.1 % of the total products (Mallard and Linstrom 2005). The formation of PH_2^+ from H_3O^+ reactions of phosphine by elimination of hydrogen (Eq. 3.54) and the formation of P^+ by the elimination of a second hydrogen (Eq. 3.55) are endothermic.

$$PH_3 + H_3O^+ \rightarrow PH_2^+ + H_2 + H_2O \tag{3.54}$$

$$PH_3 + H_3O^+ \rightarrow P^+ + 2H_2 + H_2O \tag{3.55}$$

The enthalpy of reaction Eq. 3.54 is + 2.51 eV and that of Eq. 3.55 is + 4.95 eV where the enthalpies of formation of P^+ and PH_2^+ were taken from Lias et al (1988) and are 11.33 eV and 13.76 eV respectively; the enthalpy of formation of H_3O^+ of 6.25 eV was employed and other values were taken from Mallard and Linstrom (2005). Thus only the non-dissociative reaction is anticipated at the energies available in normally operated PTR-MS (Figure 3.2 – 3.4).

The proton affinity of phosphine is less than those of $H_3O^+(H_2O)_n$ $n=1 – 3$. However entropy drives the reaction with $H_3O^+(H_2O)$ and it is exoergic and efficient proceeding with a rate constant of 1.5×10^{-9} cm^3 s^{-1} (Milligan et al 2007). Ligand switching was also observed in SIFT and reactions Eq. 3.56 and 3.57 were observed to proceed with rates of 6×10^{-10} cm^3 s^{-1} and 6×10^{-10} cm^3 s^{-1} respectively.

$$PH_3 + H_3O^+(H_2O)_2 \rightarrow PH_3(H_3O)^+ + 2H_2O \tag{3.56}$$

$$PH_3 + H_3O^+(H_2O)_3 \rightarrow PH_3(H_3O)^+ + 3H_2O \tag{3.57}$$

3.7 Implications for Mass Spectra Interpretation

A number of molecules react dissociatively with H_3O^+ and a number of the non-dissociative and dissociative products are isobaric. Careful consideration of possible contributors to a given m/z is required and unambiguous identification cannot be made without the use of alternative techniques such as GC and/or the use of a number of reagent ions. A mass list in which possible contributors to a range of m/z are identified from the calculations and analysis above is included in electronic format and serve as a summary of this research. Further investigation of product distributions as a function of E/N and as a function of

temperature and pressure at fixed E/N is required. In addition the effects of relative humidity and trace gas concentration on product distributions are of interest. Such a database would enable variation of the drift tube conditions to be used effectively as a tool for compound identification. This information would also potentially allow drift tube conditions to be optimised for a particular species of interest. The variation of both reaction efficiencies and collisional rate constants under these varied parameters requires further research as identified here.

Attached: Mass List in Electronic Format.

References

Amelynck, C., N. Schoon, T. Kuppens, P. Bultinck, E. Arjis (2005) A selected ion flow tube study of the reactions of H_3O^+, NO^+ and O_2^+ with some oxygenated biogenic volatile organic compounds, *International Journal of Mass Spectrometry*, **247**: 1-9.

Aoki, N., S. Inomata, H. Tanimoto (2007) Detection of alkyl nitrates by proton transfer reaction time-of-flight spectrometry, *International Journal of Mass Spectrometry*, **263**: 12-21.

Aprea, E., F. Biasioli, T. D. Märk, F. Gasperi (2007a) PTR-MS study of esters in water and water/ethanol solutions: Fragmentation patterns and partition coefficients, *International Journal of Mass Spectrometry*, **262**: 114-121.

Aprea, E., F. Biasioli, S. Carlin, G. Versini, T. D. Märk, F. Gasperi (2007b) Rapid white truffle headspace analysis by proton transfer reaction mass spectrometry and comparison with solid-phase microextraction coupled with gas chromatography/mass spectrometry, *Rapid Communications in Mass Spectrometry*, **21**: 2564 – 2572.

Arnold, S. T., A. A. Viggiano, R. A. Morris (1998) Rate constants and product branching fractions for the reactions of H_3O^+ and NO^+ with C_2-C_{12} alkanes, *Journal of Physical Chemistry A*, **102**: 8881-8887.

Berruyer-Penaud, F., G. Bouchoux, O. Payen, M. Sablier (2004) Structure, reactivity and thermochemical properties of protonated lactic acid, *Journal of Mass Spectrometry*, **39**: 613 – 620.

Blake, R. S., C. Whyte, C. O. Hughes, A. M. Ellis, P. S. Monks (2004) Demonstration of proton-transfer reaction time-of-flight mass spectrometry for real-time analysis of trace volatile organic compounds, *Analytical Chemistry*, **76**: 3841 – 3845.

Blake, R. S., K. P. Wyche, A. M. Ellis, P. S. Monks (2006) Chemical ionization reaction time-of-flight mass spectrometry: Multi-reagent analysis for determination of trace gas composition, *International Journal of Mass Spectrometry*, **254**: 85-93.

Bohme, D. K., G. I. Mackay, H. I. Schiff (1980) Determination of proton affinities from the kinetics of proton transfer reactions. VII. The proton affinities of O_2, H_2, Kr, O, N_2, Xe, CO_2, CH_4, N_2O, and CO, *Journal of Chemical Physics*, **73** (10): 4976-4986.

Boscaini, E., T. Mikoviny, A. Wisthaler, E. Von Hartungen, T. D. Märk (2004) Characterisation of wine with PTR-MS, *International Journal of Mass Spectrometry*, **239**: 215 – 219.

Bouchoux, G., J. Y. Salpin, D. Leblane (1996) A relationship between the kinetics and thermochemistry of proton transfer reactions in the gas phase, *International Journal of Mass Spectrometry and Ion Processes*. **153**: 37-48.

Bouchoux, G., N. Choret, R. Flammang (1997) Unimolecular chemistry of protonated diols in the gas phase: Internal cyclization and hydride ion transfer, *Journal of Physical Chemistry A*, **101**: 4271 – 4282.

Buhr, K., S, van Ruth, C, Delahunty (2002) Analysis of volatile flavour compounds by proton transfer reaction-mass spectrometry: fragmentation patterns and discrimination between isobaric and isomeric compounds, *International Journal of Mass Spectrometry*, **221:** 1-7.

Christian, T. J., B. Kleiss, R. J. Yokelson, R. Holzinger, P. J. Crutzen, W. M. Hao, T. Shirai, D. R. Blake (2004) Comprehensive laboratory measurements of biomass-burning emissions: 2. First comparison of open path FTIR, PTR-MS, and GC-MS/FID/ECD, *Journal of Geophysical Reasearch*, **109** (D02311): 1-12.

Custer, T. G., S. Kato, R. Fall, V. M. Bierbaum (2003) Negative-ion CIMS: analysis of volatile leaf wound compounds including HCN, *International Journal of Mass Spectrometry*, **223 – 224**: 427 – 446.

De Gouw, J., C. J. Howard, T. G. Custer, B. M. Baker, R. Fall (2000) Proton-transfer chemical-ionisation mass spectrometry allows real-time analysis of volatile organic compounds released from cutting and drying of crops, *Environmental Science and Technology*, **34**: 2640-2648.

De Gouw, J., P. D. Goldan, C. Warneke, W. C. Kuster, J. M. Roberts, M. Marchewka, S. B. Bertman, A. A. P. Pszenny, W. C. Keene (2003) Validation of proton transfer reaction-mass spectrometry (PTR-MS) measurements of gas-phase organic compounds in the atmosphere during the New England Air Quality Study (NEAQS) in 2002, *Journal of Geophysical Research*, **108** (D21): 4682, art.-nr.: 10.1029/2003JD003863.

De Gouw, J., C. Warneke (2007) Measurements of volatile organic compounds in the earth's atmosphere using proton-transfer-reaction mass spectrometry, *Mass Spectrometry Reviews*, **26**: 223-257.

Dotan, I., D. L. Albritton, W. Lindinger, M. Pahl (1976) Mobilities of CO_2^+, N_2H^+, H_3O^+, $H_3O^+.H_2O$, and $H_3O^+.(H_2O)_2$ ions in N_2, *The Journal of Chemical Physics*, **65** (11): 5028-5030.

Dotan, I., W. Lindinger, D. L. Albritton (1977) Mobilities of H_2O^+ and $H_3O^+.nH_2O$ (n = 0, 1, 2) ions in He, *Journal of Chemical Physics*, **67** (12): 5968-5969.

Duckett, S., B. Gilbert (2000) *Foundations of Spectroscopy*. Oxford University Press, New York.

Ellis, H., R. D. Harrison, H. D. B. Jenkins (1999) *Nuffield Advanced Science Revised Book of Data*. Longman, Singapore.

Fall, R., T, Karl, A, Hansel, A, Jordan, W, Lindinger (1999) Volatile organic compounds emitted after leaf wounding: On-line analysis by proton-transfer-reaction mass spectrometry, *Journal of Geophysical Research*, **104**: 15963 – 15974.

Fall, R., T. Karl, A. Jordans, W. Lindinger (2001) Biogenic C5 VOCs: release from leaves after freeze-thaw wounding and occurrence in air at a high mountain observatory, *Atmospheric Environment*, **35**: 3905-3916.

Feng, W. Y., C. Lifshitz (1995) The reactivity of neat and mixed proton-bound ethanol clusters, *International Journal of Mass Spectrometry and Ion Processes*, **149/150**: 13 – 25.

Glosik, J., D. Smith, P. Španěl, W. Freysinger, W. Lindinger (1993) SIFDT studies of the reactions of C^+, CH^+ and CH_2^+ with HCl and CO_2, and CH_3^+ with HCl, *International Journal of Mass Spectrometry and Ion Processes*, **129**: 131-143.

Hansel, A., A. Jordan, R. Holzinger, P. Prazeller, W. Vogel, W. Lindinger (1995) Proton transfer reaction mass spectrometry: on-line trace gas analysis at the ppb level, *International Journal of Mass Spectrometry and Ion Processes*, **149/150**: 609-619.

Hansel, A., W. Singer, A. Wisthaler, M. Schwarzmann, W. Lindinger (1997) Energy dependencies of the proton transfer reactions H_3O^+ + CH_2O $\Leftrightarrow$ CH_2OH^+ + H_2O, *International Journal of Mass Spectrometry and Ion Processes*:**167/168**: 697-703.

Hansel A., A. Jordan, C. Warneke, R. Holzinger, A. Wisthaler, W. Lindinger (1999) Proton-transfer-reaction mass spectrometry (PTR-MS): on-line monitoring of volatile organic compounds at volume mixing ratios of a few pptv, *Plasma Sources Science and Technology*, **8**: 332-336.

Harrison, A. G (1992) *Chemical Ionization Mass Spectrometry*, CRC Press, Inc., Florida.

Harwood, L. M., T. D. W. Claridge (1997) *Introduction to Organic Spectroscopy*, Oxford University Press. New York.

Hunter, E. P. L., S. G. Lias (1998) Evaluated gas phase bascities and proton affinities of molecules: An update, *Journal of Physical Chemical Reference Data*, **27** (3): 413-656.

Inomata, S., H. Tanimoto, S. Kameyama, U. Tsunogai, H. Irie, Y. Kanaya, Z. Wang (2008) Technical Note: Determination of formaldehyde mixing ratios in air with PTR-MS: laboratory experiments and field measurements, *Atmospheric Chemistry and Physics*, **8**: 273 – 284.

Jobson, B. T., M. L. Alexander, G. D. Maupin, G. G. Muntean (2005) On-line analysis of organic compounds in diesel exhaust using a proton transfer reaction mass spectrometer (PTR-MS). *International Journal of Mass Spectrometry*, **245**: 78 - 89.

Karl, T., F. Harren, C. Warneke, J. De Gouw, C. Grayless, R. Fall (2005) Senescing grass crops as regional sources of reactive volatile organic compounds, *Journal of Geophysical Research*, **110**: 1-11.

Karl, T. G., T. J. Christian, R. J. Yoelson, P. Artaxo, W. M. Hao, A. Guenther (2007) The Tropical Forest and Fire Emissions Experiment: method evaluation of volatile organic compound emissions measured by PTR-MS, FTIR, and GC from tropical biomass burning, *Atmospheric Chemistry and Physics*, **7**: 5883 - 5897.

Lagg, A., A. Taucher, A. Hansel, W. Lindinger (1994) Applications of proton transfer reactions to gas analysis, *International Journal of Mass Spectrometry and Ion Processes*, **134**: 55-56.

Lias, S. G., J. F. Liebman, R. D. Levin (1984) Evaluated gas phase basicities and proton affinities of molecules; heats of formation of protonated molecules, *Journal of Physical and Chemical Reference Data*, **13** (3): 695 -808.

Lias, S. G., J. E. Bartmess, J. F. Liebman, J. L. Holmes, R. D. Levin, W. G. Mallard (1988) Gas-phase ion and neutral thermochemistry, *Journal of Physical and Chemical Reference Data*, **17** (Supplement 1): 1-861.

Lindinger, W., A. Hansel, A. Jordan (1998) On-line monitoring of volatile organic compounds at pptv levels by means of proton-transfer-reaction mass spectrometry (PTR-MS) medical applications, food control and environmental research, *International Journal of Mass Spectrometry and Ion Processes*, **173**: 191-241.

Lindinger, C., P. Pollien, S. Ali, C. Yeretzian, I. Blank, T. Märk (2005) Unambiguous identification of volatile organic compounds by proton-transfer reaction mass spectrometry coupled with GC/MS, *Analytical Chemistry*, **77**: 4117 – 4124.

MacKay, G. I., A. C. Hopkinson, D. K. Bohme (1978) Acid catalysis in the gas phase: Dissociative proton transfer to formic and acetic acid, *Journal of the American Chemical Society*, **100** (24): 7460 – 7464.

Malekina, S. D., T. L. Bell, M. A. Adams (2007) PTR-MS analysis of reference and plant-emitted volatile organic compounds, *International Journal of Mass Spectrometry*, **262**: 203-210.

Mallard, W. G., P. J. Linstrom (2005) NIST Chemistry WebBook, NIST Standard Reference Database Number 69, February 2000, National Institute of Standards and Technology, Gaithersburg, MD.

McGlashan, M. L (1971) *Physiochemical Quantities and Units*, The Royal Institute of Chemistry, Herts.

Michel, E., N. Schoon, C. Amelynck, C. Guimbaud, V. Catoire, E. Arijis (2005) A selected ion flow tube study of reactions of H_3O^+, NO^+ and O_2^+ with methyl vinyl ketone and some atmospherically important aldehydes, *International Journal of Mass Spectrometry*, **244**: 50-59.

Midey, A. J., S. T. Arnold, A. A. Viggiano (2000) Reactions of $H_3O^+(H_2O)_n$ with Formaldehyde and Acetaldehyde, *Journal of Physical Chemistry. A*, **104**: 2706-2709.

Midey, A. J., S. Williams, S. T. Arnold, A. A. Viggiano (2002) Reactions of $H_3O^+(H_2O)_{0,1}$ with alkylbenzenes from 298 K to 1200 K, *Journal of Physical Chemistry A*, **106**: 11726-11738.

Midey, A. J., S. Williams, T. M. Miller, A. A. Viggiano (2003) Reactions of O_2^+, NO^+ and H_3O^+ with methylcyclohexane (C_7H_{14}) and cyclooctane (C_8H_{16}) from 298 K to 700 K, *International Journal of Mass Spectrometry*, **222**: 413-430.

Milligan, D. B., P. F. Wilson, C. G. Freeman, M. Meot-Ner (Mautner), M. J. McEwan (2002) Dissociative proton transfer reactions of H_3^+, N_2H^+, and H_3O^+ with acyclic, cyclic and aromatic hydrocarbons and nitrogen compounds, and astrochemical implications, *Journal of Physical Chemistry*, **106**: 9745-9755

Milligan, D. B., G. J. Francis, B. J. Prince, M. J. McEwan (2007) Demonstration of selected ion flow tube MS Detection in the parts per tillion range, *Analytical Chemistry*, **79**: 2537 – 2540.

Munson, M. S. B., F. H. Field (1966) Chemical ionisation mass spectrometry. I. General introduction, *Journal of the American Chemical Society*, **88** (12): 2621 – 2630.

Norman M., A. Hansel, A. Wisthaler (2007) O_2^+ as reagent ion in the PTR-MS instrument: Detection of gas-phase ammonia, *International Journal of Mass Spectrometry*, **265**: 382 – 387.

Prazeller, P., P. T. Palmer, E. Bocaini, T. Jobson, M. Alexander (2003) Proton transfer reaction ion trap mass spectrometer, *Rapid Communications in Mass Spectrometry*, **17**: 1593-1599.

Reiner, E. J., R. A. Poirier, M. R. Peterson, I. G. Csizmadia, A. G. Harrison (1986) Unimolecular fragmentation of some gaseous protonated amines, *Canadian Journal of Chemistry*, **64**: 1652 – 1660.

Schoon, N., C. Amelynck, E. Debie, P. Bultinck, E. Arjis (2007) A selected ion flow tube study of the reactions of H_3O^+, NO^+ and O_2^+ with a series of C_5, C_6, C_8 unsaturated biogenic alcohols, *International Journal of Mass Spectrometry*, **263**: 127-136.

Schröder, D., H. Soldi-Lose, M. Semialjac, J. Loos, H. Schwarz, G. Eerdekens, F. Arnold (2003) On gaseous $C_4H_6O_2$ compounds in the atmosphere: new insights from collision experiments of the protonated molecules in the laboratory and on aircraft, *International Journal of Mass Spectrometry*, **228**: 35 – 47.

Sekiguchi, O., V. Bakken, E. Uggerud (2004) Decomposition of Protonated Formic Acid: One Transition State – Two Product Channels, *Journal of the American Society for Mass Spectrometry*, **15**: 982 – 988.

Smith, D., N. G. Adams, M. J. Henchman (1980) Studies of the binary reactions of $H_3O^+.(H_2O)_{0,1,2}$ ions and their deuterated analogues with D_2O, H_2O and NH_3, *Journal of Chemical Physics*, **72** (9): 4951 – 4957.

Smith, D., A. M. Diskin, Y. Ji, P. Španěl (2001) Concurrent use of H_3O^+, NO^+, O_2^+ precursor ions for the detection and quantification of diverse trace gases in the presence of air and breath by selected ion-flow tube mass spectrometry, *International Journal of Mass Spectrometry*, **209**: 81-97.

Smith, D., P. Španěl (2005) Selected Ion Flow Tube Mass Spectrometry (SIFT-MS) for On-line Trace Gas Analysis, *Mass Spectrometry Reviews*, **24**: 661-700.

Španěl, P., D. Smith, M. Henchman (1995a) The reactions of some interstellar ions with benzene, cyclopropane and cyclohexane, *International Journal of Mass Spectrometry and Ion Processes*, 141: 117-126.

Španěl, P., M. Pavlik, D. Smith (1995b) Reactions of H_3O^+ and OH^- ions with some organic molecules; applications to trace gas analysis in air, *International Journal of Mass Spectrometry and Ion Processes*, **145**: 177-186.

Španěl, P., D. Smith (1995c) Reactions of hydrated hydronium ions and hydrated hydroxide ions with some hydrocarbons and oxygen-bearing molecules, *Journal of Physical Chemistry*, **99**: 15551 – 15556.

Španěl, P., D. Smith (1997) SIFT studies of reactions of H_3O^+, NO^+ and O_2^+ with a series of alcohols, *International Journal of Mass Spectrometry and Ion Processes*, 167/168: 375-388

Španěl, P., J. Yufeng, D. Smith (1997) SIFT studies of the reactions of H_3O^+, NO^+ and O_2^+ with a series of aldehydes and ketones, *International Journal of Mass Spectrometry and Ion Processes*, **165/166**: 25-37.

Španěl, P., D. Smith (1998a) SIFT studies of the reactions H_3O^+, NO^+ and O_2^+ with a series of volatile carboxylic acids and esters, *International Journal of Mass Spectrometry and Ion Processes*, **172**: 137 – 147.

Španěl, P., D. Smith (1998b) SIFT studies of reactions of H_3O^+, NO^+ and O_2^+ with several ethers, *International Journal of Mass Spectrometry and Ion Processes*, **172**: 239 – 2 47.

Španěl, P., D. Smith (1998c) Selected ion flow tube studies of the reactions of H_3O^+, NO^+ and O_2^+ with some organosulphur molecules, *International Journal of Mass Spectrometry*, **176**: 167 – 176.

Španěl. P., D. Smith (1998d) Selected ion flow tube studies of the reactions of H_3O^+, NO^+ and O_2^+ with several amines and some other nitrogen containing molecules, *International Journal of Mass Spectrometry*, **176**: 203 – 211.

Španěl, P., D. Smith (1999) Selected ion flow tube studies of the reactions of H_3O^+, NO^+ and O_2^+ with eleven amine structural isomers of $C_5H_{13}N$, *International Journal of Mass Spectrometry*, **185/186/187**: 139 – 147.

Španěl, P., S. Davies, D. Smith (1999) Quantification of breath isoprene using the Selected ion flow tube mass spectrometric analytical method, *Rapid Communications in Mass Spectrometry*, **13**: 1733 – 1738.

Španěl, P., D. Smith (2000a) Quantification of hydrogen sulphide in humid air by selected ion flow tube mass spectrometry, *Rapid Communications in Mass Spectrometry*, **14**: 1136 – 1140.

Španěl, P., D. Smith (2000b) Influence of water vapour on selected ion flow tube mass spectrometric analyses of trace gases in humid air and breath, *Rapid Communications in Mass Spectrometry*, **14**: 1898-1906.

Španěl, P., J. M. van Doren, D. Smith (2002a) A selected ion flow tube study of the reactions of H_3O^+, NO^+, and O_2^+ with saturated and unsaturated aldehydes and subsequent hydration of the product ions, *International Journal of Mass Spectrometry*, **213**: 163-176.

Španěl, P., T. Wang, D. Smith (2002b) A selected ion flow tube, SIFT, study of the reactions of H_3O^+, NO^+ and O_2^+ ions with a series of diols, *International Journal of Mass Spectrometry*, **218**: 227-236.

Spitaler, R., N. Araghipour, T. Mikoviny, A. Wisthaler, J. D. Via, T. D. Märk (2007) PTR-MS in enology: Advances in analytics and data analysis, *International Journal of Mass Spectreometry*, **266**: 1-7.

Taucher J., A. Hansel, A. Jordan, W. Lindinger (1996) Analysis of compounds in human breath after ingestion of garlic using proton-transfer-reaction mass spectrometry, *Journal of Agriculture and Food Chemistry*, **44**: 3778 – 3782.

Vlasenko, A., I. J. George, J. P. D. Abbatt (2008) Formation of volatile organic compounds in the heterogeneous oxidation of condensed-phase organic films by gas-phase OH, *Journal of Physical Chemistry A*, **112**: 1552 – 1560.

Von Hartungen, E., A. Wisthaler, T. Mikoviny, D. Jaksch, E. Boscaini, P. J. Dunphy, T. D. Märk (2004) Proton-transfer-reaction mass spectrometry (PTR-MS) of carboxylic acids. Determination of Henry's law constants and axillary odour investigations, *International Journal of Mass Spectrometry*, **239**: 243 – 248.

Wang, T., D. Smith, P. Španěl (2004) Selected ion flow tube, SIFT, studies of the reactions of H_3O^+, NO^+ and O_2^+ with compounds released by Pseudomonas and related bacteria, *International Journal of Mass Spectrometry*, **233**: 245-251.

Wang, T., W. Carroll, W. Lenny, P. Boit, D. Smith (2006) The analysis of 1-propanol and 2-propanol in humid air samples using selected ion flow tube mass spectrometry, *Rapid Communications in Mass Spectrometry*, **20**: 125-130.

Warneke, C., J. Kuczynski, A. Hansel, A. Jordan, W. Vogel, W. Lindinger (1996) Proton transfer reaction mass spectrometry (PTR-MS): propanol in human breath, *International Journal of Mass Spectrometry and Ion Processes*, **154**: 61-70.

Warneke, C., C. van der Veen, S. Luxembourg, J. A. De Gouw, A. Kok (2001) Measurements of benzene and toluene in ambient air using proton-transfer-reaction mass spectrometry: calibration, humidity dependence, and field intercomparison, *International Journal of Mass Spectrometry*, **207**: 167-182.

Warneke, C., S. L. Luxembourg, J. A. De Gouw, H. J. I. Rinne, A. B. Guenther, R. Fall (2002) Disjunct eddy covariance measurements of oxygenated volatile organic compounds fluxes from an alfalfa field before and after cutting, *Journal of Geophysical Research*, **107** (D8).

Warneke, C., J. A. De Gouw, W. C. Custer, P. D. Goldan, R. Fall (2003) Validation of atmospheric VOC measurements by proton-transfer-reaction mass spectrometry using a gas chromatographic preparation method, *Environmental Science and Technology*, **37**: 2494-2501.

Warneke, C., J. A. De Gouw, E. R. Lovejoy, P. C. Murphy, W. C. Kuster (2005a) Development of proton-transfer ion trap-mass spectrometry: On-line detection and identification of volatile organic compounds in air, *Journal of the American Society for Mass Spectrometry*, **16**: 1316-1324.

Warneke, C., S. Kato, J. A. De Gouw, P. D. Goldan, W. C. Kuster, M. Shao, E. R. Lovejoy, R. Fall, F. C. Fehsenfeld (2005b) Online volatile organic compound measurements using a newly developed proton-transfer ion-trap mass spectrometry instrument during New England air quality study – intercontinental transport and chemical transformation 2004: Performance, intercompraison, and compound identification, *Environmental Science and Technology*, **39**: 5390 – 5397.

Whitney, T. A., L. P. Klemann, F. H. Field (1971) Investigation of polytertiary alkylamines using chemical ionization mass spectrometry, *Analytical Chemistry*, **43** (8): 1048 – 1052.

Williams, T. L., N. G. Adams, L. M. Babcock (1998) Selected ion flow tube studies of $H_3O^+(H_2O)_{0,1}$ reactions with sulfides and thiols, *International Journal of Mass Spectrometry and Ion Processes*, **172**: 149 – 159.

Williams, S., A. J. Midey, S. T. Arnold, R. A. Morris, A. A. Viggiano, Y. Chiu, D. J. Levandier, R. A. Dressler, M. R. Berman (2000a) Electronic, Rovibrational and Translational Energy Effects in Ion-Alkylbenzene Charge-Transfer Reactions, *Journal of Physical Chemistry*. **104**: 10336-10346.

Williams, J., U. Pöschl, P. J. Crutzen, A. Hansel, R. Holzinger, C. Warneke, W. Lindinger, J. Lelieveld (2001) An atmospheric chemistry interpretation of mass scans obtained from a proton transfer mass spectrometer flown over the tropical rainforest of Surinam, *Journal of Atmospheric Chemistry*. **38**: 133 – 166.

Wróblewski, T., L. Ziemczonek, K. Szerement, G. P. Karwasz (2006) Proton affinities of simple organic compounds, *Czechoslovak Journal of Physics*, **56**: (Suppl. B): B1110- B1115.

Wyche, K. P., R. S. Blake, K. A. Willis, P. S. Monks, A. M. Ellis (2005) Differentiation of isobaric compounds using chemical ionization mass spectrometry, *Rapid Communications in Mass Spectrometry*, **19**: 3356 – 3362.

Wyche, K. P., R. S. Blake, A. M. Ellis, P. S. Monks, T. Brauers, R. Koppmann, A. C. Apel (2007) Technical note: performance of chemical ioniazation reaction time-of-flight mass spectrometry (CIR-TOF-MS) for the measurement of atmospherically significant oxygenated volatile organic compounds, *Atmospheric Chemistry and Physics*, **7**: 609-620.

4 Identification of (Oxygenated) Volatile Organic (Sulphur Containing) Compounds Emitted from Cattle Slurry.

4.1 Introduction

(O)VOCs impact upon the oxidative capacity of the atmosphere and contribute to ozone formation in the troposphere, aerosol and cloud condensation nuclei formation and acid rain (Chapter 1). (O)VOCs are therefore the subject of legislation and abatement policies. In 1999 the United Nations Economic Commission for Europe (UNECE) Convention on Long-range Transboundary Air Pollution was extended to include the Protocol to Abate Acidification, Eutrophication and Ground-level Ozone or Gothenburg Protocol which entered into force in May 2005. This protocol sets emission ceilings for 2010 for sulphur, NOx, VOCs and ammonia. Under the protocol the European Communities VOC emissions should be cut by 57 % compared to 1990, to 6600 thousand tonnes of VOC per year, by 2010. In the United Kingdom VOC emissions should be cut by 53 % relative to 1990, to 1200 thousand tonnes of VOC per year, by 2010. (http://www.unece.org/env/lrtap/multi_h1.htm). Thus the understanding of (O)VOC budgets is critical to understanding global climate and developing and meeting targets for (O)VOC emissions. The contribution of (O)VOCs emitted as a result of agriculture and the production, storage and application of animal waste are not well quantified.

There are 216751 thousand livestock (cattle, calves, sheep, lambs, pigs, fowl) in Great Britain (2007), 10304 thousand of which are cattle and calves (DEFRA 2007). Cattle manure from beef and dairy farms is the largest volume of manure type generated in Great Britain. A survey of 1331 farms in Great Britain (2007) sponsored by the Department for Environment, Food and Rural Affairs (Defra) and the Scottish Government, Rural and Environment Research and Analysis Directorate (SG-RERAD) revealed 76 % used cattle farmyard manure or cattle slurry while 2 % used pig farm yard manure or pig slurry, 2 % used sheep farm yard manure, 2 % used broiler/turkey litter, 2 % used layer manure and 4 % used other types of manure (Thomas 2008). Hobbs *et al* (2004) estimated that the annual emission of non-methane volatile organic compounds (NMVOC) from UK livestock in 2002 was 165 ± 56 kt NMVOCs yr^{-1} based on the ratio of ammonia and NMVOC emission rates from animal waste and breathe (NMVOCs such as alcohols, esters, aldehydes, ketones, alkanes and alkenes were not included in this estimate). Cattle formed the greatest contribution emitting 102.4 kt NMVOCs yr^{-1}. While emissions from a variety of animal wastes are of interest those from cattle slurry were considered here.

A huge number of volatiles have been identified from livestock and their waste, for example, over 331 different VOCs were identified from swine operations in North Carolina (Schiffman *et al* 2001), 70 VOCs identified from a dairy farm (Sunesson *et al* 2001) and 73 VOCs have been identified from dairy slurry wastewater lagoon (Filipy *et al* 2006). Major (O)VOCs emitted from animal wastes include carboxylic acids, oxygenated aromatics, amines, and sulphur containing volatile organic compounds (e.g. Hobbs *et al* 1997, Smith *et al* 2000, Rabaud *et al* 2003, Willig *et al* 2004, Hobbs *et al* 2004). Other (O)VOCs including alkanes, alkenes, benzyl aromatics, alcohols, aldehydes, ketones and esters have been identified in the vicinity of livestock operations and from animal waste (Schiffman *et al* 2001, Sunesson *et al* 2001, Rabaud *et al* 2003, Filipy *et al* 2006, Beck *et al* 2007, Shaw *et al* 2007, Ngwabie *et al* 2008). Alongside (O)VOCs other trace gases which can potentially be detected *via* PTR-MS, including phosphine and hydrogen sulphide, are emitted (e.g. Skjelhaugen and Donantoni 1998, Hobbs *et al* 1997, Glindemann, and Bergmann 1995, Roels and Verstraete 2001).

The (anaerobic) microbial metabolism of non-utilised carbohydrates, proteins and lipids in the gut, intestine and excreted manure and urine are responsible for the majority of (O)VOC emissions from animal waste (e.g. Spoelstra 1980, Mackie *et al* 1998, Le *et al* 2005, Le 2006). Microbial activity is also a significant sink of many of the (O)VOCs. The mechanisms of formation of (O)VOCs emitted from animal manure and animal production facilities have been the subject of a number of reviews (Spoelstra 1980, Mackie *et al* 1998, Le *et al* 2005, Le 2006). Appendix C contains a summary of the potential sources and sinks of selected compounds from animal waste. The following section contains a brief discussion of the sources of carboxylic acids, sulphur containing compounds, phenollics, phosphine and amines respectively.

Carboxylic acids (volatile fatty acids) are produced largely from the deamination of amino acids (also producing ammonia) as well as fermentation of carbohydrates and lipids (e.g. Allison 1978, Spoelstra 1980, Mackie *et al* 1998, Zhu *et al* 2000). Some of the carboxylic acids are subsequently degraded to carbon dioxide (CO_2) which is utilised by methanogens as an electron acceptor with reduction to methane (CH_4) producing energy in the absence of oxygen (e.g. Mackie *et al* 1998, Manahan 1975). The emission of carboxylic acids is to some extent dependent on the balance between degradation of carbohydrates and proteins to acids and degradation to CO_2 and methanogenesis (and use of acids in assimilatory processes). Aldehydes, alcohols and esters also arise from deamination of amino acids and metabolism of carbohydrates and may also be used as substrates for CO_2 and CH_4

production. The Aldehydes, alcohols and esters are generally thought to be present in minor amounts compared to the carboxylic acids (Spoelstra 1980).

Hydrogen sulphide is produced primarily by two mechanisms. (a) Metabolism of sulphur containing amino acids and related materials, e.g. cystine, cysteine and homocystein (Appendix C), results in hydrogen sulphide. (b) Sulphate reducing bacteria utilise sulphate as an electron acceptor in the absence of oxygen, reducing sulphate to hydrogen sulphide and producing energy (Manahan *et al* 1975). Sulphate is supplied by diet or depolymerisation and desulphation of endogenously produced sulphated glycoproteins such as mucins (Mackie *et al* 1998). In addition, in a similar manner to the carboxylic acids, VOSCs methanethiol and dimethylsulphide may be used as substrates for methanogenesis, i.e. production of CO_2 and subsequent reduction to CH_4; sulphide is also produced during this process (Lomans *et al* 2002a and b). Dimethylsulphide may be biologically degraded to methanethiol and hydrogen sulphide (Bentley and Chasteen 2004, Lomans *et al* 2002a and b). Hydrogen sulphide is also strongly absorbed to soils and reacts with *Fe(II)* to form *FeS/FeS₂* (Bremner and Banwart 1976). Some hydrogen sulphide may also be biologically methylated to form methanethiol (Bentley and Chasteen 2004, Lomans *et al* 2002a and b).

Hydrogen sulphide was originally thought to be the primary gaseous link in the sulphur cycle. However atmospheric hydrogen sulphide concentrations in the presence of oxidizing surface oceans were not sufficient to explain the transfer of sulphur from the sea through the atmosphere to the land (Lovelock *et al* 1972). The observation of dimethylsulphide in and above oceans and marine environments revealed the importance of volatile organic sulphur containing compounds (VOSCs) in the global sulphur cycle and climate and it was proposed that dimethylsulphide (DMS) fills the place originally assigned to hydrogen sulphide as natural carrier of sulphur in the atmosphere (e.g. Lovelock *et al* 1972, Charlson *et al* 1987, Kiene and Bates 1990, Cox 1997, Hewitt and Davison 1997). The PTR-MS has frequently been employed for the measurement of DMS in marine air (e.g. Warneke and Gouw 2001, Williams *et al* 2004, Williams *et al* 2001, Hayward *et al* 2002, Sinha *et al* 2007). VOSC emissions from marine environments are thought to consist largely of DMS. VOSCs are also produced to a lesser extent in freshwater sediments and as in terrestrial ecosystems, a larger range of VOSCs are emitted than from marine environments (Bentley and Chasteen 2004, Lomans *et al* 2002a and b). The terrestrial sources of DMS are thought to be small compared to oceanic emissions (e.g. Watts 2000) however agricultural emissions are uncertain and have not generally been included in global budgets of DMS (Hobbs and Mottram 2000). The fermentative decomposition of organic matter is probably the most important terrestrial source of volatile sulphur containing compounds (Charlson *et al* 1987). This flux is highly

uncertain but estimated to be ~ 2 mmol m^{-2} yr^{-1}, compared to ~3 ± 1.5 mmol m^{-2} yr^{-1} from oceans. The importance of livestock emissions of dimethylsulphide and the need for further quantification has recently been highlighted by Hobbs and Mottram (2000).

Methanethiol and dimethylsulphide appear to be the predominant VOSCs emitted from animal waste. Other VOSCs include dimethyldisulphide, dimethylsulphoxide and higher alkylthiols such as ethanethiol. VOSCs in animal wastes are largely attributed to metabolism of amino acids, such as methionine, and sulphonium salt *S*-methylmethionine (e.g. Banwart and Bremner 1975, Spoelstra 1980, Mackie *et al* 1998, Le *et al* 2005, Le 2006). The mechanisms of production in marine and freshwater sediments may provide insight into other processes occurring in stored animal wastes and the soil to which it is applied. Methanethiol and dimethylsulphide are formed predominantly by methylation of hydrogen sulphide and dimethylsulphide in sulphide rich freshwater sediments and *Sphagnum* peat bogs (Bak *et al* 1992, Kiene and Hines 1995, Lomans *et al* 2002a,b, Bentley and Chasteen 2004). Methyl donating groups are formed by e.g. aerobic degradation of lignin which may be present in animal wastes (Bak *et al* 1992, Lomans *et al* 2002b, Bentley and Chasteen 2004). DMSO and DMDS reduction may also contribute to dimethylsulphide and methanethiol formation respectively (Kiene and Hines 1995, Lomans *et al* 2002b, Bentley and Chasteen 2004).

In oceans DMS is produced from degradation of sulphonium salt dimethylsulphoniopropionate (DMSP) (e.g. Bentley and Chasteen 2004, Lomans *et al* 2002b, Kiene and Bates 1990, Charlson *et al* 1987). DMSP may alternatively be degraded to methanethiol (e.g. Bentley and Chasteen 2004, Lomans *et al* 2002b), though no PTR-MS measurements of methanethiol in marine air could be found. DMSP is an osmylyte, has a cryoprotectant ability, can act as a feeding attractant or deterrent and is an antioxidant (Bentley and Chasteen 2004). Some microorganisms likely to be found in animal waste have the ability to degrade DMSP, for example *Escherichia coli* is able to scavenge DMSP (Bentley and Chasteen 2004). However DMSP is not widely distributed in terrestrial plants and it is unlikely this is a significant source of DMS in and above animal waste.

Methanogenesis and sulphogenesis are major sinks of dimethylsulphide and methanethiol in freshwater sediments and may occur in anaerobic animal wastes (Lomans *et al* 2002 a and b). A denitrifying bacteria which converts nitrate (NO_3^-) to nitrogen (N_2) using dimethylsulphide and methanethiol producing carbon dioxide and sulphate has been isolated (Lomans *et al* 2002 a and b). Anaerobic and aerobic biological oxidation of

dimethylsulphide and methanethiol have also been observed (Lomans *et al* 2002 a and b, Bentley and Chasteen 2004).

Dimethyldisulphide and dimethylsulphoxide are produced and removed by biological (and atmospheric) oxidation and reduction of methanethiol and dimethylsulphide respectively (Segal and Starkey 1969, Kadota and Ishida 1972, Kiene and Bates 1990, Kiene and Hines 1995, Lomans *et al* 2002 a and b, Bentley and Chasteen 2004). Ethanethiol has been observed from metabolism of *S*-ethylcysteine and is a product of synthesis of methionine from methanethiol and ethionine by *Saccharaomyces cerevisiae* (Cherest *et al* 1970, Kadota and Ishida 1972). Measurements of ethanethiol in the air above animal waste could not be found. However, Le *et al* (2006) repeatedly observed high concentrations
($\sim$70 to 100 mg kg^{-1} manure) of ethanethiol (in excess of methanethiol at $\sim$1 to 5 mg kg^{-1}) in pig manure.

There have been a limited number of measurements of amine emissions from animal waste and animal production facilities (Schade and Crutzen 1995 and references therein). Those measurements performed indicate that trimethylamine is the dominant amine emitted with lesser contributions from methylamine, dimethylamine, *iso*-propylamine, ethylamine, *n*-butylamine, amyl-amine and diethylamine. Emissions of methylamine and trimethylamine and lesser emissions of dimethylamine have been observed from manure piles of varying age and wetness. The extent of emissions decreased with age as manure dried. Emissions of trimethylamine were greater than those of methylamine from wet manure and *vice versa* from old dry manure (Schade and Crutzen 1995). Trimethylamine is produced from degradation of chloine and betaine and microorganisms demethylate trimethylamine to form dimethylamine and methylamine. A number of amines may also be produced by decarboxylation of amino acids (Mackie *et al* 1998, Schade and Crutzen 1995, Spoelstra 1980). Amino acid decarboxylases are induced at pH 5 to 6, the pH of 6 to 7 which normally prevails in the gastrointestinal tract favours deamination of amino acids to give the carboxylic acids (Mackie *et al* 1998). The absence of these higher amines in significant concentrations in the few studies to date also indicates that decarboxylation is a minor pathway of amino acid metabolism (Schade and Crutzen 1995). Other factors such as diet, pH and microbial composition may result in differences in the nature (and extent) of amine emissions. Biological amination of aldehydes to give hexylamine, ethylamine and *iso*-butyl amine has also been observed (Spoelstra 1980).

Phenol and 4-methyl-phenol are produced by metabolism of amino acid tyrosine in the intestine and during anaerobic animal waste storage. Phenols produced in the intestine are

partially absorbed by the animal and detoxified by conjunction with glucuronic acid and excreted in urine. Phenols can be released from the glucoronic acids by the enzyme glucuronidase, high activities of the enzyme have been found in pig faeces and waste. (Spoelstra 1977, Spoelstra 1980, Mackie *et al* 1998). 4-methylphenol emissions generally dominate with lesser emissions of phenol and minor emissions of 4-ethyl phenol. Further metabolism of phenol may be significant under anaerobic conditions or in the presence of an inorganic electron acceptor (Spoelstra 1980).

The presence of phosphine in and from livestock manure and slurry (e.g. Glindemann and Bergmann 1995, Glindemann *et al* 1996b, Eismann *et al* 1997b, Roels *et al* 2002), manure treated soils (Eismann *et al* 1997a), the rumen and gut of cattle (Gassmann and Glindemann 1993), guano of penguins, sea lions, skua and gulls (Zhu *et al* 2006a, b), human faeces (Gassmann and Glindemann 1993) and sewage plants and sludge (Dévai *et al* 1988, Rutishauser and Bachofen 1999, Roels *et al* 2002) is well established. The mechanism of phosphine formation is not well understood. Analogy with carbon, sulphur, nitrogen and oxygen cycles might suggest the reduction of phosphorus as part of a respiratory process to release energy in a similar manner to methanogenesis or sulphogenesis. However, the oxidation of phosphates to compounds containing phosphorus in a low oxidation state, such as phosphine, is thermodynamically unfavourable requiring a high energy electron donor (Roels and Verstraete 2001). This does not exclude a biological reduction pathway and various bacteria have been shown to generate phosphine (e.g. Dévai *et al* 1998, Jenkins *et al* 2000). A strong correlation between methane and phosphine release from anaerobic manure has been demonstrated initially suggesting a direct link between phosphine and methanogenesis (Eismann 1997b). However, Rutishauser and Bachofen (1999) found that inhibiting methanogenic bacteria in sewage sludge lead to no reduction in phosphine production despite reduced methane emissions. Jenkins *et al* (2000) observed phosphine emission from sheep manure and amino acid fermentation enriching culture where no methane emission was observed supporting the findings of Rutishauser and Bachofen (1999). A correlation between hydrogen sulphide and phosphine emission from manure, although weaker than with methane, was also observed by Eismann *et al* (1997b). Glindemann and Bergmann (1995) observed a correlation between phosphine and dimethyldisulphide from pig slurry storage tanks. It is possible that the relation between phosphine and methane and sulphides solely indicates that the processes underlying phosphine production are enhanced by similar anaerobic environments rather than that there is a direct link with for example methanogenesis or sulphogenesis.

Abiotic volatilization of matrix-bound phosphine (MBP) is a potential contributing source of free phosphine. The presence of phosphine in animal feed as a result of fumigation may contribute to phosphine in and consequently from slurry. However, Eismann *et al* (1997b) found higher MBP concentrations in manure than the feed given to the cattle which produced the manure indicating the existence of another source of phosphine. Likewise, Gassmann and Glindemann (1993) found that levels of phosphine increased along the course of digestion in cattle from the rumen through the gut to fresh cow pat and cattle manure.

Iron corrosion is another possible source of phosphine from slurry. The high temperature, oxygen deprived conditions and excess of reducing agents such as iron in metallurgic iron melts favour reduction of phosphorus or phosphates to phosphide and technical iron regularly contains iron phosphide (Glindemann *et al* 1998). Glindemann *et al* (1998) have shown that corrosion of iron containing iron phosphides from, for example slurry storage tanks, releases phosphine (free and MBP) and is accelerated by acidic conditions.

Soil may act as a source or sink of phosphine. High phosphine uptake in the presence of Fe (III) has been observed. Other factors such as the level of oxygen depletion, presence of organics, and extent of soil waterlogging affect the extent of phosphine uptake by soils (Eismann *et al* 1997a). Microbial oxidation of phosphine is a possibility; biological oxidation of phosphite (in which *P* also has oxidation state -III) coupled with sulphate reduction has recently been demonstrated as a source of energy for metabolism in *Desulfotignum phosphitoxidans* (Hanrahan *et al* 2005, Schink and Friedrich 2000).

Many of the (O)VOCs released from animal waste are odorous. The identification and quantification of compounds contributing to the odour of animal waste and the investigation of abatement methods has been the subject of a number of previous investigations (e.g. Hobbs *et al* 1995, Misselbrook *et al* 1997, Hobbs *et al* 1999, Schiffman *et al* 2001, Willig *et al* 2004, Le 2006). A small number of recent studies (e.g. Hobbs *et al* 2004, Shaw *et al* 2007, Ngwabie *et al* 2008) have explored the contribution of emissions from animals and their waste to the global budget of (O)VOCs and the resulting impact on the oxidative capacity of the atmosphere, ozone formation and particulate and cloud growth. The scale of (O)VOC emissions from agriculture remain uncertain. Some examples of previous measurements of various (O)VOCs from and in the vicinity of animal wastes are collated in Appendix D.

The production and application of animal wastes is of importance to gaseous links in the carbon, nitrogen, sulphur and potentially phosphorous cycle. The fates of (O)VOCs emitted from animal waste include reaction with OH, NO_3 and O_3 as well as contribution (directly or

indirectly) to particulate and cloud condensation nuclei formation and acid rain. The rates of reaction of some relevant (O)VOCs with OH, NO_3 and O_3, the products of these atmospheric oxidation reactions and potential contributions to particle and cloud condensation nuclei formation and/or growth are given in Table 4.1. The contribution of these (O)VOCs and the products of their oxidation to cloud formation contrasts with the production of greenhouse gas methane generally associated with livestock (Hobbs and Mottram 2000).

Of the compounds considered in Table 4.1, the carboxylic acids are the longest lived with respect to reaction with OH. The fates of carboxylic acids in the troposphere are not well understood (Crunaire et al 2005). However since the acids react relatively slowly with OH , (Table 4.1) deposition plays an important role. The acids are polar and highly soluble and wet deposition is therefore a significant sink and their contribution to acid rain is well established. The residence time of acids in the troposphere is highly dependent on the level of precipitation (Chebbi and Carlier 1996).

Hydrogen sulphide and dimethylsulphide have lifetimes of one to two days with respect to OH/NO_3 oxidation (Table 4.1). Methanethiol and ethanethiol are comparably short lived with lifetimes of ~5 h. The higher oxidation state sulphur compounds, dimethyldisulphide and dimethylsulphoxide, react rapidly with OH with lifetimes of less than one hour at OH concentrations generally found in the troposphere. The predominant products from oxidation of these sulphur containing volatiles include sulphur dioxide (SO_2), sulphuric acid (H_2SO_4), methylsulphonic acid (CH_3SO_3H) and carbonyl sulphide (COS). These compounds are highly polar and soluble with relatively low vapour pressure and adsorb to existing particles. H_2SO_4 also homogenously nucleates forming cloud condensation nuclei and contributes to acid rain.

The residence time of phosphine is 1 - 2 days at average tropospheric OH concentrations (~ 12 to 13 h at 1.5×10^6 molecules cm^{-3} OH). Reaction with OH forms phosphoric acid which also contributes to cloud condensation (e.g. Frank and Rippen 1987, Fritz et al 1982, Glindemann et al 1996a, Glindemann et al 2003).

Table 4.1: The rates of reaction of various volatile trace gases emitted from animal waste with OH, NO_3 and O_3 and resulting lifetimes with respect to reaction with OH. Some of the products from the pre-dominant oxidation reactions and their impact on particulate and cloud condensation nuclei formation are given.

Compound	k_{OH} (x 10^{-11} cm^3 molecule^{-1} s^{-1})	k_{O3} (x 10^{-11} cm^3 molecule^{-1} s^{-1})	k_{NO3} (x 10^{-11} cm^3 molecule^{-1} s^{-1})	τ_{OH} (h)	Products of oxidation	Contribution to aerosol formation
Ethanoic acid (Acetic acid)	0.0700[1]			264.6	CO_2 (+ CH_3) or H_2O (+ CH_2COOH) [3, 4]	Deposition dominates the fate of carboxylic acids since chemical reaction is relatively slow. However atmospheric oxidation is non-negligable and the impact of the acids on the HO_x budget significant [3, 4]. Although mono-carboxylic acids are found mostly in the gas phase their concentration in aerosol particles is sufficient to make them a candidate for cloud condensation nuclei [5].
Propanoic acid (Propionic acid)	0.120[1]			154.3		
Butanoic acid (Butyric acid)	0.179 (298 K)[2]			103.5		
2-methyl-propanoic acid (iso-butyric acid)	0.200[1]			92.6		
Hydrogen sulphide	0.47 (298 K)[6]	0.000039 (298 K)[9]	≤ 0.003 (298±2 K)[11] <0.0001 (298 K)[6]	39.4	SO_2, ($\rightarrow H_2SO_4$)[13, 14]	The products of oxidation of these sulphur containing volatiles contribute to particulate and CCN formation. CH_3SO_3H (MSA), H_2SO_4 and SO_2 all contribute to particulates. MSA and SO_2 adsorp to cloud droplets and can be converted heterogeneously to sulphate. SO_2 also reacts to give H_2SO_4 which either adsorps to droplets (condenses on existing particles) and can be converted to sulphate or homogenously nucleates to form CCN.[e.g. 14, 22, 23]
Dimethylsulphide	0.48 (298 K)[6]	<0.0000001 (298 K)[10]	0.081 (298±2 K)[11] 0.11 (298 K)[6]	37.0 38.6	$(CH_3)_2SO$, $(CH_3)_2SO_2$, CH_3SO_3H, SO_2, H_2SO_4, OCS, HCHO, HCOOH, CH_3OH, CH_3SO_2OH, $CH_3S(O2)OONO_2$ [6, 13, 14, 15, 16, 17]	

Table 4.1 is continued on the following page.

Compound	k_{OH} (x 10^{-11} cm^3 molecule^{-1} s^{-1})	k_{O3} (x 10^{-11} cm^3 molecule^{-1} s^{-1})	k_{NO3} (x 10^{-11} cm^3 molecule^{-1} s^{-1})	τ_{OH} (h)	Products of oxidation	Contribution to aerosol formation
Dimethyldisulphide	23 (298 K)[6]		0.049 (298±2 K)[11] 0.07 (298 K)[6]	0.8	CH_3SH, CH_3SOH[6]	
Dimethylsulphoxide	21.4 (298 K)[7]			0.9	SO_2, $(CH_3)_2SO_2$, CH_3SO_3H, CH_3SO_2OH, H_2SO_4 $CH_3S(O2)OONO_2$[7, 17]	
Methanethiol (methyl mercaptan)	3.3 (298 K)[6]		0.081 (298±2 K)[11] 0.092 (298 K)[6]	5.6	SO_2, HCHO, CH_3SO_3H, $CH_3S(OH)H$, H_2SO_4, $(CH_3)SS(CH_3)$, COS [14, 18, 19, 20]	
Ethanethiol (ethyl mercaptan)	5.19 (275 K)[8]		0.121[12]	3.6	SO_2[21]	
Phosphine	1.40[24] 1.54 (275 K)[25]			13.2 12.0	$H_2O + PH_2$ $\rightarrow\rightarrow H_3PO_3$[24, 25, 26, 27]	Phosphine is less attracted to water droplets or organic aerosol than are the sulphur containing volatiles and their oxidation products. However phosphoric acid production by phosphine oxidation may be important in CCN formation in the high troposphere and stratosphere.[26, 27, 28]

Table 4.1 is continued on the following page.

Compound	k_{OH} (x 10^{-11} cm^3 molecule^{-1} s^{-1})	k_{O3} (x 10^{-11} cm^3 molecule^{-1} s^{-1})	k_{NO3} (x 10^{-11} cm^3 molecule^{-1} s^{-1})	τ_{OH} (h)	Products of oxidation	Contribution to aerosol formation
Methylamine	2.2 (298 K)[29]	0.0000000007 (298 ± 2 K)[30]		8.4	NO$_2$, HCONH$_2$, HCHO, H$_2$O, CH$_2$=NH →→→ N$_2$ / N$_2$O / HCN / NH$_3$ / NO[31]	Amines form aminium nitrate salts and aminium sulphate salts by reaction with nitric acid and sulphuric acid respectively. These reactions may not occur under atmospheric conditions since the analogous reactions of ammonia with nitric and sulphuric acid
Ethylamine	2.77 (298 K)[29]			6.7		forming ammonium nitrate and
Dimethylamine	6.62 (298 K)[29]	0.000000167 (298 ± 2 K)[30]		2.8	(CH3)2NCHO or HCHO + (CH3)2N radical →(+O$_2$)→ CH3N=CH2 →→→ N$_2$ / N$_2$O / HCN / NH$_3$ / NO[31]	ammonium sulphate compete with those of the amines. At typical ammonia and amine concentrations theory suggests trimethylamine and ethylamine would not form nitrate salts. It has been shown experimentally that
Trimethylamine	6.1 (298 K)[29]	0.000000784 (298 ± 2 K)[30]		3.0		triethylamine does not form nitrate salts unless the triethylamine concentration is equivilant to the ammonia concentration or there is a large excess of nitric acid. It is uncertain if methylamine or dimethylamine will form aminium nitrate salts.
(Amines continued)						Methylamine displaces ammonia from ammonium sulphate to form methylaminium sulphate when methylamine is at high VMRs. Aerosols formation as a result of photooxidization of several amines in the presence of NOx has been demonstrated. Aerosols were mainly as amminium salts with repartation back into the gas phase as the amine was depleted. SOA (non-salt) was not observed when primary and secondary amines such as methylamine or diethylamine were oxidized by OH or ozone. SOA (non-salt) was observed when tertiary trimethylamine

Table 4.1 is continued on the following page.

Compound	k_{OH} (x 10^{-11} cm^3 molecule^{-1} s^{-1})	k_{O3} (x 10^{-11} cm^3 molecule^{-1} s^{-1})	k_{NO3} (x 10^{-11} cm^3 molecule^{-1} s^{-1})	τ_{OH} (h)	Products of oxidation	Contribution to aerosol formation
						and triethylamine were oxidized by OH and ozone. SOA (non-salt) was more stable than the nitrate salts.[32, 14]
Phenol	2.81 (298 K)[33]		0.364 (298 K)	6.6	Catechol[36]	Forms SOA - nirtophenols and catechol formed from oxidation are aerosol precursors.[14,36, 37, 38]
2-methylphenol (o-cresol)	4.32 (294 ± 2 K)[34] 4.32 (300 ± 1 K)[35]	0.00000006 (300 ± 1 K)[35]		4.3	methyl-1,4-benzoquinone, 6-methyl-2-nitrophenol[34]	
3-methylphenol (m-cresol)	5.88 (294 ± 2 K)[34] 6.7 (300 ± 1 K)[35]	0.00000006 (300 ± 1 K)[35]	1.2 (298 K)[13]	3.2 2.8	methyl-1,4-benzoquinone, 5-methyl-2-nitrophenol, 3-methyl-2-nitrophenol[34]	
4-methylphenol (p-cresol)	4.96 (294 ± 2 K)[34] 5.2 (300 ± 1 K)[35]	0.00000006 (300 ± 1 K)[35]	1.66 (298 K)[13]	3.7 3.6	4-methyl-2-nitrophenol[34]	

Note: τ_{OH} denotes lifetime with respect to OH given the specified rate constant and an OH concentration of 1.5 x 10^6 molecules cm^{-3}. SOA denotes secondary organic aerosol. CCN denotes cloud condensation nuclei. Data are taken from [1]Dagaut et al (1988) in Chebbi and Carlier (1996), [2]Zetzsch and Stuhl (1982)*, [3]Seinfeld (1999), [4]Crunaire et al (2005), [5]Yu (2000), [6]Atkinson et al (2004), [7]Resende et al (2005)*, [8]Atkinson (1986)*, [9]Glavas and Toby (1975)*, [10]Du et al (2007), [11]Wallington et al (1986), [12]Atkinson (1991)*, [13]Ravishankara et al (1997), [14]Seinfeld and Pandis (1998), [15]Barnes et al (1994), [16]Urbanski et al (1997), [17]Librano et al (2004), [18]Hatakeyama and Aklmoto (1983), [19]Uchimaru et al (2007), [20]Bentley and Chasteen (2004), [21]Barnes et al (1986), [22]Cox (1997), [23]Charlson et al (1987), [24]Frank and Rippen (1987) in Glindemann et al (2003), [25]Fritz et al (1982) in Eismann et al (1997a) and*, [26]Glindemann et al (1996a), [27]Glindemann et al (2003), [28]Glindemann et al (2004), [29]Atkinson et al (1978a), [30]Tuazon et al (1994), [31]Schade and Crutzen (1995), [32]Murphy et al (2007), [33]Rinke and Zetzsch (1984)*, [34]Coeur-Tourneur et al (2006), [35]Atkinson et al (1978b), [36]Martín-Reviejo and Wirtz (2005), [37]Forstner et al (1997), [38]Blando and Turpin (2000). *in http://www.kinetics.nist.gov/kinetics/search.jsp (2000)

The amines react relatively rapidly with lifetimes of < 1 day (~2 to 9 h) at an *OH* concentration of 1.5×10^6 molecules cm^{-3} (Table 4.1). Oxidation may result in minor additions to the N_2O and *HCN* budgets (Schade and Crutzen 1995). The oxidation of some amines contributes to secondary organic aerosol (Murphy *et al* 2007). Amines may also react with nitric acid and/or sulphuric acid to form aminium nitrate and/or aminium sulphate salts (Murphy *et al* 2007).

Phenol and the methyl-phenols form nitrophenols and catechol on reaction with *OH* contributing to secondary organic aerosol, lifetimes with respect to *OH* are ~ 3 to 7 hours (Table 4.1).

Many of the (O)VO(S)Cs are also a health concern, for example hydrogen sulphide is an irritant and an asphyxiant. Exposure to hydrogen sulphide concentrations of 900 ppm (1350 mg m^{-3}) for less than 30 min can result in death in less than one hour (WHO 1981). In the UK the long term exposure limit (8-hour time weighted average reference period) of hydrogen sulphide is 5 ppm (7 mg m^{-3}) and the short term exposure limit (15 minute reference period) 10 ppm (14 mg m^{-3}) (HSE 2007). Phosphine causes asphyxia and death after half to one hour at 400 – 600 ppm (560 – 840 mg m^{-3}) and subtoxic doses have a cumulative effect (WHO 1988, Glindemann and Bergmann 1995). In the UK the long term exposure limit (8-hour time weighted average reference period) of phosphine is 0.1 ppm (0.14 mg m^{-3}) and the short term exposure limit (15 minute reference period) 0.2 ppm (0.28 mg m^{-3}) (HSE 2007). Phenol is a carcinogen with a long term exposure limit (8-hour time weighted average reference period) of 2 ppm (7.8 mg m^{-3}) (HSE 2007).

The majority of previous measurements of animal waste emissions (Appendix D) have utilized GC with sample pre-concentration to quantify (O)VOCs. A limited number of SIFT (Smith *et al* 2000, Dewhurst *et al* 2001) and PTR-MS (Shaw *et al* 2007, Ngwabie *et al* 2008) measurements of emissions from animals, animal housing and their waste have been performed. In this work PTR-MS was deployed for the measurement of emissions from cattle slurry. The use of PTR-MS allowed a large range of compounds to be tentatively identified with increased temporal resolution and without sample pre-treatment. The evolution of (O)VOCs during two fertilisations at a grassland site in 2004 and 2005 and in subsequent laboratory based measurements are reported.

4.2 Methodology

4.2.1 Field Measurements

4.2.1.1 Site Description and Land Management

The measurements were performed at Easter Bush, a field site in the South-East of Scotland ($3^o12'22''$ W, $55^o51'57''$ N) approximately 9 miles south of Edinburgh at an altitude of approximately 190 m above sea level. The measurement location and instrument configuration are shown in Figure 4.1.
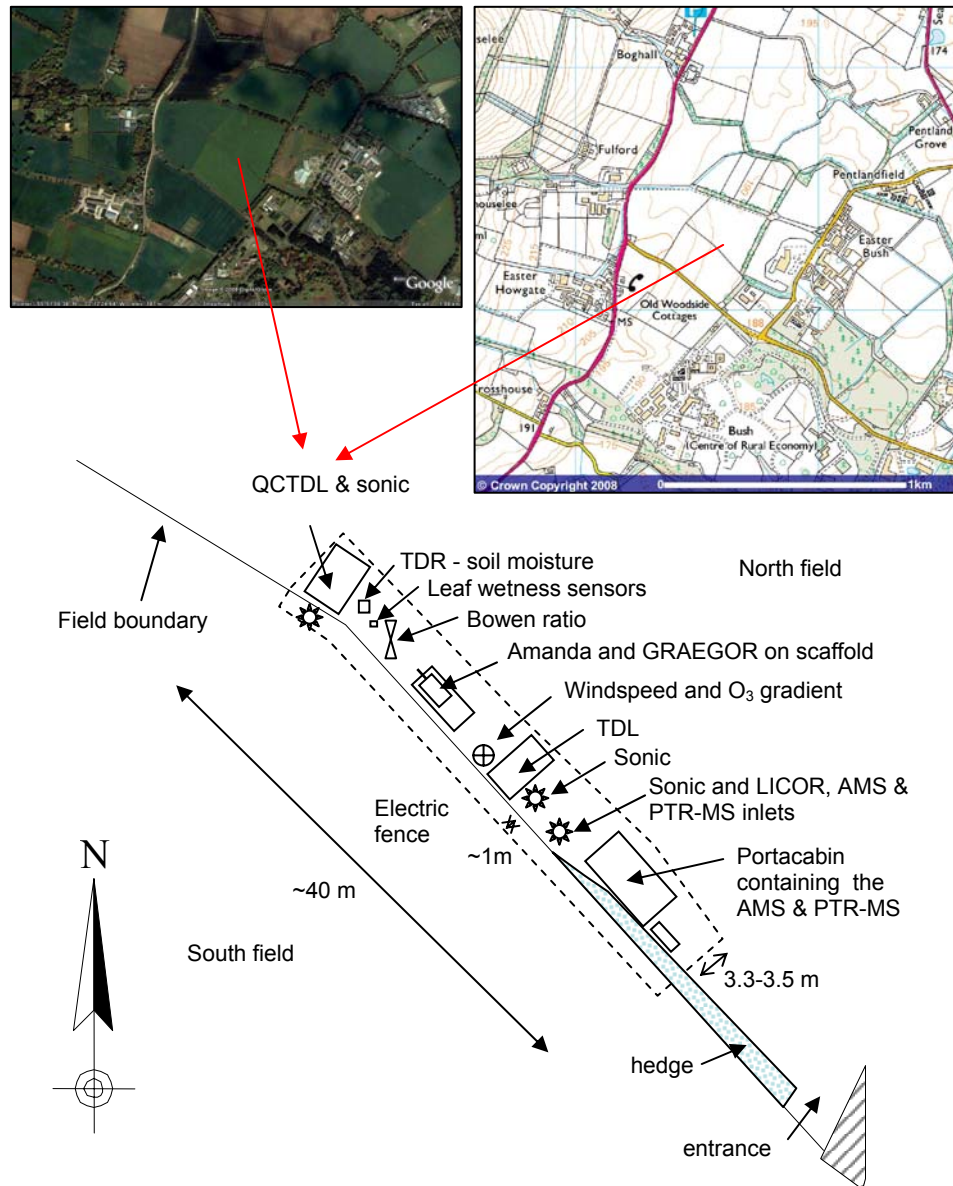
Figure 4.1: A satellite image (google_earth) and ordenance survey map of Easter Bush (http://getamap.ordnancesurvey.co.uk). The instrumental configuration at the site is shown (adapted from Twigg 2006 and Coyle 2005).

The site consists of two intensively managed grassland fields approximately 5.4 ha each which have existed as grassland for over 20 years. The fields are covered by *Lolium perenne*

(Perennial rye grass) (>90 %) interspersed with *Phleum pratense* (Timothy), *Poa annu* (Annual meadow grass), *Ranunculus repens* (Buttercup), *Trifolium repens* (White clover), *Rumenx obtusifolia* (Broad leaved dock), *Taraxacum officinale* (Dandelion), *Veronica pratense* (Field speedwell), *Chaerophyllum temulentum* (Chevril), *Dactylis glomerata* (Cocksfoot), *Holcus lanatus* (Yorkshire Fog) and *Bellis perennis* (Daisy) (Milford 2004). The instrumentation (§ 4.2.1.3 and 4.2.1.4) lies on boundary between the fields which runs northwest to southeast. During these measurements slurry was spread in the south field in which the prevailing wind is from the south west.

In previous years the fields were used for grazing and silage. In 2002 and 2003 the north field was used for grazing and cut once in 2002 and not cut in 2003. In 2002 and 2003 the south field was used for grazing and silage with two cuts in 2002 and one in 2003. The fields were similarly managed in preceding years. Both fields were regularly fertilised with mineral fertiliser (~200 – 300 kg N ha^{-1} yr^{-1}).

Long term measurements of trace gas species such as ammonia and ozone are made at Easter Bush. The results of previous measurements can be found in the literature (e.g. Coyle 2005, Milford 2004).

During 2004 neither field was cut for silage. The stocking intensities in both fields in 2004 are shown in Figure 4.2. Livestock units (LSU) per hectare are given as a measure of the stocking intensity. LSU are a measure of the feed requirements or grazing effect of animals; a value of 0.08 LSU is assigned to sheep and lambs, 1.0 LSU to dairy cows and 0.65 LSU to beef bulls (e.g. Chadwick 1995, Chesterton *et al* 2006). The fields were grazed mainly by sheep and lambs, heifers and calves were only present in the north field for a fourteen day period from the 13th of August and in the south field for a four day period from the fourth of December. The fields were both minerally fertilised; 51.75 kg N ha^{-1} was applied to the north field on the 9th of May in the form of NH_4NO_3 fertiliser (Nitram), 69 kg N ha^{-1} (Nitram) was applied to the south field on the 21st of May and 50 kg N ha^{-1} (Keimira) on the 30th of May. No organic fertiliser was applied to the north field. Cattle slurry was applied to the south field on the 28th and 29th of September only.

On the 10th of October 2005, the grass in the south field was topped and left on the field , the grass in the north field was not cut. The stocking intensities in both fields in 2005 are shown in Figure 4.3. Again both fields were grazed primarily by sheep and lambs. Heifers and calves only grazed in the north field for four days from the 3rd of June and for twenty eight days between the 30th of August and 10th of October.
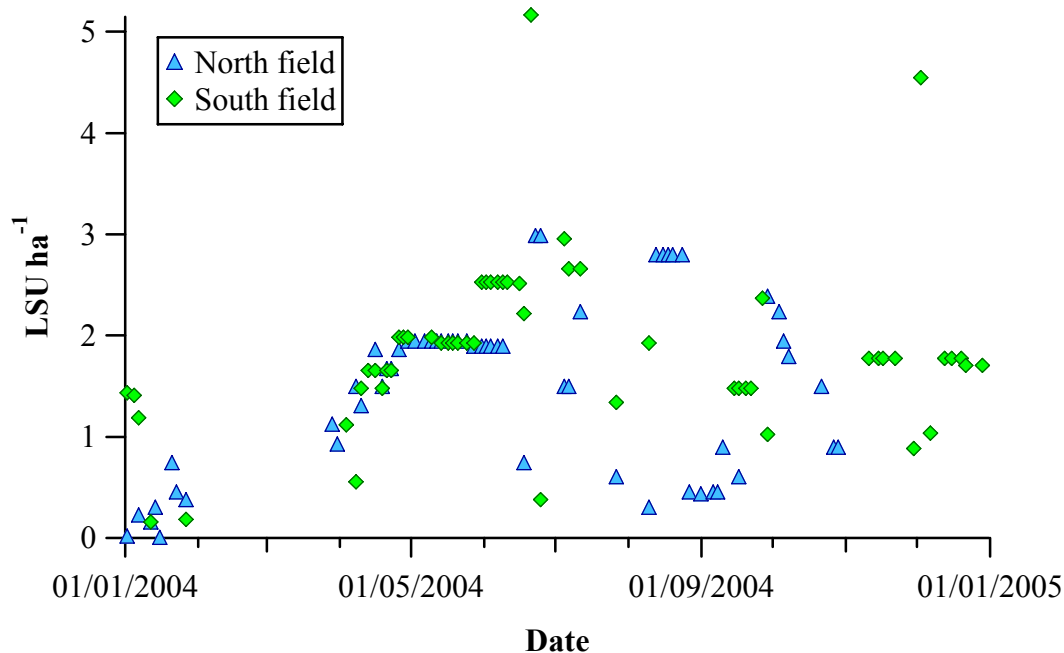
Figure 4.2: Livestock units (LSUs) per hectare in the North and South Fields at Easter Bush during 2004.

Heifers and calves grazed in the south field for nine days from the 25th of May and seven days from the 27th of October. Quantities of 69, 51.75 and 51.75 kg N ha^{-1} in the form of NH_4NO_3 fertiliser (Nitram) were applied to the north field and the same amounts to the south field on the 21st of March, 18th of April and 1st of August respectively. No organic fertiliser was applied to the north field. Cattle slurry was applied to the south field on the 27th to the 29th of April only.

4.2.1.2 Slurry

The slurry spread on the 28th and 29th of September 2004 was accumulated from Holstein-Friesian cattle between March 2004 and September 2004. The cattle were housed between March 2004 and May 2004. The housed cattle were fed full winter rations including grass silage, wholecrop wheat, draff (malt distillers grains), molasses and blended concentrate. The ratio of ingredients was varied depending on milk yield, stage of lactation and quality of the silage. The cattle were at grass with access to a buffer feed of silage and draff after milkings between May 2004 and the end of September 2004. The slurry spread on the 27th to 29th of April 2005 was obtained from housed Holstein-Fresians fed on the winter rations described above. No additives were given to the cattle or added to the slurry. The slurry was stored in above ground, glass-lined steel stores. (Private communication with Hodgson-Jones). Slurry was sprayed from a tanker in strips parallel to the field boundary and instrument inlets (Figure 4.4).
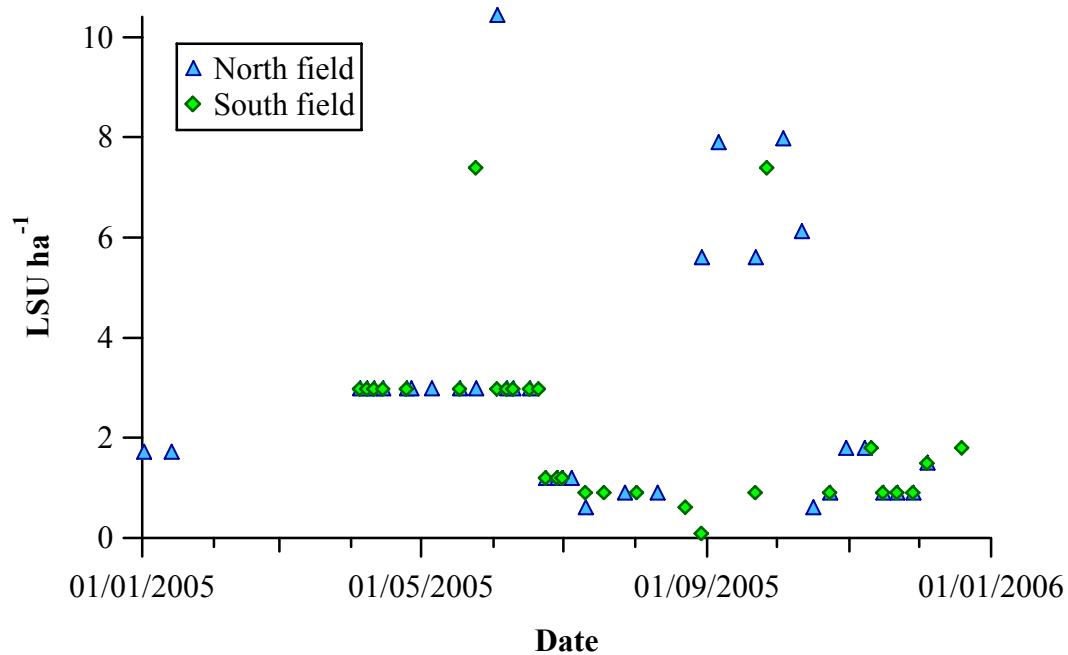
Figure 4.3: Livestock units (LSUs) per hectare in the North and South Fields at Easter Bush during 2005.
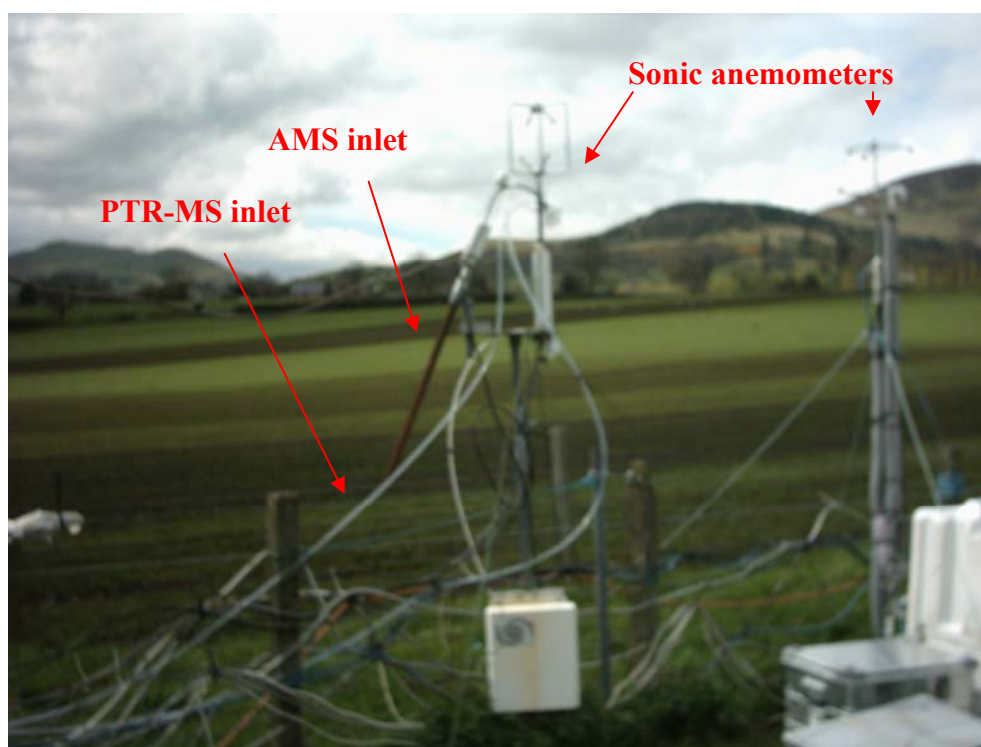
Figure 4.4: Slurry application in the South field at Easter Bush in front of the Gill sonic anemometer (left) and AMS (copper) and PTR-MS (Teflon™) inlets in April 2005.

During the 2004 and 2005 field experiments three samples of slurry were taken from the holding tank at the beginning, middle and end of slurry spreading by Dr Marsailidh Twigg (Univeristy of Ulster/CEH). The pH, dry matter content, total nitrogen, total ammoniacal nitrogen and total carbon of the slurry samples was determined by the Analytical laboratory of the Scottish Agriculture College (SAC), Bush Estate, Penicuik, Scotland. An extraction of the nitrate was carried out by Dr Marsailidh Twigg at CEH. The analysis of the slurry extract for nitrate was carried out by SAC using continuous flow colorimetery (Twigg 2006).

4.2.1.3 Instrumental Configuration During October 2004.

Meaurements were made from 24 the 24th of September 2004 to the 10th of October 2004. A V_{drift} of 600 V cm^{-1} resulting in an E of ~63.2 V cm^{-1} (l_{dt} 9.5 cm) and a P_{dt} of ~ 2.15 mbar was employed with a consequent E/N of ~129 Td. The pressure in the detection chamber was ~ 2.4 to 2.5x 10^{-9} mbar. A water flow of 8 STP cm^3 min^{-1}, V_2 150 V and V_3 75 V was applied until 27/09/04 after which a water flow of 6 STP cm^3 min^{-1}, V_2 180 V and V_3 80 V was applied. The ion source current was 8 mA throughout. The SEM was optimised at instrument start-up on 21/09/04 and 3.3 kV applied thereafter. Count rates at m/z 30 (NO^+) and m/z 32 (O_2^+) were an average of ~2.7 % and 0.49 % of count rates at m/z 19 (H_3O^+) respectively. $H_3O^+(H_2O)$ (m/z 37) count rates were ~ 1.5 % of the sum of H_3O^+ (m/z 21 x 500) and $H_3O^+(H_2O)$ count rates. $H_3^{16}O^+(H_2^{17}O)$ (m/z 39) count rates were ~ 0.43 of $H_3^{16}O^+(H_2^{16}O)$ (m/z 37) count rates as expected from isotopic abundancies (§ 2.3.3). Count rates at m/z 19 increased from ~3 x 10^6 to 4 x 10^6 cps from 24/09/04 to 27/09/04 after re-optimisation of the ion source count rates increased from 5 x 10^6 cps on 28/09/04 to ~7.5 x 10^6 cps on 10/10/04.

The PTR-MS was operated in two measurement modes. The SB (§ 2.3.3) mode was employed for two 4 minute periods at 0 and 30 minutes past the hour. The MID mode (§ 2.3.3) was employed for the remaining 26 minutes of each half hour. In the SB mode m/z 20 to m/z 500 were measured at 50 ms per m/z resulting in ~24.5 s per scan (switching time ~ 1 ms per m/z). The m/z measured and dwell times employed during MID measurements are shown in Table 4.2. Throughout the majority of measurements during and post-fertilisation (28/09/04 15:00 onward, Table 4.2) the resultant time response was ~ 6.4 s per cycle (~0.16 Hz) indicating a switching time of ~ 0.08 s per m/z. The temporal resolution of SB data was decreased compared to MID data and although a larger number of m/z were measured a reduced dwell time was employed reducing the signal to noise ratio. The instrument background was not quantified during measurements at Easter Bush in 2004. VMRs are therefore overestimates and measurements should be considered qualtitatively.

The solenoid valve of the PTR-MS inlet (§ 2.3, Figure 2.1) was attached to a ~ 14 m long Teflon™ tube (Cole-Palmer , Bishop's Stratford, Herts, UK) inlet (O.D. ¼") *via* a T-Piece. The other side of the T-Piece was connected to a pump drawing air through the inlet (~25 L min^{-1}). The 14 m inlet was taken outside of the instrument cabin and attached to a sonic anemometer ~ 2 m in height (Figure 4.4).

Table 4.2: The masses measured and corresponding dwell times in the MID mode of the PTR-MS at Easter Bush (September/October 2004).

Start date and time (GMT)	End date and time (GMT)	Monitored m/z	Dwell (ms per m/z)
28/09/04 08:00	28/09/04 09:00	21, 30, 32, 37, 55, 59, 60, 61, 73, 75, 81, 89, 91, 103, 106, 107	20
28/09/04 10:00	28/09/04 12:00	21, 30, 32, 33, 37, 55, 59, 60, 61, 73, 75, 81, 89, 91, 103, 106, 107	20
28/09/04 15:00	10/10/04 09:00	21, 30, 32, 33, 37, 39, 43, 45, 47, 55, 59, 60, 61, 73, 75, 81, 89, 91, 103, 106, 107, 109	200

4.2.1.4 Instrumental Configuration During March 2005.

Measurements were performed from the 21st of March 2005 to the 28th of April 2005. Measurements ceased on the 28th of April due to overheating of the PTR-MS pumps. Restarting and subsequent replacement of the SEM prevented measurements during slurry application on the 29th of April. The period from the 23rd of April to the 28th of April immediately prior to and during slurry application is discussed here. On the 23rd of April the inlet and drift tube temperature were increased from the normal operating temperature of 318 K to 343 K in order to minimise sticking of the relatively low voltalility compounds such as carboxylic acids expected from the slurry. A V_{drift} of 550 V cm^{-1} resulting in an E of ~57.9 V cm^{-1} (l_{dt} 9.5 cm) and a P_{dt} of ~ 2.15 mbar was employed giving an E/N of ~127 Td. The pressure in the detection chamber was ~ 2.3 to 2.4 x 10^{-9} mbar. The ion source was operated with a water flow of 8 STP cm^3 min^{-1}, V$_2$ 150 V and V$_3$ 75 V and count rates at m/z 30 (NO^+) and m/z 32 (O_2^+) were an average of 0.22 % and ~2.3 % of count rates at m/z 19 (H_3O^+) respectively. The count rates at m/z 19 were ~1 x 10^7 cps. The SEM was operated at 3.3 kV throughout and the optimum voltage monitored daily.

The PTR-MS was operated in two measurement modes: the SB (§ 2.3.3) mode was employed for two 4 minute periods at 0 and 30 minutes past the hour. The MID mode (§ 2.3.3) was employed for the remaining 26 minutes of each half hour. In the SB mode m/z 20 to m/z 140 were measured at 0.5 s per m/z resulting in ~ 61 s per scan. In the MID mode seven masses were monitored including m/z 21 (H_3O^{18+}) and m/z 37 ($H_3O^+(H_2O)$) (Table

4.3). A dwell of 5 ms per m/z was employed for m/z 21 and 37 and 10 ms per m/z on the remaining five masses of interest. This resulted in 0.6 s per cycle (1.6 Hz) and switching time was therefore ~0.08 s per m/z). In this case a larger number of m/z were measured in the SB mode and the signal to noise ratio was improved compared to MID due to the longer dwell times. However the temporal resolution in the SB mode was reduced as a result.
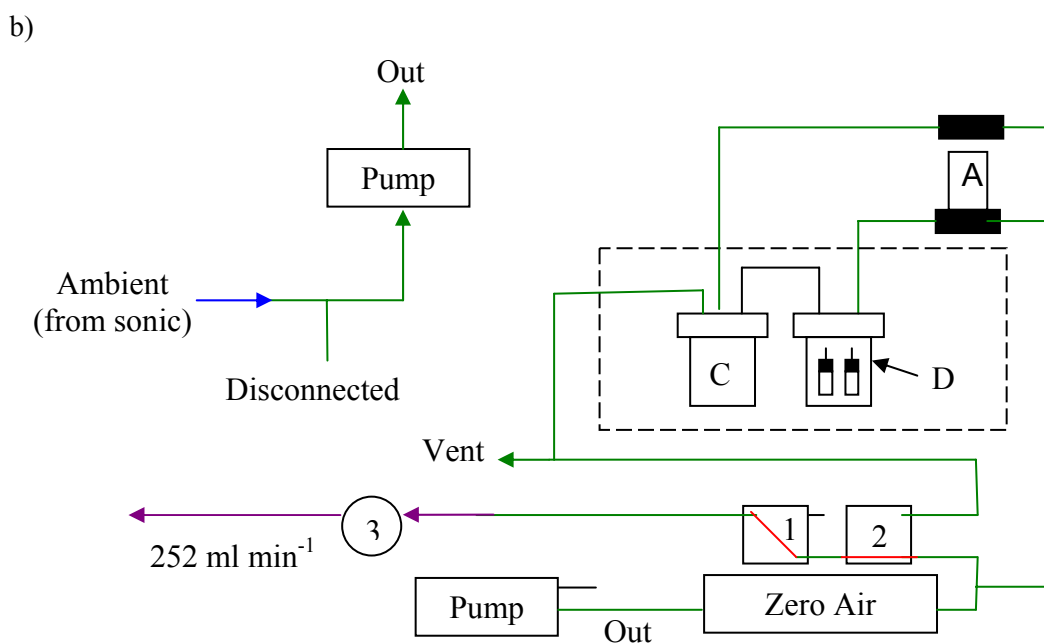
Table 4.3: Masses measured in the MID mode of the PTR-MS at Easter Bush (April 2005)

Start date and time (GMT)	End date and time (GMT)	Masses monitored
23/04/05 11:16	26/04/05 16:30	21, 37, 33, 59, 61, 69, 83
26/04/05 18:01	27/04/05 10:01	21, 37, 47, 61, 75, 89, 103
27/04/05 10:04	27/04/05 16:07	21, 37, 47, 61, 75, 109, 103
27/04/05 16:11	27/04/05 16:34	21, 37, 47, 61, 75, 109, 95
27/04/05 17:34	28/04/05 16:00	21, 37, 47, 61, 75, 109, 89

The small number of masses and diminutive dwell times were employed in order to measure fluxes *via* virtual disjunct eddy covariance (Karl *et al* 2002, Ammann *et al* 2006). However flux measurements were hampered by the relatively low measurement height and the sticky nature of the compounds corresponding to the chosen masses. The discussion here is therefore limited to identifying potential (O)VOCs emitted from the slurry.

The instrument background was measured daily between 23/04/05 and 28/04/05 using a custom built zero air generator. Cabin air was passed through Pt/Al_2O_3 powder (~0.8 g) held in a glass reactor and heated to 200°C; exhaust air was then passed through an air cooled peltier before entering the PTR-MS. The catalyst was reduced, dry 5 % Pt on Al_2O_3 (Ingenta ID: E11Pt, from Engelhard). Two measurements of the instrument background were performed: An SB of m/z 20 to m/z 140 at 0.5 s per mass and an MID measurement of the seven masses monitored during ambient measurements (Table 4.3) at 5 ms per m/z at m/z 21 and m/z 37 and 10 ms per mass at the remaining masses. Five SB scans (~5 minutes) and 500 MID cycles (~4 min 20 s) were averaged. The mean of these values was used.

The initial inlet configuration is displayed in Figure 4.5a. The diffusion system illustrated in Figure 4.5a was not sampled during these measurements and after 24/04/05 10:00 GMT the PTR-MS was connected directly to ambient (Figure 4.5c) and attached to solenoid one for zero air measurements only (Figure 4.5b). The Teflon™ (Cole-Palmer , Bishop's Stratford, Herts, UK) inlet (O.D. 3/8") running from the sonic to the PTR-MS was 13.5 m long. The flow into the PTR-MS was ~252 ml min^{-1}.

a)

Out

Pump

Ambient
(from sonic)

PTR-MS

252 ml min^{-1}

Vent

Pump

Out

Zero Air

B

A

C

D

1

2

3

b)

Out

Pump

Ambient
(from sonic)

Disconnected

Vent

252 ml min^{-1}

Pump

Out

Zero Air

A

C

D

1

2

3
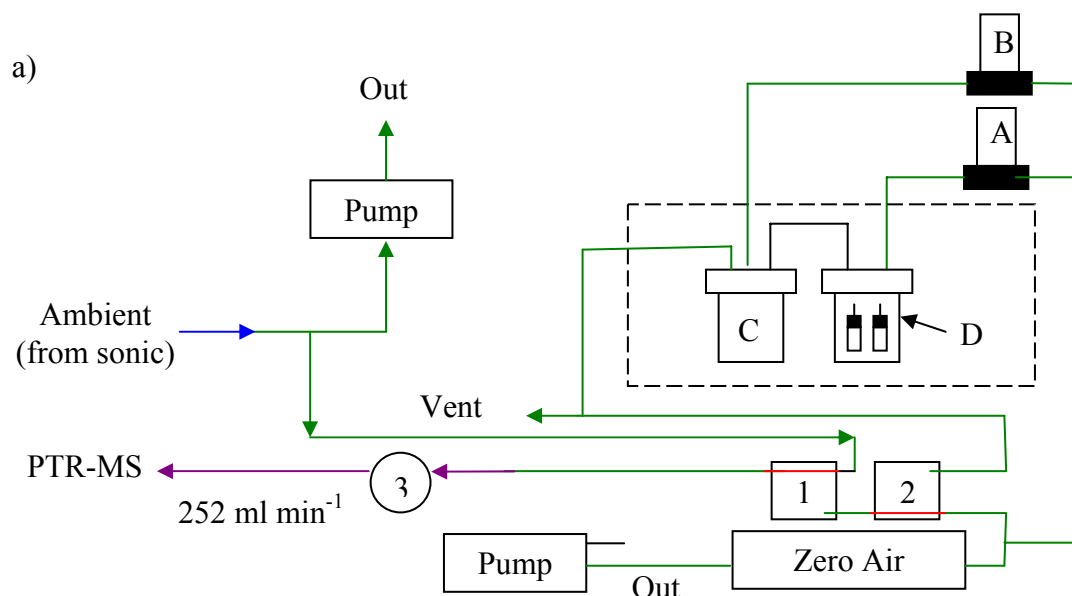
Temperature controlled oven

—— 3/8" O.D. Teflon™ tubing

—— 1/4" O.D. Teflon™ tubing

—— 1/8" O.D. Teflon™ tubing

A and B – Mass flow controllers
C – Dilution chamber
D – Diffusion chamber containing glass vials of (O)VOCs
1 and 2 – Three way solenoid valves
3 – Two way solenoid valve of PTR-MS
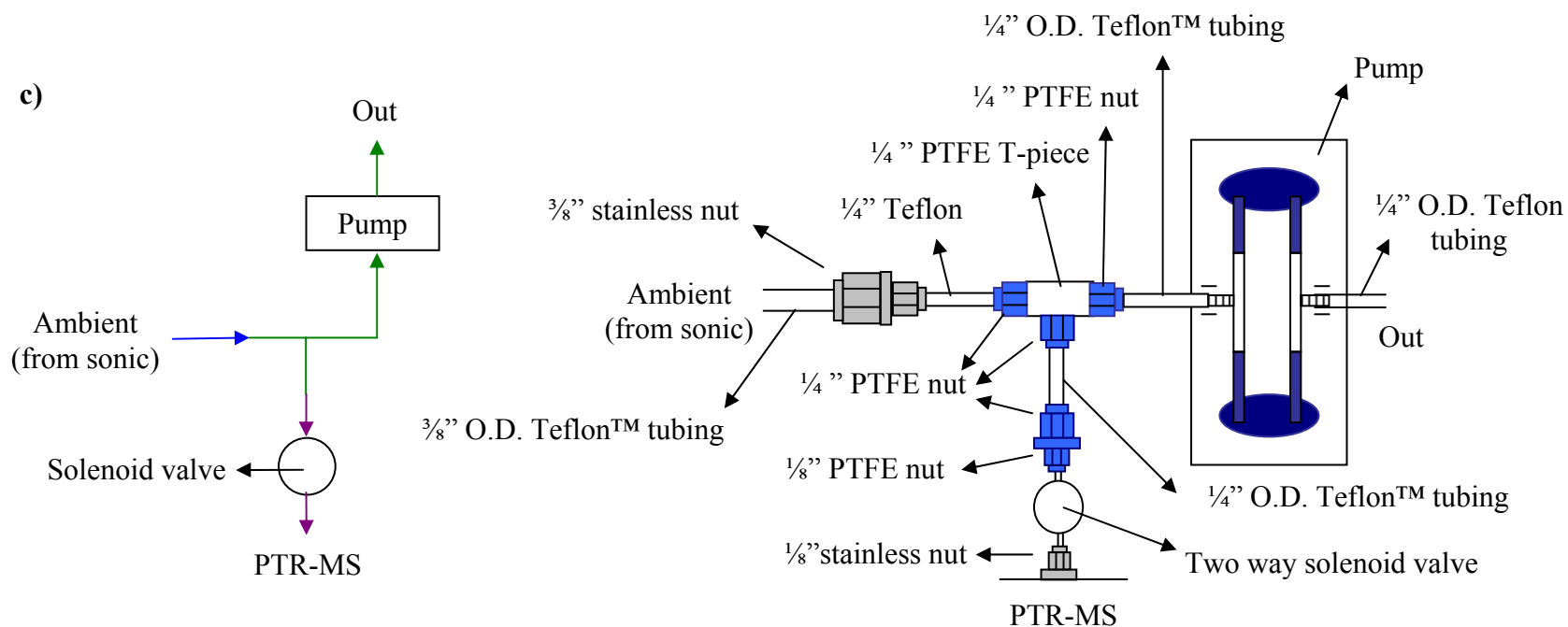
Figure 4.5: The PTR-MS inlet configuration during ambient and zero air measurements at Easter Bush: a) The configuration of the inlet until 24/04/05 10:00 GMT the inlet formation during ambient measurements is shown (solenoid one clear) during zero air measurement solenoid one was set. b) The PTR-MS inlet configuration during zero air measurements from 24/04/05 onwards. c) The inlet configuration during ambient measurements from 24/04/05 onwards.

4.2.1.5 Additional measurements during the Field Campaigns.

The field measurements were a collaboration between the Centre for Ecology and Hydrology, the University of Ulster, the University of Edinburgh and the University of Manchester. In addition to those species identified using PTR-MS a number of trace gas species, e.g. NH_3, CO_2, particulates and micrometeorological parameters, e.g. wind speed, direction, precipitation, were monitored before, during and post fertilization. A list of instrumentation used during the slurry campaigns is given in Table 4.4. A channel TDLAS and an AMANDA system were operated by Dr Marsailidh Twigg (UoU/CEH) who also analysed the resulting data. A QC-TDLAS was provided by the University of Manchester and run by Dr James Whitehead (UM/CEH) who was also responsible for subsequent data analysis (Whitehead 2006). An AMS and GREGOR were operated by Dr Richard Thomas (CEH/UM) and Dr Gavin Philips (CEH) who also performed the analysis of data from these instruments (Thomas 2007). The measurement and analysis of this micrometeorological data, trace gas species, particularly ammonia, and particulate measurements have been addressed in detail elsewhere (Twigg 2006, Whitehead 2006, Thomas 2007)

Table 4.4: Parameters measured at Easter Bush during the slurry campaigns 2004 and 2005. EC denotes Eddy Covariance, AGM - Aerodynamic Gradient Method, 04 - measured 2004 only, 05 - measured 2005 only (Twigg 2006).

Method applied	Parameter	Instrumentation	Model and Supplier
Gases:			
EC	NH_3	QC-TDLAS	Aerodyne, Inc.
AGM	NH_3 (3)	AMANDA	ECN, Petten, Netherlands
EC	NH_3 and HNO_3	Dual-TDLAS	Model TDL-D-200, Aerodyne, Inc.
AGM	NH_3, HNO_3, SO_2 (2)[05]	GRAEGOR	ECN, Petten, Netherlands
EC	VOCs	PTRMS	Ionicon Analytik, Ges.m.b.H. Innsbruck, Austria
EC	CO_2 and H_2O	Infrared Gas Analyser (IRGA)	Li7000, Li-COR, Lincoln, USA.
Aerosols:			
EC	NO_3^-, NH_4^+ [05]	AMS	Aerodyne, Inc.
AGM	NH_4^+, NO_3^- SO_3^{-05}	GRAEGOR	ECN, Netherlands

Table 4.4 is continued on the following page

Method applied	Parameter	Instrumentation	Model and Supplier
Micrometeorological			
EC	Turbulent wind components (u, v, w)and Sensible Heat Flux	Sonic Anemometer	Gill Anemometer, R010 12, Lymington, UK Metek USA-1, Elmshorn, Germany
	Net radiation	Net radiometer	NrLIte, Kipp and Zonen.
	Global radiation	Pyranometer	SKS110, Skye,
	PAR	Photosynthetically Active Radiation Sensor	SKP215
	Precipitation	Tipping bucket rain gauge	ARG100
	Temperature and Relative Humidity	Humitter	50Y,Vailsala
	Air Temperature	Thermocouples	Type-E Thermocouples,
Plant measurements:	Surface Wetness	Wetness Sensing Grid	Campbell Scientific 237 Wetness Sensing Grid, Loughbourgh, UK
	Leaf Wetness and Temperature[04]	Clip Sensors	(Burkhardt and Eiden, 1994)
Soil Measurements:	Soil Temperature	Thermocouple Probes (4)	Campbell Scientific, Loughbourgh, UK.
	Soil Flux	Soil Heat Flux Plates (2)	HPP01 Soil Heat Flux Plates, Campbell Scientific, Loughbourgh, UK>
	Soil Water Content	Time Domain Reflectometery	TDR100, Campbell Scientific, Loughbourgh, UK.

4.2.2 Cuvette Measurements

Two cuvette experiments were performed, the first from the 11th to the 14th of April 2006 the second from the 14th to the 18th of April 2006. These experiments are hereafter referred to as laboratory experiment 1 and 2 respectively. The slurry used in laboratory experiment 1 was fresh and used on the day of collection. The same batch of slurry was used in laboratory experiment 2. In the intervening period the slurry was stored in a sealed container in cool dark conditions.

A layer of slurry ~ 5 mm in depth was applied to a plastic tray with an area of 0.045 m^2 and placed on a Ohaus Ranger scale balance (Ohaus Coporation, Pine Brook US) in a Perspex^{TM} (polymethylmethacryllate) (ICI, UK) cuvette. The instrumental set-up during the cuvette experiments is shown in Figure 4.6. The cuvette contained an inlet and outlet. The outlet (20 cm of O.D. 12.5 mm polyethylene) was split by three polypropylene T-junction

compression fittings (Cole-Palmer, Bishop's Stratford, Herts, UK.) to attach inlets to the PTR-MS, an infrared gas analyser (IGRA) for CO_2 and H_2O (LiCOR 7000, Li-COR, Inc. Lincoln, US) and a Dual TDLAS. Measurements of temperature and relative humidity inside the cuvette were made using a temperature and relative humidity sensor (HMP50, Vaisala, Campbell Scientific Ltc, Loughborough, UK). The temperature, humidity, IRGA (analogue outputs) and change in weight of the slurry were logged using a program written by Dr Marsailidh Twigg in LabView© (National Instruments, US). One minute averages of weight, temperature, relative humidity, CO_2 and H_2O mixing ratios were recorded to an ASCII file in the LabView© logging program. The LabView© logging program also controlled a continuously operated fan inside the cuvette. The IRGA was operated in differential mode with the difference in concentrations in the air entering and leaving the cuvette measured, that is the air entering the cuvette was passed through the reference cell and that leaving through the measurement cell. Dr Marsailidh Twigg configured the instrument (excluding the PTR-MS inlet and instrumentation) and was responsible for the operation and logging and analysis of data from the Dual TDLAS, IGRA, balance and temperature and relative humdity sensor, details of these measurements have been described elsewhere (Twigg 2006).

The measured flow rate through the cuvette was ~12.4 l min^{-1}. The Dual TDLAS sampled air at a rate of 10 l min^{-1}. The PTR-MS drew 0.357 l min^{-1} and 0.338 l min^{-1} during laboratory experiment 1 and 2 respectively. The inlet to the PTR-MS consisted of ¼" O.D. Teflon™ tubing (Cole-Palmer, Bishop's Stratford, Herts, UK) and all fittings were PTFE.

During laboratory experiment 1, a V_{drift} of 500 V cm^{-1} resulting in an E of ~57.9 V cm^{-1} (l_{dt} 9.5 cm) and a P_{dt} of ~ 2.01 mbar was employed with a consequent E/N of ~126.5 Td (N = 4.58 x 10^{16} molecules cm^{-3}). In laboratory experiment 2, the drift tube pressure was ~2.00 mbar other parameters were unchanged resulting in an E/N of ~127.1 Td (N = 4.55 X 10^{16} molecules cm^{-3}).

During the laboratory experiments, the pressure in the detection chamber was ~ 2.17 x 10^{-9} mbar. A water flow of 7 STP cm^3 min^{-1}, V_2 50 V and V_3 50 V was applied. The ion source current was 8 mA throughout. The SEM voltage was 3.0 kV from the 11th of April until the 12th of April at 08:35 GMT when the SEM was re-optimised, a voltage of 3.1 kV was applied for the remainder of the measurements.
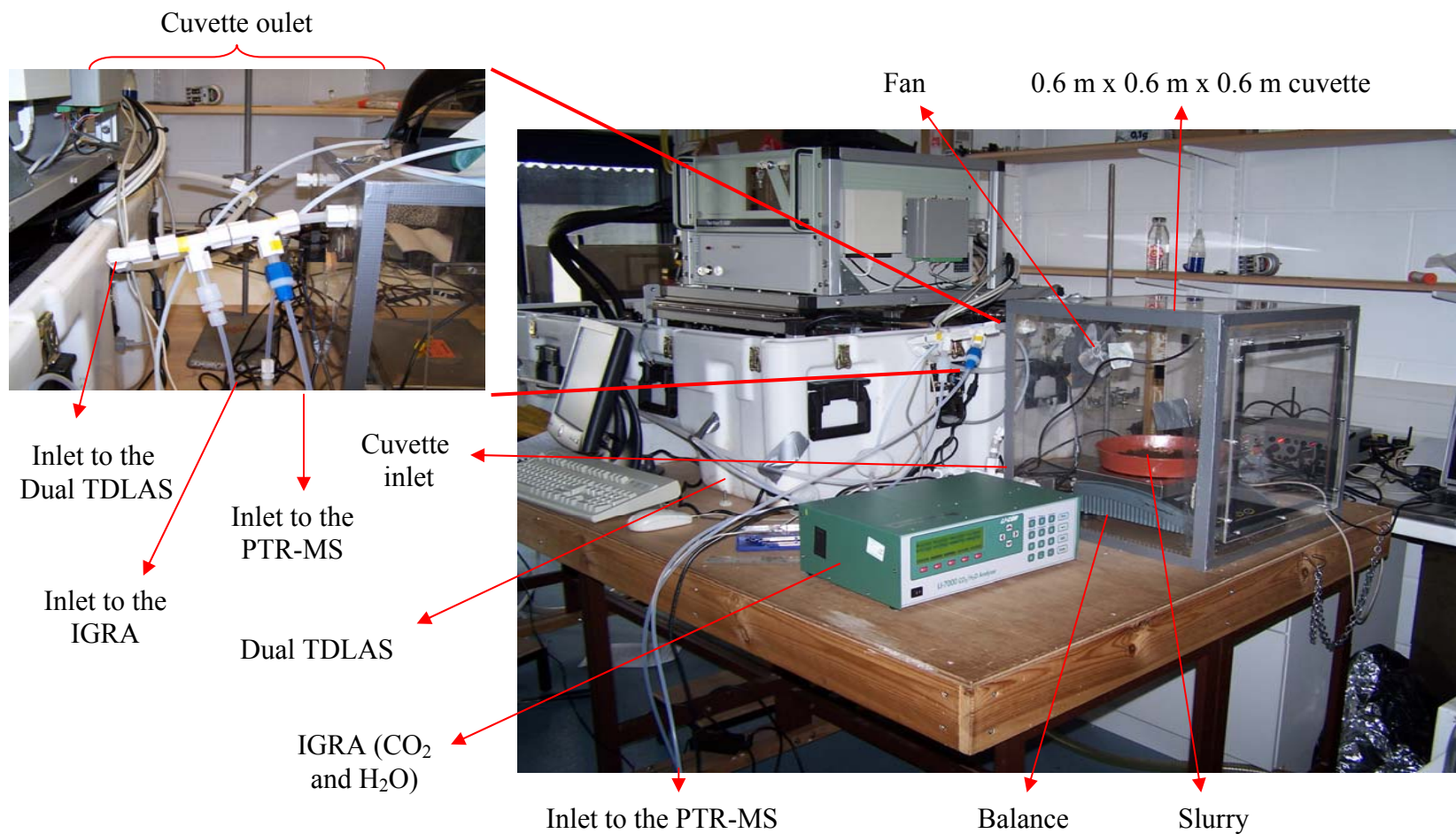
Eigure 4.6: The instrumental configuration during laboratory experiments 1 and 2.
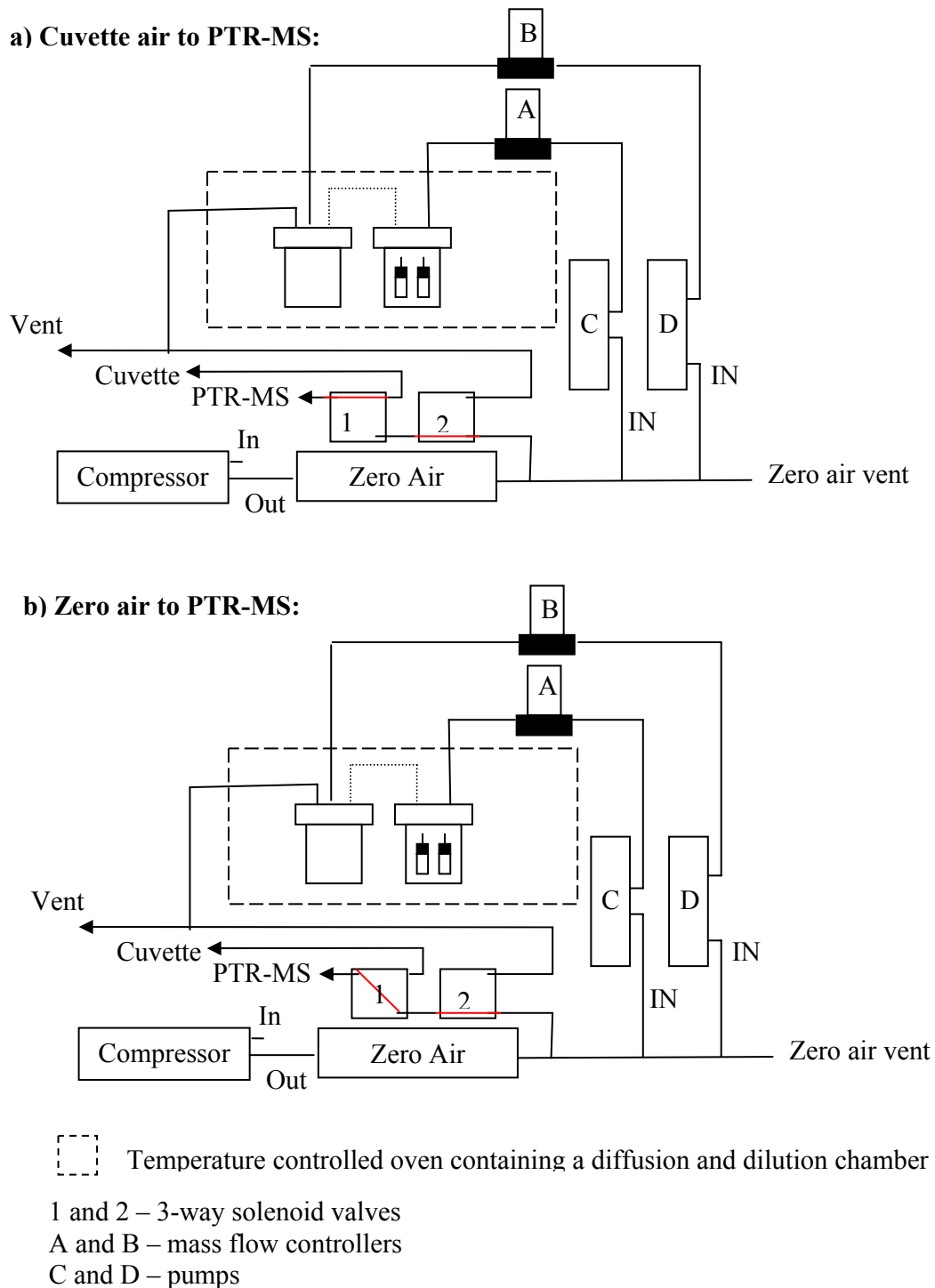
In laboratory experiment 1 count rates at m/z 30 (NO^+) and m/z 32 (O_2^+) were an average of ~0.19 (±0.01) % and 0.98 (±0.04) % of count rates at m/z 19 (H_3O^+) respectively. $H_3O^+(H_2O)$ (m/z 37) count rates were ~ 1.55 (±0.67) % of the sum of H_3O^+ (m/z 21 x 500) and $H_3O^+(H_2O)$ count rates. Count rates at m/z 19 were 1.09 x 10^7 (± 7.34 x 10^5). During laboratory experiment 2, count rates at m/z 30 (NO^+) and m/z 32 (O_2^+) were an average of ~0.18 (±0.01) % and 1.00 (±0.04) % of count rates at m/z 19 (H_3O^+) respectively. $H_3O^+(H_2O)$ (m/z 37) count rates were ~ 1.39 (±0.53) % of the sum of H_3O^+ (m/z 21 x 500) and $H_3O^+(H_2O)$ count rates. Count rates at m/z 19 were 1.0 x 10^7 (± 2.41 x 10^5) (numbers in the brackets are the standard deviations of the mean of half hourly averages).

The zero air generator described in § 4.2.1.4 was used to measure the instrument background. In this case the air was passed through 1 % Pt on Al_2O_3 pellets (3.2 mm) (Sigma Aldrich, Gillingham, Dorset, UK) mixed with activated charcoal. The inlet configuration at the PTR-MS during both measurements is shown in Figure 4.7.

In laboratory experiment 1 the PTR-MS was operated in two measurement modes. The SB (§ 2.3.3) mode was employed for two 4 minute periods at 0 and 30 minutes past the hour. The MID mode (§ 2.3.3) was employed for the remaining 26 minutes of each half hour. In the SB mode m/z 21 to m/z 141 were measured at 0.5 s per m/z resulting in ~61 s per scan (switching time ~ 1 ms per m/z). In the first seven hours of MID measurements m/z 21, 37, 33, 61, 75, 89, 95, 103 and 109 were measured and thereafter m/z 60, 58, 47, 41, 43 and 45 were added. Dwell times of 1 s per m/z were employed resulting in a response time of ~15.46 s cycle^{-1} (0.06 Hz) for the majority of measurements, a switching time of ~30 ms per m/z was observed throughout. Four measurements of instrument background were made in the SB and MID mode, measurement parameters were as during cuvette measurements. The means of 75 cycles from each MID background measurement were averaged. The means of 10 scans from each SB background measurement were averaged to quantify the instrument background.

In laboratory experiment 2, the instrument background was measured hourly. Each hour of measurements consisted of a 5 minute SB measurement of zero air followed by a 5 minute SB measurement of cuvette air, a 20 minute MID measurement of cuvette air, a 5 minute SB scan of cuvette air, a 20 minute MID measurement of cuvette air and a 5 minute MID measurement of zero air (Figure 4.8). During analysis (§ 4.2.3) the SB measurement of zero air during a given hour was subtracted from the SB measurements of cuvette air performed within the same hour and likewise for the MID measurements. In the SB modes m/z 21 to m/z 141 were measured at a speed of 0.5 s per m/z (~61 s per scan). In MID modes m/z 21,

33, 37, 41, 43, 45, 47, 58, 60, 61, 75, 89, 95, 103 and 109 were monitored with dwell times of 1 s per m/z resulting in a scan time of ~15.46 s (switching time of 30 ms per m/z).

a) Cuvette air to PTR-MS:

b) Zero air to PTR-MS:

Temperature controlled oven containing a diffusion and dilution chamber

1 and 2 – 3-way solenoid valves
A and B – mass flow controllers
C and D – pumps

Figure 4.7: The inlet and zero air configuration during the laboratory experiments. a) Solenoid one was clear and cuvette air passed in to the PTR-MS. b) Solenoid 1 was set and zero air sampled at the PTR-MS. The diffusion oven was empty and pumps C and D off during the slurry cuvette measurements.
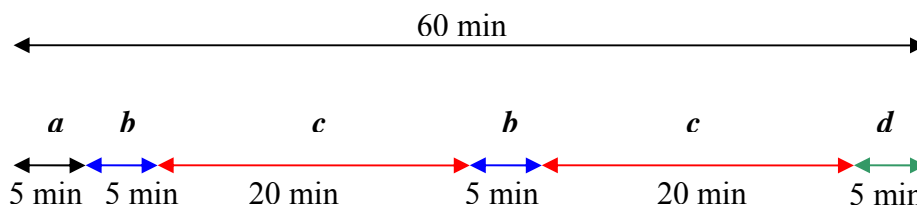
Figure 4.8: The measurement modes during each hour of laboratory experiment 2: *a* denotes an SB meaurement of zero air, *b* an SB measurement of cuvette air, *c* an MID measurement of cuvette air and *d* an MID measurement of zero air.

Temperature, fan and solenoid valve switching associated with the zero air operation and variation of measurement sample and mode were achieved using a LabJack© U12 (LabJack US) and programs developed in LabView© (National Instruments, US) and the Quadstar-32 bit (Pfeiffer Vacuum, UK) software that is employed for PTR-MS control.

The pH, total nitrogen, total ammonium, total carbon and dry matter content of the slurry sampled at the start of laboratory experiment 1 was determined by the Analytical laboratory of the Scottish Agriculture College (SAC), Bush Estate, Penicuik, Scotland. (Twigg 2006).

4.2.3 Calculation of Concentrations

In the absence of alternative techniques such GC or GC-PTR-MS compounds could not be unambiguously identified. Further it is hypothesised that more than one compound contributed to a number of m/z (§ 4.3). Therefore a compound specific approach to calculation of VMR could not be employed: VMRs were calculated from Eq. 2.73 (§ 2.6) utilising a nominal rate constant of 2×10^{-9} cm^3 s^{-1}, t calculated from Eq. 2.66 (§ 2.5) and detection efficiencies from the Boltzmann sigmoidal shown in Figure 2.16 (§ 2.7). A reduced mobility of H_3O^+ of 2.80 cm^2 V^{-1} s^{-1} (Dotan *et al* 1976) was employed for calculation of *t*. With the exception of analysis of measurements from Easter Bush 2004, detection efficiency corrected ion count rates of zero air were subtracted from ambient detection efficiency corrected count rates before use in Eq. 2.72. This approach assumes that the reaction of the trace species of interest with $H_3O^+(H_2O)$ is thermodynamically favourable (§ 2.6), if the trace species does not react with $H_3O^+(H_2O)$ *via* proton-transfer the application of Eq. 2.73 would result in inaccurate concentrations. In the case of trace species which do not react at all with $H_3O^+(H_2O)$ ions (non-polar relatively low proton affinity molecules, § 2.6), application of Eq. 2.73 would result in an underestimation of the VMR of the species. Given the inaccuracy associated with use of a nominal rate constant (variable depending on the compound), and inaccuracy and uncertainties associated with the calculation of *t* (§ 2.5) and

detection efficiencies determined in the manner described in § 2.7, VMRs determined from measurements at Easter Bush in 2005 and in laboratory experiments are semi-quantitative and are best considered qualitatively.   In the absence of instrument background measurements at Easter Bush in 2004, the VMRs are an overestimate and not quantitative. VMRs were calculated using programs written in LabView©, 'raw' (no averaging performed), 30 minute mean and hourly mean cps, ncps and VMRs (ppb) were derived.

4.3 Results and Discussion

4.3.1 Slurry Composition

The results of slurry analysis are shown in Table 4.5. Notably the pH of the slurry applied at Easter Bush in 2005 was higher than that applied in 2004 and that at the start of experiment 1. The slurry applied at Easter Bush in 2004 contained reduced dry matter. The total nitrogen content of slurry applied at Easter Bush in 2004 was approximately half that of the slurry applied in 2005 and that used in laboratory experiment 1. The total carbon content of the slurries was similar and only slightly less (~5 %) in the slurry applied at Easter Bush in 2005 compared to 2004.

Table 4.5: The chemical composition of slurry applied during laboratory experiment 1 and fertilisation at Easter Bush in 2004 and 2005.

Variable	Easter Bush 2004	Easter Bush 2005	Laboratory Experiment 1
DM (%)	3.3	10.03	12.0
pH	7.53	8.9	7.23
TN (%) (FM)	0.20	0.40	0.40
TAN (%) (FM)	0.11	0.12	0.11
TC (%) (DM)	48.4	43.07	47.5
Nitrate (µg/ml) (FM)	2.4	1.3	Not measured

Note: DM denotes dry matter, FM fresh matter, TN - total nitrogen, TAN - total ammoniacal nitrogen, TC – total carbon (Twigg 2006).

4.3.2 Micrometeorology Conditions During Fertilisations at Easter Bush in 2004 and 2005.

A detailed discussion of micometeorology during fertilisations can be found elsewhere (Twigg 2006) and are only briefly summarised here. The wind direction was predominantly from the SW during both fertilisations. However during the fertilisation in 2004 the wind direction did change to NE between the 29th of September at 08:00 (GMT) and the 30th of September at ~07:35 (GMT). Slurry was not being applied during this period. The range of temperatures during fertilisations were 6.2 to 15.2°C and 3.9 to 15.9°C in 2004 and 2005

respectively. The average temperature was 10.4^{o}C during both fertilisations. Wind speed was between 0.02 and 10.3 m s^{-1} during fertilisation in 2004 and 0.08 to 8.7 m s^{-1} in 2005.

4.3.3 Volatile Organic Compounds

As discussed in Chapter 2, 3 and also § 4.2.3, definitive identification of compounds contributing to a given m/z measured using PTR-MS and consequent quantification is not possible in the absence of alternative techniques such as GC, GC-PTR-MS or the use of a range of reagent ions. Tentative identification of the compounds contributing significantly to some of the masses observed to increase during slurry applications are discussed in the following section. Candidates for a given m/z as collated in electronic format are considered and the most likely contributor(s) identified based on previous measurements, such as those collated in Appendix D, contextual reasoning based on potential processes occurring within the slurry (Appendix D), observed product distributions, isotope ratios and the relationship between time evolution of increases related to Henrys Law constants (§ 4.3.5).

In the case of isotope ratios, the ratio of the measured mass of interest (m/z x) to m/z $x + 1$ and/or m/z $x + 2$ is compared to calculated ratios derived from the natural isotopic abundancies. Consider, for example, two potential contributors to m/z 47; ethanol and methanoic acid, the later compound contains one carbon and the former two. Natural isotopic composition of elements were taken from Rosman and Taylor (1997). The natural isotopic abundance of ^{12}C: ^{13}C is 98.94 : 1.08. Thus if m/z 47 corresponds to a one carbon molecule alone the corresponding ^{13}C isotope at m/z 48 would be 1.09 % of m/z 47 and if m/z 47 is a carbon two molecule alone m/z 48 would be 2.18 % of m/z 47. In the case of ethanol and methanoic acid there is an additional contribution to m/z 48 from the ^{17}O isotope, the natural isotopic abundance of ^{16}O:^{17}O is 99.757: 0.038. If m/z 47 were ethanol alone the ^{17}O isotope at m/z 48 would form 0.038 % of m/z 47, if methanoic acid the ^{17}O isotope at m/z 48 would be 0.076 % of m/z 47. If m/z 47 were ethanol alone, m/z 48 would therefore expected to be 2.21 % of m/z 47, if m/z 47 were methanoic acid alone m/z 48 would be 1.17 % of m/z 47. Thus by comparing the measured m/z 48 percentage of m/z 47 with these calculated values the contribution of each molecule can be estimated. Similar arguments could be applied using m/z 47 and m/z 49 and the natural isotopic abundance of ^{16}O:^{18}O of 99.757 : 0.205 to ascertain the contributions of molecules containing one and two oxygens. The use of isotopic ratios assumes that there are no other contributors to the m/z at which the isotope occurs (m/z $x + 1$ or 2) and is therefore limited in application. In all cases SB 30 minute averages were used to calculate m/z x+1 and/or m/z x+2 abundancies. Where negative concentrations

resulting from overestimation of the instrument background were observed, these values were neglected in isotope comparisons and fragment abundancies.

4.3.3.1 Carboxylic Acids, Esters and Alcohols

Relatively large concentrations of C_2 to C_5 carboxylic acids have previously been observed from livestock and their waste (§ 4.1, Appendix D). The products of the non-dissociative reaction of the C_2 to C_5 carboxylic acids with H_3O^+ results in ions at m/z 61, m/z 75, m/z 89 and m/z 103 respectively (§ 3.3). Increases in m/z 61, m/z 75, m/z 89 and m/z 103 were observed during both fertilizations at Easter Bush and during the laboratory measurements (Figure 4.9). The correlations between the non-dissociative masses are given in Table 4.6 Relatively strong correlations were observed between m/z 61 and m/z 75, m/z 89 and m/z 103. The correlation between the larger masses was greatest and the correlation with m/z 61 the weakest (excluding m/z 47).

Correlations with m/z 47, at which the non-dissociative product of the reaction of H_3O^+ with methanoic acid occurs, are also specified in Table 4.6. The production of methanoic acid by, for example, deamination of glycine may occur, though examples of previous measurements could not be found. No increase in m/z 47 was observed as a result of the fertilisations at Easter Bush. During the laboratory experiments m/z 47 increased and peaked within the first hour of slurry application, at 118 ppb and 35 ppb during experiment one and two respectively (Figure 4.9). This peak in m/z 47 occurred 6.5 to 10.5 hours before the peak in m/z 61 (§ 4.3.5) and the correlations of m/z 47 with m/z 61, m/z 75, m/z 89 and m/z 109 were poor (Table 4.6). This may suggest other compound(s) contributed more significantly to m/z 47 than methanoic acid.

The non-dissociative product of ethanol occurs at m/z 47 (§ 3.1.1, § 3.7) Alcohols are produced from microbial breakdown of amino acids and carbohydrates (Spoelstra 1980). Ethanol has previously been observed in the vicinity of livestock and their waste; Filipy *et al* (2006) measured ethanol concentrations in the range of 14.3 to 58.0 ppb next to a dairy slurry waste lagoon. Rabaud *et al* (2003) observed ethanol concentrations of 16.09 to 90.60 ppb ethanol at a dairy farm in California. Smith *et al* (2000) observed a mean concentration of 7491 ppb ethanol from the headspace of diluted pig faeces and 376 ppb from the headspace of fresh pig urine using SIFT. Ngwabie *et al* (2008) used PTR-MS to derive median ethanol concentrations of 1203.5 ppb (range 68.0 -11729.1 ppb) from m/z 47 in a dairy cowshed.
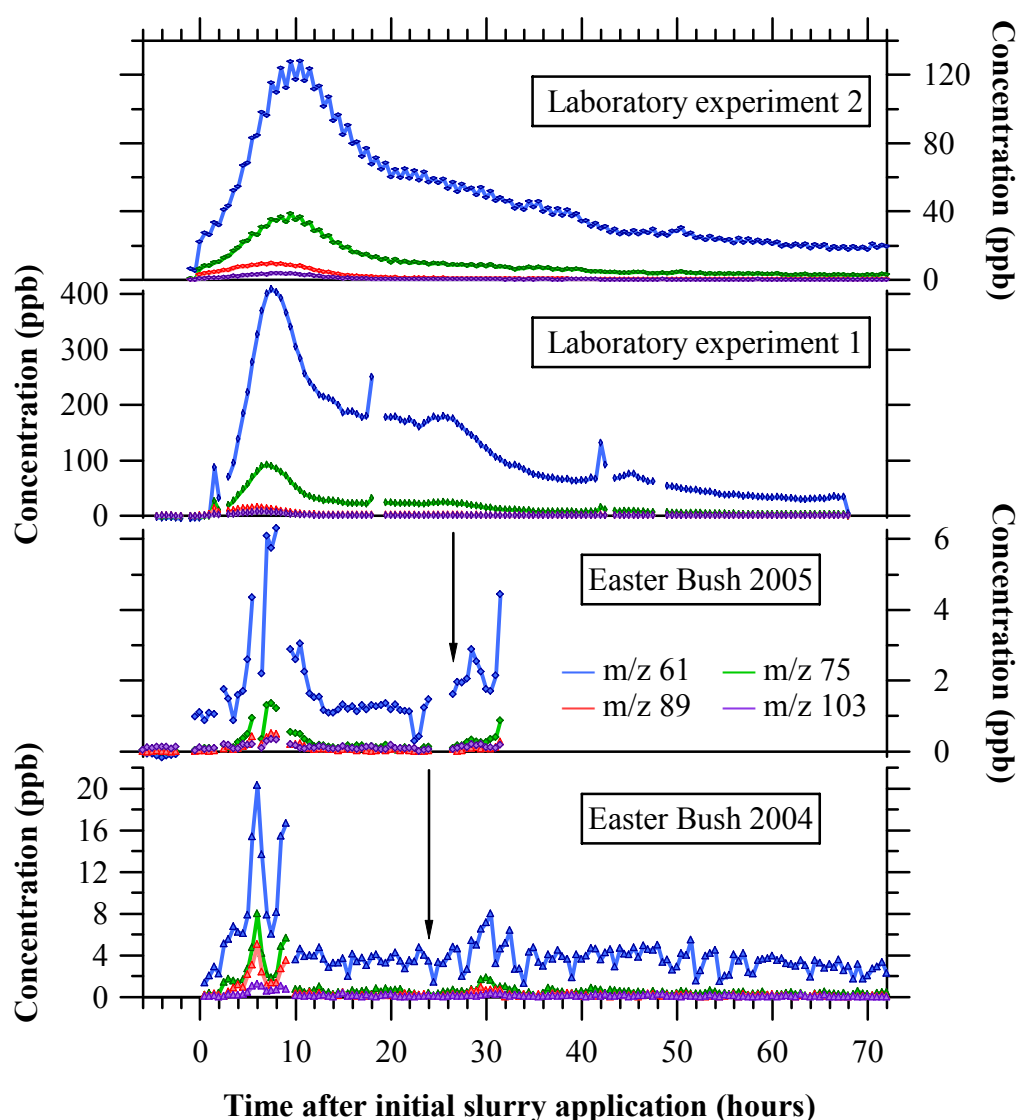
Figure 4.9: m/z 61, m/z 75, m/z 89 and m/z 103 VMRs during fertilizations at Easter Bush in 2004 and 2005 and laboratory experiments. Concentrations are half hourly means of the SB data. Concentrations are given as a function of time elapsed after initial slurry application. The starts of applications (0 hours) correspond to 08:00 (GMT) 28/09/04, 08:00 (GMT) 27/04/05, 14:30 (GMT) 11/04/06 and 13:00 (GMT) 14/04/06 for Easter bush 2004, Easter Bush 2005 and laboratory experiment 1 and 2 respectively. The arrows indicate the time fertilisation recommenced during Easter Bush measurements and indicate 07:30 (GMT) 29/09 during Easter Bush 2004 and 09:30 (GMT) 28/04 during Easter Bush 2005.

Table 4.6: Correlation coefficients (R^2) between m/z 47, 61, 75, 89 and 103. Values given in brackets were derived from half hourly means, those without brackets from hourly means. Values in bold type were derived from SB data those not in bold from MID data.

Measurement	R^2 between m/z 47 and				R^2 between m/z 61 and			R^2 between m/z 75 and		R^2 between m/z 89 and
	m/z 61	m/z 75	m/z 89	m/z 103	m/z 75	m/z 89	m/z 103	m/z 89	m/z 103	m/z 103
Easter Bush 2004	0.39, **0.27** (**0.21**)	0.17, **0.19** (**0.21**)	0.10, **0.16** (**0.09**)	0.12, **0.17** (**0.11**)	0.91, **0.95** (**0.89**)	0.85, **0.92** (**0.86**)	0.87, **0.84** (**0.77**)	0.98, **0.96** (**0.93**)	0.98, **0.87** (**0.81**)	0.99 **0.87** (**0.81**)
Easter Bush 2005	0.03, **0.01** (0.03, **0.00**)	0.00, **0.00** (0.00, **0.02**)	0.00, **0.00** (0.00, **0.03**)	0.02, **0.08** (0.02, **0.01**)	0.94, **0.96** (0.93, **0.94**)	0.74, **0.88** (0.75, **0.87**)	0.90, **0.77** (0.90, **0.64**)	0.97, **0.94** (0.97, **0.92**)	0.86, **0.75** (0.87) (**0.61**)	* **0.73** (*) (**0.60**)
Experiment 1	0.11, **0.02** (0.11, **0.02**)	0.19, **0.01** (0.18, **0.00**)	0.46, **0.01** (0.44, **0.01**)	0.31, **0.00** (0.30, **0.00**)	0.91, **0.90** (0.90, **0.90**)	0.49, **0.45** (0.48, **0.43**)	0.62, **0.59** (0.62, **0.58**)	0.75, **0.73** (0.75, **0.71**)	0.88 **0.86** (0.88) (**0.86**)	0.96 **0.94** (0.96) (**0.93**)
Experiment 2	0.00, **0.00** (0.00, **0.00**)	0.00, **0.00** (0.00, **0.00**)	0.05, **0.06** (0.05, **0.06**)	0.02, **0.02** (0.02, **0.02**)	0.92, **0.92** (0.92, **0.92**)	0.63, **0.63** (0.63, **0.63**)	0.70, **0.69** (0.70, **0.68**)	0.86, **0.86** (0.86, **0.86**)	0.92, **0.91** (0.92, **0.90**)	0.98 **0.97** (0.98) (**0.97**)

During the 0 to 5 hour period post slurry application in which elevated m/z 47 concentrations were observed, the m/z 48 concentration was 2.27 (± 0.31) % and 2.52 (±0.50) % of the m/z 47 concentration in experiment 1 and 2 respectively (Figure 4.10). Assuming no other molecules contributed to m/z 48, carbon two rather than carbon one molecule dominated at m/z 47 (§ 4.3.3) and m/z 47 is tentatively identified as consisting predominantly of ethanol.

Other potential contributors to m/z 47 (§ 3.7) such as fragments of methanol dimers (Malekina *et al* 2007, § 3.3.1), butyl ethyl ether (m/z 47 forms 55 % of total products ions in SIFT, Španěl and Smith 1998b), ethyl formate (m/z 47 forms < 5 % of total product ions in SIFT, Španěl and Smith 1998a) and ethyl nitrate (m/z 47 forms 1.8 % of total product ions in PTR-TOF-MS, $KE_{c.m.}^{r}$ 0.21 eV, P_{dt} 6.66 mbar, E ~200 V cm^{-1}, Aoki *et al* 2007) cannot be ruled out. The $^{16}O{:}^{18}O$ abundancies could not be used to verify the number of oxygens presence due to the occurrence of another compound at m/z 49 (§ 4.3.3.3).
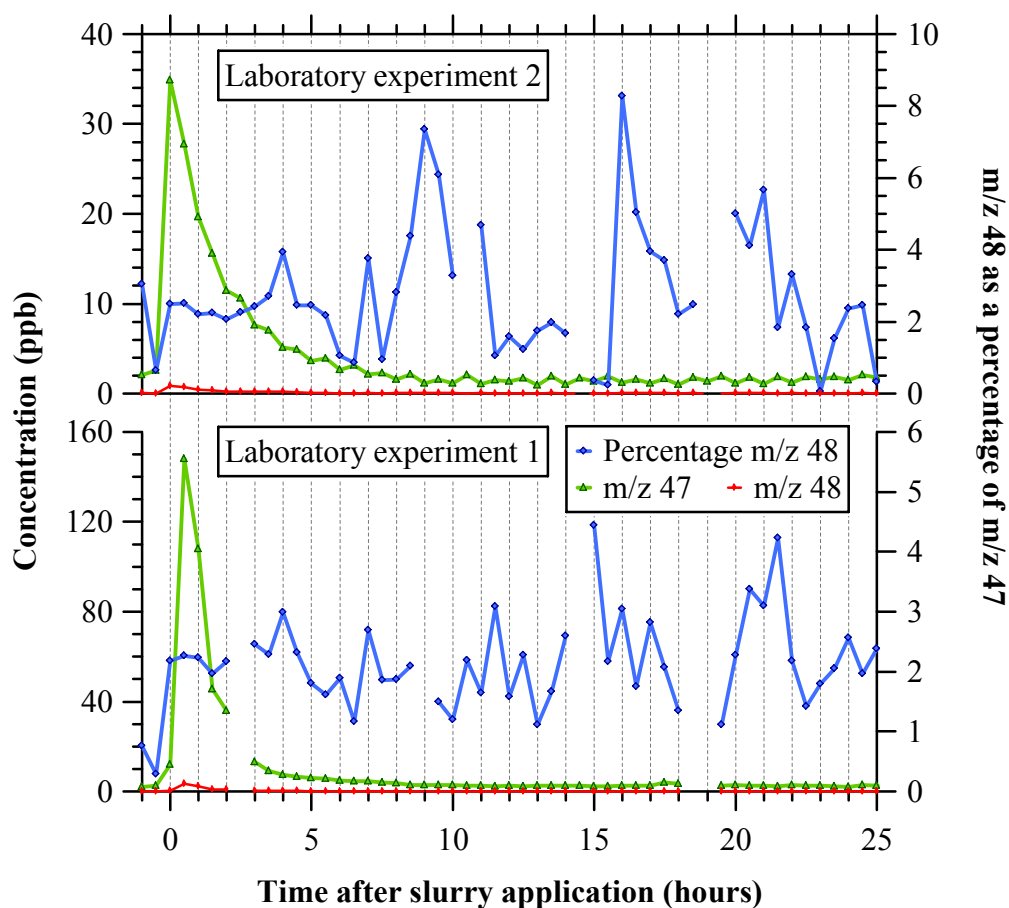

Figure 4.10: The time evolution of m/z 47 and m/z 48 and m/z 48 as a percentage of m/z 47 is shown during laboratory experiments 1 and 2. Values are 30 minute means of SB data and percentages were calculated from these values.

Propanol has also been observed in previous studies: Rabaud *et al* (2003) observed 1-propanol concentrations of 36.54 to 304.00 ppb from an industrial dairy. Sunesson *et al* (2001) observed 1-propanol in 15 out of 56 samples from dairy farms at concentrations of 0.4 to 8.1 ppb. Beck *et al* (2007) observed up to 134 ppb of propanol from dwellings and stables on cattle farms. The non-dissociative products of protonation of propanol isomers ($C_3H_8OH^+$) are isobaric with that of ethanoic acid ($C_2H_4O_2H^+$) at m/z 61. The reaction of both the propanol isomers and ethanoic acid with H_3O^+ also produce fragments at m/z 43 formed by elimination of H_2O to give $C_3H_7^+$ and $C_2H_3O^+$ respectively (§ 3.1.1 and § 3.3.1). The extent of fragmentation to m/z 43 from reaction of H_3O^+ with ethanoic acid is less than that from the propanol isomers. Product distributions of 0 to 30 % at m/z 43 (70 % to 100 % at m/z 61) have been reported from the reaction of ethanoic acid with H_3O^+ depending on the drift tube conditions (Table 3.14, § 3.3). Conversely product distributions of 0 to 20 % at m/z 61 and 73 to 100 % at m/z 43 (and 0 to 50 % at m/z 41) have been reported from propanol (Table 3.4, § 3.1). Under the drift tube conditions applied here the higher values of fragment abundances are applicable.

A strong correlation between m/z 43 and m/z 61 was observed during the fertilisations at Easter Bush and during laboratory experiments. R^2 were 0.80, 0.78, 0.88 and 0.85 during laboratory experiments 1 and 2, fertilisation at Easter Bush in 2004 (0.5 to 72 hours after initial slurry application) and at Easter Bush in 2005 (0 to 31.5 hours after initial slurry application). The concentrations of m/z 43 and m/z 61 during the fertilisations at Easter Bush and during laboratory experiments 1 and 2 are shown in Figure 4.11. The percentage of the sum of m/z 43 and m/z 61 contributed by m/z 43 is shown. These values were calculated using half hourly means of SB data and the averages and standard deviations discussed here correspond to the means of this half hourly data.

During laboratory experiment 1 an initial peak in m/z 43 was observed within the first two hours of slurry application, during the second hour a minor peak in m/z 61 was also observed. In the first hour after application, m/z 43 formed 99 % of m/z 43 and m/z 61 and in the second 60 to 70 %. A second increase in m/z 43 and m/z 61 was then observed reaching a maximum 7 to 8 hours after slurry application. After the first peak in m/z 43, the percentage of the total contributed by m/z 43 decreased reaching an approximately constant level from 10 hours after slurry application, averaging 32.6 ± 1.7 % between 10 and 67.5 hours. Similar results were observed during laboratory experiment 2. An initial increase in m/z 43 was seen within the first 30 minutes of slurry application and m/z 43 formed ~ 70 % of m/z 43 and m/z 61. m/z 43 and m/z 61 then increased reaching a maximum approximately 10.5 hours after slurry application. After the initial peak in m/z 43 the percentage

contribution of m/z 43 to the sum of m/z 43 and m/z 61 decreased to an approximately constant level averaging at 32.2 ± 1.4 % between 14 and 90 hours after slurry application.
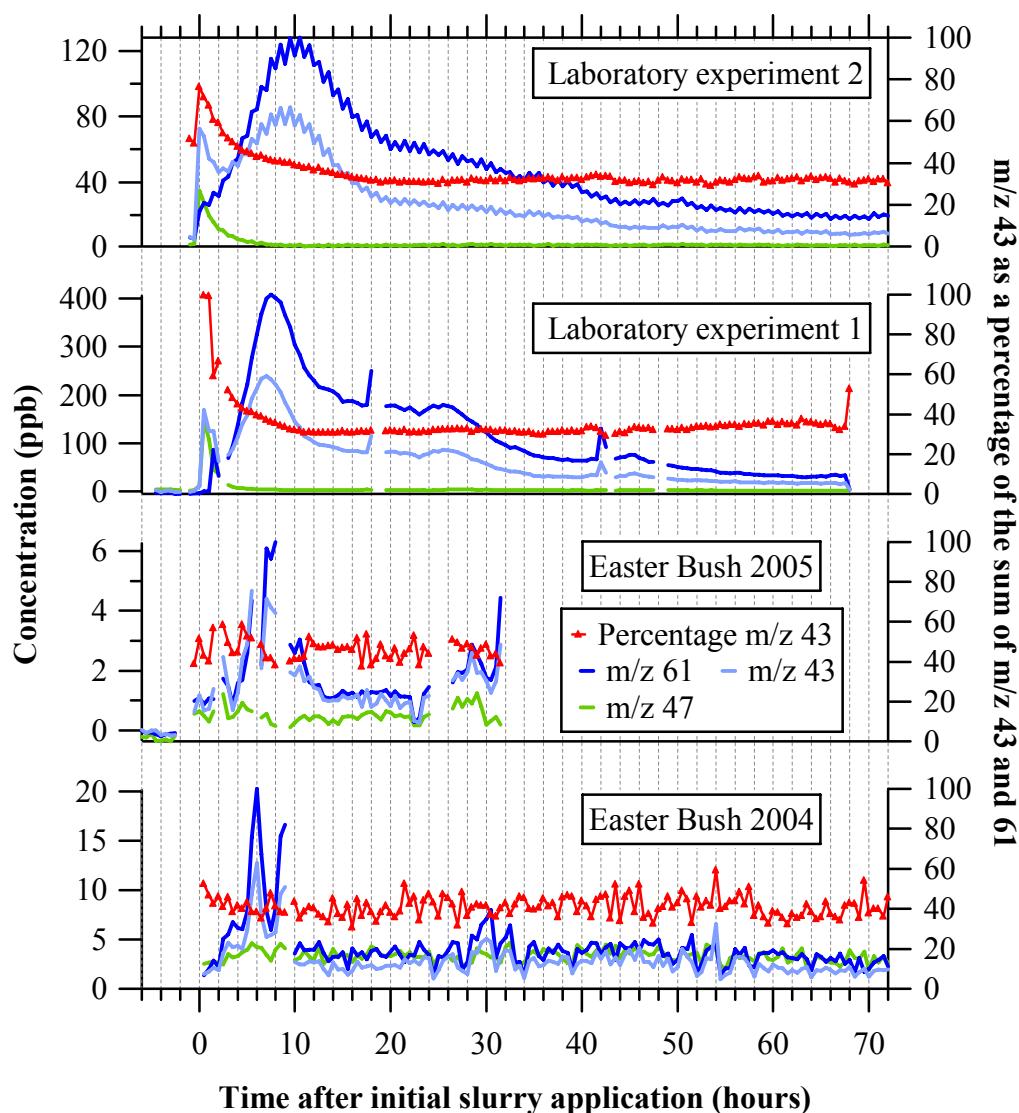
Figure 4.11: The concentrations of m/z 43, m/z 61 and m/z 47 during fertilizations at Easter Bush in 2004 and 2005 and laboratory experiments 1 and 2. Concentrations are half hourly means of the SB data. Concentrations are given as a function of time elapsed after initial slurry application. The starts of applications (0 hours) correspond to 08:00 (GMT) 28/09/04, 08:00 (GMT) 27/04/05, 14:30 (GMT) 11/04/06 and 13:00 (GMT) 14/04/06 for Easter bush 2004, Easter Bush 2005 and laboratory experiment 1 and 2 respectively. The percentage of the sum of m/z 61 and m/z 43 contributed by m/z 43 is also shown.
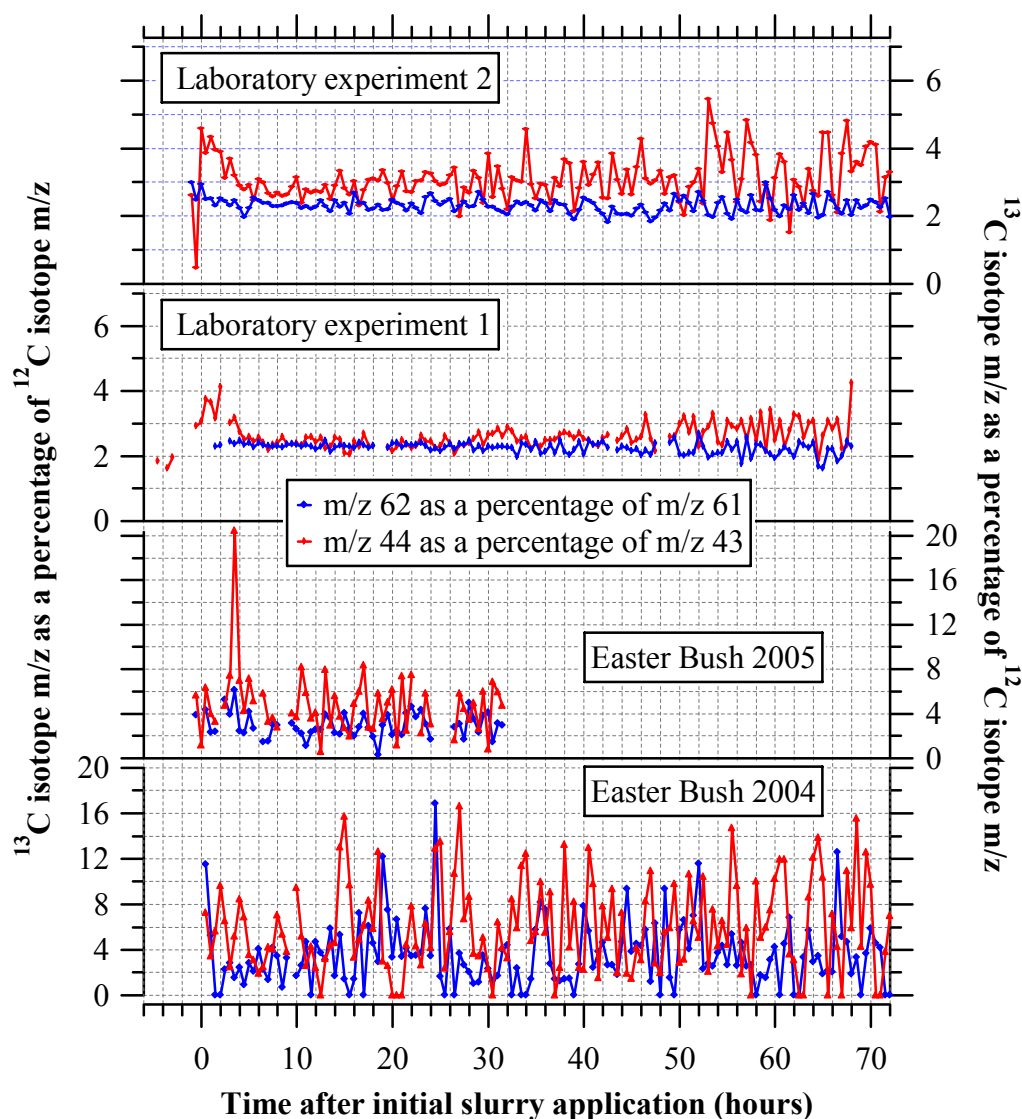
During fertilisation at Easter Bush in 2005, an initial peak in m/z 43 and m/z 61 was observed one and a half to two hours after slurry application began. m/z 43 formed 57.0 % and 58.5 % of m/z 43 and m/z 61 at one and a half and two hours after application respectively. Another peak was observed at five and a half hours after application at which

point m/z 43 formed 51.8 % of the total of m/z 43 and m/z 61. During a third peak between 6.5 and 11 hours after application, m/z 43 was 41.2 ± 1.2 %. After the beginning of fertilisation on 29/09/05 at 26.5 to 32 hours after the initial fertilization (28/09/05) m/z 43 contributed 46.2 ± 3.3 % to the sum of m/z 43 and m/z 61. The mean m/z 43 percentage of m/z 43 and m/z 61 was 46.2 ± 5.08 % for the period from 0 to 31.5 hours after slurry application. During fertilisation at Easter Bush in 2004, the mean percentage contribution of m/z 43 to the sum of m/z 43 and m/z 61 was 41.2 ± 4.8 % between 0 and 48 hours after slurry application began.

The mean of Henry's Law constants of 1-propanol collated in Mallard and Linstrom (2005) is 138 ± 19 mol kg^{-1} bar and that of ethanoic acid is 5671 ± 3032 mol kg^{-1} bar. On this basis a peak in propanol emissions may be expected prior to that of ethanoic acid (§ 4.3.5). It is possible that the initial peaks in m/z 43 observed in the laboratory experiments, and to some extent evident during fertilisation at Easter Bush in 2005, in which m/z 43 formed ~60 to 99 % of the sum of m/z 43 and m/z 61 correspond predominantly to propanol isomers with reduced fragmentation. The later peak in which the percentage contribution of m/z 43 was reduced, and during laboratory measurements eventually stabilised at ~ 32 %, may have resulted from an increasing contribution of ethanoic acid. The initial peak in m/z 43 observed in the laboratory experiments also appears to correlate with that observed at m/z 47 (Figure 4.11). The R^2 of MID concentrations (no averaging) of m/z 47 and m/z 43 for 0 to 2 hours after application during laboratory experiment 2 is 0.85. This supports the identification of m/z 47 and the initial peak in m/z 43 to C_2 and C_3 alcohols respectively.

The m/z 44 and m/z 61 as a percentage of m/z 43 and m/z 62 respectively are shown in Figure 4.12. If a C_2 molecule alone was present, the intensity at the ^{13}C mass (m/z 44 or m/z 61) would be 2.18 % of that at the ^{12}C m/z (m/z 43 and m/z 61); if only a C_3 molecule contributed, the intensity at the ^{13}C m/z would be 3.27 % of that at the ^{12}C m/z. If the ^{17}O isotope is considered in addition to the ^{13}C isotope then if $C_2H_5O_2^+$ molecules alone were at m/z 61, m/z 62 would form 2.26 % of m/z 61, if $C_3H_9O^+$ molecules alone contributed to m/z 61, m/z 62 would form 3.30 % of m /z 61. In the case of m/z 43 including the ^{17}O isotope, if $C_2H_3O^+$ alone contributed m/z 44 would form 2.21 % of m/z 43 (if $C_3H_7^+$ was the sole contributor m/z 44 would be 3.27 %).

The abundance of m/z 62 as a percentage of m/z 61 was relatively constant during laboratory experiment 1 and the mean from 1.5 to 68 hours post slurry application was 2.25 ± 0.17 %. This corresponds to 6.42 (± 15.6) % C_3 and 93.6 (± 15.6) % C_2 molecules. If considering ^{17}O isotopes and comparing possible contributions from $C_2H_5O_2^+$ and $C_3H_9O^+$ suggests m/z 61

Figure 4.12: The measured intensity of m/z 44 and m/z 62, corresponding to ^{13}C isotopes of ^{12}C isotopes at m/z 43 and m/z 61, as a percentage of these ions respectively during fertilisations at Easter Bush in 2004 and 2005 and laboratory experiments 1 and 2.

consisted of $C_2H_4O_2H^+$ alone. The mean intensity of m/z 62 as a percentage of m/z 61 was 2.29 ± 0.27 from 0 to 91 hours after slurry application in laboratory experiment 2 after slurry application. This corresponds to $10.09 (\pm 24.77)$ % C_3 and $89.91 (\pm 24.77)$ % C_2 molecules. If including ^{17}O isotopes and comparing possible contributions from $C_2H_5O_2^+$ and $C_3H_9O^+$ this suggests m/z 61 consisted of $97.12 (\pm 25.97)$ % $C_2H_5O_2^+$ and $2.88 (\pm 25.97)$ % $C_3H_9O^+$.

Thus a C_2 ion (tentatively $C_2H_4O_2H^+$) dominated at m/z 61 during both laboratory experiments and ethanoic acid is identified as the principal contributor. The C_3 contribution may be the result of minor fragmentation from propanol isomers (§ 3.1.1, Table 3.4).

A number of C_2 molecules besides ethanoic acid may have contributed to m/z 61: $C_2H_5O_2^+$ at m/z 61 is a major fragment of the esters (ethyl, propyl, *iso*-propyl, butyl, hexyl and octyl acetate) on reaction with H_3O^+ under drift tube conditions (Table 4.7, Buhr *et al* 2002, Aprea *et al* 2007a, Blake *et al* 2006). Esters are produced as a result of microbial deamination of amino acids and fermentation of carbohydrates in slurry, though emissions are thought to be less than the carboxylic acids (Spoelstra 1980). Raubaud *et al* (2003) observed 0.19 to 9.56 ppb ethyl acetate, 6.97 to 25.96 ppb butyl acetate in air samples from a commercial dairy. Sunesson *et al* (2001) observed 0.2 to 27.7 ppb ethyl acetate in 47 out of 56 samples from a dairy farm. Beck *et al* (2007) observed maximum concentrations of 19.3 ppb ethyl acetate, 7.76 ppb propyl acetate and 7.5 ppb butyl acetate in dwellings and stables of dairy farms. A $C_2H_3O^+$ fragment is also formed at m/z 43 from the reaction of these esters with H_3O^+ under drift tube conditions. The m/z 43: m/z 61 product distributions from the acetates are similar to that observed from ethanoic acid (Table 4.7, § 3.3 Table 3.14). The non-dissociative products of the reaction of ethyl, propyl and butyl acetate are minor products in the PTR-MS (Table 4.7) and are isobaric with the non-dissociative products of the C_4 to C_6 carboxylic acids (Table 4.7, § 3.3 Table 3.14).

An upper limit to the contribution of butyl acetate can be estimated by assuming that the non-dissociative product of this ester is the only contributor to m/z 117, neglecting C_6 carboxylic acids and other esters. Peak concentrations of m/z 117 during laboratory experiments 1 and 2 were 0.41 and 0.28 ppb respectively. Assuming that the non-dissociative product forms 10 % of the total product ions from butyl acetate (Table 4.7), this corresponds to maximum butyl acetate concentrations of 4.1 and 2.8 ppb during experiment 1 and 2 respectively, suggesting this is a minor contributor to m/z 61. The non-dissociative product of methyl formate also occurs at m/z 61 (Table 4.7) and may contribute though no product ion is produced at m/z 43.

The Henry's Law constants of the esters (Table 4.7) are also significantly less than that of ethanoic acid and any contribution from the esters might be expected in the initial hours of slurry application (§ 4.3.5).

In laboratory experiment 1, m/z 44 was between 3.01 and 4.12 % of m/z 43 between 0 and 3.5 h after slurry application during the initial peak in m/z 43 (Figures 4.12 and 4.11). The mean abundance of m/z 44 as a percentage of m/z 43 was 3.42 ± 0.43 during this period. The fragment of ethanoic acid (§ 3.3.1) and the acetates (Table 4.7) at m/z 43 is $C_2H_3O^+$ and that from the propanol isomers and $\geq C_5$ alcohols (§ 3.1.1) is $C_3H_7^+$. The percentage ratio of m/z 43 and m/z 44 during this initial 3.5 hours was closest to the $^{12}C{:}^{13}C$ ratio expected for a

three carbon molecule (3.27 %). The m/z 43 ion during this period is tentatively attributed to $C_3H_7^+$. At 4 to 68 hours after slurry application m/z 44 formed 2.58 ($\pm$ 0.34) % of m/z 43 suggesting a C_2 ion was the predominant contributor at 63.30 $\pm$ 23.85 % (a C_3 ion contributing 36.70 $\pm$ 23.85 %). Including ^{17}O isotopes and comparing possible contributions from $C_2H_3O^+$ and $C_3H_7^+$ the measured percentage m/z 44 suggests $C_2H_3O^+$ consists of 66.35 $\pm$ 32.69 % ($C_3H_7^+$ contributing 35.58 $\pm$ 32.69 %). It is assumed that the majority of $C_2H_3O^+$ ions produced resulted from the reaction of ethanoic acid with a possible contribution from the acetate esters discussed above.

Table 4.7: The Henry's Law constants (K_{HL}) of selected esters and product distributions from their reaction with H_3O^+. Henry's Law constants are averages of values given in Mallard and Linstrom (2005), uncertainties are standard deviations.

Ester (M)	K_{HL} (mol kg^{-1} bar)	Product ion as a Percentage of Total Product Ions			
		MH^+ (m/z)	$C_2H_5O_2^+$ (m/z 61)	$C_2H_3O^+$ (m/z 43)	Other (m/z)
Methyl formate	6.7 $\pm$ 1.6	(61): >95[a], ~94[bi], ~76[bii]	see MH^+		(33): <5[a], ~6[bi], ~24[bii]
Ethyl acetate	4.7 $\pm$ 0.3	(89):100[a], 98[c], 13.4[d], 22.4[e], 5[f]	*2[c], 49.5[d], 54.6[e], 74[f]	34.7[d], 23.0[e], 21[f]	(41): 2.5[d]
Propyl acetate	3.1 $\pm$ 0.6	(103): 2.9[d]	58.5[d]	38.6[d]	
i-Propyl acetate		(103): 3.9[e]	64.5[e]	27.7[e]	(79): 3.9[e]
Butyl acetate	4.3 $\pm$ 0.2	(117): 10.0[d]	62.5[d]	27.5[d]	
Hexyl acetate	1.9	(145)	53.5[d]	42.2[d]	(57): 4.3[d]
Octyl acetate		(173): 2.4[e]	19.5[e]	26.3[e]	(41): 7.4[e]
					(57): 29.5[e]
					(71): 13.3[e]
					(113): 1.8[e]

Note: Product distributions are taken from: [a]Španěl and Smith (1998a) measured in SIFT at P_{FT} 0.67 mbar, T_{FT} 300 K. [b]Warneke et al (1996) measured in SIFDT, values were obtained over a range of $KE_{c.m.}^r$ (~0.05 to 1.5 eV); those shown here correspond to $KE_{c.m.}^r$ of [i]0.2 eV, [ii]1 eV, T_{dt} was 298 K P_{dt} and E were not specified. [c]Španěl and Smith (1995) measured in SIFT at P_{FT} 0.67 mbar, T_{FT} 300 K. [d]Buhr et al (2002) measured in PTR-MS at V_{drift} 600 V (l_{dt}, P_{dt}, T_{dt}, E/N not specified), [e]Aprea et al (2007a) measured in PTR-MS E/N ~ 120 Td, P_{dt} 2.03 mbar and T_{dt} 323 K therefore V_{drift} ~ 55 V cm^{-1}). A helium carrier gas was used in all SIFT and SIFDT measurements. [f]Blake et al (2006) measured in CIR-TOF-MS (with H_3O^+) at E 270 V cm^{-1}, T_{dt} 313 K E/N 165 Td and therefore P_{dt} ~7.1 mbar. Values in [d] and [e] were given as relative abundances (normalised with the dominant product ion 100) and were converted to percentage product ion distributions to one decimal place. * m/z 61 may also correspond to $C_3H_9O^+$ formed by loss of CO from MH^+. It is assumed that all ions at m/z 61 correspond to $C_2H_5O_2^+$ (+C_nH_{2n}) formed by McLafferty re-arrangement of MH^+ with subsequent ejection of water to form $C_2H_3O^+$ (refer to Aprea et al 2007a, Buhr et al 2002, Španěl and Smith 1995, [a]Španěl and Smith 1998a and Harrison 1992 for a discussion of reaction pathways).

The measured m/z 43: m/z 44 and m/z 61: m/z 62 ratios have been used to derive the percentage contributions of C_2 and C_3 molecules to m/z 43 and m/z 61 respectively during laboratory experiment 1. Given the natural isotopic abundancies a value of 100 % C_2 molecules corresponds to m/z 44 forming 2.18 % of m/z 48, and 100 % C_3 to 3.27 % m/z 44. The C_2 and C_3 concentrations at m/z 43 and 61 were subsequently calculated, where percentage contributions were greater than 100 % the values were assumed to be 100 % and where less than 0 % to be 0 %. The results are shown in Figure 4.13 and Figure 4.14.
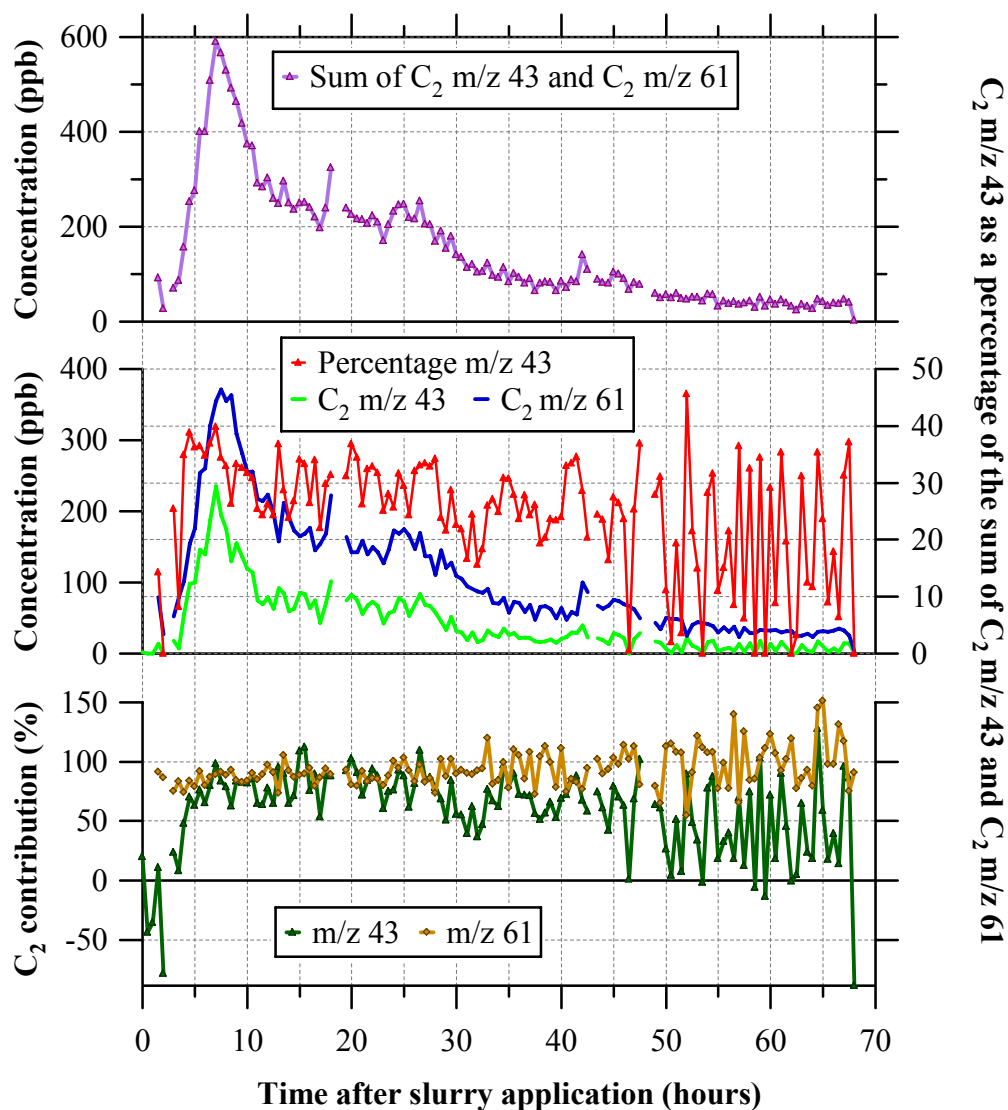
Figure 4.13: The percentage contribution of C_2 molecules to m/z 43 (dark green) and m/z 61 (brown) during laboratory experiment 1. The resulting C_2 concentrations at m/z 43 (light green) and m/z 61 (blue) and consequent C_2 m/z 43 abundance as a percentage of the sum of C_2 m/z 43 and C_2 m/z 61 (red) are shown. The sum of C_2 m/z 43 and C_2 m/z 61 (purple) is displayed. Values were calculated from 30 minute averages of SB data.
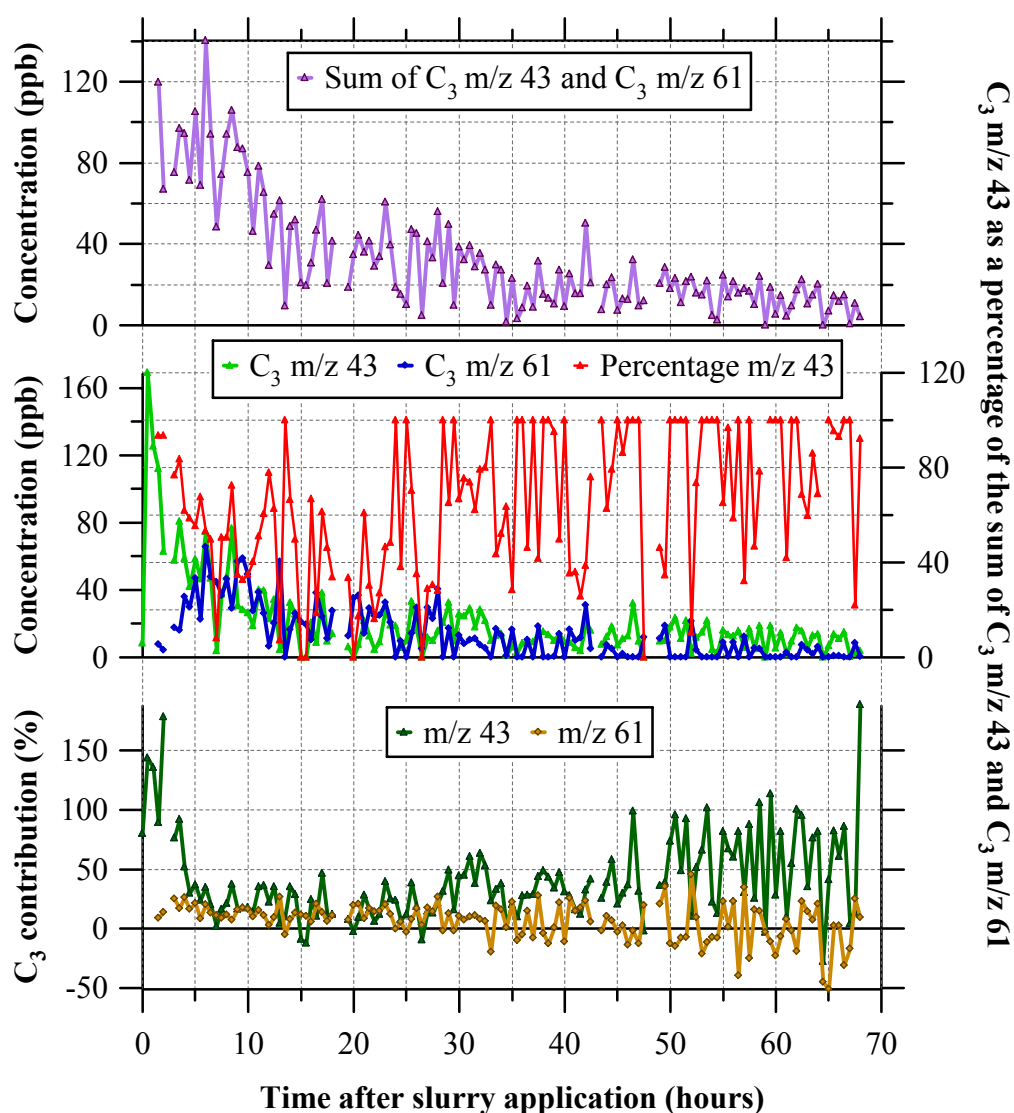
Figure 4.14: The percentage contribution of C_3 molecules to m/z 43 (dark green) and m/z 61 (brown) during laboratory experiment 1. The resulting concentrations of C_3 molecules at m/z 43 (light green) and m/z 61 (blue) and consequent C_3 m/z 43 abundance as a percentage of the sum of C_3 m/z 43 and C_3 m/z 61 (red) are shown. The sum of C_3 m/z 43 and C_3 m/z 61 is displayed (purple). Values were calculated from 30 minute averages of SB data.

These results clearly show that a C_3 molecule(s) initially dominated at m/z 43 between 0 and 4 hours after slurry application and a C_2 molecule(s) dominated during 10 and 45 hours with increased variation thereafter. The percentage contribution of C_2 and C_3 molecules to m/z 61 was relatively uniform throughout laboratory experiment 1 with the C_2 molecules dominating throughout (Figure 4.13 and 4.14).

There is a strong correlation (R^2 0.91 between 1.5 and 68 hours) between the C_2 m/z 43 and C_2 m/z 61. The C_2 m/z 43 product distributions of 20 to 40 % of the sum of C_2 m/z 43 and C_2 m/z 61 are in agreement with product distributions reported from ethanoic acid in the

literature under similar drift tube conditions to those applied here (Karl *et al* 2007, Christian *et al* 2004, Williams *et al* 2001, Table 3.14) and those from the acetate esters (Table 4.7). Variations in the ratio of C_2 m/z 43: C_2 m/z 61 may be due to varying contributions of acetate esters, with slightly differing degrees of fragmentation than that of ethanoic acid, and of methyl formate.

The C_3 m/z 43 and C_3 m/z 61 intensities were weakly correlated (R^2 0.13 between 1.5 and 68 hours), suggesting a different source molecule. At the peak in C_3 m/z 43 at 1.5 and 2 hours after slurry application, C_3 m/z 43 formed 93.50 % and 93.55 % of the sum of C_3 m/z 43 and C_3 m/z 61. This is within the m/z 43 : m/z 61 product distributions from propanol isomers cited in the literature (§ 3.1.1, Table 3.4). A peak in C_3 m/z 61 was then observed and the C_3 m/z 43 as a percentage of the sum of C_3 m/z 43 and C_3 m/z 61 decreased (Figure 4.14). This may suggest a source of C_3 molecules at m/z 61 other than propanol fragments. The propanol concentration is therefore taken to be the C_3 m/z 43 concentration rather than the sum of C_3 m/z 43 and C_3 m/z 61, with possible contributions from higher alcohols (§ 3.1.1). Varying degrees of fragmentation of propanol isomers and higher alcohols to m/z 41 have also been cited in the literature (§ 3.1.1, Table 3.4) m/z 41 contributing between 0 % and 51 % of the total product ions. There are a number of other contributors to m/z 41 and the peak concentration during laboratory experiment 1 was 129.60 ppb close to that of C_3 m/z 43 (169.11 ppb). The R^2 of C_3 m/z 43 to m/z 41 was 0.62 suggesting other contributors were present. Thus the degree of fragmentation to m/z 41 cannot be estimated. The correlation between C_3 m/z 43 and m/z 47 is 0.60, it is noteworthy that the correlation between m/z 47 and m/z 41 is 0.97.

In addition to propanol isomers and $> C_5$ alcohols, the $>C_6$ acyclic alkanes (§ D.1.1), cyclopropane (§ D.1.4), propene and $>C_5$ alkenes (§ D.1.2) form $C_3H_7^+$ product ions at m/z 43 in the PTR-MS. The sum of the mean concentrations of *n*- isomer $C_6 - C_{14}$ acyclic alkanes observed by Beck *et al* (2007) in stables on cattle farms were 20 % of the mean concentration of propanol. Conversely in dwellings on the cattle farms the mean propanol concentration was 40 % of the sum of the alkanes. The mean concentration of 1-propanol observed by Sunesson *et al* (2001) was 18 % of the sum of a range of C_9 to C_{14} acyclic alkanes measured. However, it is probable that the source of these alkanes was fuels and/or solvents used on the farms rather than animal waste. No measurements of alkanes or alkenes directly from animal wastes could be found. It is therefore assumed that the contribution of these compounds to emissions from the slurry is minimal compared to propanol and possibly the higher alcohols.

In laboratory experiment 2, the m/z 44 intensity as a percentage of m/z 43 decreased from 4.59 % at 0 hours to 2.88 % at 4 hours after slurry application (Figure 4.12). The percentage was relatively constant between 4 and 26 hours after slurry application, the mean during this period was 2.87 ± 0.26 % corresponding to 63.30 % C_3 molecules and 36.70 C_2 molecules ($\pm$ 23.86 %). The m/z 43: m/z 44 ratio was increasingly variable as the experiment proceeded and the mean between 27 and 91 hours after slurry application was 3.29 ± 0.92 %.

The measured m/z 43: m/z 44 and m/z 61: m/z 62 ratios have been used to derive the percentage contributions of C_2 and C_3 molecules to m/z 43 and m/z 61 respectively during laboratory experiment 2. The C_2 and C_3 concentrations at m/z 43 and 61 were subsequently calculated, where percentage contributions were greater than 100 % the values were assumed to be 100 % and where less than 0 % to be 0 %. The results are shown in Figure 4.15 and Figure 4.16 and are similar to those observed from laboratory experiment 1.

Given the laboratory experiment observations and on the basis of product distributions available in the literature, it is assumed that m/z 61 during Easter Bush measurement consisted of ethanoic acid (with possible contributions from the acetate esters). It is probable that a further 20 to 40 % of the total product ions from ethanoic acid occurred at m/z 43. The resultant ethanoic acid concentrations during fertilisations at Easter Bush are shown in Figure 4.17. The m/z 43 concentration remaining after subtraction of the ethanoic acid contribution is also shown. This is an approximation of propanol concentrations, additional fragmentation to m/z 41 may have occurred and higher alcohols may have contributed to m/z 43.

At the 40 % level of ethanoic acid fragmentation there appears to have been no propanol emitted during fertilisation at Easter Bush in 2004. At the 20 % level of ethanoic acid fragmentation, a small peak in propanol is observed but strong correlation with the calculated ethanoic acid concentration (Figure 4.17) may indicate underestimation of the level of ethanoic acid fragmentation. As observed during the laboratory experiments, a peak in propanol preceding that of ethanoic acid occurred during fertilisation in 2005.
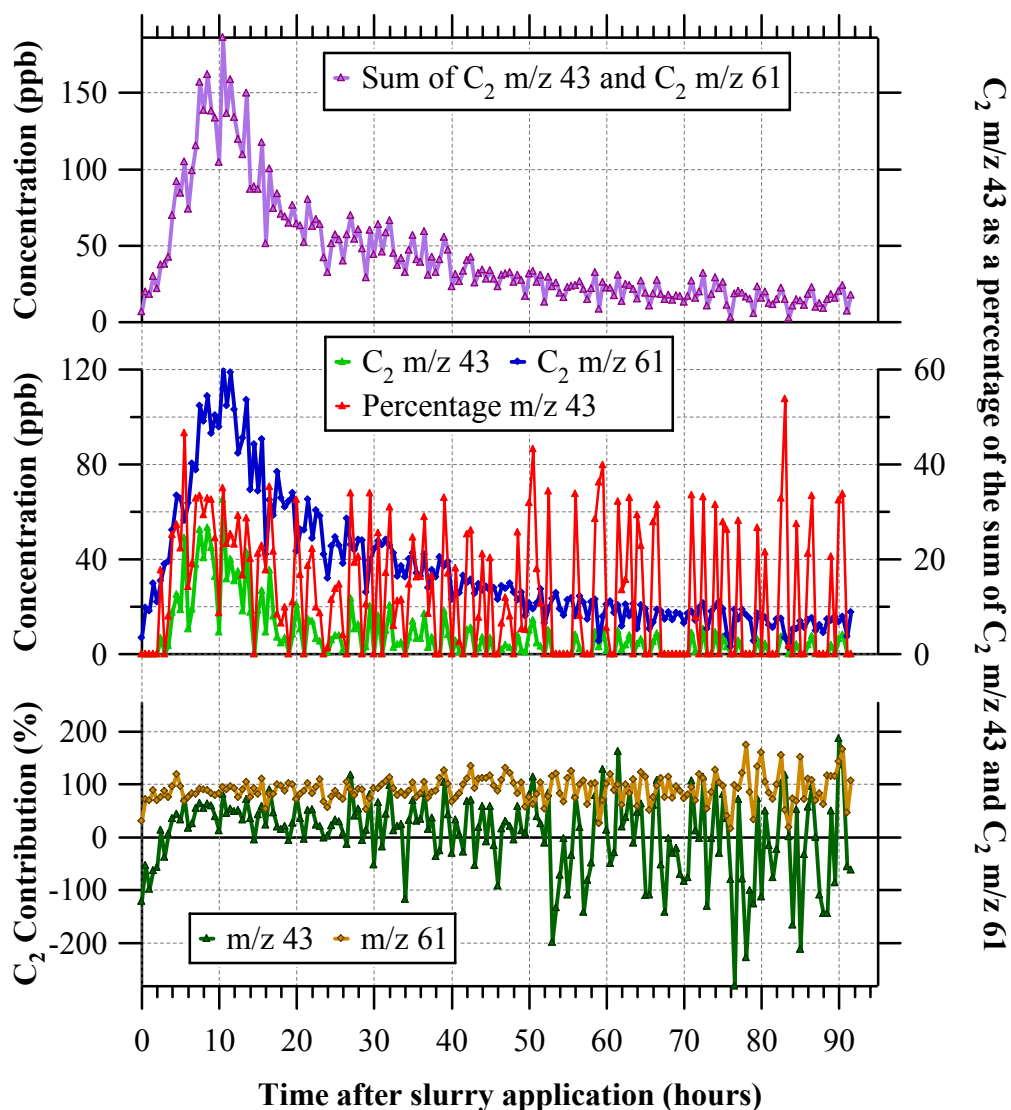
Figure 4.15: The percentage contribution of C_2 molecules to m/z 43 (dark green) and m/z 61 (brown) during laboratory experiment two. The resulting C_2 concentrations at m/z 43 (light green) and m/z 61 (blue) and consequent C_2 m/z 43 abundance as a percentage of the sum of C_2 m/z 43 and m/z 61 (red) are shown. The sum of C_2 m/z 43 and C_2 m/z 61 (purple) is displayed. Values were calculated from 30 minute averages of SB data.
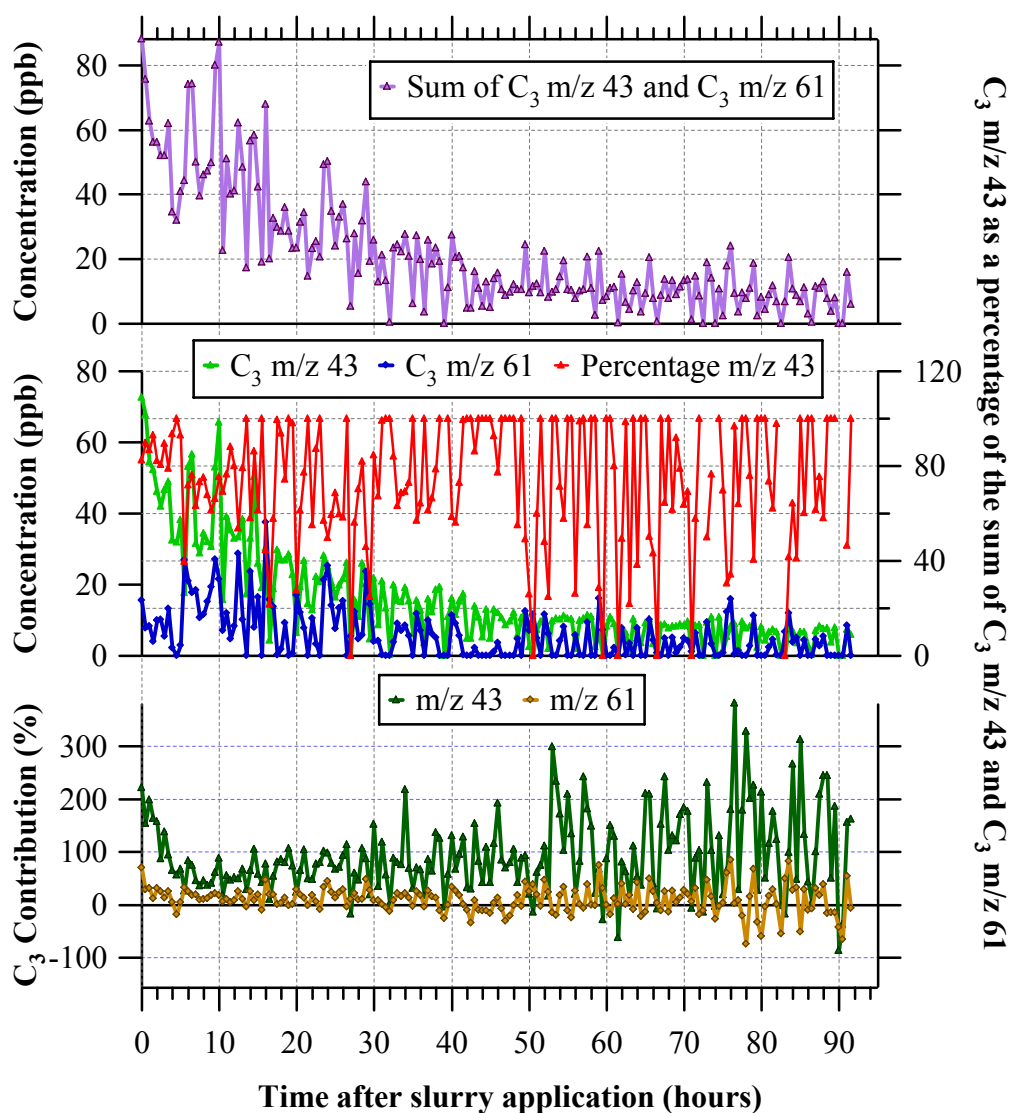
Figure 4.16: The percentage contribution of C_3 molecules to m/z 43 (dark green) and m/z 61 (brown) during laboratory experiment 2. The resulting concentrations of C_3 molecules at m/z 43 (light green) and m/z 61 (blue) and consequent C_3 m/z 43 abundance as a percentage of the sum of C_3 m/z 43 and C_3 m/z 61 (red) are shown. The sum of C_3 m/z 43 and C_3 m/z 61 is displayed (purple). Values were calculated from 30 minute averages of SB data.
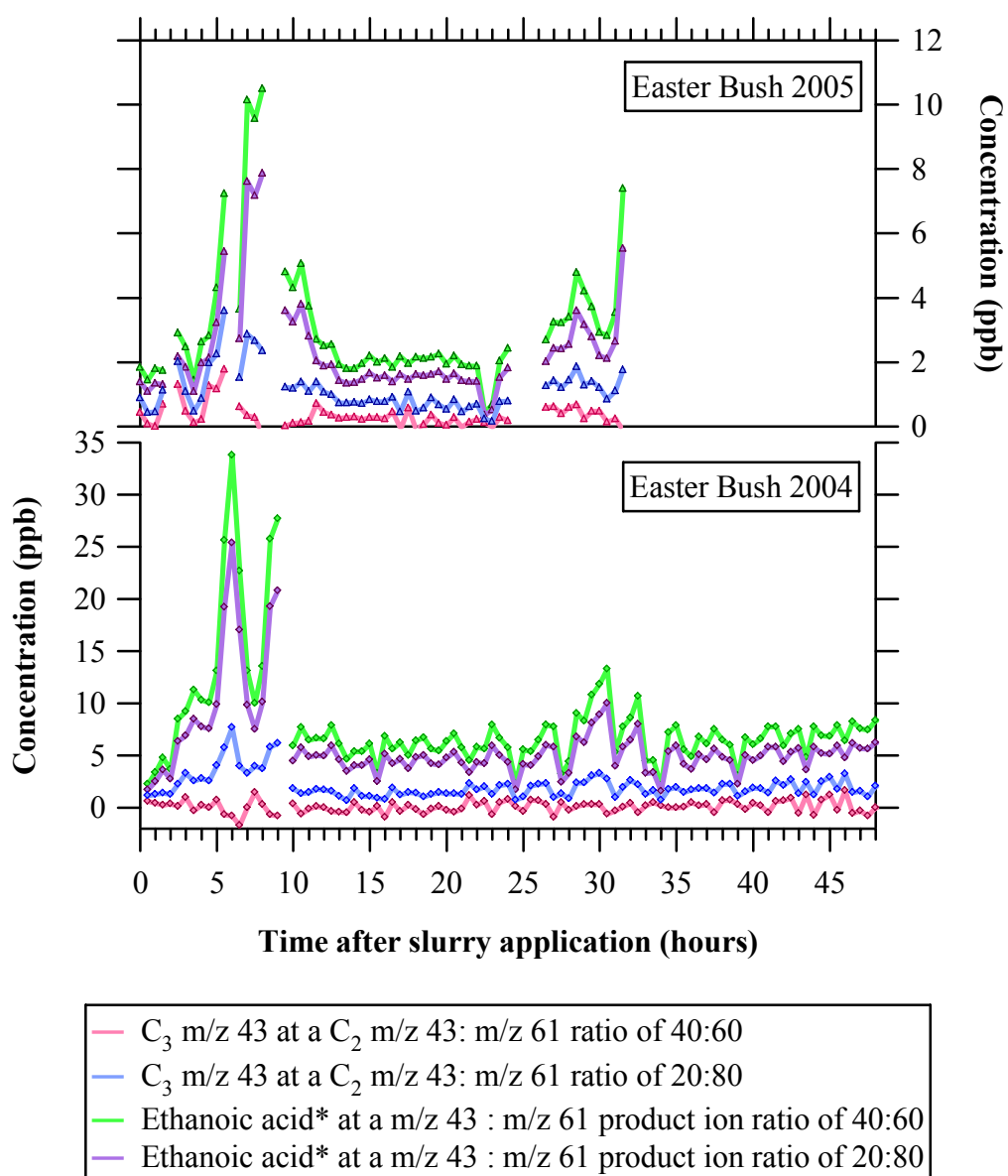
Figure 4.17: Approximate concentrations of ethanoic acid *and contributing esters during fertilisations at Easter Bush in 2004 and 2005. Concentrations were calculated assuming that m/z 61 consists of ethanoic acid alone and that a further 20 (purple) to 40 % (green) of the total product ions occurred at m/z 43. The concentrations at m/z 43 after subtraction of the ethanoic acid contribution (~25 % (blue) to ~ 67 % (pink) of m/z 61).

The non-dissociative product of the reaction of H_3O^+ with propanoic acid, $C_3H_7O_2^+$, occurs at m/z 75. Propanoic acid also reacts with H_3O^+ *via* dissociative elimination of H_2O to form $C_3H_5O^+$ at m/z 57. The m/z 57 ion forms 10 % of product under the thermal conditions of SIFT (§ 3.3.1, Table 3.13, and 31. 7 % in the PTR-MS at *EN* 145 Td (P_{dt} 2.0 mbar, T_{dt} 333 K, *E* 63.2 V cm^{-1}) (§ 3.3.1, Table 3.14). The non-dissociative product of C_4 alcohols ($C_4H_{11}O^+$) theortically corresponds to m/z 75, however in the PTR-MS these higher alcohols react completely by elimination of H_2O forming $C_4H_9^+$ at m/z 57 with minor additional

fragmentation to m/z 41 (§ 3.1.1, Table 3.4). The variation of m/z 75 and m/z 57 during laboratory experiments one and two and during fertilisations at Easter Bush in 2004 and 2005 are shown in Figure 4.18.
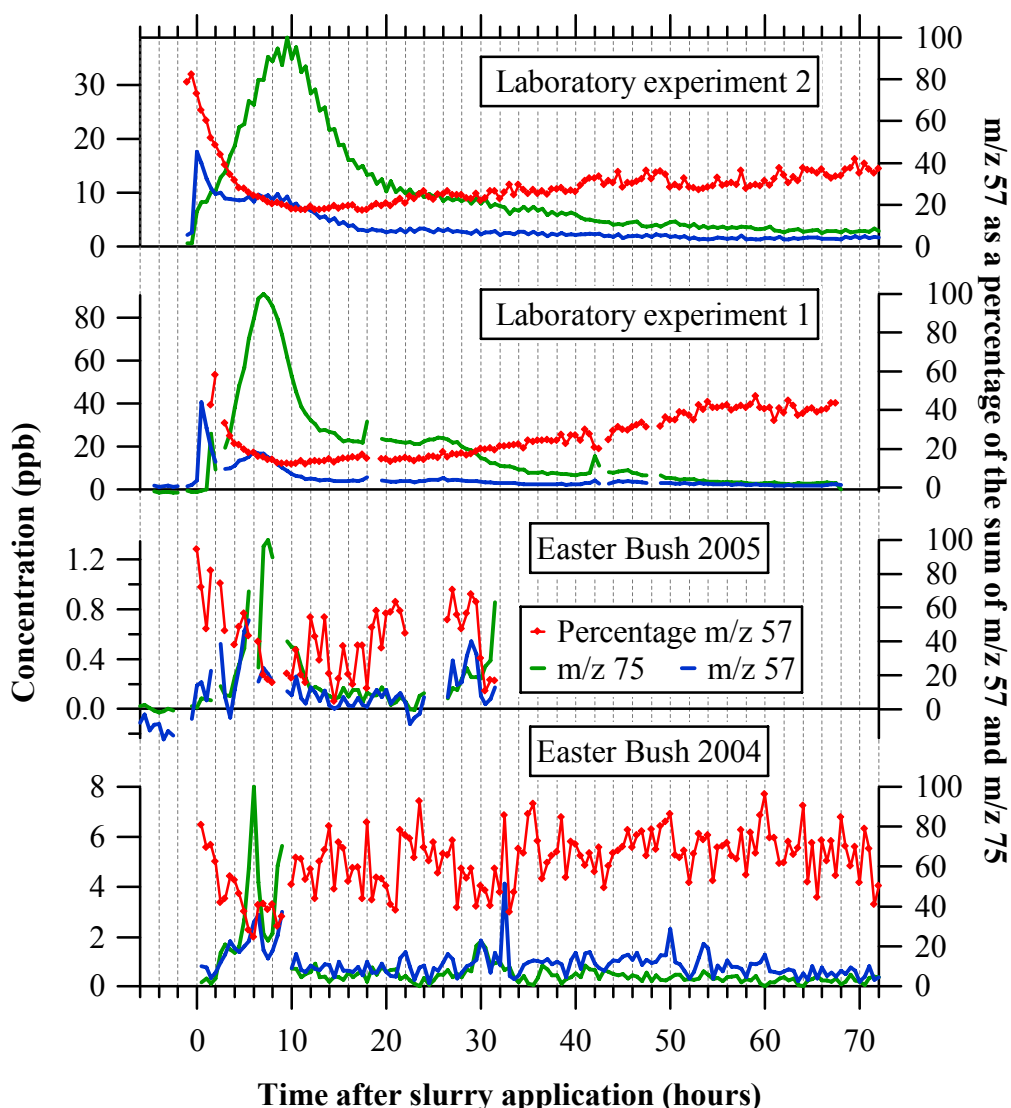
Figure 4.18: The concentrations of m/z 57 and m/z 75 during laboratory experiments one and two and fertilizations at Easter Bush in 2004 and 2005. Concentrations are half hourly means of the SB data. Concentrations are given as a function of time elapsed after initial slurry application. The starts of applications (0 hours) correspond to 08:00 (GMT) 28/09/04, 08:00 (GMT) 27/04/05, 14:30 (GMT) 11/04/06 and 13:00 (GMT) 14/04/06 for Easter bush 2004, Easter Bush 2005 and laboratory experiment 1 and 2. The percentage of the sum of m/z 75 and m/z 57 contributed by m/z 57 is also shown.

The relationships between m/z 57 and m/z 75 show similar trends to those observed between m/z 43 and m/z 61 (Figure 4.11). During laboratory experiments 1 and 2, an initial peak in m/z 57 was observed between 0 and 2 hours after slurry application. During this period m/z 57 formed 60 to 80 % of the net m/z 57 and m/z 75 intensity. A secondary peak in m/z 57 correlated with the peak in m/z 75 was subsequently observed with a maxima at ~ 7.5 and

10.0 hours after slurry application in laboratory experiment 1 and 2 respectively. The m/z 57 abundance as a percentage of count rates at m/z 57 and m/z 75 decreased following the initial peak in m/z 57 as m/z 75 increased. The m/z 57 abundance reached a minimum of ~ 12 and 17 % at the peak in m/z 75 during laboratory experiments 1 and 2 respectively, and consequently increased to ~ 40 % toward the end of the experiments.

During fertilisation at Easter Bush in 2005 an initial peak in m/z 57 was observed between one and a half to two hours after slurry application. The m/z 57 ion formed 81.9 % to 74.2 % of net m/z 57 and m/z 75. A further peak was observed at five and a half hours after application at which point m/z 57 formed 56.4 % of the total of m/z 57 and m/z 75. During a third peak between 7.5 and 10 hours after slurry application m/z 57 was 17.8 ± 2.2 %. After the beginning of fertilisation on 29/09/05 at 26.5 to 29.5 hours after the initial fertilization (28/09/05) a peak in m/z 57 was observed; m/z 57 contributing 59.0 ± 8.5 % to the sum of m/z 57 and m/z 75. A peak in m/z 75 was observed from 30 hours to 31.5 hours during which m/z 57 formed 18.5 ± 8.1 % of net m/z 57 and m/z 75. During fertilisation at Easter Bush in 2004 m/z 57 and m/z 75 peaked at 6 hours after initial slurry application. The m/z 57 abundance decreased from around 80 % at the start of fertilisation to 25 % during the peak in m/z 57 and m/z 75. The m/z 57 abundance increased following the peak in m/z 57 and m/z 75 to between 40 and 80 % for the remainder of fertilisation.

The measured ratios of m/z 75: m/z 76 during fertilisations at Easter Bush was highly variable, suggesting another contributor at m/z 76. The measured m/z 75: m/z 76 ratio during laboratory experiments 1 and 2 was used to derive the percentage contribution of C_3 and C_4 molecules to m/z 75. The results are shown in Figure 4.19. A value of 100 % C_3 molecules corresponds to an m/z 76 intensity of 3.27 % of m/z 75, a value of 100 % C_4 molecules corresponds to an m/z 76 intensity of 4.37 %. C_3 molecules dominated m/z 75 during both laboratory experiments.

In addition to propanoic acid, a well established emission from slurry (Appendix D), a number of esters form $C_3O_2H_7^+$ ions at m/z 75 in the PTR-MS. The non-dissociative products of ethyl formate and methyl acetate occur at m/z 75. In SIFT (PTR-MS measurements unavailable) m/z 75 formed 95 % of the product ions from ethyl formate (< 5 % at m/z 47) (Španěl and Smith 1998a). In PTR-MS, m/z 75 forms 91.7 % of product ions from methyl acetate (V_{drift} 600 V, l_{dt}, P_{dt}, T_{dt}, E/N not specified) (Buhr *et al* 2002) and 100 % in SIFT (Španěl and Smith 1998a).
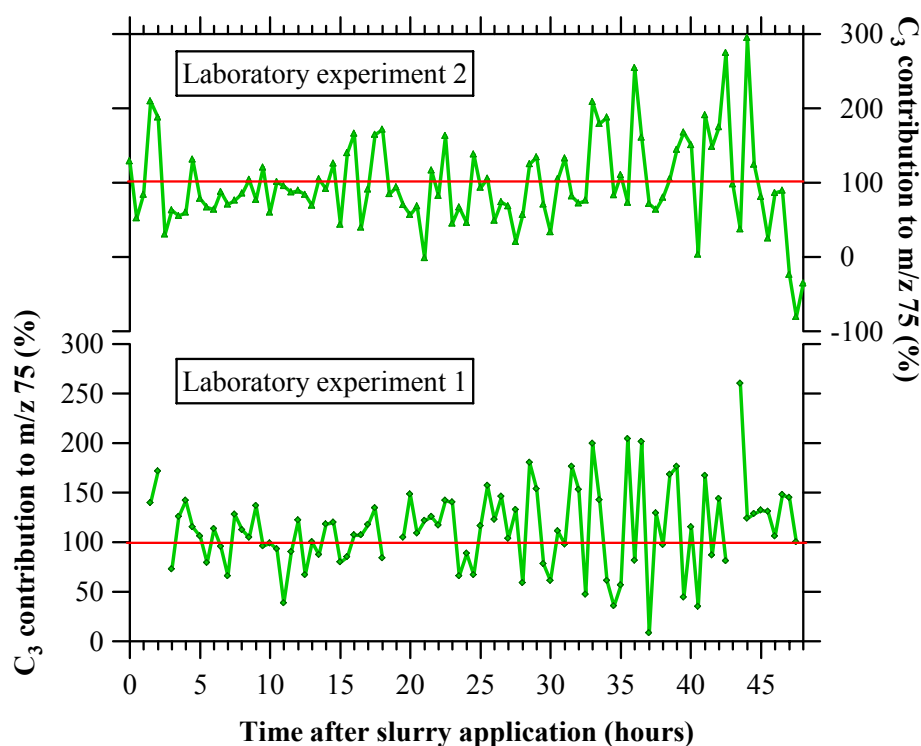
Figure 4.19: The percentage contribution of C_3 molecules to m/z 75 calculated from the measured ratio of m/z 76 to m/z 75 and ^{13}C isotopic abundancies. Values were calculated from 30 minute averages of SB data.

Ethyl, propyl and butyl propionate form $C_3O_2H_7^+$ (m/z 75) and $C_3H_5O^+$ (m/z 57) fragment ions in the PTR-MS; product distributions are shown in Table 4.8.

Table 4.8: The Henry's Law constants (K_{HL}) of selected esters and product distributions from their reaction with H_3O^+.

Ester (M)	K_{HL} (mol kg^{-1} bar)	Product ion as a Percentage of Total Product Ions			
		MH^+ (m/z)	$C_3O_2H_7^+$ (m/z 75)	$C_3H_5O^+$ (m/z 57)	Other (m/z)
Ethyl propionate	4.6	(103): 36.7[a] 95[b]	55.6[a]	7.8[a] 5[b]	
Propyl propionate	2.6	(117) 25.2[c]	44.2[c]	27.9[c]	(93): 2.7[c]
Butyl propionate		(131) 12.7[c]	66.7[c]	20.7[c]	

Note: Henry's Law constants are from Mallard and Linstrom (2005). Product distributions are taken from: [a]Buhr *et al* (2002) measured in PTR-MS at V_{drift} 600 V (l_{dt}, P_{dt}, T_{dt}, E/N not specified), [b]Španěl and Smith (1998a) measured in SIFT at P_{FT} 0.67 mbar, T_{FT} 300 K. [c]Aprea *et al* (2007a) measured in PTR-MS $E/N \sim 120$ Td, P_{dt} 2.03 mbar and T_{dt} 323 K therefore V_{drift} ~ 55 V cm^{-1}). Values in [a] and [c] were given as relative abundances (normalised with the dominant product ion 100) and were converted to percentage product ion distributions to one decimal place.

Sunesson *et al* (2001) observed concentrations of 0.07 ppb to 0.96 ppb ethyl propionate in the air of dairy farms. No measurements of the propionates directly from animal waste could be found. The non-dissociative product ion of ethyl propionate occurs at m/z 103. Peak concentrations of m/z 103 were 7.27 ppb and 10.63 ppb during laboratory experiments 1 and 2 respectively. Assuming C_5 carboxylic acids and other esters make no contribution to m/z 103, and given the product distributions in the literature (Table 4.7) indicates maximum ethyl propionate concentrations of 19.8 ppb and 10.6 ppb during laboratory experiments 1 and 2 respectively. Thus ethyl propionate appears to make little contribution to m/z 75 and m/z 57 particularly given that previous measurements (Appendix D) indicate the presence of C_5 carboxylic acids at m/z 103 is likely. The peak concentrations of m/z 117 and m/z 131 and the reported product distributions from propyl propionate and butyl propionate respectively (Table 4.7) indicate upper limit peak concentrations of 1.63 and 1.11 ppb propyl propionate and 0.76 ppb and 0.47 ppb butyl propionate from laboratory experiments 1 and 2 respectively.

The ratio of m/z 57: m/z 58 cannot be used to determine the contribution of C_3 and C_4 molecules to m/z 57 due to the occurrence of another product ion, tentatively identified as a fragment of trimethylamine, at m/z 58 (§ 4.3.3.4). Likewise the m/z 57: m/z 59 ratio cannot be used to determine the number of oxygens present due to the occurrence of another compound(s) at m/z 59. The total propanoic acid concentration may be estimated by assuming $C_3H_7O_2^+$ from propanoic acid is the sole contributor to m/z 75 and applying propanoic acid product distributions observed by von Hartungen *et al* (2004) (§ 3.3.1, Table 3.14). However if 32 % of the m/z 75 concentration is subtracted from the m/z 57 concentration, negative concentrations result from 4 hours after slurry application during the peak in m/z 75. This may reflect the contribution of molecules such as methyl acetate and/or ethyl formate to m/z 75 which do not form product ions at m/z 57. It is also probable that the degree of fragmentation during these measurements was less than that observed by von Hartungen *et al* (2004) (§3.31, Table 3.14). An *E/N* of 145 Td (P_{dt} 2.0 mbar, T_{dt} 333 K, *E* 63.2 V cm^{-1}) was employed by von Hartungen *et al* (2004), the *E/N*, and thus energy available for dissociation, was reduced at ~ 127 Td (P_{dt} ~2.0 mbar, T_{dt} 318 K, *E* ~ 57.9 V cm^{-1}) in the laboratory experiments here.

If the minima in the abundance of m/z 57 as a percentage of m/z 75 (Figure 4.19) is taken to be the product distribution of propanoic acid, the product distributions collated in Table 4.9 result. This assumes propanoic acid is the only contributor to m/z 57 (in addition to m/z 75) at this point. The abundancies at the peak in m/z 75 are also shown in Table 4.9. All of the values, except those corresponding to the minima during fertilisation at Easter Bush in 2005,

lie between the product distributions observed from propanoic acid in SIFT (10 % m/z 57: 90 % m/z 75) (§ 3.3.1, Table 3.13) and those observed in the PTR-MS at E/N of 145 Td (P_{dt} 2.0 mbar, T_{dt} 333 K, E 63.2 V cm^{-1}) by Von Hartungen et al (2004) (§ 3.3.1, Table 3.4). The concentrations of m/z 75 and m/z 57 at the m/z 57 abundance minima were close to zero (0.08 ppb and 0.003 ppb respectively), the distribution observed at the peak in m/z 75 is closer to those observed during fertilisation at Easter Bush in 2004 and the laboratory experiments. These values of product ion distributions were used to derive propanoic acid concentrations (assuming propanoic acid was the only contributor to m/z 75) during the fertilisations at Easter Bush and the laboratory experiments and are displayed in Figure 4.20. The remaining concentrations at m/z 57 are shown in Figure 4.20.

Table 4.9: The minimum abundancies of m/z 57 as a percentage of m/z 57 and m/z 75 and, in brackets, those at the peak in m/z 75 concentrations. The times after intial applications of slurry at which the abundancies were observed are shown. The minima values are those from the periods from 0 hours after slurry application onward during the laboratory experiments and fertilisation at Easter Bush in 2005, and from 0 to 72 hours after application during fertilisation at Easter Bush in 2004.

Measurement	Product abundance (%)		Time after slurry application (hours)
	m/z 57	m/z 75	
Laboratory experiment 1	12 (16)	88 (84)	10.0 (7.0)
Laboratory experiment 2	17 (19)	83 (81)	17.5 (9.5)
Easter Bush 2005	4 (17)	96 (83)	14.5 (7.5)
Easter Bush 2004	25 (25)	75 (75)	6.0 (6.0)

The concentrations at m/z 57 remaining after subtraction of the approximated propanoic acid contribution (Figure 4.20) may correspond to C_4 alcohols which occur predominantly at m/z 57 in the PTR-MS with some minor fragmentation to m/z 41 (§ 3.1.1, Table 3.4). The m/z 57 ion is also the dominant product from 1-pentanol and C_6 to C_9 alcohols form fragments at m/z 57 (§ 3.1.1, Table 3.4). A large number of esters produce ions at m/z 57 in the PTR-MS (Aprea et al 2007a, Buhr et al 2002). C_4 to C_{13} alkenes form $C_4H_9^+$ ions at m/z 57 on reaction with H_3O^+ (§ D.1.2, Table D.8). Butyl nitrate isomers (Aoki et al 2007) and propenal also form product ions at m/z 57. Given the underlying microbial processes determining emissions from slurry, the alcohols and esters are perhaps the most likely candidates. C_4 to C_8 alcohols and a range of esters have been observed and quanitifed, using GC based techniques, in the vicinity of animals and their waste (e.g. Rabaud et al 2003, Filipy et al 2006, Beck et al 2007, Sunneson et al 2001).

The formation of $[MHH_2O]^+$ ions has been observed from non-dissociated alcohol ions (§ 3.1.2) and the non-dissociative and dissociative products of the carboxylic acids (§ 3.3.2). In the case of ethanoic acid this association complex occurs at m/z 79 and in the case propanoic

acid at m/z 93. The m/z 79 and m/z 93 ions did not increase above levels observed prior to fertilisation at Easter Bush in 2005 or post fertilisation at Easter Bush in 2004. Increases in m/z 79 and m/z 93 ions were observed during both laboratory experiments (Figure 4.21). Concentrations at these m/z were not well correlated with those of the acids. Other possible contributors to m/z 79 include benzene (§ D.2.1), dimethylsulphoxide, a dimethyldisulphide fragment (§ 3.4.1, Table 3.17), a thioethanol fragment (§ 3.4.1, Table 3.16) and benzaldehyde (Malekina *et al* 2007). Toluene occurs at m/z 93 (§ D.2.1).
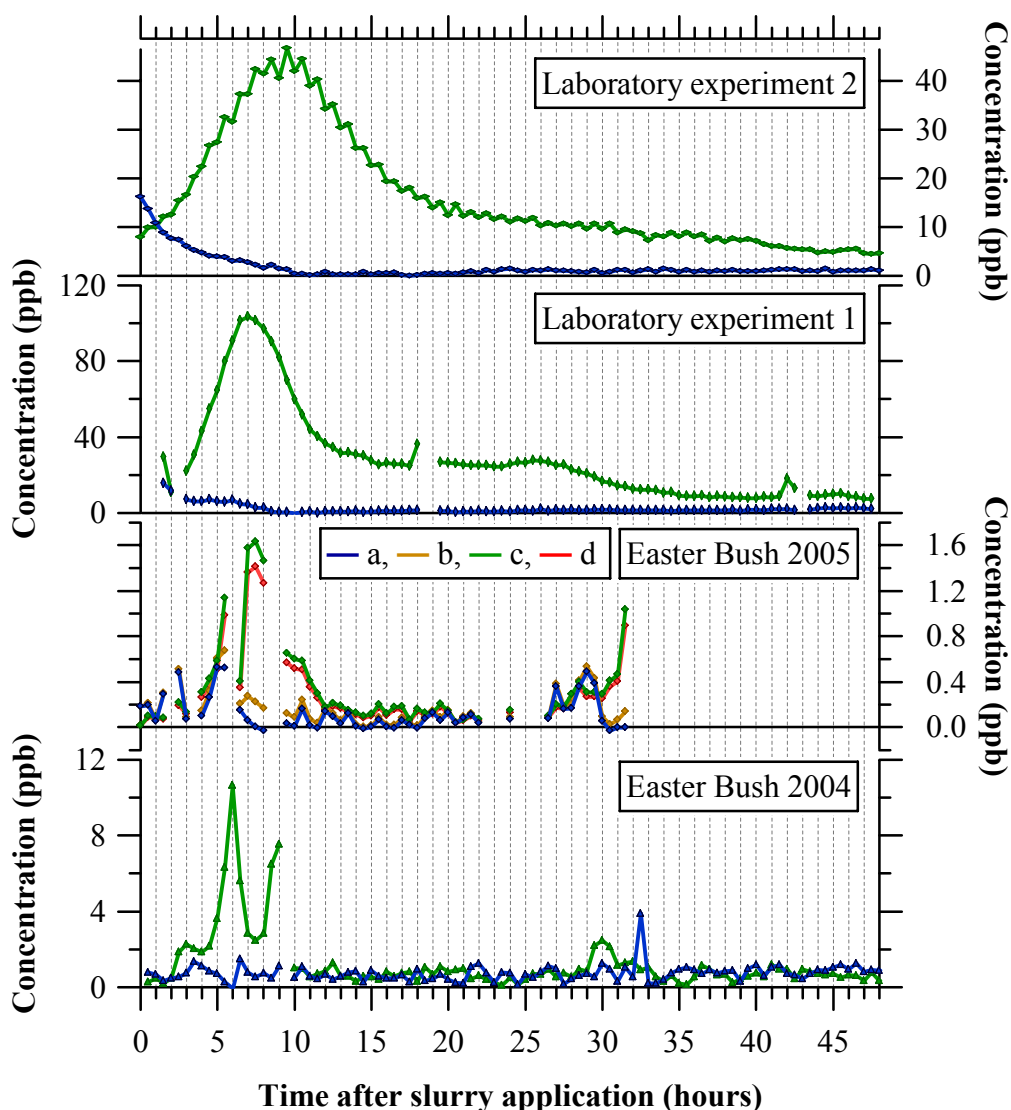
Figure 4.20: Concentrations of propanoic acid (green, red) calculated by assuming that m/z 75 corresponds to propanoic acid alone and deriving an approximation of the product distribution from propanoic acid from the minimum in the measured m/z 57: m/z 75 ratio (a), or, the measured m/z 57: m/z 75 ratio at the peak in m/z 75 concentrations (b). Concentrations remaining at m/z 57 (blue, brown) after subtraction of the propanoic acid contribution derived from the minima in m/z 57: m/z 75 ratio (c) or the m/z 57: m/z 75 ratio at the peak in m/z 75 concentrations (d) are shown.
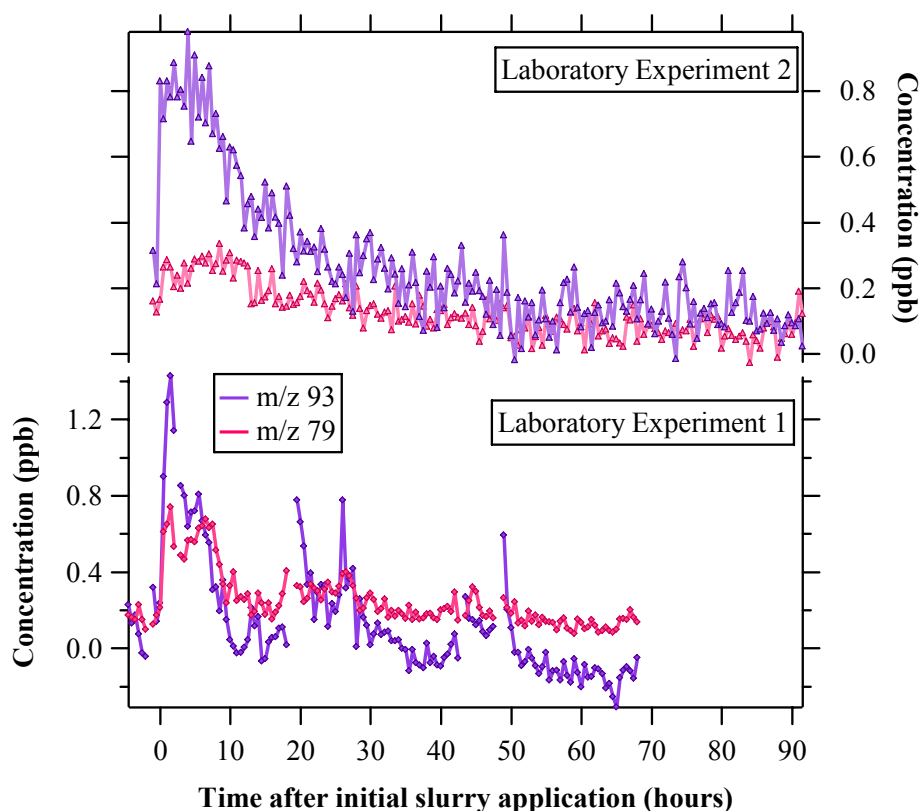
Figure 4.21: The concentrations of m/z 79 and m/z 93 during laboratory experiments 1 and 2. The subtraction of instrument background from m/z 79 during experiment 2 resulted in negative concentrations and was therefore excluded.

4.3.3.2 Aromatics

Increases in m/z 95 and m/z 109 were observed during both fertilisations at Easter Bush and during laboratory experiments 1 and 2 and are displayed in Figure 4.22. The m/z 95 and m/z 109 concentrations were strongly correlated during all measurements. During laboratory experiment 1, the R^2 from 0 hours after slurry application was 0.95; during laboratory experiment 2, the R^2 from 0 hours onwards was 0.89. The R^2 of m/z 95 with m/z 109 was 0.87 from 0 hours after the initial slurry application onward during fertilisation at Easter Bush, 2005. The R^2 of m/z 95 with m/z 109 during Easter Bush, 2004 from 0 to 48 hours after the initial slurry application was slightly lower at 0.66.

These strong correlations between m/z 95 and m/z 109 suggest a similar source. Phenol and the methyl phenol isomers occur at m/z 95 and m/z 109 respectively. Phenol and 4-methyl-phenol have been observed from animal waste (Appendix D), are both produced from the metabolism of amino acid tyrosine (§ 4.1, Appendix C) and possess similar Henrys Law constants (§ 4.3.5).
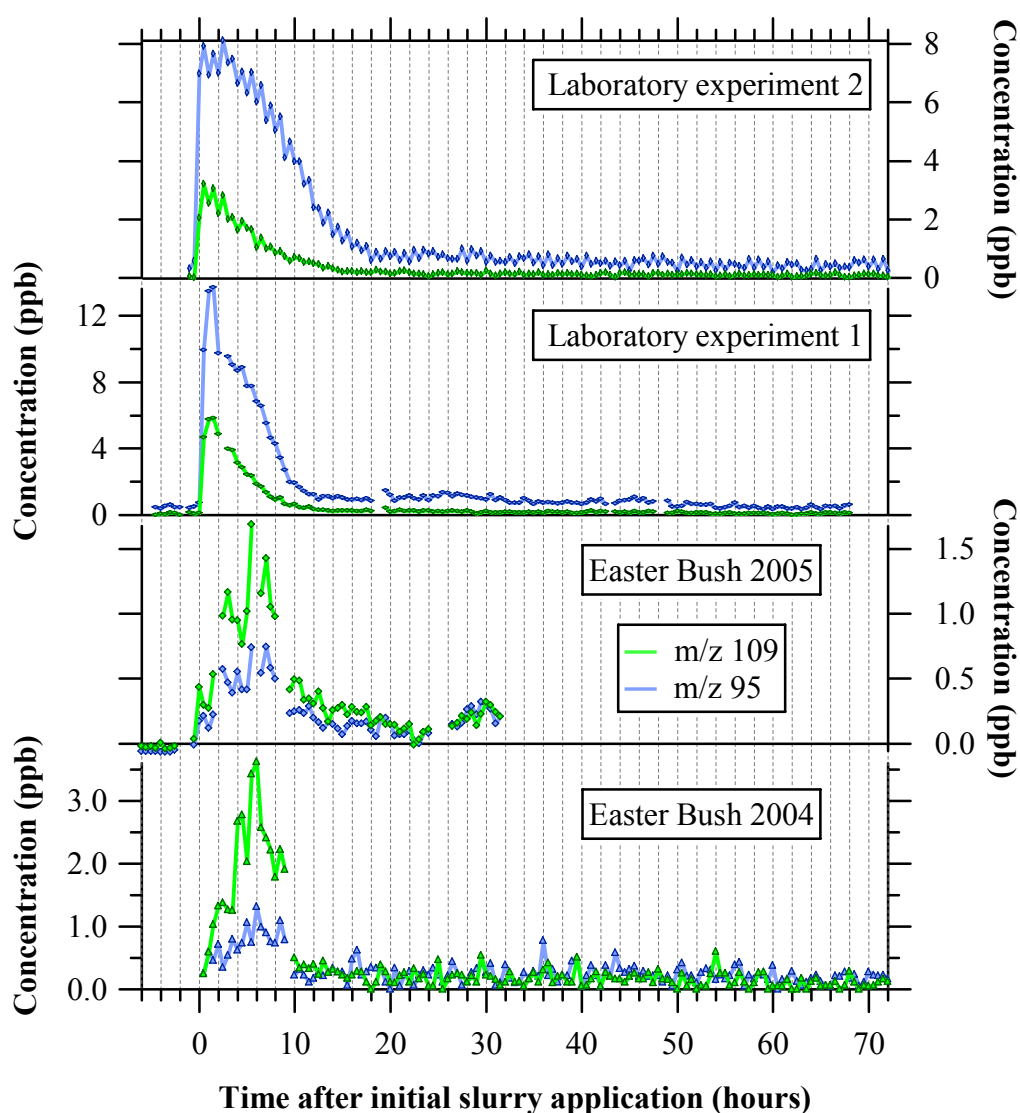
Figure 4.22: m/z 95 and m/z 109 concentrations during fertilizations at Easter Bush in 2004 and 2005 and laboratory experiments 1 and 2. Concentrations are half hourly means of the SB data.

Dimethyldisulphide may also contribute to m/z 95 and has been observed from some animal waste in similar magnitudes to phenol (Appendix D). Dimethyldisulphide is produced from the oxidation of methanethiol. The m/z 49 ion, tentatively identified as methanethiol, peaked at 0.6, 1.1 and 5.7 ppb during fertilisations at Easter Bush in 2005, laboratory experiment 1 and laboratory experiment 2 respectively (§ 4.3.3.3). No increase in m/z 49 was observed during fertilisation at Easter Bush in 2004 (§ 4.3.3.3) which suggests any contribution of dimethyldisulphide to m/z 95 was negligible. In the PTR-MS, a fragment at m/z 79 has also been observed from the reaction of dimethyldisulphide with H_3O^+ (Table 3.17, § 3.4.1), however, several other molecules contribute to m/z 79 (§ 4.3.3.1).

If m/z 95 consisted of phenol alone, the ^{13}C isotope at m/z 96 would be expected to form ~ 6.55 % (6.58% including the ^{17}O isotope contribution) of m/z 95. If m/z 95 was comprised of dimethyldisulphide alone the ^{13}C and ^{33}S isotopes at m/z 96 would be expected to form ~ 3.78 % of m/z 96. The m/z 95 and m/z 96 ions were strongly correlated in laboratory experiment 1 (R^2 0.95 from 0 to 68 hours after slurry application) supporting the assumption that the ^{13}C isotope of m/z 95 is the only contributor at m/z 96. The measured m/z 96 as a percentage of m/z 95 concentration during laboratory experiment 1 is shown in Figure 4.23. During 0 to 9.5 hours after slurry application m/z 96 formed 6.03 ± 1.08 % of m/z 95 suggesting phenol was the dominant contributor to m/z 95.
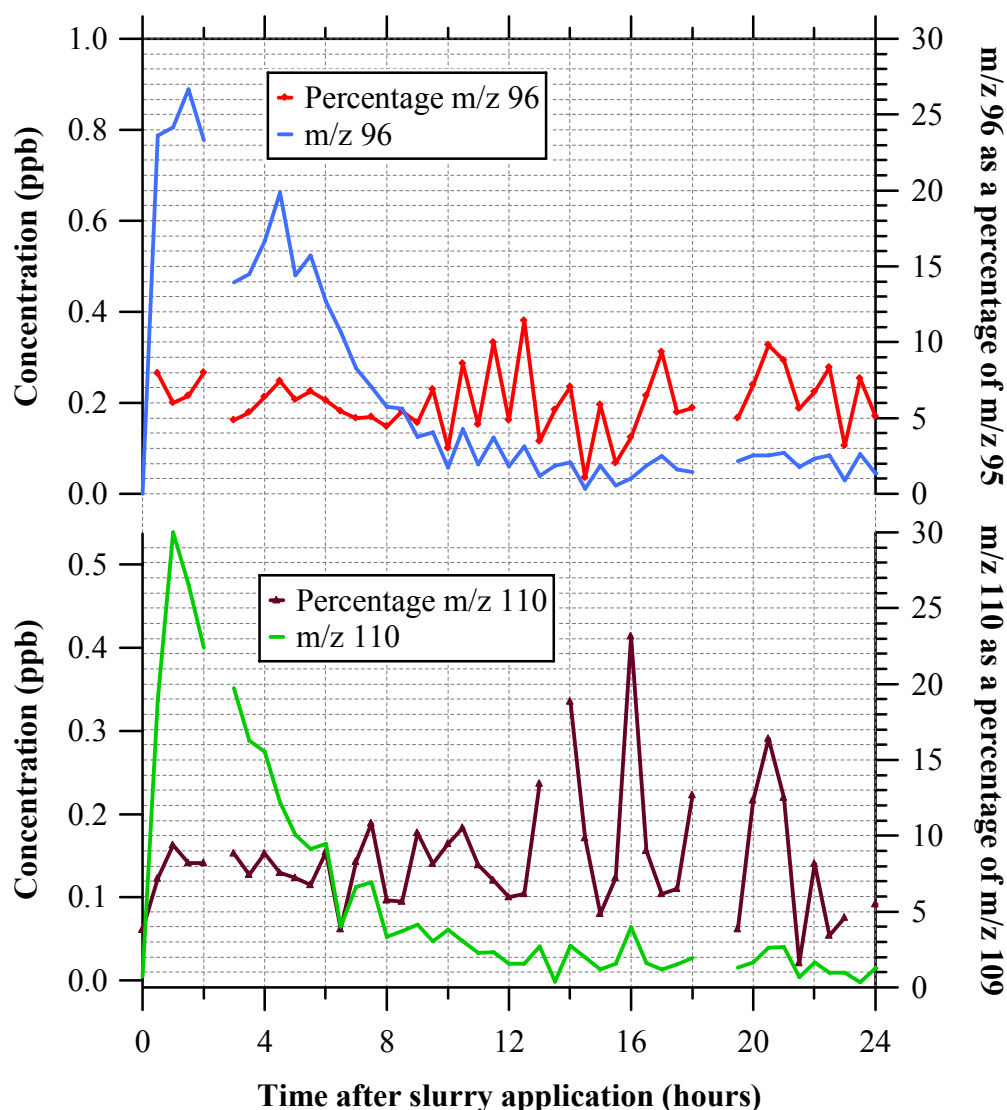
Figure 4.23: The time evolution of m/z 96 during laboratory experiment 1 and the m/z 96 intensity as a percentage of m/z 95 are shown in the upper graph. The m/z 110 concentrations and m/z 110 as a percentage of m/z 109 during laboratory experiment 1 are displayed in the lower graph. Values shown are 30 minute means of SB data and percentages were calculated from these values.

If phenol were the sole contributor to m/z 95, the ^{18}O isomer at m/z 97 would form 0.205 % of m/z 95. If dimethyldisulphide were the lone contributor to m/z 95, the ^{34}S isotope at m/z 97 would form 9.04 % of m/z 95. During laboratory experiment 1 from 0 to 9.5 hours after the slurry application, m/z 97 formed 8.78 ± 3.41 % of m/z 96. However, as shown in Figure 4.24, there appears to have been a background contributor other than the m/z 95 isomer at m/z 96.
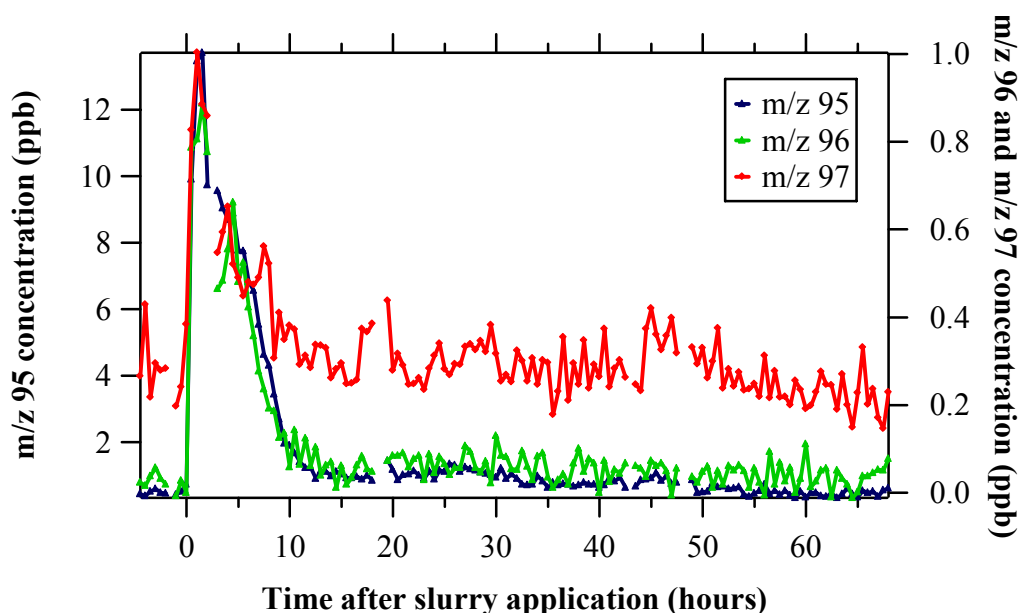
Figure 4.24: The concentrations of m/z 95, m/z 96 and m/z 97 during laboratory experiment 1.

In the case of m/z 109, if methyl phenol was the sole contributor the ^{13}C isotope at m/z 110 would form 7.64 % of m/z 109 (7.68 % including the ^{17}O isotope). During laboratory experiment 1 measured concentrations at m/z 110 formed 7.82 ± 1.72 % of m/z 109 between 0.5 and 9.5 hours after slurry application during which m/z 109 concentrations peaked (Figure 4.23)

During laboratory experiment 2, m/z 96 formed 6.75 ± 1.00 % of m/z 95 from 0 to 14 hours post slurry application, during which m/z 95 concentrations peaked, suggesting phenol dominated m/z 95 (Figure 4.25). As in laboratory experiment 1, another contributor to m/z 97 besides the m/z 95 isotope appears to have been present and this isotope ratio is not considered. The m/z 110 ion formed 6.65 ± 1.95 % from 0 to 14 hours post slurry application (Figure 4.25).
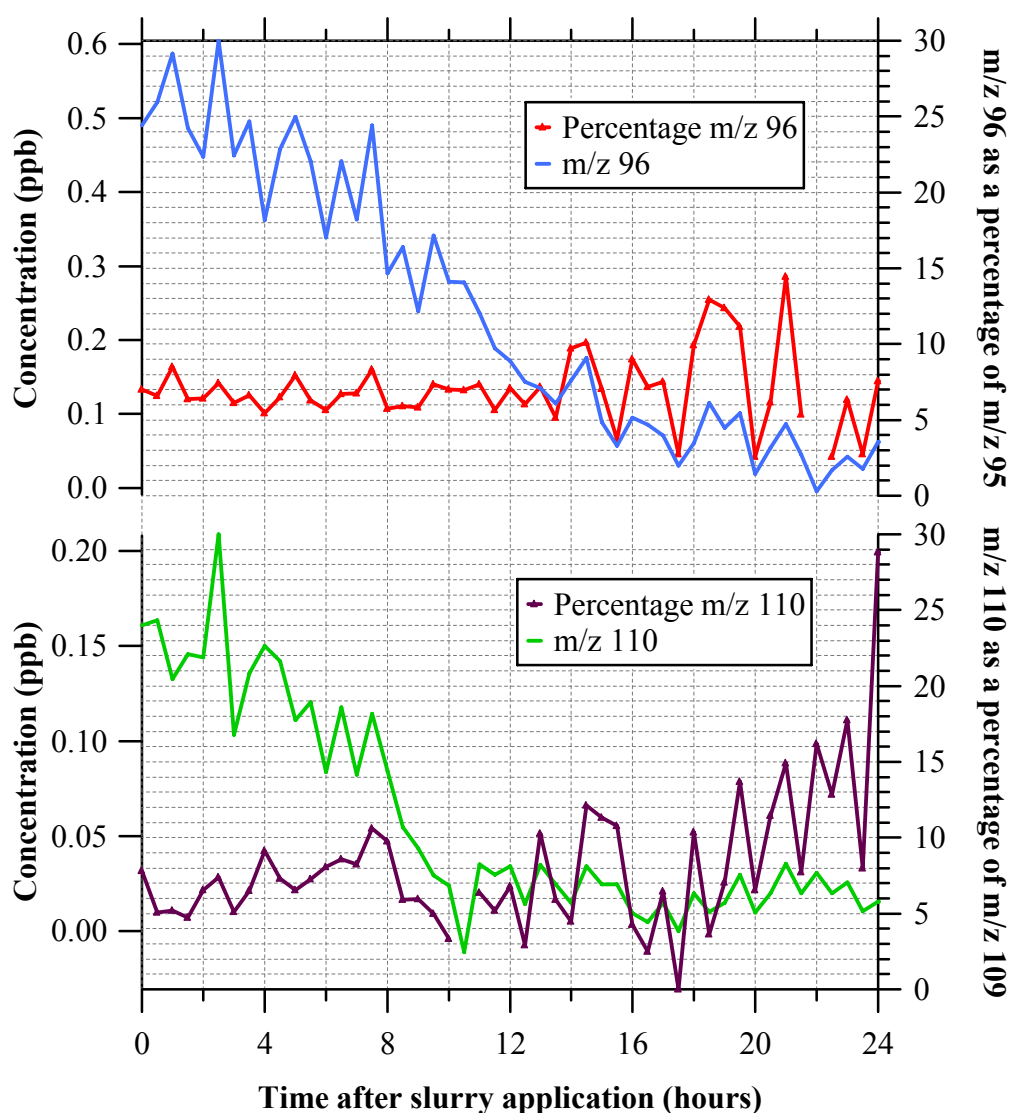
Figure 4.25: The time evolution of m/z 96 during laboratory experiment 2 and the m/z 96 intensity as a percentage of m/z 95 are shown in the upper graph. The m/z 110 concentrations and m/z 110 as a percentage of m/z 109 during laboratory experiment 2 are displayed in the lower graph. Values shown are 30 minute means of SB data and percentages were calculated from these values.

The measured m/z 95: m/z 96 and m/z 109: m/z 110 ratios during fertilisation at Easter Bush in 2004 and 2005 were more variable. The ratios during fertilisation at Easter Bush in 2005 are shown in Figure 4.26. The m/z 96 ion formed a mean of 5.68 ± 2.86 % of m/z 95 and m/z 110 a mean of 6.81 ± 2.04 % of m/z 109 during 2.5 to 8 hours after the initial slurry application, during which m/z 95 and m/z 109 peaked.
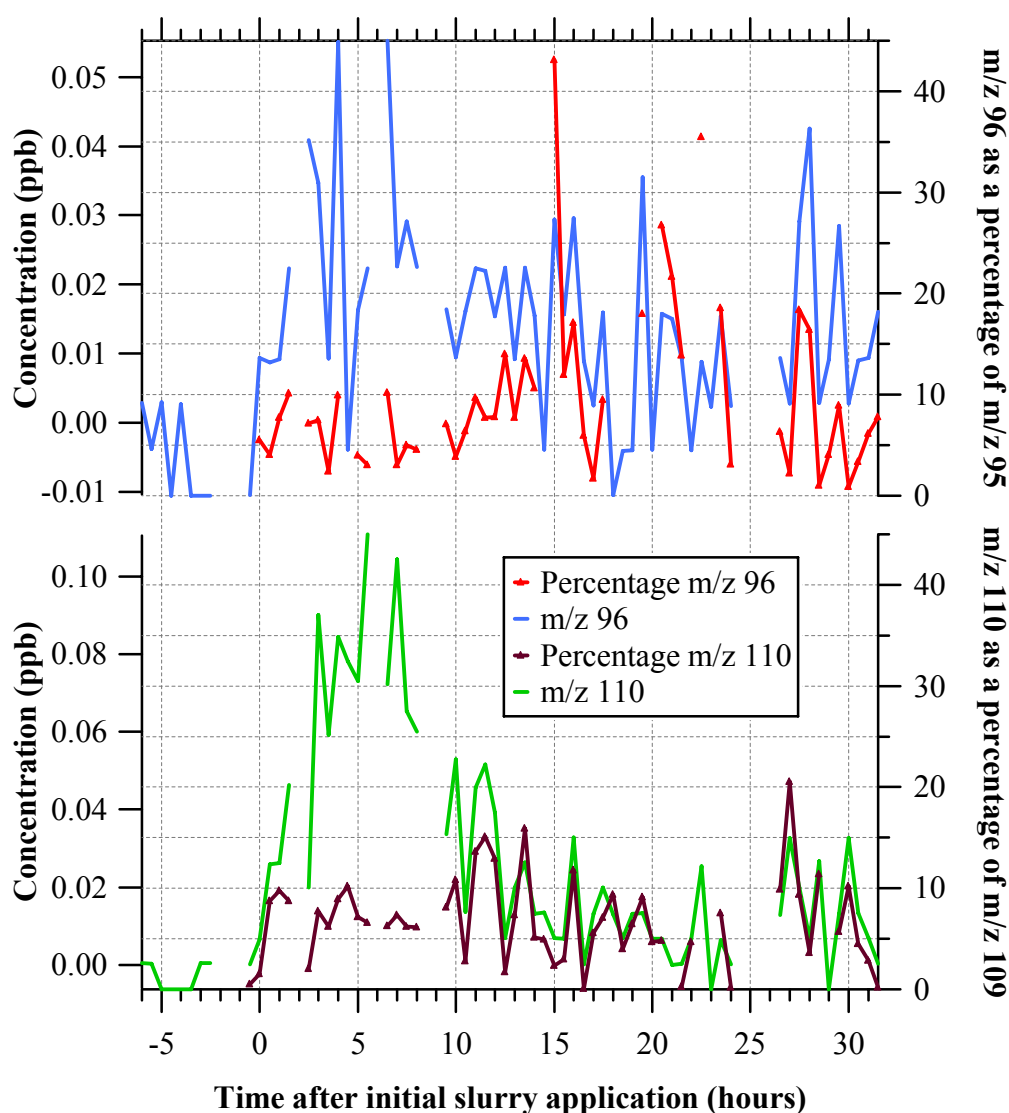
Figure 4.26: The time evolution of m/z 96 during fertilisation at Easter Bush 2005 and the m/z 96 intensity as a percentage of m/z 95 are shown in the upper graph. The m/z 110 concentrations and m/z 110 as a percentage of m/z 109 during fertilisation at Easter Bush 2005 are displayed in the lower graph. Values shown are 30 minute means of SB data and percentages were calculated from these values.

The m/z 95 and m/z 109 ions are tentatively identified as consisting predominantly of phenol and 4-methylphenol respectively. Contributions to m/z 109 from 2- and 3-methylphenol are possible. On the basis of previous measurements of emissions from animal waste (Le 2006, Le *et al* 2005 and references therein), it is likely that concentrations of these isomers are small compared to 4-methylphenol produced from tyrosine degradation. During the fertilisations at Easter Bush, the concentrations of 4-methylphenol (m/z 109) were greater than those of phenol (m/z 95) which is consistent with previous measurements from animal waste (§ 4.1, Appendix D). During the laboratory experiments, the phenol (m/z 95) concentrations exceeded those of 4-methylphenol (m/z 109). The length of slurry storage is

known to effect the relative concentrations of phenollic compounds emitted. This may have contributed here though generally decreases in 4-methyl-phenol and increases in phenol with length of storage have been reported (e.g. Spoelstra 1980, Le 2006 and references therein).

4-ethylphenol is also produced from the degradation of tyrosine (Mackie *et al* 1998, Spoelstra 1977, Le 2006) as well as from *p*-coumoaric acid from plant material (Spoelstra 1980). Product distributions from 4-ethylphenol in the PTR-MS could not be found, only the non-dissociative product, at m/z 123, is formed from reaction with H_3O^+ in SIFT (§ 3.2, Table 3.20). No increase in m/z 123 was observed as a result of fertilisation at Easter Bush in 2004 or 2005. Peaks in m/z 123 were observed during both laboratory experiments (Figure 4.27). 4-ethylphenol is produced from tyrosine in lesser quantities than phenol and 4-methylphenol (Mackie *et al* 1998, Spoelstra 1980) and previous measurements have shown reduced emission of 4-ethylphenol from animal waste (e.g. Hobbs *et al* 1997, Hobbs *et al* 2004) and in the vicinity of animals and there waste (e.g. Sunesson *et al* 2000). Maximum concentrations of m/z 123 during both laboratory experiments were less than those of m/z 95 and m/z 109. It is noteworthy that the correlation of m/z 123 with m/z 95 and m/z 109 was relatively poor i.e. $R^2 < 0.62$.

Protonated benzoic acid may also contribute to m/z 123 (product distributions unknown). Benzoic acid is produced from microbial metabolism of amino acids phenylanaline and tyrosine (Spoelstra 1980, Mackie *et al* 1998). The other ethylphenol isomers and/or phenylethanols may also contribute to m/z 123.

The measured ratio of m/z 123 : m/z 124 and m/z 123 : m/z 125 could not be used to aid identification of contributors to m/z 123 due to the presence of compounds other than the m/z 123 isotopes at m/z 124 and m/z 125.

Indole and 3-methyl indole (skatole) are produced from the degradation of tryptophan (e.g. Spoelstra 1980, Mackie *et al* 1998) and have been observed in air above animal waste (e.g. Willig *et al* 2004, Hobbs *et al* 1998, Hobb *et al* 2004). No measurements of the product distributions from indole or 3-methyl indole in the PTR-MS could be found. However both compounds form only the non-dissociative products at m/z 118 and m/z 123 respectively from reaction with H_3O^+ in SIFT (Wang *et al* 2004). No increases in m/z 132 where observed during fertilisations at Easter Bush in 2004 and 2005 or during the laboratory experiments. No increases in m/z 118 were observed as a result of the fertilisations at Easter Bush, however increases were seen during the laboratory experiments (Figure 4.27). The concentrations at m/z 118 correlated strongly with those at m/z 95 and m/z 109. The R^2

between m/z 118 and m/z 95 was 0.96 and was 0.91 between m/z 118 and m/z 109 from 0 hours after slurry application onwards of laboratory experiment one. During laboratory experiment 2, from 0 hours after slurry application onwards, the R^2 between m/z 118 and m/z 95 was 0.84 and between m/z 118 and m/z 109 was 0.90. The concentrations of indole and skatole have been observed to decrease during prolonged storage (Spoelstra 1980) and this may have contributed to the absence of increases in m/z 118 during fertilisations at Easter Bush.
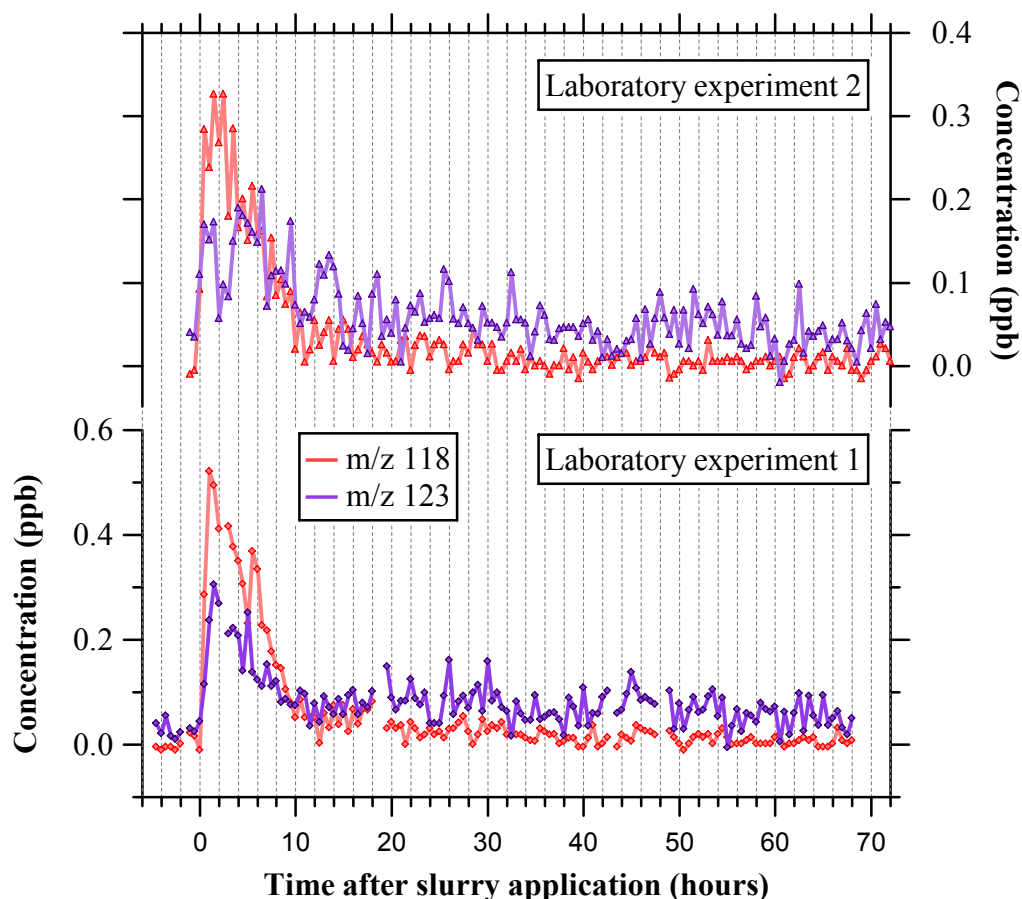
Figure 4.27: The m/z 118 and m/z 123 concentrations during fertilizations at Easter Bush in 2004 and 2005 and laboratory experiments 1 and 2. Concentrations are half hourly means of the scanbargraph data. Concentrations are given as a function of time elapsed after initial slurry application.

4.3.3.3 Sulphur Containing Compounds

Hydrogen sulphide and volatile sulphur containing organic compounds have been observed in the rumen gas of cattle (Dewhurst *et al* 2001), in livestock breathe (Williams *et al* 1999, Hobbs and Mottram 2000) from animal wastes (Appendix D, Banwart and Bremner 1975), in livestock housing (Kim *et al* 2007) and in the viscinity of livestock and their waste (Filipy *et al* 2006).

The reaction of H_3O^+ with hydrogen sulphide produces only the non-dissociative product at m/z 35 in the PTR-MS. The Gibbs free energy of the reaction with H_3O^+ is relatively small (-0.14 eV), the reverse reaction occurs and concentrations may be an underestimation (§ 3.4.1). The ^{18}O isotope of methanol also occurs at m/z 35. The concentrations of m/z 35 with the ^{18}O isotope of methanol subtracted are shown in Figure 4.28 and are denoted m/z 35* hereafter. The methanol isotope contribution was calculated from the m/z 33 concentration assuming m/z 33 consists of methanol alone and that the ^{18}O isotope is 0.205 % of m/z 33.

The non-dissociative products of the reaction of H_3O^+ with dimethylsulphide and ethanethiol occur at m/z 63. Though under slightly differing drift tube conditions dimethylsulphide has been shown to form the non-dissociative product alone in the PTR-MS (§ 3.4.1, Table 3.17). Ethanethiol reacts non-dissociatively with H_3O^+ in SIFT (§ 3.4.1, Table 3.17). Product distributions from the reaction of ethanethiol with H_3O^+ in the PTR-MS could not be found (refer to § 3.4 for further discussion). The ^{18}O isotope of m/z 61 also occurs at m/z 63, an upper limit of this contribution has been approximated and subtracted by assuming that m/z 61 corresponds to $C_2H_5O_2^+$ alone, the resultant m/z 63 concentrations are shown in Figure 4.28 and are denoted m/z 63* hereafter.

Methanethiol reacts with H_3O^+ to produce the non-dissociative product, at m/z 49, in SIFT (§ 3.4.1, Table 3.16). Product distributions in the PTR-MS could not be found and fragmentation under the higher energy conditions cannot be ruled out (§ 3.4). The concentrations at m/z 49 are also shown in Figure 4.28. The ^{18}O isotope of ethanol (m/z 47) was subtracted from m/z 49, denoted m/z 49*, though in this case the isotope contribution was comparably negligible.

In both laboratory experiments no hydrogen sulphide (m/z 35*) was detected. Hydrogen sulphide (m/z 35 *) was observed during both fertilisations at Easter Bush. Higher concentrations of m/z 35* were observed during fertilisation in 2004 than 2005. It is possible that the lack of instrument background measurement in 2004 contributed to this difference. However, the concentrations of close to zero either side of the peaks suggest otherwise. The maximum m/z 35* concentration during fertilisation at Easter Bush in 2005, before background subtraction, was 0.58 ppb and after background subtraction 0.57 ppb. The concentrations of sulphur containing volatiles emitted have been shown to depend on the length of waste storage, diet, concentrations of sulphur containing amino acids in feed, and pH (e.g. Le 2005, Le et al 2007, Stevens and Laughlin 1993). The lower pH of slurry applied during fertilisation at Easter Bush in 2004 (§ 4.3.1) may have contributed to the higher concentrations of hydrogen sulphide as well as the variations in diet (§ 4.2.1.2).

Characteristaion of the PTR-MS for hydrogen sulphide in a similar manner to methanal (Inomata *et al* 2008, § 3.2.3) over a range of drift tube conditions is required for quantification (§ 3.4).
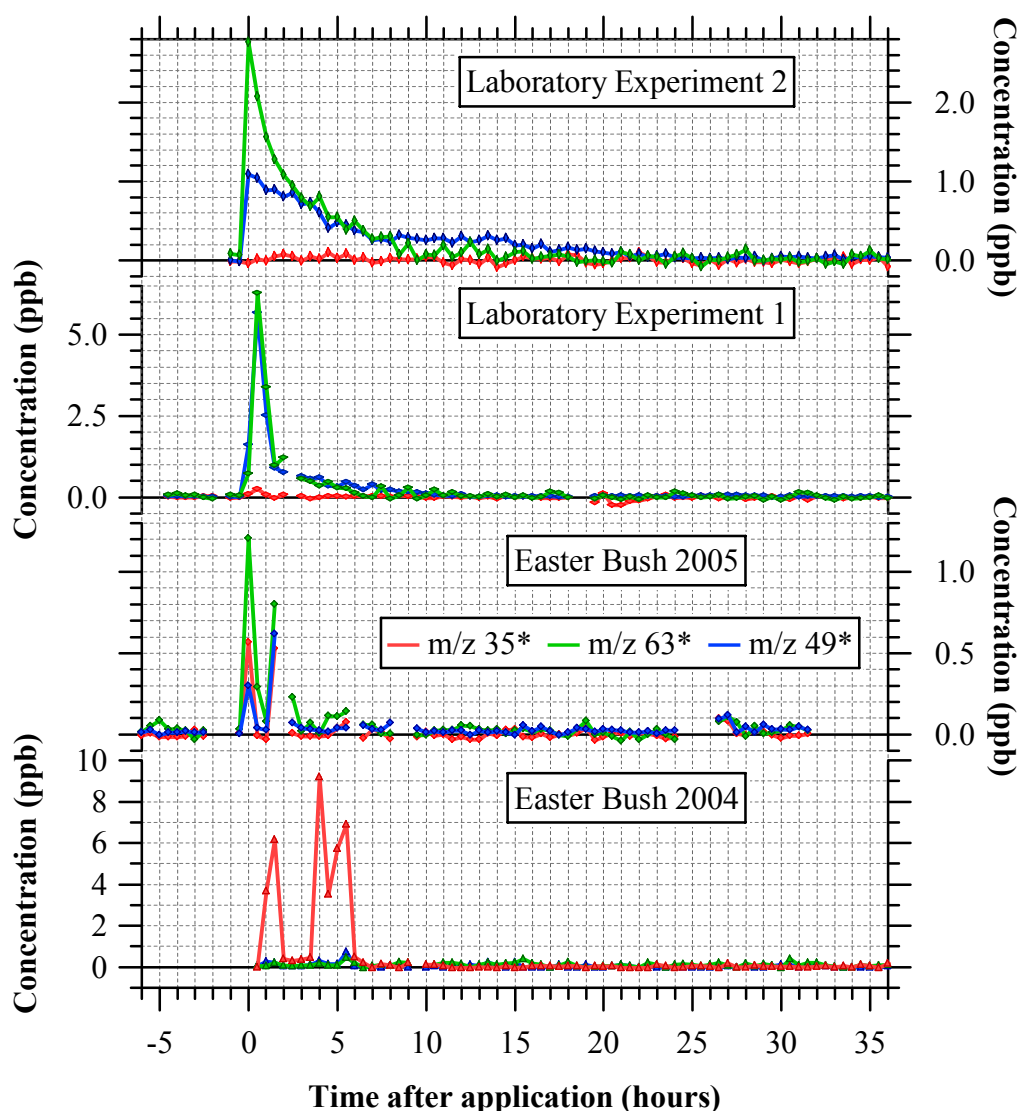
Figure 4.28: Concentrations of m/z corresponding to sulphur containing compounds during fertilisations at Easter Bush in 2004 and 2005 and during laboratory experiments. Values are 30 minute averages of SB data.

The m/z 49 ion, tentatively identified as methanethiol, and m/z 63, identified as dimethylsulphide and/or ethanethiol, were produced during both laboratory experiments and during fertilization at Easter Bush in 2005. Neither m/z 49 nor m/z 63 increased during fertilisation at Easter Bush in 2004.

Hydrogen sulphide is produced primarily as a result of microbial sulphate reduction for assimilatory and dissimilatory processes and amino acid degradation (Appendix C). VOSCs

are also likely to be produced primarily as a result of metabolism of sulphur containing amino acids (Appendix C). These processes are anaerobic and the aeration and agitation of the slurry reduces the production of these sulphur containing compounds (Banwart and Bremner 1975, Stevens and Laughlin 1993) The aeration and agitation during transportation and the process of fertilisation may be responsible for the low concentrations relative to those from anaerobically stored unstirred slurry listed in Appendix D. The extent of adsorption by soils (Appendix C), biological oxidation (Appenidx C) in addition to environmental factors such as concentrations of OH and the consequent lifetime of the relatively short lived VOSCs with respect to atmospheric oxidation may also effect the concentrations of sulphur containing volatiles from animal waste.

In addition to hydrogen sulphide, phosphine may contribute to m/z 35. Initially phosphine concentrations in the range of 8318.4 to 273934 ppb were reported from sediments of sewage plants and shallow lakes (Appendix D). However, such concentrations have not been observed in subsequent measurements and would be fatal if inhaled (WHO 1988, Glindemann and Bergmann 1995). Phosphine concentrations in the range of ~0 to 33 ppb have been observed in measurements from animal waste over the last decade (Appendix D). Where phosphine and hydrogen sulphide have been measured concurrently, hydrogen sulphide concentrations have greatly exceeded those of phosphine (Eismann *et al* 1997b, Jenkins *et al* 2000, Roels and Versttraete 2005). In example: Eismann *et al* (1997b) observed average concentrations of 86 pl phosphine and 4206 µl hydrogen sulphide from 1 kg of manure. Thus, given the underestimation of hydrogen sulphide mixing ratios in the PTR-MS, it is probable that the contribution of phosphine to m/z 35 was negligible. In future, the sample could be intermittently, passed through a solid $NaOH$ filter to remove hydrogen sulphide (as employed in some GC analysis, e.g. Glindemann and Bergmann 1995) to establish the phosphine concentration.

4.3.3.4 Amines

Previous measurements reported in the literature indicate that trimethylamine and methylamine are the dominant amines emitted in the vicinity of animals and their waste (Appendix C and D). The non-dissociative product of the reaction of H_3O^+ with methylamine is isobaric with O_2^+ at m/z 32 and cannot be measured in the PTR-MS. In SIFT the product ions from the reaction of trimethylamine with H_3O^+ consist of 90 % the non-dissociated product at m/z 60 and 10 % at m/z 58 produced by elimination of H_2 from protonated trimethylamine (§ 3.5, Table 3.21). Product distributions of trimethylamine in the PTR-MS could not be found. Concentrations of m/z 60 and m/z 58 during laboratory

experiments 1 and 2 and fertilisation at Easter Bush in 2004 and 2005, are shown in Figure 4.29.
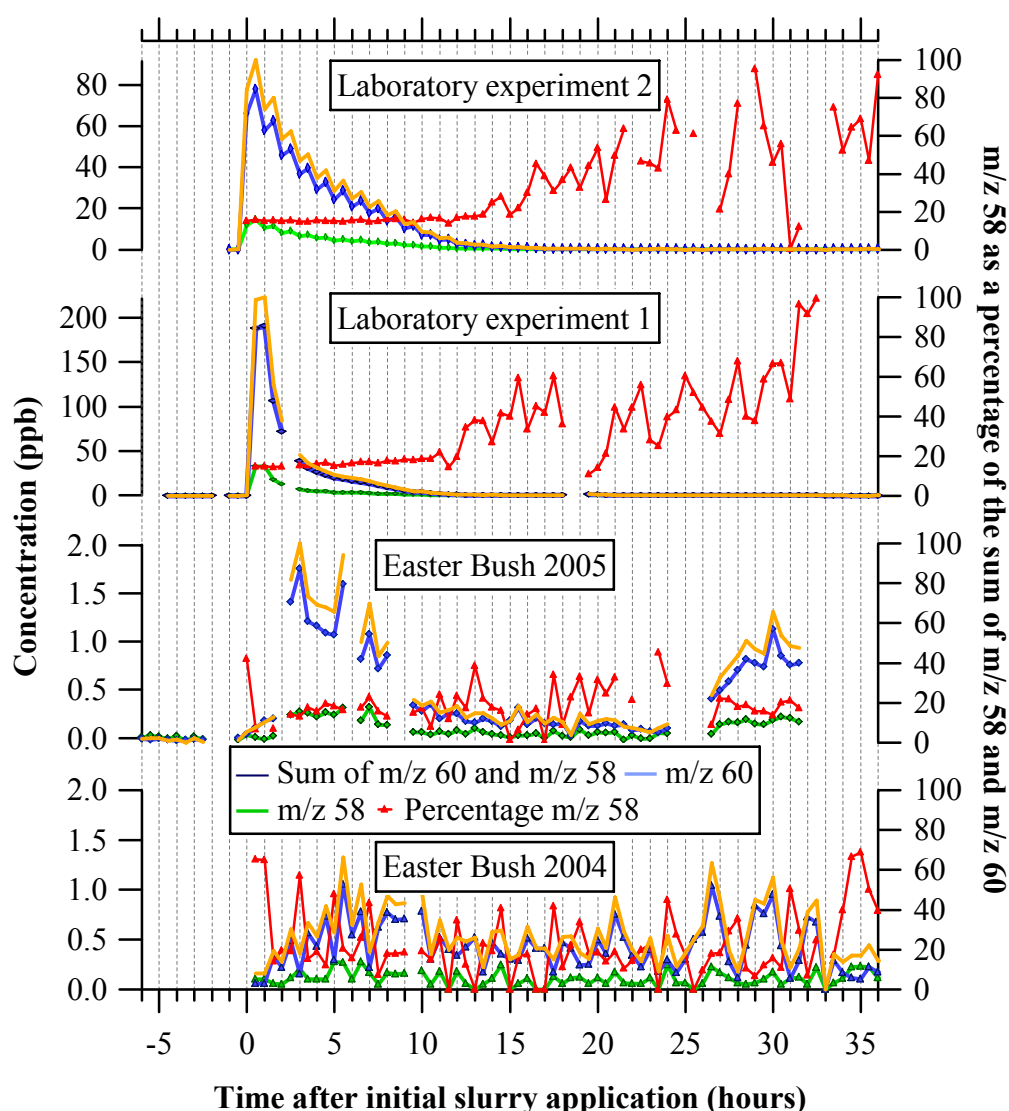
Figure 4.29: Concentrations at m/z 58 (green) and m/z 60 (blue) and their sum (amber) during fertilizations at Easter Bush in 2004 and 2005 and laboratory experiments 1 and 2 as a function of time elapsed after initial slurry application. Concentrations are half hourly means of the SB data. The abundance of m/z 58 as a percentage of the sum of m/z 58 and m/z 60 is also shown (red).

A comparison of m/z 60 and m/z 58 concentrations pre-fertilisation with those during fertilisation at Easter Bush in 2005 (Figure 4.30) clearly shows an increase in both m/z as a result of slurry application. The contributions of the ^{18}O isotope of m/z 57 and ^{13}C isotope of m/z 59 have been removed from m/z 58 and m/z 60 respectively. An upper estimate of the m/z 57 ^{18}O isotope contribution was calculated by treating all of the m/z 57 signal as a molecule containing two oxygens ($C_3H_5O^+$, § 4.3.3.1). The m/z 59 ^{13}C isotope contribution was calculated by treating m/z 59 as a C_3 molecule.
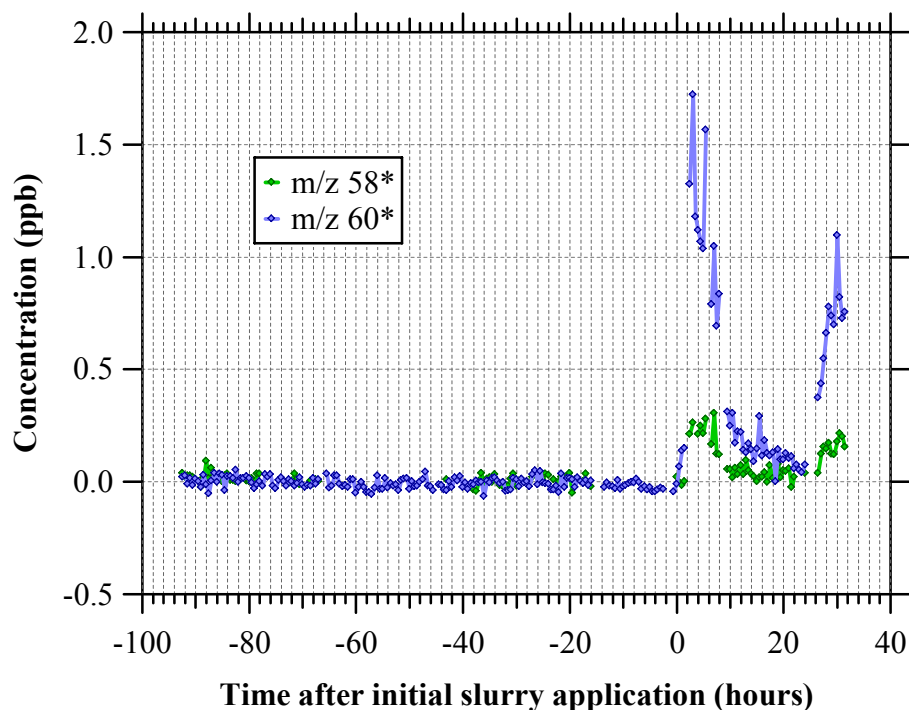
Figure 4.30: The m/z 58 and m/z 60 concentrations during fertilization at Easter Bush in 2005 as a function of the time elapsed after the start of slurry application. Concentrations are half hourly means of the scanbargraph data. * denotes the removal of the ^{18}O isotope of m/z 57 and ^{13}C isotope of m/z 59 from m/z 58 and m/z 60 respectively assuming m/z 57 contains two oxygens and m/z 59 contains three carbons.

In contrast, no increase in either m/z 58 or m/z 60 is apparent from half hourly SB data from fertilisation at Easter Bush in 2004 (Figure 4.31). The speed per m/z during SB measurements was reduced (50 ms) at Easter Bush in 2004 compared to the other SB measurements (0.5 s) (§ 4.2). In the MID measurements, in which the dwell was exceptionally longer than in SB measurements at Easter Bush in 2004, there is some evidence of a minor increase in m/z 60 (Figure 4.31).
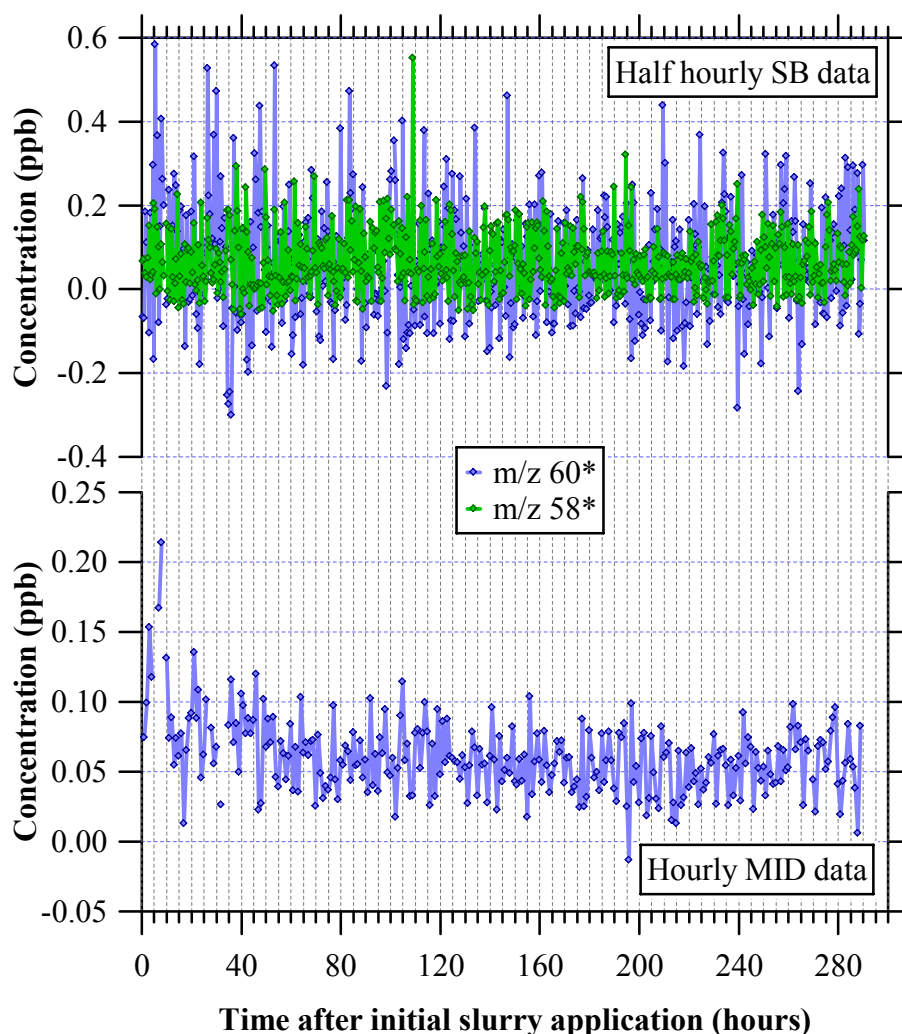
Figure 4.31: Concentrations at m/z 58 and m/z 60 concentrations during fertilization at Easter Bush in 2005 as a function of the time elapsed after the start of slurry application. Concentrations in the upper graph are half hourly means of the SB data, concentrations in the lower graph are hourly averages of MID data.

Strong correlations were observed between m/z 60 and m/z 58. R^2 from zero hours after slurry application onwards during laboratory experiment 1 and 2 were 1.0. The R^2 from zero hours after the start of slurry application onward during fertilisation at Easter Bush in 2005 was 0.86. This supports the identification of m/z 60 as trimethylamine. The ion at m/z 58 formed 16.51 ± 1.37 % of the sum of m/z 60 and m/z 58 during the peak in m/z 60 from 0.5 to 10.5 hours after slurry application in laboratory experiment 1(Figure 4.29). The ion m/z 58 formed 15.73 ± 1.03 % of the sum of m/z 60 and m/z 58 from during the peak in m/z 60 from 0 to 13.5 hours after slurry application in laboratory experiment 2 (Figure 4.29). During the first peak in m/z 60 from 2.5 to 10 hours after the start of slurry application at Easter Bush in 2005, m/z 58 formed 16.71 ± 2.68 % of the sum of m/z 60 and m/z 58, during the second peak from 27 to 31.5 hours post initial slurry application it was 18.53 ± 2.81 %.

Assuming m/z 58 consists of the trimethylamine fragment alone, these product distributions would suggest a greater degree of fragmentation of trimethylamine compared to that observed in SIFT (§ 3.5, Table 3.21) as expected given the elevated energies in PTR-MS.

1-propylamine and 2-propylamine may also contribute to m/z 60 as both compounds have been observed in small amounts from animal waste and are possibly produced from the decarboxylation of α-Aminobutyrate (Spoelstra 1980, Mackie *et al* 1998, Appenidx C). In SIFT (at 300 K and ~0.67 mbar) these primary amines do not fragment to m/z 58, instead fragmentation to m/z 18 (NH_4^+) occurs (§ 3.5, Table 3.19). m/z 18 was not measured, a number of the $>C_3$ primary and secondary amines have been shown to form NH_4^+ fragments on reaction with H_3O^+ (§ 3.5, Table 3.19). Ammonia occurs at m/z 18 and large amounts of NH_4^+ are produced by the hollow cathode ion source. The contribution of these primary amines can not be determined but the strong correlation between m/z 58 and m/z 60 may suggest the tertiary amine, trimethylamine, dominates. As discussed in § 3.4.1 the propylamines may fragment to m/z 58 at the higher energies of PTR-MS (relative to SIFT), higher amines may also form ions at m/z 58 at the elevated energies. The secondary amine methylethylamine also reacts with H_3O^+ to produce the non-dissociative product at m/z 60 and a fragment at m/z 58; in SIFT m/z 60 forms 95 % of total product ions and m/z 58 5 % (Španěl and Smith 1998c, § 3.5, Table 3.20). No measurements of methylethylamine from animal waste could be found. On the basis of previous measurements from animal waste and given the strong correlation between m/z 58 and m/z 60 the sum of m/z 60 and m/z 58 is tentatively identified as the trimethylamine concentration. Ngwabie *et al* (2008) report trimethylamine concentrations of 2.8 to 69.9 ppb from dairy cowsheds utilising PTR-MS, though count rates at m/z 60 alone were considered.

4.3.4 Ammonia

The emissions of ammonia observed during fertilisations at Easter Bush in 2004 and 2005 and laboratory experiments have been discussed in detail by Twigg (2006) and Whitehead (2006). The concentrations observed are displayed in Figure 4.32. Some correlations with the (O)VOCs were observed. For example, during fertilisation in 2005 and both laboratory experiments, ammonia showed a strong correlation with trimethylamine (Figure 4.32). As clearly observed during fertilisation at Easter Bush in 2004 (Figure 4.32), similar variations in the carboxylic acids to that of ammonia were observed but on a delayed timescale which may be related to the larger solubility's of the acids (§ 4.3.5). The C_3 m/z 43 (tentatively propanol) and ethanol concentrations also showed some correlation with ammonia as did the VOSCs; however these compounds generally peaked before ammonia.
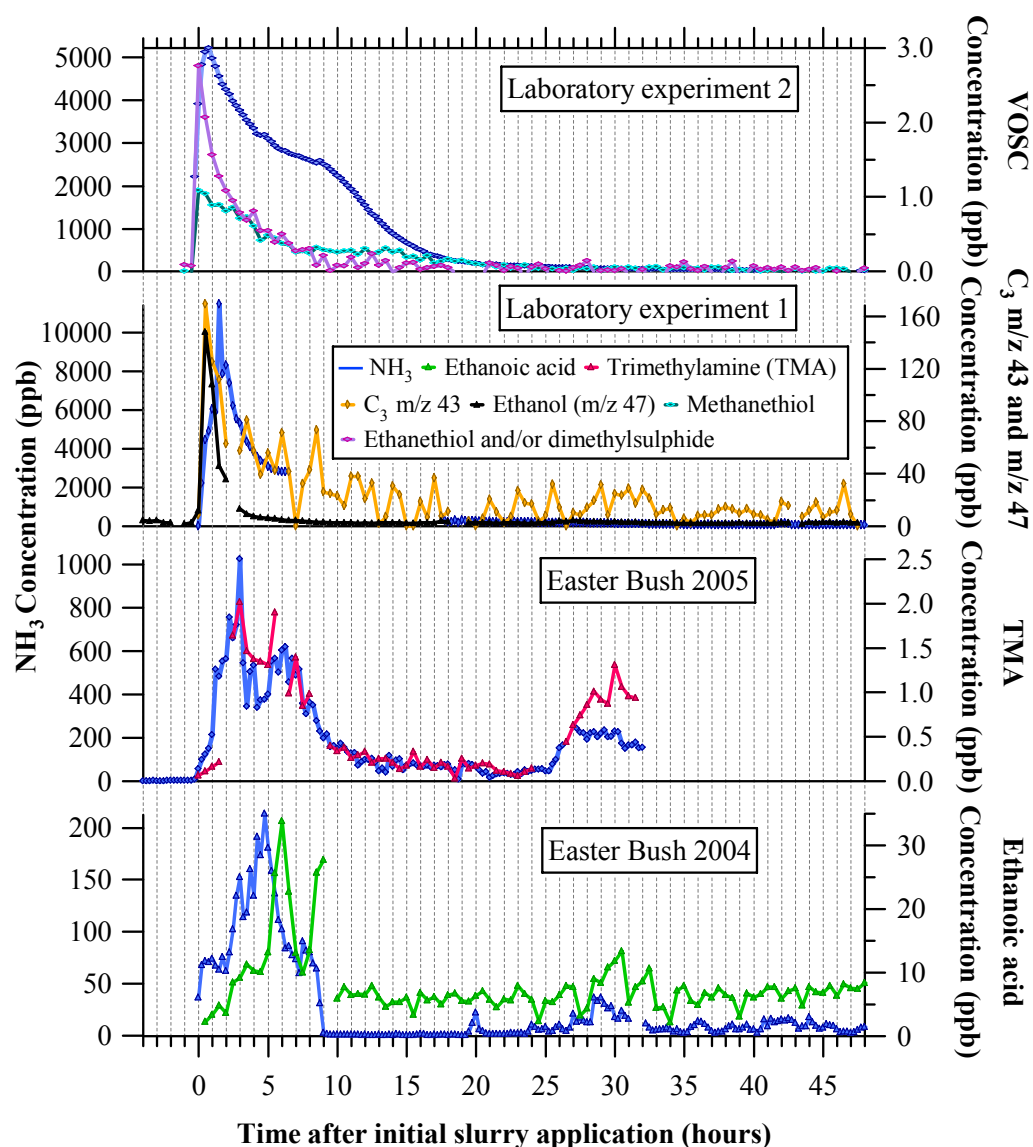
Figure 4.32: Ammonia (NH$_3$) concentrations during fertilisations at Easter Bush in 2004 and 2005 and during laboratory experiments; values are 15 minute averages. (O)VOC concentrations are 30 minute means derived from SB data. Ethanoic acid concentrations were calculated from C_2 concentrations at m/z 61 and m/z 43 using isotopic abundancies as outlined in § 4.3.3.1. Ethanol concentrations are those at m/z 47. The C_3 signal at m/z 43 (tentatively propanol) is calculated from isotopic abundancies as outlined in § 4.3.3.1. Trimethylamine (TMA) concentrations correspond to the sum of signal at m/z 58 and m/z 60. Methanthiol concentrations are those at m/z 49 with the ^{18}O isotope of ethanol removed. Dimethylsulphide and/or ethanethiol concentrations are those at m/z 63 with the ^{18}O isotope of m/z 61 from m/z 63 (assuming m/z 61 contains two oxygen atoms) removed.

4.3.5 Time Evolution of Trace Gases

The time evolution of trace gases from slurry may be partially (in addition to for example underlying microbial processes) dependent on the moisture content of the slurry and the Henry's Law constant of the trace gas (Liang and Liao 2004, Twigg 2006). Lower solubility

gases might be expected to peak before those with higher solubility. The time of peaks in trace gases as a function of Henry's Law constants during laboratory experiment 1 and 2 are shown in Figures 4.33.

(a)

R^2 = 0.82

Laboratory Experiment1

Time of Peak (Hours)

Henry's Law Constant (mol kg^{-1} bar)

(b)

R^2 = 0.82

Laboratory Experiment 2

Time of Peak (Hours)

Henry's Law Constant (mol kg^{-1} bar)
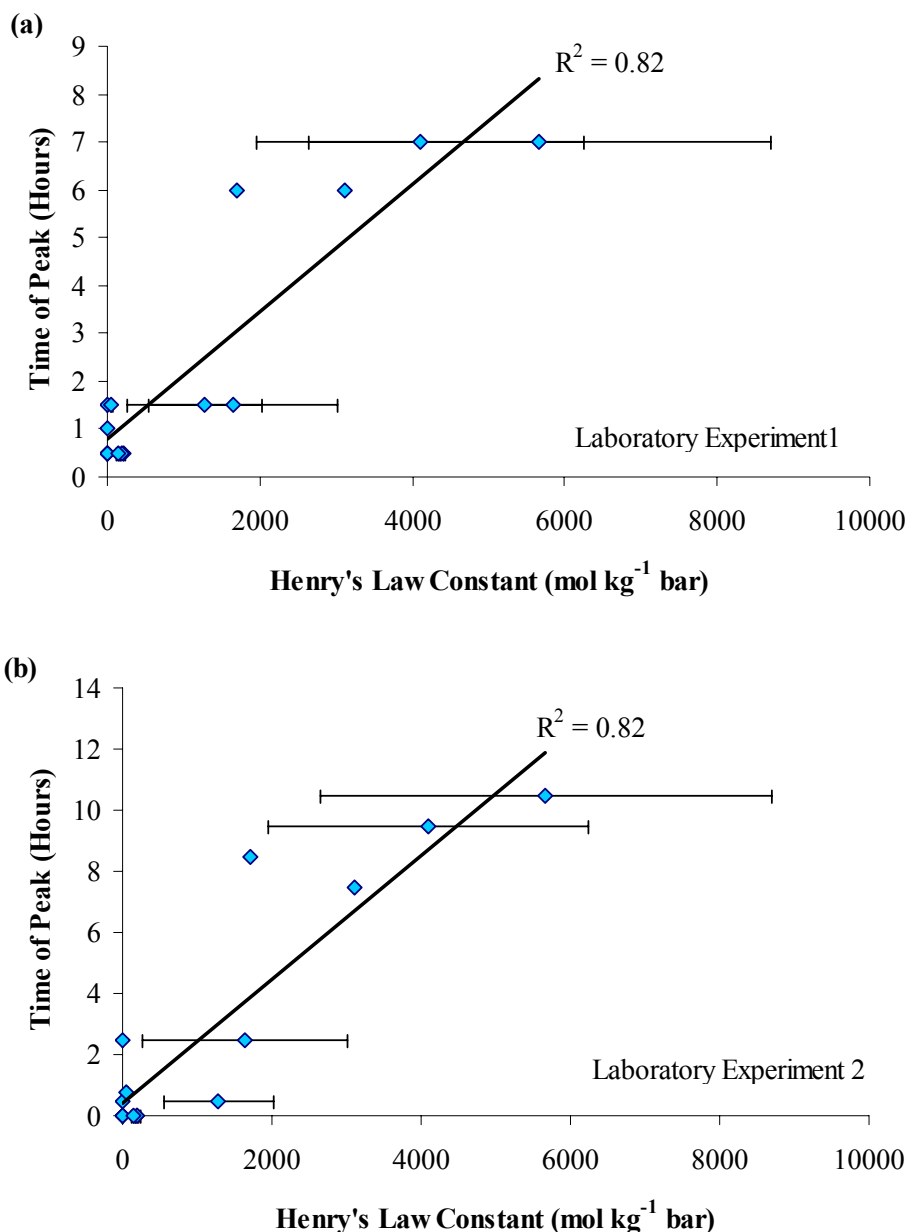
Figure 4.33: The variation in time of peaks in trace gas species as a function of the Henry's Law constants of the species during laboratory (a) experiment 1 and (b) experiment 2. The following trace species are plotted: ammonia, methanol (m/z 33), ethanol (m/z 47), hydrogen sulphide (m/z 35*), methanethiol (m/z 49), ethanethiol (m/z 63), dimethylsulphide (m/z 63), butanoic acid (m/z 89 – ignoring other contributors to m/z 89 and neglecting fragmentation to m/z 71), pentanoic acid (m/z 103) (m/z 89 – ignoring other contributors to m/z 103 and neglecting fragmentation to m/z 85), ethanoic acid (C_2 m/z 43 and C_2 m/z 61, § 4.3.3.1), butanoic acid (derived from m/z 75 and m/z 57 refer to § 4.3.3.1), trimethylamine (m/z 58 and m/z 60), phenol (m/z 95), 4-methylphenol (m/z 109), dimethyldisulphide (m/z 95), propanol (C_3 m/z 43 refer to § 4.3.3.1). Henry's Law constants are means of values taken from Mallard and Linstrom (2005) uncertainties are ± standard deviations.

In both cases a relationship between Henry's Law constant and the time of the peak in trace gas species is apparent. The plotted data are shown in Table 4.10. The correlation observed further supports the identification of compounds in § 4.3.3.

Table 4.10: The Henry's Law constants of various trace species and the time of peaks in trace gas species in hours after initial slurry application of laboratory experiment 1 and 2. Values correspond to those in Figures 4.33. Henry's Law constants are means of values taken from Mallard and Linstrom (2005).

Compound	Mean K_{HL} (mol kg^{-1} bar)	Standard deviation of K_{HL}	Time of peak (hours)	
			Exp 1	Exp 2
Ethanoic acid	5671	3032	7	10.5
Propanoic acid	4100	2146	7	9.5
Butanoic acid	3117		6	7.5
Pentanoic acid	1700		6	8.5
Methanol	204	34	0.5	0
Ethanol	184	35	0.5	0
Propanol	138	19	0.5	0
Hydrogen sulphide	0.09	0.03		
Methanethiol	0.38	0.20	0.5	0
Dimethylsulphide	0.48	0.19	0.5	0
Ethanethiol	0.29	0.06	0.5	0
Trimethylamine	10		1	0.5
Phenol	1640	1383	1.5	2.5
4-methylphenol	1284	738	1.5	0.5
Dimethyldisulphide	0.9	0.07	1.5	2.5
Ammonia	56	16	1.5	0.75

4.4 Summary

Using the discussions in Chapter 3 and resultant mass list (available in digital format) alongside contextual reasoning and the use of isotopic ratios, a number of compounds have been identified in the air during slurry applications. The identification and semi-quantitative analysis is subject to the provisions made in the text as in several cases ions are isobaric. Conclusive identification of compounds would require measurement using alternative techniques such as GC alongside or on-line with the PTR-MS.

Peaks in m/z tentatively assigned to alcohols, were identified during the initial hours of slurry applications. During the cuvette experiments peaks at m/z 47 and 43 were observed, the former was assigned to ethanol and the later in part to propanol, C_5 and higher alcohols may have also contributed to this fraction of m/z 43. No increase in m/z 47 was observed as a result of slurry application at Easter Bush in 2004 or 2005. Increases in m/z 43 attributed, in part, to propanol were observed during fertilisation at Easter Bush in 2005. A peak in m/z 57, after removal of an approximate propanoic acid contribution, was also observed a

fraction of which may have been contributed to by $\geq C_5$ alcohols. Later peaks in carboxylic acids, primarily acetic acid (m/z 61 and a calculated fraction of m/z 43) and to a lesser extent propanoic acid (m/z 75 and a fraction of m/z 57) and the C_4 and C_5 acids were observed during both laboratory experiments and during fertilisations at Easter Bush. As discussed in detail other compounds including trimethylamine (m/z 60 & m/z 58), phenol (m/z 95), methyl-phenols (m/z 109), methanethiol (m/z 49), ethanethiol and/or dimethylsulphide (m/z 63) were tentatively identified. The time of peak of trace gas species were correlated with their Henry's law constants. Some correlations were observed between ammonia and the trace gas species measured with the PTR-MS.

Clarification of compound identity using alternative techniques, product distribution measurements, calibration of the PTR-MS and subsequent measurements of fluxes using virtual disjunct eddy covariance would be desirable. Concurrent quantification of the trace gas species such as carboxylic acids in the feed, animal waste and animal breath would be valuable as well as measurements of other trace gas species such as methane. These measurements would ideally be combined with further laboratory measurements to investigate controlling factors such as pH, age of animal waste and type of animal waste.

References

Allison, M. J (1978) Production of branched-chain volatile fatty acids by certain anaerobic bacteria, *Applied and Environmental Microbiology*, **35** (5): 872 - 877.

Ammann, C., A. Brunner, C. Sprig, A. Neftel (2006) Technical note: Water vapour concentration and flux measurements with PTR-MS, *Atmospheric Chemistry and Physics*, **6**: 4643 – 4651.

Aoki, N., S. Inomata, H. Tanimoto (2007) Detection of C_1-C_5 alkyl nitrates by proton transfer reaction time-of-flight mass spectrometry, *International Journal of Mass Spectrometry*, **263**: 12-21.

Aprea, E., F. Biasioli, T. D. Märk, F. Gasperi (2007a) PTR-MS study of esters in water and water/ethanol solutions: Fragmentation patterns and partition coefficients, *International Journal of Mass Spectrometry*, **262**: 114-121.

Aprea, E., F. Biasioli, S. Carlin, G. Versini, T. D. Märk, F. Gasperi (2007b) Rapid white truffle headspace analysis by proton transfer reaction mass spectrometry and comparison with solid-phase microextraction coupled with gas chromatography/mass spectrometry, *Rapid Communications in Mass Spectrometry*, **21**: 2564 – 2572.

Atkinson, R., R. A. Perry, J. N. Pitts, Jr., (1978a) Rate constants for the reactions of the OH radical with $(CH_3)_2NH$, $(CH_3)_3N$ and $C_2H_5NH_2$ over the temperature range 298 - 426 K, *Journal of Chemical Physics*, **68** (4): 1850 – 1853.

Atkinson, R., K. R. Darnall, J. N. Pitts, Jr. (1978b) Rate constants for the reactions of OH radicals and ozone with cresols at 300 ± 1 K, *The Journal of Physical Chemistry*, **82** (26): 2082-2759.

Atkinson, R. (1986) Kinetics and mechanisms of the gas-phase reactions of the hydroxyl radical with organic compounds under atmospheric conditions, *Chemical Reviews* , **86** (1): 69 -201.

Atkinson, R. (1991) Kinetics and mechanisms of the gas-phase reactions of the NO_3 radical with organic compounds, *Journal of Physical Chemical Reference Data*, **20**: 459 – 507.

Atkinson, R., D. L. Baulch, R. A. Cox, J. N. Crowley, R. F. Hampson, R. G. Hynes, M. E. Jenkin, M. J. Rossi, J. Troe (2004) Evaluated kinetic and photochemical data for atmospheric chemistry: Volume I – gas phase reactions of O_x, HO_x, NO_x and SO_x species, *Atmospheric Chemistry and Physics*, **4**: 1461–1738.

Bak, F., K. Finster, F. Rothfuß (1992) Formation of dimethylsulphide and methanethiol from methoxylated aromatic compounds and inorganic sulfide by newly isolated anaerobic bacteria, *Archives of Microbiology*, **157**: 529 - 534.

Banwart and Bremner (1975) Identification of sulfur gases evolved from animal manures, *Journal of Environmental Quality*, **4** (3): 363 - 366.

Barnes, I., V. Bastian, K. H. Becker, E. H. Fink, W. Nelsen (1986) Oxidation of sulphur compounds in the atmosphere: I. rate constants of OH radical reactions with sulphur dioxide, hydrogen sulphide, aliphatic thiols and thiophenol, *Journal of Atmospheric Chemistry*, **4**: 445 – 466.

Barnes, I., K. H. Becker, I. Patgroescu (1994) The tropospheric oxidation of dimethyl sulfide: A new source of carbonyl sulfide, *Geophysical Research Letters*, **21** (22): 2389 – 2392.

Beck, J. P., A. Heutelbeck, H. Dunkelberg (2007) Volatile organic compounds in dwelling houses and stables of dairy and cattle farms in northern Germany, *Science of the Total Environment*, **372**, 440 – 454.

Bentley, R., T. G. Chasteen (2004) Environmental VOSCs - formation and degradation of dimethyl sulfide, methanethiol and related materials, *Chemosphere*, **55**: 291 - 317.

Blake, R. S., K. P. Wyche, A. M. Ellis, P. S. Monks (2006) Chemical ionization reaction time-of-flight mass spectrometry: Multi-reagent analysis for determination of trace gas composition, *International Journal of Mass Spectrometry*, **254**: 85-93.

Blando, J. D., B. J. Turpin (2000) Secondary organic aerosol formation in cloud and fog droplets: a literature evaluation of a plausibility, *Atmospheric Enviuronment*, **34**: 1623 – 1632.

Bremner, J. M., W. L. Banwart (1976) Sorption of sulphur gases by soils, *Soil Biology and Biochemistry*, **8** (2): 79 – 83.

Buhr, K., S, van Ruth, C, Delahunty (2002) Analysis of volatile flavour compounds by proton transfer reaction-mass spectrometry: fragmentation patterns and discrimination between isobaric and isomeric compounds, *International Journal of Mass Spectrometry*, **221:** 1-7.

Chadwick, L. (1995) *Farm Management Handbook, 16th edition*, SAC, Edinburgh.

Charlson, R. J., J. E. Lovelock, M. O. Andreae, S. G. Warren (1987) Oceanic phytoplankton, atmospheric sulphur, cloud albedo and climate, *Nature*, **326**: 655-661.

Chebbi, A., P. Carlier (1996) Carboxylic acids in the troposphere, occurrence, sources and sinks: A Review, *Atmospheric Environment*, **30** (24): 4233 - 4249.

Cherest, H., G. Talbot, H. De Robichon-Szulmajster (1970) Role of homocysteine synthetase in an alternate route for methionine biosynthesis in *Saccharomyces cerevisiae*, *Journal of Bacteriology*, **102** (2): 448 - 461.

Chesterton, C, I. Condliffe, S. Peel, M. Davies, B. McLean (2006), *Revised Calculation of Livestock Units for Higher Level Stewardship Agreements*, DEFRA, UK.

Christian, T. J., B. Kleiss, R. J. Yokelson, R. Holzinger, P. J. Crutzen, W. M. Hao, T. Shirai, D. R. Blake (2004) Comprehensive laboratory measurements of biomass-burning emissions: 2. First comparison of open path FTIR, PTR-MS, and GC-MS/FID/ECD, *Journal of Geophysical Reasearch*, **109** (D02311): 1-12.

Coeur-Tourneur, C., F. Henry, M-A. Janquin, L. Brutier (2006) Gas-phase reaction of Hydroxyl radicals with *m-, o-* and *p-*cresol, *International Journal of Chemical Kinteics*, **38**: 553 – 562.

Cox, R. A. (1997) Atmospheric sulphur and climate – what have we learned ?, *Philosophical Transactions: Biological Sciences*, **352** (1350): 251 – 254.

Coyle, M. (2005) *The Gaseous Exchange of Ozone at Terrestial Surfaces: Non-stomatal Deposition to Grassland*. Thesis (PhD). University of Edinburgh.

Crunaire, S., A. Tomas, P. Coddeville, C. Fittschen, B. Lemoine (2005) Simulation chamber study of the oxidation of acetic acid by OH radicals - Detection of reaction products by CW-CRDS in the near-infrared range, *Geophysical Research Abstracts*, **7**.

Dagaut, P., T. J. Wallington, R. Liu, M. Kurylo (1988) The gas phase reaction of hydroxy radicals with a series of carboxylic acids over the temperature range 240 - 440 K, *International Journal of Chemical Kinetics*, **20**: 331 – 338.

DEFRA (2007) *Agriculture in the United Kingdom 2007*, UK.

Dévai, I., L. Felföldy, I. Wittner, S. Plósz (1988) Detection of phosphine: new aspects of the phosphorous cycle in the hydrosphere, *Letters to Nature*, **333**: 343 - 345.

Dewhurst, R. J., R. T. Evans, T. T. Mottram, P. Španěl, D. Smith (2001) Assessment of the rumen processes by selected-ion-flow-tube mass spectrometric analysis of rumen gases, *Journal of Dairy Science*, **84**: 1438-1444.

Dotan, I., D. L. Albritton, W. Lindinger, M. Pahl (1976) Mobilities of CO_2^+, N_2H^+, H_3O^+, $H_3O^+.H_2O$, and $H_3O^+.(H_2O)_2$ ions in N_2, *The Journal of Chemical Physics*, **65** (11): 5028-5030.

Du, L., Y. Xu, M. Ge, L. Jia, L. Yao, W. Wang (2007) Rate constant of the gas phase reaction of dimethylsulphide (CH_3SCH_3) with ozone, *Chemical Physics Letters*, **436**: 36-40.

Eismann, F., D. Glindemann, A. Bergmann, P. Kuschk (1997a) Soils as a source and sink of phosphine, *Chemosphere*, **35** (3): 523 - 533.

Eismann, F., D. Glindemann, A. Bergmann, P. Kuschk (1997b) Balancing phosphine in manure fermentation, *Journal of Environmental Science and Health Part B - Pesticides food Contaminants and Agricultural Wastes*, **32** (6): 955 - 968.

Fall, R (1999) Chapter 2: Biogenic Emissions of Volatile Organic Compounds from Higher Plants. In: *Reactive Hydrocarbons in the Atmosphere*, edited by C. N. Hewitt, pages 41-91. Academic Press, London.

Filipy, J., B. Rumberg, G. Mount, H. Westberg, B. Lamb (2006) Identification and quantification of volatile organic compounds from a dairy, *Atmospheric Environment*, **40**: 1480 – 1494.

Forstner. H. J. L ., R. C. Flagan, J. H. Seinfeld (1997) Secondary organic aerosol from the photooxidation of aromatic hydrocarbons: Molecular composition, *Environmental Science Technology*, **31**: 1345 – 1358.

Frank and Rippen (1987) Verhalten von phosphin in der atmosphäre, *Lebensmitteltechnik*, **7-8**: 409 – 411.

Fritz, B., K. Lorenz, W. Steinert, R. Zellner (1982) Laboratory kinetic investigations of the tropospheric oxidation of selected industrial emissions, Physiochemical Behaviour of Atmospheric Pollutants. In *Physiochemical Behaviour of Atmospheric Pollutants*, edited by B. Versino, H. Ott, Reidel, Europe.

Gassmann, G., D. Glindemann (1993) Phosphane (PH_3) in the biosphere, *Angewandte Chemie: International Edition in English*, **32** (5): 761 - 763.

Glavas, S., S. Toby (1975) Reaction between ozone and hydrogen sulphide, *Journal of Physical Chemistry*, **79** (8): 779-782.

Glindemann, D., A. Bergmann (1995) Spontaneous emission of phosphane from animal slurry treatment processing, *Zentralblatt für Hygiene and Umweltmedizin*, **198**: 49-56.

Glindemann, D., A. Bergmann, U. Stottmeister, G. Gassmann (1996a) Phosphine in the Lower Terrestrial Troposphere, *Naturwissenschaften*, **83**: 131 – 133.

Glindemann, D., U. Stottmeister, A. Bergmann (1996b) Free phosphine from the anaerobic biosphere, *Environmental Science and Pollution Research*, **3** (1): 17-19.

Glindemann, D., F. Eismann, A. Bergmann, P. Kuschk, U. Stottmeister (1998) Phosphine by bio-corrosion of phosphide-rich iron, *Environmental Science and Pollution Research*, **5**: 71-74.

Glindemann, D., M. Edwards, P. Kuschk (2003) Phosphine gas in the upper troposphere, *Atmospheric Environment*, **37**: 2429 – 2433.

Glindemann, D., M. Edwards, O. Schrems (2004) Phosphine and methylphosphine production by simulated lightning – a study for the volatile phosphorus cycle and cloud formation in the earth atmosphere, *Atmospheric Environment*, **38**: 6867 – 6874.

Hanrahan, G., T. M. Salmassi, C. S. Khachikian, K. L. Foster (2005) Reduced inorganic phosphorus in the natural environment: significance, specification and determination, *Talanta*, **66**: 435 – 444.

Harrison, A. G (1992) *Chemical Ionization Mass Spectrometry*, CRC Press, Inc., Florida.

Hatakeyama, S., H. Aklmoto (1983) Reactions of OH radicals with methanethiol, dimethyl sulfide and dimethyl disulfide in air, *Journal of Chemical Physics,* **87**:2387 – 2395.

Hayward, S., C. N. Hewitt, J. H. Sartin, S. M. Owen (2002) Performance characteristics and applications of proton transfer reaction-mass spectrometer for measuring volatile organic compounds in ambient air, *Environmental Science and Technology*, **36**: 1554-1560.

Hewitt, C. N., B. Davison (1997) Field measurements of dimethylsulphide and its oxidation products in the atmosphere, *Philosophical Transactions: Biological Sciences*, **352** (1350): 183 – 189.

Hobbs, P. J., T. H. Misselbrook, B. F. Pain (1995) Assesment of odours from livestock wastes by a photoionization detector, an electronic nose, olfactometry and gas chromatography-mass spectrometry, *Journal of Agricultural Engineering Research*, **60**: 137 – 144.

Hobbs, P. J., T. H. Misselbrook, B. F. Pain (1997) Characterisation of odourous compounds and emissions from slurries produced from weaner pigs fed dry feed and liquid diets, *Journal of the Science of Food and Agriculture*, **73**: 437 - 445.

Hobbs, P, J., T. H. Misselbrook, B. F. Pain (1998) Emission rates of odorous compounds from pig slurries, *Journal of the Science of Food and Agribulture*, **77**: 341 - 348.

Hobbs, P. J., T. H. Misselbrook, T. R. Cumby (1999) Product and emission of odours and gases from ageing pig waste, *Journal of Agricultural Engineering Research*, **72**: 291 - 298.

Hobbs, P., T. Mottram (2000) New directions: Significant contributions of dimethyl sulphide from livestock to the atmosphere, *Atmospheric Environment*, **34**: 3649 – 3650.

Hobbs, P. J., J. Webb, T. T. Mottram, B. Grant, T.M Misselbrook (2004) Emissions of volatile organic compounds originating from UK livestock agriculture, *Journal of the Science of Food and Agriculture*, **84**: 1414 – 1420.

Health and Safety Executive (HSE) (2007) *Table 1: List of approved workplace exposure limits (as consolidated with amendments October 2007)*, UK: http://www.hse.gov.uk, (EH40/2005 Workplace exposure limits).

Inomata, S., H. Tanimoto, S. Kameyama, U. Tsunogai, H. Irie, Y. Kanaya, Z. Wang (2008) Technical Note: Determination of formaldehyde mixing ratios in air with PTR-MS: laboratory experiments and field measurements, *Atmospheric Chemistry and Physics*, **8**: 273 – 284.

Jenkins, R. O., T. -A. Morris, P. J. Craig, A. W. Ritchie, N. Ostah (2000) Phosphine generation by mixed- and monoseptic-cultures of anaerobic bacteria, *The Science of the Total Environment*, **250**: 73 - 81.

Kadota, H., Y. Ishida (1972) Production of volatile sulfur compounds by microorganisms, *Annual Reviews,* **26**: 127-138.

Karl, T. G., C. Sprig, J. Rinne, C. Stroud, P. Prevost, J. Greenberg, R. Fall, A. Guenther (2002) Virtual disjunct eddy covariance measurements of organic compound fluxes from a subalpine forest using proton transfer reaction mass spectrometry, *Atmospheric Chemistry and Physics*, **2**: 279 – 291.

Karl, T. G., T. J. Christian, R. J. Yoelson, P. Artaxo, W. M. Hao, A. Guenther (2007) The Tropical Forest and Fire Emissions Experiment: method evaluation of volatile organic compound emissions measured by PTR-MS, FTIR, and GC from tropical biomass burning, *Atmospheric Chemistry and Physics*, **7**: 5883 - 5897.

Kiene, R. P., T. S. Bates (1990) Biological removal of dimethyl sulphide from sea water, *Nature*, **345**: 702 - 705.

Kiene, R. P., M. E. Hines (1995) Microbial formation of dimethylsulphide in anoxic *Sphagnum* peat, *Applied and Environmental Microbiology*, **61** (7): 2720 - 2726.

Kim, K. Y., H. J. Ko, H. T. Kim, Y. S. Kim, Y. M. Roh, C. M. Lee, H. S. Kim, C. N. Kim (2007) Sulfuric odorous compounds emitted from pig-feeding operations, *Atmospheric Environment*, **41**: 4811 – 4818.

Le, P. D., A. J. A. Aarnink, N. W. M. Ogink, P. M. Becker, M. W. A. Verstegen (2005) Odor from animal production facilities: Its relation to diet, *Nutrition Research Reviews*, **18** (1): 3-30.

Le, P. D. (2006) *Odor from pig production: its relation to diet*, Thesis (PhD) Wageningen Institute of Animal Science, Wageningen University, The Netherlands.

Le, P. D., A. J. A. Aarnink, A. W. Jongbloed, C. M. C. van der Peet Schwering, N. W. M. Ogink, M. W. A. Verstegen (2007) Effects of crystalline amino acid supplementation to the diet on odor from pig manure, *Journal of Animal Science*, **85**: 791-801.

Liang, H-M., C-M. Liao (2004) Dynamic transport of livestock generated VOC-odor in a ventilated airspace with mixing heterogeneity, *Atmospheric Environment*, **38**: 345-355.

Librano, V., G. Tringali, J. Hjorth, S. Coluccia (2004) OH-initiated oxidation of DMS/DMSO: reaction products at high NO_x levels, *Environmental Pollution*, **127**: 403 - 410.

Lomans, B. P., A. Pol, H. J. M. Op den Camp (2002a) Microbial cycling of volatile organic sulfur compounds in anoxic environments, *Water Science and Technology*, **45** (10): 55-60.

Lomans, B. P., C. van der Drift, A. Pol, H. J. M. Op den Camp (2002b) Microbial cycling of volatile organic sulfur compounds, *Cellular and Molecular Life Sciences*, **59**: 575 - 588.

Lovelock, J. E., R. J. Maggs, R. A. Rasmussen (1972) Atmospheric dimethyl sulphide and the natural sulphur cycle, *Nature*, **237**: 452 – 453.

Mackie, R. I., P. G. Stroot, V. H. Varel (1998) Biochemical identification and biological origin of key odor components in livestock waste, *Journal of Animal Science*, **76**: 1331 – 1342.

Malekina, S. D., T. L. Bell, M. A. Adams (2007) PTR-MS analysis of reference and plant-emitted volatile organic compounds, *International Journal of Mass Spectrometry*, **262**: 203-210.

Mallard, W. G., P. J. Linstrom (2005) NIST Chemistry WebBook, NIST Standard Reference Database Number 69, February 2000, National Institute of Standards and Technology, Gaithersburg, MD.

Manahan, S. E. (1975) *Environmental Chemistry, Second Edition*, William Grant Press, Massachusetts.

Martín-Reviejo, M., K. Wirtz (2005) Is benzene a precursor for secondary organic aerosol?, *Environmental Science and Technology*, **39**: 1045 – 1054.

Milford, C. (2004) *Dynamics of Atmospheric Ammonia Exchange with Intensively-Managed Grassland*. Thesis (PhD), University of Edinburgh.

Misselbrook, T. H., P. J. Hobbs, K. C. Persaud (1997) Use of an electronic nose to measure odour concentration following application of cattle slurry to grassland, *Journal of Agricultural Engineering Research*, **66**: 213 – 220.

Murphy, S. M., A. Sorooshian, J. H. Kroll, N. L. Ng, P. Chhabra, C. Tong, J. D. Surratt, E. Knipping, R. C. Flagan, J. H. Seinfeld (2007) Secondary organic aerosol formation from atmospheric reactions of aliphatic amines, *Atmospheric Chemistry and Physics*, **7**: 2313-2337.

Ngwabie, N. M., G. W. Schade, T. G. Custer, S. Linke, T. Hinz (2008) Abundances and flux estimates of volatile organic compounds from a dairy cowshed in Germany, *Journal of Environmental Quality*, **37**: 565 – 573.

Rabaud, N. E., S. E. Ebeler, L. L. Ashbaugh, R. G. Flocchini (2003) Characterization and quantification of odorous and non-odorous volatile organic compounds near a dairy in California, *Atmospheric Environment*, **37**: 933 - 940.

Ravishankara, A. R., Y. Rudich, R. Talukdar, S. B. Barone (1997) Oxidation of atmospheric reduced sulphur compounds: perspective from laboratory studies, *Philosophical Transactions: Biological Sciences*, **352** (1350): 171 - 182.

Resende, S. M., J. C. de Bona, P. D. S. Sombrio (2005) Theoretical study of the role of adducts in the atmospheric oxidation of dimethyl sulfoxide by OH, O_2 and O_3 and the kinetics of the reaction DMSO + OH, *Chemical Physics*, **309**: 283 – 289.

Rinke, M., C. Zetzsch (1984) Rate constants for the reactions of OH radicals with aromatics - benzene, phenol, aniline, and 1,2,4-trichlorobenzene, *Berichte Der Bunsen-Gesellschaft-Physical Chemistry Chemical Physics*, **88** (1): 55-62.

Roels, J., W. Verstraete (2001) Biological formation of volatile phosphorus compounds, *Bioresource Technology*, **79**: 243 - 250.

Roels, J., H. V. Langenhove, W. Verstraete (2002) Determination of phosphine in biogas and sludge at ppt-levels with gas chromatography-thermionic specific detection, *Journal of Chromatography A*, **952**: 229 – 237.

Roels, J., G. Huyghe, W. Verstraete (2005) Microbially mediated phosphine emission, *Science of the Total Environment,* **338**: 253 - 265.

Rosman, K. J. R., P. D. P. Taylor (1997) *Isotopic Compositions of the Elements 1997*, International Union of Pure and Applied Chemistry.

Rutishauser, B. V., R. Bachofen (1999) Phosphine formation from sewage sludge cultures, *Ecology/Environmental Microbiology*, **5**: 525 – 531.

Schade, G. W., P. J. Crutzen (1995) Emission of aliphatic amines from animal husbandry and their reactions: Potential source of N_2O and HCN, *Journal of Atmospheric Chemistry*, **22:** 319 -346.

Schiffman, S. S., J. L. Bennett, J. H. Raymer (2001) Quantification of odors and odorants from swine operations in North Carolina, *Agricultural and Forest Meteorology*, **108**: 213 – 240.

Schink, B., M. Friedrich (2000) Phosphite oxidation by sulphate reduction, *Nature,* **406**: 37.

Seinfeld, J. H., S. N. Pandis (1998) *Atmospheric Chemistry and Physics From Air Pollution to Climate Change*, John Wiley & Sons, Inc., United States of America.

Seinfeld, J. H. (1999) Chapter 8: Global Atmospheric Chemistry of Reactive Hydrocarbons. In: Reactive Hydrocarbons in the Atmosphere, edited by C. N. Hewitt, pages 41-91. Academic Press, London.

Segal, W., R. L. Starkey (1969) Microbial decomposition of methionine and identity of the resulting sulfur products, *Journal of Bacteriology*, **98** (3): 908 - 913.

Shaw, S. L., F. M. Mitloehner, W. Jackson, E. J. Depeters, J. G. Fadel, P. H. Robinson, R. Holzinger, A. H. Goldstein (2007) Volatile organic compound emissions from dairy cows and their waste as measured by proton-transfer-reaction mass spectrometry, *Environmental Science and Technology*, **41**: 1310 – 1316.

Sinha, V., J. Williams, M. Meyerhöfer, U. Riebesell, A. I. Paulino, A. Larsen (2007) Air-sea fluxes of methanol, acetone, acetaldehyde, isoprene and DMS from a Norwegian fjord following a phytoplankton bloom in a mesocosm experiment, *Atmospheric Chemistry and Physics*, **7**: 739-755.

Skjelhaugen, O. J., L. Donantoni (1998) Combined aerobic and electrolytic treatment of cattle slurry, *Journal of Agricultural Enginering Research*, **70**: 209 - 219.

Smith, D., P. Spanel, J. B. Jones (2000) Analysis of volatile emissions from porcine faeces and urine using selected ion flow tube mass spectrometry, *Bioresource Technology*, **75**: 27 - 33.

Španěl, P., D. Smith (1995) Reactions of H_3O^+ and OH^- ions with some organic molecules; applications to trace gas analysis in air, *International Journal of Mass Spectrometry and Ion Processes*, **145**: 177-186.

Španěl, P., D. Smith (1998a) SIFT studies of the reactions H_3O^+, NO^+ and O_2^+ with a series of volatile carboxylic acids and esters, *International Journal of Mass Spectrometry and Ion Processes*, **172**: 137 – 147.

Španěl, P., D. Smith (1998b) SIFT studies of reactions of H_3O^+, NO^+ and O_2^+ with several ethers, *International Journal of Mass Spectrometry and Ion Processes*, **172**: 239 – 247.

Spanel. P., D. Smith (1998c) Selected ion flow tube studies of the reactions of H_3O^+, NO^+ and O_2^+ with several amines and some other nitrogen containing molecules, *International Journal of Mass Spectrometry*, **176**: 203 – 211.

Spoelstra, S. F. (1977) Simple phenols and indoles in anaerobically stored piggery wastes, *Journal of the Science of Food and Agriculture,* **28**: 415 - 423.

Spoelstra, S. F. (1980) Origin of objectionable odorous components in piggery wastes and the possibility of applying indicator components for studying odour development, *Agriculture and Environment*, **5**: 241 - 260.

Stevens, R. J., R. J. Laughlin (1993) Effects of diet and storage time on the concentration of sulphide in dairy-cow slurry, *Bioresource Technology*, **45**: 13-16.

Sunesson, A-L., J. Gullberg, G. Blomquist (2001) Airborne chemical compounds on dairy farms, *Journal of Environmental Monitoring*, **3**: 210-216.

Thomas, R. M. (2007) *Measurement of Speciated Aerosol Fluxes.* Thesis (PhD). University of Manchester.

Thomas, M. (2008) *The British Survey of Fertiliser Practice. Fertiliser Use On Farm Crops For Crop Year 2007*, DEFRA, UK.

Tuazon, E. C., R. Atkinson, S. M. Aschmann, J. Arey (1994) Kinetics of products of the gas-phase reactions of O_3 with amines and related-compounds, *Research on Chemical Intermediates*, **20** (3-5): 303-320.

Twigg, M. (2006) *Application of Tunable Diode Laser Absorption Spectroscopy for the Investigation of Surface-Atmosphere Exchange of Ammonia*, Thesis (PhD). University of Ulster.

Uchimaru, T., A. M. El-Nahas, M. Sugie, K. Tokuhashi, A. Sekiya (2007) DFT/Ab initio study on the pathways for the reaction of CH_3SH with NO_3 Radical, *Chemistry Letters,* **36** (3): 400 – 401.

Urbanski, S. P., R. E. Stickel, Z. Zhao, P. H. Wine (1997) Mechanistic and kinetic study of formaldehyde production in the atmospheric oxidation of dimethyl sulphide, *Journal of the Chemical Society., Faraday Transactions,* **93** (16): 2813 - 2819.

Von Hartungen, E., A. Wisthaler, T. Mikoviny, D. Jaksch, E. Boscaini, P. J. Dunphy, T. D. Märk (2004) Proton-transfer-reaction mass spectrometry (PTR-MS) of carboxylic acids. Determination of Henry's law constants and axillary odour investigations, *International Journal of Mass Spectrometry*, **239**: 243 – 248.

Wallington, T. J., R. Atkinson, A. M. Winer, J. N. Pitts, Jr. (1986) Absolute rate constants for the gas phase reactions of the NO_3 radical with CH_3SH, CH_3SCH_3, CH_3SSCH_3, H_2S, SO_2 and CH_3OCH_3 over the temperature range 280 - 350 K, *The Journal of Physical Chemistry*, **90** (21): 5393 - 5396.

Wang, T., P. Spanel, D. Smith, (2004) A selected ion flow tube, SIFT, study of the reactions of H_3O^+, NO^+ and O_2^+ ions with several N- and O-containing heterocyclic compounds in support of SIFT-MS, *International Journal of Mass Spectrometry*, **237**: 167-174.

Warneke, C., J. Kuczynski, A. Hansel, A. Jordan, W. Vogel, W. Lindinger (1996) Proton transfer reaction mass spectrometry (PTR-MS): propanol in human breath, *International Journal of Mass Spectrometry and Ion Processes*, **154**: 61-70.

Warneke, C., J. A. de Gouw (2001) Organic trace gas composition of the marine boundary layer over the northwest Indian Ocean in April 2000, *Atmospheric Environment*, **35**: 5923 – 5933.

Watts, S. F. (2000) The mass budgets of carbonyl sulfide, dimethyl sulfide, carbon disulfide and hydrogen sulfide, *Atmospheric Environment*, **34**: 761 – 779.

Williams, J., N-Y. Wang, R. J. Cicerone, K. Yagi, M. Kurihara, F. Terada (1999) Atmospheric methyl halides and dimethyl sulphide from cattle, *Global Biogeochemical Cycles*, **13** (2): 485 – 491.

Williams, J., U. Pöschl, P. J. Crutzen, A. Hansel, R. Holzinger, C. Warneke, W. Lindinger, J. Lelieveld (2001) An atmospheric chemistry interpretation of mass scans obtained from a proton transfer mass spectrometer flown over the tropical rainforest of Surinam, *Journal of Atmospheric Chemistry*. **38**: 133 – 166.

Williams, J., R. Holzinger, V. Gros, X. Xu, E. Atlas, D. W. R. Wallace (2004) Measurements of organic species in air and seawater from the tropical Atlantic, *Geophysical Research Letters*, **31**: L23S06, 1 – 5.

Willig, S., M. Lacorn, R. Claus (2004) Development of a rapid and accurate method for the determination of key compounds of pig odor, *Journal of Chromatography A*, **1038**: 11 – 18.

Whitehead, J. D. (2006) *Atmospheric Ammonia Measurements using a Quantum Cascade Tunable Diode Laser Absorption Spectrometer*. Thesis (PhD). University of Manchester.

World Health Organisation (WHO) (1981) *Hydrogen Sulfide*. Geneva: United Nations Environment Programme, the International Labour Organisation and the World Health Organization (Environmental Health Criteria 19).

World Health Organisation (WHO) (1988) *Phosphine and selected metal phosphides*. Geneva: United Nations Environment Programme, the International Labour Organisation and the World Health Organization (Environmental Health Criteria 73).

Yu. S. (2000) Role of organic acids (formic, acetic, pyruvic and oxalic) in the formation of cloud condensation nuclei (CCN): a review, *Atmospheric Research*, **53**: 185 - 217.

Zetzsch, C., F. Stuhl (1982) *Rate Constants for Reactions of OH with Carbonic Acids*, European Symposium of Physio-Chemical Behaviour of Atmospheric Pollutants.

Zhu, J. (2000) A review of microbiology in swine manure odor control, *Agriculture, Ecosystems and Environment*, **78**: 93 - 106.

Zhu. R., L. Sun, D. Kong, J. Geng, N. Wang, Q. Wang, X. Wang (2006a) Matrix-bound phosphine in Antarctic biosphere*, Chemosphere*, **64**: 1429 - 1435.

Zhu, R., D. Kong, L. Sun, J. Geng, X. Wang, D. Glindemann (2006b) Tropospheric phosphine and its sources in coastal Antartica, *Environmental Science and Technology*, **40**: 7656 - 7661.

5 Conclusions and Future Work

A large number of uncertainties and inaccuracies are associated with the calculation of concentrations in the PTR-MS and, where possible, instrument calibration is therefore the preferable procedure for trace gas quantification. However, often a large number of trace gas species are measured together and calibration for every species is impossible. In addition, it is difficult to produce stable and low concentrations of trace gases, such as carboxylic acids, with relatively low volatility and highly polarity. The uncertainty in resultant concentrations is higher than the ~20 % often associated with standards of compounds such as the hydrocarbons. Several unsuccessful attempts were made as part of this research to generate low concentrations of alcohols and alkylbenzenes using custom built diffusion and permeation tube systems for automated calibration of the PTR-MS. Generation of standards was hampered by the short period (1-2 months) of measurement campaigns available for stabilization and development, the difficulty in achieving sufficiently high dilutant flows for the low concentrations required and pressure differential for mass flow controller operation from a zero air system, access to high precision balances, and losses of trace gases in, for example, solenoid valves.

It is therefore important to reduce inaccuracies associated with the calculation of concentrations. The largest sources of inaccuracy and uncertainty are the detection efficiencies (including variation in abilities to traverse the drift tube in addition to the area from the drift tube exit to detection), the manner in which corrections are made for the effects of humidity and the derivation of the rate constant. The models for collisional rate constant calculation and effects of the electric field on it have been considered in Chapter 2. A Microsoft® Excel file for the calculation of collisional rate constants using the various models discussed is attached in an electronic form. This includes the calculation of collisional rate constant for the reaction of H_3O^+ with over 400 molecules. The use of a model to account for the probable decrease in collisional rate constant with increasing translational energy of the ion resulting from the electric field (though unaffected dipole rotational temperature) available in the literature, but not previously applied to the PTR-MS, is suggested. Experimental investigation of the ability of this model to calculate the decrease of the collisional rate constant as a function of centre-of-mass kinetic energy and of the point at which the hard sphere radius becomes important, and the collisional rate constant increases, for various ion-molecule systems is required. This is complicated by the effects of the electric field on reaction efficiency as distinct from those on the collisional rate constant. Measurements of rate constants for the reaction of trace gas species with $H_3O^+(H_2O)_n$ in air

buffer in the presence of an electric field as a function of centre-of-mass kinetic energy, temperature (at fixed centre-of-mass kinetic energy) and pressure would be of interest.

In either the case that concentrations are calculated or calibrated quantification of compounds requires the appropriate assignment of m/z to particular molecular sources. There are many isobaric molecules and non-dissociated and dissociated ions this is particularly important in tropospheric air samples that contain a complex and changing mixture of trace gas species. There have been a limited number of measurements of product distributions from molecules in the PTR-MS and where available drift tube conditions are not always stated. A large number of measurements of product distributions resulting from the reaction of H_3O^+ with trace gas species in SIFT are available in the literature. However, it is important to note that product distributions in the SIFT do not directly apply to the PTR-MS. In the PTR-MS the electric field results in increased ion (primarily translational) energy. In addition to the use of an electric field, the energy of reaction may be increased by increasing temperature, as in VT-SIFT measurements, or by use of a lower proton affinity ion and thereby greater reaction exoergicity. A method has been proposed to approximate the change in energy in these measurements relative to reaction with H_3O^+ at 298 K. This theoretically allows interpolation from VT-SIFT measurements and measurements with alternate protonating ions to hypothesise fragmentation in the PTR-MS. The enthalpies of various dissociation reactions have been calculated and used alongside these data to aid assessment of the viability of fragmentation pathways in the PTR-MS. The assumptions and shortcoming of this technique have been discussed. These include the generally greater pressure and polyatomic, as opposed to monatomic, buffer employed in PTR-MS compared to SIFT measurements and consequent affects on the product distributions from three-body reactions. In addition, the distribution of the increased energy in VT-SIFT differs from that in PTR-MS. Fragmentation patterns in EI-MS have also been discussed to assist identification of possible fragments, but due to the large energies involved, many of these fragments are not observed in PTR-MS and the extent of any like fragmentation differs. Attention has been paid to compounds likely to occur during slurry applications, such as carboxylic acids, alcohols, amines and sulphur containing compounds. In example, ethanol forms only the non-dissociated ion from reaction with H_3O^+ in SIFT whilst in PTR-MS based techniques, 0 to 100 % of product ions have been observed at m/z 47 with up to 50 % of product ions at m/z 29 and varying amounts at m/z 19 and 31 depending on drift tube conditions and alcohol concentrations. In the case of higher alcohols, in addition to fragmentation by elimination of water observed in SIFT, dissociation to $C_iH_{2i+1}^+$ ions and a smaller alcohol is observed from C_5 alcohols and to a greater extent from higher alcohols.

Product distributions from other groups of compounds, namely alkanes, alkenes, dienes and aromatics have been discussed and are attached in electronic format. It is from these compounds which most measurements in VT-SIFT and reactions with other reagent ions have been made and to which the discussed methodology has been applied. The results of these developments and similar considerations for other compounds such as esters and ethers have been used to compile a list of possible contributors to selected m/z in a mass list attached in electronic format. There is a need for the measurement of product distributions from the reaction of H_3O^+ with various trace gas species in the PTR-MS over a range of humidities as a function of E/N and thereby centre-of-mass kinetic energies, temperature at fixed E/N and pressure at fixed E/N. Experimental derivation of the extent of protonated dimer and trimer formation as a function of trace gas concentration is required. Such information would enable fragmentation to used as a tool in identification of compounds at a given m/z and optimisation of instrumental parameters to quantify a given compound of interest. Ambiguity as to product distributions, such as uncertainty as to the degree of fragmentation of 2-methyl-1, 3-butadiene (isoprene) to m/z 39 and m/z 41, and potential resultant inaccuracies in concentrations could have important implications for atmospheric (O)VOC budgets.

The results of Chapter 3 have been applied alongside isotopic ratios, comparison with GC measurements in the literature and also available information regarding underlying biochemical processes, to identify compounds emitted during slurry application to a grassland field and in slurry cuvette measurements in Chapter 4. An early peak in propanol (fraction of m/z 43) and possibly higher alcohols followed by later peaks in carboxylic acids, primarily acetic acid (m/z 61 and a fraction of m/z 43) and to a lesser extent propanoic acid (m/z 75 and a fraction of m/z 57) and higher acids, was generally observed. A large increase in m/z 60 and m/z 58, tentatively identified as trimethylamine with possible contributions from other C_3H_9N amines, was seen during fertilisation at Easter Bush in 2005 and during cuvette experiments though not during fertilisation at Easter Bush in 2004. Increases in m/z 95 and m/z 109, cautiously identified as phenol and methyl-phenols respectively, were observed during all measurements. During cuvette experiments, increases in m/z 95 exceeded those of m/z 109 while the reverse was observed during both slurry applications at Easter Bush. Increases in m/z 35 were observed during both slurry applications at Easter Bush though not during cuvette experiments; m/z 35 was tentatively identified as hydrogen sulphide with possible contributions from phosphine. Increases in m/z 49, tentatively assigned as methanethiol and m/z 63 as dimethylsulphide and/or ethanethiol, were observed during the cuvette experiments and during fertilisation at Easter Bush in 2005. Some

correlations were observed between ammonia concentrations and trace gas species, particularly trimethylamine and on a delayed timescale, the carboxylic acids. A correlation between the Henry's law constant of trace gas species and the time of peak was observed. Further laboratory based experiments to investigate the effects of controlling factors such as pH, length of slurry storage, diet, wind speed and animal waste type would be of value. Concurrent measurements of concentrations of (O)VOCs and the other trace species concentrations in the diet, animal waste and animal breath as well as methane measurements would be valuable. The slurry measurements further highlight the need for measurements of product distributions in the PTR-MS. In example, it is possible that at the higher energies of PTR-MS the propylamines, as well as the secondary and tertiary C_3H_9N amines, fragment to m/z 58; higher amines may also fragment to m/z 58 *via* alkide abstraction. Methanethiol may fragment to m/z 47 (by elimination of hydrogen) and ethanethiol to m/z 29 (by elimination of H_2S) with an underestimation of concentrations resulting if calculated from m/z 49 and 63 respectively.

The large number of possible contributors to a number of m/z in the mass list highlights the need for GC measurements alongside or on-line with the PTR-MS. A methodology for GC measurements of various carboxylic acids and 2-methyl-1, 3-butadiene (isoprene) at high concentrations has been developed. An automated (with the exception of liquid nitrogen filling) pre-concentration system consisting of an adsorption trap (operated with a water cooled peltier and subsequently heated using nickel chromium wire and a 48 V, ~4 A, transformer *via* a relay) followed by a cryotrap (with similar subsequent heating) for use with the GC to enable measurement at trace concentrations has been developed. Although automation *via* a LabJack© U12 (LabJack US) and program written in LabView© (National Instruments, US) has been demonstrated, modifications have followed and this has not yet been deployed successfully.

During measurements from slurry, concomitant GC measurements could enable, for example, different C_3H_9N amine contributions to m/z 60 and m/z 58 to be identified. The presence of esters, hydrocarbons, alcohols and carboxylic acids could be determined by GC and, given knowledge of product distributions from them, there resultant contribution to m/z 61, 75, 89, 103 and 43, 57, 71 and 85 determined. At present the ability of PTR-MS to quantify hydrogen sulphide is uncertain. The measurement of forward and reverse reaction rates of hydrogen sulphide with H_3O^+ and/or characterisation of the PTR-MS for hydrogen sulphide at various humidities and drift tube conditions with verification of resultant concentrations by for example GC is needed. Intermittent removal of hydrogen sulphide

using an alkaline filter such as NaOH to establish contributions of phosphine to m/z 35 would be of interest.

If the contributions from various molecules could be established and trace species quantified, virtual disjunct eddy covariance flux measurements of select trace gas species during slurry applications using the PTR-MS would be desirable. Virtual disjunct eddy covariance flux measurements of the more volatile, less polar sulphur containing compounds, amines and possibly phosphine would be more feasible than measurement of carboxylic acid fluxes. Flux measurement of the acids is further complicated by the number of other potential contributors to the corresponding m/z. Virtual disjunct eddy covariance flux measurements have been made above an oak forest and in urban areas during this work and a program has been developed in LabView© (National Instruments, US) for flux calculation, correction and loss evaluation.

OTHER WORK

RESEARCH PROJECTS/FIELD EXPERIMENTS

Project	Location	Dates
Butene Isomerisation Over Zeolite Ferrierite Under Microwave and Conventional Heating.	Keele University, UK	June – August 2002
Synthesis and Characterisation of SBA-15 and Al-SBA-15.	Keele University, UK	2002/2003
Butene Reformation Over Undopped, Ceria Moped and Molybdenum Oxide Doped Nickel/Yittria Stabilized Catalysts.	Keele University, UK	2002/2003
Investigation of the influence of Aluminium, Iron, Zinc and Copper on the Formation of Amyloid Fibrils of $A\beta_{1-42}$.	Keele University, UK	June - August 2003
(O)VOC measurements over fertilised grassland at Easter Bush near Edinburgh.	Edinburgh, UK	September – October 2004
(O)VOC flux measurements over the city of Gotebörg, Sweden (Göte – 2005 / BIAFLUX)	Gothenburg, Sweden	February 2005
(O)VOC measurements over grassland before and during slurry application at Easter Bush, near Edinburgh.	Edinburgh, UK	March – April 2005
(O)VOC flux measurements over an Oak forest (ACCENT BIAFLUX).	Alice Holt, UK	July – August 2005
(O)VOC flux measurements at Calton Hill, Edinburgh (CityFlux) .	Edinburgh, UK	November - December 2005
(O)VOC flux and truck based measurements over Manchester (CityFlux)	Manchester, UK	May 2006
PTR-MS instrument configuration for measurements in Central London (CityFlux)	London, UK	October/ November 2006
Development of a program for the calculation, correction and loss evaluation of (O)VOC fluxes measured *via* virtual disjunct eddy covariance using PTR-MS	Edinburgh, UK	February 2004 onwards
Construction of automated pre-concentration for GC analysis of (O)VOCs	Edinburgh, UK	October 2004 onwards

PUBLICATIONS:

Zholobenko, V. L., E. R. House (2003) Zeolite based catalysts for microwave-induced transformations of hydrocarbons, *Catalysis Letters*, **89**: 35 - 40.

House, E. R., J. Collingwood, A. Khan, O. Korchazkina, G. Berthon, C. Exley (2004) Aluminium, iron, zinc and copper influence the *in vitro* formation of amyloid fibrils of Aβ$_{42}$ in a manner which may have consequences for metal chelation in Alzheimer's disease, *Journal of Alzheimers Disease*, **6**: 291 - 301.

CONFERENCES / NON-PEER REVIEWED PUBLICATIONS:

Conference	Dates
European Research Course on Atmospheres (ERCA), Grenoble, Talk, "Measurement of OVOCs in the Troposphere"	12/01/04 – 13/02/04
Royal Meteorological Society (Atmospheric Chemistry Section), Leicester University.	01/04/04
Talk, "Measurement of Oxygenated Volatile Organic Compounds in the Troposphere" University of Edinburgh.	11/05/04
ACCENT BIAFLUX International Workshop, Edinburgh.	08/09/04 – 10/09/04
Talk, "Measurement of Oxygenated Volatile Organic Compounds in the Troposphere Using PTR-MS and GC" University of Edinburgh.	21/10/05
Conference and training session on Proton Transfer Reaction Mass Spectrometry, Austria	29/01/05 – 03/02/05
Talk, " Measurement of Volatile Organic Compounds from the Lipstick Tower" Gotebörg and University of Edinburgh	02/11/05 11/11/05
Poster and abstract, "Measurement of Organic Aerosol Precursors over an Oak Forest" ileaps international conference, Boulder , Colorado, USA.	23/01/06
Talk, "Measurement of (O)VOCs over Two Urban Areas" CEH Edinburgh	22/02/06
Talk, "VOC fluxes above Gotebörg and Edinburgh", CityFlux Meeting, CEH.	24/02/06

Appendix A.

The Derivation of the Equation for Calculation of the Volume Mixing Ratio of Trace Gas Components in the PTR-MS

In the drift tube of the PTR-MS many trace gas components undergo reaction with H_3O^+ ions:

$$M_a + H_3O^+ \xrightarrow{k_a} M_aH^+ + H_2O \qquad \text{(A.1)}$$

$$M_b + H_3O^+ \xrightarrow{k_b} M_bH^+ + H_2O \qquad \text{(A.2)}$$

$$M_i + H_3O^+ \xrightarrow{k_i} M_iH^+ + H_2O \qquad \text{(A.3)}$$
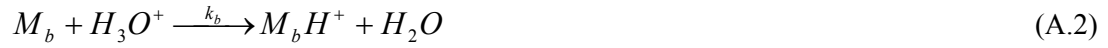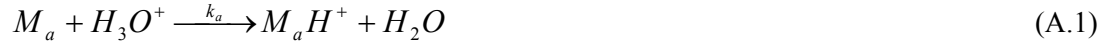
The rate equation for the reaction of i trace gas species with H_3O^+ is:

$$-\frac{d[H_3O^+]}{dt} = [H_3O^+]\sum_i k_i[M_i] \qquad \text{(A.4)}$$

The desired component is the concentration of a single trace species, e.g. M_a (Eq.A.1), the rate equation for the reaction of a single trace gas species is:

$$\frac{d[M_aH^+]}{dt} = k_a[M_a][H_3O^+] \qquad \text{(A.5)}$$

An expression for H_3O^+ is obtained by rearrangement and integration of Eq A.4 between time $t{=}0$ and $t{=}t$ (Eq. A.6 – A.8). $\sum_i [M_i]$ is treated as a constant since reaction time is short and a small fraction of the total trace gas concentration (which is much greater than the H_3O^+ concentration) reacts (§ 2.2).

$$\int_{t=0}^{t=t} d[H_3O^+]\frac{1}{[H_3O^+]} = -\sum_i k_i[M_i]\int_{t=0}^{t=t} dt \qquad \text{(A.6)}$$

$$\ln[H_3O^+]_t = -\sum_i k_i[M_i]t + \ln[H_3O^+]_0 \qquad \text{(A.7)}$$

$$[H_3O^+]_t = [H_3O^+]_0 \exp\left(-t\sum_i k_i[M_i]\right) \qquad \text{(A.8)}$$

where $[H_3O^+]_0$ denotes concentration at time, $t,{=}0$ and $[H_3O^+]_t$ that at time t. Substitution of Eq. A.8 into Eq. A.5 gives:

$$\frac{d[M_aH^+]}{dt} = k_a[M_a][H_3O^+]_0 \exp\left(-t\sum_i k_i[M_i]\right) \qquad \text{(A.9)}$$

Rearrangement and integration of Eq. A.9 gives:

$$[M_aH^+] = \frac{k_a[M_a]}{\sum_i k_i[M_i]}[H_3O^+]_0\left(1 - \exp - t\sum_i k_i[M_i]\right)$$ (A.10)

Rearrangement of Eq. A.7 gives:

$$\sum_i k_i[M_i] = -\frac{1}{t}\ln\frac{[H_3O^+]_t}{[H_3O^+]_0}$$ (A.11)

Substitution of Eq. A.11 gives:

$$[M_aH^+]_t = \frac{tk_a[M_a]}{-\ln([H_3O^+]_t/[H_3O^+]_0)}[H_3O^+]_0\left(1 - \exp - t\sum_i k_i[M_i]\right)$$ (A.12)

The total RH^+ concentration, $\sum_i[M_iH^+]$, is given by:

$$\sum_i[M_iH^+]_t = [H_3O^+]_0 - [H_3O^+]_t$$ (A.13)

Substitution of $[H_3O^+]_t$ *via* Eq.A.8 into Eq. A.13 gives:

$$\sum_i[M_iH^+]_t = [H_3O^+]_0 - [H_3O^+]_0\exp - t\sum_i k_i[M_i] = [H_3O^+]_0(1 - \exp - t\sum_i k_i[M_i])$$ (A.14)

Substitution of Eq. A.14 into Eq. A.12 and rearrangement to make $[R_a]$ the subject gives:

$$[R_a] = \frac{[M_aH^+]}{\sum_i[M_iH^+]}\frac{1}{k_at}\left(\ln\frac{[H_3O^+]_0}{[H_3O^+]_t}\right)$$ (A.15)

Substituting for $[H_3O^+]_0$ *via* Eq. A.13 gives:

$$[M_a] = \frac{[M_aH^+]}{\sum_i[M_iH^+]}\frac{1}{k_at}\left(\ln 1 + \left[\frac{\sum_i[M_iH^+]}{[H_3O^+]_t}\right]\right)$$ (A.16)

This logarithmic function can take the form:

$$\ln(1 + x) = x - \frac{x^2}{2} + \frac{x^3}{3} - \dots \quad \text{for} \quad x \le |1|$$ (A.17)

and since $[H_3O^+] \gg \sum_i[M_iH^+]$ (§2.2) therefore $\sum_i[M_iH^+]/[H_3O^+]$ is small the non

linear terms can be neglected and so Eq A.16 becomes:

$$[M_a] = \frac{1}{kt}\frac{[M_aH^+]_t}{[H_3O^+]_t}$$ (A.18)

These concentrations in Eq. A.18 at time t refer to concentrations at the drift tube exit. Due to ion losses between the drift tube and quadrupole, the mass dependent transmission of the quadrupole and variability in deflection to and detection at the SEM (§ 2.8) detected ion

count rates are related to the drift tube exit concentration by detection efficiency coefficients, $T_{H_3O^+}$ and $T_{M_aH^+}$:

$$(H_3O^+) = [H_3O^+]_{l_d} T_{H_3O^+} \tag{A.19}$$

$$(M_aH^+) = [M_aH^+]_{l_d} T_{M_aH^+} \tag{A.20}$$

where ( ) denotes detected ion count rates and $[]_{l_d}$ denotes concentrations at the drift tube exit as in Eq. A.19. Thus the volume mixing ratio of M is calculated from:

$$[M_a] = \frac{(M_aH^+)}{(H_3O^+)} \frac{T_{H_3O^+}}{T_{M_aH^+}} \frac{1}{kt} \frac{10^9}{N} \tag{A.21}$$

where N is the number density of particles in the drift tube. Division by N gives a value of $[M_a]$ in parts per part air, which is multiplied by 1 x 10^9 to give the volume mixing ratio in units of parts per billion (by volume), ppb.

Appendix B. (References in Chapter 2)

Ion-Dipole Potential Energy of Interaction

A dipole consists of two charges, $+q$ and $-q$, separated by a distance, R. R is the sum of d_1 and d_2 as defined in Figure B.1. A dipole moment, μ_D, is the product of the charge of the dipole, q and the distance between the charges, R.
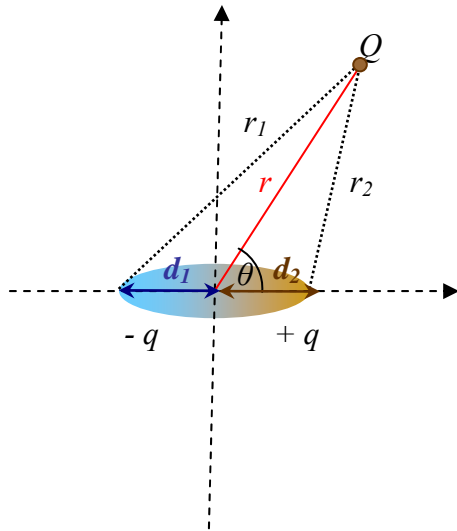
Figure B.1: Co-ordinates for calculation of the interaction between an ion of charge Q and a dipole with charges $+q$ and $-q$. The distance between the charges, R, $= d_1+d_2$ (Adapted from Shirts, 1986).

The potential energy between two charges is given by Coulomb's law:

$$U = \frac{q_a q_b}{4\pi\varepsilon_0 r} \tag{B.1}$$

U is the potential energy of interaction between two charges q_a and q_b separated by a distance, r. The potential energy of interaction between a dipole and ion is the sum of the interactions between $+q$ and Q and $-q$ and Q, from Coulombs law

$$U = \frac{+qQ}{4\pi\varepsilon_0 r_2} + \frac{-qQ}{4\pi\varepsilon_0 r_1} \tag{B.2}$$

At large r, d_1 and d_2 are assumed to be equal since any differences are small relative to r. In this case d_1 and d_2 are equal to $-R/2$ and $R/2$ respectively. Applying the Law of cosines, expressions for r_1 and d_2 in terms of R and r can be obtained (Shirts, 1986) (Figure B.2)

$$c^2 = a^2 + b^2 - 2ab\cos\theta$$
$$r_1^2 = r^2 + (-R/2)^2 - 2r(-R/2)\cos\theta$$
$$r_1^2 = r^2 + (R^2/4) + rR\cos\theta$$

$$c^2 = a^2 + b^2 - 2ab\cos\theta$$
$$r_2^2 = r^2 + (R/2)^2 - 2r(R/2)\cos\theta$$
$$r_2^2 = r^2 + (R^2/4) - rR\cos\theta$$
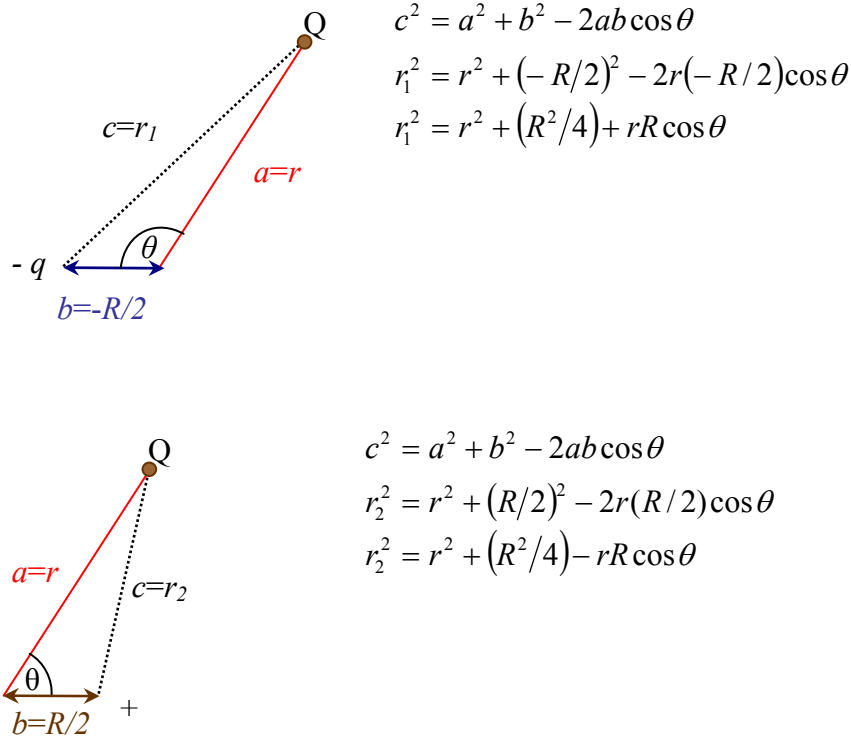
Figure B.2: The derivation of expressions for r_1 and r_2 as defined in Figure B.1.

Expressions for r_1 (Eq. B.3) and r_2 (Eq. B.4) can be substituted into Eq. B.2 to give Eq. B.5:

$$r_1 = (r^2 + R^2/4 + rR\cos\theta)^{1/2} \tag{B.3}$$

$$r_2 = (r^2 + R^2/4 - rR\cos\theta)^{1/2} \tag{B.4}$$

$$U = \frac{+qQ}{4\pi\varepsilon_0}\left(r^2 + \frac{R^2}{4} - rR\cos\theta\right)^{-1/2} + \frac{-qQ}{4\pi\varepsilon_0}\left(r^2 + \frac{R^2}{4} + rR\cos\theta\right)^{-1/2} \qquad (B.5)$$

Factorising out r gives

$$U = \frac{qQ}{4\pi\varepsilon_0 r}\left[\left(1 + \frac{R^2}{4r^2} - \frac{R}{r}\cos\theta\right)^{-1/2} - \left(1 + \frac{R^2}{4r^2} + \frac{R}{r}\cos\theta\right)^{-1/2}\right] \qquad (B.6)$$

Applying

$$(1+x)^{-1/2} = 1 - x/2 + 3x^2/8 + \ldots\ldots \qquad (B.7)$$

to the first inner bracket of Eq. B.6 and neglecting all terms with powers greater than 2 :

$$x = \frac{R^2}{4r^2} - \frac{R}{r}\cos\theta \qquad (B.8)$$

$$\frac{x}{2} = \frac{R^2}{8r^2} - \frac{R}{2r}\cos\theta \qquad (B.9)$$

$$x^2 = \left(\frac{R^2}{4r^2} - \frac{R}{r}\cos\theta\right)^2 = \frac{R^4}{4^2 r^4} + \frac{R^2}{r^2}\cos^2\theta - 2\times\frac{R^2}{4r^2}\times -\frac{R}{r}\cos\theta \approx \frac{R^2}{r^2}\cos^2\theta \qquad (B.10)$$

$$\frac{3x^2}{8} = \frac{3R^2}{8r^2}\cos^2\theta \qquad (B.11)$$

and so

$$\left(1 + \frac{R^2}{4r^2} - \frac{R}{r}\cos\theta\right)^{-1/2} = \left(1 - \left(\frac{R^2}{8r^2} - \frac{R}{2r}\cos\theta\right) + \frac{3R^2}{8r^2}\cos^2\theta\right) \qquad (B.12)$$

Treating the second bracket of Eq. B.6 in the same manner and substituting in to Eq. B.6 gives:

$$U = \frac{qQ}{4\pi\varepsilon_0 r}\left[\left(1 - \frac{R^2}{8r^2} + \frac{R}{2r}\cos\theta + \frac{3R^2}{8r^2}\cos^2\theta + .\right) - \left(1 - \frac{R^2}{8r^2} - \frac{R}{2r}\cos\theta + \frac{3R^2}{8r^2}\cos^2\theta + .\right)\right]$$

$$= \frac{qQ}{4\pi\varepsilon_0 r}\left(\frac{R}{r}\cos\theta + \ldots\right) \qquad (B.13)$$

By definition $\mu_D = qR$ giving:

$$U = \frac{\mu_D Q}{4\pi\varepsilon_0 r^2}\cos\theta(1 + ..) \approx \frac{\mu_D Q}{4\pi\varepsilon_0 r^2}\cos\theta \qquad (B.14)$$

Appendix C. (References in chapter 4)

Table C.1: Some potential sources and sinks of a selection of trace volatile compounds in animal waste and during its application to grassland.

Compound	Sources	Sinks
Ethanoic acid (Acetic acid)	**Deamination of amino acids alanine, glycine, serine glutamate, aspartate (also producing ammonia).** Deamination is the major pathway of amino acid metabolism at pH 6 to 7. Bacteria involved in deamination of carboxylic acids include *Eubacteria, Peptostreptocococcus, Bacterioides, Streptococcus, Escherichia, Megasphaera, Propionibacterium, Lactobacilli and Clostridium.* (Mackie *et al* 1998, Zhu *et al* 2000) **Fermentation of carbohydrates** (Mackie *et al* 1998) **Synthesis of acetic acid from CO_2 and H_2.** This is a common pathway in anaerobic ecosystems though there is no experimental evidence of this synthesis in wastes (Spoelstra 1980).	**Carboxylic acids are utilized for production of CO_2 and subsequently CH_4 by methanogens**. The amount of carboxylic acid depends on the balance between degradation of carbohydrates, proteins, lipids and methanogenesis (e.g. Mackie *et al* 1998) Dry and wet depositions are the dominant fates of carboxylic acids in the troposphere since chemical oxidation is slow (Table 4.1). Effective residence times (due to wet and dry deposition) are variable and are strongly controlled by precipitation estimates range from several hours to more than a week (Chebbi and Carlier 1996)
Propanoic acid (Propionic acid)	**Deamination of amino acids; threonine, glutamate, aspartate (also producing ammonia)**. (Mackie *et al* 1998, Zhu *et al* 2000) **Fermentation of carbohydrates** (Mackie *et al* 1998)	As above
Butanoic acid (Butyric acid)	**Deamination of amino acids; glutamate, aspartate (also producing ammonia)**. (Mackie *et al* 1998, Zhu *et al* 2000) **Fermentation of carbohydrates** (Mackie *et al* 1998)	As above
2-Methyl-Propanoic acid (*iso*-butyric acid)	**Deamination of amino acid valine (also producing ammonia)** (Allison 1978, Spoelstra 1980, Mackie *et al* 1998).	As above
Pentanoic acid (Valeric acid)	**Deamination of amino acids (also producing ammonia)**. (Mackie *et al* 1998, Zhu *et al* 2000) **Fermentation of carbohydrates** (Mackie *et al* 1998)	As above
3-methylbutanoic acid (*iso*-Valeric acid)	**Deamination of amino acid leucine (also producing ammonia)** (Allison 1978, Spoelstra 1980, Mackie *et al* 1998).	As above

Table C.1 is continued on the following page

Compound	Sources	Sinks
2-methylbutanoic acid	**Deamination of amino acid *iso*-leucine (also producing ammonia)** (Allison 1978, Spoelstra 1980, Mackie *et al* 1998).	As above
Hydrogen Sulphide	**Bacterial metabolism of sulphur containing amino acids** (and related compounds) cystine, cysteine (also forming ammonia and pyruvate), homocystein and thioglycolate (Spoelstra *et al* 1980, Mackie *et al* 1998, Kadota and Ishida 1972). Bacteria producing hydrogen sulphide from amino acid degradation include *Escherichia Coli* (cysteine and homocysteine) *Pseudonomas* sp. NCMB 1520 (cysteine), *Clostridium oedematicus* (Thioglycolate) (Kadota and Ishida 1972, Lomans *et al* 2002b). **Biological degradation of DMS to MT to H_2S *via* aerobic enzymatically catalysed pathways.** (refer to DMS and MT sinks) (Bentley and Chasteen 2004, Lomans *et al* 2002a and b). **Sulphate (and sulphite) reduction by sulphate reducing bacteria in oxygen depleted environments** (Manahan *et al* 1975, Zhu *et al* 2000, Kadota and Ishida 1972, Mackie *et al* 1998, Spoelstra 1980, Lomans *et al* 2002b). This can be assimilatory for synthesis of organic sulphur compounds (Zhu *et al* 2000, Mackie *et al* 1998, Lomans *et al* 2002b). Bacteria performing this reduction for assimilation include *Megasphaera, enterobacteria, Veillonella* (Mackie *et al* 1998). *Saccharomyces sake* produce hydrogen sulphide in the biosynthesis of cysteine from sulphate (repressed by methionine) (Kadota and Ishida 1972). *Saccharomyces cerevisiae* produce hydrogen sulphide from sulphate, sulphite and thiosulphate in the absence of methionine (Kadota and Ishida 1972). Alternatively reduction can be dissimilatory in order to dispose of an excess of reduction equivalents and produce energy (Manahan 1975, Zhu *et al* 2000, Mackie *et al* 1998, Lomans *et al* 2002b). Sulphate is supplied by diet or depolymerisation and desulphation of endogenously produced sulphated glycoproteins such as mucins (Mackie *et al* 1998).	**Biological methylation of hydrogen sulphide to form methanethiol** under high sulphide (HS-/H2S) concentrations in the presence of methyl donating groups e.g. methylated aromatics (refer to methanethiol sources) (Bentley and Chasteen 2004, Lomans *et al* 2002a and b, Bak *et al* 1992). **Oxidation to elemental sulphur (S^0) or sulphate** A variety of bacteria, found in soil and water can oxidize hydrogen sulphide to elemental sulphur. These include *Beggiatoa* and *Thiothrix*. Photosynthetic bacteria belonging to the families *Chromatiaceae* and *Chlorobiaceae* oxidize hydrogen sulphide to elemental sulphur and sulphate in the presence of light and the absence of oxygen. (Lomans *et al* 2002a,b, WHO 1981). **Hydrogen sulphide is strongly adsorbed by soils** (Bremmner and Banwart 1976, Spoelstra 1980). **Reaction with Fe (II) forming FeS/FeS_2** (Lomans *et al* 2002a and b). Atmospheric oxidation (Table 4.1).

Table C.1 is continued on the following page.

Compound	Sources	Sinks
Hydrogen Sulphide (continued)	Hydrogen availability may influence competition between sulphodigenesis and methanogenesis non- limiting hydrogen allowing both to occur concomitantly (Mackie *et al* 1998) *Desulfovibro* is a major hydrogenotrophic sulphur reducer (Manahan *et al* 1975, Mackie *et al* 1998). Sulphate reducing organisms have been found in amounts of 10^3 to 10^4 per ml in piggery waste (Spoelstra 1980). **Methanogenesis of DMS and MT producing sulphide, methane and carbon dioxide and/or sulphate reduction by DMS/MT leading to sulphide and carbon dioxide** (Lomans *et al* 2002a, b).	
Dimethylsulphide	**Microbial decomposition of amino acids and sulphonium salts.** For example; methionine is decomposed to dimethylsulphide (indirectly probably *via* methanethiol) by e.g. *Scopulariopsis brevicaulis, Schizophylum commune* and *Pseudomonas* sp. NCMB 1520 (Kadota and Ishida 1972, Spoelstra *et al* 1980, Kiene and Hines 1995). Decomposition of amino acid cysteine is a source of dimethyl sulphide (Hobbs *et al* 2004). Sulphonium salts may degraded to dimethylsulphide occurs enzymatically and non-enzymatically (Bentley and Chasteen 2004). Decomposition of *S*-methylmethionine, the sulphonium salt of methionine, by, for example, *Scropulariopsis brevicaulis* results in mainly dimethylsulphide (Kadota and Ishida 1972, Lomans 2002a, b, Bentley and Chasteen 2004, Kiene and Hienes 1995). Dimethylsulphide is also produced from trimethylsulphonium by *Pseudomonas* MS isolated from soil (Kadota and Ishida 1972, Bentley and Chasteen 2004). *S*-methylmethionine is thought to be a significant precursor of dimethylsulphide in terrestrial areas (Bentley and Chasteen 2004).	**Methanogenesis** - dimethylsulphide is converted to methane and methanethiol which is subsequently disproportionated to methane, carbon dioxide and hydrogen sulphide (Lomans *et al* 2002 a and b). **Sulphate reducing bacteria** - one strain of bacteria belonging to genus *Desulfotomaculum* has been isolated which oxidises dimethylsulphide to carbon dioxide and sulphide. Syntrophic metabolism between methanogens and sulphate reducers exists in sulphate rich freshwater sediments in which reduction equivalents derived from oxidation of dimethylsulphide are scavenged by sulphate reducing bacteria (Lomans *et al* 2002 a and b). **Use by denitrifying bacteria** – nitrate (NO_3^-) is converted to nitrogen (N_2) using dimethylsulphide and also producing carbon dioxide and sulphate (SO_4^{2-}) (Lomans *et al* 2002 a and b).

Table C.1 is continued on the following page.

Compound	Sources	Sinks
Dimethylsulphide (continued)	**Degradation of sulphonium salt dimethylsulphoniopropionate (DMSP), previously known as dimethyl-beta-propiothetin** (e.g. Bentley and Chasteen 2004, Lomans *et al* 2002 a and b, Kiene and Bates 1990, Charlson *et al* 1987, Kadota and Ishida 1972). DMSP is degraded to dimethylsulphide by DMSP lyase. DMSP lyase is present in aerobic and anaerobic bacteria, eukaryotic algae, phytoplankton and some plants (Bentley and Chasteen 2004). Acrylate is also produced and is further metabolised (Bentley and Chasteen 2004, Lomans *et al* 2002a and b). DMSP is an osmylyte in many algae, dinaflagellates, coccolithophores, halophillic plants species has a cryoprotectant ability, can act as a feeding attractant or deterrent, and is an antioxidant scavenging OH (Bentley and Chasteen 2004). DMSP is biosynthesised from methionine (Bentley and Chasteen 2004). This is the predominant source of dimethylsulphide production in oceans (Bentley and Chasteen 2004, Kiene and Bates 1990, Charlson *et al* 1987) and has a lesser role in freshwater sediments (Bentley and Chasteen 2004, Lomans *et al* 2002a and b). DMSP may be alternatively or methyl donation from DMSP may occur (Bentley and Chasteen 2004, Lomans *et al* 2002a and b). DMSP is not widespread in terrestrial plants (Bentley and Chasteen 2004). degraded to MMPA and methanethiol (refer to methanethiol sources).	Atmospheric oxidation (Table 4.1). **Oxidation** - Microorganisms mainly belonging to the generas *Thiobacillus*, *Methylophaga* and *Hyphomicrobium* degrade dimethylsulphide by anoxygenic photooxidation with H_2O to sulphide and formaldehyde (*via* methanethiol). The sulphide and formaldehyde may be further oxidised to sulphuric acid and carbon dioxide in order to release energy (*Thiobacillus*) or the formaldehyde may be incorporated in cell biomass (*Hyphomicrobium*) (sulphide may be oxidised to sulphuric acid). *Rhodovulvum sulfidophilum* normally use sulphide as an electron donor but can use DMS oxidizing to DMSO photoautotrophically catalysed by DMS dehydrogenase. The reduction of DMSO to DMS by DMS reductase is also reversible to some extent. **(**Kiene and Bates 1990, Bentley and Chasteen 2004, Lomans *et al* 2002 a and b). Oxidation of dimethylsulphide with O_2 to give DMSO also occurs: Marine methanotrophs containing a methane oxidase convert dimethylsulphide to DMSO with an oxygen requirements. Soil bacteria, *Acinetobacter* sp strain 20 B has also been shown to produce DMSO and small amount of $DMSO_2$ from dimethylsulphide. Ammonia monoxygenase can produce DMSO from DMS: CH_3-S-CH_3 (in place of ammonia) + $O_2+2e^-+2H^+\rightarrow$ CH_3-SO-CH_3 (analogous to NH_2OH) + H_2O. (Kiene and Bates 1990, Bentley and Chasteen 2004, Lomans *et al* 2002 a,b).

Table C.1 is continued on the following page.

Compound	Sources	Sinks
Dimethylsulphide (continued)	**Methylation of methanethiol in the presence of methyl donating groups such as methylated aromatic compounds (anaerobic).** Aromatics from e.g. degradation of lignin (aerobic), a very abundant biopolymer, donate methyl (CH_3^+) to methanethiol forming dimethylsulphide. The residual aromatic remaining after methyl donation is degraded to acetate or acetate and butyrate. This process has been observed in marine and freshwater sediments and *Sphagnum* peat bogs. Methylation is performed by anaerobic homoacetogenic bacteria (*Pelobacter* type), *Holophaga foetida*, *Parasporobacterium paucivrans, Sporobacter termitidis, Sporobacterium olearium*. Aside from methylated aromatics, thiol S-methyltransferases (TMT) enzymes catalysing transfer of methyl groups from *S*-Adenosylmethionin (produced, for example, from methionine *via* reaction with ATP and water) to methanethiol giving dimethylsulphide and *S*-Adenosylhomocyteine have been isolated. TMT enzymes are important in *Sphagnum* peat bogs, salt marshes and freshwater sediments. (Bentley and Chasteen 2004, Lomans *et al* 2002 a and b, Bak *et al* 1992, Kiene and Hines 1995). **DMSO reduction.** DMSO is reduced to DMS by DMSO reductases requiring a molybdenum cofactor. DMSO reductases are widely distributed and DMSO reducing capacity is widespread among aerobic and anaerobic bacteria, plants and animals. DMSO reductases have been found e.g. in *Escherichia Coli*, *Rhodobacter sphaeroides* and *Rhodobacter capsulates*. The reaction is to some extent reversible. DMSO reduction with lactate produces dimethylsulphide and acetate (Bentley and Chasteen 2004, Lomans *et al* 2002 a and b, Kiene and Hines 1995).	

Table C.1 is continued on the following page.

Compound	Sources	Sinks
Dimethyldisulphide	**Chemical oxidation of methanethiol**, for example, methanethiol produced from decomposition of methionine is partially oxidised to dimethyldisulphide. (Segal and Starkey 1969, Kadota and Ishida 1972, Lomans *et al* 2002 a and b).	**Reduction to methanethiol** (Lomans *et al* 2002 a, b) Atmospheric oxidation (4.1).
Dimethylsulphoxide	**DMS oxidation by photoautotrophic anoxygenic bacteria *via* enzyme DMS dehydrogenase to DMSO (/phototrophic oxidation of MT)** - refer to dimethylsulphide sinks (Kiene and Bates 1990, Bentley and Chasteen 2004, Lomans *et al* 2002 a and b) **Biological oxidation of DMS with O_2 to give DMSO** – refer to dimethylsulphide sinks. (Kiene and Bates 1990, Bentley and Chasteen 2004, Lomans *et al* 2002 a and b). Atmospheric oxidation of DMS (Table 4.1).	**Biological DMSO reduction by DMSO reductases** – refer to DMS sources (Bentley and Chasteen 2004, Lomans *et al* 2002 a and b, Kiene and Hines 1995). Atmospheric oxidation (Table 4.1).
Methanethiol (methyl mercaptan)	**Microbial (bacteria, actinomycetes and filamentous fungi) decomposition of amino acid methionine by deamination (producing ammonia) followed by demethiolation.** This decomposition is catalysed by enzyme L-methionine-γ-lase and requires a pyridoxal phosphate cofactor. The enzyme has been purified to homogeneity from *Pseudonomas putida*, *Brevibacterium linens* and *Trichomonas vaginalis* and the *P. putida* and the enzyme has been cloned in *Escherichia Coli*. α-ketobutyric acid is also produced and decomposition to CO_2 and H_2O is sometimes then observed. Some of the methanethiol produced is chemically oxidised to dimethyldisulphide (refer to dimethyldisulphide sources) the quantity varying with different cultures. *Aspergillus sp., Aspergillus oryzae, Fusarium culmorum, Streptomyces griseus. Streptomyces lavandulae, Pseudomonas sp., Psudomonas fluorescens, Proteus vulgaris, Escherichia coli, Pseudomonas aeruginosa, Clostridium tetani, Clostridium perfringens, Scopulariopsis brevicaulis, Microsporum gypseum, Aspergillus niger* and *Schizophyllum commune* produce methanethiol from methionine. (Segal and Starkey 1969, Mackie *et al* 1998, Spoelstra 1980, Kadota and Ishida 1972, Lomans *et al* 2002 a and b, Bentley and Chasteen 2004, Kiene and Hines 1995).	**Methylation of methanethiol to form dimethylsulphide** – refer to dimethylsulphide sources. (Bentley and Chasteen 2004, Lomans *et al* 2002 a and b, Bak *et al* 1992, Kiene and Hines 1995). **Methanogensis to methane, carbonyl sulphide and sulphide.** This is syntrophic with sulphate reduction using methanethiol. This is a major removal process in freshwater sediments. (Lomans *et al* 2002 a and b). **Conversion to carbon dioxide and sulphide by sulphate reducing bacteria.** Syntrophic metabolism between methanogens and sulphate reducers exists in sulphate rich freshwater sediments in which reduction equivalents derived from oxidation of DMS are scavenged by sulphate reducing bacteria. Methanethiol accumulation is only observed in sediments in the presence of methanogenate inhibitors and inhibitors of sulphate reducing bacteria in sulphate rich sediments. Inhibition of either methnogenesis or sulphogenesis alone does not prevent methanethiol conversion to hydrogen sulphide in sediments. (Lomans *et al* 2002 a and b). **Phototrophic oxidation to give DMSO** (Lomans *et al* 2002 a and b).

Table C.1 is continued on the following page.

Compound	Sources	Sinks
Methanethiol (continued)	**Bacterial (e.g. *Pseudonomas crucivae, Saccharomyces cerevisiae, Neurospora*) decomposition of *S*-methylcysteine producing ammonia, pyruvate and methanethiol.** This is catalysed by enzyme *S*-alkylcysteine lyase and a pyrioxidal phosphate cofactor is required. The reaction is also catalysed by methionine γ-lyase using *S*-methylcysteine as a substrate. Some of the methanethiol produced is chemically oxidised to dimethyldisulphide (refer to dimethyldisulphide sources) the quantity varying with different cultures. (Kadota and Ishida 1972, Lomans *et al* 2002 a and b, Bentley and Chasteen 2004). **Methylmercaptopropionate (MMPA) demethiolation.** MMPA is produced by anaerobic or aerobic degradation of dimethylsulphoniopropionate (DMSP). This is an alternative to degradation of DMSP to dimethylsulphide and acrylate (refer to DMS sources). This is the predominant source of methanethiol production in oceans and has a lesser role in freshwater sediments. (Lomans *et al* 2002 a and b, Bentley and Chasteen 2004). **Dimethyldisulphide reduction to methanethiol,** (some of the methanethiol is metabolised to methane and hydrogen sulphide). (Lomans *et al* 2002 a and b). **Methylation of hydrogen sulphide in the presence of high sulphide concentrations and methyl donating groups**. Methylated aromatic compounds acts as methyl donors in anaerobic environments. The reaction may occur for detoxification of sulphide or degradation of methylated aromatics. This is a major mechanism of methanethiol formation in freshwater sediments rich in sulphide (i.e. sulphate as is major precursor) and methyl donators. Methyl donating aromatics are	**Use by denitrifying bacteria** – nitrate (NO_3^-) is converted to nitrogen (N_2) using methanethiol and producing CO_2 and sulphate (SO_4^{2-}) (Lomans *et al* 2002 a and b). **Aerobic biotic degradation to hydrogen sulphide and formaldehyde.** Formaldehyde is subsequently used in assimilatory processes or further oxidised to carbon dioxide (and hydrogen sulphide to sulphate or sulphuric acid) (Lomans *et al* 2002 a and b, Bentley and Chasteen 2004). Atmospheric oxidation (Table 4.1).

Table C.1 is continued on the following page.

Compound	Sources	Sinks
Methanethiol (continued)	produced from lignin a very abundant biopolymer (aerobically). The residual aromatic remaining after methyl donation is degraded to acetate or acetate and butyrate. The process is observed in marine and freshwater sediments, *Sphagnum* peat bogs. Methylation is performed by anaerobic homoacetogenic bacteria (*Pelobacter* type) and has been studied with other organisms including *Holophaga foetida, Parasporobacterium paucivrans, Sporobacter termitidis, Sporobacterium olearium*. Aside from methylated aromatics thiol S-methyltransferases (TMT) enzymes (refer to dimethylsulphide sources) catalyse transfer of methyl groups from S-Adenosylmethionine to sulphide giving methanethiol and S-Adenosylhomocyteine. (Lomans *et al* 2002 a and b, Bentley and Chasteen 2004, Bak *et al* 1992). **Enzyme(s) described as C-S lyase, cysteine sulphoxide lyase, allinase or allin lyase using S-alkyl-L-cysteine sulphoxides produce several products including thiosulphinates.** (Bentley and Chasteen 2004). **Sulphate reducing bacteria have been shown to produce trace methanethiol** (Spoelstra 1980). This may be a result of processes listed above or a process connected to sulphate reduction.	
Ethanethiol (ethyl mercaptan)	**Sulphate reducing bacteria have been shown to produce traces of ethanethiol** (Spoelstra 1980) **Metabolism of *S*-ethylcysteine by *Saccharaomyces cerevisiae*** (Kadota and Ishida 1972).**Ethanethiol is a product of synthesis of methionine from methanethiol and ethionine by *Saccharaomyces cerevisiae*** (Cherest *et al* 1970, Kadota and Ishida 1972).	Atmospheric oxidation (Table 4.1).
Phosphine	**Microbial reduction of organic and/or inorganic phosphates** in slurry (alike reduction of sulphate to hydrogen sulphide, nitrate to ammonia, carbon dioxide to methane). However unlike methanogenesis and sulphodigenesis reduction of phosphates to phosphine with electron donors commonly utilised in nature (e.g. lactate, hydrogen) is endergonic rather than energy producing. This does not exclude a biological reduction pathway, given some energy input (Roels and Verstraete 2001, Roels *et al* 2005) or an as yet unidentified highly	**Microbial oxidation of phosphine ?** It is possible such an energy producing process occurs. The oxidation of phosphite (in which P also has oxidation state –III) coupled with sulphate reduction has been demonstrated as a source of energy for metabolism in *Desulfotignum phosphitoxidans*. Such roles of reduced phosphorus in microorganisms may be an evolutionary trait resulting from the reductive environment on primitive earth (Hanrahan *et al* 2005, Schink and Friedrich 2000).

Table C.1 is continued on the following page.

Compound	Sources	Sinks
Phosphine (continued)	energetic electron donor. Monoseptic cultures of bacteria including *Escherichia coli, Clostridium sporogenes, Clostridium acetobutyticum, Clostridium cochliarium, Salmonella gallinarum, Salmonalla arizonae* have been shown to generate phosphine (Dévai *et al* 1998, Jenkins *et al* 2000). Although phosphine evolution has been shown to correlate with methane emissions (Eismann 1997b), phosphine has been observed in the absence of methane (Jenkins *et al* 2000) and experimental evidence (e.g. methanogen inhibition) indicates there is no direct link to methanogenesis (Rutishauser and Bachofen 1999). Weaker correlations of phosphine evolution with hydrogen sulphide (e.g. Eismann *et al* 1997b) and dimethyl disulphide (Glindemann and Bergmann 1995) have been observed a link with sulphidogenesis may exist. It is possible that the relation between phosphine and methane and sulphides solely indicates that the processes underlying phosphine production are enhanced by similar environmental conditions. **Abiotic release of matrix bound phosphine (MBP).** However free phosphine released is sometime less than the decrease in MBP (suggesting sinks and possibly a negative flux - not necessarily ruling out microbial production) (e.g. Eismann *et al* 1997b). On other occasions abiotic release has been insufficient to account for free phosphine suggesting another source such as microbial reduction (laboratory experiment with mixed cultures and mediums - sinks such as soil and iron fillings not present) (Jenkins *et al* 2000). **Animal feed as a result of its fumigation with phosphine** may contribute to total phosphine though is not a sole source. MBP in fresh manure exceeds that in the feed (Eismann *et al* 1997b). Phosphine has been shown to increase along the course of digestion in cattle from the rumen through the gut to fresh cow pat and cattle manure suggesting an additional source (Gassmann and Glindemann 1993).	**Soil** – whether soils act as a source or sink of phosphine can strongly depend on the nature of iron species present in the soil (amongst other factors such as level of oxygen depletion, presence of organics). It is hypothesised that soil catalyses Fe (III) removal of phosphine. Addition of sodium azide does not effect phosphine removal from Fe(III) containing soils, suggesting Fe(III) reducing bacteria are not involved. The extent of phosphine emission differs in waterlogged and dry soils, removal continuing for longer from waterlogged soils indicating diffusion into the aqueous phase is rate limiting. Soil uptake could be important particularly at times when photooxidation by OH is not occurring (at night) (Eismann *et al* 1997a). A half life of phosphine in the presence of maize field soil without Fe(III) addition of 42 minutes, and 8 minutes with Fe(III) addition was obtained by Eismann *et al* (1997a). This compares with an average atmospheric half-life of 28 h for an average OH concentration of 5×10^5 molecules cm^{-3} (Frank and Rippen 1987 in Glindemann *et al* 2003 and Eismann *et al* 1997a). Fe(II) had no effect on half-life (i.e. ~42 min) during soil contact (Eismann *et al* 1997a). Atmospheric oxidation (Table 4.1).

Table C.1 is continued on the following page.

Compound	Sources	Sinks
Phosphine (continued)	**The corrosion of iron containing iron phosphides from, for example, slurry storage tanks** (Glindemann *et al* 1998, Roels and Verstraete 2004). Corrosion of zero valent aluminium (Roels and Verstraete 2004). **Soil -** soils act as source and sinks of phosphine emissions from soil increase after manure application then decrease with time. The release of phosphine from soils is dependent on a balance of natural generation and depletion MBP acting as a trace of the balance released under acidic conditions (Eismann *et al* 1997a, Glindemann *et al* 2005)	
Methylamine	**Metabolism of trimethylamine by microorganisms** (Schade and Crutzen 1998). **Amino acid glycine decarboxylation.** Amino acid decarboxylases are induced at pH 5 to 6 and may be involved in intracellular pH regulation (compared to deamination of amino acids giving carboxylic acids at pH 6 -7). Bacterial genera with decarboxylase activity include *Bacteroides, Bifidobacterium, Selenomonas, Streptococcus* and the enterobacteria. (Spoelstra 1980, Mackie *et al* 1998, Schade and Crutzen 1998). **Produced from minor precursors hordenine and sarcosine** (Schade and Crutzen 1998).	Atmospheric oxidation (Table 4.1). May compete with ammonia for nitric and sulphuric acid to form aminium nitrate and aminium sulphate salts respectively (Seinfield and Pandis 1998, Murphy *et al* 2007) (Table 4.1).
Dimethylamine	**Metabolism of trimethylamine by microorganisms** (Schade and Crutzen 1998). **Produced from minor precursors hordenine and sarcosine** (Schade and Crutzen 1998).	Atmospheric oxidation (Table 4.1). May compete with ammonia for nitric and sulphuric acid to form aminium nitrate and aminium sulphate salts respectively (Seinfield and Pandis 1998, Murphy *et al* 2007) (Table 4.1).
1-Propylamine	**Production by various bacteria demonstrated.** (Spoelstra 1980). **Possibly resulting from decarboxylation of amino acid α-Aminobutyrate** (Mackie *et al* 1998) Amino acid decarboxylase, an enzyme that catalyses formation of propylamine (and other amines not tabulated here) from amino acids has been isolated in *Proteus vulgaris* and *Bacillus sphaericus* (Spoelstra 1980).	Atmospheric oxidation (Table 4.1). May compete with ammonia for nitric and sulphuric acid to form aminium nitrate and aminium sulphate salts respectively (Seinfield and Pandis 1998, Murphy *et al* 2007) (Table 4.1).

Table C.1 is continued on the following page.

Compound	Sources	Sinks
2-Propylamine	**Possibly decarboxylation of α-Aminobutyrate** (Mackie *et al* 1998). 2-propylamine has been observed in small amounts from animal wastes possibly resulting from amino acid degradation (Schade and Crutzen 1998).	Atmospheric oxidation (Table 4.1). May compete with ammonia for nitric and sulphuric acid to form aminium nitrate and aminium sulphate salts respectively (Seinfield and Pandis 1998, Murphy *et al* 2007) (Table 4.1).
Trimethylamine	**Chloine degradation** (Schade and Crutzen 1998). **Betaine degradation** (Schade and Crutzen 1998). Aromatic amino acids are metabolized by a variety of anaerobes including *Bacteroides, Lactobacillus, Clostridium and Bifidobacterium* (Mackie *et al* 1998).	**Demethylation by microorganisms to form dimethylamine and methylamine** (Schade and Crutzen 1998). Atmospheric oxidation (Table 4.1). May compete with ammonia for sulphuric acid to form aminium sulphate salts (Murphy *et al* 2007) (Table 4.1).
4-methylphenol (*p*-cresol)	**Metabolism of amino acid tyrosine by intestinal anaerobes including bacteroides, Lactobacillus, Clostridium, Bifidobacterium and as well as during anaerobic storage of wastes. Tyrosine may be alternatively metabolised to phenol, 4-ethyl phenol or phenol propionate** (Spoelstra 1977, Spoelstra 1980, Mathus *et al* 1995, Mackie *et al* 1998, Zhu 2000). Refer to phenol sources.	Atmospheric oxidation (Table 4.1).

Appendix D. (References in chapter 4)

Table D.1: Some previous measurements of selected volatile compounds emitted from animal waste and animal production facilities.

Compound	Previous Measurement		Animal waste	Measurement method	Reference
	Concentrations ppb (μg m^{-3})*	Emission Rates			
Ethanoic acid (Acetic acid)	**2887 ± 1363** (7098)		**Headspace of fresh pig faeces** from 6 pigs diluted with de-ionised water & pH adjusted to 4.0 using 0.1 M HCl.	**SIFT-MS**	Smith *et al* (2000)
	616 ± 616 (1515)		**Headspace of fresh pig urine** from 6 pigs, pH adjusted to 4.0 using 0.1 M HCl.	**SIFT-MS**	Smith *et al* (2000)
		5.7 g m^{-3} day^{-1}	**Headspace of fresh cattle slurry**, pH 7.1, 53.7 ± 9.5 g kg^{-1} dry matter, 1.09 ± 0.7 kg m^{-3} NH$_4$.	Slurry placed in a 40 m^3 emissions chamber with 1 m s^{-1} circulation of air over the slurry surface. Slurry kept at 15 ^{o}C and the emission chamber at 20°C, periodic sampling analysed by **GC-MS** with pre-concentration.	Hobbs *et al* (2004)
		Trace	**Headspace of laying hen manure**, pH 8.3, 501.2 ± 144.8 g kg^{-1} dry matter, 7.52 ± 0.66 kg m^{-3} NH$_4$.	As above	Hobbs *et al* (2004)
	15.1 to 168.7 **(37.1 to 414.9**)		**Air at three sampling sites at a commercial dairy farm in California** two of which were next to a waste water lagoon, acetic acid was observed in 4 out of 48 samples.	**GC-MS** with simultaneous olfactometry (samples collected on adsorption tubes).	Rabaud *et al* (2003)

Table D.1 is continued on the following page.

Compound	Previous Measurement		Animal waste	Measurement method	Reference
	Concentrations Ppb (μg m^{-3})*	Emission Rates			
Ethanoic acid (continued)	1912 (**4700**)		**Headspace of pig slurry from pigs fed dry feed pellets collected over 28 days** and stored in enclosed stainless steel trays in a water bath at 15°C for 1 month before placing in an emissions chamber. Slurry analysed before odour and emissions chamber experiment: total solids 5.93 kg, pH 7.1 (pH 7.9 after odour and emissions chamber measurements) ammonium N 458 g, Nitrate N 4.97 g, total N 800 g.	Slurry placed in a 40 m^3 emissions chamber (can reduce from 40 to 15 m3 over 3 h period) with 1.0 m^3 s^{-1} circulation of air over manure surface at 20°C. Tedlar samples taken and analysed by **GC-MS** with preconcentration.	Hobbs *et al* (1997)
	935.4 (**2300**)		**Headspace of pig slurry from pigs fed liquid feed with water to feed ratio of 3:1 (w/w) collected over 28 days** and stored in enclosed stainless steel trays in a water bath at 15°C for 1 month before placing in an emissions chamber. Slurry analysed before odour and emissions chamber experiment: total solids 6.04 kg, pH 7.5 (pH 8.5 after odour and emissions chamber measurements) ammonium N 556 g, Nitrate N 2.20 g, total N 858 g.	As above	Hobbs *et al* (1997)
	732.1 (**1800**)		**Headspace of pig slurry from pigs fed liquid feed with water to feed ratio of 4:1 (w/w) collected over 28 days** and stored in enclosed stainless steel trays in a water bath at 15°C for 1 month before placing in an emissions chamber. Slurry analysed before odour and emissions chamber experiment: total solids 4.77 kg, pH 7.6 (pH 8.4 after odour and emissions chamber measurements) ammonium N 502 g, Nitrate N 5.90 g, total N 785 g.	As above	Hobbs *et al* (1997)

Table D.1 is continued on the following page.

Compound	Previous Measurement		Animal waste	Measurement method	Reference
	Concentrations ppb ($\mu g\ m^{-3}$)*	Emission Rates			
Ethanoic acid (continued)	3.4 µg litre-1		**Air samples from the middle of a pig house** (44 pigs, 5.3 m^3 of air per pig). VMR in the air were primarily determined by concentrations of the acid in faeces and slurry: 19.2 mg g^{-1} dry matter in faeces, 2.0 mg g^{-1} dry matter in slurry.	**GC-FID** with pre-concentration.	Willig *et al* (2004)
Propanoic acid	**2621 ± 1383** (7935)		**Headspace of fresh pig faeces** from 6 pigs diluted with de-ionised water & pH adjusted to 4.0 using 0.1 M HCl.	**SIFT-MS**	Smith *et al* (2000)
	825.8 **(2500)**		**Headspace of pig slurry from pigs fed dry feed pellets collected over 28 days** and stored in enclosed stainless steel trays in a water bath at 15^oC for 1 month before placing in an emissions chamber. Slurry analysed before odour and emissions chamber experiment: total solids 5.93 kg, pH 7.1 (pH 7.9 after odour and emissions chamber measurements) ammonium N 458 g, Nitrate N 4.97 g, total N 800 g.	Slurry placed in a 40 m^3 emissions chamber (can reduce from 40 to 15 m3 over 3 h period) with 1.0 $m^3\ s^{-1}$ circulation of air over manure surface at 20^oC. Tedlar samples taken and analysed by **GC-MS** with preconcentration.	Hobbs *et al* (1997)
	23 **(70)**		**Headspace of pig slurry from pigs fed liquid feed with water to feed ratio of 3:1 (w/w) collected over 28 days** and stored in enclosed stainless steel trays in a water bath at 15^oC for 1 month before placing in an emissions chamber. Slurry analysed before odour and emissions chamber experiment: total solids 6.04 kg, pH 7.5 (pH 8.5 after odour and emissions chamber measurements) ammonium N 556 g, Nitrate N 2.20 g, total N 858 g.	As above	Hobbs *et al* (1997)

Table D.1 is continued on the following page.

Compound	Previous Measurement		Animal waste	Measurement method	Reference
	Concentrations ppb (μg m^{-3})*	Emission Rates			
Propanoic acid (continued)	6.6 **(20)**		**Headspace of pig slurry from pigs fed liquid feed with water to feed ratio of 4:1 (w/w) collected over 28 days** and stored in enclosed stainless steel trays in a water bath at 15°C for 1 month before placing in an emissions chamber. Slurry analysed before odour and emissions chamber experiment: total solids 4.77 kg, pH 7.6 (pH 8.4 after odour and emissions chamber measurements) ammonium N 502 g, Nitrate N 5.90 g, total N 785 g.	As above	Hobbs *et al* (1997)
	577 ± 313 (1747)		**Headspace of fresh pig urine** from 6 pigs, pH adjusted to 4.0 using 0.1 M HCl.	**SIFT-MS**	Smith *et al* (2000)
	2.3 μg litre-1		**Air samples from the middle of a pig house** (44 pigs, 5.3 m^3 of air per pig). VMR in the air were primarily determined by concentrations of the acid in faeces and slurry: 7.7 mg g^{-1} dry matter in faeces, 1.1 mg g^{-1} dry matter in slurry.	**GC-FID** with pre-concentration.	Willig *et al* (2004)
		0.15 g m^{-3} day^{-1}	**Headspace of fresh cattle slurry**, pH 7.1, 53.7 ± 9.5 g kg^{-1} dry matter, 1.09 ± 0.7 kg m^{-3} NH$_4$.	Slurry placed in a 40 m^3 emissions chamber with 1 m s^{-1} circulation of air over the slurry surface. Slurry kept at 15 ^{o}C and the emission chamber at 20°C, periodic sampling analysed by **GC-MS** with preconcentration.	Hobbs *et al* (2004)

Table D.1 is continued on the following page.

Compound	Previous Measurement		Animal waste	Measurement method	Reference
	Concentrations ppb (μg m^{-3})*	Emission Rates			
Propanoic acid (continued)		Trace	**Headspace of laying hen manure**, pH 8.3, 501.2 $\pm$ 144.8 g kg^{-1} dry matter, 7.52 $\pm$ 0.66 kg m^{-3} NH$_4$.	As above	Hobbs *et al* (2004)
Butanoic acid (Butyric acid)	**1402 $\pm$ 804**** (5055)		**Headspace of fresh pig faeces** from 6 pigs diluted with de-ionised water & pH adjusted to 4.0 using 0.1 M HCl.	**SIFT-MS**	Smith *et al* (2000)
	106 $\pm$ 134** (382)		**Headspace of fresh pig urine** from 6 pigs, pH adjusted to 4.0 using 0.1 M HCl.	**SIFT-MS**	Smith *et al* (2000)
	0.8 μg litre-1		**Air samples from the middle of a pig house** (44 pigs, 5.3 m^3 of air per pig). VMR in the air were primarily determined by concentrations of the acid in faeces and slurry: 7.0 mg g^{-1} dry matter in faeces, 0.7mg g^{-1} dry matter in slurry.	**GC-FID** with pre-concentration	Willig *et al* (2004)
	305.1 **(1100)**		**Headspace of pig slurry from pigs fed dry feed pellets collected over 28 days** and stored in enclosed stainless steel trays in a water bath at 15°C for 1 month before placing in an emissions chamber. Slurry analysed before odour and emissions chamber experiment: total solids 5.93 kg, pH 7.1 (pH 7.9 after odour and emissions chamber measurements) ammonium N 458 g, Nitrate N 4.97 g, total N 800 g.	Slurry placed in a 40 m^3 emissions chamber (can reduce from 40 to 15 m3 over 3 h period) with 1.0 m^3 s^{-1} circulation of air over manure surface at 20°C. Tedlar samples taken and analysed by **GC-MS** with preconcentration.	Hobbs *et al* (1997)

Table D.1 is continued on the following page.

Compound	Previous Measurement		Animal waste	Measurement method	Reference
	Concentrations ppb (μg m^{-3})*	Emission Rates			
Butanoic acid (continued)	1109 **(4000)**		**Headspace of pig slurry from pigs fed liquid feed with water to feed ratio of 3:1 (w/w) collected over 28 days** and stored in enclosed stainless steel trays in a water bath at 15°C for 1 month before placing in an emissions chamber. Slurry analysed before odour and emissions chamber experiment: total solids 6.04 kg, pH 7.5 (pH 8.5 after odour and emissions chamber measurements) ammonium N 556 g, Nitrate N 2.20 g, total N 858 g.	As above	Hobbs *et al* (1997)
	Not detected		**Headspace of pig slurry from pigs fed liquid feed with water to feed ratio of 4:1 (w/w) collected over 28 days** and stored in enclosed stainless steel trays in a water bath at 15°C for 1 month before placing in an emissions chamber. Slurry analysed before odour and emissions chamber experiment: total solids 4.77 kg, pH 7.6 (pH 8.4 after odour and emissions chamber measurements) ammonium N 502 g, Nitrate N 5.90 g, total N 785 g.	As above	Hobbs *et al* (1997)
		0.06 g m^{-3} day^{-1}	**Headspace of fresh cattle slurry**, pH 7.1, 53.7 $\pm$ 9.5 g kg^{-1} dry matter, 1.09 $\pm$ 0.7 kg m^{-3} NH$_4$.	Slurry placed in a 40 m^3 emissions chamber with 1 m s^{-1} circulation of air over the slurry surface. Slurry kept at 15 ^{o}C and the emission chamber at 20°C, periodic sampling analysed by **GC-MS** with pre-concentration.	Hobbs *et al* (2004)

Table D.1 is continued on the following page.

Compound	Previous Measurement		Animal waste	Measurement method	Reference
	Concentrations ppb (μg m^{-3})*	Emission Rates			
Butanoic acid (continued)		Trace	**Headspace of laying hen manure**, pH 8.3, 501.2 $\pm$ 144.8 g kg^{-1} dry matter, 7.52 $\pm$ 0.66 kg m^{-3} NH$_4$.	As above	Hobbs *et al* (2004)
2-methyl-propanoic acid (*iso*-butyric acid)	55.5 **(200)**		**Headspace of pig slurry from pigs fed dry feed pellets collected over 28 days** and stored in enclosed stainless steel trays in a water bath at 15°C for 1 month before placing in an emissions chamber. Slurry analysed before odour and emissions chamber experiment: total solids 5.93 kg, pH 7.1 (pH 7.9 after odour and emissions chamber measurements) ammonium N 458 g, Nitrate N 4.97 g, total N 800 g.	Slurry placed in a 40 m^3 emissions chamber (can reduce from 40 to 15 m3 over 3 h period) with 1.0 m^3 s^{-1} circulation of air over manure surface at 20°C. Tedlar samples taken and analysed by **GC-MS** with preconcentration.	Hobbs *et al* (1997)
	None detected		**Headspace of pig slurry from pigs fed liquid feed with water to feed ratio of 3:1 (w/w) collected over 28 days** and stored in enclosed stainless steel trays in a water bath at 15°C for 1 month before placing in an emissions chamber. Slurry analysed before odour and emissions chamber experiment: total solids 6.04 kg, pH 7.5 (pH 8.5 after odour and emissions chamber measurements) ammonium N 556 g, Nitrate N 2.20 g, total N 858 g.	As above	Hobbs *et al* (1997)

Table D.1 is continued on the following page.

Compound	Previous Measurement		Animal waste	Measurement method	Reference
	Concentrations Ppb (µg m^{-3})*	Emission Rates			
2-methyl-propanoic acid (continued)	None detected		**Headspace of pig slurry from pigs fed liquid feed with water to feed ratio of 4:1 (w/w) collected over 28 days** and stored in enclosed stainless steel trays in a water bath at 15°C for 1 month before placing in an emissions chamber. Slurry analysed before odour and emissions chamber experiment: total solids 4.77 kg, pH 7.6 (pH 8.4 after odour and emissions chamber measurements) ammonium N 502 g, Nitrate N 5.90 g, total N 785 g.	As above	Hobbs *et al* (1997)
		0.07 g m^{-3} day^{-1}	**Headspace of fresh cattle slurry**, pH 7.1, 53.7 ± 9.5 g kg^{-1} dry matter, 1.09 ± 0.7 kg m^{-3} NH$_4$.	Slurry placed in a 40 m^3 emissions chamber with 1 m s^{-1} circulation of air over the slurry surface. Slurry kept at 15 ^{o}C and the emission chamber at 20°C, periodic sampling analysed by **GC-MS** with pre-concentration.	Hobbs *et al* (2004)
		None detected	**Headspace of laying hen manure**, pH 8.3, 501.2 ± 144.8 g kg^{-1} dry matter, 7.52 ± 0.66 kg m^{-3} NH$_4$.	As above	Hobbs *et al* (2004)
	0.1 µg litre-1		**Air samples from the middle of a pig house** (44 pigs, 5.3 m^3 of air per pig). VMR in the air were primarily determined by concentrations of the acid in faeces and slurry: 0.9 mg g^{-1} in faeces, 0.2 mg g^{-1} in slurry.	**GC-FID** with pre-concentration	Willig *et al* 2004

Table D.1 is continued on the following page.

Compound	Previous Measurement		Animal waste	Measurement method	Reference
	Concentrations ppb (µg m^{-3})*	Emission Rates			
Pentanoic acid (Valeric acid)	**397 ± 111**** (1657)		**Headspace of fresh pig faeces** from 6 pigs diluted with de-ionised water & pH adjusted to 4.0 using 0.1 M HCl.	**SIFT-MS**	Smith *et al* (2000)
	21.06 **(87.92)**		**Air at three sampling sites at a commercial dairy farm in California** two of which were next to a waste water lagoon, pentanoic acid was observed in 1 out of 48 samples.	**GC-MS** with simultaneous olfactometry (samples collected on adsorption tubes).	Rabaud *et al* (2003)
	47.9 **(200)**		**Head space of pig slurry from pigs fed dry feed pellets collected over 28 days** and stored in enclosed stainless steel trays in a water bath at 15^{0}C for 1 month before placing in an emissions chamber. Slurry analysed before emissions chamber experiment: total solids 5.93kg, pH7.1 (pH7.9 after odour and emissions chamber measurements) ammonium N458g, Nitrate N 4.97g, total 800g.	Slurry placed in a 40 m^3 emissions chamber (can reduce from 40 to 15 m^3 over 3 h period) with 1.0 m^3 s^{-1} circulation of air over manure surface at 20^{0}C. Tedlar samples taken and analysed by **GC-MS** with preconcentration.	m^3
	Not detected		**Headspace of pig slurry from pigs fed liquid feed with water to feed ratio of 3:1 (w/w) collected over 28 days** and stored in enclosed stainless steel trays in a water bath at 15°C for 1 month before placing in an emissions chamber. Slurry analysed before emissions chamber experiment: total solids 6.04 kg, pH 7.5 (pH 8.5 after odour and emissions chamber measurements) ammonium N 556 g, Nitrate N 2.20 g, total N 858 g.	As above	Hobbs *et al* (1997)

Table D.1 is continued on the following page.

Compound	Previous Measurement		Animal waste	Measurement method	Reference
	Concentrations ppb (μg m^{-3})*	Emission Rates			
Pentanoic acid (Valeric acid) continued	Not detected		**Headspace of pig slurry from pigs fed liquid feed with water to feed ratio of 4:1 (w/w) collected over 28 days** and stored in enclosed stainless steel trays in a water bath at 15°C for 1 month before placing in an emissions chamber.Slurry analysed before emissions chamber experiment: total solids 4.77 kg, pH 7.6 (pH 8.4 after odour and emissions chamber measurements) ammonium N 502 g, Nitrate N 5.90 g, total N 785 g.	As above	Hobbs *et al* (1997)
	0.2 μg litre-1		**Air samples from the middle of a pig house** (44 pigs, 5.3 m^{3} of air per pig). VMR in the air were primarily determined by concentrations of the acid in faeces and slurry: 2.0 mg g^{-1} in faeces, 0.2 mg g^{-1} in slurry.	**GC-FID** with pre-concentration.	Willig *et al* (2004)
		0.01 g m^{-3} day^{-1}	**Headspace of fresh cattle slurry**, pH 7.1, 53.7 $\pm$ 9.5 g kg^{-1} dry matter, 1.09 $\pm$ 0.7 kg m^{-3} NH$_4$.	Slurry placed in a 40 m^{3} emissions chamber with 1 m s^{-1} circulation of air over the slurry surface. Slurry kept at 15°C and the emission chamber at 20°C, periodic sampling analysed by **GC-MS** with pre-concentration.	Hobbs *et al* (2004)
	None detected		**Headspace of laying hen manure**, pH 8.3, 501.2 $\pm$ 144.8 g kg^{-1} dry matter, 7.52 $\pm$ 0.66 kg m^{-3} NH$_4$.	As above	Hobbs *et al* (2004)

Table D.1 is continued on the following page

Compound	Previous Measurement		Animal waste	Measurement method	Reference
	Concentrations ppb ($\mu g\ m^{-3}$)*	Emission Rates			
3-methyl-butanoic acid (*iso*-Valeric acid)	0.2 µg litre-1		**Air samples from the middle of a pig house** (44 pigs, 5.3 m^3 of air per pig). VMR in the air were primarily determined by concentrations of the acid in faeces and slurry: 1.7 mg g^{-1} in faeces, 0.3 mg g^{-1} in slurry.	**GC-FID** with pre-concentration.	Willig *et al* (2004)
	263.5 **(1100)**		**Headspace of pig slurry from pigs fed dry feed pellets collected over 28 days** and stored in enclosed stainless steel trays in a water bath at 15°C for 1 month before placing in an emissions chamber. Slurry analysed before emissions chamber experiment: total solids 5.93 kg, pH 7.1 (pH 7.9 after emissions chamber measurements) ammonium N 458 g, Nitrate N 4.97 g, total N 800 g.	Slurry placed in a 40 m^3 emissions chamber (can reduce from 40 to 15 m3 over 3 h period) with 1.0 $m^3\ s^{-1}$ circulation of air over manure surface at 20°C. Tedlar samples taken and analysed by **GC-MS** with preconcentration.	Hobbs *et al* (1997)
	191.6 **(800)**		**Headspace of pig slurry from pigs fed liquid feed with water to feed ratio of 3:1 (w/w) collected over 28 days** and stored in enclosed stainless steel trays in a water bath at 15°C for 1 month before placing in an emissions chamber. Slurry analysed before emissions chamber experiment: total solids 6.04 kg, pH 7.5 (pH 8.5 after emissions chamber measurements) ammonium N 556 g, Nitrate N 2.20 g, total N 858 g.	As above	Hobbs *et al* (1997)

Table D.1 is continued on the following page.

Compound	Previous Measurement		Animal waste	Measurement method	Reference
	Concentrations ppb (μg m^{-3})*	Emission Rates			
3-methyl-butanoic acid (iso-Valeric acid (continued)	Not detected		**Headspace of pig slurry from pigs fed liquid feed with water to feed ratio of 4:1 (w/w) collected over 28 days** and stored in enclosed stainless steel trays in a water bath at 15°C for 1 month before placing in an emissions chamber. Slurry analysed before emissions chamber experiment: total solids 4.77 kg, pH 7.6 (pH 8.4 after emissions chamber measurements) ammonium N 502 g, Nitrate N 5.90 g, total N 785 g.	As above	Hobbs *et al* (1997)
		0.22 g m^{-3} day^{-1}	**Headspace of fresh cattle slurry**, pH 7.1, 53.7 ± 9.5 g kg^{-1} dry matter, 1.09 ± 0.7 kg m^{-3} NH$_4$.	Slurry placed in a 40 m^3 emissions chamber with 1 m s^{-1} circulation of air over the slurry surface. Slurry kept at 15°C and the emission chamber at 20°C, periodic sampling analysed by **GC-MS** with pre-concentration.	Hobbs *et al* (2004)
	Not detected		**Headspace of laying hen manure**, pH 8.3, 501.2 ± 144.8 g kg^{-1} dry matter, 7.52 ± 0.66 kg m^{-3} NH$_4$.	As above	Hobbs *et al* (2004)
2-methyl-butanoic acid		0.14g m^{-3} day^{-1}	**Headspace of fresh cattle slurry,** pH 7.1, 53.7 ± 9.5 g kg^{-1} dry matter, 1.09 ± 0.7 kg m^{-3} NH$_4$.	Slurry placed in a 40 m^3 emissions chamber with 1 m s^{-1} circulation of air over the slurry surface. Slurry kept at 15°C and the emission chamber at 20°C, periodic sampling analysed by **GC-MS** with pre-concentration.	Hobbs *et al* (2004)

Table D.1 is continued on the following page

Compound	Previous Measurement		Animal waste	Measurement method	Reference
	Concentrations ppb (µg m^{-3})*	Emission Rates			
2-methyl-butanoic acid (continued)		Not detected	**Headspace of laying hen manure**, pH 8.3, 501.2 ± 144.8 g kg^{-1} dry matter, 7.52 ± 0.66 kg m^{-3} NH$_4$.	As above	Hobbs *et al* (2004)
Phosphine		86 pl kg^{-1}	**Fresh swine manure stored anerobically** for 43 weeks with samples of the headspace collected weekly using a syringe.	GC (NPD) with cryotrapping preconcentration.	Eismann *et al* (1997b)
		7 (spring) to 376 (fall) µg day^{-1}	**Large-scale anerobic manure fermentation plants.** 3 parallel samples taken on three subsequent days in every season except winter.	GC (NPD) with cryotrapping preconcentration.	Eismann *et al* (1997b)
		18 (spring) to 6707 (fall) µg day-1	**Large-scale anerobic manure fermentation plants.** 3 parallel samples taken on three subsequent days in every season.	GC (NPD) with cryotrapping preconcentration.	Eismann *et al* (1997b)
		9.56 ng m^{-2} h^{-1}	Closed chamber measurements next to a **gentoo penguin colony**. MBP found in the guano of this species. Sampling as above.	GC (NPD) with cryotrapping preconcentration.	Zhu *et al* (2006 a, b)
		39.96 ng m^{-2} h^{-1}	Closed chamber measurements next to a **seal colony**. MBP found in the guano of this species. Sampling as above.	GC (NPD) with cryotrapping preconcentration.	Zhu *et al* (2006 a, b)
		63.58 ng m^{-2} h^{-1}	Closed chamber measurements next to an **empire penguin colony**. MBP found in the guano of this species. Sampling as above.	GC (NPD) with cryotrapping preconcentration.	Zhu *et al* (2006 a, b)
	0 to 0.212 **(0 to 0.295)**		Tedlar samples of **animal (pig and cattle) slurry biogas**.	GC (NPD) with cryotrapping preconcentration.	Glindemann, and Bergmann (1995) Roels, and Verstraete (2001)

Table D.1 is continued on the following page

Compound	Previous Measurement		Animal waste	Measurement method	Reference
	Concentrations ppb (μg m^{-3})*	Emission Rates			
Phosphine (continued)	0.017 to 14.6 **(0.024 to 20.3)**		Tedlar samples of **animal (pig and cattle) slurry putrification gas.**	GC (NPD) with cryotrapping preconcentration.	Glindemann, and Bergmann (1995) Roels, and Verstraete (2001)
	0 to 0.039 **(0 to 0.055)**		**Composting gas, cattle manure biosolids** collected. Three samples (seasonal) collected in tedlar bags.	GC (NPD) with cryotrapping preconcentration.	Glindemann *et al* (1996b), Glindemann *et al* (2005)
	0.022 to 0.728 **(0.031 to 1.015)**		**Composting gas, swine manure biosolids** Four samples (seasonal) collected in Tedlar bags.	GC (NPD) with cryotrapping preconcentration.	Glindemann *et al* (1996b), Glindemann *et al* (2005)
	0 to 0.0093 **(0 to 0.013)**		**Biogas of cattle manure.** Four samples (seasonal) collected in Tedlar bags.	GC (NPD) with cryotrapping preconcentration.	Glindemann *et al* (1996b), Glindemann *et al* (2005)
	0.0882 to 0.171 **(0.123 to 0.238)**		**Putrefaction gas of cattle manure storage.** Three samples (seasonal) collected in tedlar bags.	GC (NPD) with cryotrapping preconcentration.	Glindemann *et al* (1996b), Glindemann *et al* (2005)
	0 to 1.164 **(0 to 1.623)**		**Biogas, swine manure digestion** Four samples (seasonal) collected in Tedlar bags.	GC (NPD) with cryotrapping preconcentration.	Glindemann *et al* (1996b), Glindemann *et al* (2005)
	0.037 to 6.45 **(0.051 to 8.995)**		**Putrefaction gas, swine manure storage.** Fourteen samples (2 storage plants, 4 seasons) taken in Tedlar bags.	GC (NPD) with cryotrapping preconcentration.	Glindemann *et al* (1996b), Glindemann *et al* (2005)

Table D.1 is continued on the following page.

Compound	Previous Measurement		Animal waste	Measurement method	Reference
	Concentrations ppb (μg m^{-3})*	Emission Rates			
Phosphine (continued)	0.0014 to 33.7 **(0.002 to 47)**		**Biogas, putrefaction gas, three swine and cattle farming plants.**	Unknown	Glindemann *et al* (2005)
	8318.4 to 273934 **(11600 to 382000)**		**Biogas released from sediments of sewage plants and shallow lakes.**	GC N-P FID	Dévai *et al* (1988)
		280 pg kg^{-1} 2 h 370 pg kg^{-1} 5 h 200 pg kg^{-1} 24 h	**Swine manure applied to a soil sample (0.2 g of manure per g soil) and stored anerobically** at 37°C. Concentrations in the headspace at 2, 5 and 24 h after manure application given.	GC (NPD) with cryotrapping preconcentration used to analyse syringe samples.	Eismann *et al* (1997a)
		410 pg kg^{-1} 2 h 480 pg kg^{-1} 5 h 290 pg kg^{-1} 24 h	**Swine manure applied to a soil (0.2 g of manure per g soil) and stored aerobically** at 37°C. Concentrations in the the headspace measured by taking syringe samples. Concentrations at 2, 5 and 24 h after manure application given.	GC (NPD) with cryotrapping preconcentration.	Eismann *et al* (1997a)
Hydrogen sulphide	**~1400000** (1952294) decreasing to **~500000** (697248) after 45 weeks **~300000** (418349) decreasing to **~150000** (209174) after 46 weeks		30 m^3 (filled over four weeks) of **untreated cattle slurry stored (anerobically) for 45 weeks** in a 60 m^3 tank. Total solids 6.4 %, volatile solids 84 % COD ~40 g l^{-1} (w.23) pH 7.7, total-N 26 g kg^{-1} total solids, NH$_4$-N 13 g kg^{-1} total solids. 30 m^3 (filled over four weeks) of **aerated and stored (45 weeks) cattle slurry** in a 60 m^3 tank. Total solids 6.3 %, volatile solids 83 % COD ~35 g l^{-1} (w.23) pH 7.9, total-N 25 g kg^{-1} total solids, NH$_4$-N 13 g kg^{-1} total solids.	A 20 litre can was three quarter filled for 1 minute and gas concentrations measured using a Dräger hand pump. As above	Skjelhaugen and Donantoni (1998) Skjelhaugen and Donantoni (1998)

Table D.1 is continued on the following page.

Compound	Previous Measurement		Animal waste	Measurement method	Reference
	Concentrations ppb ($\mu g\ m^{-3}$)*	Emission Rates			
Hydrogen sulphide *(continued)*	10757 **(15000)**		**Headspace of pig slurry from pigs fed dry feed pellets collected over 28 days** and stored in enclosed stainless steel trays in a water bath at 15°C for 1 month before placing in an emissions chamber. Slurry analysed before emissions chamber experiment: total solids 5.93 kg, pH 7.1 (pH 7.9 after emissions chamber measurements) ammonium N 458 g, Nitrate N 4.97 g, total N 800 g.	Slurry placed in a 40 m^3 emissions chamber (can reduce from 40 to 15 m^3 over 3 h period) with 1.0 m^3 s^{-1} circulation of air over manure surface at 20 ^{o}C. Tedlar samples taken and analysed by GC-MS.	Hobbs *et al* (1997)
	172105 **(240000)**		**Headspace of pig slurry from pigs fed liquid feed with water to feed ratio of 3:1 (w/w) collected over 28 days** and stored in enclosed stainless steel trays in a water bath at 15°C for 1 month before placing in an emissions chamber. Slurry analysed before emissions chamber experiment: total solids 6.04 kg, pH 7.5 (pH 8.5 after emissions chamber measurements) ammonium N 556 g, Nitrate N 2.20 g, total N 858 g.	As above	Hobbs *et al* (1997)
	2151 **(3000)**		**Headspace of pig slurry from pigs fed liquid feed with water to feed ratio of 4:1 (w/w) collected over 28 days** and stored in enclosed stainless steel trays in a water bath at 15°C for 1 month before placing in an emissions chamber. Slurry analysed before odour and emissions chamber experiment: total solids 4.77 kg, pH 7.6 (pH 8.4 after odour and emissions chamber measurements) ammonium N 502 g, Nitrate N 5.90 g, total N 785 g.	As above	Hobbs *et al* (1997)

Table D.1 is continued on the following page

Compound	Previous Measurement		Animal waste	Measurement method	Reference
	Concentrations ppb (μg m^{-3})*	Emission Rates			
Hydrogen sulphide (continued)		214.7 ($\pm$83.9) mg m^{-2} min^{-1}	**Mean of emission rates from 8 groups of pigs** (12 pigs/group): 4 female groups 4 male groups of the four of each sex two groups were growers, two were finishers, of these two groups one was fed standard commercial diet and the other a reduced crude protein diet.	Slurry placed in a 40 m^3 emissions chamber with 28 m^3 leaked over 2 h. 1.0 m^3 s^{-1} circulation of air over slurry surface. Slurry held at 15°C and the chamber was at 20°C. Samples analysed by GC-MS with preconcentration.	Hobbs *et al* (1998
		0.48 μg 20 g^{-1}	**Fresh (<24 h old) manure from dairy cattle (*Bos taurus*)**, homogenised sample obtained by adding sufficient water to obtain a thick slurry and by blending this slurry for 5 minutes with a mixer. In air dried manure pH 5.7, organic carbon 41.6 % total N 2.15 %, total S 0.231 % ash 9.7 % water content 87.1 % in homogenised slurry used (4.5 % in air dried).	GC analysis of 0.1 - 2.0 ml samples every 2 days from 65 ml or 265 ml bottles containing the manure. Incubations were at 23 ^{o}C and the bottles were sealed with laboratory air for 30 days.	Banwart and Bremner (1975)
		22.8 μg 20 g^{-1}	**Fresh (<24 h old) manure from poultry (*Gallus domesticus*)**, homogenised sample obtained by adding sufficient water to obtain a thick slurry and by blending this carbon 30.0 % total N 5.26 %, total S 0.558 % ash 28.1% water content 78.8 % in homogenised slurry used (5.6 % in air dried).	As above	Banwart and Bremner (1975)

Table D.1 is continued on the following page.

Compound	Previous Measurement		Animal waste	Measurement method	Reference
	Concentrations ppb (μg m^{-3})*	Emission Rates			
Hydrogen sulphide (continued)		31.1 μg 20 g^{-1}	**Fresh (<24 h old) manure from sheep (*Ovis aries*)**, homogenised sample obtained by adding sufficient water to obtain a thick slurry and blending for 5 minutes. In air dried manure pH 8.1, organic carbon 40.3 % total N 2.24 %, total S 0.348 % ash 15.4 % water content 87.1 % in homogenised slurry used (3.2 % in air dried).	As above	Banwart and Bremner (1975)
		1.28 μg 20 g^{-1}	**Fresh (<24 h old) manure from swine (*Sus scrofa*)**, homogenised sample obtained by adding sufficient water to obtain a thick slurry and by blending for 5 minutes. In air dried manure pH 5.9, organic carbon 41.5 % total N 3.67 %, total S 0.260 % ash 15.3 % water content 82.2 % in homogenised slurry used (5.8 % in air dried).	As above	Banwart and Bremner (1975)
Dimethylsulphide	**123 ± 73** (313)		**Headspace of fresh pig urine** values are means of samples from 6 pigs each with samples of unchanged pH, adjusted to pH 4 (using 0.1M HCl) and pH 8.0 (using 0.1 M NaOH).	**SIFT-MS**	Smith *et al* (2000)
	2357 ± 1304 (5990)		**Headspace of fresh pig faeces** from 6 pigs diluted with de-ionised water means of samples from the six pigs with unchanged pH, acidic (pH4 using 0.1M HCl) and alkaline (pH 8.0 using 0.1 M NaOH) given.	**SIFT-MS**	Smith *et al* (2000)

Table D.1 is continued on the following page.

Compound	Previous Measurement		Animal waste	Measurement method	Reference
	Concentrations Ppb ($\mu g\ m^{-3}$)*	Emission Rates			
Dimethylsulphide (continued)		0.20 µg per 20 g	**Fresh (<24 h old) manure from dairy cattle (*Bos taurus*)**, homogenised sample obtained by adding sufficient water to obtain a thick slurry & blending for 5 minutes. In air dried manure pH 5.7, organic carbon 41.6 % total N 2.15 %, total S 0.231 % ash 9.7 % H_2O content 4.5 % (87.1 % in homogenised slurry used).	GC analysis of 0.1 - 2.0 ml samples every 2 days from 65 ml or 265 ml bottles containing the manure. Incubations were at 23 ^{o}C and the bottles were sealed with laboratory air for 30 days.	Banwart and Bremner (1975)
		1.74 µg per 20 g	**Fresh (<24 h old) manure from poultry (*Gallus domesticus*)**, homogenised sample obtained by adding sufficient water to obtain a thick slurry & blending for 5 minutes. In air dried manure pH 7.1, organic carbon 30.0 % total N 5.26 %, total S 0.558 % ash 28.1% H_2O content 5.6 % (78.8 % in homogenised slurry).	As above	Banwart and Bremner (1975)
		1.59 µg per 20 g	**Fresh (<24 h old) manure from sheep (*Ovis aries*)**, homogenised sample obtained by adding sufficient water to obtain a thick slurry and by blending this slurry for 5 minutes with a mixer. In air dried manure pH 8.1, organic carbon 40.3 % total N 2.24 %, total S 0.348 % ash 15.4 % water content 87.1 % in homogenised slurry used (3.2 % in air dried).	As above	Banwart and Bremner (1975)

Table D.1 is continued on the following page.

Compound	Previous Measurement		Animal waste	Measurement method	Reference
	Concentrations ppb (µg m^{-3})*	Emission Rates			
Dimethylsulphide (continued)		0.36 µg per 20 g	**Fresh (<24 h old) manure from swine (*Sus scrofa*)**, homogenised sample obtained by adding sufficient water to obtain a thick slurry and by blending this slurry for 5 minutes with a mixer. In air dried manure pH 5.9, organic carbon 41.5 % total N 3.67 %, total S 0.260 % ash 15.3 % water content 82.2 % in homogenised slurry used (5.8 % in air dried).	As above	Banwart and Bremner (1975)
	5509 (**14000**)		**Headspace of pig slurry from pigs fed dry feed pellets collected over 28 days** and stored in enclosed stainless steel trays in a water bath at 15°C for 1 month before placing in an emissions chamber. Slurry analysed before emissions chamber experiment: total solids 5.93 kg, pH 7.1 (pH 7.9 after emissions chamber measurements) ammonium N 458 g, Nitrate N 4.97 g, total N 800 g.	Slurry placed in a 40 m^3 emissions chamber (can reduce from 40 to 15 m^3 over 3 h period) with 1.0 m^3 s^{-1} circulation of air over manure surface at 20 ^{o}C. Tedlar samples taken and analysed by GC-MS.	Hobbs *et al* (1997)
	None detected		**Headspace of pig slurry from pigs fed liquid feed with water to feed ratio of 3:1 (w/w) collected over 28 days** and stored in enclosed stainless steel trays in a water bath at 15°C for 1 month before placing in an emissions chamber. Slurry analysed before emissions chamber experiment: total solids 6.04 kg, pH 7.5 (pH 8.5 after emissions chamber measurements) ammonium N 556 g, Nitrate N 2.20 g, total N 858 g.	Slurry placed in a 40 m^3 emissions chamber (can reduce from 40 to 15 m^3 over 3 h period) with 1.0 m^3 s^{-1} circulation of air over manure surface at 20 ^{o}C. Tedlar samples taken and analysed by GC-MS.	Hobbs *et al* (1997)

Table D.1 is continued on the following page.

Compound	Previous Measurement		Animal waste	Measurement method	Reference
	Concentrations ppb (μg m^{-3})*	Emission Rates			
Dimethylsulphide (continued)	None detected		**Headspace of pig slurry from pigs fed liquid feed with water to feed ratio of 4:1 (w/w) collected over 28 days** and stored in enclosed stainless steel trays in a water bath at 15°C for 1 month before placing in an emissions chamber. Slurry analysed before emissions chamber experiment: total solids 4.77 kg, pH 7.6 (pH 8.4 after emissions chamber measurements) ammonium N 502 g, Nitrate N 5.90 g, total N 785 g.	Slurry placed in a 40 m^3 emissions chamber (can reduce from 40 to 15 m^3 over 3 h period) with 1.0 m^3 s^{-1} circulation of air over manure surface at 20 ^{o}C. Tedlar samples taken and analysed by GC-MS.	Hobbs *et al* (1997)
Dimethyldisulphide		None detected	**Headspace of fresh cattle slurry**, pH 7.1, 53.7 ± 9.5 g kg^{-1} dry matter, 1.09 ± 0.7 kg m^{-3} NH$_4$.	Slurry placed in a 40 m^3 emissions chamber with 1 m s^{-1} circulation of air over the slurry surface. Slurry kept at 15°C and the emission chamber at 20°C, periodic sampling analysed by **GC-MS** with pre-concentration.	Hobbs *et al* (2004)
		683 g m^{-3} day^{-1}	**Headspace of laying hen manure**, pH 8.3, 501.2 ± 144.8 g kg^{-1} dry matter, 7.52 ± 0.66 kg m^{-3} NH$_4$	As above	Hobbs *et al* (2004)

Table D.1 is continued on the following page.

Compound	Previous Measurement		Animal waste	Measurement method	Reference
	Concentrations ppb (µg m^{-3})*	Emission Rates			
Dimethyldisulphide (continued)	3114 **(12000)**		**Headspace of pig slurry from pigs fed dry feed pellets collected over 28 days** and stored in enclosed stainless steel trays in a water bath at 15°C for 1 month before placing in an emissions chamber. Slurry analysed before odour and emissions chamber experiment: total solids 5.93 kg, pH 7.1 (pH 7.9 after odour and emissions chamber measurements) ammonium N 458 g, Nitrate N 4.97 g, total N 800 g.	Slurry placed in a 40 m^3 emissions chamber (can reduce from 40 to 15 m^3 over 3 h period) with 1.0 m^3 s^{-1} circulation of air over manure surface at 20 ^{o}C. Tedlar samples taken and analysed by GC-MS.	Hobbs *et al* (1997)
	None detected		**Headspace of pig slurry from pigs fed liquid feed with water to feed ratio of 3:1 (w/w) collected over 28 days** and stored in enclosed stainless steel trays in a water bath at 15°C for 1 month before placing in an emissions chamber. Slurry analysed before emissions chamber experiment: total solids 6.04 kg, pH 7.5 (pH 8.5 after emissions chamber measurements) ammonium N 556 g, Nitrate N 2.20 g, total N 858 g.	As above	Hobbs *et al* (1997)
	None detected		**Headspace of pig slurry from pigs fed liquid feed with water to feed ratio of 4:1 (w/w) collected over 28 days** and stored in enclosed stainless steel trays in a water bath at 15°C for 1 month before placing in an emissions chamber. Slurry analysed before emissions chamber experiment: total solids 4.77 kg, pH 7.6 (pH 8.4 after emissions chamber measurements) ammonium N 502 g, Nitrate N 5.90 g, total N 785 g.	As above	Hobbs *et al* (1997)

Table D.1 is continued on the following page.

Compound	Previous Measurement		Animal waste	Measurement method	Reference
	Concentrations ppb (μg m^{-3})*	Emission Rates			
Dimethyldisulphide (continued)		0 μg per 20 g	**Fresh (<24 h old) manure from dairy cattle (*Bos taurus*)**, homogenised sample obtained by adding sufficient water to obtain a thick slurry and by blending this slurry for 5 minutes with a mixer. In air dried manure pH 5.7, organic carbon 41.6 % total N 2.15 %, total S 0.231 % ash 9.7 % water content 87.1 % in homogenised slurry used (4.5 % in air dried).	GC analysis of 0.1 - 2.0 ml samples every 2 days from 65 ml or 265 ml bottles containing the manure. Incubations were at 23 $^{\circ}$C and the bottles were sealed with laboratory air for 30 days.	Banwart and Bremner (1975)
		1.70 μg per 20 g	**Fresh (<24 h old) manure from poultry (*Gallus domesticus*)**, homogenised sample obtained by adding sufficient water to obtain a thick slurry and by blending this slurry for 5 minutes with a mixer. In air dried manure pH 7.1, organic carbon 30.0 % total N 5.26 %, total S 0.558 % ash 28.1% water content 78.8 % in homogenised slurry used (5.6 % in air dried).	As above	Banwart and Bremner (1975)
		0.13 μg per 20 g	**Fresh (<24 h old) manure from sheep (*Ovis aries*)**, homogenised sample obtained by adding sufficient water to obtain a thick slurry and by blending for 5 minutes. In air dried manure pH 8.1, organic carbon 40.3 % total N 2.24 %, total S 0.348 % ash 15.4 % H$_2$O content 3.2 % (87.1 % in homogenised slurry).	As above	Banwart and Bremner (1975)

Table D.1 is continued on the following page.

Compound	Previous Measurement		Animal waste	Measurement method	Reference
	Concentrations ppb ($\mu g\ m^{-3}$)*	Emission Rates			
Dimethyldisulphide (continued)		0.08 μg per 20 g	**Fresh (<24 h old) manure from swine (*Sus scrofa*)**, homogenised sample obtained by adding sufficient water to obtain a thick slurry and blending for 5 minutes. In air dried manure pH 5.9, organic carbon 41.5 % total N 3.67 %, total S 0.260 % ash 15.3 H_2O content 5.8 % (82.2 % in homogenised slurry).	As above	Banwart and Bremner (1975)
Dimethylsulphoxide	36.24 to 126.65 **(115.70 to 404.36)**		**Air at three sampling sites at a commercial dairy farm in California** two of which were next to a waste water lagoon, dimethylsulphoxide was observed in 18 out of 48 samples.	**GC-MS** with simultaneous olfactometry (samples collected on adsorption tubes).	Rabaud *et al* (2003)
Methanethiol (methyl mercaptan)	Typically **100** (196)		**Headspace of fresh pig urine** values are means of samples from 6 pigs each with samples of unchanged pH, adjusted to pH4 (by addition of 0.1M HCl) and pH 8.0 (using 0.1 M NaOH).	**SIFT-MS**	Smith *et al* (2000)
	376 ng litre-1		**Air samples from the middle of a pig house** (44 pigs, 5.3 m^3 of air per pig). VMR in the air were primarily determined by concentrations of the acid in faeces and slurry: 3139 mg g-1 dry matter in slurry.	**RF-HPLC with fluorescence detection.**	Willig *et al* (2004)

Table D.1 is continued on the following page

Compound	Previous Measurement		Animal waste	Measurement method	Reference
	Concentrations ppb (μg m^{-3})*	Emission Rates			
Methanethiol (continued)	18336 **(36000)**		**Headspace of pig slurry from pigs fed dry feed pellets collected over 28 days** and stored in enclosed stainless steel trays in a water bath at 15°C for 1 month before placing in an emissions chamber. Slurry analysed before odour and emissions chamber experiment: total solids 5.93 kg, pH 7.1 (pH 7.9 after odour and emissions chamber measurements) ammonium N 458 g, Nitrate N 4.97 g, total N 800 g.	Slurry placed in a 40 m^3 emissions chamber (can reduce from 40 to 15 m^3 over 3 h period) with 1.0 m^3 s^{-1} circulation of air over manure surface at 20 ^{o}C. Tedlar samples taken and analysed by GC-MS.	Hobbs *et al* (1997)
	None detected		**Headspace of pig slurry from pigs fed liquid feed with water to feed ratio of 3:1 (w/w) collected over 28 days** and stored in enclosed stainless steel trays in a water bath at 15°C for 1 month before placing in an emissions chamber. Slurry analysed before emissions chamber experiment: total solids 6.04 kg, pH 7.5 (pH 8.5 after emissions chamber measurements) ammonium N 556 g, Nitrate N 2.20 g, total N 858 g.	As above	Hobbs *et al* (1997)
	None detected		**Headspace of pig slurry from pigs fed liquid feed with water to feed ratio of 4:1 (w/w) collected over 28 days** and stored in enclosed stainless steel trays in a water bath at 15°C for 1 month before placing in an emissions chamber. Slurry analysed before chamber experiment: total solids 4.77 kg, pH 7.6 (pH 8.4 after chamber measurements) ammonium N 502 g, Nitrate N 5.90 g, total N 785 g.	As above	Hobbs *et al* (1997)

Table D.1 is continued on the following page

Compound	Previous Measurement		Animal waste	Measurement method	Reference
	Concentrations ppb ($\mu g\ m^{-3}$)*	Emission Rates			
Methanethiol (continued)		0.34 µg per 20 g	**Fresh (<24 h old) manure from dairy cattle (*Bos taurus*)**, homogenised sample obtained by adding sufficient water to obtain a thick slurry and by blending this slurry for 5 minutes with a mixer. In air dried manure pH 5.7, organic carbon 41.6 % total N 2.15 %, total S 0.231 % ash 9.7 % water content 87.1 % in homogenised slurry used (4.5 % in air dried).	GC analysis of 0.1 - 2.0 ml samples every 2 days from 65 ml or 265 ml bottles containing the manure. Incubations were at 23 ^{o}C and the bottles were sealed with laboratory air for 30 days.	Banwart and Bremner (1975)
		51.5 µg per 20 g	**Fresh (<24 h old) manure from poultry (*Gallus domesticus*)**, homogenised sample obtained by adding sufficient water to obtain a thick slurry and by blending this slurry for 5 minutes with a mixer. In air dried manure pH 7.1, organic carbon 30.0 % total N 5.26 %, total S 0.558 % ash 28.1% water content 78.8 % in homogenised slurry used (5.6 % in air dried).	As above	Banwart and Bremner (1975)
		16.7 µg per 20 g	**Fresh (<24 h old) manure from sheep (*Ovis aries*)**, homogenised sample obtained by adding sufficient water to obtain a thick slurry and by blending this slurry for 5 minutes with a mixer. In air dried manure pH 8.1, organic carbon 40.3 % total N 2.24 %, total S 0.348 % ash 15.4 % H_2O content 3.2 % (87.1 % in homogenised slurry).	As above	Banwart and Bremner (1975)

Table D.1 is continued on the following page.

Compound	Previous Measurement		Animal waste	Measurement method	Reference
	Concentrations ppb ($\mu g\ m^{-3}$)*	Emission Rates			
Methanethiol (continued)		1.35 μg per 20 g	**Fresh (<24 h old) manure from swine (*Sus scrofa*)**, homogenised sample obtained by adding sufficient water to obtain a thick slurry and by blending this slurry for 5 minutes. In air dried manure pH 5.9, organic carbon 41.5 % total N 3.67 %, total S 0.260 % ash 15.3 % H_2O content 5.8 % (82.2 % in homogenised slurry).	As above	Banwart and Bremner (1975)
Methylamine		4×10^{-16} to 13×10^{-16} moles $m^{-2}\ h^{-1}$	**Air above manure piles regularly loaded with fresh manure from beef cattle.**		Schade and Crutzen (1995) and references therein.
Dimethylamine		0.6×10^{-16} to 5×10^{-16} moles $m^{-2}\ h^{-1}$	**Air above manure piles regularly loaded with fresh manure from beef cattle.**		Schade and Crutzen (1995) and references therein.
Trimethylamine		0.5×10^{-16} to 13×10^{-16} moles $m^{-2}\ h^{-1}$	**Air above manure piles regularly loaded with fresh manure from beef cattle.**		Schade and Crutzen (1995) and references therein.
Phenol	1246 **(4800)**		**Headspace of pig slurry from pigs fed dry feed pellets collected over 28 days** and stored in enclosed stainless steel trays in a water bath at 15°C for 1 month before placing in an emissions chamber. Slurry analysed before odour and emissions chamber experiment: total solids 5.93 kg, pH 7.1 (pH 7.9 after odour and emissions chamber measurements) ammonium N 458 g, Nitrate N 4.97 g, total N 800 g.	Slurry placed in a 40 m^3 emissions chamber (can reduce from 40 to 15 m^3 over 3 h period) with 1.0 m^3 s^{-1} circulation of air over manure surface at 20 ^{o}C. Tedlar samples taken and analysed by GC-MS.	Hobbs *et al* (1997)

Table D.1 is continued on the following page.

Compound	Previous Measurement		Animal waste	Measurement method	Reference
	Concentrations ppb (µg m^{-3})*	Emission Rates			
Phenol (continued)	960.2 **(3700)**		**Headspace of pig slurry from pigs fed liquid feed with water to feed ratio of 3:1 (w/w) collected over 28 days** and stored in enclosed stainless steel trays in a water bath at 15°C for 1 month before placing in an emissions chamber. Slurry analysed before emissions chamber experiment: total solids 6.04 kg, pH 7.5 (pH 8.5 after emissions chamber measurements) ammonium N 556 g, Nitrate N 2.20 g, total N 858 g.	As above	Hobbs *et al* (1997)
	1116 **(4300)**		**Headspace of pig slurry from pigs fed liquid feed with water to feed ratio of 4:1 (w/w) collected over 28 days** and stored in enclosed stainless steel trays in a water bath at 15°C for 1 month before placing in an emissions chamber. Slurry analysed before emissions chamber experiment: total solids 4.77 kg, pH 7.6 (pH 8.4 after emissions chamber measurements) ammonium N 502 g, Nitrate N 5.90 g, total N 785 g.	As above	Hobbs *et al* (1997)
		0.01 g m^{-3} day^{-1}	**Headspace of fresh cattle slurry**, pH 7.1, 53.7 ± 9.5 g kg^{-1} dry matter, 1.09 ± 0.7 kg m^{-3} NH$_4$.	Slurry placed in a 40 m^3 emissions chamber with 1 m s^{-1} circulation of air over the slurry surface. Slurry kept at 15°C and the chamber at 20°C Samples analysed by **GC-MS** with preconcentration.	Hobbs *et al* (2004)

Table D.1 is continued on the following page.

Compound	Previous Measurement		Animal waste	Measurement method	Reference
	Concentrations ppb (μg m^{-3})*	Emission Rates			
Phenol (continued)		Trace	**Headspace of laying hen manure**, pH 8.3, 501.2 $\pm$ 144.8 g kg^{-1} dry matter, 7.52 $\pm$ 0.66 kg m^{-3} NH$_4$.	As above	Hobbs *et al* (2004)
		0.21 ($\pm$0.247) mg m^{-2} min^{-1}	**Mean of emission rates from 8 groups of pigs** (12 pigs/group): 4 female groups 4 male groups of the four of each sex two groups were growers, two were finishers, of these two groups one was fed standard commercial diet and the other a reduced crude protein diet.	Slurry placed in a 40 m^3 emissions chamber. 1.0 m^3 s^{-1} circulation of air over slurry surface. Slurry held at 15°C and the chamber at 20°C. Samples analysed by GC-MS with preconcentration.	Hobbs *et al* (1998)
4-methylphenol (*p*-cresol)	150 ng litre-1		**Air samples from the middle of a pig house** (44 pigs, 5.3 m^3 of air per pig). VMR in the air were primarily determined by concentrations of the acid in faeces and slurry: 360 mg g^{-1} in faeces, 226 mg g^{-1} in slurry.	**RF-HPLC with fluorescence detection.**	Willig *et al* 2004
		2.80 g m^{-3} day^{-1}	**Headspace of fresh cattle slurry**, pH 7.1, 53.7 $\pm$ 9.5 g kg^{-1} dry matter, 1.09 $\pm$ 0.7 kg m^{-3} NH$_4$.	Slurry placed in a 40 m^3 emissions chamber with 1 m s^{-1} circulation of air over the slurry surface. Slurry kept at 15°C and the emission chamber at 20°C, periodic sampling analysed by **GC-MS** with pre-concentration.	Hobbs *et al* (2004)
		Trace	**Headspace of laying hen manure**, pH 8.3, 501.2 $\pm$ 144.8 g kg^{-1} dry matter, 7.52 $\pm$ 0.66 kg m^{-3} NH$_4$.	As above	Hobbs *et al* (2004)

Table D.1 is continued on the following page

Compound	Previous Measurement		Animal waste	Measurement method	Reference
	Concentrations ppb (μg m^{-3})*	Emission Rates			
4-methylphenol (continued)	1583 **(7000)**		**Headspace of pig slurry from pigs fed dry feed pellets collected over 28 days** and stored in enclosed stainless steel trays in a water bath at 15°C for 1 month before placing in an emissions chamber. Slurry analysed before emissions chamber experiment: total solids 5.93 kg, pH 7.1 (pH 7.9 after emissions chamber measurements) ammonium N 458 g, Nitrate N 4.97 g, total N 800 g.	Slurry placed in a 40 m^3 emissions chamber (can reduce from 40 to 15 m^3 over 3 h period) with 1.0 m^3 s^{-1} circulation of air over manure surface at 20 ^{o}C. Tedlar samples taken and analysed by GC-MS.	Hobbs *et al* (1997)
	1312 **(5800)**		**Headspace of pig slurry from pigs fed liquid feed with water to feed ratio of 3:1 (w/w) collected over 28 days** and stored in enclosed stainless steel trays in a water bath at 15°C for 1 month before placing in an emissions chamber. Slurry analysed before emissions chamber experiment: total solids 6.04 kg, pH 7.5 (pH 8.5 after odour and emissions chamber measurements) ammonium N 556 g, Nitrate N 2.20 g, total N 858 g.	As above	Hobbs *et al* (1997)
	1040 **(4600)**		**Headspace of pig slurry from pigs fed liquid feed with water to feed ratio of 4:1 (w/w) collected over 28 days** and stored in enclosed stainless steel trays in a water bath at 15°C for 1 month before placing in an emissions chamber. Slurry analysed before emissions chamber experiment: total solids 4.77 kg, pH 7.6 (pH 8.4 after odour and emissions chamber measurements) ammonium N 502 g, Nitrate N 5.90 g, total N 785 g.	As above	Hobbs *et al* (1997)

Table D.1 is continued on the following page.

Compound	Previous Measurement		Animal waste	Measurement method	Reference
	Concentrations ppb (μg m^{-3})*	Emission Rates			
4-methylphenol (continued)		0.44 (± 0.397) mg m^{-2} min^{-1}	**Mean of emission rates from 8 groups of pigs** (12 pigs/group): 4 female groups 4 male groups of the four of each sex two groups were growers, two were finishers, of these two groups one was fed standard commercial diet and the other a reduced crude protein diet.	Slurry placed in a 40 m^3 emissions chamber with 28 m^3 leaked over 2 h. 1.0 m^3 s^{-1} circulation of air over slurry surface. Slurry held at 15°C and the chamber was at 20°C. Samples analysed by GC-MS with preconcentration.	Hobbs *et al* (1998)